1987

PLASMA DIAGNOSTICS WITH MICROWAVES

WILEY SERIES IN PLASMA PHYSICS

SANBORN C. BROWN, ADVISORY EDITOR
RESEARCH LABORATORY OF ELECTRONICS
MASSACHUSETTS INSTITUTE OF TECHNOLOGY

HEALD AND WHARTON · PLASMA DIAGNOSTICS WITH MICROWAVES
MCDANIEL · COLLISION PHENOMENA IN IONIZED GASES

PLASMA DIAGNOSTICS WITH MICROWAVES

M. A. Heald

Department of Physics
Swarthmore College
Swarthmore, Pennsylvania

C. B. Wharton

General Atomic Division
General Dynamics Corporation
San Diego, California

John Wiley & Sons Inc., New York · London · Sydney

Library of Congress Catalog Card Number: 64–23839
PRINTED IN THE UNITED STATES OF AMERICA

To Jane and Gloria, who have played well
the roles of both wife and midwife
during this long labor.

Preface

The subject of plasma diagnostics is concerned with making significant, nonperturbing measurements and expressing them in numbers. The term "diagnostics," of course, comes from the medical profession. The word was first borrowed by scientists engaged in testing nuclear explosions about fifteen years ago to describe measurements in which they deduced the progress of various physical processes from the observable external symptoms. The word crept into the jargon of the then-classified Sherwood Program, the AEC program of controlled nuclear fusion research. Now the term "plasma diagnostics" is applied to a wide variety of plasma measurements. The term implies that the diagnostic measurement does not itself change the state of the plasma, that two or more diagnostic measurements may thus be made simultaneously and, in most cases, that time-resolved data can be obtained from a single transient event.

In the case of microwave diagnostics, the interpretation often is difficult and requires not only an understanding of the formal theory of electromagnetic interactions with plasmas, but also development of an intuitive skill in selecting meaningful simplifications. Many of the cases of wave propagation are much too complicated to permit exact formulation and solution; a feeling for how things scale from similar, more tractable cases is often essential. Consequently, we shall find it necessary to develop a fairly complete basic theory of many facets of wave interactions on which to base our scaling and approximating to specific cases.

Historically, the subject of microwave diagnostics is not new. The laboratory experiments of Balthazar van der Pol (1920) to demonstrate that charged particles have a large influence on electromagnetic wave propagation did much to settle an important controversy of the day,

whether or not an ionosphere was responsible for distant radio propagation. His calculations of plasma conductivity and refractive index yielded the same equations to be found in our Chapter 1 for the Lorentz plasma, including a density-dependent term that was later named the *plasma frequency* by Tonks and Langmuir (1929). Subsequently, workers in the field of ionospheric propagation, with such landmarks as Appleton (1932) and Mitra (1952), have perfected to a high degree the use of radio-wave probes for sounding the ionosphere.

The improved microwave technology following World War II opened new expanses of the frequency spectrum. The pioneering theoretical work of Margenau (1946) and experimental work of Biondi and Brown (1949) and others in the M.I.T. group, in developing resonant cavity techniques, rekindled interest in plasma measurements with electromagnetic waves. Faraday-rotation measurements with waves beamed through controlled fusion plasmas, performed by R. F. Post and others in Berkeley in 1952, stimulated the development of microwave diagnostics as a standard measuring technique in Project Sherwood research (Wharton et al., 1955; Heald, 1956).

Laboratory experimental techniques have come a long way since the days of van der Pol, who measured the shift in standing waves on a Lecher wire terminated by small capacitive discs immersed in the plasma. His microwave source was a Blondlot arc, running under kerosene, producing a few milliwatts of damped 200 Mc wave trains. Nevertheless, embellishments of those early day techniques are still used for diagnosing low-density plasmas, and several of the experiments described in Chapters 5 and 6 have recognizable similarities.

Our aim in writing this book has been to bring together, on the one hand, a summary of the basic theory of the interaction of electromagnetic waves with plasmas and, on the other, a description of the practical experimental techniques that exploit this interaction. The book is written mainly in the context of the plasmas of controlled fusion research, which are characteristically *hot* (implying a high degree of ionization and low interparticle collision rates) and *large* (relative to the wavelength of an electromagnetic wave at the plasma frequency ω_p). However, most of the material is relevant also to the plasmas found in the fields of M.H.D. power generation, space vehicle propulsion and communication, ionospheric radio propagation, microwave devices, classical gas discharges, and radio astronomy. We have limited the detailed discussions to "high-frequency" techniques that use waves at frequencies of the order of the electron plasma frequency. Also, we have given somewhat more attention to free-space beam techniques than to those employing resonant cavities and waveguides.

The formal theory of electromagnetic interactions in plasma often makes use of mathematical techniques that are beyond the experimentalist's training. We make no apologies about writing the book from an experimentalist's viewpoint, so that many of the theoretical discussions are somewhat cavalier and inelegant. On the other hand, we have endeavored to go beyond the mere displaying of useful theoretical formulas. The theory presented is developed sufficiently to indicate the assumptions and ranges of validity of the more sophisticated theoretical presentations in the literature as well as to serve as a primer for these treatments. Thus for instance, we present a hydromagnetic treatment of wave propagation in Section 3.3 although, in general, more useful "practical" results are obtained by the corresponding kinetic treatment of Section 3.4. The hope, then, is that this volume may be of some value to those seeking an introduction to plasma physics beyond the narrow topic of microwave diagnostics, without offending the specialist seeking solutions to specific problems.

The similarities and differences of electromagnetic and spacecharge wave propagation in bounded plasmas and in infinite, homogeneous plasmas are carefully delineated, including the dependence of wave properties on temperature and magnetic field strength. Because the effects of finite temperature on spacecharge wave propagation have been included, we are able to give an introduction to wave growth and electrostatic instabilities and to collisionless (Landau) damping. Some of the effects of instabilities and turbulence on wave scattering and electromagnetic radiation are also discussed.

There is considerable experimental material included. We have attempted to present the broad picture of wave propagation and radiation experiments, still retaining enough detail to permit an experimentalist new in the field to proceed with a diagnostic experiment. The descriptions of the techniques, therefore, are fairly complete. Numerous illustrative examples have been chosen from the literature and from our own work. Some of the latter are new and are published here for the first time.

Our subject is specialized; this volume was not visualized as a text in formal courses, although portions of it may well fit into certain courses. No formal problems have been included although problem material is present. In the plasma physics field, workers will come from a number of diverse backgrounds. An argument or notation that is familiar and elementary to a microwave tube engineer, for example, may not be familiar to a specialist in gaseous discharges. And the terminology of fluid mechanics or ionosphere research may be unfamiliar to workers in the former fields, and vice versa. The literature abounds with different notational conventions, often not explicitly stated. Consequently, we

have attempted to maximize this book's use for reference and individual study by defining many terms, by cross-referencing, and by including or giving references to elementary and applied material from diverse fields that might be passed over in a textbook.

The first six chapters are devoted to the propagation of externally generated waves in a plasma, the first five being primarily theoretical. Chapter 1 presents the well-known Appleton-Hartree theory of wave propagation, including a brief discussion of the effect of heavy-ion motion. The next two chapters examine the role of collision processes, especially electron-ion Coulomb collisions, and summarize the modifications that occur when electron thermal speeds are comparable with the wave phase velocity. Chapters 4 and 5 consider the boundaries and spatial nonuniformity of real plasmas. Chapter 4 deals with the propagation of free-space beams, and includes a discussion of the choice of antenna systems with which to probe a plasma sample of given size. Chapter 5 meanwhile deals with a plasma confined in a resonant cavity or waveguide, or acting as a waveguiding structure itself, for either electromagnetic or spacecharge waves. Finally Chapter 6 gives an extensive discussion of the practical applications of these *active* microwave probing techniques.

Chapters 7 and 8 present, respectively, the theory of microwave radiation generated by a plasma, by both thermal and nonthermal processes, and the practical application of *passive* radiometric techniques.

Chapter 9 is devoted to extensive descriptions and photographs of much of the hardware and special circuits useful for microwave diagnostics, but not readily available commercially. With some regret we have omitted a listing of commercial suppliers of generators, detectors, and components, although references to listings in the literature have been cited. While this information is of great use to an experimentalist entering the field, we feared that a list would soon be obsolete and subject to unintended favoritism.

A brief survey of a number of other plasma diagnostic techniques besides microwaves is given in Chapter 10. The main emphasis has been placed on techniques that yield information similar to that obtainable with microwaves, that is, plasma electron properties, although other techniques were included for completeness. Correlative measurements are indicated where possible.

A summary of wave propagation in general dielectric materials is given in Appendix A. This can serve as a starting point for those readers unfamiliar with microwaves or needing a review. A brief summary of some of the properties of tensors and matrices is given in Appendix B, since these operations are used repeatedly throughout the text.

An unusually large number of references is cited, many from the very recent research literature. To a large extent, this book is a review of

research in progress rather than a text in a well established field. Therefore we have felt it necessary, especially in the theoretical chapters, to provide the means of following up our introductory discussions with more detailed research papers. It is inevitable that many of these references will be superseded by new work in the near future.

A bibliography of important general references is given at the end of the book. Literature references in the text are identified by author and year. Bibliographic details are then given in listings following the general bibliography. The references for Chapters 1 to 8 and the appendices are compiled into a single alphabetical author list. However, since the material covered in Chapters 9 and 10 is somewhat foreign to that of the other chapters, separate reference lists are given for these two chapters. The reference lists may be used as an author index.

We have attempted to follow the notation and terminology of plasma waves admirably systematized by the M.I.T. group (Allis et al., 1963), except in a few cases where strong tradition decrees otherwise. Familiarity with our notation for general wave propagation may be obtained by a quick glance through Appendix A. We have tried to avoid obscure normalized parameters, so often found in theoretical journal papers, in an attempt to preserve some physical insight into the equations. Because we make much use of complex notation for familiar coefficients (such as conductivity, dielectric constant, and refractive index) we have used the special symbol $\cup$ (as $\breve{\sigma}$, $\breve{\kappa}$, and $\breve{\mu}$) to indicate explicitly when a quantity is complex. Considerable use is made of vector and tensor notation; a brief review is given in Appendix B.

Rationalized mks units have been used throughout. However, numerical graphs and formulas are often stated in the vernacular of centimeters, gigacyles, and kilogauss. In particular, energies normally are stated in electron volts, or in units of the Rydberg energy constant ($R_y = 13.6$ eV) when this is relevant to the physics. Temperatures are expressed in energy units (kT); those of other preference may note that 1 electron volt $\approx 1.16 \times 10^4$ degrees Kelvin.

In preparing this book we have been assisted greatly by our colleagues at the Plasma Physics Laboratory (Project Matterhorn) of Princeton University, at the Lawrence Radiation Laboratory of the University of California, and at the John Jay Hopkins Laboratory of General Atomic in San Diego, as well as by numerous other associates who have taken the time to point out some of our errors and shortcomings. Professor S. C. Brown, of M.I.T., has read the manuscript and contributed helpful suggestions.

Swarthmore, Pennsylvania — M. A. HEALD
San Diego, California — C. B. WHARTON

Contents

1 Electromagnetic Wave Propagation in a Cold Plasma, 1

1.1 Introduction, 1

1.2 Plasma oscillations and the plasma frequency, 2

1.3 Electromagnetic wave propagation (no magnetic field), 4
- 1.3.1 Elementary case neglecting collisions, 4
- 1.3.2 Conductivity with collisional damping: Lorentz conductivity, 6
- 1.3.3 Propagation in a Lorentz plasma (no magnetic field), 6
- 1.3.4 Low-loss plasmas ($\nu \ll \omega_p$): the three frequency regions, 7
- 1.3.5 The critical electron density, 12

1.4 Wave propagation with magnetic field, 12
- 1.4.1 Wave propagation along the magnetic field: circularly polarized waves, 12
- 1.4.2 Faraday rotation of angle of polarization, 19
- 1.4.3 Arbitrary direction of propagation: coordinate systems, 20
- 1.4.4 Magnetic field at angle θ with respect to propagation: Appleton's equation, 21
- 1.4.5 Wave polarization, 24
- 1.4.6 Propagation across the magnetic field, 25
- 1.4.7 The conductivity tensor, 29
- 1.4.8 Conductivity in rotating coordinates, 31
- 1.4.9 Summary of principal waves, 34

1.4.10 Propagation at an oblique angle: the QL and QT approximations, 38
1.4.11 Index, velocity, and ray surfaces, 45
1.4.12 Refractive index contour maps, 49
1.5 Ion motion effects, 50
1.5.1 Conductivity with ion motions, 51
1.5.2 Principal waves including ion motions, 52
1.5.3 Oblique propagation with ion motions, 56

2 Collision Processes, 57

2.1 Introduction, 57
2.2 Elementary considerations of collision processes, 58
2.2.1 Collision cross sections and frequencies, 58
2.2.2 Velocity dependence of cross sections, 62
2.3 Effect of collisions on electron motion, 64
2.4 Analysis of particle interactions, 66
2.4.1 Boltzmann equation, 67
2.4.2 Elementary Boltzmann theory of plasma conductivity, 69
2.4.3 Effective collision frequency, 71
2.5 Coulomb interactions, 76
2.5.1 Debye shielding, 76
2.5.2 Coulomb collisions, 79
2.5.3 Effective coulomb collision frequencies, 82
2.5.4 The logarithmic term, 85
2.6 Nonlinear effects, 89
2.6.1 Criterion for linearity, 89
2.6.2 Breakdown, 91
2.6.3 Luxembourg effect, 91
2.6.4 Other nonlinearities, 92
2.6.5 Incoherent scattering, 93

3 Waves in Warm Plasma, 95

3.1 Introduction, 95
3.2 Magnetic permeability of a plasma, 96
3.3 Hydromagnetic calculation of plasma waves, 98
3.3.1 Moment equations, 98
3.3.2 Hydromagnetic dispersion relations, 100
3.4 Kinetic (Boltzmann) theory of waves, 104
3.4.1 Propagation along the field, 108
3.4.2 Propagation across the field, 111

3.4.3 No magnetic field, 112
3.4.4 Plasma or electrostatic waves, 112
3.5 Landau damping and wave absorption, 113
3.6 Relativistic plasmas, 115

4 Wave Propagation Through Bounded Plasmas, 117

4.1 Introduction, 117
4.2 Simple adiabatic analysis of a plasma slab, 120
4.2.1 Average electron density, 120
4.2.2 Adiabatic measurement of density profile, 123
4.2.3 Reflections from cutoffs and resonances, 125
4.3 The slab with sharp boundaries, 127
4.4 Inhomogeneous plasmas, 130
4.4.1 Isotropic inhomogeneous plasmas, 133
4.4.2 Anisotropic inhomogeneous plasmas, 136
4.5 The geometrical optics of a uniform cylindrical plasma column, 137
4.5.1 Transmission loss by refraction, 137
4.5.2 Other sources of loss, 141
4.6 The antenna problem, 141
4.6.1 Fresnel zones, 142
4.6.2 Collimation, 146
4.6.3 Optimization of antennas, 148
4.6.4 Validity of the geometrical-optics, slab model, 150

5 Guided Wave Propagation, 155

5.0 Introduction, 155
5.1 Measurements on plasmas contained in resonant cavities, 155
5.1.1 Measurement of plasma admittance, 158
5.1.2 Measurement of plasma density and collision frequency, 159
5.1.3 Special cavity modes for high density plasmas, 162
5.1.4 Experimental techniques, 163
5.2 Waveguides containing plasmas, 163
5.3 The ω-β diagram, 167
5.4 Nonuniform plasma in a waveguide, 168
5.5 Spacecharge waves, 170
5.5.1 Spacecharge waves in a cold, drifting plasma, 171
5.5.2 Spacecharge waves in plasma columns of finite radius, 174

5.5.3 Spacecharge waves in a plasma column in a magnetic field, 179
5.5.4 Surface spacecharge waves on a drifting plasma column, 182
5.6 Spacecharge waves in a warm plasma, 183
5.6.1 No magnetic field, 183
5.6.2 Spacecharge waves in a warm, magnetized plasma, 188

6 Microwave Propagation Experiments, 192

6.1 Transmission-attenuation and reflection experiments, 192
6.1.1 Microwave circuits for transmission and reflection measurement, 192
6.1.2 Transient plasmas, 194
6.2 Frequency diversity, 197
6.2.1 Frequency diplexers, 199
6.2.2 Polarization diplexers, 200
6.3 Phase-shift measurements, 200
6.3.1 Microwave interferometer, 200
6.3.2 Rf modulation envelope, 204
6.3.3 "Fringe-shift" or zebra-stripe interferometer, 206
6.3.4 Polar plot display, 210
6.4 Density distribution: profile measurements, 212
6.5 Magnetic field effects, 219
6.5.1 Ordinary and extraordinary waves; density profiles, 220
6.5.2 Faraday rotation, 223
6.5.3 Whistler mode propagation, 225
6.5.4 Propagation at angle θ to magnetic field, 227
6.5.5 Doppler-shifted gyrofrequency in drifting plasmas, 228
6.6 Propagation through fluctuating plasmas, 229
6.7 Microwave scattering experiments, 232
6.7.1 Incoherent scattering, 232
6.7.2 Scattering from plasma fluctuations, 234
6.7.3 Scattering from small plasma columns, 240

7 Microwave Radiation from Plasma, 242

7.1 Introduction, 242
7.2 Strict blackbody radiation, 242
7.3 Bremsstrahlung in a transparent medium, 245
7.3.1 Radiation by a single electron, 246

7.3.2 The Gaunt factor, 248
7.3.3 Quantum considerations, 250
7.3.4 Electron shielding, 252
7.3.5 The Gaunt factor and $\ln\Lambda$, 253
7.3.6 Summary of microwave bremsstrahlung, 254
7.3.7 Atom bremsstrahlung and total radiation, 256
7.4 Radiation transport and the gray body, 257
7.4.1 Energy flow in an inhomogeneous medium, 257
7.4.2 The Einstein coefficients, 259
7.4.3 The partially transparent plasma, 261
7.4.4 Correlation of emission and conductivity theories, 262
7.5 Radiation from a slab and Kirchhoff's law, 263
7.5.1 Effect of antenna gain, 264
7.5.2 Surface reflection, 266
7.5.3 Kirchhoff's law, 270
7.6 Cyclotron radiation, 272
7.6.1 Total radiation, 272
7.6.2 Radiation anisotropy (nonrelativistic), 273
7.6.3 Line shape (nonrelativistic), 274
7.6.4 Radiation by a single relativistic electron, 275
7.6.5 Spectrum (relativistic), 276
7.6.6 Effect of collective electron motion, 278
7.7 Cerenkov radiation, 280
7.8 Coherent radiation, 285

8 Plasma Radiation Experiments, 287

8.1 Radiation from dense plasmas: blackbody radiation, 287
8.2 Radiation from a plasma in a magnetic field, 291
8.2.1 Magnetic mirror radiation experiments, 292
8.2.2 Absorption-radiation experiment in a pulsed mirror machine, 293
8.2.3 Absorption-radiation measurements in a waveguide or cavity, 297
8.3 Swept-frequency radiometers, 299
8.4 Radiation of nonthermal origin, 299
8.4.1 Instability-generated radiation, 300
8.4.2 Nonthermal cyclotron radiation, 302

9 Microwave Hardware and Techniques, 305

9.1 Transmission lines, 305
9.1.1 Waveguide considerations, 305

9.1.2 Open waveguide transmission lines, 310
9.1.3 Free-space radiation, 312
9.2 Special components, 313
9.2.1 Phase shifters, 314
9.2.2 Hybrid junctions, 315
9.2.3 Polarization and frequency diplexers, 316
9.2.4 Filters, 318
9.2.5 Circular polarizers, 319
9.2.6 Resonant cavities, 324
9.3 Antennas and radiators, 329
9.3.1 Horns, 329
9.3.2 Lenses, 331
9.3.3 Dielectric rod antennas, 334
9.3.4 Reflecting antennas, 336
9.3.5 Slot radiators, 338
9.3.6 Antenna pattern measurements, 341
9.4 Signal sources, 344
9.4.1 Klystrons, 344
9.4.2 Traveling wave oscillators and amplifiers, 344
9.4.3 Magnetrons, 345
9.4.4 Tunnel diodes, 345
9.4.5 Harmonic generators, 345
9.5 Signal detection, 346
9.5.1 Video crystal detectors, 346
9.5.2 Superheterodyne receivers, 349
9.5.3 Parametric mixer-amplifiers, 351
9.5.4 Miscellaneous receiver systems, 352
9.5.5 Microwave radiometers, 353
9.5.6 Measurement of receiver performance, 355
9.6 Vacuum system considerations, 356
9.6.1 Vacuum materials, 356
9.6.2 Transmission-line windows, 357
9.6.3 Movable probes, 360
9.6.4 Microwave absorbers, 361
9.7 Circuitry considerations, 362
9.7.1 Electronic circuits, 362
9.7.2 Circuit interference and stray pickup, 364

10 General Plasma Diagnostic Techniques, 366

10.1 Tabulation of some useful diagnostic techniques, 366
10.2 Optical and infrared probing, 368

10.3 Conductivity probes, 374
10.4 Langmuir probes, 378
10.4.1 Single Langmuir probe, no magnetic field, 378
10.4.2 Single probe with a magnetic field, 383
10.4.3 Single probe: miscellaneous effects, 384
10.4.4 Double floating probes, 384
10.4.5 Double probes, no magnetic field, 384
10.4.6 Double probes in a magnetic field, 385
10.4.7 Double probes: miscellaneous effects, 386
10.5 Plasma wave and resonant probes, 386
10.6 Magnetic probes, 387
10.7 Ballistic probes, 387
10.8 Optical spectroscopy, 388
10.8.1 Constituent identity and state, 388
10.8.2 Stark broadening, 388
10.8.3 Doppler broadening, 389
10.8.4 Doppler shift, 390
10.9 Bremsstrahlung and recombination continuum, 391

Appendix A Review of Electromagnetic Wave Propagation, 392

A.1 Basic relations for a linear medium, 392
A.1.1 Complex dielectric constant or conductivity, 394
A.1.2 Complex propagation constants, 396
A.2 Microscopic relations, 400
A.2.1 The microscopic field in a dielectric, 401
A.2.2 The microscopic field in a plasma, 402
A.3 Propagation in an anisotropic medium, 403

Appendix B Tensor and Matrix Algebra, 406

B.1 Vectors, tensors, and matrices, 406
B.2 Addition, multiplication, and inversion of tensors, 408

General References, 411
References for Chapters 1–8, 412
References for Chapter 9, 430
References for Chapter 10, 435
Subject Index, 439

I often say that when you can measure what you are speaking about, and express it in numbers, you know something about it; but when you cannot express it in numbers, your knowledge is of a meagre and unsatisfactory kind; it may be the beginning of knowledge, but you have scarcely, in your thought, advanced to the state of Science, *whatever the matter may be.*

LORD KELVIN (1824–1907)

CHAPTER 1

Electromagnetic wave propagation in a cold plasma

1.1 Introduction

A real-life plasma is a very complicated phenomenon. Viewed as a medium for the propagation of electromagnetic waves, a plasma in a magnetic field is refractive, lossy, dispersive, resonant, anisotropic, nonreciprocal, nonlinear, and inhomogeneous. We begin by accepting as many simplifications as possible and then in later chapters introduce refinements to the elementary treatment.

In this chapter we consider the theory of electromagnetic wave propagation in an infinite, uniform, Lorentz plasma. A *Lorentz plasma* denotes a simplified model in which it is assumed that the electrons interact with each other only through collective spacecharge forces, and that the heavy positive ions and neutral molecules are at rest. In effect, the ions and neutrals are regarded as a continuous stationary fluid through which the electrons move with viscous friction. In addition, we use a simplified analysis that infers the properties of the plasma medium from the motion of individual representative particles, thereby making implicit assumptions about the nature of the interparticle collision processes. Both these simplifications ignore statistical correlations in the positions and velocities of the plasma electrons, refinements which are considered in Chapters 2 and 3. In particular, as implied by the adjective "cold," we first neglect effects which depend explicitly on electron temperature.[1] These refinements can usually be incorporated as small corrections to the effective

[1] Nevertheless, as pointed out in Chapter 3, it cannot be assumed that the electron thermal velocities are zero. Therefore the term "temperate" is perhaps more appropriate than "cold."

plasma parameters within the format of the simplified theory. Thus the simple model gives results which are at least qualitatively correct for more complicated models. The effects of plasma boundaries and inhomogeneity are considered in Chapters 4 and 5.

1.2 Plasma oscillations and the plasma frequency

Before proceeding with the basic topic of electromagnetic wave propagation, it is helpful to consider briefly the phenomenon of electron plasma or spacecharge oscillations. The physical nature of plasma oscillations can be seen from a simple argument originally given by Tonks and Langmuir (1929). We consider an initially uniform electron gas of density n. By some external means, let a one-dimensional perturbation occur such that electrons at position x are displaced in the x direction by a small increment $\xi(x)$, as shown in Fig. 1.1. The local density of electrons then departs from the uniform density n by the increment

$$\delta n = -n\frac{d\xi}{dx}. \tag{1.2.1}$$

Since the net charge density ρ was originally zero, the perturbed charge density is

$$\delta\rho = -e\,\delta n = ne\frac{d\xi}{dx}, \tag{1.2.2}$$

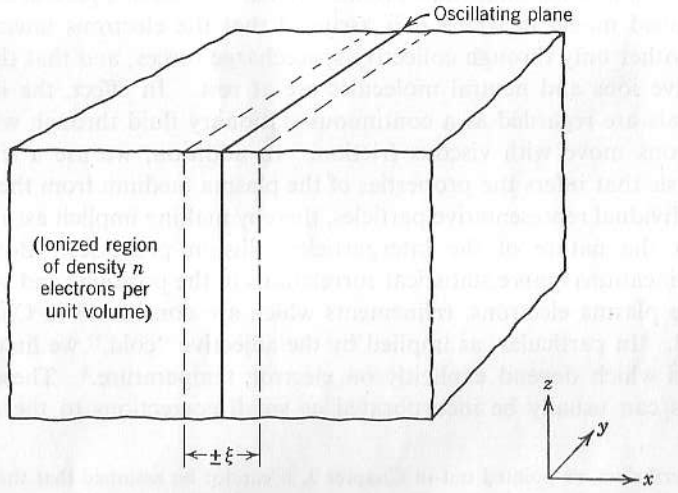

FIG. 1.1 Geometry of one-dimensional perturbation leading to plasma oscillation.

where the electron charge is $-e$. The new net charge is related to the existing electric field by Gauss's law

$$\epsilon_0\frac{dE}{dx} = ne\frac{d\xi}{dx}, \tag{1.2.3}$$

which can be integrated immediately, giving

$$E = \frac{ne}{\epsilon_0}\xi \tag{1.2.4}$$

within an arbitrary constant. The electric force on each electron is then

$$F = -eE = -\frac{ne^2}{\epsilon_0}\xi. \tag{1.2.5}$$

For simplicity, we neglect the viscous damping forces which arise from collisions between the electron and heavy particles. Newton's equation of motion is then

$$m\ddot{\xi} + \frac{ne^2}{\epsilon_0}\xi = F_{ext}, \tag{1.2.6}$$

where m is the electron mass, $\ddot{\xi} \equiv \partial^2\xi/\partial t^2$ is the electron acceleration, and F_{ext} is the external force required to produce the perturbation. If this external force is suddenly removed, (1.2.6) shows that the electrons oscillate about their equilibrium positions with simple harmonic motion at the *plasma frequency*

$$\omega_p = \left(\frac{ne^2}{\epsilon_0 m}\right)^{1/2}. \tag{1.2.7}$$

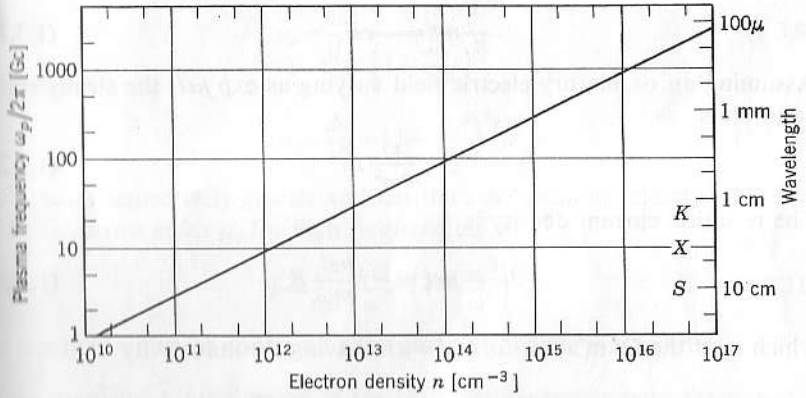

FIG. 1.2 Cyclic plasma frequency $\omega_p/2\pi$ as a function of electron density.

Numerically,

$$\frac{\omega_p}{2\pi}\,[\text{cps}] = 8979(n[\text{cm}^{-3}])^{1/2}. \tag{1.2.8}$$

Figure 1.2 shows this relation for the microwave region. This oscillatory behavior is known as a plasma oscillation. The generalization of this argument to three dimensions has been discussed by Dawson (1959).

The arbitrariness of the spatial distribution of $\xi(x)$ in the above argument implies that a plasma oscillation does not transfer energy; that is, a disturbance does not propagate beyond the region in which it is excited. This property ceases to be true if a significant electron temperature exists (Chapter 3), or if the plasma is bounded or contains gradients of electron density (Chapter 5). In the case of bounded plasmas, depolarizing effects displace the macroscopic resonance frequency from the plasma frequency (for example, to $\omega_p/\sqrt{2}$ for the transverse dipole mode of a cylinder, $\omega_p/\sqrt{3}$ for a sphere). The disturbance is carried along as a convected wave in a drifting plasma (see Section 5.5).

1.3 Electromagnetic wave propagation (no magnetic field)

1.3.1 ***Elementary case neglecting collisions.*** The interaction of an electromagnetic wave with an electron gas can be presented in the following simplified form, which continues to neglect collisional damping. Instead of prescribing a spatial displacement $\xi(x)$, as in the previous section, we prescribe a net electric field $E(t)$. This net electric field is the sum of an external field imposed by sources outside the plasma and the internal field associated with the electron spacecharge by (1.2.4). Neglecting all other external forces, we have for the equation of motion, in place of (1.2.6),

$$m\ddot{\xi} = -eE. \tag{1.3.1}$$

Assuming an oscillatory electric field varying as $\exp j\omega t$, the steady-state solution is

$$\xi = \frac{e}{m\omega^2}E. \tag{1.3.2}$$

The resulting current density is

$$J = -ne\dot{\xi} = -j\frac{ne^2}{m\omega}E, \tag{1.3.3}$$

which is of the Ohm's-law form $J=\sigma E$, having a conductivity

$$\sigma = -j\frac{ne^2}{m\omega}. \tag{1.3.4}$$

For wave propagation in a linear medium, as shown in Appendix A, a complex conductivity may be replaced by a *complex dielectric constant* which, in this case, is

$$\breve{\kappa} = 1 - j\frac{\sigma}{\epsilon_0\omega} = 1 - \frac{ne^2}{\epsilon_0 m\omega^2} = 1 - \frac{\omega_p^2}{\omega^2}, \tag{1.3.5}$$

where ω_p is the plasma frequency defined by (1.2.7), and the symbol $\cup$ is used to denote explicitly a complex quantity.

This analysis may be applied to a plane electromagnetic wave traveling in the z direction and varying as $\exp(j\omega t - \breve{\gamma}z)$, where $\breve{\gamma} = \alpha + j\beta$ is the complex *propagation coefficient*, and α and β are the *attenuation* and *phase coefficients*.[2] The dispersion relation for such a wave is

$$\breve{\gamma} = j\breve{\kappa}^{1/2}\frac{\omega}{c}. \tag{1.3.6}$$

For low frequencies $\omega < \omega_p$, the effective dielectric constant κ is negative, and the wave is attenuated without phaseshift:

$$\alpha = \left(\frac{\omega_p^2}{\omega^2} - 1\right)^{1/2}\frac{\omega}{c} \xrightarrow[\omega^2 \ll \omega_p^2]{} \frac{\omega_p}{c}$$
$$\beta = 0 \tag{1.3.7}$$

If a wave impinges upon the plasma region from outside, it is totally reflected at the boundary. However, for high frequencies $\omega > \omega_p$, the wave is propagated without attenuation:

$$\alpha = 0$$
$$\beta = \left(1 - \frac{\omega_p^2}{\omega^2}\right)^{1/2}\frac{\omega}{c} \xrightarrow[\omega^2 \gg \omega_p^2]{} \frac{\omega}{c}. \tag{1.3.8}$$

The *phase* and *group velocities*, in this case, are

$$v_\phi = \frac{\omega}{\beta} = \frac{1}{\left(1 - \frac{\omega_p^2}{\omega^2}\right)^{1/2}}c \tag{1.3.9}$$

$$v_g = \frac{d\omega}{d\beta} = \left(1 - \frac{\omega_p^2}{\omega^2}\right)^{1/2}c, \tag{1.3.10}$$

which are respectively greater and less than the vacuum velocity of light c. The *refractive index* μ, for high frequencies,

$$\mu = \frac{c}{v_\phi} = \frac{\beta c}{\omega} = \left(1 - \frac{\omega_p^2}{\omega^2}\right)^{1/2}, \tag{1.3.11}$$

is less than unity, in contrast to the index of ordinary dielectrics.

[2] See Appendix A for a review of the basic electromagnetic wave theory and a discussion of our notation.

1.3.2 ***Conductivity with collisional damping: Lorentz conductivity.*** The influence of discrete positive ions and neutral molecules in a plasma can be represented to good approximation by including a viscous damping term, proportional to velocity, in the electron equation of motion. With this addition to (1.3.1), the equation of motion becomes

$$m\ddot{\xi} = -eE - \nu m\dot{\xi}. \tag{1.3.12}$$

The form of the damping term $\nu m\dot{\xi}$ anticipates the fact, discussed at length in Chapter 2, that direct physical meaning can be given to the parameter ν as a *collision frequency* (strictly, *collision frequency for momentum transfer*). In brief, we argue that on the average an electron loses its directed momentum $m\dot{\xi}$ at each collision. Thus, if the electron averages ν collisions per second, $-\nu m\dot{\xi}$ represents the time rate of change of momentum and, hence, the statistical average force exerted on the electron by the massive ion-neutral component of the plasma. More careful examination of the averaging process (Section 2.3) shows that this form of damping term is strictly correct only when the collision frequency is independent of electron velocity, a rather special case. For the present, we need only regard ν as a phenomenological damping constant, having the dimensions of radian frequency.

The steady-state solution of (1.3.12) for oscillatory fields, obtained by the substitution $\partial/\partial t \to j\omega$, is

$$\xi = \frac{eE}{m\omega(\omega - j\nu)}. \tag{1.3.13}$$

The current density $J = -ne\dot{\xi}$ yields a complex conductivity

$$\check{\sigma} \equiv \sigma_r + j\sigma_i = \frac{ne^2}{m(\nu + j\omega)} = \frac{ne^2}{m}\,\frac{\nu - j\omega}{\nu^2 + \omega^2} \tag{1.3.14}$$

which is known as the *Lorentz conductivity*. The equivalent complex *Lorentz dielectric constant* is

$$\check{\kappa} \equiv \kappa_r - j\kappa_i = 1 - j\frac{\check{\sigma}}{\epsilon_0\omega} = 1 - \frac{{\omega_p}^2}{\omega(\omega - j\nu)}$$

$$= \left(1 - \frac{{\omega_p}^2}{\omega^2 + \nu^2}\right) - j\left(\frac{{\omega_p}^2\,\nu/\omega}{\omega^2 + \nu^2}\right). \tag{1.3.15}$$

1.3.3 ***Propagation in a Lorentz plasma (no magnetic field).*** The propagation of plane electromagnetic waves in a uniform medium (of relative permeability unity) may be expressed in terms of a complex dielectric constant $\check{\kappa}$;

$$\check{\gamma} = \alpha + j\beta = j\check{\kappa}^{1/2}\,\frac{\omega}{c}, \tag{1.3.16}$$

where $\check{\gamma}$ is the complex propagation coefficient occurring in the phase factor $\exp(j\omega t - \check{\gamma}z)$, and α and β are the attenuation and phase coefficients, respectively.[3] It is useful also to define a *complex refractive index*

$$\check{\mu} \equiv \mu - j\chi = -j\check{\gamma}\,\frac{c}{\omega} = \check{\kappa}^{1/2} \tag{1.3.17}$$

where μ and χ are the (*real*) *refractive index* and *attenuation index*, respectively. Thus

$$\alpha = \chi\,\frac{\omega}{c} \tag{1.3.18}$$

$$\beta = \mu\,\frac{\omega}{c}. \tag{1.3.19}$$

The sign of the square roots in (1.3.16) and (1.3.17) is taken such that β and μ are positive. For a resume of the relevant basic theory of electromagnetic waves, see Appendix A.

Using the Lorentz dielectric constant (1.3.15) in appendix formulas (A.46) and (A.47), we obtain explicitly:

$$\mu = \mathrm{Re}(\check{\kappa}^{1/2}) = \left\{\frac{1}{2}\left(1 - \frac{{\omega_p}^2}{\omega^2 + \nu^2}\right) + \frac{1}{2}\left[\left(1 - \frac{{\omega_p}^2}{\omega^2 + \nu^2}\right)^2 + \left(\frac{{\omega_p}^2}{\omega^2 + \nu^2}\,\frac{\nu}{\omega}\right)^2\right]^{1/2}\right\}^{1/2} \tag{1.3.20}$$

$$\chi = -\mathrm{Im}(\check{\kappa}^{1/2}) = \left\{-\frac{1}{2}\left(1 - \frac{{\omega_p}^2}{\omega^2 + \nu^2}\right) + \frac{1}{2}\left[\left(1 - \frac{{\omega_p}^2}{\omega^2 + \nu^2}\right)^2 + \left(\frac{{\omega_p}^2}{\omega^2 + \nu^2}\,\frac{\nu}{\omega}\right)^2\right]^{1/2}\right\}^{1/2} \tag{1.3.21}$$

The propagation coefficients α and β are obtained from (1.3.18) and (1.3.19). Evaluation of the effective collision frequency ν is discussed in Sections 2.4.3 and 2.5.3.

1.3.4 ***Low-loss plasmas*** $(\nu \ll \omega_p)$***: the three frequency regions.*** We consider as a function of frequency the electrical properties of a plasma characterized by the parameters plasma frequency ω_p (proportional to square root of electron density $n^{1/2}$) and effective collision frequency ν (in general, a function of electron density and temperature; see Sections 2.4.3 and 2.5.3), assuming the Lorentz conductivity (1.3.14) and no magnetic field. In the case of a highly ionized, high-temperature plasma for which $\nu \ll \omega_p$, we can distinguish three frequency regions.

[3] Thus $\check{\gamma} = j\check{k}$, where $\check{k}$ is the complex angular wave number used by many authors. See Appendix A.

LOW FREQUENCIES $\omega < \nu$. In this region the conductivity is largely real and, to a first approximation, is

$$\sigma \approx \frac{ne^2}{m\nu}, \tag{1.3.22}$$

a familiar relation from the elementary kinetic theory of conductors. Expanding in the limit $\omega \ll \nu$, $\nu^2 \ll \omega_p{}^2$ and making use of the approximations (A.48) and (A.49) in Appendix A, we obtain:

$$\mu \approx \left(\frac{\omega_p{}^2}{2\omega\nu}\right)^{1/2}\left(1-\frac{\omega}{2\nu}\right) \tag{1.3.23}$$

$$\chi \approx \left(\frac{\omega_p{}^2}{2\omega\nu}\right)^{1/2}\left(1+\frac{\omega}{2\nu}\right) \tag{1.3.24}$$

The *attenuation length* or *skin-depth* δ is

$$\delta = \frac{1}{\alpha} = \frac{c}{\chi\omega} \approx \frac{c}{\omega_p}\left(\frac{2\nu}{\omega}\right)^{1/2}\left(1-\frac{\omega}{2\nu}\right). \tag{1.3.25}$$

We observe that μ and χ are nearly equal, and δ is approximately $(2/\mu_0\omega\sigma_r)^{1/2} \propto \omega^{-1/2}$ as in the familiar metallic skin-effect problem. We note, incidentally, that for a highly ionized gas the temperature variation of the electron-ion collision frequency is such that the low-frequency conductivity *increases* with the three-halves power of the temperature (see Section 2.5.3). A one-kilovolt plasma is approximately equivalent to room-temperature copper.

INTERMEDIATE FREQUENCIES $\nu < \omega < \omega_p$. In this region the plasma will not propagate an electromagnetic wave, after the manner of a waveguide beyond cutoff. Expanding, now, in the limit $\nu^2 \ll \omega^2 \ll \omega_p{}^2$, and using (A.52) and (A.53), we obtain:

$$\mu \approx \frac{\nu\omega_p}{2\omega^2}\left(1-\frac{5\nu^2}{8\omega^2}+\frac{\omega^2}{2\omega_p{}^2}\right) \tag{1.3.26}$$

$$\chi \approx \frac{\omega_p}{\omega}\left(1-\frac{3\nu^2}{8\omega^2}-\frac{\omega^2}{2\omega_p{}^2}\right) \tag{1.3.27}$$

$$\delta \approx \frac{c}{\omega_p}\left(1+\frac{3\nu^2}{8\omega^2}+\frac{\omega^2}{2\omega_p{}^2}\right) \tag{1.3.28}$$

Thus, the penetration depth of this evanescent wave is practically constant in the interior of this frequency region, and is comparable to the wavelength of a free-space wave at the plasma frequency—a few millimeters in typical laboratory plasmas.

HIGH FREQUENCIES $\omega > \omega_p$. Here, the plasma becomes a relatively low-loss dielectric. In the limit $\nu^2 \ll \omega^2 - \omega_p{}^2$ and $\nu^2 \ll \omega^2(\omega^2-\omega_p{}^2)^2/\omega_p{}^4$, using (A.50) and (A.51), we obtain:

$$\mu \approx \left(1-\frac{\omega_p{}^2}{\omega^2}\right)^{1/2}\left[1+\frac{\nu^2\omega_p{}^2(\omega^2-\frac{3}{4}\omega_p{}^2)}{2\omega^2(\omega^2-\omega_p{}^2)^2}\right] \approx \left(1-\frac{\omega_p{}^2}{\omega^2}\right)^{1/2} \tag{1.3.29}$$

$$\chi \approx \frac{\nu\omega_p{}^2}{2\omega^3}\left(1-\frac{\omega_p{}^2}{\omega^2}\right)^{-1/2} \tag{1.3.30}$$

$$\delta \approx \frac{c}{\omega_p}\left(\frac{2\omega^2}{\nu\omega_p}\right)\left(1-\frac{\omega_p{}^2}{\omega^2}\right)^{1/2} \tag{1.3.31}$$

Note that the refractive index is quite insensitive to collisional damping and that the attenuation is very small for the assumed conditions.

Numerical values of α, β, μ, and χ are shown as functions of frequency in Fig. 1.3 for a typical laboratory plasma. Fig. 1.4 shows the attenuation length δ as a function of frequency for two different collision frequencies (or temperatures). The magnitudes of the quantities plotted change smoothly and slowly at the boundaries of the three frequency regions with the exception of the attenuation parameters, α, χ, and δ, across the plasma resonance, $\omega = \omega_p$. Expansion of the complete expression (1.3.21) for χ in the neighborhood of $\omega = \omega_p$ shows that the attenuation length δ changes

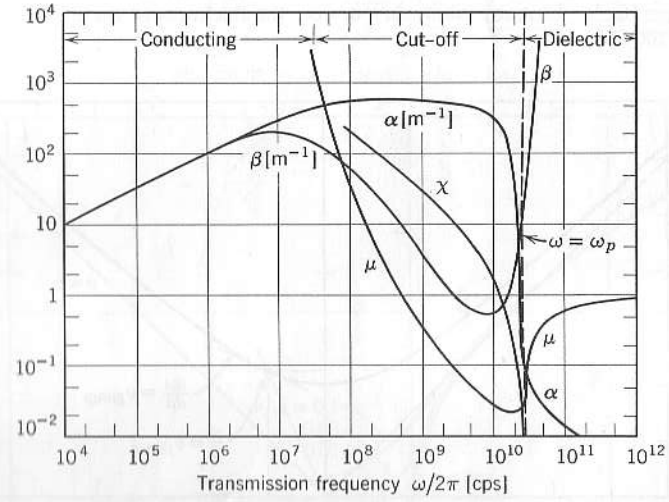

FIG. 1.3 Propagation constants as a function of frequency for a typical laboratory plasma in hydrogen gas. Electron density 10^{13} cm^{-3}; electron temperature 10 eV. The three frequency domains are shown at the top. Symbols are defined in the text.

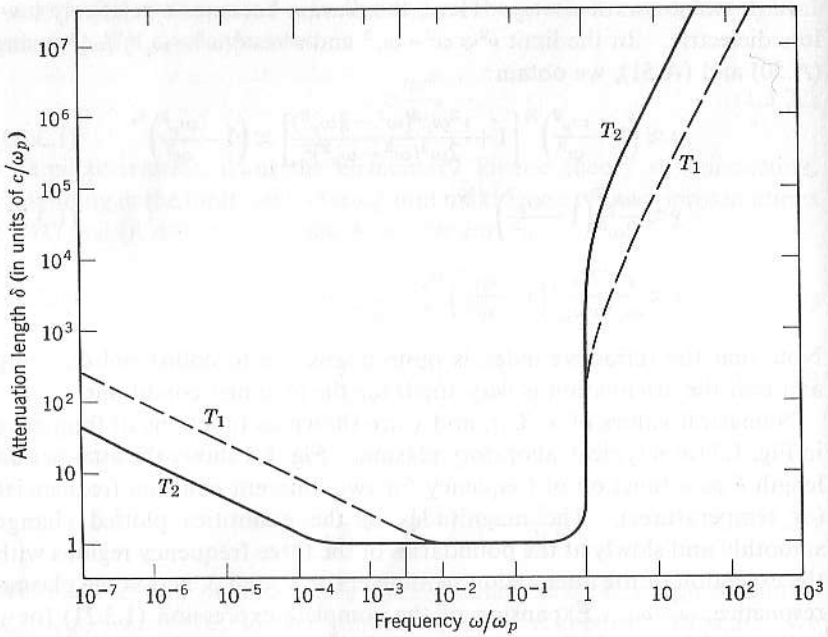

FIG. 1.4 Attenuation length δ of electromagnetic wave in a highly ionized plasma, as a function of frequency, for two temperatures $T_2 \approx 10T_1$, such that $\nu_1/\omega_p = 3 \cdot 10^{-3}$ and $\nu_2/\omega_p = 10^{-4}$. In many laboratory devices the thickness of the plasma is of the order of 100 c/ω_p.

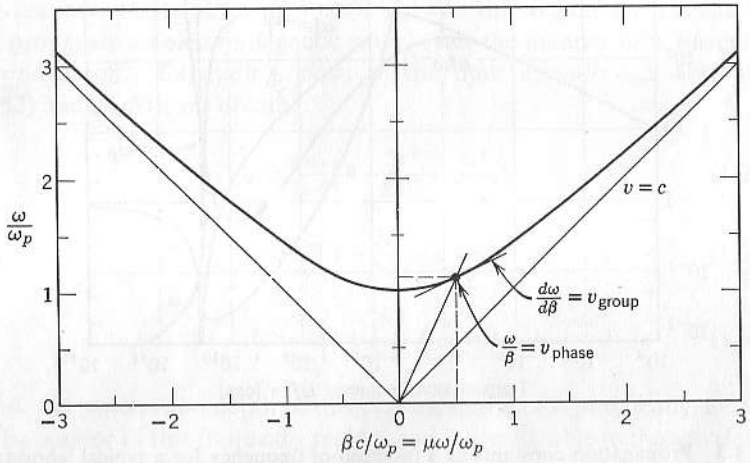

FIG. 1.5 The ω-β or Brillouin diagram for a loss-free plasma (high frequencies).

by the large factor $(2\omega_p/\nu)^{1/2}$ in the small frequency change $(2\nu\omega_p)^{1/2}$. Thus, a fractional change of a few per cent in frequency or, alternatively, in electron density (ω_p^2) can change a low-loss plasma from opaque to transparent.

An alternative way to plot the phase characteristics of a low-loss plasma is the ω-β diagram, Fig. 1.5. This representation is most useful when the frequency is the variable and the dielectric properties of the medium are fixed, such as in ionospheric observations or in waveguide or microwave tube technology. Since the phase and group velocities of the wave

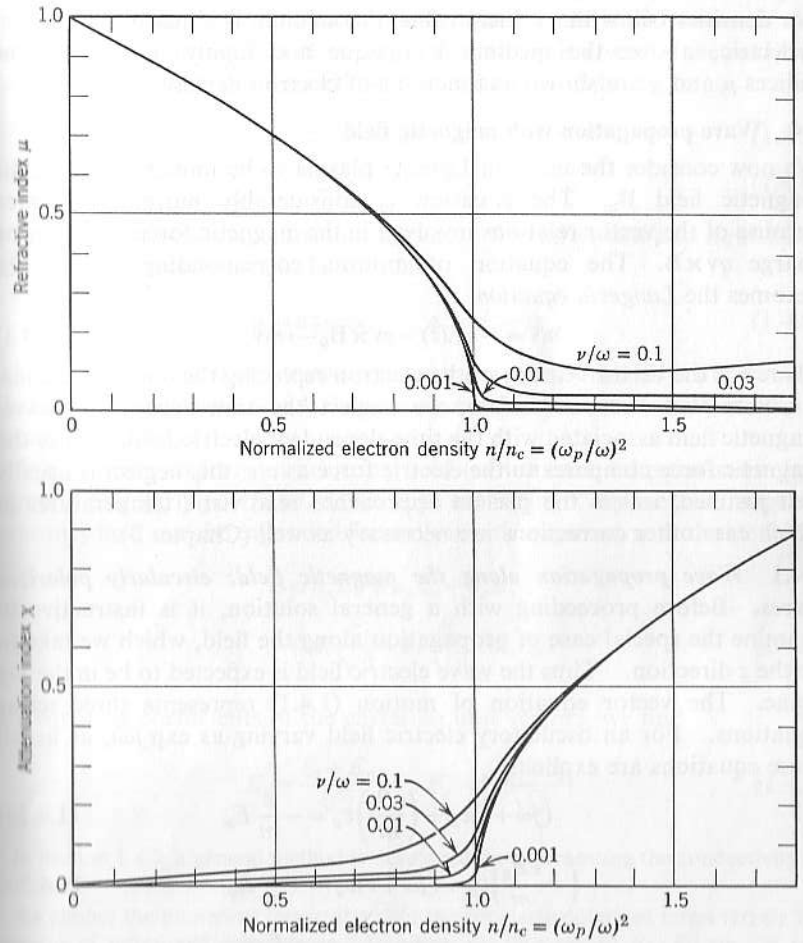

FIG. 1.6 Refractive and attenuation indices as functions of electron density.

are $v_\phi = \omega/\beta$ and $v_g = d\omega/d\beta$, the value of the diagram in obtaining these quantities is seen immediately. Further use of ω-β diagrams, normalized to various quantities, is made in connection with spacecharge waves in Chapter 5.

1.3.5 ***The critical electron density.*** For rf measurements in a time-varying laboratory plasma, the physical situation is better described with the following emphasis. Consider a fixed test frequency ω, to which there corresponds a *critical density* n_c, defined by the plasma frequency relation

$$\omega^2 = \frac{n_c e^2}{\epsilon_0 m}. \tag{1.3.32}$$

For densities below this critical value, the medium is a nearly transparent dielectric; above, the medium is opaque and highly reflecting. The indices μ and χ are shown as functions of electron density in Fig. 1.6.

1.4 Wave propagation with magnetic field

We now consider the uniform Lorentz plasma to be immersed in a static magnetic field $\mathbf{B}_0$. The situation is considerably more complicated because of the vector relations involved in the magnetic force on a moving charge $q\mathbf{v}\times\mathbf{B}$. The equation of motion, corresponding to (1.3.12), becomes the *Langevin equation*

$$m\dot{\mathbf{v}} = -e\mathbf{E}(t) - e\mathbf{v}\times\mathbf{B}_0 - \nu m\mathbf{v} \tag{1.4.1}$$

where $\mathbf{v}$ is the vector velocity of the electron replacing the one-dimensional ξ. Note that here, as before, we neglect the time-dependent (wave) magnetic field associated with the time-dependent electric field. Since the magnetic force compares to the electric force as v/c, this neglect is usually well justified, unless the plasma approaches relativistic temperatures in which case other corrections are necessary as well (Chapter 3).

1.4.1 ***Wave propagation along the magnetic field: circularly polarized waves.*** Before proceeding with a general solution, it is instructive to examine the special case of propagation along the field, which we take to be the z direction. Thus the wave electric field is expected to be in the x-y plane. The vector equation of motion (1.4.1) represents three scalar equations. For an oscillatory electric field varying as $\exp j\omega t$, as usual, these equations are explicitly

$$(j\omega+\nu)v_x + \left(\frac{eB_0}{m}\right)v_y = -\frac{e}{m}E_x \tag{1.4.2a}$$

$$\left(-\frac{eB_0}{m}\right)v_x + (j\omega+\nu)v_y = -\frac{e}{m}E_y \tag{1.4.2b}$$

$$(j\omega+\nu)v_z = -\frac{e}{m}E_z. \tag{1.4.2c}$$

The third equation is not coupled to the other two. Physically, it would represent a possible electromagnetic wave propagating perpendicular to the magnetic field or, alternatively, a spacecharge oscillation of the sort discussed in Section 1.2. In either case, the transverse motion is not affected and thus (1.4.2c) may be ignored. The first two equations are coupled together by the $\mathbf{v}\times\mathbf{B}$ term in a way that obscures the dependence of $\mathbf{v}$ on $\mathbf{E}$, needed to evaluate the conductivity and propagation constants.[4]

The x-y symmetry of (1.4.2a) and (1.4.2b) suggests consideration of *rotating* or *circularly polarized fields*. The notation used to express such vectors can be a matter of some subtlety. Consider a vector rotating with time in a right-handed sense about the z axis. The y component is equal in magnitude to the x component and lags it by 90°. In terms of the usual convention that the actual physical quantity is given by the *real part* of a complex quantity (phasor), we may write, for instance,

$$E_x = E_0 \exp j\omega t \tag{1.4.3}$$

$$E_y = -jE_0 \exp j\omega t \tag{1.4.4}$$

where E_0 is a time-independent amplitude. Similarly, left- and right-hand rotating unit vectors would be written

$$\mathbf{a}_l = \mathbf{a}_x + j\mathbf{a}_y \qquad \mathbf{a}_r = \mathbf{a}_x - j\mathbf{a}_y, \tag{1.4.5}$$

where $\mathbf{a}_x$, $\mathbf{a}_y$ are the unit vectors in the x and y directions. It is understood that any quantity with which these unit vectors are used contains the time factor $\exp(+j\omega t)$.

We can now express an arbitrary field (of unrestricted polarization) in terms of circularly polarized, rather than cartesian, components. Such an arbitrary field may be expanded formally in either system, with the identity[5]

$$\begin{aligned}\mathbf{E} &\equiv \mathbf{a}_x E_x + \mathbf{a}_y E_y + \mathbf{a}_z E_z \\ &\equiv \mathbf{a}_l \frac{E_l}{\sqrt{2}} + \mathbf{a}_r \frac{E_r}{\sqrt{2}} + \mathbf{a}_z E_z.\end{aligned} \tag{1.4.6}$$

By equating coefficients of the cartesian unit vectors, we find

$$E_x = \frac{E_l + E_r}{\sqrt{2}} \qquad E_y = j\frac{E_l - E_r}{\sqrt{2}}, \tag{1.4.7}$$

[4] In Section 1.4.7, a general method is developed for representing the conductivity as a tensor.

[5] We choose the numerical factor of $\sqrt{2}$ in the circularly polarized terms largely for reasons of notational convenience. In effect, we thus regard E_x, E_l, etc., as *rms* amplitudes. Other conventions will be found in the literature.

and, conversely,[6]

$$E_l=\frac{E_x-jE_y}{\sqrt{2}} \qquad E_r=\frac{E_x+jE_y}{\sqrt{2}}. \tag{1.4.8}$$

Note that a *wave* traveling in the $+z$ direction with right-hand circular polarization in time has a left-handed space dependence.

In the steady state, the electron velocities resulting from circularly polarized electric fields will also be circularly polarized,

$$\mathbf{v}_l=(\mathbf{a}_x+j\mathbf{a}_y)\frac{v_l}{\sqrt{2}} \tag{1.4.9}$$

$$\mathbf{v}_r=(\mathbf{a}_x-j\mathbf{a}_y)\frac{v_r}{\sqrt{2}}. \tag{1.4.10}$$

For these circularly polarized velocities the $\mathbf{v}\times\mathbf{B}_0$ term may be evaluated as

$$\mathbf{v}\times\mathbf{B}_0=\frac{vB_0}{\sqrt{2}}(\mathbf{a}_x\pm j\mathbf{a}_y)\times\mathbf{a}_z=\frac{vB_0}{\sqrt{2}}(-\mathbf{a}_y\pm j\mathbf{a}_x)$$

$$=\pm j\frac{vB_0}{\sqrt{2}}(\mathbf{a}_x\pm j\mathbf{a}_y)=\pm jB_0\mathbf{v}; \tag{1.4.11}$$

that is, the term appears formally as being "parallel" to $\mathbf{v}$ so that (1.4.2a) and (1.4.2b) become independent of each other,

$$\left(j\omega+\nu+j\frac{eB_0}{m}\right)v_l=-\frac{e}{m}E_l \tag{1.4.12a}$$

$$\left(j\omega+\nu-j\frac{eB_0}{m}\right)v_r=-\frac{e}{m}E_r. \tag{1.4.12b}$$

Using $-ne\mathbf{v}=\mathbf{J}=\sigma\mathbf{E}$, we then obtain two conductivities for the circularly polarized fields

$$\check{\sigma}_l=\frac{ne^2}{m}\frac{1}{\nu+j(\omega+\omega_b)} \tag{1.4.13}$$

$$\check{\sigma}_r=\frac{ne^2}{m}\frac{1}{\nu+j(\omega-\omega_b)}, \tag{1.4.14}$$

in which we have introduced

$$\omega_b\equiv\frac{|e|B_0}{m} \tag{1.4.15}$$

[6] It is worth noting that this formalism is equivalent to using complex (phasor) notation in the real x-y plane, as well as in the usual complex time domain. Note in (1.4.3) and (1.4.4) $E_x=\mathrm{Re}[E_0\exp j\omega t]$ and $E_y=\mathrm{Re}[-jE_0\exp j\omega t]=\mathrm{Im}[E_0\exp j\omega t]$.

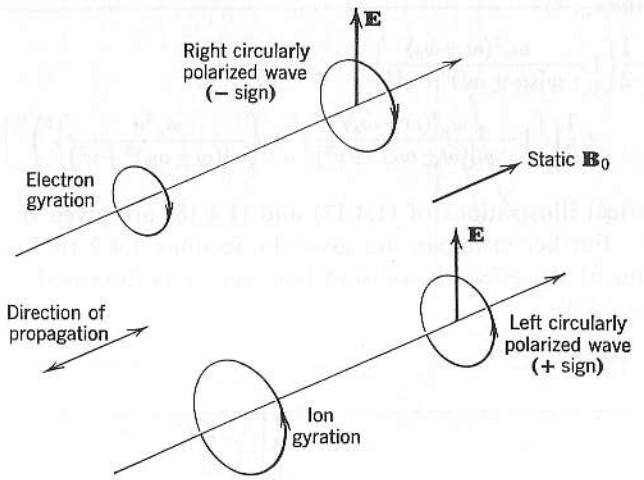

FIG. 1.7 Geometry of circularly polarized waves propagating parallel or antiparallel to magnetic field. The handedness is defined with respect to the magnetic field.

for the *electron cyclotron frequency* or *gyrofrequency*, the angular frequency with which an electron gyrates in a magnetic field.[7] The equivalent complex dielectric constants are readily obtained by the usual relation (A.22)

$$\check{\kappa}_{l,r}=1-j\frac{\check{\sigma}_{l,r}}{\omega\epsilon_0}=1-\frac{\omega_p^2/\omega}{(\omega\pm\omega_b)-j\nu}$$

$$=\left\{1-\frac{\omega_p^2(\omega\pm\omega_b)}{\omega[(\omega\pm\omega_b)^2+\nu^2]}\right\}-j\left\{\frac{\omega_p^2\nu}{\omega[(\omega\pm\omega_b)^2+\nu^2]}\right\}. \tag{1.4.16}$$

Circularly polarized electromagnetic waves, traveling in the $\pm z$ direction, set up circularly polarized electric fields, to which the conductivities or dielectric constants just calculated apply. The geometry of these waves is shown in Fig. 1.7. Therefore, the refractive and attenuation indices of these *cyclotron waves* may be calculated from the dielectric constant using (A.46) and (A.47):

$$\mu_{l,r}=\mathrm{Re}(\check{\kappa}_{l,r}^{\frac{1}{2}})$$

$$=\left[\frac{1}{2}\left\{1-\frac{\omega_p^2(\omega\pm\omega_b)}{\omega[(\omega\pm\omega_b)^2+\nu^2]}\right\}+\frac{1}{2}\left(\left\{1-\frac{\omega_p^2(\omega\pm\omega_b)}{\omega[(\omega\pm\omega_b)^2+\nu^2]}\right\}^2+\left\{\frac{\omega_p^2\nu}{\omega[(\omega\pm\omega_b)^2+\nu^2]}\right\}^2\right)^{\frac{1}{2}}\right]^{\frac{1}{2}} \tag{1.4.17}$$

[7] This quantity is not to be confused with the *Larmor frequency*, which occurs in other physical problems involving precession of electrons in a magnetic field, and is defined as $eB/2m$ (that is, one-half the cyclotron frequency).

$$\chi_{l,r} = -\mathrm{Im}(\kappa_{l,r}^{1/2})$$
$$= \left[-\frac{1}{2}\left\{1 - \frac{\omega_p^2(\omega \pm \omega_b)}{\omega[(\omega \pm \omega_b)^2 + \nu^2]}\right\} \right. \tag{1.4.18}$$
$$\left. + \frac{1}{2}\left(\left\{1 - \frac{\omega_p^2(\omega \pm \omega_b)}{\omega[(\omega \pm \omega_b)^2 + \nu^2]}\right\}^2 + \left\{\frac{\omega_p^2 \nu}{\omega[(\omega \pm \omega_b)^2 + \nu^2]}\right\}^2\right)^{1/2}\right]^{1/2}$$

Numerical illustrations of (1.4.17) and (1.4.18) are given by Figs. 1.8 and 1.9. Further examples are given in Sections 1.4.9 to 1.4.12. The evaluation of the effective collision frequency ν is discussed in Sections 2.4.3 and 2.5.3.

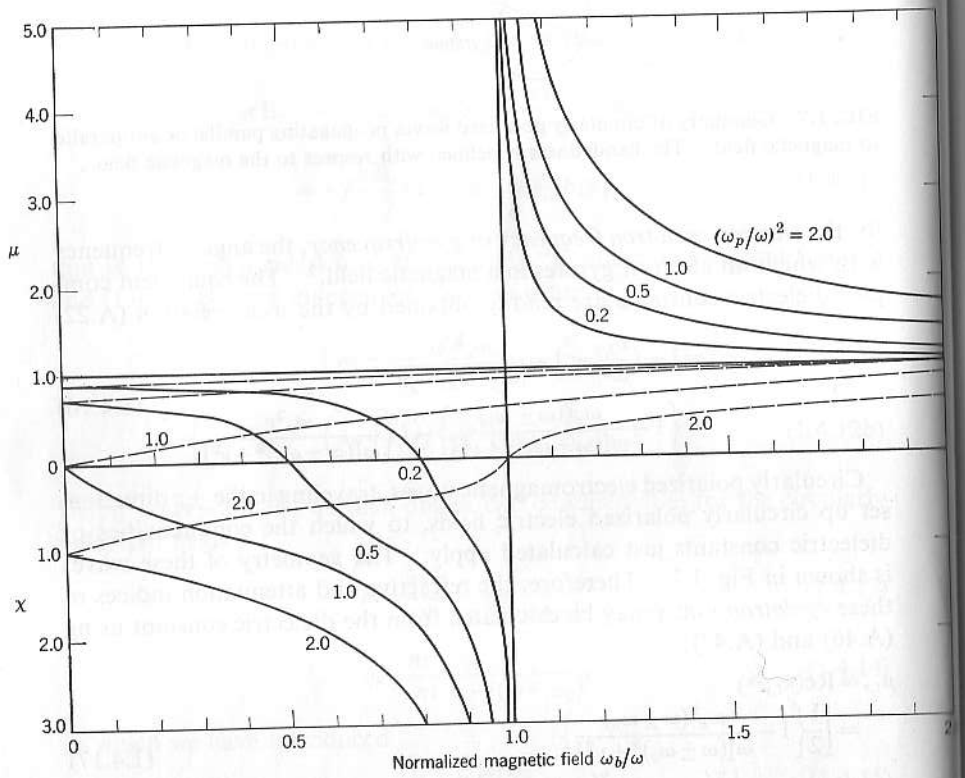

FIG. 1.8 Refractive and attenuation indices as functions of magnetic field for circularly polarized waves propagated along the field, for various plasma densities. Right-hand polarization (sense of electron gyration), *solid* curves; left-hand, *dashed*. No collisions ($\nu/\omega = 0$).

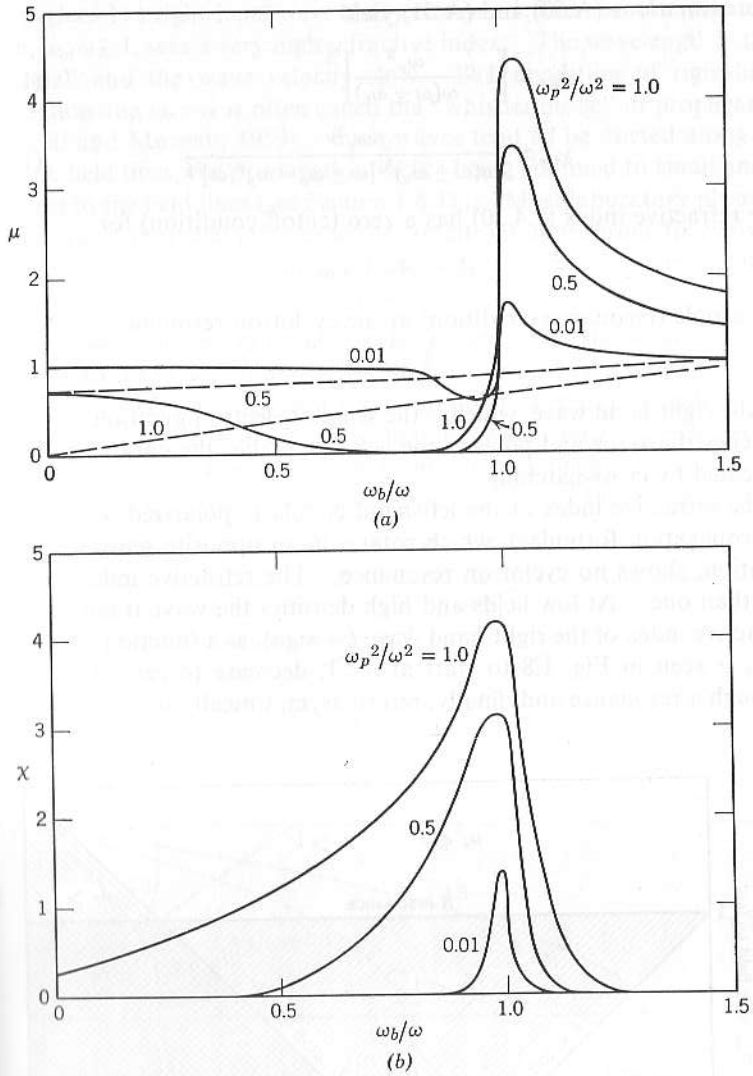

FIG. 1.9 As Fig. 1.8 but nonzero collision rate, $\nu/\omega = 0.01$.

If the collision frequency is sufficiently small, as in Fig. 1.8, simplified expressions may be obtained. For propagating frequencies ($\kappa_r > 0$) in the limit

$$\nu^2 \ll \left\{ \begin{matrix} (\omega \pm \omega_b)^2 \\ |\omega(\omega \pm \omega_b) - \omega_p^2|, \end{matrix} \right. \tag{1.4.19}$$

approximations (A.50) and (A.51) yield

$$\mu_{l,r} \approx \left[1 - \frac{\omega_p^2}{\omega(\omega \pm \omega_b)}\right]^{1/2} \tag{1.4.20}$$

$$\chi_{l,r} \approx \frac{\omega_p^2 \nu}{2\omega(\omega \pm \omega_b)^{3/2}[\omega \pm \omega_b - \omega_p^2/\omega]^{1/2}}. \tag{1.4.21}$$

The refractive index (1.4.20) has a zero (cutoff condition) for

$$\omega_p^2/\omega^2 = 1 \pm \omega_b/\omega, \tag{1.4.22}$$

and a pole (resonance condition) at the cyclotron resonance

$$\omega = \omega_b \tag{1.4.23}$$

for the right-hand wave, which is the sense of electron gyration. Fig. 1.10 sketches the zeros and poles in the ω_p^2—ω_b plane; the cut-off regions are indicated by cross-hatching.

The refractive index of the left-hand circularly polarized wave (+ sign in propagation formulas), which rotates in an opposite sense to electron gyration, shows no cyclotron resonance. The refractive index is always less than one. At low fields and high densities the wave is cut off. The refractive index of the right-hand wave (− sign), as a function of magnetic field, is seen in Fig. 1.8 to start at $\mu < 1$, decrease to zero (cut off), go through a resonance and, finally, return asymptotically to unity. At high

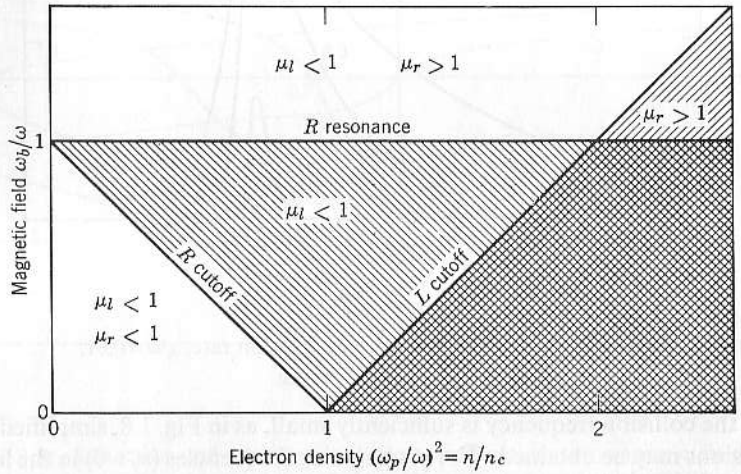

FIG. 1.10 Propagating regions of left and right circularly polarized waves along magnetic field (no collisions). Waves are cut off in shaded regions.

fields ($\omega_b/\omega > 1$) a right-hand wave always sees $\mu > 1$, and near the resonance region, $\omega_b/\omega \gtrsim 1$, sees a very high refractive index. The wavelength is then very small and the wave velocity slow. This condition of right-hand polarization and $\omega_b > \omega$ is often called the "whistler mode" of propagation (Helliwell and Morgan, 1959). Such waves tend to be ducted along the magnetic field lines, the propagation vector being confined to small angles in respect to the field lines (see Section 1.4.11). Most laboratory plasmas, however, have appreciable losses at the conditions appropriate for whistler propagation, and the wave attenuation is very large. Further mention of the whistler mode is made in Chapter 6.

1.4.2 ***Faraday rotation of angle of polarization.*** The significance of the independence of (1.4.12a) and (1.4.12b) for circularly polarized waves is that a general wave, with arbitrary state of polarization, propagates along the magnetic field in a plasma in a manner which may be analyzed by (*a*) resolving the actual wave into two counterrotating circularly polarized waves, (*b*) following the independent propagation of these components,

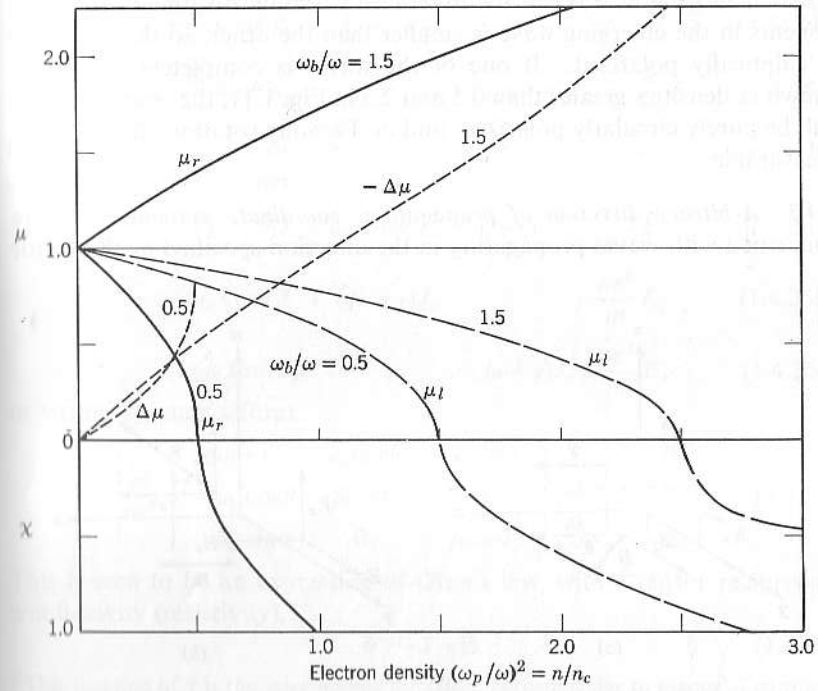

FIG. 1.11 Faraday rotation index $\Delta\mu = \mu_l - \mu_r$, neglecting collisions, for $\omega_b/\omega = 0.5$ and 1.5.

and (*c*) superposing the two components to obtain the resultant wave at any desired point. Specifically, if a linearly polarized, plane wave is incident on a magnetized plasma along the field, its direction of linear polarization will be rotated. The wave may be thought of as consisting of two counterrotating waves of equal amplitude. As these waves pass through the plasma, they travel at different velocities, as determined by the upper and lower signs of (1.4.20). After the wave emerges from the plasma, its plane of linear polarization has been rotated, since one of the circularly polarized components has traveled electrically farther than the other. The rotation angle is

$$\Psi=\tfrac{1}{2}(\beta_l-\beta_r)d=(\mu_l-\mu_r)\pi d/\lambda=(\Delta\mu)\pi d/\lambda \qquad (1.4.24)$$

where d is the distance traveled in the plasma. An example is given in Fig. 1.11. Note that this rotation is with respect to the magnetic field and independent of the sense of propagation along the field. Thus, the propagation is nonreciprocal (Goldstein, 1958).

The attenuation of the two counterrotating components will also be different in general. When the difference is significant, one of the components in the emerging wave is smaller than the other, so that the wave is elliptically polarized. If one of the waves is completely cut off, as shown at densities greater than 0.5 and 2.5 in Fig. 1.11, the emerging wave will be purely circularly polarized, and no Faraday rotation effects will be measurable.

1.4.3 ***Arbitrary direction of propagation: coordinate systems.*** We are concerned with waves propagating in the direction specified by the vector

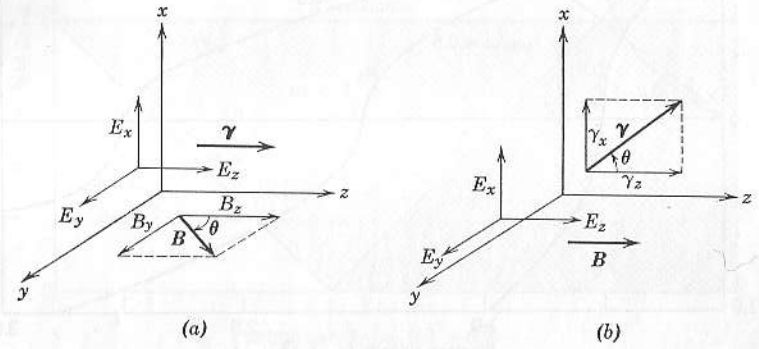

FIG. 1.12 Alternative coordinate systems for propagation in an arbitrary direction to the magnetic field.

propagation constant γ.[8] The vector nature of the equation of motion (1.4.1) forces us to define a coordinate system with care. Two such coordinate systems are common. We shall have occasion to use both. In one case, the z axis is aligned with the wave propagation direction γ, and the static magnetic field $\mathbf{B}_0$ is taken in the y-z plane (Fig. 1.12a). In the other, the z axis is aligned with $\mathbf{B}_0$, and γ is taken in the x-z plane (Fig. 1.12b). In both cases, θ is, in magnitude, the angle between γ and $\mathbf{B}_0$. Thus, $\theta=0$ corresponds to propagation *along* the field, $\theta=90°$ to propagation *across* it.

1.4.4 ***Magnetic field at angle θ with respect to propagation: Appleton's equation.*** We now seek a general solution for propagation at an arbitrary angle with respect to the magnetic field, using the coordinate system of Fig. 1.11a in which the propagation is in the z direction with phase factor $\exp(j\omega t-\check{\gamma}z)$, and the static magnetic field lies in the y-z plane [$\mathbf{B}_0=B_0\,(0,\sin\theta,\cos\theta)$]. Expansion of the force equation (1.4.1) yields:

$$(j\omega+\nu)v_x+\frac{eB_0}{m}\cos\theta\,v_y-\frac{eB_0}{m}\sin\theta\,v_z=-\frac{e}{m}E_x \qquad (1.4.25a)$$

$$-\frac{eB_0}{m}\cos\theta\,v_x+\quad(j\omega+\nu)v_y\qquad\qquad=-\frac{e}{m}E_y \qquad (1.4.25b)$$

$$\frac{eB_0}{m}\sin\theta\,v_x\qquad\qquad+\;(j\omega+\nu)v_z=-\frac{e}{m}E_z \qquad (1.4.25c)$$

Identifying the cyclotron frequency (1.4.15) and replacing velocity by current density ($\mathbf{J}=-ne\mathbf{v}$), we have

$$(j\omega+\nu)J_x+\omega_b\cos\theta\,J_y-\omega_b\sin\theta\,J_z=\frac{ne^2}{m}E_x \qquad (1.4.26a)$$

$$-\omega_b\cos\theta\,J_x+\;(j\omega+\nu)J_y\qquad\qquad=\frac{ne^2}{m}E_y \qquad (1.4.26b)$$

$$\omega_b\sin\theta\,J_x\qquad\qquad+\;(j\omega+\nu)J_z=\frac{ne^2}{m}E_z \qquad (1.4.26c)$$

or written in matrix form

$$\frac{m}{ne^2}\begin{bmatrix} j\omega+\nu & \omega_b\cos\theta & -\omega_b\sin\theta \\ -\omega_b\cos\theta & j\omega+\nu & 0 \\ \omega_b\sin\theta & 0 & j\omega+\nu \end{bmatrix}\begin{bmatrix} J_x \\ J_y \\ J_z \end{bmatrix}=\begin{bmatrix} E_x \\ E_y \\ E_z \end{bmatrix}. \qquad (1.4.27)$$

This is seen to be an expression of Ohm's law, with a tensor reciprocal-conductivity (resistivity),[9]

$$\check{\sigma}^{-1}\cdot\mathbf{J}=\mathbf{E}. \qquad (1.4.28)$$

[8] The direction of γ is the *wave-normal* direction, perpendicular to planes of constant phase. It is not necessarily the direction of energy flow. See Section 1.4.11.

[9] An elementary discussion of tensor algebra is given in Appendix B.

In principle we could invert the matrix $\check{\boldsymbol{\sigma}}^{-1}$ by standard methods to obtain the conductivity tensor $\check{\boldsymbol{\sigma}}$, find the equivalent dielectric constant tensor $\check{\boldsymbol{\kappa}}=\mathbf{1}-j\check{\boldsymbol{\sigma}}/\omega\epsilon_0$, and then substitute in the anisotropic dispersion relation (A.74). This approach is followed in Section 1.4.7. Here, however, we use a different but equivalent approach, which is somewhat less complicated algebraically. It is possible to obtain a formal expression for the conductivity tensor in terms of the propagation constant from Maxwell's equations. We then demand that the two expressions for the conductivity tensor be self-consistent.

We assume plane waves having the phase factor $\exp(j\omega t-\check{\gamma}z)$, where $\check{\gamma}=\alpha+j\beta=j\check{\mu}\omega/c$ is the complex propagation constant, in a medium carrying explicit current density $\mathbf{J}$ (dielectric constant and relative permeability unity). In component form, Maxwell's curl equations become [see (A.70) and (A.71)]:

$$\check{\gamma}E_y=-j\omega\mu_0H_x \tag{1.4.29a}$$

$$-\check{\gamma}E_x=-j\omega\mu_0H_y \tag{1.4.29b}$$

$$0=-j\omega\mu_0H_z \tag{1.4.29c}$$

$$\check{\gamma}H_y=J_x+j\omega\epsilon_0E_x \tag{1.4.30a}$$

$$-\check{\gamma}H_x=J_y+j\omega\epsilon_0E_y \tag{1.4.30b}$$

$$0=J_z+j\omega\epsilon_0E_z \tag{1.4.30c}$$

We note that the wave can have no longitudinal component of $\mathbf{H}$, regardless of the direction of the static magnetic field; however, a longitudinal component of $\mathbf{E}$ is not excluded so that the Poynting vector need not be in the direction of $\boldsymbol{\gamma}$ (see Section 1.4.11). Eliminating H_x, H_y, we have, in matrix notation,

$$j\omega\epsilon_0\begin{bmatrix}\check{\mu}^2-1 & 0 & 0\\ 0 & \check{\mu}^2-1 & 0\\ 0 & 0 & -1\end{bmatrix}\begin{bmatrix}E_x\\ E_y\\ E_z\end{bmatrix}=\begin{bmatrix}J_x\\ J_y\\ J_z\end{bmatrix}, \tag{1.4.31}$$

which is an expression for Ohm's law in the form

$$\check{\boldsymbol{\sigma}}\cdot\mathbf{E}=\mathbf{J}. \tag{1.4.32}$$

Now for (1.4.28) and (1.4.32) to be self-consistent

$$\mathbf{E}=\check{\boldsymbol{\sigma}}^{-1}\cdot\mathbf{J}=\check{\boldsymbol{\sigma}}^{-1}\cdot\check{\boldsymbol{\sigma}}\cdot\mathbf{E}$$

or

$$(\check{\boldsymbol{\sigma}}^{-1}\cdot\check{\boldsymbol{\sigma}}-\mathbf{1})\cdot\mathbf{E}=0 \tag{1.4.33}$$

where $\mathbf{1}$ is the unit or identity tensor. Equation (1.4.33) represents three simultaneous homogeneous equations; the determinant of the coefficients must vanish to yield a solution. Substituting from (1.4.27) and (1.4.31) and carrying out the matrix multiplication (see Appendix B), we have

$$\frac{j\omega}{\omega_p^2}\begin{vmatrix}(j\omega+\nu)(\check{\mu}^2-1)+j\omega_p^2/\omega & \omega_b(\check{\mu}^2-1)\cos\theta & \omega_b\sin\theta\\ -\omega_b(\check{\mu}^2-1)\cos\theta & (j\omega+\nu)(\check{\mu}^2-1)+j\omega_p^2/\omega & 0\\ \omega_b(\check{\mu}^2-1)\sin\theta & 0 & -(j\omega+\nu)+j\omega_p^2/\omega\end{vmatrix}=0. \tag{1.4.34}$$

We now have a straightforward but complicated equation to solve for $\check{\mu}$, the complex refractive index.

It is helpful to define some normalized quantities to simplify the algebra:

$$\begin{aligned} X&\equiv\omega_p^2/\omega^2 & Y&\equiv\omega_b/\omega\\ \Upsilon&\equiv 1-j\nu/\omega & Y_L&\equiv Y\cos\theta\\ M^2&\equiv\check{\mu}^2-1 & Y_T&\equiv Y\sin\theta\end{aligned} \tag{1.4.35}$$

The determinantal equation (1.4.34) becomes

$$-\frac{M^6}{X}\begin{vmatrix}\Upsilon+X/M^2 & -jY_L & -jY_T/M^2\\ jY_L & \Upsilon+X/M^2 & 0\\ -jY_T & 0 & -(\Upsilon-X)/M^2\end{vmatrix}=0. \tag{1.4.36}$$

It is most convenient to solve for X/M^2. Rewriting and factoring out $M^4(\Upsilon-X)/X$, we have the quadratic

$$\left(\frac{X}{M^2}\right)^2+\left(2\Upsilon-\frac{Y_T^2}{\Upsilon-X}\right)\left(\frac{X}{M^2}\right)+\left[\Upsilon\left(\Upsilon-\frac{Y_T^2}{\Upsilon-X}\right)-Y_L^2\right]=0, \tag{1.4.37}$$

the solution of which is

$$\frac{X}{M^2}=-\left[\Upsilon-\frac{Y_T^2}{2(\Upsilon-X)}\right]\mp\left[\frac{Y_T^4}{4(\Upsilon-X)^2}+Y_L^2\right]^{1/2}; \tag{1.4.38}$$

and finally

$$\check{\mu}^2=1+M^2=1-\frac{X}{\left[\Upsilon-\frac{Y_T^2}{2(\Upsilon-X)}\right]\pm\left[\frac{Y_T^4}{4(\Upsilon-X)^2}+Y_L^2\right]^{1/2}}. \tag{1.4.39}$$

Thus the result of solving the determinantal equation (1.4.34) is

$$\check{\mu}^2=(\mu-j\chi)^2=1-\frac{\omega_p^2/\omega^2}{\left[1-j\frac{\nu}{\omega}-\frac{(\omega_b^2/\omega^2)\sin^2\theta}{2(1-\omega_p^2/\omega^2-j\nu/\omega)}\right]\pm\left[\frac{(\omega_b^4/\omega^4)\sin^4\theta}{4(1-\omega_p^2/\omega^2-j\nu/\omega)^2}+\frac{\omega_b^2}{\omega^2}\cos^2\theta\right]^{1/2}}. \tag{1.4.40}$$

This equation is *Appleton's equation*, and was first derived to describe propagation of radio waves in the ionosphere (Appleton, 1932; Ratcliffe, 1959). It gives the propagation indices for plane waves in a magnetized cold plasma that is uniform over dimensions that are large, compared to a wavelength. The sense of the $\pm$ sign has been chosen to agree with that of (1.4.16) for the special case of propagation along the field ($\theta=0$). Equation (1.4.40) is often called the *Appleton-Hartree* equation, a somewhat ambiguous identification that recalls Hartree's incorrect version, based on an analysis including the so-called Lorentz polarization correction (see Appendix, Section A.2.2).[10] Numerical examples of Appleton's equation are given in Sections 1.4.10 to 1.4.12. The effective collision frequency ν is to be evaluated by the methods discussed in Sections 2.4.3 and 2.5.3.

1.4.5 ***Wave polarization.*** A *characteristic wave* is defined as one which does not change its state of polarization as it propagates through the medium. Ratios of field components are then independent of position. A more general wave may be represented as a sum of characteristic waves. For instance, we saw in Sections 1.4.1 and 1.4.2 that circularly polarized waves propagate along the magnetic field without alteration, while a linearly polarized wave experiences Faraday rotation. The concept of characteristic waves is closely related to the concept of normal modes or eigenfunctions arising in the formal mathematical theory of oscillatory systems.

Characteristic electromagnetic waves in a magnetized plasma, in general, are elliptically polarized. By assuming plane waves with all field components varying with the same phase factor $\exp(j\omega t-\check{\gamma}z)$, we have implicitly assumed characteristic waves in deriving Appleton's equation in the previous section. The state of polarization of these waves as a function of the plasma parameters remains to be found. Since, by (1.4.29), the waves are always transverse-magnetic, it is useful to define a *wave polarization coefficient*

$$\check{R}\equiv-\frac{H_y}{H_x}. \tag{1.4.41}$$

If $\check{R}$ is real, the wave is linearly polarized; if $\check{R}$ is complex, the wave is elliptically polarized. In particular, $\check{R}=\mp j$ for left- and right-handed

[10] Hartree's formula is, in the notation of (1.4.35),

$$\check{\mu}^2=1-\frac{X}{\left[(\Upsilon+\tfrac{1}{2}X)-\dfrac{Y_T{}^2}{2(\Upsilon-\frac{1}{2}X)}\right]\pm\left[\dfrac{Y_T{}^4}{4(\Upsilon-\frac{1}{2}X)^2}+Y_L{}^2\right]^{1/2}}.$$

circular polarization, respectively. By (1.4.29) and (1.4.30), it follows that

$$\check{R}=-\frac{H_y}{H_x}=\frac{E_x}{E_y}=\frac{J_x}{J_y}. \tag{1.4.42}$$

To evaluate this ratio, we recall that (1.4.33) is a system of simultaneous equations for the components of **E**, with coefficients written out explicitly in the determinant (1.4.34). The second of the three equations yields immediately

$$\check{R}=\frac{E_x}{E_y}=\frac{(j\omega+\nu)(\check{\mu}^2-1)+j\omega_p{}^2/\omega}{\omega_b(\check{\mu}^2-1)\cos\theta}. \tag{1.4.43}$$

Using the solution (1.4.40), we obtain

$$\check{R}_\pm=\frac{j}{(\omega_b/\omega)\cos\theta}\left\{\left[\frac{(\omega_b{}^2/\omega^2)\sin^2\theta}{2(1-\omega_p{}^2/\omega^2-j\nu/\omega)}\right]\mp\left[\frac{(\omega_b{}^4/\omega^4)\sin^4\theta}{4(1-\omega_p{}^2/\omega^2-j\nu/\omega)^2}+\frac{\omega_b{}^2}{\omega^2}\cos^2\theta\right]^{1/2}\right\}. \tag{1.4.44}$$

An interesting property is

$$(\check{R}_+)(\check{R}_-)=1. \tag{1.4.45}$$

For the special case studied in Section 1.4.1 of propagation along the field, $\check{R}\to\mp j$ as required.

The coefficient $\check{R}$ specifies the wave polarization except for the longitudinal component E_z. From the third equation of (1.4.33) [using (1.4.34)], we may evaluate a longitudinal polarization coefficient

$$\check{S}\equiv\frac{E_z}{E_x}=\frac{\omega_b(\check{\mu}^2-1)\sin\theta}{-(j\omega+\nu)+j\omega_p{}^2/\omega}=\frac{j(\omega_p{}^2/\omega^2)(\omega_b/\omega)\sin\theta}{\left(1-\dfrac{\omega_b{}^2}{\omega^2}-j\dfrac{\nu}{\omega}\right)\left\{\left[1-j\dfrac{\nu}{\omega}-\dfrac{(\omega_b{}^2/\omega^2)\sin^2\theta}{2(1-\omega_p{}^2/\omega^2-j\nu/\omega)}\right]\pm\left[\dfrac{(\omega_b{}^4/\omega^4)\sin^4\theta}{4(1-\omega_p{}^2/\omega^2-j\nu/\omega)^2}+\dfrac{\omega_b{}^2}{\omega^2}\cos^2\theta\right]^{1/2}\right\}}. \tag{1.4.46}$$

The wave polarizations vary in a complicated manner with the many parameters. Curves for $\check{R}$ have been published in connection with ionospheric investigations (Snyder and Helliwell, 1952; Consoli et al., 1961).

1.4.6 ***Propagation across the magnetic field.*** The important special cases of propagation *along* ($\theta=0$) and *across* ($\theta=90°$) the magnetic field are

easily obtained from the general Appleton equation (1.4.40). The $\theta=0$ case has already been discussed at length in Sections 1.4.1 and 1.4.2. For $\theta=90°$, again two characteristic waves are obtained:

ordinary
$$\breve{\mu}_{ord}^2=1-\frac{\omega_p^2/\omega^2}{1-j\nu/\omega} \tag{1.4.47}$$

extraordinary
$$\begin{aligned}\breve{\mu}_{ex}^2&=1-\frac{\omega_p^2/\omega^2}{1-j\dfrac{\nu}{\omega}-\dfrac{\omega_b^2/\omega^2}{1-\omega_p^2/\omega^2-j\nu/\omega}}\\&=\left\{1-\frac{\omega_p^2[(\omega^2-\omega_p^2)(\omega^2-\omega_p^2-\omega_b^2)+\nu^2\omega^2]}{\omega^2(\omega^2-\omega_p^2-\omega_b^2-\nu^2)^2+\nu^2(2\omega^2-\omega_p^2)^2}\right\}\\&\quad -j\left\{\frac{\nu\omega_p^2[\omega_p^4+\omega^2(\omega^2-2\omega_p^2+\omega_b^2+\nu^2)]}{\omega[\omega^2(\omega^2-\omega_p^2-\omega_b^2-\nu^2)^2+\nu^2(2\omega^2-\omega_p^2)^2]}\right\}.\end{aligned} \tag{1.4.48}$$

The labels *ordinary* and *extraordinary* are conventional in ionospheric terminology, but are in conflict with the terminology of crystal optics and some magnetohydrodynamic literature (Allis, Buchsbaum, and Bers, 1963). Examination of (1.4.40) and (1.4.44) shows that the ordinary wave is linearly polarized with **E** parallel to the magnetic field. The ordinary wave is so named because it has the same dispersion relation as if no magnetic field were present [compare (1.3.15) and (1.4.47)].[11] The field-free case was discussed at some length in Sections 1.3.3 and 1.3.4.

The extraordinary wave is polarized with **E** perpendicular to the magnetic field and is linearly polarized in the sense that it is excited by a linearly polarized wave outside the plasma. However, from (1.4.46), we find that there is a component of **E** in the direction of propagation; thus, actually, **E** is elliptically polarized in the plane perpendicular to the magnetic field and including the direction of propagation. To obtain explicitly the indices μ and χ, if $\breve{\mu}^2\equiv L-jM$, then by (A.46) and (A.47)

$$\begin{Bmatrix}\mu\\ \chi\end{Bmatrix}=\left[\frac{\pm L+(L^2+M^2)^{1/2}}{2}\right]^{1/2}. \tag{1.4.49}$$

In the limit where collisional damping may be neglected, (1.4.48) reduces to

$$\begin{aligned}\breve{\mu}_{ex}&=\left[1-\frac{\omega_p^2(\omega^2-\omega_p^2)}{\omega^2(\omega^2-\omega_p^2-\omega_b^2)}\right]^{1/2}\\&=\left[\frac{(1-\omega_p^2/\omega^2)^2-\omega_b^2/\omega^2}{1-\omega_p^2/\omega^2-\omega_b^2/\omega^2}\right]^{1/2}.\end{aligned} \tag{1.4.50}$$

[11] This independence no longer holds when finite electron thermal velocities are considered; see Chapter 3.

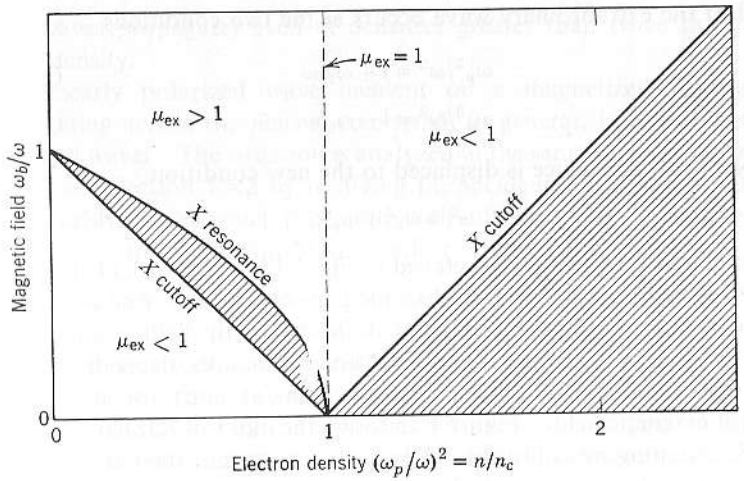

FIG. 1.13 Propagating regions for extraordinary wave across magnetic field ($\theta=90°$), neglecting collisions. The wave is cut off in the shaded regions.

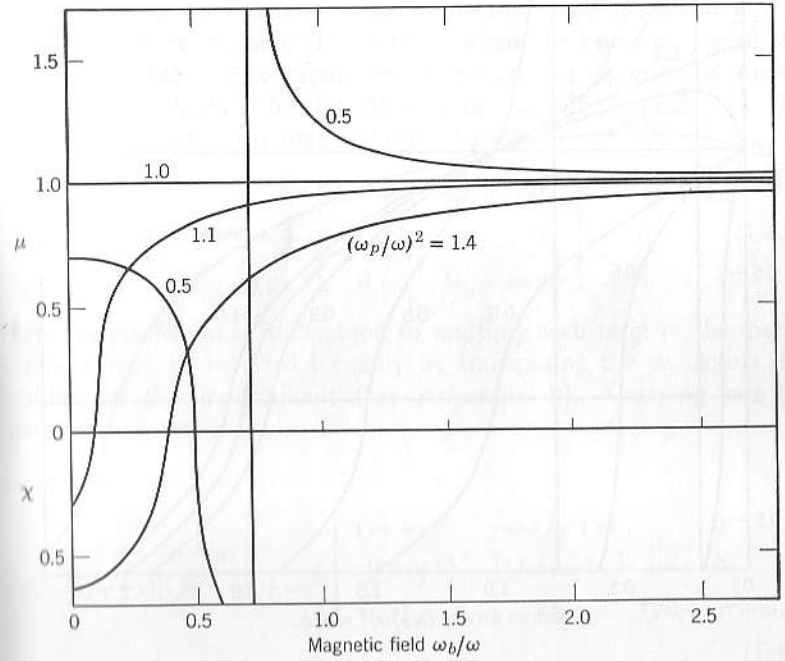

FIG. 1.14 Refractive and attenuation indices as functions of magnetic field, at various plasma densities, for extraordinary wave propagating across the field, neglecting collisions.

Cutoff of the extraordinary wave occurs at the two conditions

$$\omega_p^2/\omega^2 = 1 + \omega_b/\omega \tag{1.4.51}$$

$$\omega_p^2/\omega^2 = 1 - \omega_b/\omega. \tag{1.4.52}$$

The cyclotron resonance is displaced to the new condition

$$\omega^2 = \omega_b^2 + \omega_p^2. \tag{1.4.53}$$

The poles and zeros of $\check{\mu}$ are sketched in Fig. 1.13. Figure 1.14 shows the refractive index plotted vs. ω_b, assuming no collisions. For $\omega_p^2/\omega^2 > 1$, the index is real (waves propagate) if the magnetic field is sufficiently large. For $\omega_p^2/\omega^2 < 1$, there are cutoffs and resonances, depending on the value of ω_b. At $\omega_p^2/\omega^2 = 1$ the index remains at unity for all nonzero values of magnetic field. Figure 1.15 shows the index of refraction plotted vs. ω_p^2, assuming no collisions. For $\omega_b > \omega$, note that the index remains

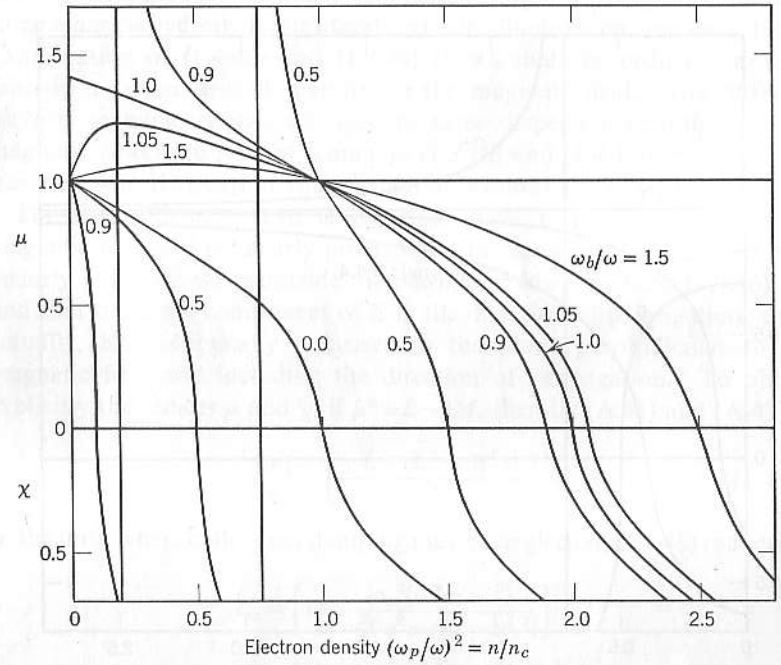

FIG. 1.15 Refractive and attenuation indices as functions of electron density, at various magnetic field strengths, for extraordinary wave propagating across the field, neglecting collisions.

real (waves propagate) even at densities greater than twice the normal cutoff density.

A linearly polarized wave incident on a magnetized plasma and propagating across the field is converted, in general, into an elliptically polarized wave. The situation is analyzed in the same way as the Faraday rotation of Section 1.4.2 by resolving the incident wave into component characteristic waves which propagate with different velocities. The effect is analogous to the Cotton-Mouton effect in classical optics.

1.4.7 ***The conductivity tensor.*** We seek a general conductivity relation between current density **J** and electric field **E**, for a plasma in a magnetic field. Because of the vector nature of the magnetic force $q\mathbf{v}\times\mathbf{B}$, this conductivity is anisotropic with respect to the magnetic field and is therefore a tensor. Although the conductivity tensor is a general relation, valid, within the assumptions of this chapter, for arbitrary electric fields of any origin,[12] it offers in particular an alternative procedure to that of Section 1.4.4 for calculating the propagation constants of characteristic electromagnetic waves in a plasma.

To derive the conductivity tensor, it is more convenient to use the second coordinate system of Fig. 1.12, in which the z axis is aligned with the magnetic field. The expansion of the general equation of motion (1.4.1) is thus identical to (1.4.25) with the simplification $\theta \to 0$. The reciprocal conductivity is obtained immediately from (1.4.27) as

$$\check{\sigma}^{-1} = \frac{m}{ne^2}\begin{bmatrix} j\omega+\nu & \omega_b & 0 \\ -\omega_b & j\omega+\nu & 0 \\ 0 & 0 & j\omega+\nu \end{bmatrix}, \tag{1.4.54}$$

where the coefficient is understood to multiply each term of the matrix. A matrix may be inverted formally by transposing the co-factors, and dividing by the determinant (see Appendix B). Carrying out this operation, we obtain

$$\check{\sigma} = (\check{\sigma}^{-1})^{-1}$$

$$= \frac{ne^2/m}{(j\omega+\nu)[(j\omega+\nu)^2+\omega_b^2]}\begin{bmatrix} (j\omega+\nu)^2 & -\omega_b(j\omega+\nu) & 0 \\ \omega_b(j\omega+\nu) & (j\omega+\nu)^2 & 0 \\ 0 & 0 & (j\omega+\nu)^2+\omega_b^2 \end{bmatrix}; \tag{1.4.55}$$

[12] Refinements are considered in Chapter 3 which introduce *spatial dispersion*, whereby the conductivity is itself a function of wave direction and propagation constants.

and thus the general tensor conductivity is

$$\check{\sigma}=\begin{bmatrix}\sigma_\perp & +j\sigma_\times & 0\\ -j\sigma_\times & \sigma_\perp & 0\\ 0 & 0 & \sigma_\parallel\end{bmatrix} \tag{1.4.56}$$

where

$$\sigma_\perp \equiv -j\frac{ne^2}{m}\frac{\omega-j\nu}{(\omega-j\nu)^2-\omega_b{}^2} \tag{1.4.57}$$

$$\sigma_\times \equiv -j\frac{ne^2}{m}\frac{\omega_b}{(\omega-j\nu)^2-\omega_b{}^2} \tag{1.4.58}$$

$$\sigma_\parallel \equiv -j\frac{ne^2}{m}\frac{1}{\omega-j\nu}. \tag{1.4.59}$$

The corresponding tensor dielectric constant is

$$\check{\kappa}=\mathbf{1}-j\frac{\check{\sigma}}{\omega\epsilon_0}=\begin{bmatrix}\kappa_\perp & -j\kappa_\times & 0\\ +j\kappa_\times & \kappa_\perp & 0\\ 0 & 0 & \kappa_\parallel\end{bmatrix} \tag{1.4.60}$$

where

$$\kappa_\perp \equiv 1-\frac{(\omega_p{}^2/\omega^2)(1-j\nu/\omega)}{(1-j\nu/\omega)^2-\omega_b{}^2/\omega^2} \tag{1.4.61}$$

$$\kappa_\times \equiv \frac{(\omega_p{}^2/\omega^2)(\omega_b/\omega)}{(1-j\nu/\omega)^2-\omega_b{}^2/\omega^2} \tag{1.4.62}$$

$$\kappa_\parallel \equiv 1-\frac{\omega_p{}^2/\omega^2}{1-j\nu/\omega}. \tag{1.4.63}$$

Having now obtained general expressions for the conductivity and dielectric constant, we may find wave propagation constants by using the dispersion relation for plane waves in an anisotropic medium (A.74). Without loss of generality we take the propagation direction to lie in the x-z plane with direction cosines $(\sin\theta, 0, \cos\theta)$; then (A.74) becomes

$$\begin{vmatrix}\kappa_\perp-\check{\mu}^2\cos^2\theta & -j\kappa_\times & \check{\mu}^2\sin\theta\cos\theta\\ +j\kappa_\times & \kappa_\perp-\check{\mu}^2 & 0\\ \check{\mu}^2\sin\theta\cos\theta & 0 & \kappa_\parallel-\check{\mu}^2\sin^2\theta\end{vmatrix}=0. \tag{1.4.64}$$

This equation is quadratic in $\check{\mu}^2$

$$A\check{\mu}^4+B\check{\mu}^2+C=0, \tag{1.4.65}$$

with coefficients

$$\begin{aligned}A &\equiv \kappa_\perp\sin^2\theta+\kappa_\parallel\cos^2\theta\\ B &\equiv -(\kappa_\perp{}^2-\kappa_\times{}^2)\sin^2\theta-\kappa_\perp\kappa_\parallel(1+\cos^2\theta)\\ C &\equiv \kappa_\parallel(\kappa_\perp{}^2-\kappa_\times{}^2).\end{aligned} \tag{1.4.66}$$

Alternatively the equation may be solved for $\tan^2\theta$, yielding

$$\tan^2\theta=-\frac{\kappa_\parallel[\check{\mu}^2-(\kappa_\perp+\kappa_\times)][\check{\mu}^2-(\kappa_\perp-\kappa_\times)]}{(\check{\mu}^2-\kappa_\parallel)[\kappa_\perp\check{\mu}^2-(\kappa_\perp{}^2-\kappa_\times{}^2)]}. \tag{1.4.67}$$

This latter form is particularly convenient, as it permits one to extract easily the propagation formulas for the special cases of $\theta=0$ and 90°. Also one finds cutoff and resonance conditions as a function of angle by setting $\check{\mu}^2=0$ or ∞, respectively.

Both (1.4.65) and (1.4.67) are alternative forms of Appleton's equation (1.4.40). Further discussion and numerical examples are given in Sections 1.4.9 to 1.4.12.

1.4.8 ***Conductivity in rotating coordinates.*** Some algebraic simplification of the conductivity and dielectric constant tensors is obtained by expressing them in the rotating coordinates introduced in Section 1.4.1 (Åström, 1950; Turner, 1954). By (1.4.6) an arbitrary electric field is resolved into the independent component vectors

$$\begin{aligned}\mathbf{E}_l &= (\mathbf{a}_x+j\mathbf{a}_y)\,E_l/\sqrt{2}\\ \mathbf{E}_r &= (\mathbf{a}_x-j\mathbf{a}_y)\,E_r/\sqrt{2}\\ \mathbf{E}_z &= \mathbf{a}_z E_z\end{aligned} \tag{1.4.68}$$

rather than the usual cartesian components (E_x, E_y, E_z). Continuing in the coordinate system with z axis aligned with the magnetic field, and using (1.4.12), we find for the equations of motion

$$\begin{aligned}[(j\omega+\nu)+j\omega_b]v_l &= -\frac{e}{m}E_l\\ [(j\omega+\nu)-j\omega_b]v_r &= -\frac{e}{m}E_r\\ (j\omega+\nu)v_z &= -\frac{e}{m}E_z,\end{aligned} \tag{1.4.69}$$

or in matrix form with $\mathbf{J}=-ne\mathbf{v}$

$$j\frac{m}{ne^2}\begin{bmatrix}\omega+\omega_b-j\nu & 0 & 0\\ 0 & \omega-\omega_b-j\nu & 0\\ 0 & 0 & \omega-j\nu\end{bmatrix}\begin{bmatrix}J_l\\ J_r\\ J_z\end{bmatrix}=\begin{bmatrix}E_l\\ E_r\\ E_z\end{bmatrix}. \tag{1.4.70}$$

Inverting the matrix yields the *conductivity tensor in rotating coordinates*

$$\check{\sigma}' = \begin{bmatrix} \sigma_l & 0 & 0 \\ 0 & \sigma_r & 0 \\ 0 & 0 & \sigma_\parallel \end{bmatrix} \tag{1.4.71}$$

with

$$\sigma_l \equiv -j\frac{ne^2}{m}\frac{1}{(\omega - j\nu)+\omega_b} \tag{1.4.72}$$

$$\sigma_r \equiv -j\frac{ne^2}{m}\frac{1}{(\omega - j\nu)-\omega_b} \tag{1.4.73}$$

$$\sigma_\parallel \equiv -j\frac{ne^2}{m}\frac{1}{\omega - j\nu}. \tag{1.4.74}$$

Comparison with (1.4.57) to (1.4.59) shows

$$\sigma_\perp = \frac{\sigma_l + \sigma_r}{2} \qquad \sigma_l = \sigma_\perp - \sigma_\times$$

$$\sigma_\times = \frac{-(\sigma_l - \sigma_r)}{2} \qquad \sigma_r = \sigma_\perp + \sigma_\times. \tag{1.4.75}$$

The equivalent dielectric constant tensor in rotating coordinates is also diagonal,

$$\check{\kappa}' = \mathbf{1} - j\frac{\check{\sigma}'}{\omega\epsilon_0} = \begin{bmatrix} \kappa_l & 0 & 0 \\ 0 & \kappa_r & 0 \\ 0 & 0 & \kappa_\parallel \end{bmatrix} \tag{1.4.76}$$

with

$$\kappa_l \equiv 1 - \frac{\omega_p^2/\omega^2}{(1 - j\nu/\omega)+\omega_b/\omega} \tag{1.4.77}$$

$$\kappa_r \equiv 1 - \frac{\omega_p^2/\omega^2}{(1 - j\nu/\omega)-\omega_b/\omega} \tag{1.4.78}$$

$$\kappa_\parallel \equiv 1 - \frac{\omega_p^2/\omega^2}{1 - j\nu/\omega} \tag{1.4.79}$$

and the relations

$$\kappa_\perp = \frac{\kappa_l + \kappa_r}{2} \qquad \kappa_l = \kappa_\perp + \kappa_\times$$

$$\kappa_\times = \frac{\kappa_l - \kappa_r}{2} \qquad \kappa_r = \kappa_\perp - \kappa_\times. \tag{1.4.80}$$

In this notation, Appleton's equation in the form (1.4.67) becomes

$$\tan^2\theta = -\frac{\kappa_\parallel(\check{\mu}^2 - \kappa_l)(\check{\mu}^2 - \kappa_r)}{(\check{\mu}^2 - \kappa_\parallel)(\kappa_\perp\check{\mu}^2 - \kappa_l\kappa_r)}. \tag{1.4.81}$$

The conversion of the conductivity or dielectric constant tensors from fixed to rotating coordinates may be accomplished directly by a unitary matrix transformation (Turner, 1954). Consider a vector which is given in terms of the usual cartesian components. There exists a transformation matrix $\mathbf{U}$ which operates on the vector to express it in components in a second coordinate system without changing its physical meaning. For example, the equivalence stated in (1.4.6) is given in matrix notation by

$$\frac{1}{\sqrt{2}}\begin{bmatrix} 1 & -j & 0 \\ 1 & j & 0 \\ 0 & 0 & \sqrt{2} \end{bmatrix}\begin{bmatrix} E_x \\ E_y \\ E_z \end{bmatrix} = \begin{bmatrix} E_l \\ E_r \\ E_z \end{bmatrix}, \tag{1.4.82}$$

which is of the form

$$\mathbf{U}\cdot\mathbf{E} = \mathbf{E}'. \tag{1.4.83}$$

The reverse transformation is

$$\frac{1}{\sqrt{2}}\begin{bmatrix} 1 & 1 & 0 \\ j & -j & 0 \\ 0 & 0 & \sqrt{2} \end{bmatrix}\begin{bmatrix} E_l \\ E_r \\ E_z \end{bmatrix} = \begin{bmatrix} E_x \\ E_y \\ E_z \end{bmatrix}, \tag{1.4.84}$$

of the form

$$\mathbf{U}^{-1}\cdot\mathbf{E}' = \mathbf{E}. \tag{1.4.85}$$

$\mathbf{U}$ and $\mathbf{U}^{-1}$ are reciprocal matrices such that

$$\mathbf{U}^{-1}\cdot\mathbf{U} = \mathbf{U}\cdot\mathbf{U}^{-1} = \mathbf{1}. \tag{1.4.86}$$

Consider the relation $\mathbf{J} = \check{\sigma}\cdot\mathbf{E}$; then, with the primes denoting the rotating coordinate system,

$$\check{\sigma}'\cdot\mathbf{E}' = \mathbf{J}' = \mathbf{U}\cdot\mathbf{J} = \mathbf{U}\cdot\check{\sigma}\cdot\mathbf{E} = \mathbf{U}\cdot\check{\sigma}\cdot\mathbf{U}^{-1}\cdot\mathbf{E}'$$

and we obtain the transformation relation for the conductivity tensor

$$\check{\sigma}' = \mathbf{U}\cdot\check{\sigma}\cdot\mathbf{U}^{-1}. \tag{1.4.87}$$

If in cartesian coordinates in general

$$\check{\sigma} \equiv \begin{bmatrix} \sigma_{xx} & \sigma_{xy} & \sigma_{xz} \\ \sigma_{yx} & \sigma_{yy} & \sigma_{yz} \\ \sigma_{zx} & \sigma_{zy} & \sigma_{zz} \end{bmatrix}, \tag{1.4.88}$$

then in the rotating coordinates using (1.4.82) to (1.4.85)

$$\check{\boldsymbol{\sigma}}' = \begin{bmatrix} \frac{(\sigma_{xx}+\sigma_{yy})+j(\sigma_{xy}-\sigma_{yx})}{2} & \frac{(\sigma_{xx}-\sigma_{yy})-j(\sigma_{xy}+\sigma_{yx})}{2} & \frac{\sigma_{xz}-j\sigma_{yz}}{\sqrt{2}} \\ \frac{(\sigma_{xx}-\sigma_{yy})+j(\sigma_{xy}+\sigma_{yx})}{2} & \frac{(\sigma_{xx}+\sigma_{yy})-j(\sigma_{xy}-\sigma_{yx})}{2} & \frac{\sigma_{xz}+j\sigma_{yz}}{\sqrt{2}} \\ \frac{\sigma_{zx}+j\sigma_{zy}}{\sqrt{2}} & \frac{\sigma_{zx}-j\sigma_{zy}}{\sqrt{2}} & \sigma_{zz} \end{bmatrix}, \tag{1.4.89}$$

which for (1.4.56) simplifies to

$$\check{\boldsymbol{\sigma}}' = \begin{bmatrix} \sigma_\perp - \sigma_\times & 0 & 0 \\ 0 & \sigma_\perp + \sigma_\times & 0 \\ 0 & 0 & \sigma_\parallel \end{bmatrix} \tag{1.4.90}$$

in agreement with (1.4.71) to (1.4.75). By the same transformation, the dielectric constant is obtained in the form (1.4.76).

1.4.9 ***Summary of principal waves.*** Before further consideration of the general case of propagation in an arbitrary direction, it is helpful to collect and summarize results for propagation in the *principal directions* along ($\theta=0$) and across ($\theta=90°$) the magnetic field. Since there are two characteristic waves for each direction, we have four *principal waves*. From the "$\tan^2\theta$" form of Appleton's equation, (1.4.81), we obtain the indices by setting the numerator or the denominator equal to zero. Thus, in terms of the dielectric constant elements (1.4.77) to (1.4.80):

$\theta=0$:

$$\check{\mu}_l^{\,2} = \kappa_l \tag{1.4.91}$$

$$\check{\mu}_r^{\,2} = \kappa_r \tag{1.4.92}$$

$\theta=90°$:

$$\check{\mu}_{ord}^2 = \kappa_\parallel \tag{1.4.93}$$

$$\check{\mu}_{ex}^2 = \frac{\kappa_l\kappa_r}{\kappa_\perp} = \frac{\kappa_\perp^{\,2}-\kappa_\times^{\,2}}{\kappa_\perp} \tag{1.4.94}$$

For simplicity, we here neglect collisions ($\nu/\omega \to 0$). We introduce special frequencies:

$$\text{cutoffs} \quad \begin{cases} \omega_1 \equiv -(\omega_b/2)+[(\omega_b/2)^2+\omega_p^{\,2}]^{1/2} & (1.4.95) \\ \omega_2 \equiv +(\omega_b/2)+[(\omega_b/2)^2+\omega_p^{\,2}]^{1/2} & (1.4.96) \end{cases}$$

$$\text{resonance} \quad \omega_{uh} \equiv (\omega_b^{\,2}+\omega_p^{\,2})^{1/2} \tag{1.4.97}$$

where ω_b and ω_p are, of course, the electron cyclotron and plasma frequencies of (1.4.15) and (1.2.7). The resonance at ω_{uh} is known as the

upper hybrid (cf. Section 1.5.2). In terms of these special frequencies the principal propagation formulas become:

$\theta=0$:

$$\check{\mu}_{l,r} = \left[\frac{(\omega \mp \omega_1)(\omega \pm \omega_2)}{\omega(\omega \pm \omega_b)}\right]^{1/2} \tag{1.4.98}$$

$\theta=90°$:

$$\check{\mu}_{ord} = \left(\frac{\omega^2-\omega_p^{\,2}}{\omega^2}\right)^{1/2} \tag{1.4.99}$$

$$\check{\mu}_{ex} = \left[\frac{(\omega^2-\omega_1^{\,2})(\omega^2-\omega_2^{\,2})}{\omega^2(\omega^2-\omega_{uh}^2)}\right]^{1/2} \tag{1.4.100}$$

This formulation permits quick identification of the frequencies for cutoff ($\mu \to 0$) and resonance ($\mu \to \infty$) for the respective waves. Figure 1.16 sketches qualitatively the behavior of the propagation indices as functions of frequency. The plasma medium may be thought of as a sort of filter with pass- and stopbands (Mower, 1956).

A useful point of view in laboratory plasma physics is to regard electron density, rather than wave frequency, as the independent variable. All quantities may then be normalized to the (fixed) wave frequency. In particular, the density may be normalized to the critical density n_c, defined in Section 1.3.5 ($n/n_c=\omega_p^{\,2}/\omega^2$). Accordingly, the special frequencies of (1.4.95) to (1.4.97) correspond to the special densities:

$$\text{cutoffs} \quad \begin{cases} n_1/n_c \equiv 1+\omega_b/\omega & (1.4.101) \\ n_2/n_c \equiv 1-\omega_b/\omega & (1.4.102) \end{cases}$$

$$\text{resonance} \quad n_h/n_c \equiv 1-\omega_b^{\,2}/\omega^2 \tag{1.4.103}$$

The propagation indices of the principal waves become:

$\theta=0$:

$$\check{\mu}_l = \left(\frac{n_1-n}{n_1}\right)^{1/2} \tag{1.4.104}$$

$$\check{\mu}_r = \left(\frac{n_2-n}{n_2}\right)^{1/2} \tag{1.4.105}$$

$\theta=90°$:

$$\check{\mu}_{ord} = \left(\frac{n_c-n}{n_c}\right)^{1/2} \tag{1.4.106}$$

$$\check{\mu}_{ex} = \left[\frac{(n_1-n)(n_2-n)}{n_c(n_h-n)}\right]^{1/2} \tag{1.4.107}$$

Figure 1.17 shows qualitatively the behavior of the propagation indices as functions of density. Note, in particular, that for strong magnetic fields such that $\omega_b > \omega$, n_2 and n_h become negative, so that the respective cutoffs

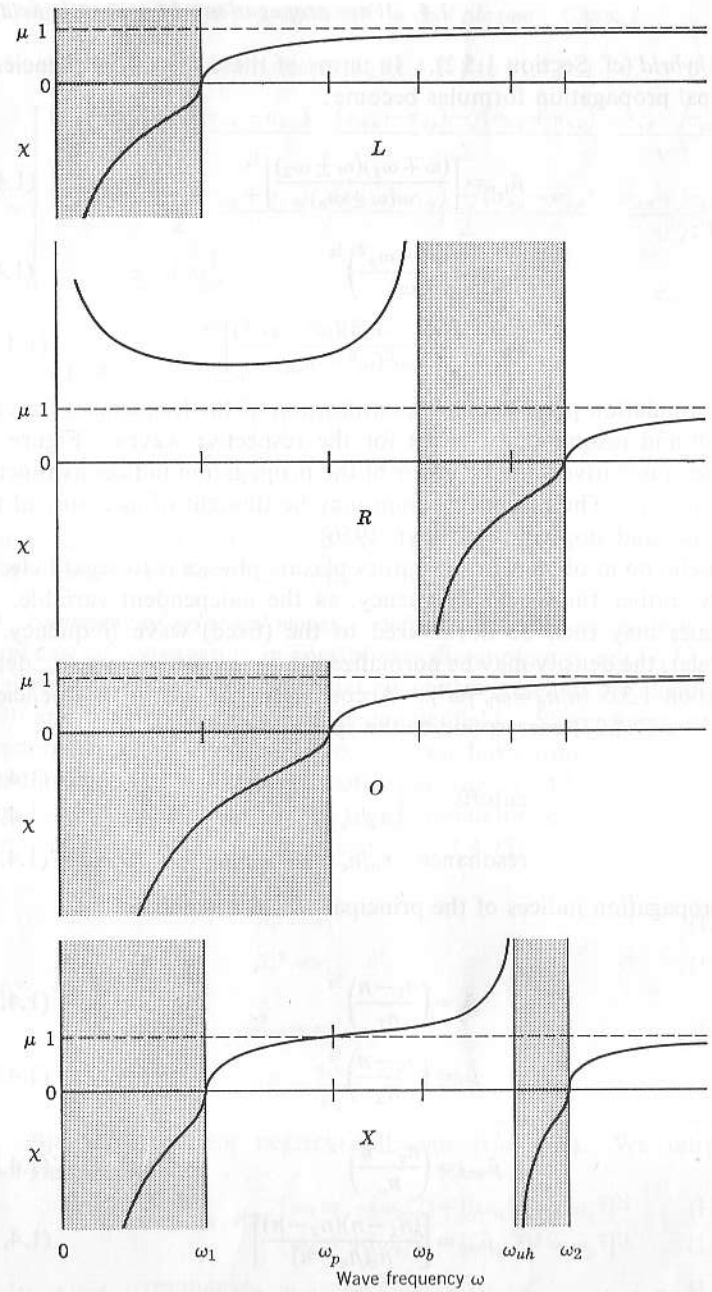

FIG. 1.16 Qualitative variations of refractive index with frequency for principal waves, showing stopbands (shaded) and passbands. The locations of cutoffs and resonances are unchanged as ω_b is greater or less than ω_p.

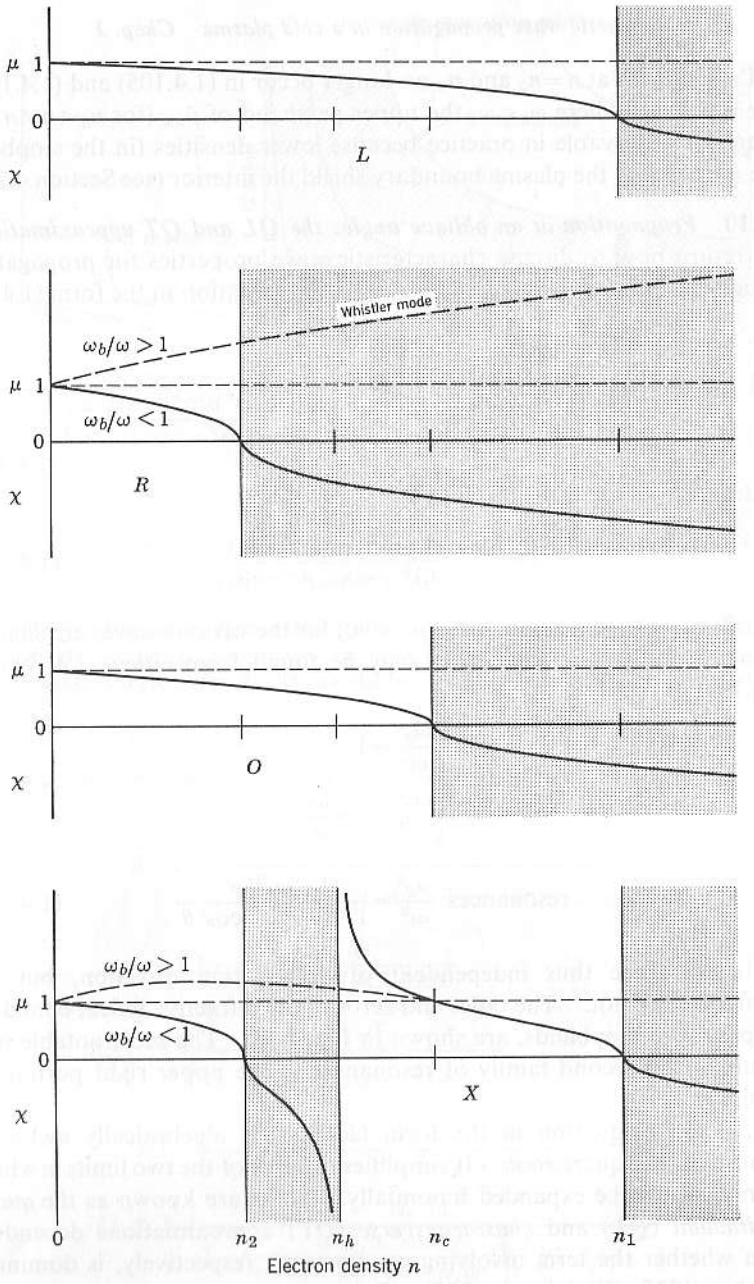

FIG. 1.17 Qualitative variation of refractive index with electron density for principal waves. Note disappearance of stopbands for R and X waves when $\omega_b/\omega > 1$.

and resonances at $n=n_2$ and n_h no longer occur in (1.4.105) and (1.4.107). For low fields where $\omega_b<\omega$, the upper passband of $\check{\mu}_{ex}$ (for $n_h<n<n_1$) is often not observable in practice because lower densities (in the stopband $n_2<n<n_h$) near the plasma boundary shield the interior (see Section 4.2.3).

1.4.10 ***Propagation at an oblique angle: the QL and QT approximations.*** We return now to discuss characteristic wave properties for propagation at an arbitrary angle described by Appleton's equation in the form (1.4.40)

$$\check{\mu}^2=1-\frac{\omega_p{}^2/\omega^2}{\left[1-j\frac{\nu}{\omega}-\frac{(\omega_b{}^2/\omega^2)\sin^2\theta}{2(1-\omega_p{}^2/\omega^2-j\nu/\omega)}\right]\pm\left[\frac{(\omega_b{}^4/\omega^4)\sin^4\theta}{4(1-\omega_p{}^2/\omega^2-j\nu/\omega)^2}+\frac{\omega_b{}^2}{\omega^2}\cos^2\theta\right]^{1/2}} \tag{1.4.108}$$

or the equivalent form (1.4.81)

$$\tan^2\theta=-\frac{\kappa_\parallel(\check{\mu}^2-\kappa_l)(\check{\mu}^2-\kappa_r)}{(\check{\mu}^2-\kappa_\parallel)(\kappa_\perp\check{\mu}^2-\kappa_l\kappa_r)}. \tag{1.4.109}$$

Cutoffs ($\mu\to 0$) and resonances ($\mu\to\infty$) for the various waves are sharply defined only as $\nu/\omega\to 0$. They may be found from either (1.4.108) or (1.4.109):

$$\text{cutoffs}\quad\begin{cases}\dfrac{\omega_p{}^2}{\omega^2}=1\\[2ex]\dfrac{\omega_p{}^2}{\omega^2}=1\pm\dfrac{\omega_b}{\omega}\end{cases} \tag{1.4.110}$$

$$\text{resonances}\quad\frac{\omega_p{}^2}{\omega^2}=\frac{1-\omega_b{}^2/\omega^2}{1-(\omega_b{}^2/\omega^2)\cos^2\theta}. \tag{1.4.111}$$

The cutoffs are thus independent of propagation direction, but the resonances are not. The poles and zeros of the refractive index, bounding the pass- and stopbands, are shown in Fig. 1.18. The most notable new feature is the second family of resonances in the upper right portion of the figure.

Appleton's equation in the form (1.4.108) is algebraically awkward because of the square root. It simplifies in either of the two limits in which the radical can be expanded binomially. These are known as the *quasi-longitudinal* (*QL*) and *quasi-transverse* (*QT*) approximations depending upon whether the term involving $\cos\theta$ or $\sin\theta$, respectively, is dominant (Booker, 1935; Whitehead, 1952). Putting

$$\check{\rho}\equiv\frac{(\omega_b/\omega)(\sin^2\theta/\cos\theta)}{2(1-\omega_p{}^2/\omega^2-j\nu/\omega)}=\frac{\kappa_\parallel\kappa_\perp-\kappa_l\kappa_r}{\kappa_\parallel\kappa_\times}\frac{\sin^2\theta}{2\cos\theta} \tag{1.4.112}$$

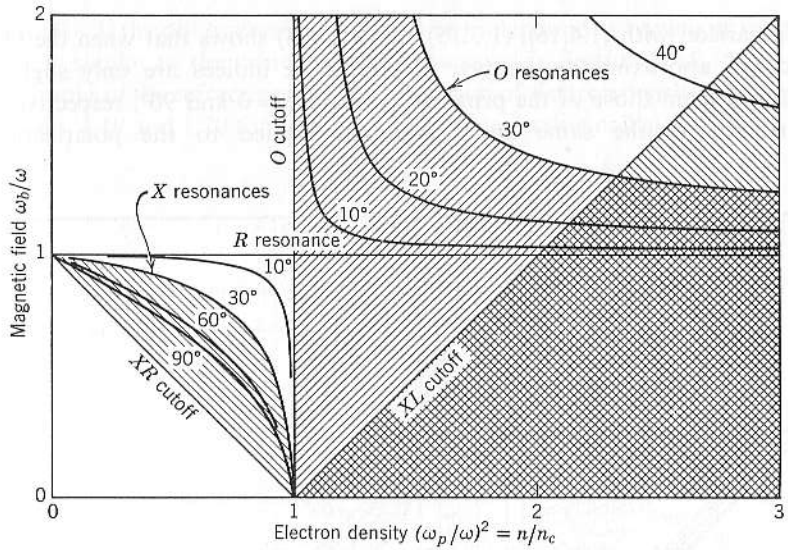

FIG. 1.18 Cutoffs and resonances for oblique propagation, neglecting collisions. *L* and *R* refer to the QL approximation, *O* and *X* to the QT. As an example, the nonpropagating regions for $\theta=30°$ are shaded (positive slope for *O*, negative slope for *X*).

and expanding binomially to first order, we have:

QL ($|\check{\rho}^2|\ll 1$):

$$\check{\mu}_{l,r}^2\approx 1-\frac{\omega_p{}^2/\omega^2}{1-j\frac{\nu}{\omega}\pm\frac{\omega_b}{\omega}\cos\theta(1\mp\check{\rho}+\frac{1}{2}\check{\rho}^2+\ldots)}$$

$$\approx 1-\frac{\omega_p{}^2/\omega^2}{1-j\nu/\omega\pm(\omega_b/\omega)\cos\theta} \tag{1.4.113}$$

QT ($|\check{\rho}^2|\gg 1$):

$$\check{\mu}_{ord}^2\approx 1-\frac{\omega_p{}^2/\omega^2}{1-j\frac{\nu}{\omega}+\frac{\omega_b}{2\omega}\cos\theta(\check{\rho}^{-1}+\ldots)}$$

$$\approx 1-\frac{\omega_p{}^2/\omega^2}{1-j\nu/\omega+(1-\omega_p{}^2/\omega^2-j\nu/\omega)\cot^2\theta} \tag{1.4.114}$$

$$\check{\mu}_{ex}^2\approx 1-\frac{\omega_p{}^2/\omega^2}{1-j\frac{\nu}{\omega}-\frac{(\omega_b{}^2/\omega^2)\sin^2\theta}{1-\omega_p{}^2/\omega^2-j\nu/\omega}(1+\frac{1}{4}\check{\rho}^{-2}+\ldots)}$$

$$\approx 1-\frac{\omega_p{}^2/\omega^2}{1-j\frac{\nu}{\omega}-\frac{(\omega_b{}^2/\omega^2)\sin^2\theta}{1-\omega_p{}^2/\omega^2-j\nu/\omega}} \tag{1.4.115}$$

Comparison with (1.4.16), (1.3.15), and (1.4.48) shows that when the QL and QT approximations apply, the refractive indices are only slightly changed from those of the principal waves at $\theta=0$ and 90°, respectively. Furthermore, the same approximations applied to the polarization

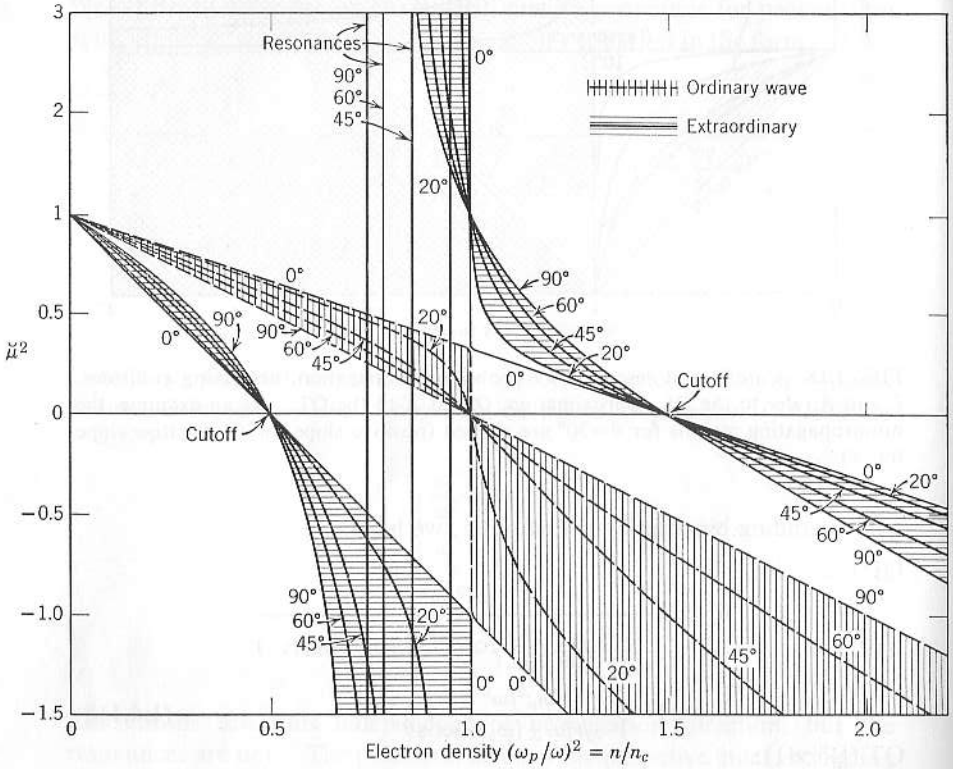

FIG. 1.19 Refractive indices for characteristic waves at various angles θ; $\omega_b/\omega=0.5$, $\nu/\omega=0$. The shaded regions indicate the domains of the ordinary and extraordinary waves.

relation (1.4.44) show that the QL waves are very nearly left and right circularly polarized,[13] and the QT waves nearly linearly polarized (wave **E** in the plane of $\mathbf{B}_0$ and γ for the ordinary wave, **E** perpendicular to this plane for the extraordinary). Except for a small range of conditions such

[13] The handedness of the circular polarization is defined with respect to the magnetic field direction, not the wave propagation direction.

that $|\check{\rho}|\sim 1$, the oblique waves may thus be understood as having properties closely similar to the principal waves discussed in Section 1.4.9.

Graphs of the refractive index as a function of electron density are shown in Figs. 1.19 and 1.20 for $\omega_b/\omega<1$ and >1, neglecting collisions ($\nu/\omega\to 0$).

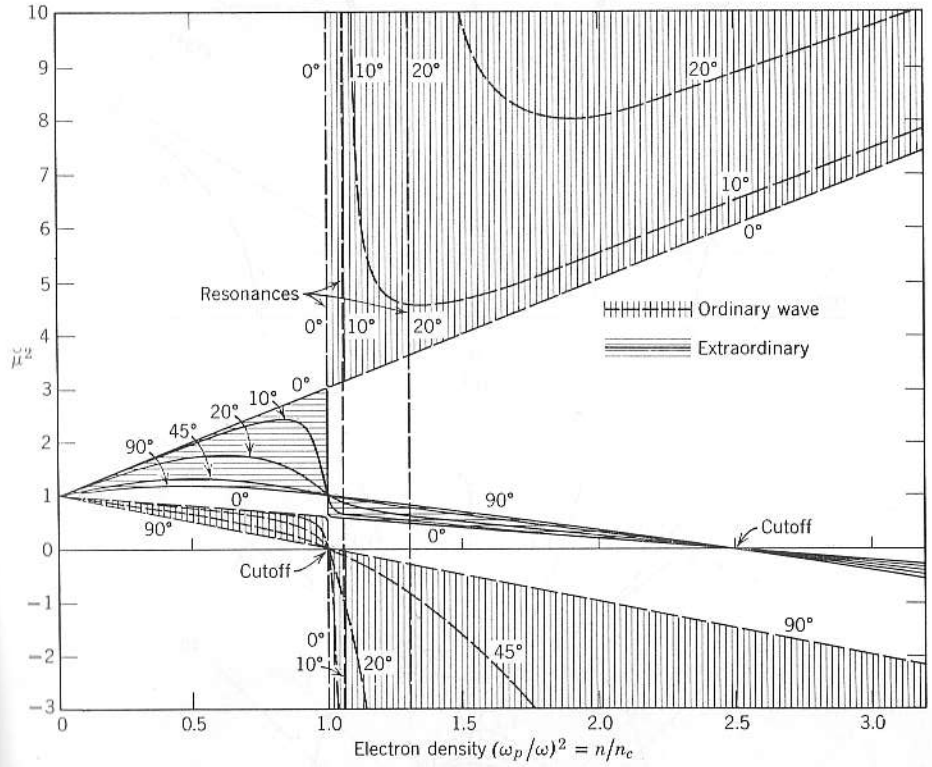

FIG. 1.20 Same as Fig. 1.19, but $\omega_b/\omega=1.5$.

Curves for propagation angles other than those shown lie within the cross-hatched regions, and can be estimated by interpolation.

An interesting anomaly appears at $\omega_p^2/\omega^2=1$. The 0° curves are seen to interchange. The curve for the left-hand wave drops down abruptly and becomes the right-hand wave; the right-hand wave goes through a resonance to become the left-hand wave. This purely mathematical difficulty arises from the fact that at $\omega_p^2/\omega^2=1$ the QL condition $|\check{\rho}^2|\ll 1$

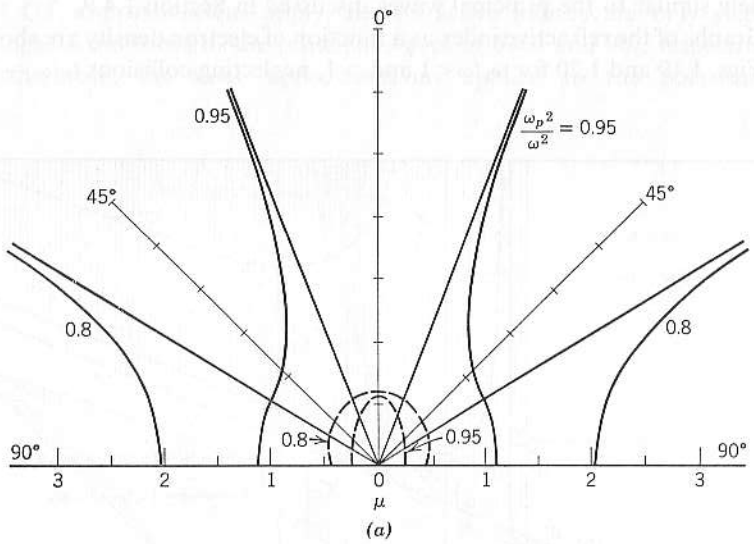

(a)

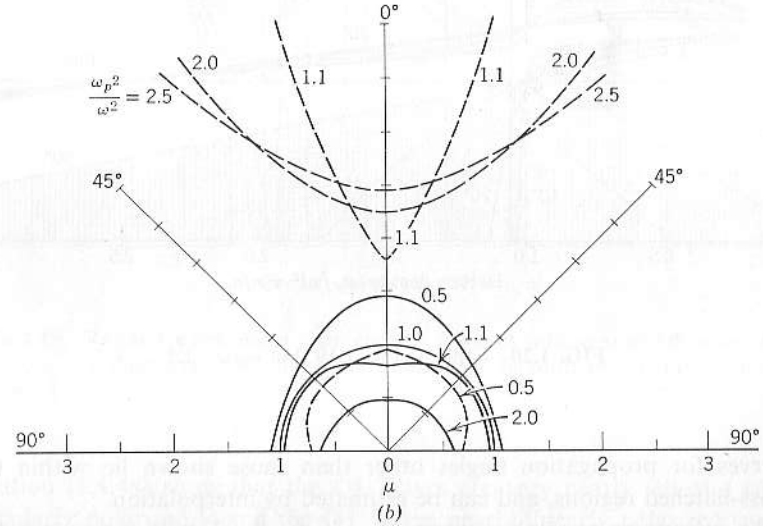

(b)

FIG. 1.21 Polar plots of refractive index (index or slowness surfaces), (*a*) $\omega_b/\omega = 0.5$, (*b*) $\omega_b/\omega = 1.5$. Ordinary wave, *dashed* curves; extraordinary, *solid*; no collisions.

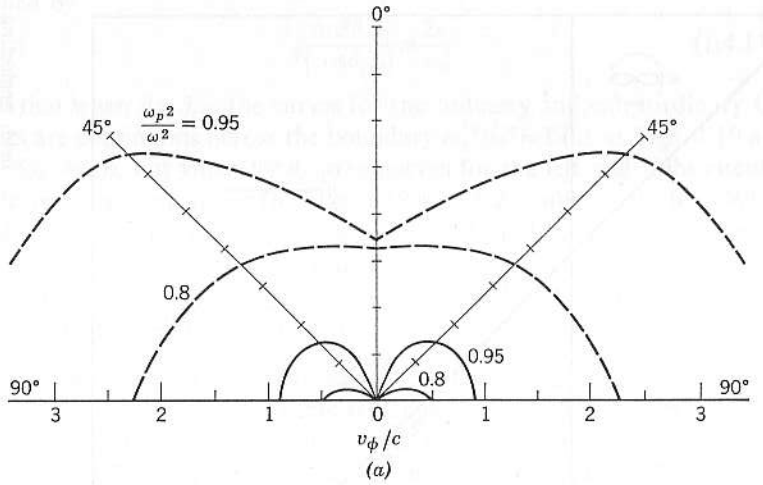

(a)

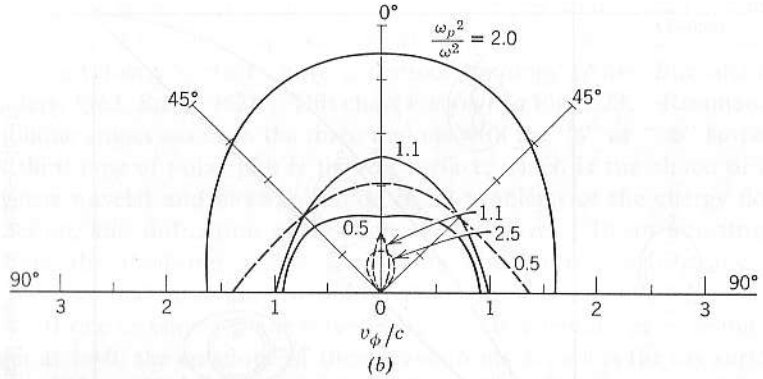

(b)

FIG. 1.22 Polar plots of reciprocal refractive index (phase-velocity or wave-normal surfaces), (*a*) $\omega_b/\omega = 0.5$, (*b*) $\omega_b/\omega = 1.5$. Ordinary wave, *dashed* curves; extraordinary, *solid*; no collisions.

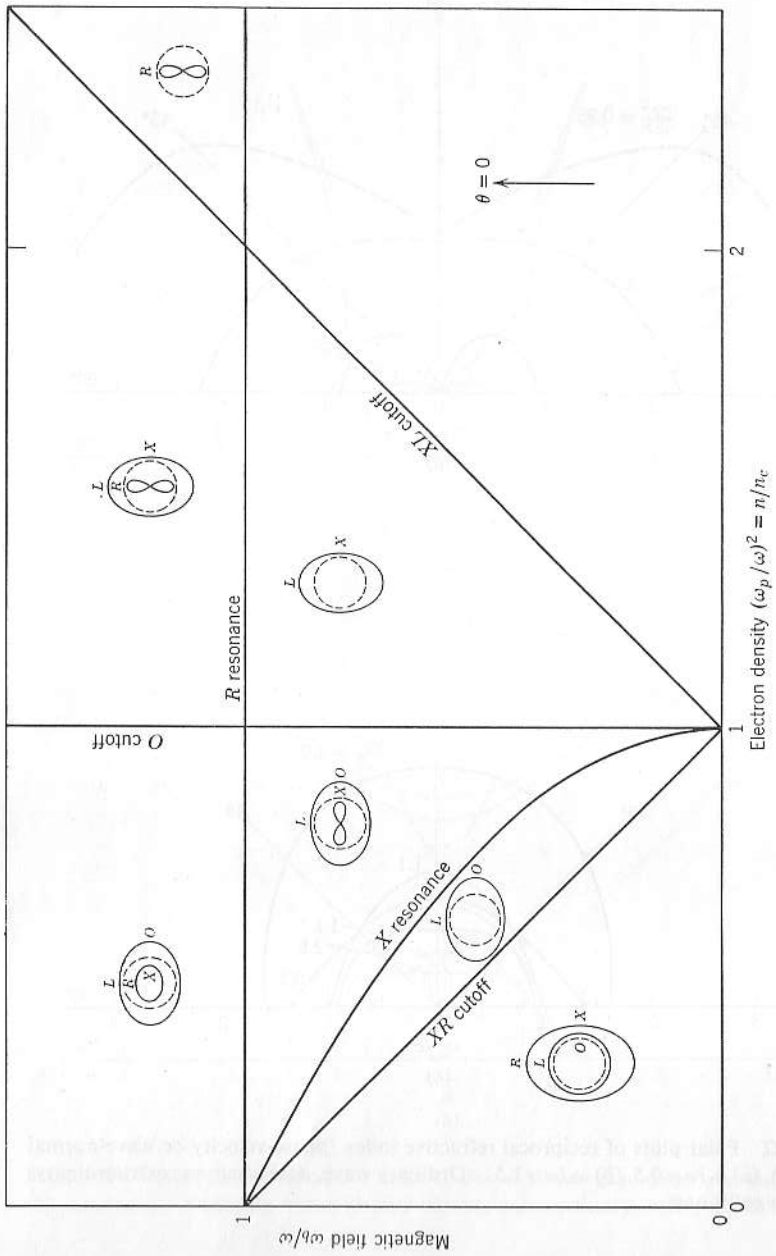

FIG. 1.23 Typical shape of phase-velocity surfaces for various regions of electron density and magnetic field, neglecting collisions. The dashed circles represent the vacuum velocity of light. The polar axis (magnetic field direction) is toward the top of the figure. The notations O, X, L, and R designate the ordinary and extraordinary (QT), and left- and right-hand (QL) waves. Similar information, plotted differently, is given in Figs. 1.19 and 1.20.

cannot be obtained without collisions. There is thus a *critical angle* defined by

$$\frac{\sin^2\theta_{crit}}{|\cos\theta_{crit}|} \equiv \frac{2\nu}{\omega_b} \tag{1.4.116}$$

such that when $\theta > \theta_{crit}$ the curves for the ordinary and extraordinary QT waves are continuous across the boundary $\omega_p^2/\omega^2 = 1$ (as in Figs. 1.19 and 1.20 for $\theta \neq 0$), but when $\theta < \theta_{crit}$ the curves for the left and right circular QL waves are continuous (in Figs. 1.19 and 1.20 only for $\theta = 0$). When $\theta = \theta_{crit}$, the two curves intersect at $\omega_p^2/\omega^2 = 1$, and the two characteristic waves couple to each other. Further discussion of propagation characteristics when collisions are significant is found in Ratcliffe (1959), Chapters 9–10, and Budden (1961), Chapter 6.

1.4.11 ***Index, velocity, and ray surfaces.*** The refractive index $\mu = \mathrm{Re}(\check{\mu})$ may be displayed with polar plots as a function of θ, the angle between the propagation direction and the static magnetic field (Clemmow and Mullaly, 1955). Figure 1.21 shows representative cases. In classical crystal optics this type of figure is known as the *refractive-index* or *slowness* surface.[14]

Alternatively, one may make a similar polar plot for the reciprocal refractive index—that is, the phase velocity v_ϕ/c. Figure 1.22 shows in this format the same cases as Fig. 1.21. This type of figure is known as the *phase-velocity* or *wave-normal* surface.

A useful catalog of wave propagation characteristics as functions of electron density, magnetic field, and direction of propagation can be made by dividing the density–magnetic field plane into regions in each of which the phase-velocity surfaces have a distinct topology (Allis, Buchsbaum, and Bers, 1963; Stix, 1962). This chart is shown in Fig. 1.23. Resonances at oblique angles occur in the three regions with the "8" or "∞" surface.

A third type of polar plot is the *ray* surface, which is the shape of the Huygens wavelet and has application in all problems of the energy flow, refraction, and diffraction of monochromatic waves. In an anisotropic medium the Poynting vector $\mathbf{E}\times\mathbf{H}$ (ray direction) is not parallel to the wave-normal direction γ whenever there is a component of $\mathbf{E}$ parallel to γ. If one considers plane wave fronts of all orientations crossing an origin at $t = 0$, the envelope of these wave fronts at $t = 1$ is the ray surface (Hines, 1951). The ray direction is displaced from the wave-normal direction (γ) toward the magnetic field direction ($\mathbf{B}_0$) by an angle α where

$$\tan\alpha = \frac{1}{\mu}\frac{d\mu}{d\theta}. \tag{1.4.117}$$

[14] The term "surface" is used since the plot may be visualized in three dimensions as a figure of revolution about the $\theta = 0$ axis, symmetric about the $\theta = 90°$ plane.

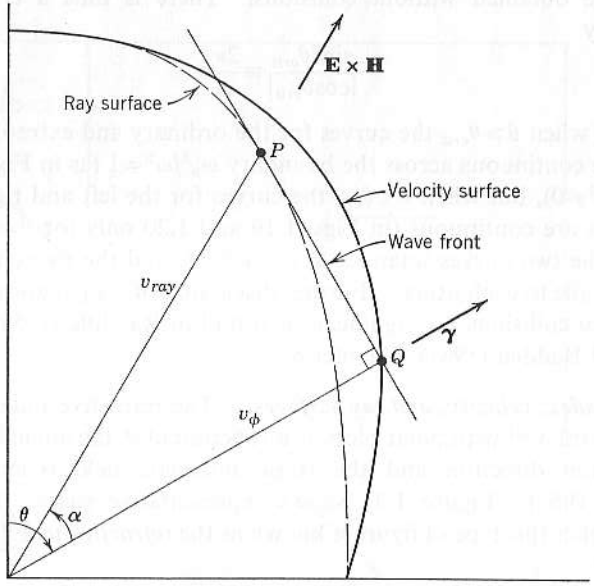

FIG. 1.24 Relation between phase-velocity and ray surfaces. The wave front is perpendicular to the radius vector to Q and tangent at P. The magnitudes of the radius vectors are the phase velocity v_ϕ and the ray velocity v_{ray}.

The radius vector to the ray surface in any ray direction is the *ray velocity*

$$v_{ray}=v_\phi\left[1+\frac{1}{\mu^2}\left(\frac{d\mu}{d\theta}\right)^2\right]^{1/2}. \tag{1.4.118}$$

The ray surface is related to the phase-velocity surface in that the tangent planes of the ray surface are everywhere perpendicular to radius-vectors of the velocity surface (Fig. 1.24). The ray direction corresponding to a given wave-normal direction (γ) is also the normal to the tangent plane of the refractive index surface.

In a dispersive, as well as anisotropic, medium the group velocity, which arises from the dependence $\mu(\omega)$, is parallel to the ray velocity, which arises from the dependence $\mu(\theta)$. For a loss-free but otherwise general medium the dispersion relation [such as (A.74)] is a functional relationship between the angular frequency ω and the vector propagation coefficient $\boldsymbol{\beta}=\gamma/j$. One may express the vector $\boldsymbol{\beta}$ in terms of its components in either cartesian (x, y, z) or spherical (β, θ, ϕ) coordinates,

$$\boldsymbol{\beta}=(\beta_x, \beta_y, \beta_z)=(\beta, \theta, \phi). \tag{1.4.119}$$

In direct extension of the definition (A.42), the anisotropic group velocity is given by (Stix, 1962)

$$\begin{aligned}\mathbf{v}_g=\nabla_\beta\omega&=\mathbf{a}_x\frac{\partial\omega}{\partial\beta_x}+\mathbf{a}_y\frac{\partial\omega}{\partial\beta_y}+\mathbf{a}_z\frac{\partial\omega}{\partial\beta_z}\\&=\mathbf{a}_\beta\left(\frac{\partial\omega}{\partial\beta}\right)_\theta+\mathbf{a}_\theta\frac{1}{\beta}\left(\frac{\partial\omega}{\partial\theta}\right)_\beta\end{aligned} \tag{1.4.120}$$

where ∇_β is the gradient operator in $\boldsymbol{\beta}$-space and $\mathbf{a}_x, \ldots, \mathbf{a}_\theta$ are the unit vectors in the $x, \ldots, \theta$ directions. By expanding the derivative $(\partial\omega/\partial\theta)_\beta$, one obtains[15]

[15] The dispersion relation $f(\omega, \beta, \theta)=0$ is mathematically similar to an equation of state. Appropriate methods of handling the partial derivatives are developed in thermodynamics texts. See, for example, Sears (1953) and Crawford (1949).

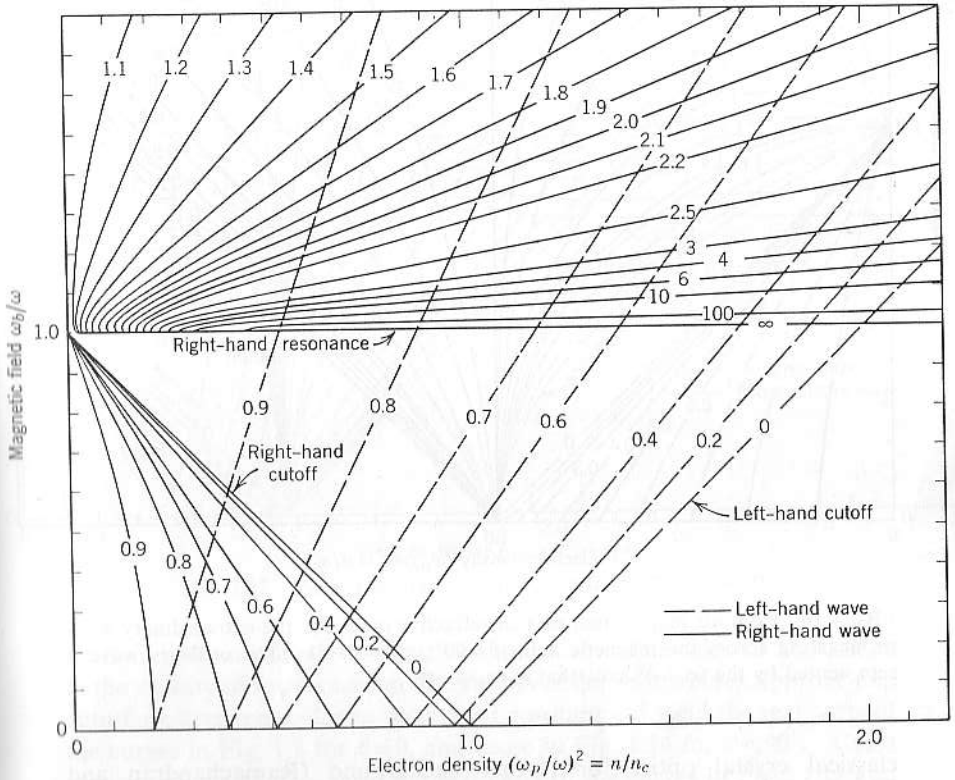

FIG. 1.25 Contour map of real part of refractive index for the left- and right-hand circularly polarized waves propagating along the magnetic field (cyclotron waves) $(\nu/\omega=10^{-3})$.

$$\mathbf{v}_g = \left(\frac{\partial\omega}{\partial\beta}\right)_\theta \left[\mathbf{a}_\beta - \mathbf{a}_\theta \frac{1}{\mu}\left(\frac{\partial\mu}{\partial\theta}\right)_\omega\right] = \left(\frac{\partial\omega}{\partial\beta}\right)_\theta \frac{\mathbf{v}_{ray}}{v_\phi}, \tag{1.4.121}$$

where $\mathbf{v}_{ray}$ has the magnitude (1.4.118) and the direction implied by (1.4.117).

The problem of energy flow in an anisotropic, dispersive, lossy medium becomes exceedingly complicated. The reader is referred to treatments of

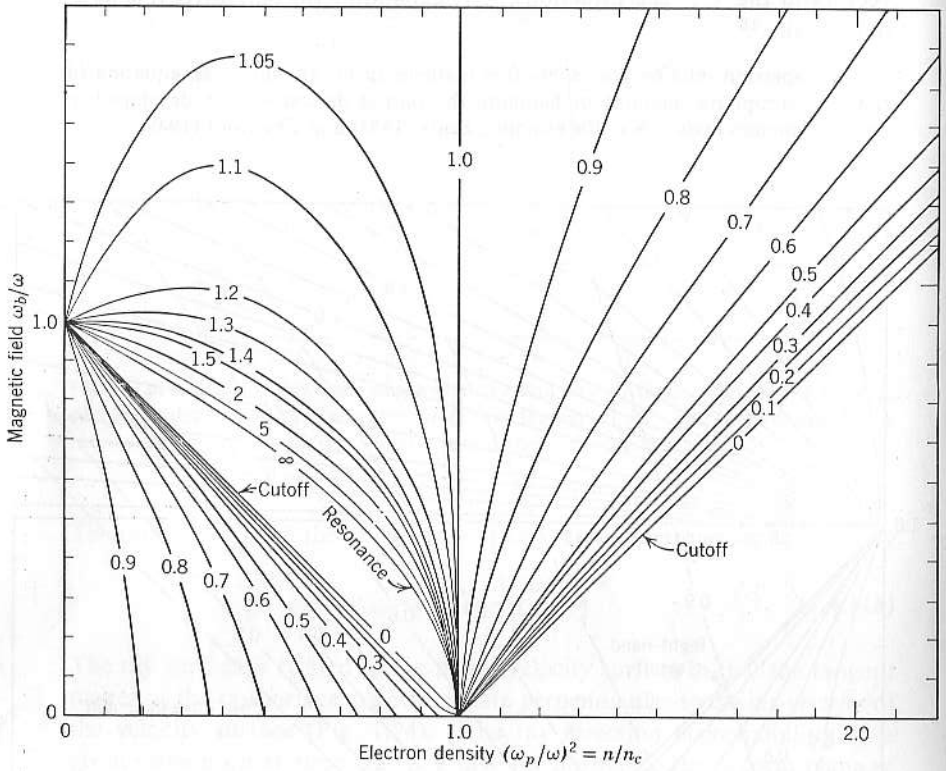

FIG. 1.26 Contour map of real part of refractive index for the extraordinary wave propagating across the magnetic field ($\theta = 90°$; $\nu/\omega = 10^{-3}$). The ordinary wave is represented by the $(\omega_p/\omega)^2$ axis (that is, $\omega_b/\omega = 0$).

classical crystal optics for further background (Ramachandran and Ramaseshan, 1961). The problem in the plasma context is discussed at length by Budden (1961), Stix (1962), and Brandstatter (1963). A famous example is the guiding or ducting of waves in the "whistler mode" along

the magnetic field (Helliwell and Morgan, 1959; Rao and Booker, 1963), discussed further in Section 6.5.3.

1.4.12 ***Refractive index contour maps.*** The zeros and poles of the refractive index were shown in the ω_p^2–ω_b plane as a function of propagation angle in Fig. 1.18. For a particular angle of propagation, lines of constant refractive index then make up a contour map. The cases of

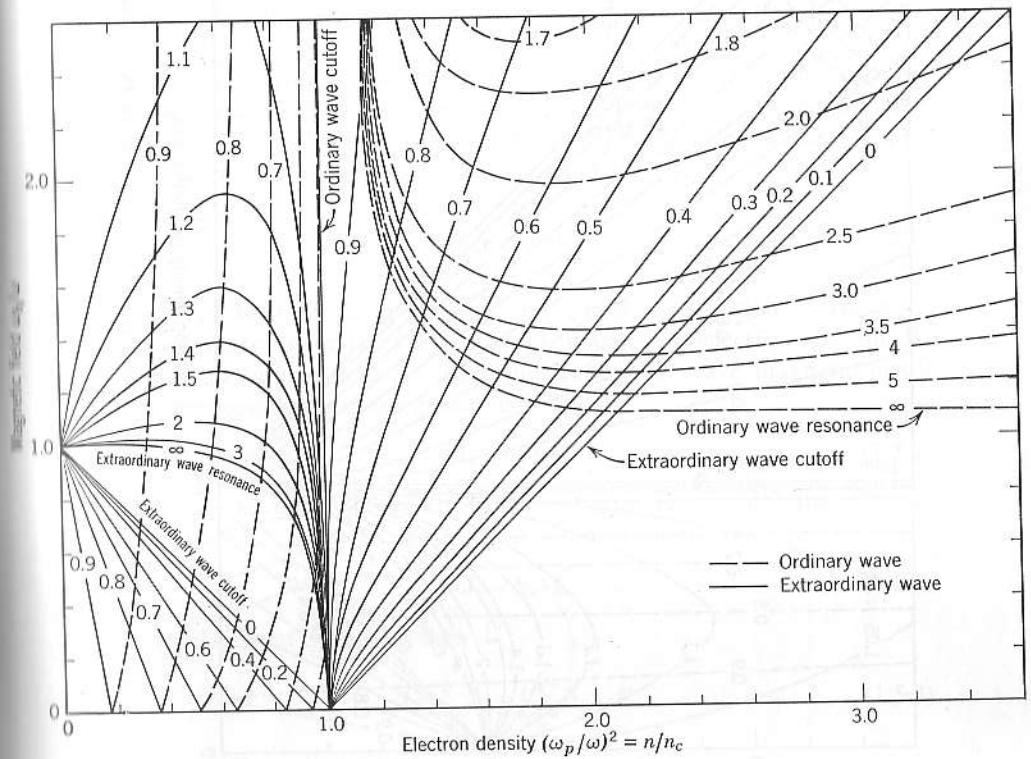

FIG. 1.27 Refractive index contour map for $\theta = 20°$ ($\nu/\omega = 0$).

$\theta = 0$ and 90° are shown in Figs. 1.25 and 1.26. The ridge of high index in the vicinity of resonance and the valleys of depressed index approaching cutoff are apparent. Cross sections at constant ω_p^2 yield the real parts of the curves in Fig. 1.8 for $\theta = 0$, and those in Fig. 1.14 for $\theta = 90°$. Cross sections at constant ω_b yield the real parts of the curves in Figs. 1.11 and 1.15, respectively.

Contour maps for propagation at other angles are shown in Figs. 1.27 and 1.28. Here the "ordinary" resonance is seen emerging in the upper

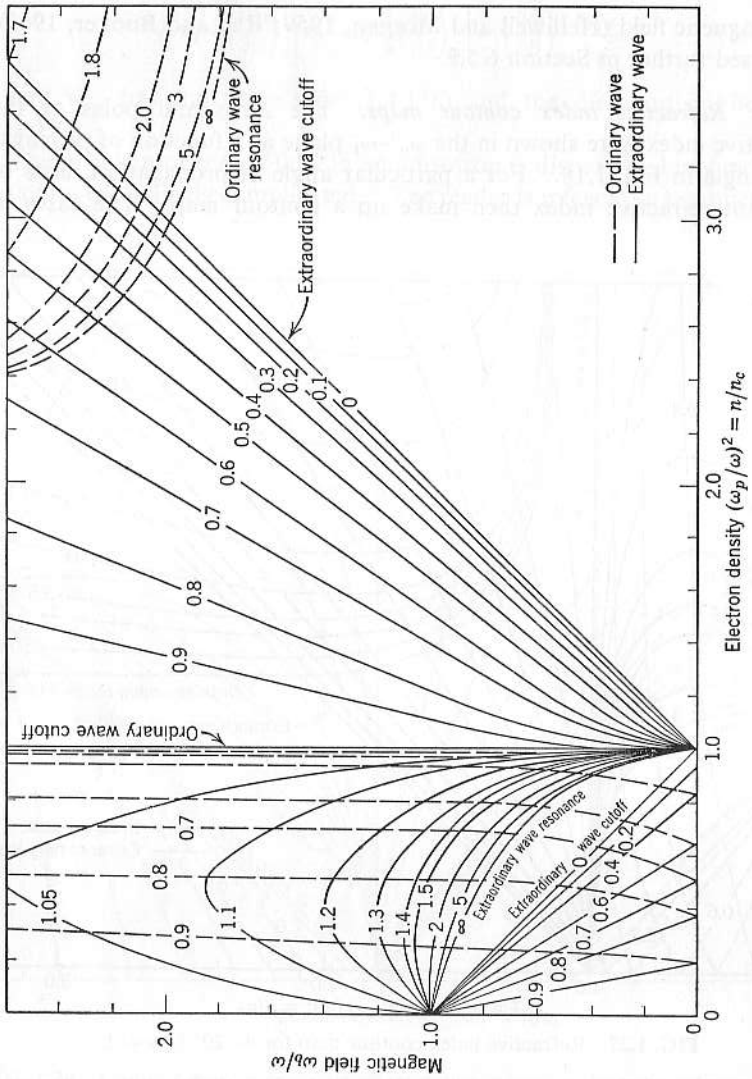

FIG. 1.28 Refractive index contour map for $\theta = 45°$ ($\nu/\omega = 0$).

right corner. It does not extend to low density for any magnetic field, so that the only possibility of coupling to it from outside a plasma is by evanescent waves through thin cut-off regions or by mode conversion (see Section 4.2.3).

1.5 Ion motion effects

Our discussion thus far has neglected motion of the heavy positive ions. In the high-frequency domain, which is our principal interest, the ion

current is very small relative to the electron current, on account of the greater inertia of the ions. However, at lower frequencies (for example, near the ion cyclotron frequency) the ion current can be dominant. Coincidentally, it usually happens that those frequencies for which ion motion is significant imply wavelengths comparable to the size of laboratory plasmas and, hence, boundary conditions must be considered simultaneously (Stix, 1962). In contrast, our basic viewpoint for high-frequency waves is that of such small wavelengths that the laboratory plasma can be treated as an infinite medium.

1.5.1 ***Conductivity with ion motions.*** The contribution of ion currents may be evaluated by a straightforward extension of the methods of Sections 1.4.7 and 1.4.8 (Åström, 1950; Allis, Buchsbaum, and Bers, 1963). The equation of motion of the kth particle species is

$$m_k \frac{d\mathbf{v}_k}{dt} = q_k(\mathbf{E} + \mathbf{v}_k \times \mathbf{B}_0) - m_k \nu_k \mathbf{v}_k, \tag{1.5.1}$$

where m_k is the mass, q_k the charge, and ν_k an effective collision frequency or damping term for the kth species; $\mathbf{E}$ is the wave electric field and $\mathbf{B}_0$ the static magnetic field (as usual, neglecting the wave magnetic field). The corresponding current density is

$$\mathbf{J}_k = n_k q_k \mathbf{v}_k, \tag{1.5.2}$$

where n_k is the density of the kth species. As in Section 1.4.7, the relations (1.5.1) and (1.5.2) can be expressed as a tensor Ohm's law

$$\mathbf{J}_k = \check{\boldsymbol{\sigma}}_k \cdot \mathbf{E}. \tag{1.5.3}$$

The total current density is then

$$\mathbf{J} = \sum_k \mathbf{J}_k = \left(\sum_k \check{\boldsymbol{\sigma}}_k\right) \cdot \mathbf{E}, \tag{1.5.4}$$

and the total conductivity[16]

$$\check{\boldsymbol{\sigma}} = \sum_k \check{\boldsymbol{\sigma}}_k. \tag{1.5.5}$$

The corresponding total tensor dielectric constant is

$$\check{\boldsymbol{\kappa}} = \mathbf{1} - j\frac{\check{\boldsymbol{\sigma}}}{\omega\epsilon_0} = \mathbf{1} - j\frac{\sum_k \check{\boldsymbol{\sigma}}_k}{\omega\epsilon_0}. \tag{1.5.6}$$

[16] This argument is often phrased in terms of mobility instead of conductivity. See footnote 3 in Appendix A.

In the circularly polarized coordinate system and notation of Section 1.4.8, the elements of the diagonalized dielectric constant tensor, replacing (1.4.77) to (1.4.79), are

$$\kappa_l = 1 - \sum_k \frac{\omega_{pk}^2}{\omega(\omega + \omega_{bk} - j\nu_k)} \tag{1.5.7}$$

$$\kappa_r = 1 - \sum_k \frac{\omega_{pk}^2}{\omega(\omega - \omega_{bk} - j\nu_k)} \tag{1.5.8}$$

$$\kappa_\parallel = 1 - \sum_k \frac{\omega_{pk}^2}{\omega(\omega - j\nu_k)} \tag{1.5.9}$$

where the generalized plasma and cyclotron frequencies are

$$\omega_{pk}^2 = \frac{n_k q_k^2}{\epsilon_0 m_k} \tag{1.5.10}$$

$$\omega_{bk} = -\frac{q_k B_0}{m_k}. \tag{1.5.11}$$

1.5.2 ***Principal waves including ion motions.*** For the important special case of a two-component electron-ion plasma with equal densities $n_e = n_i = n$ and negligible collision rate $\nu_e = \nu_i = 0$,

$$\kappa_l = 1 - \frac{(\omega_p')^2}{(\omega + \omega_{be})(\omega - \omega_{bi})} \tag{1.5.12}$$

$$\kappa_r = 1 - \frac{(\omega_p')^2}{(\omega - \omega_{be})(\omega + \omega_{bi})} \tag{1.5.13}$$

$$\kappa_\parallel = 1 - \frac{(\omega_p')^2}{\omega^2} \tag{1.5.14}$$

where ω_{be} and ω_{bi} are the absolute magnitudes of the electron and ion cyclotron frequencies, and

$$(\omega_p')^2 = \omega_p^2(1 + m_e/m_i) \tag{1.5.15}$$

is simply the plasma frequency for the reduced mass of the electron-ion system $(m_e^{-1} + m_i^{-1})^{-1} \approx m_e$. Propagation in the principal directions may be summarized in the format of Section 1.4.9. The special frequencies and densities defined by (1.4.95) to (1.4.97) and (1.4.101) to (1.4.103) are modified slightly. These modified definitions, which include the effects of motion of a single species of positive ion, are

special frequencies:

$$\omega_1 \equiv -\left(\frac{\omega_{be} - \omega_{bi}}{2}\right) + \left[\left(\frac{\omega_{be} + \omega_{bi}}{2}\right)^2 + (\omega_p')^2\right]^{1/2} \tag{1.5.16}$$

$$\omega_2 \equiv +\left(\frac{\omega_{be} - \omega_{bi}}{2}\right) + \left[\left(\frac{\omega_{be} + \omega_{bi}}{2}\right)^2 + (\omega_p')^2\right]^{1/2} \tag{1.5.17}$$

$$\omega_{uh}^2 \approx (\omega_p')^2 + \omega_{be}^2 - \omega_{ih}^2 + \omega_{bi}^2 - O(\omega_{ih}^4/\omega_{uh}^2) \tag{1.5.18}$$

$$\omega_{ih}^2 \approx \frac{(\omega_p')^2 + \omega_{be}\omega_{bi}}{(\omega_p')^2 + \omega_{be}^2 + \omega_{bi}^2}\,\omega_{be}\omega_{bi} + O\left(\frac{\omega_{ih}^4}{\omega_{uh}^2}\right) \tag{1.5.19}$$

special densities:

$$n_c'/n_c \equiv \omega_p^2/(\omega_p')^2 = (1 + m_e/m_i)^{-1} \tag{1.5.20}$$

$$n_1/n_c \equiv (1 + \omega_{be}/\omega)(1 - \omega_{bi}/\omega) \tag{1.5.21}$$

$$n_2/n_c \equiv (1 - \omega_{be}/\omega)(1 + \omega_{bi}/\omega) \tag{1.5.22}$$

$$n_h/n_c \equiv \frac{(1 - \omega_{be}^2/\omega^2)(1 - \omega_{bi}^2/\omega^2)}{1 - \omega_{be}\omega_{bi}/\omega^2} \tag{1.5.23}$$

The refractive indices for the principal waves are

$\theta = 0$:

$$\check{\mu}_l^2 = \frac{(\omega - \omega_1)(\omega + \omega_2)}{(\omega + \omega_{be})(\omega - \omega_{bi})} = \frac{n_1 - n}{n_1} \tag{1.5.24}$$

$$\check{\mu}_r^2 = \frac{(\omega + \omega_1)(\omega - \omega_2)}{(\omega - \omega_{be})(\omega + \omega_{bi})} = \frac{n_2 - n}{n_2} \tag{1.5.25}$$

$\theta = 90°$:

$$\check{\mu}_{ord}^2 = \frac{\omega^2 - (\omega_p')^2}{\omega^2} = \frac{n_c' - n}{n_c'} \tag{1.5.26}$$

$$\check{\mu}_{ex}^2 = \frac{(\omega^2 - \omega_1^2)(\omega^2 - \omega_2^2)}{(\omega^2 - \omega_{ih}^2)(\omega^2 - \omega_{uh}^2)} = \frac{(n_1 - n)(n_2 - n)}{(1 - \omega_{be}\omega_{bi}/\omega^2)(n_h - n)} \tag{1.5.27}$$

There is a new resonance for the left-hand wave at the ion cyclotron frequency, as we would expect intuitively. In addition, there is the new *lower hybrid resonance* for the extraordinary wave at ω_{lh}, where ω_{lh} and the modified ω_{uh} are the two positive solutions of the equation (Auer, Hurwitz, and Miller, 1958)

$$\omega^4 - [(\omega_p')^2 + \omega_{be}^2 + \omega_{bi}^2]\omega^2 + \omega_{be}\omega_{bi}[(\omega_p')^2 + \omega_{be}\omega_{bi}] = 0, \tag{1.5.28}$$

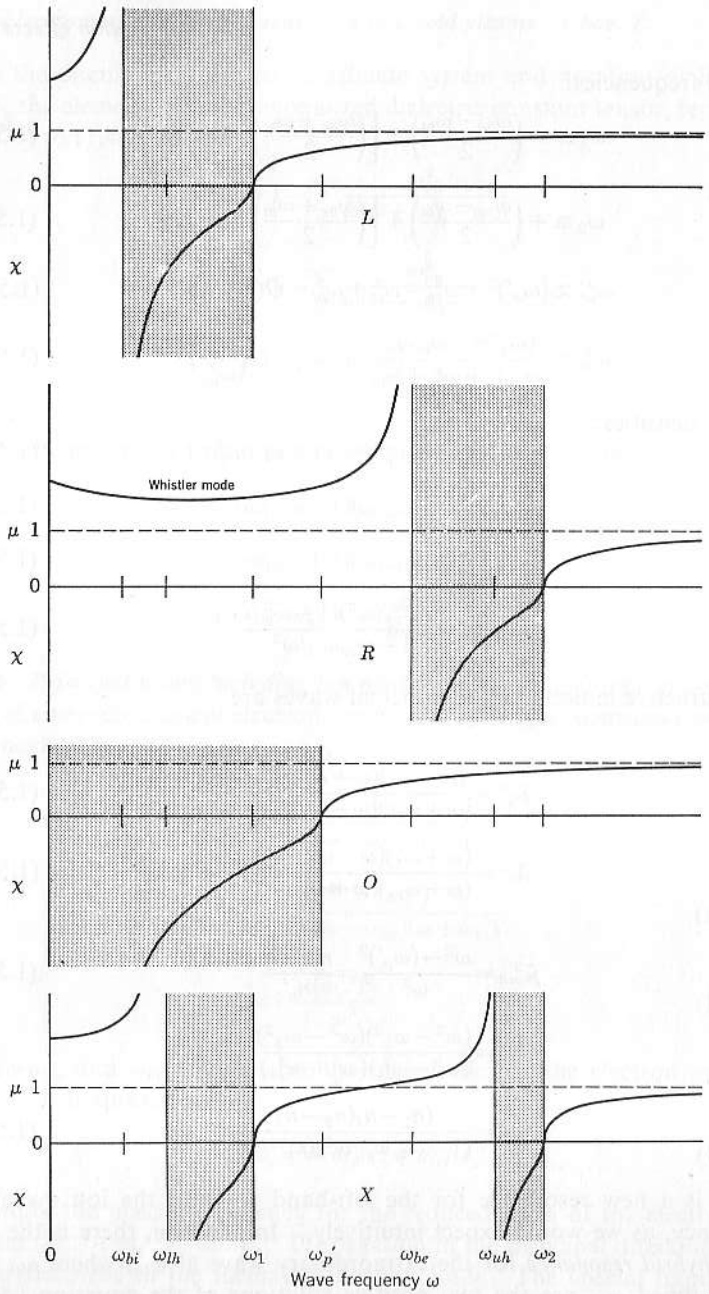

FIG. 1.29 Qualitative variation of refractive index with frequency for principal waves, including ion motions. Compare Fig. 1.16.

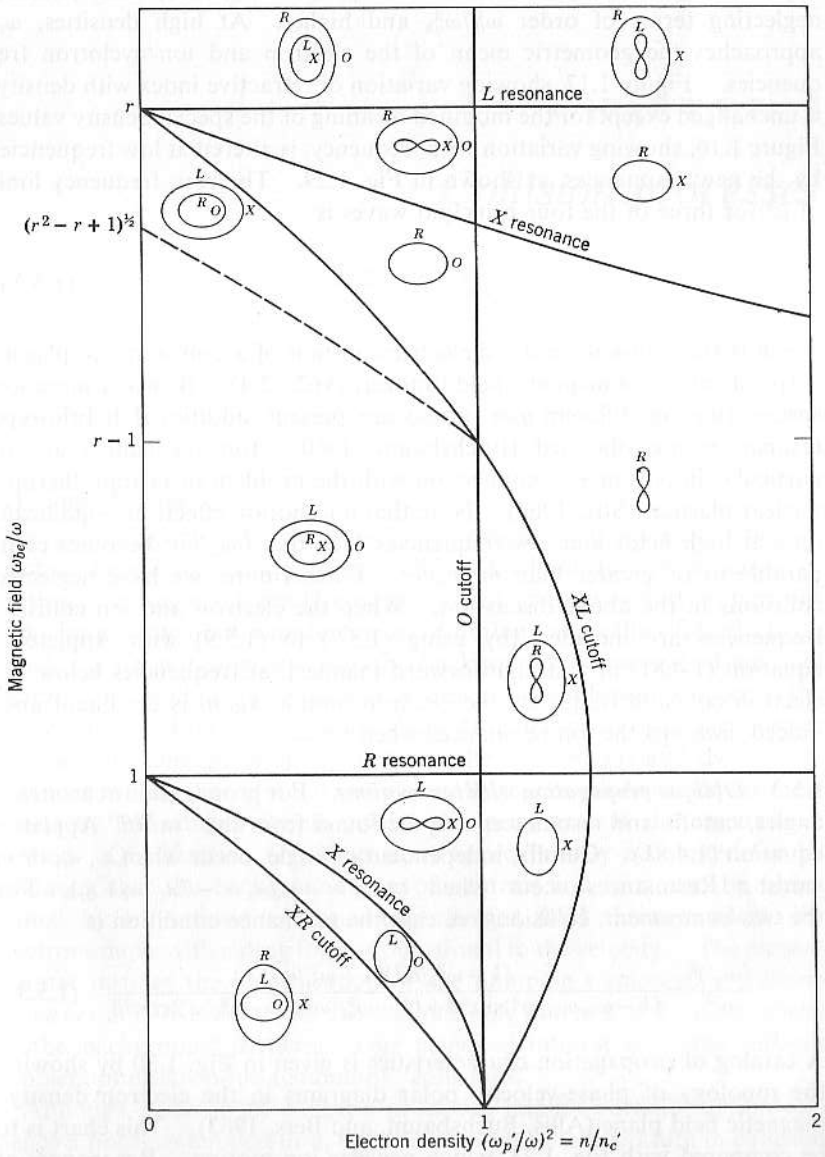

FIG. 1.30 Characteristic shape of phase-velocity surfaces for various regions of density and field, including ion motions with $r = \omega_{be}/\omega_{bi}$. Compare with Fig. 1.23. The labeling of O and X waves changes across the dashed line, which corresponds to the condition $\kappa_l \kappa_r = \kappa_\perp \kappa_\parallel$.

approximate solutions of which are given in (1.5.18) and (1.5.19), neglecting terms of order $\omega_{lh}^4/\omega_{uh}^2$ and higher. At high densities, ω_{lh} approaches the geometric mean of the electron and ion cyclotron frequencies. Figure 1.17, showing variation of refractive index with density, is unchanged except for the modified meaning of the special density values. Figure 1.16, showing variation with frequency, is altered at low frequencies by the new resonances, as shown in Fig. 1.29. The zero frequency limit of $\check{\mu}^2$ for three of the four principal waves is

$$\check{\mu}_{dc}^2 = 1 + \frac{(\omega_p')^2}{\omega_{be}\omega_{bi}}, \tag{1.5.29}$$

which is the well-known d-c dielectric constant of a collision-free plasma perpendicular to a magnetic field (Spitzer, 1962, §2.4). If two or more ion species (having different q/m ratios) are present, additional hybrid-type resonances are obtained (Buchsbaum, 1960). Ion resonances are of particular importance in connection with the problem of heating thermonuclear plasmas (Stix, 1962). Note that ion-motion effects are significant only at high fields and low frequencies such that $(\omega_{be}/\omega)^2$ becomes comparable to or greater than $m_i/m_e \gg 1$. Furthermore, we have neglected collisions in the above discussion. When the electron and ion collision frequencies are included [by using (1.5.7) to (1.5.9) with Appleton's equation (1.4.81) in a straightforward manner], at frequencies below the electron collision frequency the electron motion again is dominant and, indeed, swamps the ion resonances when $\nu > \omega_{bi}$.

1.5.3 ***Oblique propagation with ion motions.*** For propagation at arbitrary angles, cutoffs and resonances may be found from the "$\tan^2\theta$" Appleton equation (1.4.81). Cutoffs, independent of angle, occur when $\kappa_\parallel$, κ_l, or κ_r vanish. Resonances occur when $\tan^2\theta = -\kappa_\parallel/\kappa_\perp = -2\kappa_\parallel/(\kappa_l + \kappa_r)$. For the two-component, collision-free case the resonance condition is

$$\frac{(\omega_p')^2}{\omega^2} = \frac{(1-\omega_{be}^2/\omega^2)(1-\omega_{bi}^2/\omega^2)}{(1-\omega_{be}\omega_{bi}/\omega^2)\sin^2\theta + (1-\omega_{be}^2/\omega^2)(1-\omega_{bi}^2/\omega^2)\cos^2\theta}. \tag{1.5.30}$$

A catalog of propagation characteristics is given in Fig. 1.30 by showing the topology of phase-velocity polar diagrams in the electron density–magnetic field plane (Allis, Buchsbaum, and Bers, 1963). This chart is to be compared with Fig. 1.23, which neglects ion motion. Resonances at oblique angles occur in the five regions having "8" or "∞" velocity surfaces. Note that the scale of Fig. 1.30 is greatly distorted by the assumption of a very small ratio m_i/m_e. In a practical case, $m_e \ll m_i$ and the effects of ion motion are negligible unless $\omega_{be} \gg \omega$.

CHAPTER 2
Collision processes

2.1 Introduction

The preceding chapter developed the propagation characteristics of electromagnetic waves in a uniform ionized medium from the equation of motion of a single, "typical" electron. This analysis would be rigorous if the ionized medium were to consist of nothing more than free electrons which (*1*) do not interact with the background of neutral atoms and charged ions, and (*2*) possess thermal speeds negligible with respect to the phase velocity of the wave. Both of these qualifications refer to processes that permit exchange of energy between the electron gas and the electromagnetic wave. Therefore, it was physically reasonable to anticipate these effects by including a simple viscous damping term in the equation of motion. Qualification (*1*), at least, is approximately accounted for by assuming that the background gas, of neutrals and ions, can be represented by a continuous, stationary, charged fluid through which the electrons move with a drag force proportional to the velocity. The present chapter justifies the identification of the damping term with a *collision frequency* and investigates its physical meaning in terms of the discreteness of the background particles. Our principal interest is in the difficult problem of electron-ion (coulomb) "collisions."

Although mention of collision processes implies particle motion and hence a nonzero temperature, the role of electron temperature in collision processes is essentially different from that implied in qualification (*2*) above. It is appropriate to describe as "cold" those plasmas for which qualification (*2*) is well satisfied. The cases of "warm" and "hot" plasmas are considered in Chapter 3. We again assume that the positive ions are so massive that they do not move under the action of the wave field.

2.2 Elementary considerations of collision processes

2.2.1 ***Collision cross sections and frequencies.*** Consider the interaction of a *test* particle (an electron, let us say) with a group of *field* particles (atoms and molecules, or ions). Initially, we assume that the mean free path is sufficiently long and the interparticle force sufficiently short-range that a collision can be treated as a discrete two-body interaction. This assumption is notably troublesome in the case of the long-range coulomb force.

For a specific central-force law between two particles there exists, in general, a relation between the impact parameter b, the relative velocity v, and the scattering angle of the test particle ϕ (see Fig. 2.1). The analysis in the general case is most readily carried out in center-of-mass coordinates and then transformed to the laboratory system. We shall be principally interested in the case where the field particle has large mass and small velocity compared to the test particle. In this case, v and ϕ are simply the speed and scattering angle of the test particle in laboratory coordinates. The probability per unit path length for the test particle to be scattered

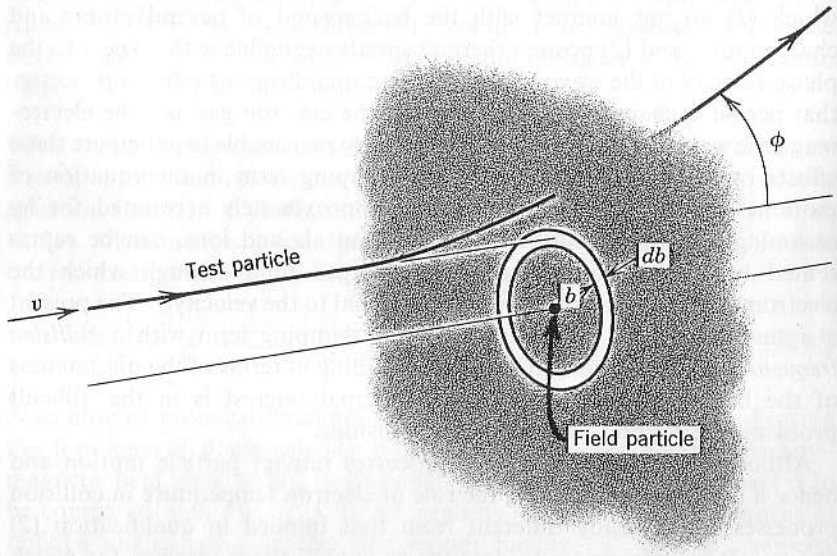

FIG. 2.1 Geometry of a collision. The impact parameter b is the distance of closest approach if there were no interparticle force. The scattering angle ϕ is the deflection of the orbit asymptote.

through an angle between ϕ and $\phi+d\phi$ is

$$dP_\phi = n_f\, 2\pi\, b(v,\phi)\, db = n_f\, 2\pi\, b(v,\phi)\, \frac{\partial b}{\partial \phi}\, d\phi, \tag{2.2.1}$$

where n_f is the number of field particles per unit volume. It is customary to write this probability in terms of a *differential cross section* $q_\Omega(v,\phi)$, having dimensions of area per unit solid-angle, such that

$$dP_\phi = n_f\, q_\Omega(v,\phi)\, 2\pi \sin\phi\, d\phi \tag{2.2.2}$$

where $2\pi \sin\phi\, d\phi = d\Omega$ is the element of solid-angle.

The *total cross section* q_t is obtained by integration over all angles:

$$q_t(v) = 2\pi \int_0^\pi q_\Omega(v,\phi) \sin\phi\, d\phi, \tag{2.2.3}$$

an integral which, in some cases, diverges at the lower limit.

The total probability of collision per unit path length is[1]

$$P(v) = \int_\phi dP_\phi = n_f q_t(v). \tag{2.2.4}$$

For test particles having a speed v, the total probability of collision per unit time, synonymous with the *total collision frequency* ν_t, is

$$\nu_t(v) = n_f\, q_t(v)\, v. \tag{2.2.5}$$

The *mean free path* is

$$\lambda_t(v) = \frac{1}{P(v)} = \frac{v}{\nu_t(v)} = \frac{1}{n_f\, q_t(v)}. \tag{2.2.6}$$

Next consider the energy and momentum exchange in a collision. For simplicity, assume that a test particle of mass m and velocity v

[1] In classical gas discharge terminology, it is customary to define a normalized *probability of collision* P_c as the probability per unit path in the field gas at 1 mm-Hg pressure and 0°C (Brown, 1959). Thus

$$P_c = \frac{L}{760}\, q_t,$$

$$P = P_c p \left(\frac{273}{T+273}\right),$$

where L is Loschmidt's constant (2.7×10^{19} cm^{-3}), and p and T are the actual pressure and absolute temperature of the field gas. This formulation is not useful in the case of highly ionized plasmas where particle densities and temperatures, rather than pressures, are the experimentally important quantities.

impinges upon a stationary field particle of mass M.[2] From conservation of momentum and energy, one obtains for an elastic collision (Symon, 1960, pp. 171–75),

$$\text{Fractional energy lost by test particle} \quad \frac{2r[1-\cos\phi(1-r^2\sin^2\phi)^{1/2}+r\sin^2\phi]}{(1+r)^2} \tag{2.2.7}$$

$$\text{Fractional forward momentum lost by test particle} \quad \frac{1-\cos\phi(1-r^2\sin^2\phi)^{1/2}+r\sin^2\phi}{1+r} \tag{2.2.8}$$

where ϕ is the angle through which the test particle is scattered and $r=m/M$. In the interesting case of $m\ll M$:

$$\text{Fractional energy lost} \quad \frac{2m}{M}(1-\cos\phi) \tag{2.2.9}$$

$$\text{Fractional forward momentum lost} \quad 1-\cos\phi \tag{2.2.10}$$

To obtain the average energy and forward momentum lost, it is necessary to average over the scattering angle ϕ. Thus

$$\langle 1-\cos\phi\rangle=\frac{\int q_\Omega(v,\phi)(1-\cos\phi)\sin\phi\, d\phi}{\int q_\Omega(v,\phi)\sin\phi\, d\phi}. \tag{2.2.11}$$

In problems of energy and momentum transfer, the important collision cross section is the *cross section for momentum transfer*

$$q_m(v)=2\pi\int q_\Omega(v,\phi)(1-\cos\phi)\sin\phi\, d\phi=\langle 1-\cos\phi\rangle q_t(v). \tag{2.2.12}$$

Relations equivalent to (2.2.4) to (2.2.6) exist for the momentum-transfer cross section. In particular, there is the *collision frequency for momentum transfer*,

$$\nu_m=n_f\, q_m(v)\, v, \tag{2.2.13}$$

which is generally the physically important collision frequency in problems of wave propagation. Indeed, for convenience, we shall normally omit the subscript m hereafter for this quantity.

The functional forms $q_\Omega(v,\phi)$, or equivalently $b(v,\phi)$, may be computed, in principle, from the dynamics of the specific interparticle force law. As an example, consider an electron (regarded as a mass-point) colliding with

[2] A more general discussion of collision geometries, using center-of-mass coordinates and allowing for field particle velocity, is given by Allis (1956, Section 3*b*). The neglect of target particle velocity is reasonable except in unusual cases where the ion temperature exceeds the electron temperature by a factor of the order of $(M/m)^{1/2}$.

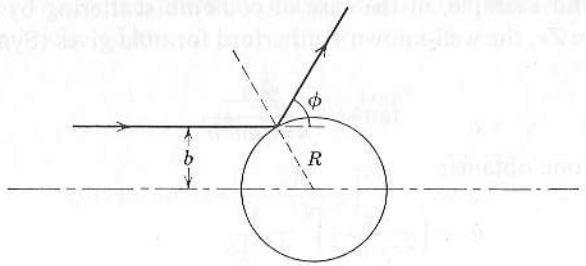

FIG. 2.2 Geometry of the "electron-molecule" hard-sphere collision.

a massive hard-sphere molecule of radius R. If the electron impinges with an impact parameter b, it is easily seen (Fig. 2.2) that it is deflected by an angle ϕ for which

$$\cos\phi=\frac{2b^2}{R^2}-1. \tag{2.2.14}$$

Thus, we obtain for the three cross sections:

$$q_\Omega=\frac{b\,\partial b/\partial\phi}{\sin\phi}=\frac{R^2}{4} \tag{2.2.15}$$

$$q_t=\frac{\pi R^2}{2}\int_0^\pi \sin\phi\, d\phi=\pi R^2 \tag{2.2.16}$$

$$q_m=\frac{\pi R^2}{2}\int_0^\pi (1-\cos\phi)\sin\phi\, d\phi=\pi R^2 \tag{2.2.17}$$

$$\langle 1-\cos\phi\rangle=q_m/q_t=1 \tag{2.2.18}$$

Both total cross sections are equal to the geometrical cross section, independent of velocity, and the average energy lost per collision is $2m/M$, a well-known result. When the problem is treated by quantum mechanics, the total cross section is found to be greater by a factor of two to four, depending on velocity, on account of diffraction of the electron wave (Mott and Massey, 1949, pp. 38–40). For short-range electron-molecule (or electron-atom) collisions, with forces falling off more rapidly than $1/r^3$, it has been shown by Mott (Massey and Burhop, 1952, p. 3) that the total cross section q_t (2.2.3) is bounded on account of quantum effects. Furthermore, for most common atoms or molecules and electrons of low to moderate energy (~ 1 eV), scattering is approximately isotropic, and the total and momentum-transfer cross sections do not differ appreciably.

As a second example, in the case of coulomb scattering by a massive ion of charge Ze, the well-known Rutherford formula gives (Symon, 1960, pp. 135–38)

$$\tan\tfrac{1}{2}\phi=\frac{Ze^2}{4\pi\epsilon_0 mv^2 b}, \tag{2.2.19}$$

from which one obtains:

$$q_\Omega=\left(\frac{Ze^2}{8\pi\epsilon_0 mv^2}\right)^2\frac{1}{\sin^4\tfrac{1}{2}\phi} \tag{2.2.20}$$

$$q_t=8\pi\left(\frac{Ze^2}{8\pi\epsilon_0 mv^2}\right)^2\int_0^1\frac{d(\sin\tfrac{1}{2}\phi)}{\sin^3\tfrac{1}{2}\phi} \tag{2.2.21}$$

$$q_m=16\pi\left(\frac{Ze^2}{8\pi\epsilon_0 mv^2}\right)^2\int_0^1\frac{d(\sin\tfrac{1}{2}\phi)}{\sin\tfrac{1}{2}\phi} \tag{2.2.22}$$

In this case, both integrated cross sections diverge at the lower limit (large b), on account of the dominance of small-angle deflections, so that an appropriate cutoff on the impact parameter must be applied. The same result is found from the quantum-mechanical treatment. The momentum transfer cross section q_m (2.2.12) deweights small-angle deflections by the factor $(1-\cos\phi)$ and, accordingly, diverges only logarithmically. The long-range nature of the coulomb force leads to many complications to which we shall return in Section 2.5.2.

While our discussion has emphasized elastic collisions, most experimental situations clearly also involve inelastic collisions such as excitation, ionization, and dissociation (Francis, 1960; Brown, 1959). These processes can also, of course, be described in terms of cross sections and collision frequencies. The over-all collision frequency is then the sum of the component collision frequencies for each relevant process,

$$\nu=n_1q_1v+n_2q_2v+\ldots=\nu_1+\nu_2+\ldots. \tag{2.2.23}$$

Thus, for instance, collisions with impurity particles having a large cross section q may contribute significantly to the over-all collision frequency even though they are present in small concentration n.

2.2.2 ***Velocity dependence of cross sections.*** In order to discuss the dependence of cross sections on velocity, it is useful to assume a simple inverse-power *force* law of the form (Kihara et al., 1960; Mott-Smith, 1960)

$$F(r)=\frac{K}{r^s}, \tag{2.2.24}$$

where s is usually an integer, and further to assume that the momentum-transfer cross section is determined approximately by the impact parameter for which the potential energy equals the kinetic energy of the incident particle. Thus

$$\frac{K}{(s-1)b^{s-1}}=\tfrac{1}{2}mv^2 \tag{2.2.25}$$

and

$$q_m(v)=\pi b^2=\pi\left[\frac{2K}{(s-1)mv^2}\right]^{2/(s-1)}\propto v^{-4/(s-1)}, \tag{2.2.26}$$

$$\nu_m(v)\propto v^{(s-5)/(s-1)}. \tag{2.2.27}$$

Table 2.1 lists the results of this model for a number of interesting cases.

TABLE 2.1 VELOCITY DEPENDENCE OF COLLISION PARAMETERS

Interaction	Force	Velocity dependence: Cross section q	Collision frequency $\nu=nqv$	Mean free path $\lambda=1/nq$
Electron-neutral	Empirical (nitrogen)	v	v^2	$1/v$
	Hard sphere (step function)	1	v	1
	Polarization $(1/r^5)$	$1/v$	1	v
	Dipole $(1/r^3)$	$1/v^2$	$1/v$	v^2
Electron-ion	Coulomb $(1/r^2)$	$1/v^4$	$1/v^3$	v^4

In reality, interparticle forces are not, in general, simple inverse powers of distance. Furthermore, the situation is complicated by resonances and quantum mechanical effects, especially at energies such that the deBroglie wavelength of the electron is comparable to the dimension of the cross section (more precisely, to the product of impact parameter and scattering angle, $b\phi$) (Mott and Massey, 1949; Massey and Burhop, 1952; and Vogt and Wannier, 1954). Thus, one must in general resort to

experiment to determine cross sections empirically, including the dependence on electron velocity and on scattering angle (Rose and Clark, 1961; Brown, 1959).

Thus far, monoenergetic test particles have been assumed. If they have some velocity distribution, not necessarily Maxwellian, cross sections and collision frequencies must be suitably averaged over velocities. For instance, the average momentum-transfer collision frequency is

$$\overline{\nu_m} = n_f \overline{q_m v} = n_f \frac{\int q_m(v)\, v f(v)\, d^3\mathbf{v}}{\int f(v)\, d^3\mathbf{v}} \tag{2.2.28}$$

where $f(v)$ is the velocity distribution function for the test particles and the bar over a quantity denotes this particular form of average. It should be noted, however, that this direct average of the collision frequency is not the only one with useful physical significance. Section 2.4.3 discusses other forms of velocity averaging which are more important for our purposes.

2.3 Effect of collisions on electron motion

Since $mv\nu$, where ν is the momentum-transfer collision frequency (2.2.13), represents the average rate of change of forward momentum due to collisions, it is possible to write the equation of motion for an "average" electron in the form

$$m\ddot{\xi} = -m\nu\dot{\xi} - eE_0 \exp j\omega t, \tag{2.3.1}$$

identical to (1.3.12) with $E = E_0 \exp j\omega t$. This model, of an electron moving through a viscous medium, follows directly in the limit where the electron makes a large number of collisions during one oscillation of the wave field (that is, $\omega \ll \nu$). However, we wish to consider the full range of conditions, including $\omega \gtrsim \nu$, for which the validity of (2.3.1) is not obvious. To do this, we again consider an average electron, but distinguish between the ordered velocity component produced by the wave field and the random component of thermal motion (Appleton and Chapman, 1932). The equation of motion for the *ordered component*, during the time interval between collisions, is

$$m\ddot{\xi} = -eE_0 \exp j\omega t. \tag{2.3.2}$$

We assume the boundary condition that this ordered velocity is zero at the instant of collision, t_1. Thus

$$\begin{aligned}\dot{\xi} &= j\frac{eE_0}{m\omega}[\exp(j\omega t) - \exp(j\omega t_1)] \\ &= j\frac{eE_0}{m\omega}\exp(j\omega t)[1 - \exp(-j\omega\tau)],\end{aligned} \tag{2.3.3}$$

where $\tau = t - t_1$. This equation is, of course, valid only for the interval $t_1 < t < t_2$, where t_2 is the time of the next collision.

In order to find the average ordered velocity, it is necessary to know the statistical distribution of the time intervals τ, in the past, at which the electrons made their last collision. This distribution is entirely equivalent to that of the time intervals τ, in the future, when the electrons make their next collision. Consider a group of electrons, N_0 in number, at an arbitrary instant of time. The number N of these that have not undergone a collision after an interval τ is obtained from

$$\frac{dN}{dt} = -\nu N, \tag{2.3.4}$$

giving

$$N = N_0 \exp(-\nu\tau). \tag{2.3.5}$$

Therefore, the fraction making the previous collision within the interval τ to $\tau + d\tau$, in the past, is

$$\frac{dN}{N_0} = \nu \exp(-\nu\tau)\, d\tau, \tag{2.3.6}$$

the familiar Poisson distribution.

Combining (2.3.3) and (2.3.6), we obtain for the statistical average of the ordered velocity component at time t

$$\begin{aligned}(\dot{\xi})_{ave} &= j\frac{eE_0}{m\omega}\exp(j\omega t)\int_0^\infty [1 - \exp(-j\omega\tau)]\nu \exp(-\nu\tau)\, d\tau \\ &= -\frac{eE_0}{m(\nu + j\omega)}\exp j\omega t.\end{aligned} \tag{2.3.7}$$

But if we had written the equation of motion (2.3.2) with a damping term $g\dot{\xi}$,

$$m\ddot{\xi} = -g\dot{\xi} - eE_0 \exp j\omega t, \tag{2.3.8}$$

we obtain

$$\dot{\xi} = -\frac{eE_0}{g + jm\omega}\exp j\omega t. \tag{2.3.9}$$

Comparison of (2.3.9) with (2.3.7) leads to the identification

$$g = m\nu. \tag{2.3.10}$$

It should be noted that (2.3.7) assumes that ν is either independent of velocity or that the random velocity is large compared to the ordered component. In the latter case, a common one, ν is an appropriate average over the electron velocity distribution (Section 2.4.3). Comparison with (2.3.1) shows that the assumption that the ordered velocity is zero after a collision is equivalent to the identification of ν as the momentum-transfer

collision frequency. It should be noted that collision frequency ν compares with the *radian* wave frequency ω, not the *cyclic* wave frequency $\omega/2\pi$.

2.4 Analysis of particle interactions

The dynamics of a macroscopic system (such as a plasma) consisting of a large number of interacting microscopic systems (electrons, ions, and neutral molecules) can be analyzed at several levels of detail. The most important of these are the *orbit*, *kinetic*, and *hydromagnetic* theories.

It is obviously impossible to follow the exact dynamics of each of the microsystems, a hopeless many-body problem. One may, however, follow the behavior of a "typical" microsystem and infer therefrom the behavior of the macrosystem. This approach, often known as *orbit theory*, is essentially that employed in Chapter 1 (Rosenbluth and Longmire, 1957). It is useful when the interactions among the microsystems are either (*1*) weak enough to be negligible in some sense, or (*2*) strong enough to be represented by a self-consistent interaction between the average microsystem and a fluid representation of the rest of the microsystems. In either case, the statistical fluctuations of the interactions are necessarily ignored.

The statistical features of the problem are preserved in the *kinetic theory* approach (Jancel and Kahan, 1955; Delcroix, 1960). We consider explicitly the particle distribution function f, defined such that at time t there are

$$f(\mathbf{r}, \mathbf{v}, t)\, dx\, dy\, dz\, dv_x\, dv_y\, dv_z$$

microsystems of a given class (electrons, let us say) located in the element of phase space between $(\mathbf{r}, \mathbf{v})$ and $(\mathbf{r}+d\mathbf{r}, \mathbf{v}+d\mathbf{v})$. In the absence of collisions, at a time $t+dt$ precisely these same particles, and none others, will occupy the element of phase space at $(\mathbf{r}+\mathbf{v}dt, \mathbf{v}+\mathbf{a}dt)$, where $\mathbf{a}=\mathbf{F}/m$ is the acceleration imposed by external forces (common to all particles). By a Taylor expansion

$$f(\mathbf{r}+\mathbf{v}dt, \mathbf{v}+\mathbf{a}dt, t+dt)=f(\mathbf{r}, \mathbf{v}, t)+\sum_{i=1}^{3} v_i \frac{\partial f}{\partial x_i}\, dt+\sum_{i=1}^{3} a_i \frac{\partial f}{\partial v_i}\, dt+\frac{\partial f}{\partial t}\, dt. \tag{2.4.1}$$

Thus, it follows that the total rate of change of f along a stream line is

$$\frac{df}{dt}=\sum v_i \frac{\partial f}{\partial x_i}+\sum a_i \frac{\partial f}{\partial v_i}+\frac{\partial f}{\partial t}$$

$$=\mathbf{v}\cdot\nabla_r f+\mathbf{a}\cdot\nabla_v f+\frac{\partial f}{\partial t}, \tag{2.4.2}$$

where ∇_r and ∇_v are respectively the gradient operators in configuration and velocity space.[3] If no collisions (or other processes such as ionization and recombination) occur, we have the *kinetic* or *Vlasov equation* (Vlasov, 1938)

$$\frac{df}{dt}=\frac{\partial f}{\partial t}+\mathbf{v}\cdot\nabla_r f+\mathbf{a}\cdot\nabla_v f=0, \tag{2.4.3}$$

which is closely related to the Liouville theorem on the conservation of density-in-phase of statistical mechanics. It may also be regarded as a generalized equation of continuity. If collisions or other statistical processes do occur, then there may be a net change $(\partial f/\partial t)_{coll}$ in the number of particles in the given element of phase space, and

$$\frac{\partial f}{\partial t}+\mathbf{v}\cdot\nabla_r f+\mathbf{a}\cdot\nabla_v f=\left(\frac{\partial f}{\partial t}\right)_{coll}, \tag{2.4.4}$$

which is the *Boltzmann equation*.

In general, it is macroscopic quantities, corresponding to integrations over the distribution function, that are of physical interest. It is often possible to carry out these integrations without specifying the exact nature of the distribution function, thereby obtaining a set of *hydromagnetic* equations in the macroscopic variables (such as velocity of mass motion, pressure, and current density). These equations are often known as Boltzmann *transport* equations, although this modifier is sometimes used for (2.4.4). The hydromagnetic description will be used in Chapter 3 (Spitzer, 1962; Bernstein and Trehan, 1960).

2.4.1 ***Boltzmann equation.*** Since the collisionless Boltzmann, or Vlasov, equation (2.4.3) implies the particle dynamics (Bernstein and Trehan, 1960), it is entirely equivalent to orbit theory in cases where collisions may legitimately be neglected. However, some problems may be mathematically more tractable in the kinetic theory treatment. An example is the "warm" plasma case of Chapter 3, for which electron thermal speeds are no longer assumed negligible with respect to the phase velocity of the wave.

A major problem in the use of the Boltzmann equation is the evaluation of the collision term $(\partial f/\partial t)_{coll}$, which is in general an integral not only over $f(\mathbf{r}, \mathbf{v}, t)$ for the class of particles in question, but also over the corresponding distribution functions for all other classes of particles with which interactions occur (Allis, 1956; Bernstein and Trehan, 1960). Thus, strictly speaking, we have an *integro*-differential equation.

A common simplification is to assume that, in the absence of external

[3] We call attention to the common use of the notation $\partial/\partial\mathbf{r}$ and $\partial/\partial\mathbf{v}$ for the configuration and velocity space gradients.

forces, collisional processes produce a return to equilibrium with a characteristic relaxation time constant τ. Thus

$$f(t)-f_0=[f(0)-f_0]\exp(-t/\tau)$$

or

$$\left\{\frac{\partial[f(t)-f_0]}{\partial t}\right\}_{coll}=\left[\frac{\partial f(t)}{\partial t}\right]_{coll}=-\frac{[f(t)-f_0]}{\tau}, \tag{2.4.5}$$

where $f(0)$ is the initial perturbed distribution and f_0 the equilibrium, the latter assumed unaffected by collisions. The relaxation time τ, in general a function of v, is usually taken to be the reciprocal of the momentum-transfer collision frequency ν; thus, we substitute in the Boltzmann equation (2.4.4)

$$(\partial f/\partial t)_{coll}=-\nu(v)\,(f-f_0). \tag{2.4.6}$$

A second major problem is the mathematical complexity of solving the Boltzmann equation. It is usually necessary to expand the distribution function in a series, and retain only low-order terms. Two such expansions are commonly used. The *Chapman-Enskog* technique (Chapman and Cowling, 1951) assumes only small departure from local thermodynamic equilibrium due to some perturbing agent of strength measured by a parameter α; thus

$$f(\mathbf{r}, \mathbf{v}, t)=f_0(\mathbf{r}, v^2)+\alpha f_1(\mathbf{r}, \mathbf{v}, t)+\alpha^2 f_2(\mathbf{r}, \mathbf{v}, t)+\ldots, \tag{2.4.7}$$

where

$$f_0(\mathbf{r}, v^2)=n(\mathbf{r})\left(\frac{m}{2\pi kT}\right)^{3/2}\exp\left(-\frac{mv^2}{2kT}\right), \tag{2.4.8}$$

the Maxwell distribution. This expansion does not converge rapidly in problems where the perturbed distribution is anisotropic. Where there exists a preferred direction in space, it is useful to expand in *spherical harmonics in velocity space* (Allis, 1956):

$$\begin{aligned} f(\mathbf{r}, \mathbf{v}, t)&=\sum_l f_l(\mathbf{r}, \mathbf{v}, t)P_l(\cos\phi)\\ &=f_0(v^2)+f_1(\mathbf{r}, v^2, t)\cos\theta+f_2(\mathbf{r}, v^2, t)\frac{3\cos^2\theta-1}{2}+\ldots \end{aligned} \tag{2.4.9}$$

where f_0 is assumed isotropic but not necessarily Maxwellian.

The volume element of velocity space, often written in the alternate notations,

$$d^3\mathbf{v}=d^3v=d\mathbf{v}=dv_x\,dv_y\,dv_z, \tag{2.4.10}$$

becomes explicitly in this case

$$d^3\mathbf{v}=v^2\sin\theta\,dv\,d\theta\,d\phi \tag{2.4.11}$$

where v, θ, ϕ are the spherical coordinates in velocity space. Most physical problems are symmetric with respect to the azimuthal angle ϕ; the trivial integration then yields the simplification[4]

$$d^3\mathbf{v}\rightarrow 2\pi v^2\sin\theta\,dv\,d\theta=-2\pi v^2\,dv\,d(\cos\theta). \tag{2.4.12}$$

It is useful to evaluate some moments of the distribution function f for the spherical harmonic expansion. Recalling that spherical harmonics are orthogonal, we obtain the normalization condition

$$\begin{aligned} \int f(\mathbf{r}, \mathbf{v})\,d^3\mathbf{v}&=\int_0^\infty\int_{-1}^1 f(\mathbf{r}, \mathbf{v})\,2\pi v^2\,d(\cos\theta)\,dv\\ &=4\pi\int_0^\infty f_0(\mathbf{r}, v^2)\,v^2\,dv=n(\mathbf{r}) \end{aligned} \tag{2.4.13a}$$

where $n(\mathbf{r})$ is the particle density. Frequently it is more convenient to separate the space and velocity dependence, replacing $f(\mathbf{r}, \mathbf{v})$ by $n(\mathbf{r})f(\mathbf{v})$ with the normalization

$$\int f(\mathbf{v})\,d^3\mathbf{v}=4\pi\int_0^\infty f_0(v^2)\,v^2\,dv=1. \tag{2.4.13b}$$

The average value of the velocity component in the preferred direction,

$$v_x=v\cos\theta, \tag{2.4.14}$$

is

$$\begin{aligned} \overline{v_x}&=\int_0^\infty\int_{-1}^1 (v\cos\theta)f(\mathbf{r}, \mathbf{v})2\pi v^2\,d(\cos\theta)\,dv\\ &=\frac{4\pi}{3}\int_0^\infty f_1(\mathbf{r}, v^2)\,v^3\,dv. \end{aligned} \tag{2.4.15}$$

2.4.2 ***Elementary Boltzmann theory of plasma conductivity.*** Consider a spatially uniform plasma subject to a weak oscillating electric field $E_0\exp j\omega t$ in the x direction (Burnett, 1931; Margenau, 1946, 1958; Sampson and Enoch, 1963). There is no static magnetic field. The Boltzmann equation for the electron distribution function becomes

$$\frac{\partial f}{\partial t}-\frac{eE_0\exp j\omega t}{m}\frac{\partial f}{\partial v_x}=\left(\frac{\partial f}{\partial t}\right)_{coll}. \tag{2.4.16}$$

Note that the magnetic field associated with the oscillatory electric field is neglected, and that the electric field is assumed uniform in space (infinite wavelength). In the absence of the electric field the equilibrium distribution, maintained by unspecified agencies, is $f_0(v)$, assumed isotropic

[4] If the azimuthal angle ϕ is significant, we make the expansion (2.4.9) in the spherical harmonics $P_l^m(\cos\theta)\exp jm\phi$, P_l^m being the *associated* Legendre function.

but not necessarily Maxwellian. Using the spherical harmonic expansion (2.4.9) to first order, we have

$$f(\mathbf{v}, t)=f_0(v)+\frac{v_x f_1(v)}{v}\exp j\omega t, \tag{2.4.17}$$

in which the time dependence of f_1 is shown explicitly and $\cos\theta$ is written as v_x/v. Evaluating the collision term in the form (2.4.6) and substituting (2.4.17) in (2.4.16), we may solve for

$$f_1=\frac{eE_0/m}{\nu(v)+j\omega}\frac{\partial f_0}{\partial v}, \tag{2.4.18}$$

where the small nonlinear term in $\partial(v_x f_1/v)/\partial v_x$ has been discarded. The fact that f_1 is complex signifies that the electron velocity perturbation is not in phase with the electric field, an entirely reasonable result. The resulting current density for electrons of charge $-e$ is

$$\begin{aligned}\breve{J}&=-ne\bar{v}_x=-ne\int v_x f(\mathbf{v}, t)\,d^3\mathbf{v}\\&=-\frac{4\pi}{3}ne\exp(j\omega t)\int f_1(v)\,v^3\,dv\\&=-\frac{4\pi ne^2}{3m}E_0\exp(j\omega t)\int\frac{1}{\nu(v)+j\omega}\frac{df_0}{dv}v^3\,dv\end{aligned} \tag{2.4.19}$$

using (2.4.15) and the alternative normalization (2.4.13b). Equation (2.4.19) is equivalent to the complex conductivity

$$\begin{aligned}\breve{\sigma}&=-\frac{4\pi}{3}\frac{ne^2}{m}\int_0^\infty\frac{1}{\nu(v)+j\omega}\frac{df_0(v)}{dv}v^3\,dv\\&=\frac{4\pi}{3}\frac{ne^2}{m}\int_0^\infty\frac{d}{dv}\left[\frac{v^3}{\nu(v)+j\omega}\right]f_0(v)\,dv,\end{aligned} \tag{2.4.20}$$

the latter form obtained by an integration by parts. The corresponding complex dielectric constant is

$$\begin{aligned}\breve{\kappa}&=1-j\frac{\breve{\sigma}}{\epsilon_0\omega}\\&=1+\frac{ne^2}{\epsilon_0 m\omega}\frac{4\pi}{3}\int\frac{1}{\omega-j\nu(v)}\frac{df_0(v)}{dv}v^3\,dv.\end{aligned} \tag{2.4.21}$$

Two important special cases of (2.4.20) and (2.4.21) may be obtained, readily, as follows.

Collision frequency independent of velocity:

$$\breve{\sigma}=\frac{ne^2}{m}\frac{1}{\nu+j\omega}, \tag{2.4.22}$$

$$\breve{\kappa}=1-\frac{ne^2}{\epsilon_0 m\omega}\frac{1}{\omega-j\nu}=1-\frac{\omega_p{}^2}{\omega(\omega-j\nu)}, \tag{2.4.23}$$

independent of $f_0(v)$, results which coincide with the Lorentz conductivity (1.3.14). This illustrates the well-known Maxwell condition under which the transport properties of a gas are independent of the distribution function. No such simplification exists for other dependencies on velocity.

Maxwellian velocity distribution:
Assuming

$$f_0(v)=\left(\frac{m}{2\pi kT}\right)^{3/2}\exp\left(-\frac{mv^2}{2kT}\right), \tag{2.4.24}$$

one obtains for (2.4.20)

$$\breve{\sigma}=\frac{8}{3\sqrt{\pi}}\frac{ne^2}{m}\int_0^\infty\frac{1}{\nu(u)+j\omega}u^4\exp(-u^2)\,du, \tag{2.4.25}$$

where u is the velocity normalized to the most probable speed,

$$u=v/(2kT/m)^{1/2}. \tag{2.4.26}$$

In the case of a static magnetic field, a similar analysis summarized by Allis (1956) yields for the elements of the diagonalized (rotating coordinate) conductivity tensor (1.4.71):

$$\sigma_\parallel=-\frac{4\pi}{3}\frac{ne^2}{m}\int_0^\infty\frac{1}{\nu(v)+j\omega}\frac{df_0(v)}{dv}v^3\,dv, \tag{2.4.27}$$

$$\sigma_{l,r}=-\frac{4\pi}{3}\frac{ne^2}{m}\int_0^\infty\frac{1}{\nu(v)+j(\omega\pm\omega_b)}\frac{df_0(v)}{dv}v^3\,dv. \tag{2.4.28}$$

The corresponding dielectric constant tensor is then given by (1.4.76).

2.4.3 ***Effective collision frequency.*** The previous section has demonstrated that only for the special case of collision frequency independent of velocity does the conductivity take on the simple Lorentz form

$$\breve{\sigma}=\frac{ne^2}{m}\frac{1}{\nu+j\omega}. \tag{2.4.29}$$

Since most real collision processes are not of this special case, the conductivity depends upon the integral (2.4.20) involving the functions of velocity $\nu(v)$ and $f_0(T, v)$.[5] Because of the relative simplicity of the Lorentz formula, and the vast literature employing it, it is convenient to define an effective collision frequency $\nu_{eff}(T, \omega)$ which may be used directly in the Lorentz formula. This approach is easily followed in the limits of

[5] The electron temperature T may here be regarded more generally as any appropriate scaling parameter of the velocity distribution, specifying the distribution even in non-Maxwellian cases.

very low and very high frequencies, with the results summarized in Table 2.2. In both limiting cases the frequency dependence drops out.

TABLE 2.2 EFFECTIVE COLLISION FREQUENCIES FOR EXTREME WAVE FREQUENCIES

	Direct-current limit, $\omega \ll \nu$	Radio-frequency limit, $\omega \gg \nu$
Lorentz conductivity, Eq. (2.4.29)	$\frac{ne^2}{m}\frac{1}{\nu}$	$\frac{ne^2}{m}\left(\frac{\nu}{\omega^2}-j\frac{1}{\omega}\right)$
Boltzmann conductivity, Eq. (2.4.20)	$-\frac{4\pi ne^2}{3m}\int \frac{1}{\nu(v)}\frac{df(v)}{dv}v^3\,dv$	$-\frac{4\pi ne^2}{3m}\int\left[\frac{\nu(v)}{\omega^2}-j\frac{1}{\omega}\right]\frac{df(v)}{dv}v^3\,dv$
Effective collision frequency	$\frac{1}{\nu_{eff}}=-\frac{4\pi}{3}\int\frac{1}{\nu(v)}\frac{df(v)}{dv}v^3\,dv$	$\nu_{eff}=-\frac{4\pi}{3}\int\nu(v)\frac{df(v)}{dv}v^3\,dv$

In particular, we shall be interested in the effective collision frequency in the *high* frequency limit, a useful parameter which we identify by the special notation

$$\langle\nu\rangle=-\frac{4\pi}{3}\int\nu(v)\frac{df(v)}{dv}v^3\,dv$$
$$=\frac{4\pi}{3}\int\frac{d}{dv}[v^3\nu(v)]\,f(v)\,dv, \tag{2.4.30}$$

where $f=f_0$ is the unperturbed electron velocity distribution function. This is, in fact, a kind of average collision frequency, like (2.2.28), but obtained with a different weighting of the velocity distribution. For a Maxwellian distribution (2.4.24), the general form (2.4.30) reduces to

$$\langle\nu\rangle=\frac{8}{3\sqrt{\pi}}\left(\frac{m}{2kT}\right)^{5/2}\int\nu(v)\exp\left(-\frac{mv^2}{2kT}\right)v^4\,dv. \tag{2.4.31}$$

Assuming a simple power law [see (2.2.27)]

$$\nu(v)=Cv^l, \tag{2.4.32}$$

we may write (2.4.31) in terms of gamma functions (Jahnke and Emde, 1945) as

$$\langle\nu\rangle=C\left(\frac{2kT}{m}\right)^{l/2}\frac{\Gamma\left(\frac{5+l}{2}\right)}{\Gamma\left(\frac{5}{2}\right)}. \tag{2.4.33}$$

For the same assumptions, the direct average collision frequency (2.2.28) is

$$\bar{\nu}=\int\nu(v)\,f(v)\,4\pi v^2\,dv$$
$$\xrightarrow[\text{distribution}]{\text{Maxwell}} C\left(\frac{2kT}{m}\right)^{l/2}\frac{\Gamma\left(\frac{3+l}{2}\right)}{\Gamma\left(\frac{3}{2}\right)}. \tag{2.4.34}$$

Thus

$$\langle\nu\rangle=\frac{3+l}{3}\bar{\nu}, \tag{2.4.35}$$

special cases of which have been quoted in the literature (Molmud, 1959; Phelps, 1960). For each l, there will exist some characteristic velocity for which the velocity-dependent collision frequency equals one or the other of the averages (2.4.33) and (2.4.34). Figure 2.3 shows these characteristic velocities v_1 and v_2 defined such that

$$\nu(v_1)=\langle\nu\rangle \qquad \nu(v_2)=\bar{\nu}. \tag{2.4.36}$$

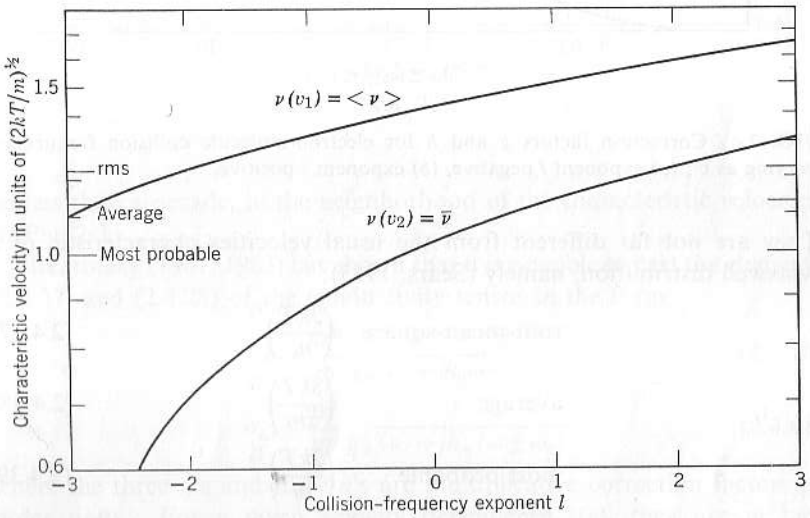

FIG. 2.3 Characteristic velocities for which $\nu(v)$ equals the high-frequency effective collision frequency $\langle\nu\rangle$ or the simple average collision frequency $\bar{\nu}$, as a function of the power-law exponent l.

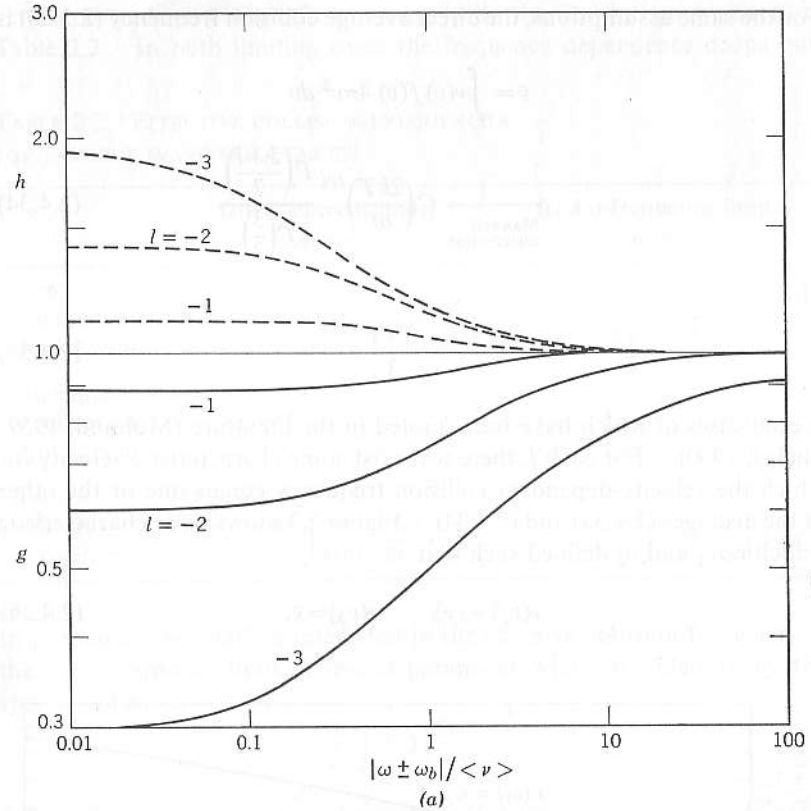

FIG. 2.4 Correction factors g and h for electron-molecule collision frequencies varying as v^l; (*a*) exponent l negative, (*b*) exponent l positive.

They are not far different from the usual velocities characteristic of a Maxwell distribution, namely (Sears, 1953):

$$\text{root-mean-square} \quad \left(\frac{3kT}{m}\right)^{1/2} \tag{2.4.37}$$

$$\text{average} \quad \left(\frac{8kT}{\pi m}\right)^{1/2} \tag{2.4.38}$$

$$\text{most probable} \quad \left(\frac{2kT}{m}\right)^{1/2} \tag{2.4.39}$$

This mathematical analysis in terms of an assumed power law (2.4.32) is physically meaningful so long as the empirical collision frequency approximates the power law over the range of velocities for which the integrands of (2.4.30) and (2.4.34) are large. For practical purposes, this range may

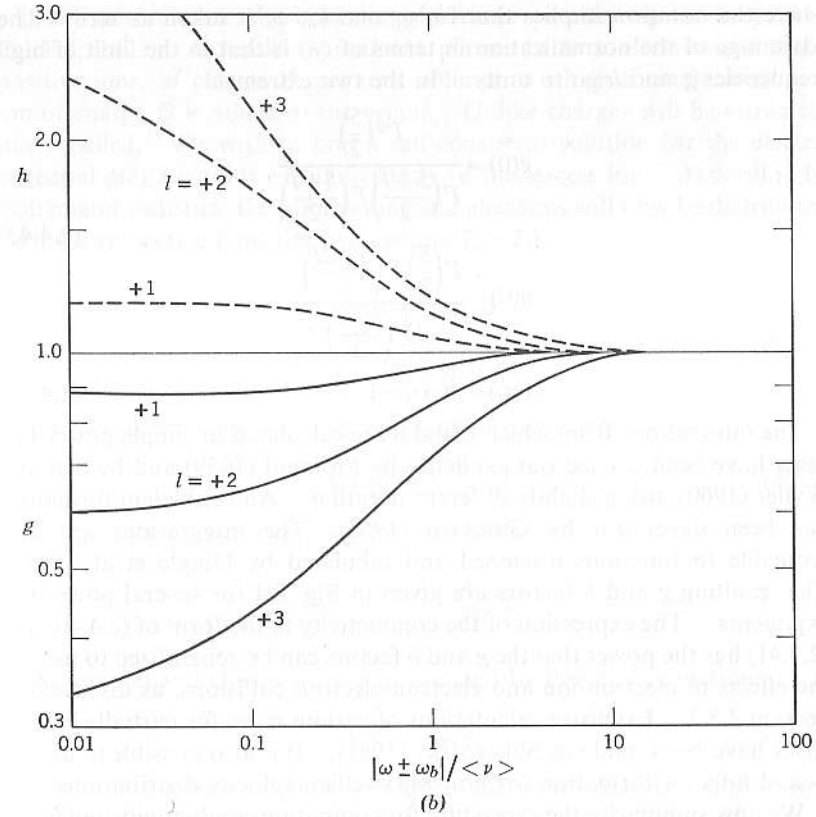

be less than a decade, in the neighborhood of the characteristic velocities of Fig. 2.3.

Shkarofsky (1961, 1963) has shown that it is possible to cast the elements (2.4.27) and (2.4.28) of the conductivity tensor in the form

$$\check{\sigma}_{\parallel} = \frac{ne^2}{m} \frac{1}{g_0\langle\nu\rangle + jh_0\omega} \tag{2.4.40}$$

$$\check{\sigma}_{l,r} = \frac{ne^2}{m} \frac{1}{g_{\pm}\langle\nu\rangle + jh_{\pm}(\omega \pm \omega_b)}, \tag{2.4.41}$$

where the three g's and three h's are multiplicative correction factors of order unity. For a given velocity dependence $\nu(v)$, they are in fact functions of a single argument:

$$\begin{aligned} g_{\pm,0} &= g(|\omega \pm \omega_b|/\langle\nu\rangle) \\ h_{\pm,0} &= h(|\omega \pm \omega_b|/\langle\nu\rangle), \end{aligned} \tag{2.4.42}$$

where the notation implies that for g_0 and h_0, ω_b is taken as zero. The advantage of the normalization in terms of $\langle\nu\rangle$ is that in the limit of high frequencies g and h go to unity. In the two extremes

$$g(0)=\frac{\Gamma^2\left(\frac{5}{2}\right)}{\Gamma\left(\frac{5+l}{2}\right)\Gamma\left(\frac{5-l}{2}\right)}$$
$$h(0)=\frac{\Gamma\left(\frac{5}{2}\right)\Gamma\left(\frac{5-2l}{2}\right)}{\Gamma^2\left(\frac{5-l}{2}\right)}, \tag{2.4.43}$$

$$g(\infty)=h(\infty)=1. \tag{2.4.44}$$

The integrations from which g and h are calculated in simple power-law cases have been carried out explicitly by Molmud (1959) and by Sen and Wyller (1960), using slightly different notation. An equivalent formalism has been developed by Gurevich (1956). The integrations are also reducible to functions discussed and tabulated by Dingle et al. (1957). The resulting g and h factors are given in Fig. 2.4 for several power-law exponents. The expression of the conductivity in the form of (2.4.40) and (2.4.41) has the power that the g and h factors can be generalized to include the effects of electron-ion and electron-electron collisions, as discussed in Section 2.5.3. Extensive calculations of various cases for partially ionized gases have been made by Shkarofsky (1961). It is also possible to use the g- and h-factor formalism for non-Maxwellian velocity distributions.

We now summarize the procedure for computing conductivity and hence propagation constants, as functions of ω, ω_b, $\nu(v)$, and $f(T, v)$. In general, one must perform the integrations (2.4.27) and (2.4.28). In practice, one can usually make use of one of the special cases given in Fig. 2.4 for simple power-law velocity dependence and a Maxwellian distribution. To do the latter, one computes $\langle\nu(T, l)\rangle$ from (2.4.33) and evaluates three g's and three h's as functions of the respective arguments $\omega/\langle\nu\rangle$, $(\omega+\omega_b)/\langle\nu\rangle$, and $|\omega-\omega_b|/\langle\nu\rangle$. For given ω and ω_b, the conductivity tensor elements may then be computed from (2.4.40) and (2.4.41), replacing the simple Lorentz elements (1.4.72) to (1.4.74). The corresponding dielectric constant tensor elements follow trivially from (1.4.76) and (1.4.80). The propagation constants may then be found from the Appleton equation (1.4.65) or (1.4.81).

2.5 Coulomb interactions

2.5.1 ***Debye shielding.*** We wish to investigate the manner in which the long-range coulomb forces in a plasma act to maintain charge neutrality,

a problem similar to the behavior of ions in an electrolyte (Debye and Huckel, 1923). Consider a uniform plasma with n electrons and n/Z positive ions, of charge Z, per unit volume to which a single *additional* ion of charge Q is added at the origin. Unlike charges will be attracted, like repelled. We wish to find a self-consistent solution for the electric potential $\psi(r)$ at radius r in the vicinity of this excess ion. According to Boltzmann statistics, the plasma ions and electrons will now be distributed with the respective densities (we assume $T_e=T_i$)

$$n_i(r)=\frac{n}{Z}\exp(-Ze\psi/kT),$$
$$n_e(r)=n\exp(e\psi/kT). \tag{2.5.1}$$

The resulting net charge density is (except at the origin)

$$\rho(r)=-ne[\exp(e\psi/kT)-\exp(-Ze\psi/kT)], \tag{2.5.2}$$

which in the high-temperature limit $Ze\psi\ll kT$ becomes

$$\rho(r)\to-\frac{(1+Z)ne^2\psi}{kT}. \tag{2.5.3}$$

The potential and charge density are related by Poisson's equation

$$\nabla^2\psi=-\rho/\epsilon_0. \tag{2.5.4}$$

Writing the Laplacian operator in spherical coordinates and substituting the approximation (2.5.3), we have

$$\frac{1}{r^2}\frac{d}{dr}\left(r^2\frac{d\psi}{dr}\right)=\frac{(1+Z)ne^2\psi}{\epsilon_0 kT}, \tag{2.5.5}$$

the appropriate solution of which is

$$\psi(r)=\frac{Q}{4\pi\epsilon_0}\frac{\exp(-r/\lambda_D)}{r} \tag{2.5.6}$$

where

$$\lambda_D=\left[\frac{\epsilon_0 kT}{(1+Z)ne^2}\right]^{1/2}. \tag{2.5.7a}$$

For many applications in plasma physics, involving dynamic processes at frequencies of the order of ω_p or higher, it is appropriate to ignore correlations in ion position, that is, to regard the positive ions as a smeared-out continuous background charge (Dawson and Oberman,

1963). This limit corresponds to setting $Z=0$ in (2.5.7a), obtaining the more common definition of the *debye shielding length*,

$$\lambda_D=\left(\frac{\epsilon_0 kT}{ne^2}\right)^{1/2}$$
$$=743\left(\frac{kT[\text{eV}]}{n[\text{cm}^{-3}]}\right)^{1/2}\text{ cm}, \qquad (2.5.7b)$$

as plotted in Fig. 2.5.

The significance of this result is that the plasma shields any local excess charge so that at a distance of a few debye lengths its effect is no longer felt. The debye length is a measure of the thickness of the sheath formed at the boundary between a plasma and a conductor. The debye length may also be thought of as the magnitude of charge separation in a plasma for which the resulting electrostatic energy density equals the particle thermal energy density (Spitzer, 1962, §2.1). Hence, significant departures from electrical neutrality are not to be expected over distances larger than λ_D. Note also that

$$\sqrt{2}\,\lambda_D=v_{mp}/\omega_p, \qquad (2.5.8)$$

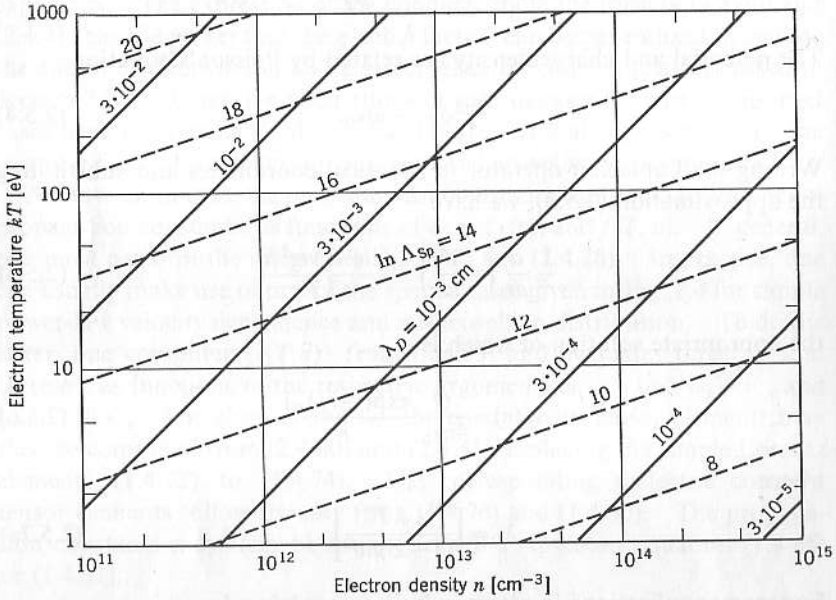

FIG. 2.5 The debye shielding length (2.5.7*b*), solid curves; and the logarithm of Spitzer's cutoff ratio (2.5.18) for $Z=1$, dashed curves. (See also Fig. 5.20.) Note corrections to ln Λ_{Sp} in Table 2.3.

where v_{mp} is the most probable electron speed (2.4.39) and ω_p is the plasma frequency. The debye length λ_D and plasma frequency ω_p represent two fundamental, interrelated scaling parameters of a plasma, measuring the distance and time scales over which the plasma establishes electrical neutrality. A necessary condition for the validity of the debye shielding picture is that the number of electrons N_D in a sphere of radius equal to the debye length be large, where

$$N_D=\frac{4\pi}{3}\lambda_D{}^3 n=\frac{1}{6\sqrt{\pi}}\left(\frac{4\pi\epsilon_0}{e^2}\right)^{3/2}\frac{(kT)^{3/2}}{n^{1/2}}$$
$$=1.7\cdot10^9\frac{(kT[\text{eV}])^{3/2}}{(n[\text{cm}^{-3}])^{1/2}}. \qquad (2.5.9)$$

2.5.2 ***Coulomb collisions.*** We now consider the coulomb interaction between electrons and ions as a collision process. The differential cross section was given in (2.2.20). It was observed that the total cross section (2.2.21), and even the momentum-transfer cross section (2.2.22), diverge for small scattering angles. We wish to estimate the relative importance of discrete close encounters as against the cumulative effect of many distant encounters in deflecting a test particle. When a light test particle impinges on a stationary massive target, the cross section for a deflection of *at least* ϕ is, from (2.2.19),

$$q_\phi=\pi\left(\frac{Ze^2}{4\pi\epsilon_0 mv^2}\right)^2\cot^2\tfrac{1}{2}\phi, \qquad (2.5.10)$$

and the corresponding collision frequency is

$$\nu_\phi=\pi nZ\left(\frac{e^2}{4\pi\epsilon_0 m}\right)^2\frac{\cot^2\frac{1}{2}\phi}{v^3}. \qquad (2.5.11)$$

In particular, the collision frequency for close collisions with $\phi\geqslant90°$ is

$$\nu_{90+}=\pi nZ\left(\frac{e^2}{4\pi\epsilon_0 m}\right)\frac{1}{v^3}, \qquad (2.5.12)$$

which is a measure of the frequency of large-angle scattering.

We now estimate the rate at which 90° deflections are produced by multiple small-angle scattering. The collision frequency for deflections between ϕ and $\phi+d\phi$ is

$$d\nu_\phi=\pi nZ\left(\frac{e^2}{4\pi\epsilon_0 m}\right)^2\frac{\cos\frac{1}{2}\phi}{v^3\sin^3\frac{1}{2}\phi}\,d\phi, \qquad (2.5.13)$$

which becomes in the limit of small deflections

$$d\nu_\phi\to8\pi nZ\left(\frac{e^2}{4\pi\epsilon_0 m}\right)^2\frac{d\phi}{v^3\phi^3}. \qquad (2.5.14)$$

In a time τ there are $\tau\, d\nu_\phi$ collisions resulting in deflections between ϕ and $\phi+d\phi$, and the expectation value of the resulting total deflection is

$$\phi^2=\phi_1{}^2+\phi_2{}^2+\ldots=\int_{\phi_{min}}^{\phi_{max}}\phi^2\,\tau\,d\nu_\phi$$

$$=\tau\,8\pi nZ\left(\frac{e^2}{4\pi\epsilon_0 m}\right)^2\frac{1}{v^3}\int_{\phi_{min}}^{\phi_{max}}\frac{d\phi}{\phi}$$

$$=\tau\,8\pi nZ\left(\frac{e^2}{4\pi\epsilon_0 m}\right)^2\frac{1}{v^3}\ln\frac{\phi_{max}}{\phi_{min}}, \tag{2.5.15}$$

where ϕ_{min} and ϕ_{max} represent the range of small deflections considered. Since the limits enter only logarithmically, they may be rather grossly approximated. Let $\phi_{max}=90°$, which does not greatly violate the small-angle approximation of (2.5.14). For ϕ_{min} we take the angle for which the impact parameter equals the debye length λ_D, since for $b>\lambda_D$ the shielding effectively masks the deflecting ion (Cohen, Spitzer, and Routly, 1950)[6]; from (2.2.19)

$$\frac{\phi_{min}}{2}=\frac{Ze^2}{12\pi\epsilon_0 kT\lambda_D}=\frac{2\sqrt{\pi}}{3}\left(\frac{e^2}{4\pi\epsilon_0 kT}\right)^{3/2}Zn^{1/2}, \tag{2.5.16}$$

in which the kinetic energy $\frac{1}{2}mv^2$ has been replaced by its mean thermal value $\frac{3}{2}kT$. The argument of the logarithmic term becomes

$$\frac{\phi_{max}}{\phi_{min}}=\frac{3\sqrt{\pi}}{8}\left(\frac{4\pi\epsilon_0 kT}{e^2}\right)^{3/2}\frac{1}{Zn^{1/2}}=\frac{\pi}{4}\Lambda_{Sp}\approx\Lambda_{Sp}, \tag{2.5.17}$$

where Λ_{Sp} is a parameter defined by Spitzer (1962, §5.2) as the ratio of the debye length to the mean impact parameter for a 90° collision $\bar{b}_{90}$. Specifically

$$\Lambda_{Sp}=\frac{\lambda_D}{\bar{b}_{90}}=\frac{2}{2\sqrt{\pi}}\left(\frac{4\pi\epsilon_0 kT}{e^2}\right)^{3/2}\frac{1}{Zn^{1/2}}=\frac{3}{\sqrt{2}}\frac{kT}{\hbar\omega_p}\left(\frac{kT}{Z^2R_y}\right)^{1/2}$$

$$=1.55\cdot10^{10}\frac{(kT[\mathrm{eV}])^{3/2}}{Z\,(n[\mathrm{cm}^{-3}])^{1/2}}. \tag{2.5.18}$$

Under common laboratory conditions $\ln\Lambda_{Sp}\sim10$ (see Fig. 2.5). Note that the number of electrons in a "debye sphere" (2.5.9) is $\frac{1}{9}Z\Lambda_{Sp}$.

The time required to achieve a cumulative deflection of 90° is, from (2.5.15),

$$\tau_{90}=\frac{\pi}{32}\left(\frac{4\pi\epsilon_0 m}{e^2}\right)^2\frac{v^3}{Zn\ln\Lambda_{Sp}}, \tag{2.5.19}$$

[6] The debye length cutoff is preferable to setting the impact parameter equal to the mean interionic spacing $n^{-1/3}$, for which case the logarithmic term is $\ln[(3\pi^4/16)^{1/3}\Lambda_{Sp}{}^{2/3}]$.

and the number of times per second a deflection by 90° is achieved is

$$\nu_{90-}=\frac{1}{\tau_{90}}=\frac{32}{\pi}\left(\frac{e^2}{4\pi\epsilon_0 m}\right)^2\frac{Zn\ln\Lambda_{Sp}}{v^3}$$

$$=\frac{32\ln\Lambda_{Sp}}{\pi^2}\nu_{90+}. \tag{2.5.20}$$

Thus, the deflection rate (collision frequency) due to cumulative small-angle deflections is, typically, of the order of thirty times larger than that due to individual large-angle deflections.

A more rigorous analysis in terms of velocity-space diffusion theory, in which velocity changes rather than angular deflections are considered, has been carried through by Chandrasekhar (1943) and by Spitzer (1962, §§5.2–5.3). In particular, Spitzer defines a "90° deflection time," the reciprocal of which is

$$\nu_D=8\pi\left(\frac{e^2}{4\pi\epsilon_0 m}\right)^2\frac{Zn\ln\Lambda_{Sp}}{v^3}$$

$$=\frac{\pi^2}{4}\nu_{90-}; \tag{2.5.21}$$

this is to be regarded as an improved version of (2.5.20). In this theory the argument of the logarithm emerges as the ratio between maximum and minimum impact parameter and the definition $\Lambda_{Sp}=\lambda_D/\bar{b}_{90}$ given by (2.5.18) follows logically. However, these particular limits must be modified under a variety of circumstances, discussed in Section 2.5.4. In the following section we use the general symbol Λ to denote the appropriate ratio.

In summary, we can divide electron-ion coulomb collisions into three classes (Bernstein and Trehan, 1960).

(*1*) *Impact parameter* $b<$ *impact parameter for* 90° *deflection* $\bar{b}_{90}$. In this case of close encounters, the electron-ion interaction may validly be considered as a discrete two-particle collision and treated by the usual collision integrals of kinetic theory (Allis, 1956; Desloge and Matthysse, 1960).

(*2*) $\bar{b}_{90}<b<$ *Debye length* λ_D. This case is characterized by many-body encounters involving a succession of uncorrelated small-angle deflections, and is best handled by a diffusion equation of the Fokker-Planck type (Chandrasekhar, 1943; Cohen et al., 1950; Allis, 1956; Bernstein and Trehan, 1960; and Desloge, 1963). As we have seen, in situations of interest ($\Lambda_{Sp}\gg1$) this case *2* is strongly dominant over case *1*. Case *1* may be included by a small change in integration limits.

(3) $b > \lambda_D$. The effect of the debye shielding is to eliminate statistical (uncorrelated) particle encounters. Particle motions on this scale represent correlated processes such as the propagation of waves.

2.5.3 ***Effective coulomb collision frequencies.*** It remains to be found how to incorporate into the conductivity formalism (2.4.40) and (2.4.41) the effects of electron-ion and electron-electron collisions. From the Fokker-Planck equation, or directly from the Boltzmann equation, it can be shown that an electron-ion collision frequency[7]

$$\nu_{ei}(v) = \tfrac{1}{2}\nu_D = 4\pi\left(\frac{e^2}{4\pi\epsilon_0 m}\right)^2 \frac{Zn \ln\Lambda}{v^3}$$

$$= 8.0 \cdot 10^{15} \frac{Zn[\mathrm{cm}^{-3}] \ln\Lambda}{(v[\mathrm{cm/sec}])^3} \ \mathrm{sec}^{-1} \qquad (2.5.22)$$

plays exactly the same role in the calculation of conductivity as the more straightforward electron-molecule momentum-transfer collision frequency

[7] ν_D, defined in (2.5.21), is the reciprocal of Spitzer's "90° deflection time."

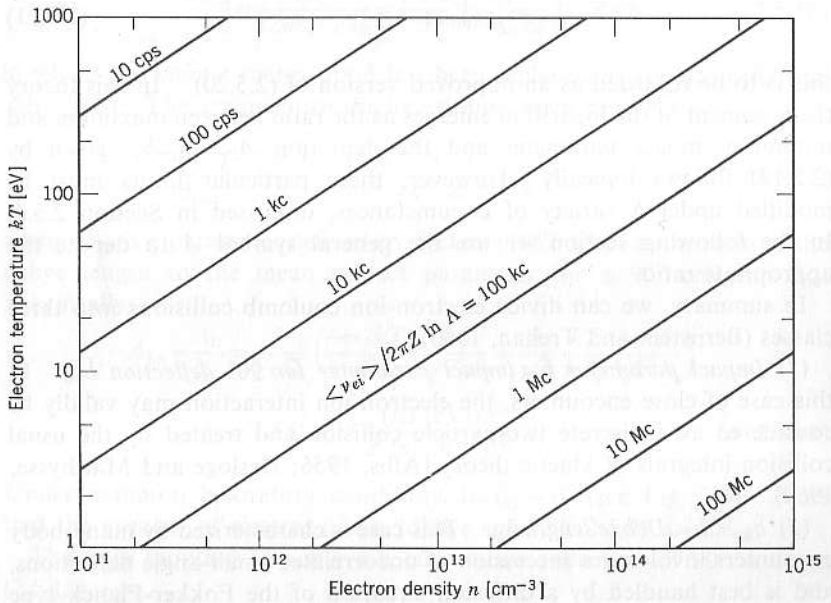

FIG. 2.6 The effective electron-ion collision frequency (2.5.23). The numbers shown are $\langle\nu_{ei}\rangle/2\pi Z \ln\Lambda$. The appropriate value of $\ln\Lambda$ must be found from (2.5.30) and Figs. 2.8 and 2.9. The 2π normalization facilitates comparison with the wave cyclic-frequency $\omega/2\pi$ in propagation formulas. See also Fig. 2.10.

$\nu_{em}(v)$ (2.2.13) (Ginsburg, 1944; Cohen et al., 1950; Allis, 1956; and Shkarofsky, 1961). Thus, from (2.4.33) for $l = -3$ the effective electron-ion collision frequency at high frequencies is for a Maxwellian velocity distribution (see Fig. 2.6)[8]

$$\langle\nu_{ei}\rangle = \frac{4(2\pi)^{1/2}}{3}\left(\frac{e^2}{4\pi\epsilon_0}\right)^2 \frac{Zn \ln\Lambda}{m^{1/2}(kT)^{3/2}}$$

$$= 2.90 \cdot 10^{-6} \frac{Zn[\mathrm{cm}^{-3}] \ln\Lambda}{(kT[\mathrm{eV}])^{3/2}} \ \mathrm{sec}^{-1}. \qquad (2.5.23)$$

In performing this integration, we have followed common practice by ignoring the velocity variation implicit in Λ.[9] The proper evaluation of $\ln\Lambda$ is discussed in the next section. In the common case of a partially ionized gas we have from (2.2.23)

$$\nu_{total}(v) = \nu_{em}(v) + \nu_{ei}(v), \qquad (2.5.24)$$

$$\langle\nu_{total}\rangle = \langle\nu_{em}\rangle + \langle\nu_{ei}\rangle, \qquad (2.5.25)$$

the latter form following because of the linearity of the operation defined by (2.4.30). The critical degree of ionization above which coulomb collisions are dominant is given by $\langle\nu_{ei}\rangle = \langle\nu_{em}\rangle$, which of course depends on the velocity dependence of the particular electron-molecule interaction and is usually a strong function of temperature. At room temperature the critical ionization for common gases in low-pressure discharges may be as small as $\sim 10^{-7}$; at $kT = 1$ eV, $\sim 10^{-4}$ (Lin et al., 1955; Anderson and Goldstein, 1955).

Using (2.5.23) and (2.4.43) in the d-c limit of the conductivity (2.4.40), we obtain $g(0) = 3\pi/32$ and

$$\sigma_{dc} = \frac{ne^2}{m}\frac{1}{g(0)\langle\nu_{ei}\rangle}$$

$$= \frac{4\sqrt{2}}{\pi^{3/2}}\frac{(4\pi\epsilon_0)^2}{m^{1/2}e^2}\frac{(kT)^{3/2}}{Z \ln\Lambda}$$

$$= 3.3 \cdot 10^2 \frac{(kT[\mathrm{eV}])^{3/2}}{Z \ln\Lambda} \ \mathrm{mho/cm}, \qquad (2.5.26)$$

[8] For $l = -3$, it may be seen from (2.4.30) that in the general case of $f(v)$ not necessarily Maxwellian

$$\langle\nu_{ei}\rangle = (4\pi/3)Cf(0)$$

where $f(0)$ is the value of the electron velocity distribution function for $v = 0$. Thus, the high-frequency effective collision frequency is insensitive to departures from the Maxwellian distribution affecting only the high energy end.

[9] If the velocity dependence of Λ_{Sp}, $\Lambda(v) = \lambda_D(T)/b_{90}(v) \propto v^2$, is retained in the integration, we obtain (2.5.23) with the logarithmic term replaced by $\ln[(2/3\gamma)\Lambda_{Sp}] \approx \ln(0.37\Lambda_{Sp})$, where $\gamma = 1.78$ is Euler's constant and where $\Lambda_{Sp} = \lambda_D/\bar{b}_{90}$ is Spitzer's average defined by (2.5.18). Other refinements are discussed in Section 2.5.4.

which is precisely the result obtained by Spitzer (Cohen et al., 1950; Spitzer, 1962, §5.4; and Maecker et al., 1955). The density dependence cancels out except in $\ln\Lambda$.

Our discussion of coulomb collisions has thus far assumed a completely ionized plasma with infinitely massive, stationary (cold) positive ions. The electrons have been assumed to interact with each other only in a long-range, collective sense. We now consider the randomizing effect of electron-electron collisions, which effect is quite different from that of collisions between electrons and other species. It is clear, on physical grounds, that like-particle collisions cannot extract momentum or energy from this component of the plasma. They do, however, cause a diffusion in velocity space, which modifies the perturbation part of the velocity distribution function. From a mathematical point of view, since the electron distribution function also enters for the scatterer, the Boltzmann equation is inherently nonlinear. The effect depends on the ionic charge Z since the relative density of ions to electrons varies as $1/Z$ and the cross section as Z^2. Neglecting electron-electron collisions is equivalent to the limit of large Z. Numerical calculations of special cases have been undertaken by a number of authors (Spitzer and Härm, 1953; Hwa, 1958; and Kelly, 1960). Shkarofsky (1961) has shown that it is possible in principle to retain the formalism (2.4.40) and (2.4.41) involving the g and h correction factors (2.4.42). Extensive calculations, based on an expansion of the collision term in generalized Laguerre polynomials, have been tabulated. The g and h factors become functions not only of $|\omega \pm \omega_b|/\langle\nu\rangle$ but also of ionic charge Z and the degree of ionization of the gas. Figure 2.7 shows the correction factors for a fully ionized gas with and without electron-electron collisions, that is, for $Z=1$ and ∞, respectively. In the case of no magnetic field ($\omega_b=0$), Spitzer and Härm (1953) and Kelly (1960) have used a numerical factor γ_E to express the ratio of the conductivity including electron-electron collisions to that for a Lorentz gas

$$\gamma_E(\omega/\langle\nu\rangle, Z)=\frac{\sigma(\omega/\langle\nu\rangle, Z)}{\sigma(\omega/\langle\nu\rangle, \infty)}. \tag{2.5.27}$$

At extreme frequencies

$$\begin{aligned}\gamma_E(0, 1)&=0.582,\\ \gamma_E(\infty, Z)&=1.\end{aligned} \tag{2.5.28}$$

The ratio remains of order unity at intermediate frequencies. As shown by Hwa (1958) and Kelly (1960), the major physical effect of electron-electron collisions on wave propagation is to broaden and damp the cyclotron resonance somewhat. Electron-electron collision effects may safely be neglected at high frequencies such that $|\omega \pm \omega_b|/\langle\nu\rangle \gg 1$.

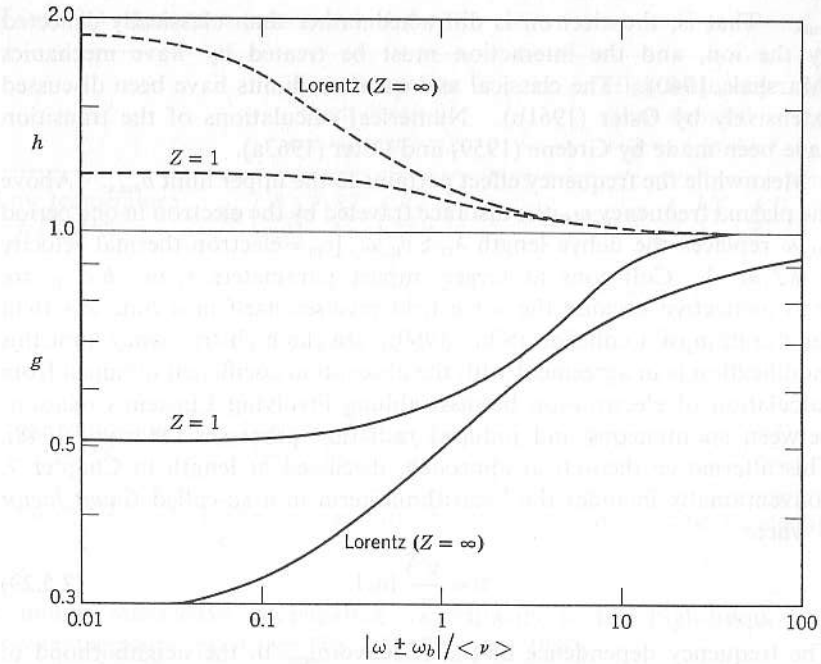

FIG. 2.7 Effect of electron-electron collisions on the correction factors g and h for a fully ionized gas with no magnetic field. The Lorentz gas calculation ignores electron-electron collisions; they are included in the curves for singly charged ions.

2.5.4 ***The logarithmic term.*** Most formulations of the electron-ion interaction process involve an integration over the impact parameter b that yields a result proportional to $\ln(b_{max}/b_{min})$. The ratio $\Lambda=b_{max}/b_{min}$ and its logarithm are divergent unless we invoke physical arguments to cut off the range of integration (Theimer, 1963). The arguments sketched in Section 2.5.2 led to the identification of b_{max} with the debye length λ_D (because of shielding) and of b_{min} with the mean impact parameter for a 90° deflection $\bar{b}_{90}$ (because of the relative ineffectiveness of close encounters). The argument of the logarithmic term then becomes Spitzer's $\Lambda_{Sp}=\lambda_D/\bar{b}_{90}$, as given by (2.5.18). Aside from numerical refinements to Λ_{Sp} of order unity, there are two general effects which alter the form of Λ, one depending on electron temperature and one on wave frequency (De Witt, 1958). We discuss these in turn.

The temperature effect pertains to the lower limit b_{min}. At electron temperatures above about 80 eV the deBroglie wavelength $\hbar/mv$ exceeds the 90° impact parameter $b_{90}=Ze^2/4\pi\epsilon_0 mv^2$ and replaces it as the limit

b_{min}. That is, the electron is diffracted rather than classically deflected by the ion, and the interaction must be treated by wave mechanics (Marshak, 1940). The classical and quantum limits have been discussed extensively by Oster (1961b). Numerical calculations of the transition have been made by Greene (1959) and Oster (1963a).

Meanwhile the frequency effect pertains to the upper limit b_{max}. Above the plasma frequency ω_p, the distance traveled by the electron in one period v_{th}/ω replaces the debye length $\lambda_D \approx v_{th}/\omega_p$ [v_{th} = electron thermal velocity $\sim(kT/m)^{1/2}$]. Collisions at larger impact parameters $v_{th}/\omega < b < \lambda_D$ are then ineffective because the wave field reverses itself in a time less than the duration of a collision (Silin, 1960). In the high-frequency limit this modification is in agreement with the absorption coefficient obtained from calculation of electron-ion bremsstrahlung involving Einstein's relations between spontaneous and induced radiation processes (Martyn, 1948). This alternative theoretical approach, discussed at length in Chapter 7, conventionally includes the logarithmic term in a so-called *Gaunt factor* $\mathcal{G}$ where

$$\mathcal{G} = \frac{\sqrt{3}}{\pi} \ln\Lambda. \tag{2.5.29}$$

The frequency dependence of the effective b_{max} in the neighborhood of $\omega \sim \omega_p$ has been examined by Dawson and Oberman (1962, 1963). The situation is complicated by the reactive properties of the plasma and the possibility of excitation of longitudinal plasma waves near $\omega = \omega_p$.

Thus far, we have not carefully distinguished between the ratio $\Lambda(v)$ appropriate for electrons of one particular velocity and the corresponding ratio $\Lambda(T)$ properly averaged for the thermal velocity distribution. Because of the logarithm, the velocity dependence of $\ln\Lambda(v)$ is weak, and a good approximation to $\ln\Lambda(T)$ is obtained simply by the substitution for v of a thermal velocity of order $(kT/m)^{1/2}$. The significance of more careful analysis is clouded by the fact that the physically invoked cutoffs (for example, $b_{max} \approx \lambda_D$) are uncertain within a numerical factor of order unity. However, in certain cases, it is possible to choose a limiting procedure that does not explicitly require an ad hoc cutoff (Oster, 1961b; Kihara and Aono, 1963).

Table 2.3 summarizes the asymptotic values of $\ln\Lambda(T)$ for the various limiting cases, to be used in the effective electron-ion collision frequency (2.5.23) assuming a Maxwellian distribution. The numerical coefficients shown are the results of refined calculations, but some may still be in error by small factors (Oster, 1961b; Dawson and Oberman, 1962). The low-frequency, low-temperature result is seen to differ from Spitzer's approximation by a factor of about one fourth. The most important limit for

TABLE 2.3 LIMITING FORMS OF $\ln\Lambda$ *

	Low frequency (high density) $\omega \ll \omega_p$ $(n \gg n_c)$	High frequency (low density) $\omega \gg \omega_p$ $(n \ll n_c)$
Low temperature $kT \ll Z^2 R_y$	$\ln\left(\frac{8}{e\gamma^4}\right)^{1/2} \frac{kT}{\hbar\omega_p}\left(\frac{kT}{Z^2R_y}\right)^{1/2}$ $= \ln\frac{1}{3e^{1/2}}\left(\frac{2}{\gamma}\right)^2 \Lambda_{Sp}$ $= \ln(0.25)\Lambda_{Sp}$	$\ln\Lambda_0 = \ln\frac{4}{\gamma^{5/2}}\frac{kT}{\hbar\omega}\left(\frac{kT}{Z^2R_y}\right)^{1/2}$ $= \ln\frac{1}{3}\left(\frac{2}{\gamma}\right)^{5/2}\frac{\omega_p}{\omega}\Lambda_{Sp}$ $= \ln(0.45)\frac{\omega_p}{\omega}\Lambda_{Sp}$
High temperature $kT \gg Z^2 R_y$	$\ln\left(\frac{8}{e\gamma}\right)^{1/2}\frac{kT}{\hbar\omega_p} = \ln(1.29)\frac{kT}{\hbar\omega_p}$	$\ln\frac{4}{\gamma}\frac{kT}{\hbar\omega} = \ln(2.24)\frac{kT}{\hbar\omega}$

* $e = 2.718$; $\gamma = 1.781$ (Euler's constant); $R_y = 13.6$ eV (Rydberg energy constant); $\Lambda_{Sp} = \lambda_D/b_{90}$, see (2.5.18).

common microwave propagation experiments is the high-frequency, low-temperature result (see Fig. 2.8) (Scheuer, 1960)

$$\Lambda_0 = \frac{1}{3}\left(\frac{2}{\gamma}\right)^{5/2}\frac{\omega_p}{\omega}\Lambda_{Sp} = \frac{4}{\gamma^{5/2}}\frac{kT}{\hbar\omega}\left(\frac{kT}{Z^2R_y}\right)^{1/2}$$
$$= 6.2\cdot 10^4 \frac{(kT[\mathrm{eV}])^{3/2}}{Z\,\omega/2\pi[\mathrm{Gc}]} \tag{2.5.30}$$

where $\gamma = 1.781$ is Euler's constant and $R_y = 13.6$ eV is the Rydberg energy constant. Figure 2.9 shows the corrections to be applied to (2.5.30) in the transition regions between the limiting cases of Table 2.3. The temperature dependence is taken from Greene's (1959) revised calculations. The frequency–electron-density dependence is taken from Dawson and Oberman (1962). The "bump" in the neighborhood of $\omega = \omega_p$ is due to the generation of plasma oscillations. These two corrections are independent in the Rayleigh-Jeans approximation ($\hbar\omega \ll kT$) (Oster, 1963a). The resulting collision frequency and attenuation coefficient, in the unshielded limit $\omega \gg \omega_p$, are shown in Fig. 2.10.

To summarize the effect of coulomb collisions on microwave propagation in a plasma without magnetic field, we recall that the formalism of (2.4.40) is used with the effective coulomb collision frequency (2.5.23). The g and h correction factors are given to good approximation by the $l = -3$ case of Figs. 2.4 and 2.5. The $\ln\Lambda$ term appearing in (2.5.23) is evaluated using the Λ_0 of (2.5.30) and Fig. 2.8 modified if necessary by

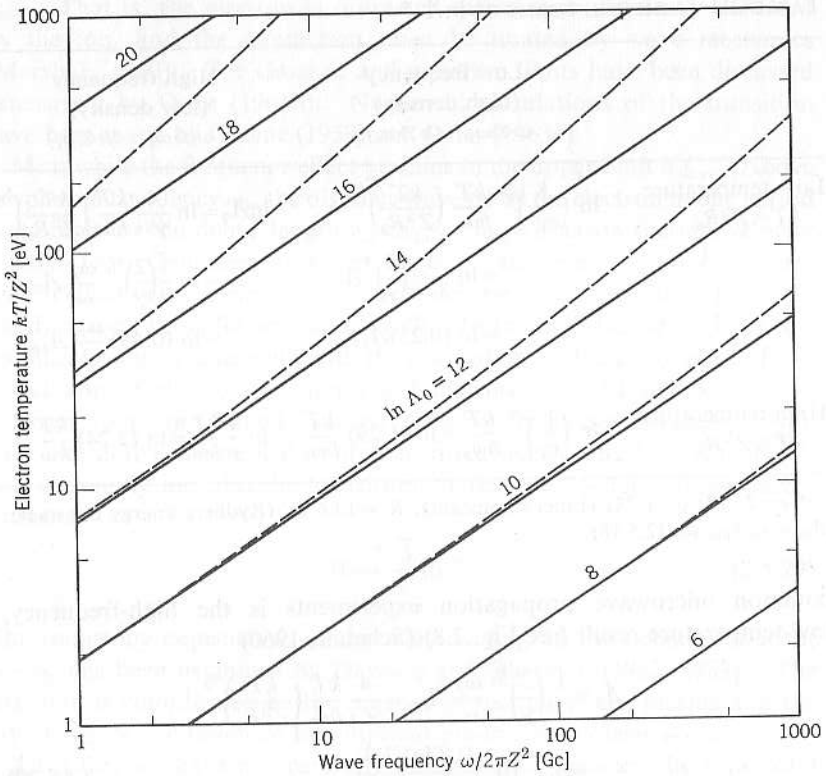

FIG. 2.8 The logarithm $\ln \Lambda_0$ of the high-frequency, low-temperature cutoff ratio (2.5.30), for ions of charge Z. The temperature correction of Fig. 2.9 is shown here by the dashed curves; the density correction must still be obtained from Fig. 2.9.

the two independent corrections given in Fig. 2.9. For most practical purposes one may use for Λ the asymptotic limits of Table 2.3 throughout the range of parameters, changing from one limit to the other at the points where the asymptotic forms are equal, namely,

$$kT = \gamma^3 Z^2 R_y = (77 \text{ eV}) Z^2 = (890{,}000^\circ \text{ K}) Z^2 \tag{2.5.31}$$

$$\frac{\omega_p^2}{\omega^2} = \frac{n}{n_c} = \frac{\gamma}{2e} = 0.328 \approx \frac{1}{3}. \tag{2.5.32}$$

Finally, we note that further modifications of Λ are required in strong magnetic fields for which the gyroradius is smaller than the debye length, that is, when $\omega_b \gtrsim \omega_p$ (Sweet, 1959). The situation is complicated not only by excitation of longitudinal plasma waves but also by the fact that the cutoff conditions are no longer isotropic in a magnetic field, so that

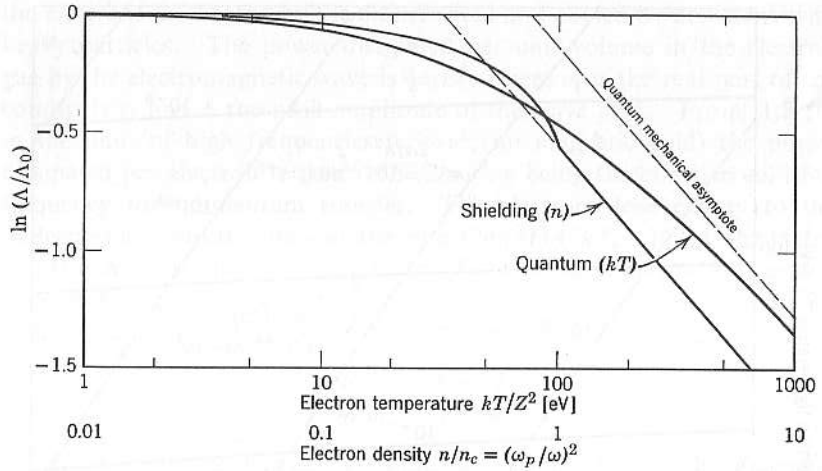

FIG. 2.9 Quantum and shielding correction terms to be applied to the low-temperature, high-frequency $\ln \Lambda_0$ of (2.5.30). The value of each correction subtracts from $\ln \Lambda_0$, which may be read from the solid lines of Fig. 2.8. The two corrections are independent. From Greene (1959, revised) and Dawson and Oberman (1962).

different forms of Λ enter the collision frequency terms of the various elements of the dielectric constant tensor (Silin, 1962; Eleonskii et al., 1962; and Oberman and Shure, 1963). However, for most practical purposes the field-free values may be used.

2.6 Nonlinear effects

A number of nonlinear processes occur in plasmas, leading, for example, to harmonic generation and interaction between two waves (Ginzburg and Gurevich, 1960). The best known, the so-called Luxembourg effect, arises from a change in the effective collision frequency as a result of electron heating by the electromagnetic wave. Thus, it vanishes for the special case of collision frequency independent of velocity. Other types of nonlinearities arise directly from the electron dynamics and the non-transverse electric fields in a nonuniform plasma or a plasma in a magnetic field. Further discussion of nonlinearities can be found in Chapter 6.

2.6.1 ***Criterion for linearity.*** A rough criterion for the validity of the linearized theory, already noted in Section 2.4, is that the velocity increment due to the electric field be small compared to the random thermal velocities; that is,

$$\frac{e^2 E^2}{m^2 \omega^2} \ll \frac{kT}{m}. \tag{2.6.1}$$

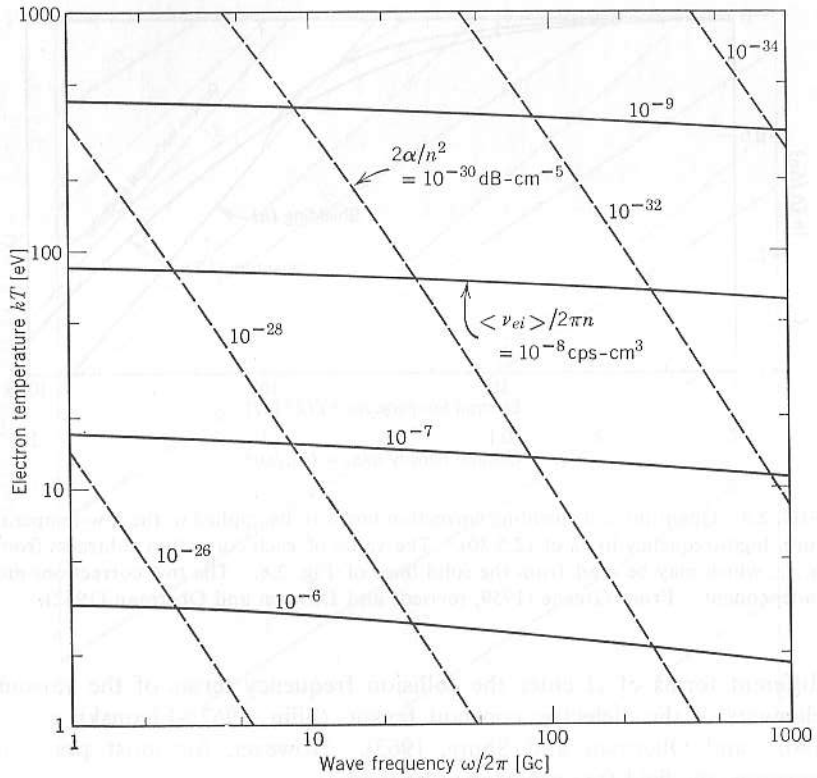

FIG. 2.10 *Solid curves.* Effective electron-ion collision frequency for a hydrogenic plasma ($Z=1$), as a function of frequency and temperature, assuming no shielding ($\omega \gg \omega_p$) but including the temperature correction of Fig. 2.9. The numbers given on the contours are to be multiplied by the electron density n in cm^{-3} to obtain the cyclic (not radian) frequency $\nu/2\pi$ in cps. Compare Fig. 2.6. *Dashed curves.* The corresponding power attenuation coefficient $2\alpha = 2\chi\omega/c$ in the high-frequency limit of (1.3.30). The numbers given are to be multiplied by $(n[\text{cm}^{-3}])^2$ to obtain 2α in decibels/cm. Attenuations derivable from this graph are in general very small because of the restriction on electron density implied by the condition $\omega_p \ll \omega$. For plasmas with ionic charge Z use the scaling relations:

$$[\nu(\omega, kT)]_Z = Z^{-2}[\nu(\omega/Z^2, kT/Z^2)]_{Z=1}$$
$$[\alpha(\omega, kT)]_Z = Z^{-6}[\alpha(\omega/Z^2, kT/Z^2)]_{Z=1}$$

This criterion permits the discard of the nonlinear term in the Boltzmann equation expansion (2.4.18), but is not sufficiently restrictive to prevent significant heating of the electron gas. In each collision with heavy particles an electron's coherent motion is randomized. The heating effect, although small, is thus cumulative. From a calorimetric viewpoint

the electrons are heated by the electric field and cooled by collisions with heavy particles. The power dissipated per unit volume in the electron gas by the electromagnetic wave is $\frac{1}{2}\sigma_r E^2$, where σ_r is the real part of the conductivity and E the peak amplitude of the wave field. From (1.3.14) in the limit of high frequencies ($\omega^2 \gg \nu^2$; no magnetic field) the power dissipated per electron is then $\nu e^2 E^2/2m\omega^2$, ν being the effective collision frequency for momentum transfer. The electrons lose energy to the molecules and positive ions at the rate $(2m/M)\nu(\frac{3}{2}kT_e - \frac{3}{2}kT_0)$, the factor $2m/M$ coming from (2.2.9) and T_e and T_0 being the electron and heavy-particle temperatures. In the steady state, these two terms are equal. Thus, if the wave is to produce negligible heating

$$\frac{e^2E^2}{m^2\omega^2} \ll \frac{6m}{M}\frac{kT}{m}, \tag{2.6.2}$$

which is more severe than (2.6.1) by the mass ratio m/M. With a magnetic field, σ_r is resonant at the cyclotron frequency for some modes and (2.6.2) must be modified accordingly. The condition (2.6.2) may be put in a crude but handy form for propagation experiments in the laboratory by noting that the intensity of a wave is $E^2/2\eta$, where $\eta \approx 377$ ohms is the wave impedance of the plasma medium, and by furthermore assuming arbitrarily that an area of dimension one wavelength is illuminated (Section 4.6.2). Then the total power radiated is of order $P \sim E^2\lambda^2/2\eta$, and the criterion for negligible heating is

$$P \ll \frac{12\pi^2 m^2 c^2 kT}{Me^2\eta} \approx 90\frac{kT[\text{eV}]}{A}\ \text{watts}, \tag{2.6.3}$$

A being the atomic number of the molecules or ions involved. Note especially that this criterion fails near both the plasma and cyclotron frequencies, where the nonlinearity is enhanced.

2.6.2 ***Breakdown.*** The production of a gas-discharge plasma by high-frequency breakdown is well known. This topic has been discussed at length by many authors, including Brown (1956) and Francis (1960, Chapter 4). Since our principal concern is the use of microwaves for diagnostic purposes, we omit further discussion.

2.6.3 ***Luxembourg effect.*** The Luxembourg effect is the process whereby an amplitude-modulated high-power wave (the "disturbing" wave) causes a corresponding modulation of the collision frequency and hence the attenuation coefficient of the plasma medium. Thus, this modulation is transferred to a second, low-power wave (the "wanted" wave) as it passes

through the disturbed region. The effect was first encountered in connection with radio-broadcast waves in the ionosphere (Bailey and Martyn, 1934). It is necessary not only that the electron–heavy particle collision frequency be velocity dependent (as it is for most real gases) but also that the modulation be slow enough that the electron temperature can follow it. Extending the calorimetric argument of Section 2.6.1, we see that the temperature variation is given by the differential equation

$$\frac{d(kT_e)}{dt}=\frac{e^2}{3m\omega^2}\nu(T_e)E^2(t)-\frac{2m}{M}\nu(T_e)(kT_e-kT_0), \qquad (2.6.4)$$

$E(t)$ being the modulated amplitude of the disturbing high-frequency field. If the functional dependence of ν (the effective collision frequency for momentum transfer, Section 2.4.3) on T_e is specified, (2.6.4) may be integrated to give the time variation of ν and hence of the amplitude attenuation coefficient α (Anderson and Goldstein, 1955). If the "disturbing" wave is suddenly turned on or off, ν and α relax to their equilibrium values with the time constant $[(2m/M)\nu]^{-1}$ (Spitzer, 1940). Or, if the disturbing wave is sinusoidally modulated such that the attenuation varies over the range $\alpha \pm \Delta\alpha$, a wanted wave passing through a disturbed region of length d emerges with an amplitude-modulation index $\frac{1}{2}\Delta\alpha\, d$.

When the plasma is in a magnetic field, the real conductivity is resonant at the cyclotron frequency for certain modes. The evaluation used for σ_r in (2.6.1) is no longer correct, and significant heating is caused by a nearly resonant disturbing wave at power levels well below the criterion of (2.6.2) and (2.6.3). Experimental techniques exploiting the Luxembourg effect have been used extensively to measure the velocity dependence of collision frequencies (Rao et al., 1961). It might also be noted that modifications of plasma properties by means other than a disturbing electromagnetic wave (for instance, electron-stream-driven longitudinal plasma oscillations) can modulate a wanted probing wave (Rosen, 1960; Baranger and Mozer, 1961). This aspect is discussed further in Section 2.6.5 and Sections 6.6 and 6.7.

2.6.4 ***Other nonlinearities.*** The presence of an electromagnetic wave changes the electron velocity distribution function $f(\mathbf{v})$ which, in turn, may alter the propagation characteristics. These matters may be investigated in detail by kinetic theory methods (Epstein, 1960, 1962; Chen, 1962; and Sodha and Palumbo, 1963). We have already discussed the change of collision frequency due to electron heating, the Luxembourg effect. However, in addition, the $\mathbf{a}\cdot\nabla_v f(\mathbf{v})$ term of the Boltzmann equation (2.4.4) is inherently nonlinear in time, a feature discarded in the expansion (2.4.18). Consequently, if the criterion (2.6.1) is violated, a single wave propagating in such a medium generates harmonics (Rosen, 1961).

We have assumed throughout that the oscillating electric field, and consequently the electron velocity distribution function, are uniform in space. This assumption is invalid when a-c spacecharge is associated with the wave, as is generally the case for the nontransverse-electric waves in plasmas in magnetic fields and for inhomogeneous plasmas (Sections 1.4.5 and 4.4). The assumption also obviously ignores the wave nature of the electric field, a matter of importance even in the linear theory, and discussed at length in Chapter 3. When $\mathbf{E}$ and $f(\mathbf{v})$ are space dependent, for one or more reasons, additional terms in the Boltzmann equation are nonlinear (Ginzburg, 1959; Wetzel, 1961; Whitmer and Barrett, 1961, 1962; and Baird and Coleman, 1961). The density modulation, for example, may cause phase modulation of a probing wave, analogous to the Luxembourg amplitude modulation. Finally, we note that the $\mathbf{v}\times\mathbf{B}$ force arising from the wave (a-c) magnetic field is inherently nonlinear, but may usually be neglected for nonrelativistic plasmas.

2.6.5 ***Incoherent scattering.*** In conclusion, we discuss briefly the process of *incoherent scattering*, which arises from thermal fluctuations rather than nonlinearities in the usual sense. Under the influence of an electromagnetic wave, a free electron oscillates and reradiates, a process known as Thomson scattering, the classical analog of the Compton effect (Heitler, 1954, §§5, 22, and 33). This reradiation from an assembly of initially stationary electrons is coherent and produces the change in phase velocity described macroscopically by the refractive index (Ratcliffe, 1959, Chapter 3). At a finite temperature, however, thermal fluctuations in the electron density give rise also to an incoherent scattering of the incident wave. The total power radiated into unit solid angle per unit volume of the scattering medium is

$$j=\tfrac{1}{2}r_0^2 nI\sin^2\Theta \qquad (2.6.5)$$

where $r_0=e^2/4\pi\epsilon_0 mc^2=2.8\cdot10^{-15}$ meter is the classical electron radius, n the average density of scattering electrons, I the intensity (watts/m^2) of the incident wave, and Θ the angle between wave polarization and direction of observation (Fejer, 1960). There is no frequency or temperature dependence of the total power so long as the incident wavelength is large compared to the debye length. The corresponding amplitude attenuation coefficient of the primary wave, $\alpha=\frac{2}{3}\pi r_0^2 n$, is negligible for most laboratory plasmas (Sampson, 1959).

The frequency spectrum of the scattered radiation is temperature dependent, and may be obtained from detailed calculations, which are especially complicated by a magnetic field (Renau et al., 1961; Farley et al., 1961). Harmonics of the incident frequency are generated (Vachaspati, 1962). Experimental measurements of backscatter from the ionosphere

have been used to determine electron density and temperature as a function of altitude (Bowles, 1961; Bowles et al., 1962).

Modifications in the scattered intensity occur when the plasma is in a nonequilibrium state. For instance, the electron and ion temperatures may differ (Salpeter, 1963) or electron-stream-driven plasma oscillations may be present (Drummond, 1962). A laboratory experiment has been performed by Kino and Allen (1961). The presence of nonthermal fluctuations in the plasma also influences the low-frequency conductivity (Yoshikawa, 1962). A more complete discussion is given in Section 6.7.

CHAPTER 3

Waves in warm plasma

3.1 Introduction

The preceding chapters have assumed a cold plasma in which electron thermal motion could be neglected.[1] Specifically, the wave nature of the electromagnetic field has been ignored; that is, the phase velocity and wavelength of the wave have been assumed infinite. We shall use the term "warm" to designate the case in which the temperature is considered explicitly but for which nonrelativistic mechanics is still appropriate. The term "hot" will be reserved for the relativistic case. Several new phenomena, described below, appear when the plasma is assumed warm.

(*1*) Spatial variations (gradients) in density and temperature over the wavelength drive particle currents, which are in addition to those driven directly by the electric field. This effect, in addition to modifying the propagation of electromagnetic waves, provides a new class of waves variously known as *plasma*, *electrostatic*, *spacecharge*, or *electroacoustical* waves. In suitable limits these waves are longitudinal, analogous to sound waves in un-ionized gases. In this class are the modes commonly referred to as "plasma oscillations" (Bohm and Gross, 1949). In the presence of a magnetic field or density gradients, spacecharge waves may couple to electromagnetic waves, as discussed in Chapter 5.

[1] Even in a cold plasma, however, the electron velocity must be greater than the velocity increments produced by the electromagnetic field (Section 2.3) if the presence of the wave is not to distort the distribution function significantly. In recognition of this lower bound on velocity, the term "temperate plasma" has been used (Allis, Buchsbaum, and Bers, 1963). In a sense, however, this is more an upper bound on the electric field than a lower bound on thermal velocity.

(*2*) A group of electrons having thermal speeds close to the wave phase velocity can exchange energy with the wave by the processes of Landau damping and Cerenkov radiation, processes which on a macroscopic scale take place in the linear accelerator and traveling-wave tube. For electromagnetic waves, a slow phase velocity (high index of refraction) is found only when a static magnetic field is present. The electroacoustic waves may be slow even without the field.

(*3*) The presence of a static magnetic field introduces a new scale of length, the gyroradius, which may be comparable to the wavelength. Under this condition the relation between current and electric field (that is, the conductivity) is in general no longer a function of a point in the plasma, but depends upon the spatial variation of the field and the past history of the particles reaching that point (Drummond, 1958; Drummond et al., 1961).

This chapter summarizes the results of theoretical analyses which take these effects into account.

3.2 Magnetic permeability of a plasma

To calculate propagation constants in a cold plasma, we have considered all particle motions explicitly. Thus the plasma represents a continuous medium having the dielectric constant and magnetic permeability of free space and the complex tensor conductivity $\check{\sigma}$ defined by $\mathbf{J}=\check{\sigma}\cdot\mathbf{E}$. Alternatively, it is possible, for a particular frequency ω, to regard the plasma as a dielectric medium having zero explicit conductivity, the permeability of free space, and the complex dielectric constant

$$\check{\kappa}=\mathbf{1}+\frac{\check{\sigma}}{j\omega\epsilon_0}. \tag{3.2.1}$$

With the introduction of finite electron temperature in the presence of a static magnetic field, we recognize that the gyrating particles possess magnetic moments and exhibit diamagnetism (Åström, 1958; Neufeld, 1963). An intuitive approach to including the effects of finite temperature would be to compute an appropriate magnetic permeability, which could then be used in addition to the cold-plasma dielectric constant in the dispersion relation obtained from Maxwell's equations.

The magnetic moment of an electron orbiting in a magnetic field is

$$p=IA=-\left(\frac{e\omega_b}{2\pi}\right)(\pi r_b{}^2)=-\frac{\frac{1}{2}mv_\perp{}^2}{B} \tag{3.2.2}$$

where I and A are the current and area generating the magnetic moment,

$r_b=2\pi v_\perp/\omega_b$ is the gyroradius, and $v_\perp$ is the velocity component perpendicular to the magnetic field.[2] The magnetization vector (magnetic moment per unit volume) for a thermal distribution of electrons is thus

$$\mathbf{M}=-\frac{nkT}{B^2}\mathbf{B}. \tag{3.2.3}$$

By definition

$$\begin{aligned}\mathbf{H}&=\frac{\mathbf{B}}{\mu_0}-\mathbf{M}\\&=\left(1+\mu_0\frac{nkT}{B^2}\right)\frac{\mathbf{B}}{\mu_0},\end{aligned} \tag{3.2.4}$$

where the coefficient in parentheses is formally the reciprocal relative permeability. Clearly, no simple proportionality exists between **H** and **B**, so that permeability is not in general a valid concept. However, in the special case where the static magnetic field B_0 is large compared to the wave magnetic field, and the two field components are spatially orthogonal, as in propagation along the static field, the relative permeability κ_m is essentially constant:

$$\begin{aligned}\kappa_m&=\left(1+\mu_0\frac{nkT}{B_0{}^2}\right)^{-1}\\&=\left[1+\left(\frac{\omega_p}{\omega_b}\right)^2\frac{kT}{mc^2}\right]^{-1}\\&=(1+\tfrac{1}{2}\beta)^{-1}.\end{aligned} \tag{3.2.5}$$

The parameter

$$\beta=\frac{2\mu_0nkT}{B_0{}^2} \tag{3.2.6}$$

represents the ratio of material to magnetic field pressure, and occurs frequently in the theory of plasma confinement (Glasstone and Lovberg, 1960, p. 52).[3] Note that β is the square of the ratio of the gyroradius to the wavelength of a free-space wave at the plasma frequency. For plane, transverse waves in a medium with zero conductivity, Maxwell's equations give the dispersion equation

$$\mu^2=\kappa\kappa_m, \tag{3.2.7}$$

[2] In passing, we note that the magnetic moment of a gyrating particle is an adiabatic invariant of the motion, a feature exploited in magnetic mirror devices (Glasstone and Lovberg, 1960, p. 337; Lenard, 1959). This is essentially a consequence of the conservation of angular momentum.

[3] This parameter, conventionally represented by the ambiguous symbol β, is not to be confused with the relativistic velocity ratio v/c, nor with the phase propagation coefficient.

where μ is the index of refraction and κ the dielectric constant. Hence we infer in this special case, using (1.4.20),

$$\mu^2=\left[1-\frac{(\omega_p/\omega)^2}{1\pm(\omega_b/\omega)}\right]\Big/\left[1+\left(\frac{\omega_p}{\omega_b}\right)^2\frac{kT}{mc^2}\right]. \tag{3.2.8}$$

This naive argument cannot be expected to have the validity of a treatment which considers explicitly the effect of the wave on the electron velocity distribution—that is, considers particle motion and thus conductivity rather than dielectric and diamagnetic properties. In particular, the permeability argument ignores resonance effects when $\omega\sim\omega_b$. The correct treatment is outlined in Section 3.4, from which it may be seen that the temperature correction in (3.2.8) is of the right order of magnitude.

3.3 Hydromagnetic calculation of plasma waves

The kinetic (Boltzmann) theory for waves of finite wavelength in a warm plasma is mathematically difficult. To provide insight we first attack the problem using the hydromagnetic approximation, mentioned in Section 2.4. This treatment necessarily excludes the phenomenon of Landau damping; therefore, we must require that the value of the electron velocity distribution function be small at the wave phase velocity. In addition, we shall assume only high-frequency oscillations so that the ion motion may be neglected. We neglect collisions and all nonlinear terms.

3.3.1 ***Moment equations.*** Given the Boltzmann equation (2.4.4)

$$\frac{\partial f}{\partial t}+\mathbf{v}\cdot\nabla_r f+\mathbf{a}\cdot\nabla_v f=\left(\frac{\partial f}{\partial t}\right)_{coll}, \tag{3.3.1}$$

we multiply through by any function $A(\mathbf{v})$ and integrate over all velocity space. The integrals for the left-hand side are (Spitzer, 1962, appendix)

$$\int A(\mathbf{v})\frac{\partial f}{\partial t}\,d^3\mathbf{v}=\frac{\partial}{\partial t}(n\bar{A}) \tag{3.3.2}$$

$$\int A(\mathbf{v})\,v_x\frac{\partial f}{\partial x}\,d^3\mathbf{v}=\frac{\partial}{\partial x}(n\overline{v_xA}) \tag{3.3.3}$$

$$\int A(\mathbf{v})\,a_x\frac{\partial f}{\partial v_x}\,d^3\mathbf{v}=-n\,\overline{\frac{\partial}{\partial v_x}(a_xA)}, \tag{3.3.4}$$

where

$$n(\mathbf{r},t)=\int f(\mathbf{r},\mathbf{v},t)\,d^3\mathbf{v} \tag{3.3.5}$$

and the bar denotes an average over the velocity distribution as, for instance,

$$\bar{A}(\mathbf{r},t)=\frac{\int A(\mathbf{v})f(\mathbf{r},\mathbf{v},t)\,d^3\mathbf{v}}{n(\mathbf{r},t)}. \tag{3.3.6}$$

If first $A(\mathbf{v})$ is taken to be unity, we obtain the *equation of continuity*

$$\frac{\partial n}{\partial t}-\frac{1}{e}\nabla_r\cdot\mathbf{J}=0 \tag{3.3.7}$$

for electrons of charge $-e$ and the macroscopic current density

$$\mathbf{J}=-ne\bar{\mathbf{v}}. \tag{3.3.8}$$

The integral (3.3.4) is zero for electromagnetic forces; the integral over the collision term is also zero, since collisions cannot alter the local density. Second, we take $A(\mathbf{v})$ to be the momentum $m\mathbf{v}$, and assume that the acceleration arises only from electromagnetic fields $\mathbf{E}$ and $\mathbf{B}$, to obtain the *equation of momentum transport*[4]

$$-\frac{m}{e}\frac{\partial\mathbf{J}}{\partial t}+\nabla\cdot\boldsymbol{\Psi}+ne\mathbf{E}-\mathbf{J}\times\mathbf{B}=0, \tag{3.3.9}$$

in which $\boldsymbol{\Psi}$ is the pressure tensor $nm\overline{\mathbf{vv}}$ arising in the integral (3.3.3), and the collision term has been neglected. Maxwell's equations provide further relations between $\mathbf{E}$, $\mathbf{B}$ and n, $\mathbf{J}$. The remaining task, characteristic of the hydromagnetic formulation, is to evaluate the pressure tensor $\boldsymbol{\Psi}$. One approach is to approximate it by a scalar pressure p. For high frequencies, pressure changes will occur adiabatically so that we would expect

$$p=(n_0{}^{1-\gamma}kT)n^\gamma, \tag{3.3.10}$$

and therefore

$$\nabla\cdot\boldsymbol{\Psi}\to\nabla p=\gamma kT\,\nabla n, \tag{3.3.11}$$

where γ is the ratio of specific heats and n_0 and T the equilibrium electron density and temperature. For strictly longitudinal plane waves the compression is essentially one-dimensional, implying $\gamma=3$ (Spitzer, 1962, §3.2). This approximation leads to the correct dispersion relation for the space-charge waves in the low magnetic field limit but does not indicate any temperature perturbation of the electromagnetic waves (Allis, Buchsbaum, and Bers, 1963). A more accurate treatment of the problem is to form an additional moment equation, which may then be rather crudely approximated. Integrating the Boltzmann equation multiplied by the dyadic $m\mathbf{vv}$, we obtain the *equation of motion of the pressure tensor.* Neglecting

[4] In the more general treatment, the corresponding equation for ions is also obtained. The sum of these two equations yields the macroscopic equation of motion; the difference, the generalized Ohm's law relation (Spitzer, 1962, §2.2). The treatment given here is appropriate for high frequencies when ion motion can be neglected, and for weak fields when a linearized equation is adequate.

all nonlinear terms and those involving the magnetic field, one obtains (Bernstein and Trehan, 1960)

$$\frac{\partial}{\partial t}\Psi-\frac{kT}{e}[\nabla\cdot\mathbf{J}\,\mathbf{1}+\nabla\mathbf{J}+(\nabla\mathbf{J})^t]=0, \tag{3.3.12}$$

the divergence of which is

$$\frac{\partial}{\partial t}(\nabla\cdot\Psi)-\frac{kT}{e}[2\nabla\nabla\cdot\mathbf{J}+\nabla\cdot\nabla\mathbf{J}]=0. \tag{3.3.13}$$

The approximations made in this equation are essentially the assumptions of low temperature and low magnetic field.[5]

3.3.2 ***Hydromagnetic dispersion relations.*** We now assume a plane wave traveling in the direction of the complex vector propagation constant $\check{\gamma}$, and expand the variables in the form

$$\begin{aligned}\mathbf{J}&=\mathbf{J}_1\exp(j\omega t-\check{\gamma}\cdot\mathbf{r})\\ \mathbf{E}&=\mathbf{E}_1\exp(j\omega t-\check{\gamma}\cdot\mathbf{r})\\ \mathbf{B}&=\mathbf{B}_0.\end{aligned} \tag{3.3.14}$$

The products of first-order quantities, and of all higher-order quantities, will be neglected. Thus the magnetic component of the wave field may be ignored. Equations (3.3.9) and (3.3.13) yield

$$-j\frac{m\omega}{e}\mathbf{J}_1-j\frac{kT}{e\omega}(2\check{\gamma}\check{\gamma}\cdot\mathbf{J}_1+\check{\gamma}\cdot\check{\gamma}\mathbf{J}_1)+n_0e\mathbf{E}_1+\mathbf{B}_0\times\mathbf{J}_1=0. \tag{3.3.15}$$

Rearranging, we have

$$\mathbf{E}_1=j\frac{\omega}{\epsilon_0{\omega_p}^2}\left[1+j\frac{\boldsymbol{\omega}_b\times}{\omega}+\frac{kT}{m\omega^2}(2\check{\gamma}\check{\gamma}\cdot+\check{\gamma}\cdot\check{\gamma})\right]\mathbf{J}_1, \tag{3.3.16}$$

where

$${\omega_p}^2=\frac{n_0e^2}{\epsilon_0m}\qquad\boldsymbol{\omega}_b=\frac{e\mathbf{B}}{m}. \tag{3.3.17}$$

The coefficient of $\mathbf{J}_1$ is a tensor resistivity, similar to $\check{\sigma}^{-1}$ in (1.4.28). It may be inverted to obtain the conductivity and dielectric constant tensors. A medium for which the dielectric constant is a function of the propagation constant is said to exhibit *spatial dispersion* (Neufeld, 1961). Without loss of generality, we take the propagation constant to lie in the x-z plane and the magnetic field along the z axis; then

$$\begin{aligned}\check{\gamma}&=j\check{\mu}\frac{\omega}{c}(\xi,0,\zeta)\\ \boldsymbol{\omega}_b&=(0,0,\omega_b)\end{aligned} \tag{3.3.18}$$

[5] We have neglected the magnetostatic field terms, which are of first order, simply because of algebraic complexity. Therefore the solution will be correct only to first order in temperature for infinitesimal field and, alternatively, for any field at zero temperature. Terms involving the product of temperature and magnetic field will not in general be correct. This restriction does not apply to the kinetic theory results quoted in Section 3.4.

where $\check{\mu}$ is the complex index of refraction and ξ, ζ are the direction cosines of $\check{\gamma}$. The coefficient of $\mathbf{J}_1$ in (3.3.16) becomes in matrix form

$$\check{\sigma}^{-1}=j\frac{\omega}{\epsilon_0{\omega_p}^2}\begin{bmatrix}1-\delta(1+2\xi^2) & -jY & -2\delta\xi\zeta\\ jY & 1-\delta & 0\\ -2\delta\xi\zeta & 0 & 1-\delta(1+2\zeta^2)\end{bmatrix} \tag{3.3.19}$$

where

$$\begin{aligned}Y&=\omega_b/\omega\\ \delta&=\check{\mu}^2kT/mc^2.\end{aligned} \tag{3.3.20}$$

It is to be noted that the parameter δ is essentially the square of the ratio of electron thermal velocity to wave phase velocity, which we require to be small (see footnote 7). The reciprocal of (3.3.19) is the conductivity

$$\check{\sigma}=-j\frac{\epsilon_0{\omega_p}^2/\omega}{(1-\delta)^2(1-3\delta)-Y^2[1-\delta(1+2\zeta^2)]}\times\begin{bmatrix}1-\delta(2+2\zeta^2)+\delta^2(1+2\zeta^2) & jY[1-\delta(1+2\zeta^2)] & 2\xi\zeta\delta(1-\delta)\\ -jY[1-\delta(1+2\zeta^2)] & 1-4\delta+3\delta^2 & -j2Y\xi\zeta\delta\\ 2\xi\zeta\delta(1-\delta) & j2Y\xi\zeta\delta & 1-\delta(2+2\xi^2)+\delta^2(1+2\xi^2)-Y^2\end{bmatrix} \tag{3.3.21}$$

where the coefficient is understood to multiply each element of the matrix. The corresponding dielectric constant is

$$\check{\kappa}=\mathbf{1}+\frac{\check{\sigma}}{j\omega\epsilon_0}. \tag{3.3.22}$$

These expressions reduce to (1.4.56) to (1.4.60) in the limit $\delta\to 0$.

The propagation constant is determined by substitution of (3.3.21) in the electromagnetic wave equation

$$\nabla\times\nabla\times\mathbf{E}+\frac{1}{c^2}\frac{\partial^2\mathbf{E}}{\partial t^2}+\mu_0\frac{\partial}{\partial t}(\check{\sigma}\cdot\mathbf{E})=0, \tag{3.3.23}$$

which for a wave of the form $\exp(j\omega t-\check{\gamma}\cdot\mathbf{r})$ in a homogeneous medium reduces to

$$\check{\gamma}\times(\check{\gamma}\times\mathbf{E})-\frac{\omega^2}{c^2}\check{\kappa}\cdot\mathbf{E}=0. \tag{3.3.24}$$

This is a system of homogeneous equations; the determinant of the coefficients must vanish to ensure a nontrivial solution. For $\check{\gamma}$ in the x-z plane, as given by (3.3.18), this condition is

$$\begin{vmatrix}1-\mu^2\zeta^2-s_{xx} & -s_{xy} & \mu^2\xi\zeta-s_{xz}\\ -s_{yx} & 1-\mu^2-s_{yy} & -s_{yz}\\ \mu^2\xi\zeta-s_{zx} & -s_{zy} & 1-\mu^2\xi^2-s_{zz}\end{vmatrix}=0, \tag{3.3.25}$$

where the elements $s_{xx}, s_{xy}, \ldots$ are the respective elements of the matrix portion of (3.3.21) multiplied by

$$\frac{(\omega_p/\omega)^2}{(1-\delta)^2(1-3\delta)-Y^2[1-\delta(1+2\zeta^2)]}.$$

For propagation along the field ($\xi=0$, $\zeta=1$), we obtain from (3.3.25) the dispersion relation

$$\left[\mu^2-1+\frac{(\omega_p/\omega)^2}{(1-\delta)+(\omega_b/\omega)}\right]\left[\mu^2-1+\frac{(\omega_p/\omega)^2}{(1-\delta)-(\omega_b/\omega)}\right]\left[1-\frac{(\omega_p/\omega)^2}{1-3\delta}\right]=0, \tag{3.3.26}$$

where $\delta=\mu^2kT/mc^2$. The first two factors are the circularly polarized electromagnetic waves; they reduce to the results obtained in Section 1.4.1 in the limit $\delta\to 0$. To first order in temperature and magnetic field (see footnote 5)

$$\mu_{l,r}^2=1-\frac{(\omega_p/\omega)^2}{1-(kT/mc^2)[1-(\omega_p/\omega)^2]\pm(\omega_b/\omega)}$$
$$\approx\left[1-\frac{(\omega_p/\omega)^2}{1\pm\omega_b/\omega}\right]\left[1-\left(\frac{\omega_p}{\omega}\right)^2\frac{kT}{mc^2}\right]. \tag{3.3.27}$$

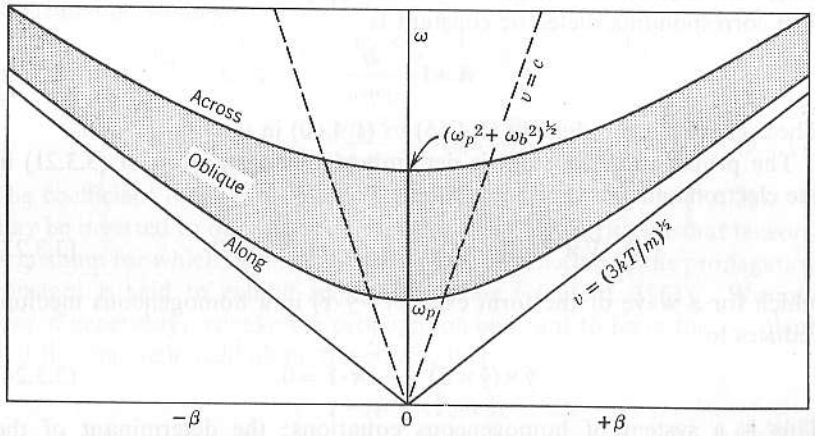

FIG. 3.1 The ω-β diagram for plasma (spacecharge) waves. The lower boundary of the shaded region pertains to waves propagating along the magnetic field, from (3.3.28); the upper boundary to waves across the field, from (3.3.35). The intercept of curves for oblique angles of propagation is at $(\omega_p^2+\omega_b^2\sin^2\theta)^{1/2}$, according to (3.4.28). The approximations used fail as the curves approach the $v=(3kT/m)^{1/2}$ asymptote. Compare Figs. 1.5, 5.19, and 5.21.

The third factor yields a wave with the dispersion relation

$$\mu^2=\frac{mc^2}{3kT}\left[1-\left(\frac{\omega_p}{\omega}\right)^2\right]$$

or

$$\omega^2=\omega_p^2+\frac{3kT}{m}\left(\frac{2\pi}{\lambda}\right)^2, \tag{3.3.28}$$

a well-known result for electron plasma oscillations (Bohm and Gross, 1949). The ω-β diagram is shown in Fig. 3.1. To fulfill the condition that thermal velocity be small compared to wave speed we note that $[1-(\omega_p/\omega)^2]$ must be small; that is, the wave only occurs for frequencies close to the plasma frequency. Examination of wave polarization shows that the electron motion is longitudinal, so that there is no coupling to the magnetic field.

For propagation across the field ($\xi=1$, $\zeta=0$), we obtain from (3.3.25) the dispersion relation

$$\left[\mu^2-1+\frac{(\omega_p/\omega)^2}{1-\delta}\right]\left\{\left[1-\frac{(\omega_p/\omega)^2(1-\delta)}{(1-\delta)(1-3\delta)-(\omega_b/\omega)^2}\right]\mu^2\right.$$
$$\left.-\left[1-\left(\frac{\omega_p}{\omega}\right)^2\frac{2-(\omega_p/\omega)^2-4\delta}{(1-\delta)(1-3\delta)-(\omega_b/\omega)^2}\right]\right\}=0. \tag{3.3.29}$$

The ordinary electromagnetic wave, which in our approximation is uncoupled to the magnetic field, has the slightly perturbed index

$$\mu_{ord}^2=1-\frac{(\omega_p/\omega)^2}{1-(kT/mc^2)[1-(\omega_p/\omega)^2]}$$
$$\approx[1-(\omega_p/\omega)^2]\left[1-\left(\frac{\omega_p}{\omega}\right)^2\frac{kT}{mc^2}\right]. \tag{3.3.30}$$

The extraordinary electromagnetic wave is coupled with a third plasma wave according to the second bracket of (3.3.29).[6] This bracket may be put over a common denominator to obtain for the dispersion relation

$$\{[1-(\omega_p/\omega)^2-(\omega_b/\omega)^2]-[4-(\omega_p/\omega)^2]\delta+3\delta^2\}\mu^2$$
$$-(\{[1-(\omega_p/\omega)^2]^2-(\omega_b/\omega)^2\}-4[1-(\omega_p/\omega)^2]\delta+3\delta^2)=0. \tag{3.3.31}$$

For small δ this equation is of the form

$$(A+a)\mu^2-(B+b)=0, \tag{3.3.32}$$

[6] Since δ contains μ^2, this bracket is in fact a cubic in μ^2, one of whose roots violates the assumption $\delta\ll 1$ and is extraneous.

where $a \ll A$ and $b \ll B$, and has the formal solution

$$\mu^2 = \frac{B}{A}\left(1 - \frac{a}{A} + \frac{b}{B} + \cdots\right). \tag{3.3.33}$$

The perturbed electromagnetic wave thus has the index

$$\mu_{ex}^2 = \left\{\frac{[1-(\omega_p/\omega)^2]^2 - (\omega_b/\omega)^2}{1-(\omega_p/\omega)^2-(\omega_b/\omega)^2}\right\}\left[1 - \left(\frac{\omega_p}{\omega}\right)^2 \frac{kT}{mc^2}\right], \tag{3.3.34}$$

where we have ignored magnetic field in the temperature term in accord with footnote 5. Since the index of refraction for the spacecharge wave is relatively large (although bounded by the requirement $\delta = \mu^2(kT/mc^2) \ll 1$), we obtain an approximation to the dispersion relation by equating the coefficient of μ^2 to zero. Since $(\omega_b/\omega)^2 \ll 1$, this coefficient, in the form given in (3.3.29), may be rewritten within our approximation

$$1 - \frac{(\omega_p/\omega)^2(1-\delta)}{(1-\delta)(1-3\delta)[1-(\omega_b/\omega)^2]},$$

whereupon the dispersion relation becomes (see Fig. 3.1)

$$(1-3\delta)[1-(\omega_b/\omega)^2] - (\omega_p/\omega)^2 \approx 1 - 3\delta - (\omega_b/\omega)^2 - (\omega_p/\omega)^2 = 0;$$

$$\mu^2 = \frac{1-(\omega_p/\omega)^2-(\omega_b/\omega)^2}{3kT/mc^2}$$

or

$$\omega^2 = \omega_p{}^2 + \omega_b{}^2 + \frac{3kT}{m}\left(\frac{2\pi}{\lambda}\right)^2. \tag{3.3.35}$$

Mathematical subtleties are involved in obtaining this dispersion relation in the limit where both temperature and magnetic field are taken to be small quantities (Gross, 1951; Bernstein, 1958). We note that this space-charge wave occurs only for frequencies near $(\omega_p{}^2 + \omega_b{}^2)^{1/2} \approx \omega_p$, within the limitations of the present theory. Since the squares of the indices of refraction are real for all cases in the present collisionless, hydromagnetic theory, it follows that the waves either propagate without attenuation or are perfectly evanescent.

3.4 Kinetic (Boltzmann) theory of waves

The kinetic theory treatment permits explicit consideration of the electron velocity distribution function. Proceeding in a manner similar to Section 2.4.2, we assume an expansion of the distribution function

$$f(\mathbf{r}, \mathbf{v}, t) = f_0(v^2) + f_1(\mathbf{r}, \mathbf{v}, t) \tag{3.4.1}$$

and electromagnetic fields

$$\begin{aligned} \mathbf{E}(\mathbf{r}, t) &= \mathbf{E}_1(\mathbf{r}, t) \\ \mathbf{B}(\mathbf{r}, t) &= \mathbf{B}_0 \end{aligned} \tag{3.4.2}$$

to obtain a linearized Boltzmann equation

$$\frac{\partial f_1}{\partial t} + \mathbf{v}\cdot\nabla_r f_1 + \boldsymbol{\omega}_b \times \mathbf{v}\cdot\nabla_v f_1 + \nu f_1 = \frac{e}{m}\,\mathbf{E}_1\cdot\nabla_v f_0, \tag{3.4.3}$$

where $\boldsymbol{\omega}_b = e\mathbf{B}_0/m$ and ν is the momentum-transfer collision frequency employed in the simple relaxation approximation of (2.4.6). The problem is now to solve (3.4.3) for $f_1(\mathbf{r}, \mathbf{v}, t)$, assuming a wave with phase factor $\exp(j\omega t - \check{\gamma}\cdot\mathbf{r})$, then to compute the current density

$$\mathbf{J}_1(\mathbf{r}, t) = -e\int \mathbf{v}\, f_1(\mathbf{r}, \mathbf{v}, t)\, d^3\mathbf{v}, \tag{3.4.4}$$

and finally to evaluate the conductivity tensor $\check{\sigma}$ such that

$$\mathbf{J}_1(\mathbf{r}, t) = \check{\sigma}(\check{\gamma}, \omega)\cdot\mathbf{E}_1(\mathbf{r}, t). \tag{3.4.5}$$

This is a calculation of considerable mathematical sophistication, which will not be reproduced here (Sitenko and Stepanov, 1957; Bernstein, 1958; Drummond, 1958; Lewis and Keller, 1962; and Johnston, 1962). The problem is treated in the books by Allis, Buchsbaum, and Bers (1963) and by Stix (1962). The complex integrals involved have been tabulated by Fried and Conte (1961). For the static magnetic field along the z axis and propagation in the x-z plane, according to (3.3.18), and assuming a Maxwellian distribution, the results are (Mower, 1959):

$$\begin{aligned}
\sigma_{xx} &= \frac{\epsilon_0\omega_p{}^2}{\omega}\int_0^\infty \left[\cos Ys - \frac{\xi^2\delta}{Y^2}(1-\cos^2 Ys)\right]\exp[\Phi(s)]\,ds \\
\sigma_{yy} &= \frac{\epsilon_0\omega_p{}^2}{\omega}\int_0^\infty \left[\cos Ys + \frac{\xi^2\delta}{Y^2}(1-\cos Ys)^2\right]\exp[\Phi(s)]\,ds \\
\sigma_{zz} &= \frac{\epsilon_0\omega_p{}^2}{\omega}\int_0^\infty (1-\zeta^2\delta s^2)\exp[\Phi(s)]\,ds \\
\sigma_{xy} &= -\sigma_{yx} = \frac{\epsilon_0\omega_p{}^2}{\omega}\int_0^\infty (-\sin Ys)\left[1 - \frac{\xi^2\delta}{Y^2}(1-\cos Ys)\right]\exp[\Phi(s)]\,ds \\
\sigma_{xz} &= \sigma_{zx} = \frac{\epsilon_0\omega_p{}^2}{\omega}\int_0^\infty \frac{\xi\zeta\delta s}{Y}(-\sin Ys)\exp[\Phi(s)]\,ds \\
\sigma_{yz} &= -\sigma_{zy} = \frac{\epsilon_0\omega_p{}^2}{\omega}\int_0^\infty \frac{\xi\zeta\delta s}{Y}(-1+\cos Ys)\exp[\Phi(s)]\,ds
\end{aligned} \tag{3.4.6}$$

$$\Phi(s) = -j(1-j\nu/\omega)s - \frac{\xi^2\delta}{Y^2}(1-\cos Ys) - \tfrac{1}{2}\zeta^2\delta s^2$$

$$\delta = \check{\mu}^2(kT/mc^2) \qquad Y = \omega_b/\omega$$

$$\xi = \sin\theta \qquad \zeta = \cos\theta$$

As in Section 1.4.8 by using the unitary matrix transformation

$$\check{\sigma}' = \mathbf{U}\cdot\check{\sigma}\cdot\mathbf{U}^{-1} \tag{3.4.7}$$

where

$$\mathbf{U} = \frac{1}{\sqrt{2}}\begin{bmatrix} 1 & -j & 0 \\ 1 & j & 0 \\ 0 & 0 & \sqrt{2} \end{bmatrix} \qquad \mathbf{U}^{-1} = \frac{1}{\sqrt{2}}\begin{bmatrix} 1 & 1 & 0 \\ j & -j & 0 \\ 0 & 0 & \sqrt{2} \end{bmatrix}, \tag{3.4.8}$$

we transform to a rotating coordinate system in which the conductivity tensor is symmetrical and is diagonal for the special case of propagation along the field. The result is (Bernstein, 1958):

$$\sigma'_{ll,\,rr} = \frac{\sigma_{xx}+\sigma_{yy}}{2} \pm j\sigma_{xy} = \frac{\epsilon_0 {\omega_p}^2}{\omega}\int_0^\infty \left[1 - \frac{\xi^2\delta}{Y^2}(1-\cos Ys)\right] \times \exp\left[-j\left(1 \pm Y - j\frac{\nu}{\omega}\right)s - \frac{\xi^2\delta}{Y^2}(1-\cos Ys) - \tfrac{1}{2}\zeta^2\delta s^2\right] ds$$

$$\sigma'_{zz} = \sigma_{zz} = \frac{\epsilon_0 {\omega_p}^2}{\omega}\int_0^\infty (1-\zeta^2\delta s^2)\exp[\Phi(s)]\,ds$$

$$\sigma'_{lr} = \sigma'_{rl} = \frac{\sigma_{xx}-\sigma_{yy}}{2} = \frac{\epsilon_0 {\omega_p}^2}{\omega}\int_0^\infty \left(-\frac{\xi^2\delta}{Y^2}\right)(1-\cos Ys)\exp[\Phi(s)]\,ds$$

$$\sigma'_{lz} = \sigma'_{zl} = \frac{1}{\sqrt{2}}(\sigma_{xz} - j\sigma_{yz}) = \frac{\epsilon_0 {\omega_p}^2}{\omega}\int_0^\infty \left(j\frac{\xi\zeta\delta s}{\sqrt{2}\,Y}\right)[1-\exp(-jYs)]\exp[\Phi(s)]\,ds$$

$$\sigma'_{rz} = \sigma'_{zr} = \frac{1}{\sqrt{2}}(\sigma_{xz} + j\sigma_{yz}) = \frac{\epsilon_0 {\omega_p}^2}{\omega}\int_0^\infty \left(-j\frac{\xi\zeta\delta s}{\sqrt{2}\,Y}\right)[1-\exp(jYs)]\exp[\Phi(s)]\,ds \tag{3.4.9}$$

The conductivity elements can readily be converted to dielectric constant elements by the usual relation $\check{\kappa} = \mathbf{1} + \check{\sigma}/j\omega\epsilon_0$. The propagation constant is obtained from the dispersion relation (3.3.24) and may be written in the form

$$A^*\check{\mu}^4 - B^*\check{\mu}^2 + C^* = 0, \tag{3.4.10}$$

where $\check{\mu}$ is the complex refractive index and

$$\begin{aligned} A^* &= \kappa_{xx}\xi^2 + \kappa_{zz}\zeta^2 + 2\kappa_{xz}\xi\zeta \\ B^* &= (\kappa_{xx}\kappa_{zz} - \kappa_{xz}^2) + (\kappa_{xx}\kappa_{yy} + \kappa_{xy}^2)\xi^2 + (\kappa_{yy}\kappa_{zz} + \kappa_{yz}^2)\zeta^2 + 2(\kappa_{yy}\kappa_{xz} - \kappa_{xy}\kappa_{yz})\xi\zeta \\ C^* &= |\kappa| \end{aligned} \tag{3.4.11}$$

with $|\kappa|$ denoting the determinant of the dielectric constant tensor. It must be remembered that the refractive index is contained implicitly in the dielectric constant elements, so that (3.4.10) is in general transcendental.

Expanded to first order in the quantity $\delta = \check{\mu}^2(kT/mc^2)$, the elements of the dielectric constant tensor are, in fixed coordinates (Sitenko and Stepanov, 1957):[7]

$$\kappa_{xx} = 1 - \frac{{\omega_p}^2}{\omega}\frac{\omega - j\nu}{(\omega-j\nu)^2 - {\omega_b}^2} \times\left\{1 + \zeta^2\delta\frac{\omega^2[(\omega-j\nu)^2+3{\omega_b}^2]}{[(\omega-j\nu)^2-{\omega_b}^2]^2} + \xi^2\delta\frac{3\omega^2}{(\omega-j\nu)^2-4{\omega_b}^2}\right\}$$

$$\kappa_{yy} = 1 - \frac{{\omega_p}^2}{\omega}\frac{\omega - j\nu}{(\omega-j\nu)^2 - {\omega_b}^2} \times\left\{1 + \zeta^2\delta\frac{\omega^2[(\omega-j\nu)^2+3{\omega_b}^2]}{[(\omega-j\nu)^2-{\omega_b}^2]^2} + \xi^2\delta\frac{\omega^2[(\omega-j\nu)^2+8{\omega_b}^2]}{(\omega-j\nu)^2[(\omega-j\nu)^2-4{\omega_b}^2]}\right\}$$

$$\kappa_{zz} = 1 - \frac{{\omega_p}^2}{\omega}\frac{1}{\omega-j\nu}\left\{1 + \zeta^2\delta\frac{3\omega^2}{(\omega-j\nu)^2} + \xi^2\delta\frac{\omega^2}{(\omega-j\nu)^2-{\omega_b}^2}\right\}$$

$$\kappa_{xy} = -\kappa_{yx} = -j\frac{{\omega_p}^2}{\omega}\frac{\omega_b}{(\omega-j\nu)^2-{\omega_b}^2} \times\left\{1 + \zeta^2\delta\frac{\omega^2[3(\omega-j\nu)^2+{\omega_b}^2]}{[(\omega-j\nu)^2-{\omega_b}^2]^2} + \xi^2\delta\frac{6\omega^2}{(\omega-j\nu)^2-4{\omega_b}^2}\right\}$$

$$\kappa_{xz} = \kappa_{zx} = -\xi\zeta\delta\frac{2\omega{\omega_p}^2(\omega-j\nu)}{[(\omega-j\nu)^2-{\omega_b}^2]^2}$$

$$\kappa_{yz} = -\kappa_{zy} = j\xi\zeta\delta\frac{\omega{\omega_p}^2\omega_b[3(\omega-j\nu)^2-{\omega_b}^2]}{(\omega-j\nu)^2[(\omega-j\nu)^2-{\omega_b}^2]^2} \tag{3.4.12}$$

The integrals of (3.4.6) are in general complex, even when collisions are neglected ($\nu \to 0$). However, the first-order expansions (3.4.12) are, neglecting collisions, pure real or imaginary in such a manner that propagation is either unattenuated or evanescent. Noncollisional damping has again been excluded.

We now catalog indices of refraction for the principal electromagnetic waves.

[7] The expansion parameter $\delta = \mu^2(kT/mc^2)$, which appears in both hydromagnetic and kinetic theories of warm plasmas, using nonrelativistic mechanics, is directly proportional to the square of the ratio of thermal velocity to that of light. If a first-order expansion of a nonrelativistic theory is to be valid, we must require $\mu^2 \gg 1$. This is of course precisely the condition under which the warm plasma results are significantly different from the cold case.

3.4.1 ***Propagation along the field*** ($\xi=0, \zeta=1$) (Platzman and Buchsbaum, 1962, 1963; Willett, 1962).

$$\check{\mu}_{l,r}^2=(\kappa_{xx}\pm j\kappa_{xy})_{\xi=0}=(\kappa'_{ll,rr})_{\xi=0}$$

$$=1-j\frac{\omega_p^2}{\omega^2}\int_0^\infty \exp\left[-j\left(1\pm Y-\frac{j\nu}{\omega}\right)s-\tfrac{1}{2}\delta s^2\right]ds$$

$$=1-j\frac{\omega_p^2}{\omega^2}\int_0^\infty (1-\tfrac{1}{2}\delta s^2+\tfrac{1}{8}\delta^2 s^4-\dots)\exp\left[-j\left(1\pm Y-\frac{j\nu}{\omega}\right)s\right]ds$$

$$=1-\frac{\omega_p^2}{\omega[(\omega-j\nu)\pm\omega_b]}$$

$$\times\left\{1+\frac{\omega^2}{[(\omega-j\nu)\pm\omega_b]^2}\mu^2\frac{kT}{mc^2}+\frac{3\omega^4}{[(\omega-j\nu)\pm\omega_b]^4}\mu^4\left(\frac{kT}{mc^2}\right)^2+\dots\right\}$$

$$\approx\left\{1-\frac{\omega_p^2}{\omega[(\omega-j\nu)\pm\omega_b]}\right\}\Big/\left\{1+\frac{\omega\omega_p^2}{[(\omega-j\nu)\pm\omega_b]^3}\frac{kT}{mc^2}\right\} \qquad (3.4.13)$$

The upper signs refer to the left-handed (ion gyration sense) circularly polarized wave; the lower to the right-handed (electron sense) wave.[8] Within the limitations of this expansion and the nonrelativistic mechanics, the temperature correction is significant for only the right-handed wave near cyclotron resonance. The effect, shown in Fig. 3.2, is to exaggerate the resonant increase in μ for $\omega\lesssim\omega_b$, in contrast to the suppression furnished by collision processes. Thus, phenomenologically, the cyclotron resonance appears to occur at a lower frequency (or higher field) (Mahaffey, 1963).

An alternative formulation of the special case of propagation along the magnetic field, neglecting collisions, expresses the dispersion relation in the form (Stix, 1962, Chap. 9)[9]

$$\mu_{l,r}^2=1-\frac{\omega_p^2}{\omega^2}\int_{-\infty}^{\infty}\frac{\omega f(v_z)\,dv_z}{\omega\pm\omega_b+\check{\mu}\omega v_z/c}, \qquad (3.4.14)$$

[8] Examination of the higher order terms in the expansion shows that a first-order approximation with the correction term

$$\left\{1-\frac{\omega\omega_p^2}{[(\omega-j\nu)\pm\omega_b]^3}\frac{kT}{mc^2}\right\}$$

in the numerator is more accurate for low densities away from resonance. The form as shown, with the correction term in the denominator, is more appropriate under conditions when $\mu^2\gg1$ and the magnitude of the correction is significant. The same remark applies also to the first-order approximation in (3.4.19) and (3.4.22). See footnote 7.

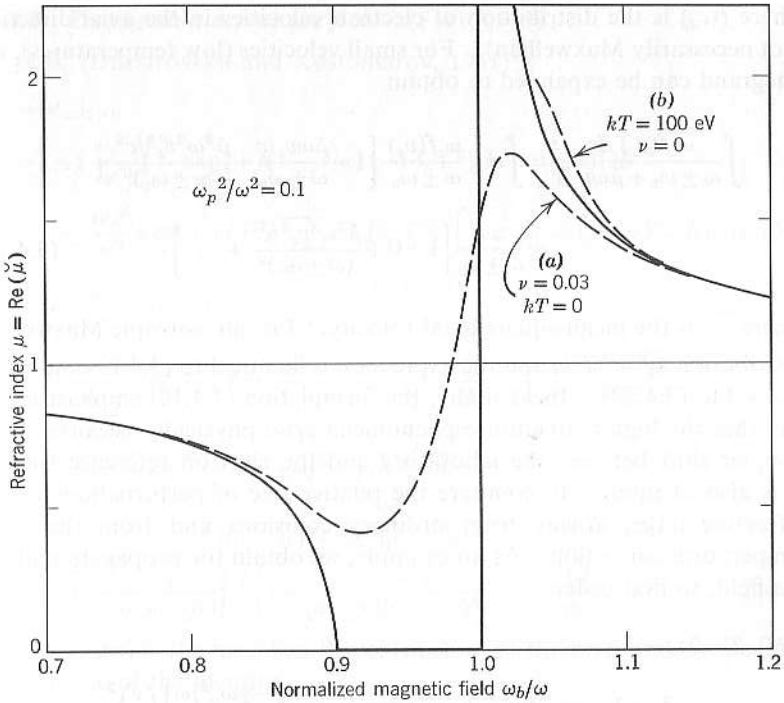

FIG. 3.2 Refractive index for the right-hand wave propagating along the magnetic field, in the vicinity of cyclotron resonance. The dashed curves show the departures from the collisionless Lorentz theory (solid curve) produced by (*a*) short-range collisions, and (*b*) high temperature. The behavior of the high-temperature curve close to $\omega_b/\omega=1$ is sensitive to careful specification of a collision rate and/or slight departures of the electron velocity distribution from Maxwellian (see Platzman and Buchsbaum, 1961; Willett, 1962).

[9] The equivalence to $\sigma'_{ll,rr}$ in (3.4.9) for a Maxwellian distribution and no collisions may be shown as follows.

$$\int_{-\infty}^{\infty}\frac{\omega f(v_z)\,dv_z}{\omega\pm\omega_b+\mu\omega v_z/c}=j\int_{-\infty}^{\infty}dv_z f(v_z)\int_0^\infty ds\exp[-j(1\pm Y+\mu v_z/c)s]$$

$$=j\int_0^\infty ds\exp[-j(1\pm Y)s]\int_{-\infty}^{\infty}dv_z\frac{1}{(2\pi)^{1/2}v_{th}}\exp\left[-\frac{v_z^2}{2v_{th}^2}-j\frac{\mu v_z s}{c}\right]$$

$$=j\int_0^\infty ds\exp\left[-j(1\pm Y)s-\frac{\tfrac{1}{2}\mu^2 v_{th}^2 s^2}{c^2}\right]\int_{-\infty}^{\infty}\frac{dv_z}{(2\pi)^{1/2}v_{th}}\exp\left[-\frac{(v_z+j\mu v_{th}^2 s/c)^2}{2v_{th}^2}\right]$$

$$=j\int_0^\infty ds\exp[-j(1\pm Y)s-\tfrac{1}{2}\delta s^2]$$

where $v_{th}=(kT/m)^{1/2}$ and $\mu^2 v_{th}^2/c^2=\delta$.

where $f(v_z)$ is the distribution of electron velocities in the axial direction (not necessarily Maxwellian). For small velocities (low temperatures), the integrand can be expanded to obtain

$$\int \frac{\omega f(v_z)\,dv_z}{\omega \pm \omega_b + \check{\mu}\omega v_z/c} = \int dv_z \frac{\omega f(v_z)}{\omega \pm \omega_b}\left[1 - \frac{\check{\mu}\omega v_z/c}{\omega \pm \omega_b} + \frac{\check{\mu}^2\omega^2 v_z^2/c^2}{(\omega \pm \omega_b)^2} + \dots\right]$$

$$= \frac{\omega}{\omega \pm \omega_b}\left[1 + 0 + \frac{\check{\mu}^2\omega^2\overline{v_z^2}/c^2}{(\omega \pm \omega_b)^2} + \dots\right], \tag{3.4.15}$$

where $\overline{v_z^2}$ is the mean-square axial velocity. For an isotropic Maxwellian distribution $\overline{v_z^2} = kT/m$ and the expression is identical to (3.4.13) and when $\omega_b \to 0$ to (3.4.22). Incidentally, the formulation (3.4.14) emphasizes the fact that the high-temperature phenomena arise physically because of the doppler shift between the laboratory and the electron reference frames. It is also of interest to compare the relative size of perturbations of the refractive index arising from ordinary collisions and from the finite temperature correction. As an example, we obtain for propagation along the field, to first order:

$\nu \neq 0,\ T = 0$:

$$\mu_{l,r}^2 = 1 - \frac{\omega_p^2}{\omega(\omega \pm \omega_b)} + \frac{\omega\omega_p^2}{(\omega \pm \omega_b)^3}\left[\frac{\omega \pm \omega_b - \frac{3}{4}\omega_p^2/\omega}{\omega \pm \omega_b - \omega_p^2/\omega}\right]\left(\frac{\nu}{\omega}\right)^2$$

$\nu = 0,\ T \neq 0$:

$$\mu_{l,r}^2 = 1 - \frac{\omega_p^2}{\omega(\omega \pm \omega_b)} - \frac{\omega\omega_p^2}{(\omega \pm \omega_b)^3}\mu^2\frac{kT}{mc^2} \tag{3.4.16}$$

We note that the corrections are in opposite directions. In the most important case, near cyclotron resonance in the right-hand mode (Fig. 3.2), approximate cancellation occurs when

$$\frac{3}{4}\left(\frac{\nu}{\omega}\right)^2 \approx \mu^2\frac{kT}{mc^2}. \tag{3.4.17}$$

Assuming electron-ion collisions, using (2.5.23), and approximating μ^2 by $\omega_p^2/\omega(\omega_b - \omega) \gg 1$, we find the finite temperature effect dominates when the inequality

$$\frac{\omega}{\omega_b - \omega}\frac{(kT[\text{eV}])^4}{n[\text{cm}^{-3}]} > 10^{-13} \tag{3.4.18}$$

is satisfied. Changes in the wave attenuation are discussed in Section 3.5.

3.4.2 *Propagation across the field* ($\xi = 1, \zeta = 0$).

$\mathbf{E}_{rf} \parallel \mathbf{B}_0$ (Dnestrovskii and Kostomarov, 1961):

$$\begin{aligned}
\check{\mu}^2 &= (\kappa_{zz})_{\zeta=0} \\
&= 1 - j\frac{\omega_p^2}{\omega^2}\int_0^\infty \exp[-j(1 - j\nu/\omega)s - (\delta/Y^2)(1 - \cos Ys)]\,ds \\
&= 1 - j\frac{\omega_p^2}{\omega^2}\exp(-\delta/Y^2)\sum_{n=-\infty}^{\infty} \mathrm{I}_n(\delta/Y^2)\int_0^\infty \exp[-j(1 - nY - j\nu/\omega)s]\,ds \\
&= 1 - \frac{\omega_p^2}{\omega^2}\exp(-\delta/Y^2)\sum_{n=-\infty}^{\infty}\frac{\mathrm{I}_n(\delta/Y^2)}{(1 - j\nu/\omega) - nY} \\
&= 1 - \frac{\omega_p^2}{\omega^2}\exp(-\delta/Y^2)\left[\frac{\mathrm{I}_0(\delta/Y^2)}{1 - j\nu/\omega} + \sum_{n=1}^{\infty}\frac{2(1 - j\nu/\omega)\mathrm{I}_n(\delta/Y^2)}{(1 - j\nu/\omega)^2 - n^2Y^2}\right] \\
&= 1 - \frac{\omega_p^2}{\omega(\omega - j\nu)}\left\{1 + \frac{\omega^2}{(\omega - j\nu)^2 - \omega_b^2}\mu^2\frac{kT}{mc^2}\right. \\
&\qquad \left. + \frac{3\omega^4}{[(\omega - j\nu)^2 - \omega_b^2][(\omega - j\nu)^2 - 4\omega_b^2]}\mu^4\left(\frac{kT}{mc^2}\right)^2 + \dots\right\} \\
&\approx \left[1 - \frac{\omega_p^2}{\omega(\omega - j\nu)}\right]\Bigg/\left\{1 + \frac{\omega\omega_p^2}{(\omega - j\nu)[(\omega - j\nu)^2 - \omega_b^2]}\frac{kT}{mc^2}\right\}
\end{aligned} \tag{3.4.19}$$

$\mathrm{I}_n(x) = \mathrm{I}_{-n}(x)$ is the modified Bessel function of the first kind, and use has been made of the identity

$$\exp(x\cos y) = \sum_{n=-\infty}^{\infty}\mathrm{I}_n(x)\exp(-jny). \tag{3.4.20}$$

$\mathbf{E}_{rf} \perp \mathbf{B}_0$:

$$\begin{aligned}
\check{\mu}^2 &= \left(\frac{\kappa_{xx}\kappa_{yy} + \kappa_{xy}^2}{\kappa_{xx}}\right)_{\zeta=0} \\
&\underset{\substack{\nu=0\\ T\to 0}}{\approx} \left\{\frac{[1 - (\omega_p/\omega)^2]^2 - (\omega_b/\omega)^2}{1 - (\omega_p/\omega)^2 - (\omega_b/\omega)^2}\right\}\Bigg/ \\
&\qquad \left\{1 + \frac{\omega_p^2[(\omega^2 - \omega_p^2)^2 + \omega_b^2(7\omega^2 - 4\omega_p^2) - 8\omega_b^4]}{(\omega^2 - 4\omega_b^2)(\omega^2 - \omega_p^2 - \omega_b^2)^2}\frac{kT}{mc^2}\right\}
\end{aligned} \tag{3.4.21}$$

The simplification of ignoring collisions in the latter form is made because of algebraic complexity.

The ordinary (parallel polarization) wave is no longer independent of magnetic field but, rather, shows resonances at all integral harmonics of the cyclotron frequency. Likewise, the extraordinary wave shows both the expected upper hybrid resonance at $\omega^2 = \omega_b^2 + \omega_p^2$ and additional resonances at harmonics of ω_b. The results obtained here may be compared with those obtained from the hydromagnetic calculation of Section 3.3.2. Further physical insight into the origin of the high-temperature modifications may be found in the discussion of Drummond (1958).

3.4.3 ***No magnetic field*** $(\omega_b=0)$:

$$\begin{aligned}\breve{\mu}^2&=(\kappa)_{\omega_b=0}\\&=1-j\frac{\omega_p^2}{\omega^2}\int_0^\infty \exp\left[-j\left(1-j\frac{\nu}{\omega}\right)s-\tfrac{1}{2}\delta s^2\right]ds\\&=1-j\frac{\omega_p^2}{\omega^2}\int_0^\infty (1-\tfrac{1}{2}\delta s^2+\tfrac{1}{8}\delta^2 s^4-\dots)\exp\left[-j\left(1-j\frac{\nu}{\omega}\right)s\right]ds\\&=1-\frac{\omega_p^2}{\omega(\omega-j\nu)}\left[1+\frac{\omega^2}{(\omega-j\nu)^2}\mu^2\frac{kT}{mc^2}+\frac{3\omega^4}{(\omega-j\nu)^4}\mu^4\left(\frac{kT}{mc^2}\right)^2+\dots\right]\\&\approx\left[1-\frac{\omega_p^2}{\omega(\omega-j\nu)}\right]\Big/\left[1+\frac{\omega\omega_p^2}{(\omega-j\nu)^3}\frac{kT}{mc^2}\right]\end{aligned}\tag{3.4.22}$$

Since for this case the refractive index never exceeds unity, the correction is numerically significant only for temperatures requiring relativistic mechanics, as discussed in Section 3.6.

3.4.4 ***Plasma or electrostatic waves.*** For propagation along the field the dispersion relation is

$$\kappa_{zz}=1+\sigma_{zz}/j\omega\epsilon_0=0.\tag{3.4.23}$$

From (3.4.6):

$$\begin{aligned}(\kappa_{zz})_{\xi=0}&=1-j\left(\frac{\omega_p}{\omega}\right)^2\int_0^\infty(1-\delta s^2)\exp\left[-j\left(1-j\frac{\nu}{\omega}\right)s-\tfrac{1}{2}\delta s^2\right]ds\\&=1-j\left(\frac{\omega_p}{\omega}\right)^2\int_0^\infty(1-\tfrac{3}{2}\delta s^2+\tfrac{5}{8}\delta^2 s^4-\dots)\exp\left[-j\left(1-j\frac{\nu}{\omega}\right)s\right]ds\\&=1-\frac{\omega_p^2}{\omega(\omega-j\nu)}\left[1+\frac{3\omega^2}{(\omega-j\nu)^2}\delta+\frac{15\omega^4}{(\omega-j\nu)^4}\delta^2+\dots\right]\\&\approx 1-\frac{\omega_p^2}{\omega(\omega-j\nu)}\left[1-\frac{3\omega^2}{(\omega-j\nu)^2}\delta\right]^{-1}\end{aligned}\tag{3.4.24}$$

Therefore to lowest order in temperature

$$\breve{\mu}^2=\frac{mc^2}{3kT}\frac{(\omega-j\nu)^2}{\omega^2}\left[1-\frac{\omega_p^2}{\omega(\omega-j\nu)}\right]\tag{3.4.25}$$

in agreement with (3.3.26). There is no magnetic field dependence, since all coherent particle motions are parallel to the field. A corresponding calculation for propagation across the field is algebraically complicated. Bernstein (1958) has shown that the dispersion relation for the plasma wave in an arbitrary direction can be put in the form

$$\begin{aligned}1+(\omega/\omega_p)^2\delta&=j\int_0^\infty\exp[\Phi(s)]\,ds\\&=j\exp[-\xi^2\delta(\omega/\omega_b)^2]\sum_{n=-\infty}^{\infty}\mathrm{I}_n[\xi^2\delta(\omega/\omega_b)^2]\\&\quad\times\int_0^\infty\exp\left[-j\left(\frac{\omega-j\nu+n\omega_b}{\omega}\right)s-\tfrac{1}{2}\zeta^2\delta s^2\right]ds,\end{aligned}\tag{3.4.26}$$

where $\delta=\breve{\mu}^2(kT/mc^2)$, $\Phi(s)$ is given in (3.4.6), and $\mathrm{I}_n(x)$ is the modified Bessel function of the first kind. This formulation is valid when the electromagnetic and plasma waves are relatively uncoupled; that is, when the phase velocity of the EM waves is large compared to that of the plasma wave at the same frequency. The special case of $\zeta=1$ leads again to (3.4.25). For propagation across the field ($\xi=1$), one obtains

$$1+(\omega/\omega_p)^2\delta=\exp[-(\omega/\omega_b)^2\delta]\left\{\mathrm{I}_0[(\omega/\omega_b)^2\delta]+2\sum_{n=1}^{\infty}\frac{\omega(\omega-j\nu)\mathrm{I}_n[(\omega/\omega_b)^2\delta]}{(\omega-j\nu)^2-n^2\omega_b^2}\right\},\tag{3.4.27}$$

which exhibits resonances at all harmonics of the gyrofrequency. Various limiting cases are considered by Bernstein (1958). Equation (3.4.27) does not converge properly in the limit of small magnetic field. An expansion of the first form of (3.4.26) for small ω_b, as well as small δ, and neglecting collisions, leads to the dispersion relation

$$\breve{\mu}^2=\frac{mc^2}{3kT}[1-(\omega_p/\omega)^2-(\omega_b/\omega)^2\xi^2],\tag{3.4.28}$$

which agrees with (3.3.28), (3.3.35), and (3.4.25), and Fig. 3.1.

A fuller discussion of spacecharge waves in warm plasmas, including the treatment of wave vectors at arbitrary angles to the magnetic field, is given in Sections 5.5 and 5.6.

3.5 Landau damping and wave absorption

Dissipative absorption of a wave appears mathematically as an imaginary term in the dielectric constant $\breve{\kappa}$ and, hence, in the square of the complex refractive index,

$$\breve{\mu}^2=(\mu-j\chi)^2=-\left(\frac{\breve{\gamma}c}{\omega}\right)^2=\breve{\kappa}=\kappa_r-j\kappa_i,\tag{3.5.1}$$

where μ and χ are the (real) refractive and attenuation indices, respectively. From (A.46) and (A.47)

$$\begin{aligned}\mu^2&=\frac{\kappa_r+(\kappa_r^2+\kappa_i^2)^{1/2}}{2}=\frac{\kappa_i^2}{4\chi^2}\xrightarrow[\kappa_i^2\ll\kappa_r^2]{}\kappa_r\left(1+\frac{\kappa_i^2}{4\kappa_r^2}\right)\\\chi^2&=\frac{-\kappa_r+(\kappa_r^2+\kappa_i^2)^{1/2}}{2}=\frac{\kappa_i^2}{4\mu^2}\xrightarrow[\kappa_i^2\ll\kappa_r^2]{}\frac{\kappa_i^2}{4\kappa_r}.\end{aligned}\tag{3.5.2}$$

The attenuation constant α, measured in nepers per meter, is

$$\alpha=\frac{\omega\chi}{c}=\frac{\kappa_i\omega}{2\mu c}\xrightarrow[\kappa_i^2\ll\kappa_r^2]{}\frac{\kappa_i}{2\kappa_r^{1/2}}\frac{\omega}{c}.\tag{3.5.3}$$

The condition $\chi^2\ll\mu^2$ is a fortiori satisfied if $\kappa_i^2\ll\kappa_r^2$.

The integrals of (3.4.6) are in general complex. This may be seen most easily in the formulation (3.4.14) in which the integrand has a simple pole at $v_z = -(\omega \pm \omega_b)c/\mu\omega$. Discarding higher order real terms in the expansion (3.4.15), we obtain for propagation in the left and right circularly polarized electromagnetic waves along the magnetic field

$$(\mu - j\chi)^2 = 1 - \frac{\omega_p^2}{\omega(\omega \pm \omega_b)} - j\pi \frac{\omega_p^2 c}{\omega^2 \mu} f\left[\frac{(\omega \pm \omega_b)c}{\omega\mu}\right], \tag{3.5.4}$$

where the one-dimensional distribution function is in the Maxwellian case

$$f(v_z) = \left(\frac{m}{2\pi kT}\right)^{1/2} \exp(-mv_z^2/2kT). \tag{3.5.5}$$

Thus, for low temperatures, the attenuation constant is, from (3.5.3) (Sagdeyev and Shafranov, 1958; Cullen, 1960),

$$\alpha \approx \left(\frac{\pi}{8}\right)^{1/2} \frac{\omega_p^2}{\omega c \mu^2} \left(\frac{mc^2}{kT}\right)^{1/2} \exp\left[-\frac{(\omega \pm \omega_b)^2}{2\omega^2\mu^2}\left(\frac{mc^2}{kT}\right)\right] \tag{3.5.6}$$

where

$$\mu^2 \approx \left[1 - \frac{\omega_p^2}{\omega(\omega \pm \omega_b)}\right].$$

This case has been studied in detail by Scarf (1962), Willett (1962), and Platzman and Buchsbaum (1962, 1963).

This result is an example of noncollisional damping known generically as phase mixing or fine scale mixing (Gershman, 1960). In the context of plasma oscillations, the phenomenon is usually called *Landau damping*. It is closely related to the inverse process of Cerenkov radiation. Physically, it arises because of synchronism between particle and wave velocities. Electrons in one region of the wave move, as a result of thermal motion, into adjoining regions where the phase of the wave is different. On the average, particles riding with the wave extract more energy from the wave (linear accelerator effect) than they give to it (traveling-wave tube effect); this energy is then gradually shared with nonsynchronous particles by collisions. Thus, thermal energy is increased at the expense of wave energy (Dawson, 1961). In the presence of a magnetic field, the effect may also be considered as arising from the doppler shift of the wave frequency as seen by the moving electron, and is frequently called *cyclotron damping*.

This dissipative process was inherently excluded in the hydromagnetic calculation of Section 3.3.2 and discarded in the first-order expansions of (3.4.12). The application of theory to experiment is complicated by the fact that the strong interaction between wave and synchronous electrons distorts the distribution function near the wave velocity, whereas collisions

tend to restore Maxwellian distribution. Hence, the magnitude of noncollisional damping depends inherently upon the collision rate (Platzman and Buchsbaum, 1961). In cases where a highly non-Maxwellian velocity distribution is somehow maintained, such that there are more fast particles than slow in the neighborhood of the wave velocity (implying a "double-humped" velocity distribution), then wave amplification or growth can occur, as calculated in Section 5.6. Examples are the traveling-wave tube and various plasma instability processes (Drummond and Pines, 1961).

Most theoretical treatments of noncollisional damping have been concerned with the longitudinal plasma waves, rather than the transverse electromagnetic waves (Landau, 1946; Bohm and Gross, 1949; and Kildal, 1961). Furthermore, the more common problem has been to assume an initial disturbance and follow its decay in time; the frequency ω, rather than the propagation constant γ, is assumed complex. The problem of determining a complex γ inherently requires consideration of *driven* waves.

To contrast with (3.5.6), we may compute the ordinary collisional attenuation, in the special cases of propagation along the magnetic field (left and right circular polarizations) or across the field (ordinary mode, putting $\omega_b = 0$). From (1.4.21),

$$\alpha = \frac{\chi\omega}{c} \approx \frac{\omega_p^2 \nu}{2c(\omega \pm \omega_b)^{3/2}(\omega \pm \omega_b - \omega_p^2/\omega)^{1/2}}. \tag{3.5.7}$$

If electron-ion collisions are dominant, as in a highly ionized gas, then $\nu \propto \omega_p^2/(kT)^{3/2}$, according to (2.5.23). For given ω, ω_p, and ω_b, there will exist some critical temperature below which collisional dissipation dominates and above which phase mixing dominates. Because of the exponential term in (3.5.6), this critical temperature is in the kilovolt region for electromagnetic waves in most laboratory plasmas, except near the gyroresonance.

It is worthwhile to note, in passing, that the real and imaginary components of the propagation constant are linked by general considerations of causality, the mathematical formulation of which is known as the Kramers-Kronig dispersion relations (Kittel, 1958; Leontovich, 1961; and Pradhan, 1962).

3.6 Relativistic plasmas

Since the expansion parameter $\delta = \mu^2(kT/mc^2)$ which appears in the kinetic treatment of "warm" plasmas, using nonrelativistic mechanics, is of order $\mu^2(v/c)^2$, it may be necessary to employ relativistic mechanics if one is to retain terms of order (kT/mc^2) for $\mu^2 \sim 1$ (Silin, 1960–1962; Graben, 1963). Also, synchrotron radiation processes imply that the interaction between a wave and plasma at multiples of the gyrofrequency should be

enhanced for a relativistic plasma (Beard, 1959). Imre (1962) has considered the problem of electromagnetic wave propagation in relativistic plasmas in detail. As an example, he obtains for propagation along the field, to first order in kT/mc^2,

$$\check{\mu}_{l,r}^2 \approx \frac{1-\dfrac{{\omega_p}^2}{\omega(\omega \pm \omega_b)}\left[1-\dfrac{5\omega}{2(\omega \pm \omega_b)}\dfrac{kT}{mc^2}\right]}{1+\dfrac{\omega{\omega_p}^2}{(\omega \pm \omega_b)^3}\dfrac{kT}{mc^2}}, \tag{3.6.1}$$

which is to be compared with (3.4.13). Johnston (1962) has developed weakly relativistic expansions, obtaining, for example, for electromagnetic waves in a plasma with no magnetic field

$$\check{\mu}^2 \approx \frac{1-\dfrac{{\omega_p}^2}{\omega^2}\left(1-\dfrac{5}{2}\dfrac{kT}{mc^2}\right)}{1+\dfrac{{\omega_p}^2}{\omega^2}\dfrac{kT}{mc^2}} \approx 1-\frac{{\omega_p}^2}{\omega^2}\left[1+\left(\frac{3}{2}-\frac{{\omega_p}^2}{\omega^2}\right)\frac{kT}{mc^2}\right], \tag{3.6.2}$$

which is to be compared with (3.4.22).

CHAPTER 4

Wave propagation through bounded plasmas

4.1 Introduction

The preceding chapters have been concerned with the propagation of electromagnetic waves in an infinite plasma. We now consider the effect of plasma boundaries on the propagation. To study high-density discharges of arbitrary size and geometry, one is generally forced to use microwave beams directed through the plasma by means of suitable antenna systems. The alternative situation in which the plasma is located within a cavity or waveguide, or is itself a waveguide, is considered in Chapter 5. The "free-space" beam technique is favorable where the dimensions of the plasma are larger than the wavelength of an electromagnetic wave at the plasma frequency. Both classes of measurements are essentially limited to frequencies $\omega \gtrsim \omega_p$, the plasma frequency (except for special techniques exploiting a static magnetic field or a detailed independent knowledge of the density profile). Thus, the beam technique is most readily analyzed when

$$\omega^2 \gg \begin{cases} {\omega_p}^2, \\ (c/D)^2, \end{cases} \tag{4.1.1}$$

where D is the dimension of the plasma. The first of these two independent conditions permits convenient simplifications in the analysis by avoiding the plasma resonance; the second is essentially a diffraction condition which permits reducing the problem of propagation of a finite beam of electromagnetic waves through a finite plasma to a one-dimensional, plane-wave problem, as a first approximation.

The propagation constant of a microwave beam in a plasma has been

shown, in Chapter 1, to depend upon the magnetic field, electron density, and collision frequency, and indirectly upon the temperature. The following basic arrangements, sketched schematically in Fig. 4.1, are useful in the case of high-temperature, highly ionized plasmas (that is, $\nu \ll \omega_p$).

(*1*) *Simple transmission or reflection.* For electron densities $n < n_c$ the plasma is transparent, while for $n > n_c$ it is opaque and totally reflecting, where $n_c = (\epsilon_0 m/e^2)\omega^2$ is the critical density.[1] The transition between

[1] In the presence of a magnetic field, the effective critical density may be altered. However, the situation is qualitatively unchanged.

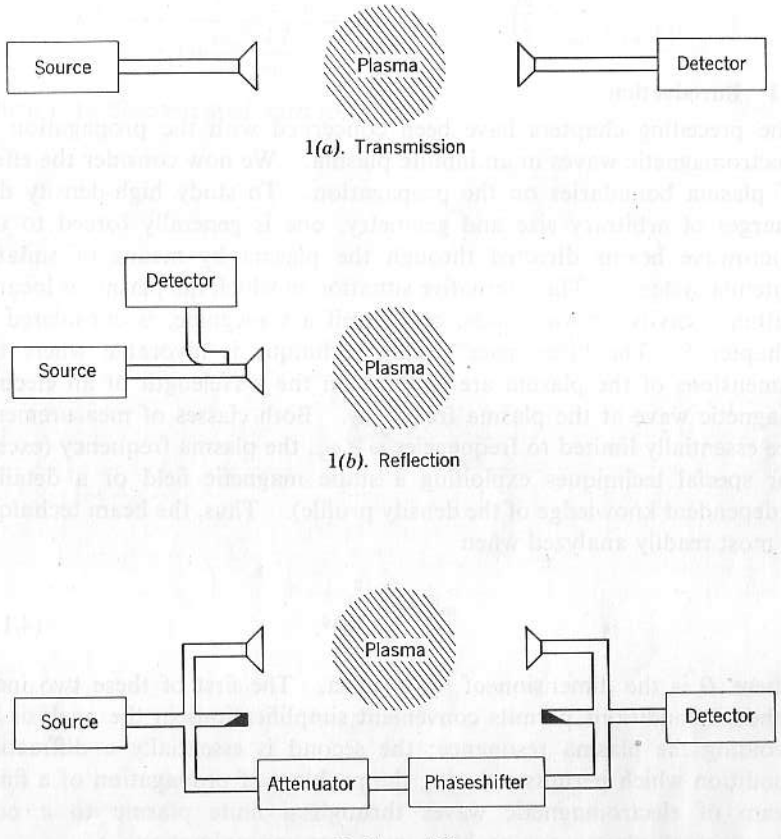

FIG. 4.1 Elementary microwave observation schemes.

these conditions is sharp. Thus, in principle, this elementary technique indicates whether the plasma density is above or below the critical value. Measurement at a given frequency is capable of determining only one value of density. The sharpness of the transition implied by the sudden change in the attenuation coefficient is not realized in practice because of the following factors.

(*a*) For densities below but approaching critical, the dielectric constant discontinuity at a sharp boundary produces an increasingly strong surface reflection (and corresponding reduction in transmission).

(*b*) If the plasma is only a few wavelengths thick, interference effects occur between the surface reflections.

(*c*) Inhomogeneous density distributions are not averaged in a simple manner.

(*d*) Refraction and scattering by the plasma occur because of inadequacies in the one-dimensional, plane-wave approximation.

If the plasma density is far above critical, an impinging signal is strongly reflected at the boundary. Therefore, motions of the effective boundary produce doppler shifts in the frequency of the reflected signal.

(*2*) *Phase shift* (*microwave bridge or interferometer*). If the signal from an auxiliary transmission path, with adjustable amplitude and phase elements, is balanced against the primary transmission signal to give a null in the absence of plasma, the output signal of the waveguide (hybrid) junction is a measure of the attenuation and phase shift in the primary path due to the plasma. In the fully transparent region of electron density, where $n \ll n_c$, a detected signal represents only phase shift which, in turn, is essentially a function of electron density only. Since the shift in phase can be calibrated, one has a continuous measurement of density between the upper limit of serious amplitude effects in the transmission path, and the lower limit of detector sensitivity. This technique is ideally suited to the observation of density as a function of time.

The propagation of the microwave beam through the bounded plasma is most readily analyzed in two limiting cases: first, the *gradual* boundary, with density varying slowly over a wavelength, to which an adiabatic analysis may be applied; and, second, the *sharp* boundary which can be attacked as a boundary-value problem. A formally similar situation occurs in quantum mechanics, in which the first case is known as the WKB approximation (Bohm, 1951). The usual *geometrical optics* limit partakes of both the above limits. It neglects reflections at the "sharp" boundaries which separate regions of different propagation characteristics and, thus, can be self-consistent only for plasmas large compared to a wavelength. The models of plasma geometry that are most useful for

analytical purposes are the plane slab and the cylinder. We recognize, however, that most experimental plasmas will fail to conform exactly to these limiting cases and simple geometries.

4.2 Simple adiabatic analysis of a plasma slab

While most experimental situations approximate cylindrical symmetry, it is often possible to treat the plasma as a slab illuminated by plane waves, and thereby reduce the problem to one dimension. We can further simplify the situation by assuming that plasma properties vary slowly near the boundaries so that reflection and interference effects are negligible, the *adiabatic* approximation.

4.2.1 ***Average electron density.*** For a high-temperature, highly ionized plasma, for which $\nu^2 \ll \omega_p^2$, dissipative attenuation is small. For simplicity, we here neglect magnetic field effects; they may be included readily by substituting the appropriate propagation formulas from Chapter 1. The phase constants for vacuum and plasma are, respectively,

$$\beta_0 = \frac{2\pi}{\lambda}$$

$$\beta_p = \left[1 - \left(\frac{\omega_p}{\omega}\right)^2\right]^{1/2} \frac{2\pi}{\lambda}$$

$$= \left[1 - \frac{n}{n_c}\right]^{1/2} \frac{2\pi}{\lambda}. \tag{4.2.1}$$

The phase advancement introduced by the plasma in a transmission path is then, in the adiabatic approximation,

$$\Delta\phi = -\int (\beta_p - \beta_0)\, dx$$

$$= \int \left\{1 - \left[1 - \frac{n(x)}{n_c}\right]^{1/2}\right\} \frac{2\pi}{\lambda}\, dx, \tag{4.2.2}$$

where the integration is carried out along the direct path from transmitting to receiving antenna. To first order in n/n_c, (4.2.2) becomes

$$\Delta\phi \xrightarrow[n \ll n_c]{} \frac{\pi}{\lambda n_c} \int n(x)\, dx$$

$$= \frac{e^2}{2\epsilon_0 mc\omega} \int n(x)\, dx. \tag{4.2.3}$$

Thus, for $n \ll n_c$, the phase shift is linearly proportional to the electron density averaged along the propagation path. For a path length L we can write the average density

$$\bar{n} = \frac{\int_0^L n(x)\, dx}{L} = \frac{2\epsilon_0 mc}{e^2} \frac{\omega\, \Delta\phi}{L},$$

$$\bar{n}[\mathrm{cm}^{-3}] = 118.4 \frac{\omega/2\pi[\mathrm{cps}]\, \Delta\phi[\mathrm{rad}]}{L[\mathrm{cm}]}. \tag{4.2.4}$$

Assuming this first order approximation, we may evaluate the dynamic range of average densities which can be measured. Because of dissipative and nonlinear effects,

$$n_{max} = \xi n_c = \xi \frac{\epsilon_0 m\omega^2}{e^2} \tag{4.2.5}$$

where ξ is a fraction which in a practical case might be 1/3. The minimum measurable density is

$$n_{min} = \frac{2\epsilon_0 mc}{e^2} \frac{\omega\, \Delta\phi_{min}}{L} \tag{4.2.6}$$

where $\Delta\phi_{min}$ is the minimum detectable phase shift, which depends upon the detector noise level and system stability. Hence

$$\frac{n_{max}}{n_{min}} = \pi \frac{\xi}{\Delta\phi_{min}} \frac{L}{\lambda} \sim \frac{1}{\Delta\phi_{min}} \frac{L}{\lambda}. \tag{4.2.7}$$

The range of measurement scales with ω, while the maximum density scales with ω^2. The situation is shown numerically in Fig. 4.2.

Similarly, in the adiabatic approximation, the total attenuation, expressed as a power transmission coefficient T, in decibels, is given by

$$T[\mathrm{dB}] = -8.686 \int \alpha\, dx, \tag{4.2.8}$$

which using (1.3.30) becomes in the limit $\nu^2 \ll \omega_p^2 \ll \omega^2$

$$T[\mathrm{dB}] = -\frac{4.3e^2}{\epsilon_0 mc\omega^2} \int \nu(x)\, n(x)\, dx, \tag{4.2.9}$$

where ν is the effective collision frequency, which generally depends on both density and temperature. The coefficient has the value $4.3e^2/\epsilon_0 mc = 0.462\ \mathrm{cm}^2/\mathrm{sec}$.

In this common limit $\nu^2 \ll \omega_p^2 \ll \omega^2$ it is to be noted that the measured phase shift depends only upon the electron density, while the attenuation depends on both density and collision rate and thus, in principle, is an indirect means of measuring temperature. There are serious limitations on both phase and amplitude measurements produced by finite size of the

plasma and the failure of practical geometries to approximate the one-dimensional, plane-wave model. The typical geometry encountered in laboratory devices is a cylindrical plasma with the microwave beam directed transverse to the discharge axis. In the frequency region for which the plasma is transparent the plasma acts like a divergent cylindrical lens, thereby influencing the amplitude of the transmitted signal. Interference effects on the transmitted amplitude occur when the plasma is only a few wavelengths in diameter (thickness). These geometrical amplitude effects are troublesome because they obscure the dissipative absorption characteristic of the plasma itself. A curved boundary increases the amount of energy reflected by surface discontinuities that does not re-enter the transmitting antenna. Depending upon the nature and geometry of the material walls surrounding the discharge, it is possible for some of this scattered energy to reach the receiving antenna. If the microwave wavelength is comparable to the discharge diameter, diffraction and surface waves around the discharge are also possible. These effects introduce errors in both phase and amplitude of the resultant signal at the receiving antenna. The amplitude measurement is generally much more vulnerable to these effects. Thus, although in principle it is possible to infer temperature from the attenuation measurement (taken together with the phase-shift/density measurement), in practice the experimental uncer-

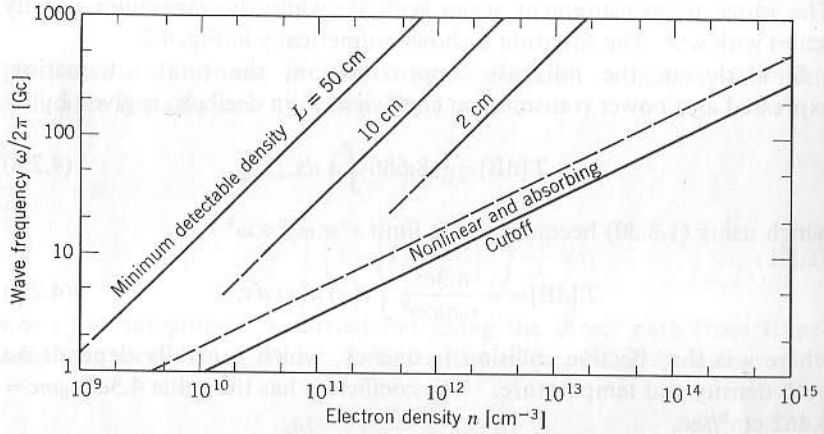

FIG. 4.2 Range of measurable electron density in pathlength L using adiabatic phase-shift analysis. The term "nonlinear," as used here, means that the phase shift is not directly proportional to average density. The minimum detectable densities assume a phase resolution of $\pi/10 = 18°$; other sensitivities can be scaled by (4.2.6).

tainties may be overwhelmingly large. In the presence of a magnetostatic field, the problems introduced by a bounded microwave beam and plasma also include the fact that, strictly speaking, we cannot everywhere achieve the simple parallel-polarization case which does not couple to the magnetic field. Spurious effects can then occur when $\omega_b \sim \omega$.

4.2.2 ***Adiabatic measurement of density profile.*** It is clear that in order to evaluate an electron density distribution from "free-space" phase-shift measurements we must know or assume two of the following three parameters.

(*1*) The shape function or *profile* for the density distribution along the transmission path (for example, rectangular, trapezoidal, cosinusoidal, etc.).

(*2*) The index of width (thickness) of this shape function.

(*3*) The numerical density coefficient of the shape function.

In the first-order binomial expansion, given above, we must assume from other considerations a characteristic thickness of the plasma; we then obtain a legitimate average electron density over this thickness. If,

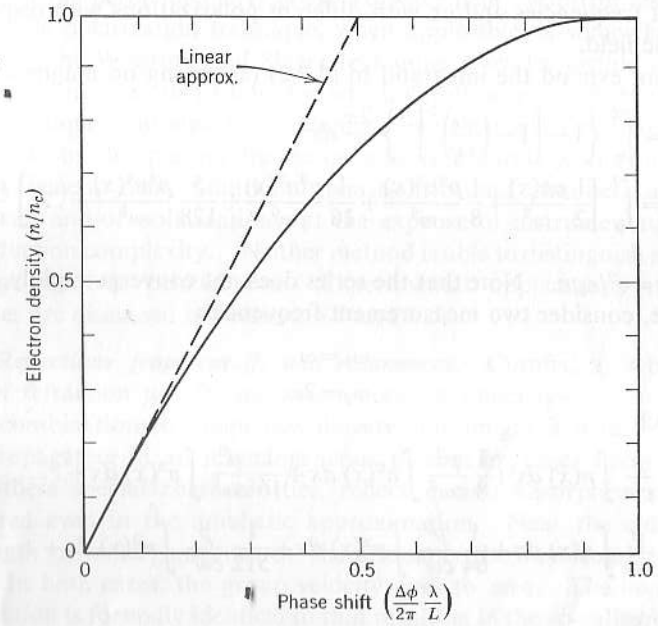

FIG. 4.3 Universal density/phase-shift curve for uniform density. See Fig. 6.20 for phase-shift curves for several spatial distributions.

however, we do not restrict our consideration to this first-order case, but still retain the adiabatic approximation, we can (*1*) expand the $\Delta\phi$ integrand to higher orders, in which case the integrals obtained are higher-order averages of the distribution function (for example, $\int n^2(x)\,dx$); or (*2*) integrate $\Delta\phi$ directly using an appropriate distribution function.

In either case, a meaningful average electron density is not obtained without an independent knowledge of the distribution function, since the phase shift is not linear with density, and the method becomes less useful for the quantitative measurement of even average densities. If, for example, we assume a constant electron density (that is, a rectangular profile which, incidentally, is somewhat contradictory to the adiabatic assumption), the integration is trivial, and we obtain a parabolic dependence of density on phase shift

$$\frac{n}{n_c}=2\left(\frac{\lambda}{L}\frac{\Delta\phi}{2\pi}\right)-\left(\frac{\lambda}{L}\frac{\Delta\phi}{2\pi}\right)^2. \tag{4.2.10}$$

Figure 4.3 is a universal graph of this relation.

Since the phase shift introduced by the plasma sample is, in general, a nonlinear function of electron density, we obtain information on the distribution of density (profile) by making simultaneous measurements at different frequencies and/or with different polarizations with respect to a magnetic field.

We can expand the integrand in (4.2.2) (assuming no magnetic field),

$$\begin{aligned}\Delta\phi&=\int_0^L\left\{1-\left[1-\left(\frac{\omega_p}{\omega}\right)^2\right]^{1/2}\right\}\frac{2\pi}{\lambda}\,dx\\&=\int_0^L\left[\frac{1}{2}\frac{pn(x)}{\omega^2}+\frac{1}{8}\frac{p^2n^2(x)}{\omega^4}+\frac{1}{16}\frac{p^3n^3(x)}{\omega^6}+\frac{5}{128}\frac{p^4n^4(x)}{\omega^8}+\dots\right]\frac{\omega}{c}\,dx,\end{aligned} \tag{4.2.11}$$

where $p=e^2/\epsilon_0 m$. Note that the series does not converge rapidly. As an example, consider two measurement frequencies

$$\omega_1=\omega$$
$$\omega_2=2\omega,$$

for which

$$\begin{aligned}\Delta\phi_1&=\frac{1}{2}\frac{p}{c\omega}\int n(x)\,dx+\frac{1}{8}\frac{p^2}{c\omega^3}\int n^2(x)\,dx+\frac{1}{16}\frac{p^3}{c\omega^5}\int n^3(x)\,dx+\dots,\\\Delta\phi_2&=\frac{1}{4}\frac{p}{c\omega}\int n(x)\,dx+\frac{1}{64}\frac{p^2}{c\omega^3}\int n^2(x)\,dx+\frac{1}{512}\frac{p}{c\omega^5}\int n^3(x)\,dx+\dots.\end{aligned} \tag{4.2.12}$$

Therefore

$$\Delta\phi_1-2\,\Delta\phi_2=\frac{3}{32}\frac{p^2}{c\omega^3}\int n^2(x)\,dx+\frac{15}{256}\frac{p^3}{c\omega^5}\int n^3(x)\,dx+\dots \tag{4.2.13}$$

and we obtain for the first two averages of the distribution

$$\frac{p}{c\omega}\int n\,dx=4\left\{\left[\Delta\phi_2-\frac{1}{6}(\Delta\phi_1-2\,\Delta\phi_2)\right]+\frac{1}{128}\frac{p^3}{c\omega^5}\int n^3\,dx+\dots\right\} \tag{4.2.14}$$

$$\frac{p^2}{c\omega^3}\int n^2\,dx=\frac{32}{3}\left\{(\Delta\phi_1-2\,\Delta\phi_2)-\frac{15}{256}\frac{p^3}{c\omega^5}\int n^3\,dx-\dots\right\}. \tag{4.2.15}$$

The usefulness of this approach is limited by the accuracy of the differential measurement $\Delta\phi_1-2\,\Delta\phi_2$. When this quantity can be successfully measured, (4.2.14) provides a refined evaluation of the average density and (4.2.15) an estimate of the mean-square density.

Procedures for obtaining profile information have been developed by Motley and Heald (1959) and by Wharton and Slager (1960). Wharton and Slager use only the magnetic-field-independent parallel-polarization case. Their data-reduction procedure is to calibrate the *peak* electron density by means of the cutoff of a "low-frequency" wave, and obtain information from the simultaneously observed phase shift of a "high-frequency" wave. Motley and Heald, using different polarizations, calibrate the *average* density with the high-frequency wave, infer profile from the low-frequency wave. Because of the greater phase-shift nonlinearity of the perpendicularly polarized wave near cyclotron resonance, the multiple polarization technique, when applicable, is somewhat more sensitive. The Wharton and Slager technique provides profile information only at the instants of time for which cutoff occurs; the Motley and Heald technique is limited to situations where the cyclotron frequency is comparable to the plasma frequency and is accurately known. Both methods benefit from additional phase-shift data channels at other frequencies and/or polarizations, at the expense of instrumentation and data-reduction complexity. Neither method is able to distinguish a hollow discharge from a peaked one. Experimental applications of these principles are discussed in Sections 6.4 and 6.5.

4.2.3 ***Reflections from cutoffs and resonances.*** Cutoffs, at which the index of refraction $\mu\to 0$, and resonances, at which $\mu\to\infty$, occur for certain combinations of frequency, density, and magnetic field. When a wave propagating in an inhomogeneous plasma impinges upon regions having these special characteristics, reflection and absorption must be considered even in the adiabatic approximation. Near the cutoff, the wavelength grows large, while near the resonance the wavelength becomes small. In both cases, the group velocity goes to zero. The analysis of this situation is formally identical to that resulting in the so-called turning-point connection formulas of the quantum-mechanical WKB approximation (Schiff, 1955). It can be shown that in the case of a *cutoff* the wave is

reflected from the anomalous region with little dissipation (Denisov, 1958; Stix, 1960). The external behavior is thus very similar to that of a sharply bounded, high-density ($n > n_c$) plasma. In the case of a *resonance*, however, the wave is largely *absorbed*. This distinction is of considerable significance for both reflection-type microwave probing measurements

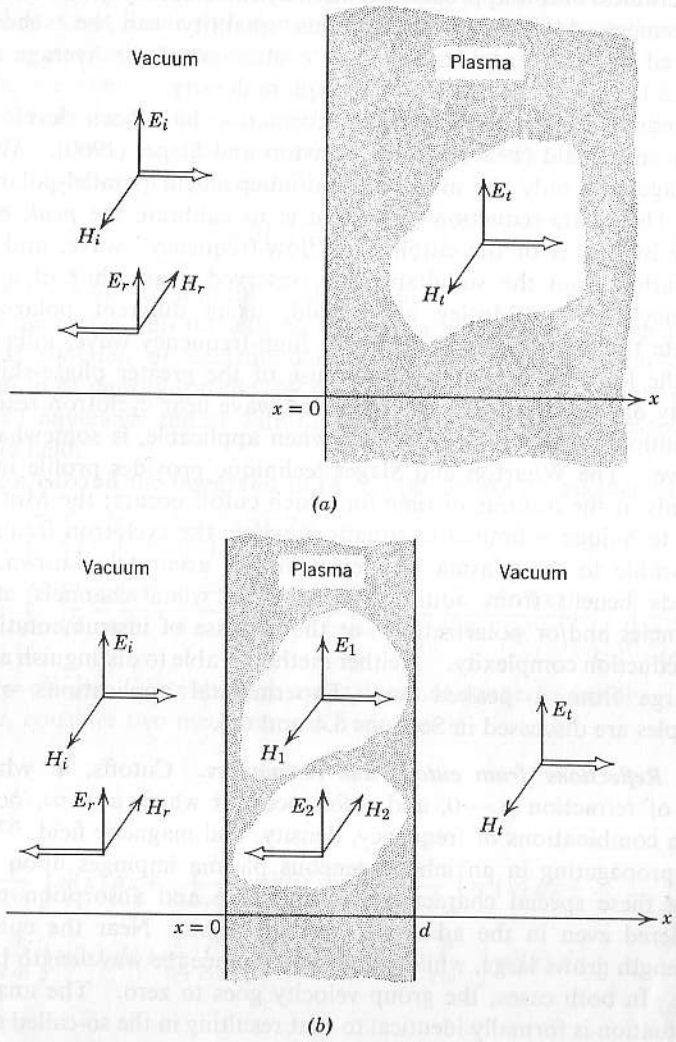

FIG. 4.4 Reflection and transmission at sharp boundaries. (*a*) Vacuum-plasma interface. (*b*) Plasma slab.

and thermal radiation measurements, as well as for the nondiagnostic question of plasma heating by electromagnetic radiation.

It will be noted from the graphs of Chapter 1 that, in general, for a given magnetic field, cutoff occurs at a lower density than the resonance. Thus, characteristically, waves entering the plasma from outside are reflected before reaching the resonance. The resonance may, in some cases, be made accessible by allowing the wave to enter the plasma in a region of high magnetic field (generally such that the cyclotron frequency $\omega_b > \omega$) which then decreases spatially within the plasma, so that the resonance is approached from the high-field side. In Section 6.5.4 an experiment using this technique is described. A situation of this sort has been exploited in the "magnetic beach" geometry for the dissipation of ion-cyclotron waves (Stix, 1958). If the regions of cutoff and resonance are close together within the plasma, relative to a wavelength, it may be possible for a sort of "tunnel effect" to occur in which the resonance region extracts energy from the evanescent wave passing through the cutoff. Tunneling or "bridging" may also take place by mode conversion processes (Ratcliffe, 1959, Chapter 17). Stix (1960, 1962) has shown that at a resonance high-temperature and ion-mass effects may reduce absorption, increase reflection, and excite other plasma modes.

4.3 The slab with sharp boundaries

We again consider the interaction of a plane wave with a slab plasma. However, in contrast with the adiabatic case of Section 4.2, we now assume a homogeneous plasma with sharp boundaries, that is, the transition between vacuum and uniform plasma occurs over a distance much less than a wavelength. There exists a well-defined reflection coefficient at each interface, and reflection and transmission coefficients are determined by boundary conditions on the wave fields at the interfaces.

Consider first the single interface of Fig. 4.4*a*. Waves traveling to the right are represented by the phase factor $\exp(j\omega t - \check{\gamma}x)$, and waves to the left, by $\exp(j\omega t + \check{\gamma}x)$ where $\check{\gamma} = \alpha + j\beta = (j\omega/c)\check{\kappa}^{1/2}$ is the complex propagation constant. In the case of a plasma, the complex dielectric constant $\check{\kappa}$, and hence $\check{\gamma}$, are known functions of electron density, collision frequency, magnetic field, etc., as developed in Chapter 1. In accordance with Maxwell's equations, the magnitudes of the electric and magnetic wave fields are related by the wave impedance

$$\check{\eta} = \frac{E}{H} = \left(\frac{\mu_0}{\check{\kappa}\epsilon_0}\right)^{1/2}, \tag{4.3.1}$$

with respective polarizations as shown in the figure. The wave impedance $\check{\eta}$ is, in general, complex on account of $\check{\kappa}$. Since the waves are transverse

and there are no surface currents at the interface, the boundary conditions require that E and H are continuous across the interface. Therefore the wave amplitudes, in the notation of Fig. 4.4*a*, are related by

$$\begin{aligned} E_i+E_r&=E_t \\ E_i-E_r&=\check{\kappa}^{1/2}E_t. \end{aligned} \tag{4.3.2}$$

It follows that the (complex) *amplitude* reflection and transmission coefficients are, respectively,

$$\begin{aligned} \check{\rho}&=\frac{E_r}{E_i}=\frac{1-\check{\kappa}^{1/2}}{1+\check{\kappa}^{1/2}}=\frac{\check{\eta}-\eta_0}{\check{\eta}+\eta_0}, \\ \check{\tau}&=\frac{E_t}{E_i}=\frac{2}{1+\check{\kappa}^{1/2}}=\frac{2\check{\eta}}{\check{\eta}+\eta_0} \end{aligned} \tag{4.3.3}$$

where $\eta_0=377$ ohms is the wave impedance of free space. Note the significance of the wave impedance that there is no reflection when the impedances of the two media are equal.[2]

The single-interface *power* reflection and transmission coefficients are, respectively,

$$\begin{aligned} r&=|\check{\rho}|^2=\frac{(1-\mu)^2+\chi^2}{(1+\mu)^2+\chi^2}, \\ t&=1-r=\mu|\check{\tau}|^2=\frac{4\mu}{(1+\mu)^2+\chi^2} \end{aligned} \tag{4.3.4}$$

where $\mu-j\chi=\check{\kappa}^{1/2}=-j\check{\gamma}c/\omega$, and the voltage standing-wave ratio is[3]

$$\mathrm{VSWR}=\frac{1+|\check{\rho}|}{1-|\check{\rho}|}=\frac{1+r^{1/2}}{1-r^{1/2}}. \tag{4.3.5}$$

[2] In a more general (nonplasma) case with the relative permeability κ_m different from unity and perhaps also complex, then $\eta=(\kappa_m\mu_0/\kappa\epsilon_0)^{1/2}$. Reflection at the interface between two media is suppressed so long as the ratio κ_m/κ is the same for both media, even though κ and κ_m themselves change by large factors. This effect is exploited in the design of microwave-absorbing wall coatings in which both κ and κ_m have imaginary (lossy) components (see Chapter 10).

[3] When the imaginary component of κ is negligible, the $\mathrm{VSWR}=1/\kappa^{1/2}=1/\mu=\eta/\eta_0$. The positive sense of polarization of the reflected wave has been chosen arbitrarily for the case $\kappa<1$. If $\kappa>1$, the sense of E_r is reversed and $\mathrm{VSWR}=\kappa^{1/2}=\mu=\eta_0/\eta$. We note, in passing, a convenient procedure for calculating the maximum transmission loss due to reflection. From standard transmission-line theory the maximum VSWR from two discontinuities is the product of the respective VSWR's (and the minimum, the quotient). Thus, the maximum transmission loss due to reflection from a slab can be obtained from standard charts assuming a single discontinuity with

$$\mathrm{VSWR}=\begin{cases} 1/\mu^2 & \mu<1 \\ \mu^2 & \mu>1. \end{cases}$$

This procedure applies only if there is no dissipative loss between discontinuities.

The situation of practical interest is that of the slab of Fig. 4.4*b*. By setting up boundary conditions similar to (4.3.2) at the two interfaces (or, alternatively, summing the infinite series of internally reflected waves), one finds (Stratton, 1941) the *amplitude* reflection and transmission coefficients

$$\check{\Gamma}=\frac{E_r}{E_i}=\frac{\check{\rho}[1-\exp(-2\check{\gamma}d)]}{1-\check{\rho}^2\exp(-2\check{\gamma}d)}, \tag{4.3.6}$$

$$\check{T}=\frac{E_t}{E_i}=\frac{(1-\check{\rho}^2)\exp[-(\check{\gamma}-j\omega/c)d]}{1-\check{\rho}^2\exp(-2\check{\gamma}d)}, \tag{4.3.7}$$

and the *power* reflection, transmission, and absorption coefficients are

$$R=\frac{r\{[1-\exp(-2\alpha d)]^2+4\exp(-2\alpha d)\sin^2(\beta d)\}}{[1-r\exp(-2\alpha d)]^2+4r\exp(-2\alpha d)\sin^2(\beta d-\psi)}, \tag{4.3.8}$$

$$T=\frac{[(1-r)^2+4r\sin^2\psi]\exp(-2\alpha d)}{[1-r\exp(-2\alpha d)]^2+4r\exp(-2\alpha d)\sin^2(\beta d-\psi)}, \tag{4.3.9}$$

$$A=1-R-T, \tag{4.3.10}$$

where ψ is the phase angle of $\check{\rho}=|\check{\rho}|\exp(j\psi)$ and

$$\begin{aligned} r^{1/2}\sin\psi&=\frac{2\chi}{(1+\mu)^2+\chi^2}, \\ r^{1/2}\cos\psi&=\frac{1-\mu^2-\chi^2}{(1+\mu)^2+\chi^2}. \end{aligned} \tag{4.3.11}$$

It is to be noted that the coefficients (4.3.8) to (4.3.10) are oscillatory functions of slab thickness d (or of frequency ω) as a result of interference of internally reflected waves. Likewise, the phase of the transmitted wave, which may be calculated from (4.3.7), is perturbed by interference. As a simplification, we may assume that the reflected waves are incoherent, thereby suppressing interference effects, and obtain[4]

[4] Interference is suppressed by considering only power relations. The fraction r of the incident wave is reflected at the first surface of the slab, the fraction $a(1-r)$ [where $a=\exp(-2\alpha d)$ is the one-way power loss through the slab] is transmitted to the second surface. Of this latter the fraction $a(1-r)^2$ escapes while the fraction $ar(1-r)$ is reflected back toward the first surface. Iteration of this analysis yields the series

$$\begin{aligned} R&=r+a^2r(1-r)^2(1+a^2r^2+a^4r^4+\ldots) \\ T&=a(1-r)^2(1+a^2r^2+a^4r^4+\ldots). \end{aligned}$$

Summation of these infinite series leads to (4.3.12) and (4.3.13).

$$R=\frac{r[1+(1-2r)\exp(-4\alpha d)]}{1-r^2\exp(-4\alpha d)}, \tag{4.3.12}$$

$$T=\frac{(1-r)^2\exp(-2\alpha d)}{1-r^2\exp(-4\alpha d)}, \tag{4.3.13}$$

$$A=\frac{(1-r)[1-\exp(-2\alpha d)]}{1-r\exp(-2\alpha d)}. \tag{4.3.14}$$

These latter relations are often useful for estimating average effects and become more realistic as $d\gg\lambda$. One may also be concerned with the case of oblique incidence, in which case the wave polarization becomes important (Graf and Bachynski, 1961).

Numerical calculations of (4.3.8) to (4.3.10) may readily be made as a function of plasma properties (French, Cloutier, and Bachynski, 1961). Figure 4.5 illustrates the case for a plasma four wavelengths thick. Figure 4.6 shows, for the same case, the phase error of the transmitted wave relative to the geometrical optics phase.

This sharp-boundary, homogeneous-plasma analysis can be extended to cylindrical geometry by expanding the incident and diffracted waves in terms of the normal-mode waves of the dielectric cylinder (Dawson and Oberman, 1959; Platzman and Ozaki, 1960). For electric-vector polarization perpendicular to a small plasma column, scattering resonances related to the plasma properties and geometry are found (Crawford et al., 1963). The finite size also modifies the frequency of longitudinal plasma oscillations (Branch and Mihan, 1955). Unless simplifying approximations can be made, numerical calculations for given experimental situations are usually difficult to carry out, even with electronic computers, since extensive summations over Bessel functions must be performed for each point. Calculation is especially difficult when the plasma diameter is not much larger than the wavelength, and when the receiving antenna is at a finite distance and subtends a nonzero angle at the plasma axis. The interaction of nearby antennas with sharp plasma boundaries, with resulting modification of reflection and transmission characteristics, has been studied in connection with precision interferometry (Kerns and Dayhoff, 1961) and with antenna matching (Redheffer, 1949).

4.4 Inhomogeneous plasmas

If the propagation properties of a plasma vary sufficiently slowly over a wavelength, the adiabatic analysis of Section 4.2 is applicable. However, this analysis explicitly excludes reflections and interference effects. At the other extreme, the case of a sharply bounded, homogeneous plasma may be solved by boundary-value methods, as outlined in Section 4.3. The treatment of the intermediate case between these two limits, especially

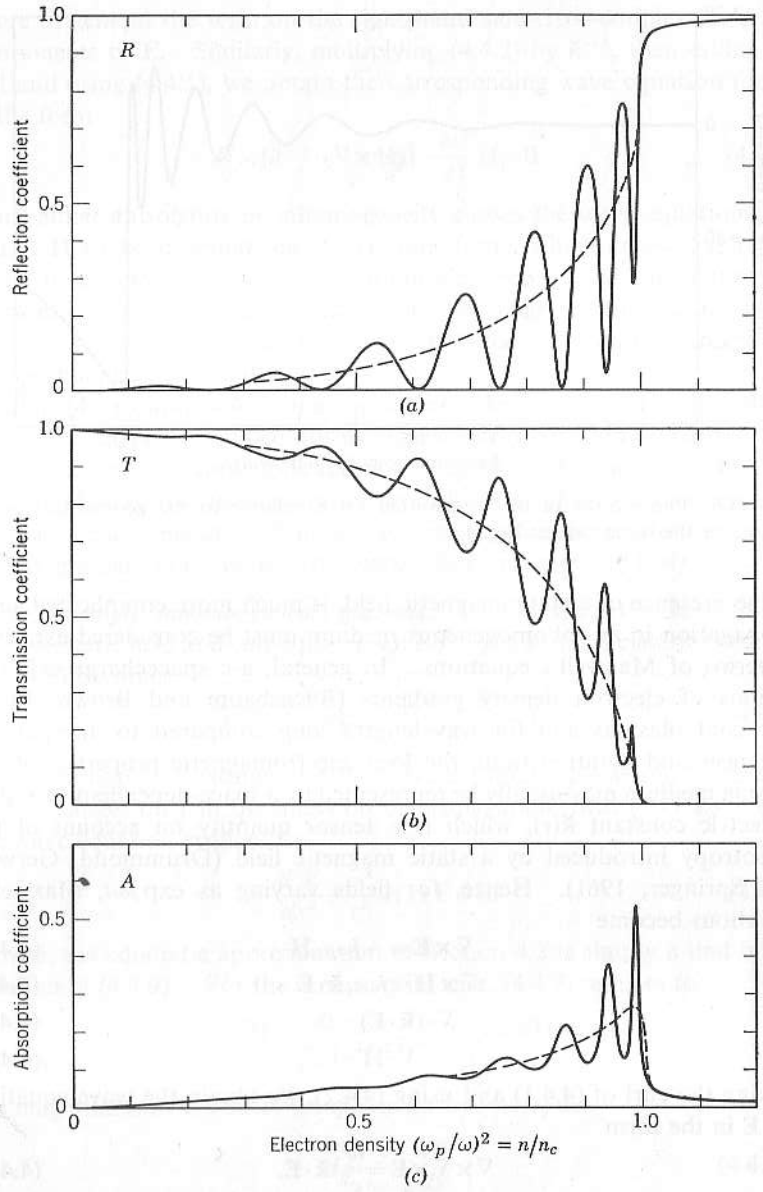

FIG. 4.5 Power reflection, transmission, and absorption coefficients, from (4.3.8) to (4.3.10), for a homogeneous slab plasma four wavelengths thick ($\nu/\omega=0.003$). The dashed curves assume incoherent internal reflections, from (4.3.12) to (4.3.14).

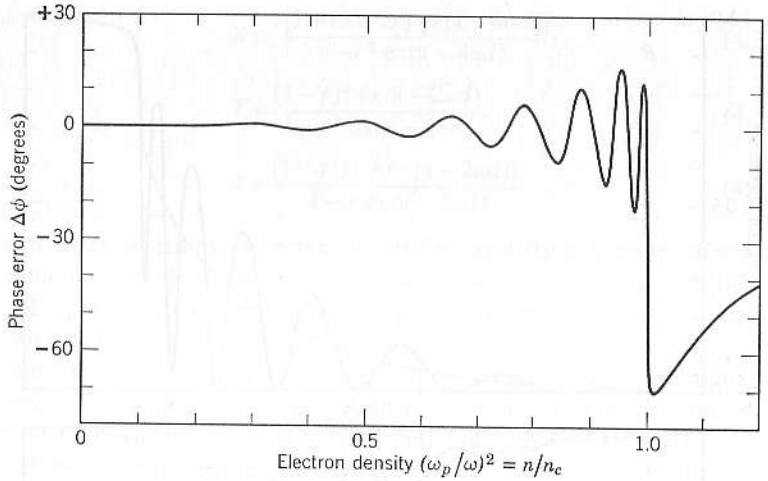

FIG. 4.6 Phase error of the transmitted wave, relative to the geometrical optics phase, for the same case as Fig. 4.5.

in the presence of a static magnetic field, is much more complicated since propagation in an inhomogeneous medium must be considered explicitly in terms of Maxwell's equations. In general, a-c spacecharge exists in regions of electron density gradients (Buchsbaum and Brown, 1957). For cold plasmas and for wavelengths long compared to interparticle distances and gyration radii, the local electromagnetic properties of the plasma medium may usually be represented by a space-dependent, complex dielectric constant $\check{\boldsymbol{\kappa}}(\mathbf{r})$, which is a tensor quantity on account of the anisotropy introduced by a static magnetic field (Drummond, Gerwin, and Springer, 1961). Hence, for fields varying as $\exp j\omega t$, Maxwell's equations become

$$\nabla\times\mathbf{E}=-j\omega\mu_0\mathbf{H} \tag{4.4.1}$$

$$\nabla\times\mathbf{H}=j\omega\epsilon_0\check{\boldsymbol{\kappa}}\cdot\mathbf{E} \tag{4.4.2}$$

$$\nabla\cdot(\check{\boldsymbol{\kappa}}\cdot\mathbf{E})=0 \tag{4.4.3}$$

$$\nabla\cdot\mathbf{H}=0. \tag{4.4.4}$$

Taking the curl of (4.4.1) and using (4.4.2), we obtain the wave equation for $\mathbf{E}$ in the form

$$\nabla\times\nabla\times\mathbf{E}=\frac{\omega^2}{c^2}\check{\boldsymbol{\kappa}}\cdot\mathbf{E}. \tag{4.4.5}$$

The vector identity $\nabla\times\nabla\times\mathbf{E}=\nabla(\nabla\cdot\mathbf{E})-\nabla^2\mathbf{E}$ allows us to rewrite the equation for $\mathbf{E}$ as

$$\nabla^2\mathbf{E}+\frac{\omega^2}{c^2}\check{\boldsymbol{\kappa}}\cdot\mathbf{E}=\nabla(\nabla\cdot\mathbf{E}), \tag{4.4.6}$$

where in general the term on the right-hand side cross-couples the three components of $\mathbf{E}$. Similarly, multiplying (4.4.2) by $\check{\boldsymbol{\kappa}}^{-1}$, then taking its curl and using (4.4.1), we obtain the corresponding wave equation for $\mathbf{H}$ in the form

$$\nabla\times[\check{\boldsymbol{\kappa}}^{-1}\cdot(\nabla\times\mathbf{H})]-\frac{\omega^2}{c^2}\mathbf{H}=0. \tag{4.4.7}$$

Thus, either anisotropy or inhomogeneity causes the wave equations for $\mathbf{E}$ and $\mathbf{H}$ to be different and to contain terms which cross-couple the scalar field components. In the nonhomogeneous case, the difference arises physically from the fact that the wave impedance (that is, the ratio of E to H) changes even when the Poynting vector (the product of E and H) is approximately constant.

From (4.4.6) and (4.4.7) one can deduce the nature of initially plane waves for various assumed forms of dielectric constant, directions of inhomogeneity, and directions and polarizations of the waves (Bachynski, 1960). The results are summarized in Table 4.1. For instance, even in the absence of a magnetic field, a wave propagating perpendicular to the density gradient is no longer transverse electromagnetic (TEM).

4.4.1 ***Isotropic inhomogeneous plasmas.*** In the special case with no magnetostatic field and consequently an isotropic, scalar dielectric constant $\check{\kappa}$, (4.4.6) becomes

$$\nabla^2\mathbf{E}+\frac{\omega^2}{c^2}\check{\kappa}\mathbf{E}+\nabla\left[\frac{(\nabla\check{\kappa})\cdot\mathbf{E}}{\check{\kappa}}\right]=0. \tag{4.4.8}$$

If, furthermore, we assume that the wave is initially plane and transverse and $\check{\kappa}$ changes only in the direction of propagation, then $(\nabla\check{\kappa})\cdot\mathbf{E}=0$ and the wave equation reduces to

$$\frac{d^2\mathbf{E}}{dx^2}+\frac{\omega^2}{c^2}\check{\kappa}(x)\,\mathbf{E}=0. \tag{4.4.9}$$

Indeed, the adiabatic approximation of Section 4.2 is simply a first-order solution of (4.4.9). For the same special case, (4.4.7) reduces to

$$\frac{d^2\mathbf{H}}{dx^2}+\frac{\omega^2}{c^2}\check{\kappa}(x)\,\mathbf{H}=\frac{1}{\check{\kappa}(x)}\frac{d\check{\kappa}}{dx}\frac{d\mathbf{H}}{dx}, \tag{4.4.10}$$

the magnitudes of $\mathbf{E}$ and $\mathbf{H}$ being related by (4.4.1) as

$$H=\frac{j}{\omega\mu_0}\frac{dE}{dx}. \tag{4.4.11}$$

If an *effective* propagation constant $\check{\gamma}(x)$ is defined such that (Osterberg, 1958)

$$\check{\gamma}(x)=-\frac{1}{E}\frac{dE}{dx}, \tag{4.4.12}$$

then (4.4.9) requires that $\check{\gamma}$ satisfy the Riccati differential equation[5]

$$-\frac{d\check{\gamma}}{dx}+\check{\gamma}^2+\frac{\omega^2}{c^2}\,\check{\kappa}(x)=0. \tag{4.4.13}$$

[5] In a homogeneous medium (4.4.13) gives the familiar result $\gamma=\pm j\kappa^{1/2}\omega/c$. The condition for the validity of the adiabatic approximation is then seen to be

$$\left|\frac{d\gamma}{dx}\right|\approx\frac{\omega}{2c}\,\frac{1}{\kappa^{1/2}}\,\frac{d\kappa}{dx}\ll\frac{\omega^2}{c^2}\,\kappa,$$

or

$$\frac{1}{\kappa}\,\frac{d\kappa}{dx}\ll\frac{2\omega}{c}\,\kappa^{1/2}\approx\frac{4\pi}{\lambda}$$

where λ is the local wavelength in the medium. That is, the relative change in κ over a wavelength must be small compared to 4π. The same condition is obtained from (4.4.17).

TABLE 4.1 EFFECT OF INHOMOGENEITY AND ANISOTROPY ON PROPAGATION OF PLANE ELECTROMAGNETIC WAVES (Bachynski, 1960)

Type of medium	Direction of inhomogeneity	Wave type*		
		O	*X*	*L*, *R*
Uniform isotropic $\boldsymbol{\kappa}^{-1}=e$	None	TEM	TEM	TEM
Uniform anisotropic $\boldsymbol{\kappa}^{-1}=\begin{pmatrix} e_\perp & e_\times & 0 \\ -e_\times & e_\perp & 0 \\ 0 & 0 & e_\parallel \end{pmatrix}$	None	TEM	TM	TEM
Inhomogeneous isotropic $\boldsymbol{\kappa}^{-1}=e(\mathbf{r})$	Along initial γ	TEM	TEM	TEM
	Along initial E	TM	TM	TM
	Along initial H	TE	TE	TE
Inhomogeneous anisotropic $\boldsymbol{\kappa}^{-1}=\begin{pmatrix} e_\perp(\mathbf{r}) & e_\times(\mathbf{r}) & 0 \\ -e_\times(\mathbf{r}) & e_\perp(\mathbf{r}) & 0 \\ 0 & 0 & e_\parallel(\mathbf{r}) \end{pmatrix}$	Along initial γ	TEM	TM	TEM
	Along initial E	NT	TM	NT
	Along initial H	TE	NT	NT

* *O*=ordinary, *X*=extraordinary (propagation across field); *L*, *R*=left/right-hand (propagation along field); TEM=transverse electromagnetic; TE=transverse electric; TM=transverse magnetic; NT=nontransverse; the propagation coefficient γ is in direction of wave normal.

If (4.4.13) can be solved for $\check{\gamma}(x)$, the wave propagation is given by

$$E(x)=E(0)\exp\left[-\int_0^x\check{\gamma}(x)\,dx\right]. \tag{4.4.14}$$

In general, (4.4.13) yields two solutions for $\check{\gamma}$, corresponding physically to waves traveling in both directions. In fact, where $\check{\kappa}$ is pure real, one solution is the complex conjugate of the other. Reflection and transmission coefficients are obtained by matching boundary conditions in a manner analogous to the uniform slab problem of Section 4.3. For the simple model of a linear variation in electron density, for instance, (4.4.9)

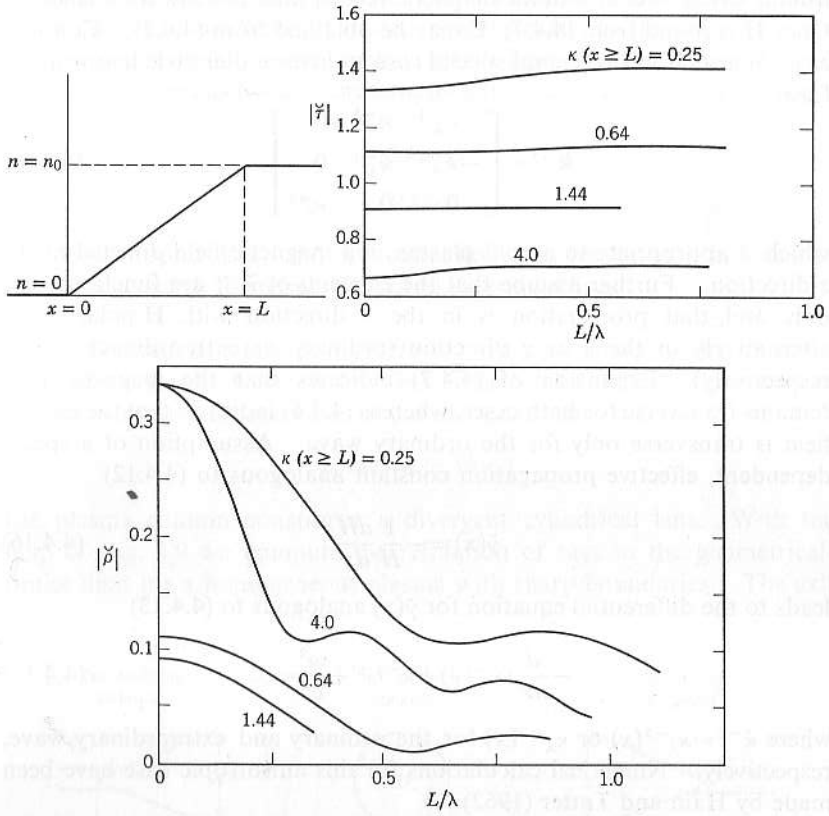

FIG. 4.7 Amplitude reflection and transmission coefficients for a linear-ramp variation of electron density n, as a function of ramp length L for real dielectric constants of the form $\kappa=1-n/n_c$; λ is free-space wavelength. (Reproduced from Albini and Jahn, 1961, by courtesy of the *Journal of Applied Physics*.)

may be solved directly in terms of Airy functions and computations made for linear ramp or trapesoidal profiles (Albini and Jahn, 1961; Wort, 1962). Figure 4.7 illustrates the dependence of reflection coefficient on ramp length and dielectric constant. Numerical calculations for other simple profiles have been made by Taylor (1961), Klein et al. (1961), and Hain and Tutter (1962). Interference effects, arising between reflections from the two sides of an inhomogeneous slab appear to be much more pronounced in the amplitude and phase of the reflected wave than for the transmitted wave. A somewhat similar problem has been considered in connection with tapered waveguides (Johnson, 1959).

4.4.2 ***Anisotropic inhomogeneous plasmas.*** In more general cases it is usually easier to deal with the magnetic vector, since it is always solenoidal. Once **H** is found from (4.4.7), **E** may be obtained from (4.4.2). Consider as a somewhat more general special case an inverse dielectric tensor in the form

$$\check{\boldsymbol{\kappa}}^{-1}=\begin{bmatrix} \kappa_\perp^{-1} & \kappa_\times^{-1} & 0 \\ -\kappa_\times^{-1} & \kappa_\perp^{-1} & 0 \\ 0 & 0 & \kappa_\parallel^{-1} \end{bmatrix}, \tag{4.4.15}$$

which is appropriate to a cold plasma in a magnetic field directed in the z direction. Further assume that the elements of $\check{\boldsymbol{\kappa}}^{-1}$ are functions of x only and that propagation is in the x direction with **H**-polarization alternatively in the y or z direction (ordinary or extraordinary waves, respectively). Expansion of (4.4.7) indicates that the magnetic field remains transverse for both cases, whereas (4.4.6) indicates that the electric field is transverse only for the ordinary wave. Assumption of a space-dependent, effective propagation constant analogous to (4.4.12)

$$\check{\gamma}(x)=-\frac{1}{H}\frac{dH}{dx}, \tag{4.4.16}$$

leads to the differential equation for $\check{\gamma}(x)$ analogous to (4.4.13)

$$-\frac{d}{dx}(\check{\kappa}^{-1}\check{\gamma})+\check{\kappa}^{-1}\check{\gamma}^2+\frac{\omega^2}{c^2}=0, \tag{4.4.17}$$

where $\check{\kappa}^{-1}=\kappa_\parallel^{-1}(x)$ or $\kappa_\perp^{-1}(x)$ for the ordinary and extraordinary wave, respectively. Numerical calculations for this anisotropic case have been made by Hain and Tutter (1962).

The problem of an inhomogeneous cylindrical plasma is again more complex, since the wave equation must be dealt with in cylindrical coordinates. With a plane wave incident upon a cylindrical plasma, it is possible in principle to calculate the phase and amplitude of the scattered

wave as a function of scattering angle (King and Wu, 1959). Since these quantities are readily measurable as a function of angle, the inverse problem of deducing the profile from scattering data provides an interesting technique for measuring plasma profiles (Shmoys, 1961; Kerker and Matijević, 1961).

4.5 The geometrical optics of a uniform cylindrical plasma column

A very approximate but useful model of common laboratory plasmas assumes a homogeneous cylindrical plasma several free-space wavelengths (of the probing microwave) in diameter, and yet neglects reflections at the boundary—the geometrical optics limit. The basic parameters of this geometry are defined in Fig. 4.8. The problem is assumed two-dimensional, the elements being of infinite extent normal to the paper. If the plasma is distant by at least a wavelength from the antenna, induction effects can be neglected and the situation treated as a radiation problem. If

$$A/\lambda \gg 1$$
$$D/\lambda \gg 1,$$

geometrical optics is a valid approximation, and we can talk in terms of rays which, except for refraction, travel in straight lines.

4.5.1 ***Transmission loss by refraction.*** We now consider the effect of refraction (Heald, 1959a; Wort, 1963). Since the index of refraction of the plasma (no magnetic field, or parallel polarization) is

$$\mu=(1-n/n_c)^{1/2}<1$$

the plasma column constitutes a divergent cylindrical lens. With the help of Fig. 4.9 we compute the refraction of rays in the geometrical-optics limit for a homogeneous plasma with sharp boundaries. The exit

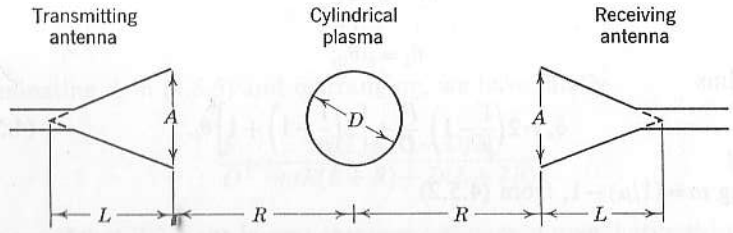

FIG. 4.8 Microwave beam geometry for a cylindrical plasma.

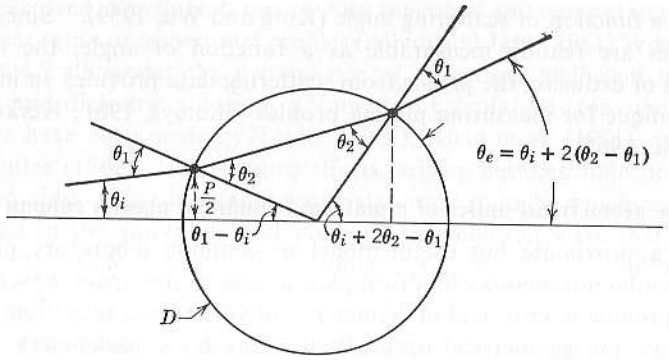

FIG. 4.9 Cylindrical refraction.

angle θ_e is given in terms of the incident angle θ_i and the entrance ordinate $P/2$ by the following simultaneous equations:

$$\theta_e = \theta_i + 2(\theta_2 - \theta_1)$$

$$\sin(\theta_1 - \theta_i) = \frac{P}{D}$$

$$\sin\theta_1 = \mu \sin\theta_2 \tag{4.5.1}$$

If now the exit ray is to strike the edge of the receiving aperture, at cartesian coordinates $(R, A/2)$ with respect to the center of the cylinder cross section, we have the following condition on θ_i and $P/2$ for the most divergent ray accepted by the receiving aperture,

$$\tan\theta_e = \frac{A - D\sin(\theta_i + 2\theta_2 - \theta_1)}{2R - D\cos(\theta_i + 2\theta_2 - \theta_1)}. \tag{4.5.2}$$

In many cases of practical interest it is reasonable to make small angle approximations. We obtain from (4.5.1)

$$\theta_1 - \theta_i = \frac{P}{D}$$

$$\theta_1 = \mu\theta_2,$$

and thus

$$\theta_e = 2\left(\frac{1}{\mu} - 1\right)\frac{P}{D} + \left[2\left(\frac{1}{\mu} - 1\right) + 1\right]\theta_i. \tag{4.5.3}$$

Setting $m = (1/\mu) - 1$, from (4.5.2)

$$(2R - D)\left[2m\frac{P}{D} + (2m+1)\theta_i\right] = A - D\left[(2m+1)\frac{P}{D} + 2(m+1)\theta_i\right]. \tag{4.5.4}$$

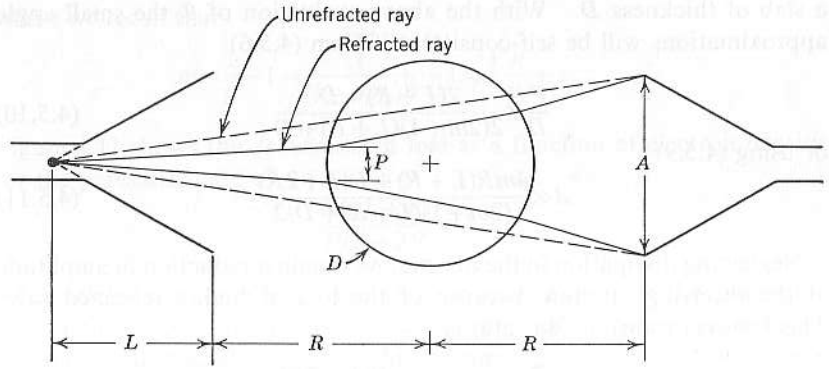

FIG. 4.10 Effect of refraction in geometrical optics approximation.

Solving for P/D, we have

$$\frac{P}{D} = \frac{A - [2(2m+1)R + D]\theta_i}{4mR + D}. \tag{4.5.5}$$

For $\mu < 1$ the largest angle involved is $(\theta_i + 2\theta_2 - \theta_1)$, and the small angle approximation is self-consistent for

$$(2m+1)\frac{P}{D} + 2(m+1)\theta_i \ll 1$$

or

$$\frac{P}{D} \ll \frac{1 - 2(m+1)\theta_i}{2m+1}. \tag{4.5.6}$$

In the geometrical optics limit, with a point source at $-(L+R)$, we have from Fig. 4.10

$$\sin\theta_i = \frac{P}{2(L+R) - D\cos(\theta_1 - \theta_i)} \tag{4.5.7}$$

or for small angles

$$\theta_i = \frac{P}{2(L+R) - D}. \tag{4.5.8}$$

Eliminating θ_i in (4.5.5) and rearranging, we have finally

$$\frac{P}{D} = \frac{A[(L+R) - D/2]}{4mR(L+R) + D(L+2R)}. \tag{4.5.9}$$

We recall that $P/2$ is the largest entrance ordinate of rays that pass into the receiving aperture. Therefore, when $P/D \ll 1$ the cylinder is equivalent to

a slab of thickness D. With the above evaluation of θ_i the small angle approximations will be self-consistent if from (4.5.6)

$$\frac{P}{D} \ll \frac{2(L+R)-D}{2(2m+1)(L+R)+D} \tag{4.5.10}$$

or using (4.5.9)

$$A \ll \frac{4mR(L+R)+D(L+2R)}{(2m+1)(L+R)+D/2}. \tag{4.5.11}$$

Neglecting dissipation in the plasma, we obtain a reduction in amplitude at the receiving aperture because of the loss of highly refracted rays. This (power) transmission ratio is

$$T=\frac{P}{P(\mu=1)}=\frac{D(L+2R)}{4mR(L+R)+D(L+2R)} \tag{4.5.12}$$

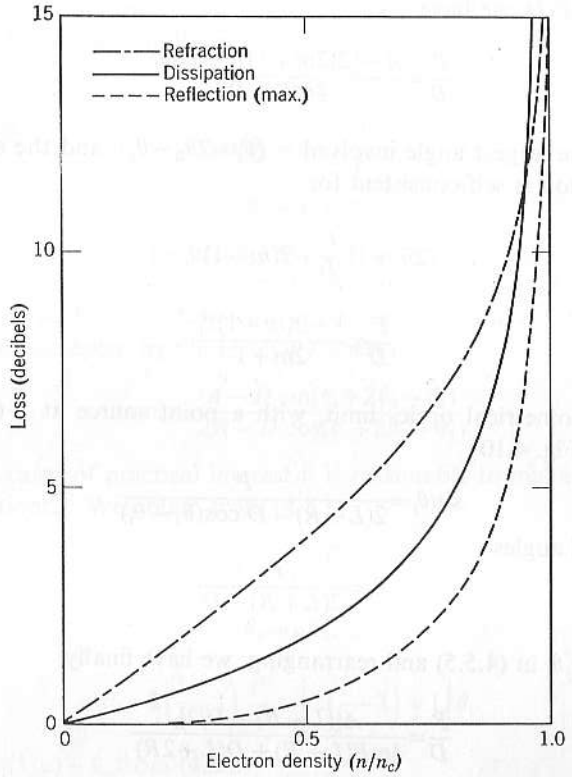

FIG. 4.11 Loss of transmitted amplitude from refraction $4R(L+R)/D(L+2R)=3.6$, dissipation $\nu D/\omega\lambda=0.1$, and reflection.

where we recall that

$$m=\frac{1}{\mu}-1=\frac{1}{(1-n/n_c)^{1/2}}-1\approx\frac{1}{2}\frac{n}{n_c}+\ldots$$

Figure 4.11 shows this transmission loss as a function of electron density for the particular case of

$$\frac{4R(L+R)}{D(L+2R)}=3.6.$$

4.5.2 ***Other sources of loss.*** For comparison, we compute the dissipative loss in the plasma due to collisions. From (1.3.30), for $n<n_c$ and low dissipation (that is, $\nu^2\ll\omega_p{}^2<\omega^2$), this transmission loss is given in decibels by

$$T[\text{dB}]=-8.686\,\alpha D=-\pi(8.686)\frac{n/n_c}{(1-n/n_c)^{1/2}}\frac{\nu D}{2\pi c}, \tag{4.5.13}$$

for rays passing near the center of the plasma. Figure 4.11 shows this relation for the numerical case

$$\frac{\nu D}{2\pi c}=\frac{\nu}{\omega}\frac{D}{\lambda}=0.1.$$

For the numerical cases chosen, the refraction loss dominates except very close to the critical density.

Finally, we consider the question of interference effects due to reflections at the sharp plasma–vacuum interfaces. In the usual case of $P/D\ll1$ the only rays received are those which pass near the center of the plasma, and we can regard the plasma as a slab of thickness D. For the case of lossless slabs, the transmission ratio (4.3.9) becomes

$$T=\frac{1}{1+\left(\frac{1-\mu^2}{2\mu}\right)^2\sin^2\left(\frac{2\pi\mu D}{\lambda}\right)} \tag{4.5.14}$$

which varies between

$$\left(\frac{2\mu}{1+\mu^2}\right)^2<T<1$$

as the relative phasing of the reflections changes. This maximum transmission loss is also shown in Fig. 4.11.

4.6 The antenna problem

The observed interaction of an electromagnetic wave with a plasma of finite size necessarily implies a "beamed" wave of finite extent and thus depends upon the antenna system used to radiate and receive the wave (Beard et al., 1962). The plane-wave model, which has been tacitly

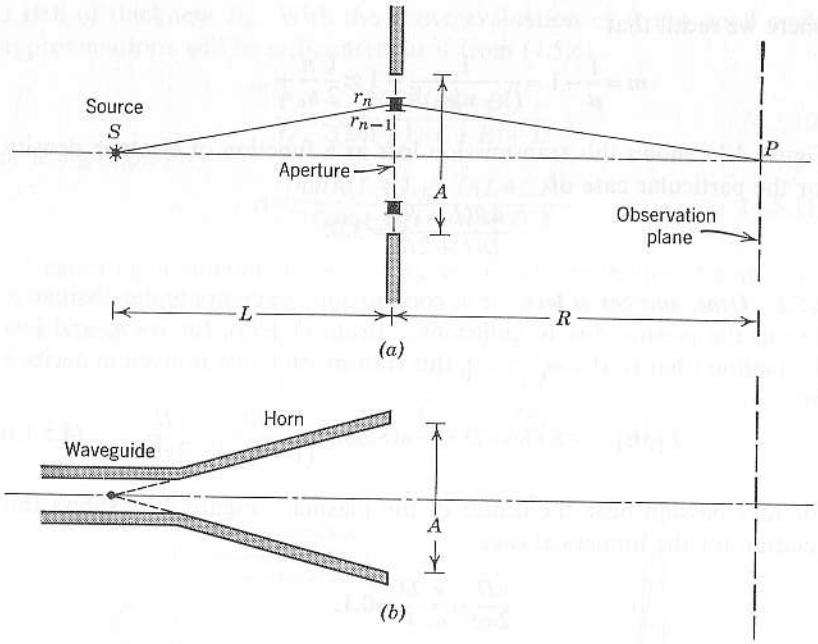

FIG. 4.12 Geometry of the physical optics of (*a*) an aperture, and (*b*) a microwave horn antenna.

assumed in the preceding discussion, is a mathematical idealization which oversimplifies the practical situation, especially when the wavelength is not much smaller than the plasma sample. Therefore, it is useful to review some of the basic principles of diffraction.

4.6.1 ***Fresnel zones.*** Consider a circular aperture, of diameter A, in an opaque screen illuminated with waves from a point S at a distance L to the left, as in Fig. 4.12*a*. We wish to investigate the nature of the radiation field in the vicinity of an observation point P on the axis a distance R to the right. In accordance with elementary Huygens-Kirchhoff-Fresnel diffraction theory, we may divide up the wave front in the aperture into *Fresnel half-period zones*, such that the radiation passing from S to P travels an additional half wavelength for each zone (Andrews, 1960). Specifically, the nth zone is a circular strip, the radius r_n of the outer edge of which is defined such that

$$(L^2+r_n^2)^{1/2}+(R^2+r_n^2)^{1/2}=L+R+n\frac{\lambda}{2}. \tag{4.6.1}$$

Setting $r_n=A/2$ and assuming $A\ll L$ and R, (4.6.1) may be expanded binomially to obtain

$$n=\frac{A^2}{4\lambda}\left(\frac{1}{L}+\frac{1}{R}\right). \tag{4.6.2}$$

If the aperture is uniformly illuminated, the contributions of adjacent zones are out of phase and of approximately equal amplitude and, thus, tend to cancel. Insight into the intensity distribution at various observation points (not necessarily on the axis) may be obtained by investigating the number of zones and the fractional area of each zone exposed by the aperture. For instance (Fig. 4.13), the intensity at P on the axis is a maximum for an aperture exposing 1, 3, 5, . . . zones, and a minimum for 2, 4, 6, . . . zones. The intensity at a point off the axis is small if roughly equal areas of odd and even numbered zones are exposed.

To a first approximation the radiation pattern of a horn antenna, of diameter A as in Fig. 4.12*b*, may be described by this analysis (Silver, 1949). We are here interested in only a qualitative description and, therefore, will not be concerned with the modifications required by a rectangular rather than circular aperture, by the polarization of an electromagnetic (transverse) wave, and by nonuniformity of illumination of the horn aperture. However, in passing, it may be noted that for the rectangular aperture with waveguide feed the diffraction field depends upon two factors each of which depends, in turn, on only one of the aperture dimensions—that is, the two dimensions are uncoupled (Schelkunoff and Friis, 1952, Chapter 16). We take A to represent the dimension controlling the radiation pattern of interest (for example, in the plane perpendicular to the axis of a cylindrical plasma as in Fig. 4.10), and

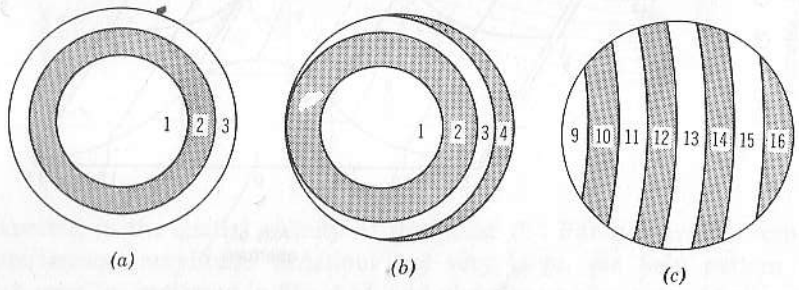

FIG. 4.13 Fresnel zones in a circular aperture; (*a*) on axis, (*b*) slightly off axis, and (*c*) far off axis (enlarged scale). (See also Fig. 9.26.)

ignore the other dimension. Furthermore, we shall assume $L \gg R$ so that L drops out of the analysis and (4.6.2) becomes[6]

$$n = A^2/4\lambda R. \tag{4.6.3}$$

Types of antennas other than horns may also be described in similar terms by suitably choosing an effective aperture dimension A.

If A, R, and λ are such that the number n of exposed Fresnel zones is in the range of one to ten, then strong interference fluctuations are to be

[6] Conversely, it may be noted that the criterion for "optimum" horn design—that is, the choice of A to maximize the gain for a fixed length L—is effectively $n \approx 1$ for $R \gg L$ (Schelkunoff and Friis, 1952).

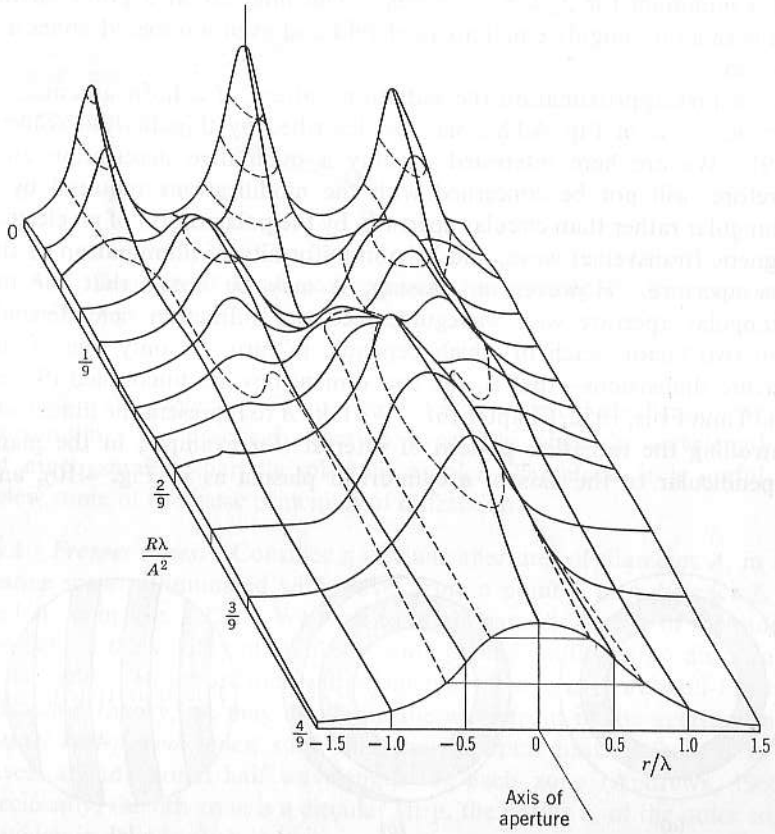

FIG. 4.14 H-plane intensity pattern in the field of a circular aperture, three wavelengths in diameter. (Reproduced from Andrews, 1947, by courtesy of *The Physical Review*.)

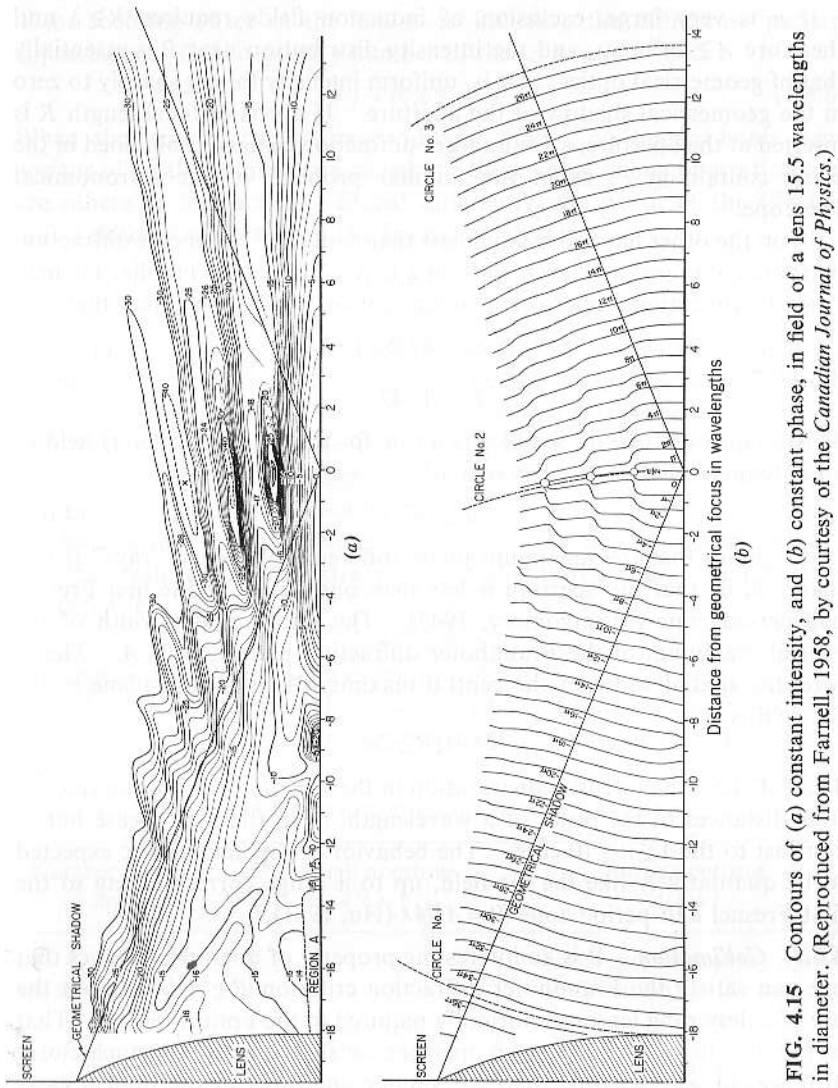

FIG. 4.15 Contours of (*a*) constant intensity, and (*b*) constant phase, in field of a lens 15.5 wavelengths in diameter. (Reproduced from Farnell, 1958, by courtesy of the *Canadian Journal of Physics*.)

expected in the spatial vicinity of the point P. For low-order Fresnel interference, amplitude variations are very large, the field pattern is "choppy" as indicated in Fig. 4.14, and phase anomalies occur (Andrews, 1947, 1950; Linfoot and Wolf, 1956). A further example is shown in Fig. 4.15 (Farnell, 1958).

If n is very large, exclusion of induction fields requires $R \gtrsim \lambda$ and therefore $A \gtrsim 2n^{1/2}\lambda \gg \lambda$, and the intensity distribution near P is essentially that of geometrical optics; that is, uniform intensity falling sharply to zero in the geometrical shadow of the aperture. If a lens of focal length R is inserted at the aperture, a Fraunhofer diffraction pattern is obtained in the plane containing P, as in the familiar problem of the astronomical telescope.

If, on the other hand, n is much less than unity, a Fraunhofer diffraction pattern is obtained at P even without a lens. This is the familiar far-field case of conventional microwave antenna theory. To the extent that

$$n \approx A^2/4\lambda R \ll 1,$$

we have

$$R \gg A^2/4\lambda.$$

This is equivalent to the well-known rule for the far (Fraunhofer) field of an antenna, which is usually written[7]

$$R \gtrsim A^2/\lambda \tag{4.6.4}$$

and signifies that the maximum phase differential between "rays" is less than $\lambda/8$, or that the aperture is less than one-fourth of the first Fresnel half-period zone (Montgomery, 1947). The total angular width of the central maximum of the Fraunhofer diffraction pattern is $2\lambda/A$. Therefore, the spatial width of the central maximum falling on a plane in the far field is

$$(2\lambda/A)R \gtrsim 2A.$$

Thus, if $A \gg \lambda$ the intensity distribution in the vicinity of P is quite smooth over distances of the order of a wavelength, as in the high n case but in contrast to the $1 \lesssim n \lesssim 10$ case. The behavior of the field can be expected to be qualitatively like the far field, up to a range corresponding to the first Fresnel half-period zone $R = A^2/4\lambda$ (Hu, 1961).

4.6.2 ***Collimation.*** It is an interesting property of microwave optics that one can satisfy the Fraunhofer diffraction criterion $R \gtrsim A^2/\lambda$ without the use of collimating lenses as normally required in the optical region. That is, the "far field" of a radiation aperture, or an obstacle, is a much closer distance, in wavelengths, than for similar apertures in the optical case. Therefore, in many situations, far-field theory can be used to describe the microwave field. Meanwhile, the use of lenses becomes less powerful since the focal length F of the lens must be

$$F \lesssim A^2/\lambda \tag{4.6.5}$$

[7] Some antenna engineers use the criterion $R \gtrsim 2A^2/\lambda$, corresponding to $\lambda/16$ or one-eighth zone. Amplitude errors due to interference are then about 2% as opposed to 5% for the criterion given above.

if the focusing effect of the lens is to influence the diffraction pattern appreciably. The so-called f number of the lens is then

$$f = F/A \lesssim A/\lambda. \tag{4.6.6}$$

When the geometrical optics condition $A/\lambda \gg 1$ no longer holds, lens designs of small f number are called for; these show strong aberration and are otherwise impractical. Stated differently, the width of the (Fraunhofer) diffraction pattern at the focus of a lens is

$$(2\lambda/A)F = 2f\lambda \tag{4.6.7}$$

with $f \gtrsim 1$ for practical lenses.

The far-field region can be effectively extended somewhat closer to the antenna aperture by using a lens to partially overcome the diffraction spreading (Sherman, 1962). The angular half-width of the central maximum of the Fraunhofer diffraction pattern is λ/A. In geometrical optics a ray leaving the edge of an aperture of width A at this angle appears to originate at a point located a distance $A^2/2\lambda$ on the source side of the aperture, and therefore the insertion of a lens of focal length $F = A^2/2\lambda$ will render this extreme ray parallel to the axis. The f number of such a lens is

$$f = A/2\lambda, \tag{4.6.8}$$

agreeing closely with the upper limit of (4.6.6).

Table 4.2 summarizes the characteristics of the radiation field for various regimes of the parameters. The best collimation ($\sim\lambda$) is obtained

TABLE 4.2 FIELD PATTERNS AND COLLIMATION OF ANTENNAS

Number of zones in aperture	Small aperture $A/\lambda \sim 1$	Large aperture $A/\lambda \gg 1$
$n \gg 10$	Induction field region	Normal geometrical ray optics (collimation $\sim A$ without lens; $\sim\lambda$ with lens)
$1 < n \lesssim 10$		Fresnel interference, "choppy" intensity distribution (collimation $\sim A$)
$n < 1$	Fraunhofer diffraction radiation pattern (collimation $2\lambda R/A \gtrsim A$)	

in the $A/\lambda \sim 1$, $n < 1$ case (antenna far field) and the $A/\lambda \gg 1$, $n \gg 10$ case with lens (geometrical optics). The latter, however, is a strongly

converging wave passing through a focus. It appears best to design the experiment so as to avoid the low-order region ($1 \lesssim n \lesssim 10$). If the number of Fresnel zones is either very large or small throughout the space occupied by plasma and receiving antenna, then the illumination will be fairly uniform and the phase fronts well-behaved.

4.6.3 ***Optimization of antennas.*** Let us assume that we are given the diameter D of a cylindrical plasma column and the wavelength λ with which we are to probe it. We further assume that λ, determined by the electron density range to be measured and perhaps the availability of short-wavelength instrumentation, is small compared to D but by no means negligible. Since we wish to obtain a reasonable average of the electron density independent of refraction (and diffraction) by the plasma, we wish to achieve maximum collimation of the microwave beam so that it effectively passes along a diameter. We have seen from a geometrical optics point of view that when $\mu < 1$ the divergent lens action improves the effective collimation by refracting nondiametric rays out of the receiving aperture. However, because of the danger of reflection from such extraneous obstacles as the vacuum system walls, and because of the desire to conserve feeble millimeter-wave power, we wish to maximize the power in received diametric rays and minimize it in nonreceived and/or non-diametric rays. That is, we wish to minimize the insertion loss between antennas while ensuring that most of the radiation passes close to the axis of the plasma (Heald, 1959a).

The most clear-cut situation is when $D \gg A \gg \lambda$, which conforms closely to infinite-slab, geometrical-optics conditions. However, our interest is in the case where perhaps $1 \lesssim D/\lambda \lesssim 10$. If $A > D$, appreciable energy passes around the plasma, reducing sensitivity and severely complicating interpretation. With $D \gtrsim A \gtrsim \lambda$, in order to avoid induction field effects and Fresnel-zone interference effects, we must have the plasma located in the far (Fraunhofer) field of the antennas, $R \gtrsim A^2/\lambda$.

It is a well-known rule of antenna engineering that for a pair of antennas to be located in the far-field region, by the usual A^2/λ criterion, the minimum insertion loss is of the order of 16dB (Montgomery, 1947). Since only about two per cent of the radiated power is received, the probability of interference from spurious reflected signals is high. We are, therefore, interested in pushing as close to the near field (Fresnel zone number $n \sim 1$) as possible without encountering severe amplitude and phase disturbances from interference. This leads to the alternative of small (nondirective) antennas relatively close to the plasma or large (directive) antennas farther back.

The concentration of rf energy produced in the field of a horn antenna depends upon two factors: the width of the wavepacket launched, and the angle of spread of the wave. Empirical plots of intensity contours in the field of millimeter horn antennas indicate that one half of the energy is confined within a beam width

$$W = \left[\left(\frac{aA}{2}\right)^2 + \left(\frac{b\lambda R}{A}\right)^2\right]^{1/2} \tag{4.6.9}$$

where a and b are correction factors depending on geometry and aperture illumination and departing only slightly from unity. For a given λ and R, this is minimized when

$$A = \left(\frac{2b}{a}\,\lambda R\right)^{1/2} \tag{4.6.10}$$

giving

$$R = \frac{a}{2b}\frac{A^2}{\lambda}$$

$$W_{min} = (ab\lambda R)^{1/2}. \tag{4.6.11}$$

This condition corresponds to an aperture of about one half a Fresnel half-period zone at R. The insertion loss between two such antennas spaced $2R$ apart is about 8dB, depending upon the other dimension of the antenna aperture. Sometimes mechanical constraints of the apparatus will prescribe R, in which case A is determined by (4.6.10). If both A and R are at the experimenter's disposal, it is necessary to consider the role of the diameter D of the plasma column. The relative beam size W/D varies as $R^{1/2}/D$, whereas the relative spreading of the field over the plasma

$$\frac{D}{W}\left(\frac{\partial W}{\partial R}\right)_{W_{min}}$$

varies as D/R. Since we wish $W \ll D \ll R$, we arbitrarily take

$$D = (W_{min}R)^{1/2} = (ab\lambda R^3)^{1/4}. \tag{4.6.12}$$

Recapitulating, given D and λ and assuming $a = b = 1$, we choose

$$R = \left(\frac{D}{\lambda}\right)^{1/3} D$$

$$A = (2\lambda R)^{1/2} = \sqrt{2}\left(\frac{\lambda}{D}\right)^{1/3} D. \tag{4.6.13}$$

This heuristic argument is founded on the vague assumption that there is some virtue in minimizing the beam width at the plasma by choice of A and then compromising in the choice of R such that

$$\frac{D}{W_{min}} = \frac{R}{D}.$$

The effect is to prescribe a situation in which the plasma is located slightly

inside the conventional far-field boundary. We have seen, however, that under these conditions diffraction anomalies should not be very severe. Note that when $D/\lambda \gg 1$, $R \ll D^2/\lambda$ and, therefore, the plasma approximates an infinite slab as far as diffraction is concerned. By reciprocity and symmetry arguments, we conclude that transmitting and receiving antennas should be identical.

The preceding discussion has been based on the assumption of simple horn antennas without lenses. It has also assumed a "long" horn ($L \gtrsim A^2/\lambda$) and $L \gtrsim 2R$, which may be impractical. Thus, two uses for lenses emerge: (*1*) to permit a less-than-long horn, in accord with conventional practice; and (*2*) to focus the beam or at least over-collimate to compensate partially for diffraction. If a horn is "long," its far-field ($R > A^2/\lambda$) pattern cannot be appreciably narrowed by addition of a lens. However, in the previous section we have discussed the use of a lens to focus the energy at a distance $R \lesssim A^2/\lambda$. The suggestion has been made to use converging lenses focused at the plasma axis (Boyd, 1959). This is chiefly based upon the geometrical-optics argument that all rays pass diametrically through the plasma, thereby removing the refraction and sampling difficulties of the "plane-wave" approach. If $A/\lambda \gg 1$ so that a good focus can be obtained, and if this focus ($\sim\lambda$) is small relative to the plasma, $D/\lambda \gg 1$—that is, a good geometrical optics situation—this procedure has merits (Papoular and Wegrowe, 1961). However, in this case, the relative rf field strength becomes very high in the vicinity of the focus, so that nonlinearities in the rf properties of the plasma may be troublesome. If, on the other hand, $D/\lambda \sim 1$, the so-called Gouy phase anomalies in the vicinity of the focus (Fig. 4.15) could severely complicate the interpretation (Linfoot and Wolf, 1956; Bekefi, 1957; and Farnell, 1958). In this case, it appears that if lenses are to be used they should be focused at the opposite antenna or beyond (Christian and Goubau, 1961). Further discussion of the practice of using lenses can be found in Sections 6.4 and 9.3.

Because of the perturbation that thick dielectric windows (glass, mica, quartz, etc.) make on the field of a millimeter-wave antenna (Redheffer, 1949), it is often useful to locate the vacuum seal at a convenient point back in the waveguide so that the antennas are wholly within the vacuum system. Such window design follows standard practice as used in microwave tube output windows and waveguide pressurizing windows; examples are given in Section 9.6. Alternatively, care must be taken to provide matching structures at the vacuum walls (Jahn, 1962).

4.6.4 ***Validity of the geometrical-optics, slab model.*** Since the geometrical-optics, plane-slab model is particularly convenient to analyze,

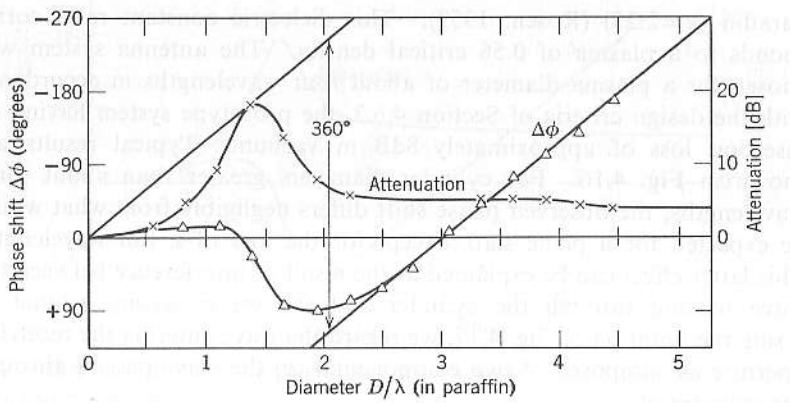

FIG. 4.16 Phase shift and attenuation as a function of cylinder diameter in paraffin analog experiment (Rosen, 1949). Wave E-field parallel to cylinder axis. Dimensions normalized to wavelength in the medium of the antennas: H-plane aperture of horn 3.1; E-plane aperture 2.6; axial length of horn (to apex) 6.8; horn separation 13.4. Measurement frequency 35 Gc.

it is of interest to investigate the validity of this model for the more practical case of a cylindrical plasma. In addition, since the nearness of the antennas, as well as of extraneous objects such as vacuum system walls, severely complicates theoretical analysis, it is often most effective to perform an analog experiment (Warder, Brodwin, and Cambel, 1962; Iams, 1950; and Lashinsky, 1963).

A plasma, with dielectric constant less than unity, can be simulated by cutting holes in a large block of low-loss dielectric, in which a scaled antenna system is imbedded. In one such experiment the phase shift and insertion loss were measured for various size cylindrical holes cut in

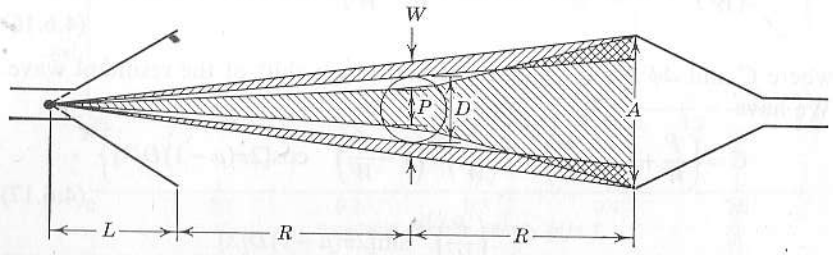

FIG. 4.17 Propagation through a dielectric cylinder, small compared to effective microwave beam.

paraffin ($\kappa=2.25$) (Rosen, 1959). This dielectric constant ratio corresponds to a plasma of 0.56 critical density. The antenna system was chosen for a plasma diameter of about four wavelengths in accordance with the design criteria of Section 4.6.3, the prototype system having an insertion loss of approximately 8dB in vacuum. Typical results are shown in Fig. 4.16. For cylinder diameters greater than about three wavelengths, the observed phase shift differs negligibly from what would be expected for a plane slab, except for the loss of a full wavelength. This latter effect can be explained as the result of interference between the wave passing through the cylinder and the wave passing around it. Using the notation of Fig. 4.17, we regard the wave entering the receiving aperture as composed of two components: (*a*) the wave passing through the cylinder of

amplitude	$(P/W)^{1/2}$
phase	$2\pi(\mu-1)D/\lambda$

(neglecting internal interference effects), where $\mu<1$ is the refractive index of the cylinder (air) relative to the paraffin, and λ is the wavelength in the paraffin; and (*b*) the unperturbed wave passing around the cylinder of

amplitude	$(1-D/W)^{1/2}$
phase	0.

W is the effective beam width at the plasma,

$$W=\frac{L+R}{L+2R}A; \tag{4.6.14}$$

and from (4.5.9)

$$\frac{P}{D}\approx\frac{A[(L+R)-D/2]}{4\left(\frac{1}{\mu}-1\right)R(L+R)+D(L+2R)}. \tag{4.6.15}$$

The resultant wave is then

$$\left(\frac{P}{W}\right)^{1/2}\exp[j2\pi(\mu-1)D/\lambda]+\left(1-\frac{D}{W}\right)^{1/2}\exp(j0)\equiv C\exp(j\Delta\phi) \tag{4.6.16}$$

where C and $\Delta\phi$ are the amplitude and phase shift of the resultant wave. We have

$$C=\left\{\frac{P}{W}+\left(1-\frac{D}{W}\right)+2\left(\frac{P}{W}\right)^{1/2}\left(1-\frac{D}{W}\right)^{1/2}\cos[2\pi(\mu-1)D/\lambda]\right\}^{1/2}, \tag{4.6.17}$$

$$\Delta\phi=\tan^{-1}\frac{\left(\frac{P}{W}\right)^{1/2}\sin[2\pi(\mu-1)D/\lambda]}{\left(\frac{P}{W}\right)^{1/2}\cos[2\pi(\mu-1)D/\lambda]+\left(1-\frac{D}{W}\right)^{1/2}}. \tag{4.6.18}$$

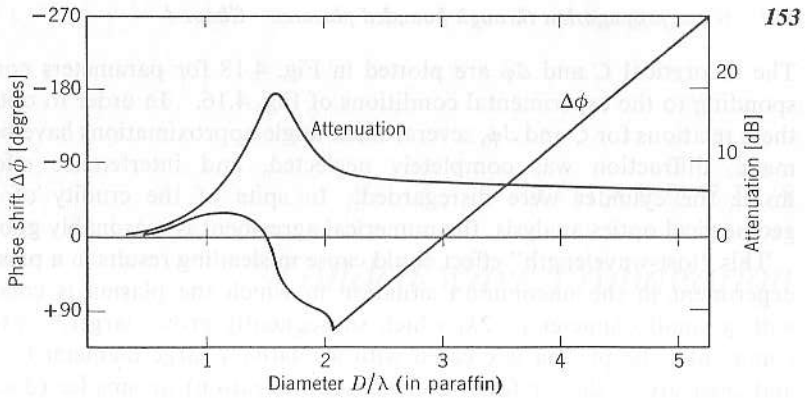

FIG. 4.18 Results of simple geometrical optics theory for the conditions of Fig. 4.16, exhibiting "loss" of 360°.

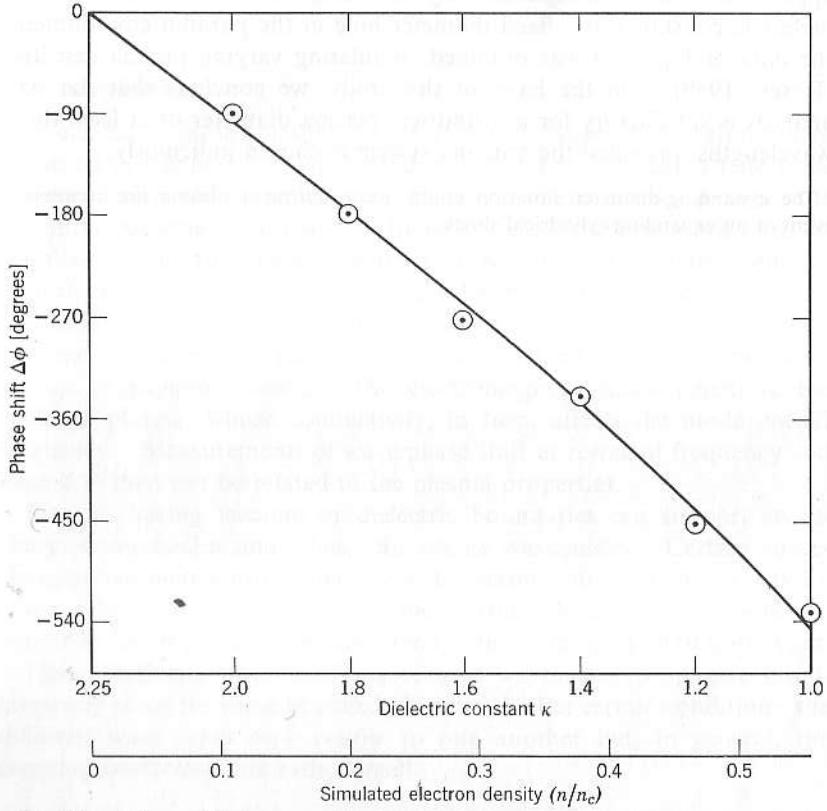

FIG. 4.19 Phase shift as a function of dielectric constant of cylinder in paraffin-analog experiment, simulating plasma of varying density. Cylinder diameter 4.6 wavelengths.

The theoretical C and $\Delta\phi$ are plotted in Fig. 4.18 for parameters corresponding to the experimental conditions of Fig. 4.16. In order to obtain these relations for C and $\Delta\phi$, several small-angle approximations have been made, diffraction was completely neglected, and interference effects inside the cylinder were disregarded. In spite of the crudity of the geometrical optics analysis, the numerical agreement is reasonably good.

This "lost-wavelength" effect could cause misleading results in a plasma experiment in the uncommon situation in which the plasma is created with a small diameter ($<2\lambda$) which subsequently grows larger.[8] More commonly, the plasma is created with a relatively large diameter ($>3\lambda$) and then grows denser (due to increased ionization) or smaller (due to some form of magnetic compression). In these cases, the transition from the vacuum (no plasma) phase-shift condition, as the plasma develops, appears to be unambiguous. By inserting rods of various known dielectric constants in a fixed diameter hole in the paraffin environment, the data of Fig. 4.19 was obtained, simulating varying plasma densities (Rosen, 1959). On the basis of this study, we conclude that the slab analysis is satisfactory for a cylindrical plasma diameter of at least three wavelengths, provided the antenna system is chosen judiciously.

[8] The expanding-diameter situation could occur during a plasma decompression event or an expanding cylindrical shock.

CHAPTER 5

Guided wave propagation

5.0 Introduction

The effects of finite plasma dimensions on wave propagation were discussed in Chapter 4. The boundaries were found to cause reflections and refraction of transmitted waves and, in some cases, to affect the radiation patterns of antennas. In most cases, the boundaries led to problems, rather than being beneficial to the propagation experiments.

In the present chapter, we discuss another class of bounded plasmas; in this case, boundaries are essential to the wave propagation. Resonant cavities and waveguides have metallic walls that carry currents and, thus, set up propagation modes. The electromagnetic fields penetrate the enclosed plasma, whose conductivity, in turn, affects the mode cut-off frequency. Measurements of wave phase shift or resonant frequency and loaded Q then can be related to the plasma properties.

Plasmas having vacuum or dielectric boundaries can support space-charge-wave modes and, thus, can act as waveguides. Certain space-charge-wave modes propagate along the plasma surface (surface waves), while others are carried within the plasma (body waves). When a magnetic field is present, the waves tend to be a combination of both types.

Electromagnetic waves and spacecharge waves may propagate simultaneously along the same bounded plasma. Under certain conditions, the different wave types may couple to one another but, in general, the coupling coefficients are rather small.

5.1 Measurements on plasmas contained in resonant cavities

The resonance properties of a cavity containing a lossy dielectric can be stated in terms of Q

$$Q=\frac{\omega_0\ (\text{energy stored})}{\text{average power loss}}=\frac{2\pi\ (\text{energy stored})}{\text{energy lost per cycle}}. \tag{5.1.1}$$

The stored energy is calculated from a volume integral of the fields contained in the cavity; the power is dissipated in both the wall losses and the dielectric losses.

When the lossy dielectric filling the cavity is a dilute plasma, of complex conductivity σ, the change in Q and the shift in resonance frequency due to introducing the plasma are given by a perturbation equation (Slater, 1946)

$$\left(\frac{1}{Q_1}-\frac{1}{Q_0}\right)-2j\frac{\Delta\omega}{\omega_0}=\frac{1}{\epsilon_0\omega_0}\frac{\int_V \sigma(r)E^2(r)\,dV}{\int_V E^2(r)\,dV} \tag{5.1.2}$$

where the 0 subscript represents unperturbed values and the 1 subscript the perturbed conditions, that is, with plasma present. The intrinsic or unloaded Q, Q_U, is not measurable, however, since we must couple to the cavity through some kind of impedance.

The equivalent coupling circuit, representing effects of the coupling orifice or loop, the wall losses, dielectric losses, and coupling line or

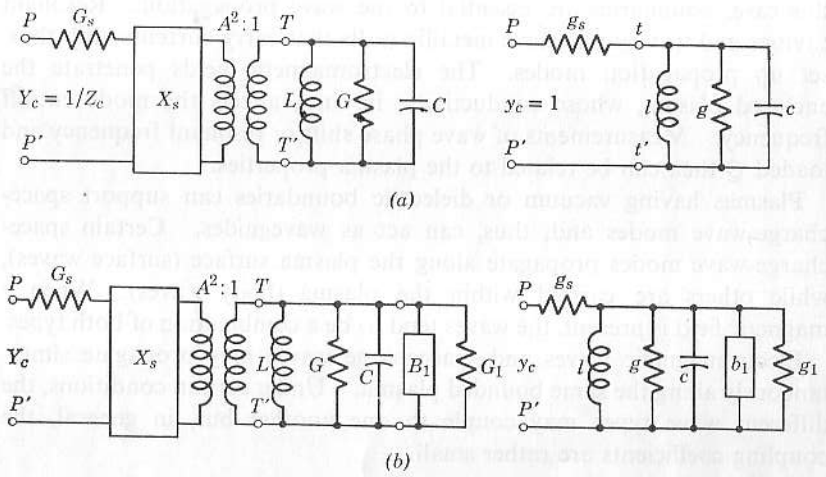

FIG. 5.1 (*a*) Equivalent circuits for an empty resonant cavity, and (*b*) one containing a plasma. The subscript 1 denotes plasma parameters. Other symbols are defined in the text.

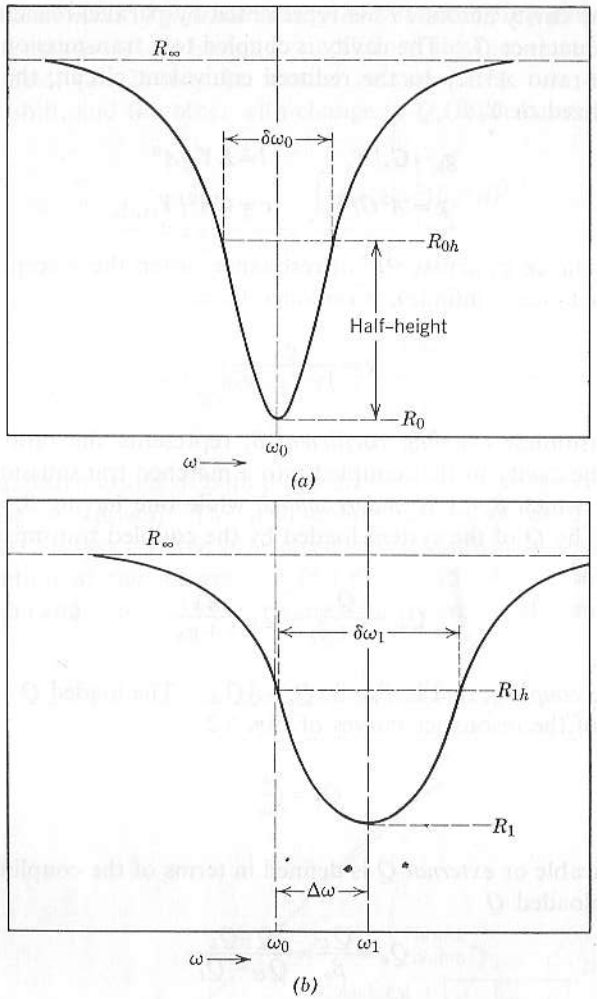

FIG. 5.2 Standing-wave ratios, expressed in decibel format, in the feed line for (*a*) an empty and (*b*) a plasma-filled resonant cavity in the vicinity of resonance, showing detuning. Symbols are defined in the text. Subscript 1 denotes plasma conditions.

waveguide losses, is sketched in Fig. 5.1. The reflection coefficients are shown in Fig. 5.2. Y_c is the matched *characteristic transmission line admittance* at PP' (Ramo and Whinnery, 1953). The network X_s represents the coupling reactance, and G_s the coupling losses. X_s is generally negligible and, in the remainder of the analysis, will be omitted (Slater,

1946). The cavity across TT' is represented by parallel reactances L and C and conductance G. The cavity is coupled to a transmission line by an admittance ratio A^2:1. In the reduced equivalent circuit, the quantities are normalized to Y_c:

$$\begin{aligned} g_s &= G_s/Y_c \qquad l = LY_c/A^2 \\ g &= A^2G/Y_c \qquad c = CA^2/Y_c. \end{aligned} \tag{5.1.3}$$

The conductance g_0 across PP' at resonance, when the susceptance of l-c is zero (reactance is infinite), is obtained from

$$g = \frac{g_0}{1-(g_0/g_s)}. \tag{5.1.4}$$

The dimensionless *coupling coefficient* β_c represents the ratio of energy stored in the cavity to that coupled into a matched transmission line. A system for which $\beta_c < 1$ is *undercoupled*, while one having $\beta_c > 1$ is *overcoupled*. The Q of the system loaded by the coupled transmission line is the *loaded* Q

$$Q_L = \frac{Q_U}{1+\beta_c} = Q_U \frac{g_0}{1+g_0}. \tag{5.1.5}$$

For *critical coupling*, that is, $\beta_c = 1$, $Q_L = \frac{1}{2}Q_U$. The loaded Q is related to the width of the resonance curves of Fig. 5.2

$$Q_L = \frac{\omega}{\delta\omega}. \tag{5.1.6}$$

The measurable or *external* Q is defined in terms of the coupling factor β_c and the unloaded Q

$$Q_e = \frac{Q_U}{\beta_c} = \frac{Q_U Q_L}{Q_U - Q_L}. \tag{5.1.7}$$

5.1.1 ***Measurement of plasma admittance.*** The effects of the plasma on the cavity resonance properties are conveniently determined by observing the complex reflection coefficient from the coupling window or the phase and standing-wave ratio in the feed waveguide (Rose and Brown, 1952). If the orifice and window are electrically thin and lossless, we are justified in neglecting X_s and G_s. Measurements of the shift in resonance frequency $\Delta\omega$, and of the loaded Q, Q_L, for the two conditions (with and without plasma) then permit the calculation of the plasma admittance $y_1 = g_1 + jb_1$. This is best done with an impedance chart, such as the Smith chart (Southworth, 1959), since explicit calculations tend to be laborious.

5.1.2 ***Measurement of plasma density and collision frequency.*** For low density plasmas ($\omega_p^2 \ll \omega^2$) having low collision rates ($\nu \ll \omega$) and no external magnetic field, (5.1.2) may be written in two parts: one dealing with frequency shift, and the other with change in Q (Buchsbaum and Brown, 1957),

$$\frac{\Delta\omega}{\omega_0} \approx \frac{1}{2}\frac{1}{1+(\nu/\omega)^2}\frac{\int_V (\omega_p^2/\omega^2)E_0^2\,dV}{\int_V E_0^2\,dV} \tag{5.1.8}$$

$$\frac{1}{Q_1} - \frac{1}{Q_0} = \Delta\left(\frac{1}{Q}\right) \approx \frac{\nu/\omega}{1+(\nu/\omega)^2}\frac{\int_V (\omega_p^2/\omega^2)E_0^2\,dV}{\int_V E_0^2\,dV}. \tag{5.1.9}$$

The spatial distributions of both the electron density and the cavity electric fields must be known. The field configurations of cavity modes, in general, are known. If the plasma density is uniform across the cavity, the evaluation of the integrals in (5.1.8) and (5.1.9) is straightforward (Buchsbaum and Brown, 1957). If the plasma consists of a small diameter

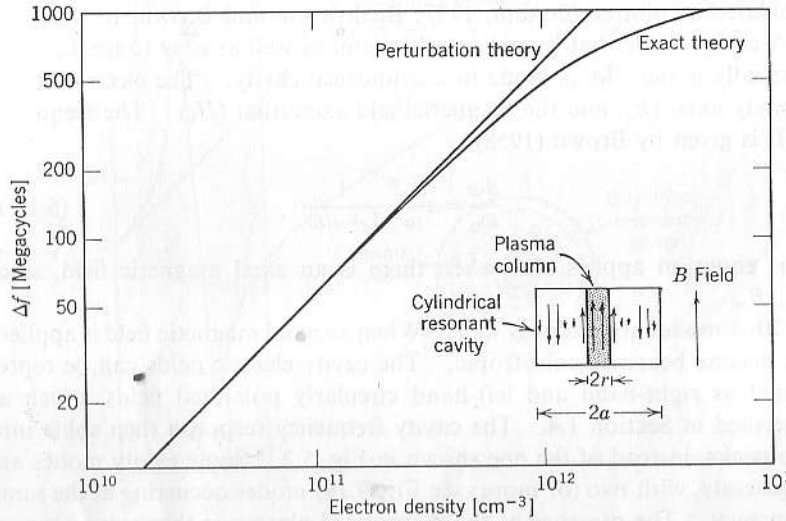

FIG. 5.3 Frequency shift of TM_{020} cylindrical cavity with a plasma post; $r/a = 1/10$, $f_0 = 5555$ Megacycles. (Courtesy S. C. Brown, M.I.T. Research Laboratory for Electronics.)

column, much smaller than the cavity diameter, it may be looked upon as a lumped admittance, shunting the cavity. As an example, consider a cylindrical cavity excited in the TM_{020} (linear accelerator) mode, containing a plasma post of diameter 1/10th that of the cavity. The curve for frequency shift vs. electron density is shown in Fig. 5.3 (Brown, 1958).

Typically, $\Delta\omega/\omega$ of 10^{-4} is easy to measure by observing an oscilloscope trace. The minimum detectable density then is about one per cent of that detectable with a transmission interferometer having a path length of 10 wavelengths and a resolution $\Delta\phi$ of 10°. Even greater sensitivity is obtainable by using heterodyning or frequency counting techniques to measure $\Delta\omega$.

When the electron density is nonuniform inside the plasma, as is nearly always the case, the frequency shift may be expressed in terms of an average density $\bar{n}$ and a geometry factor a,

$$\frac{\Delta\omega}{\omega} = -a\bar{n}. \tag{5.1.10}$$

This operation is valid only for low densities, that is, when the plasma can be treated as a perturbation in the cavity. The separation of (5.1.8) into the two parts represented by (5.1.10) is especially useful when the plasma density is to be studied as a function of time. The factor a, constant in time, then is calculated for various geometrical conditions, and the results tabulated or plotted (Oskam, 1957; Buchsbaum and Brown, 1957).

A cavity mode that is particularly useful as well as easy to treat mathematically is the TM_{010} mode in a cylindrical cavity. The electric field is entirely axial (E_z) and the magnetic field azimuthal (H_θ). The frequency shift is given by Brown (1958)

$$\frac{\Delta\omega}{\omega_0} = a\frac{\omega_p^2}{\omega^2}\frac{1}{1+\nu/\omega}. \tag{5.1.11}$$

This equation applies also when there is an axial magnetic field, since $E_z \parallel B_z$.

Other modes are useful as well. When an axial magnetic field is applied, the plasma becomes anisotropic. The cavity electric fields can be represented as right-hand and left-hand circularly polarized fields, much as described in Section 1.4. The cavity frequency response then splits into two peaks, instead of the one shown in Fig. 5.2. Some cavity modes are degenerate, with two (or more: see Fig. 9.19) modes occurring at the same frequency. The presence of the magnetized plasma in the cavity removes the degeneracy and the different modes appear at different frequencies. As an example consider the TM_{111} and TE_{011} modes. For $\omega_p/\omega \ll 1$ the frequency shifts are given by Brown (1958):

$$\left.\begin{aligned}\left(\frac{\Delta\omega}{\omega_0}\right)_+ &= \frac{a}{2}\frac{\omega_p^2}{\omega^2}\frac{1-\omega_b/\omega}{(1-\omega_b/\omega)^2+(\nu/\omega)^2} \qquad (5.1.12a)\\ \left(\frac{\Delta\omega}{\omega_0}\right)_- &= \frac{a}{2}\frac{\omega_p^2}{\omega^2}\frac{1+\omega_b/\omega}{(1+\omega_b/\omega)^2+(\nu/\omega)^2} \qquad (5.1.12b)\end{aligned}\right\}(TM_{111})$$

$$\frac{\Delta\omega}{\omega_0} = \frac{a}{2}\frac{\omega_p^2}{\omega^2}\frac{1}{1-(\omega_b/\omega)^2} \qquad (TE_{011}) \qquad (5.1.12c)$$

A study of the frequency dependence of the three modes yields information about the density spatial distribution.

For higher densities and collision rates, the frequency shift for the TE_{011} mode must be written in more complete form

$$\frac{\Delta\omega}{\omega_0} = \frac{a}{2}\frac{\omega_p^2}{\omega^2}\frac{\omega^2[\nu^2+\omega^2-\omega_b^2]}{[\nu^2+(\omega+\omega_b)^2][\nu^2+(\omega-\omega_b)^2]}. \tag{5.1.13}$$

An interesting feature of (5.1.13) is that when $\omega_b^2 = \omega^2+\nu^2$ there is no frequency shift Δf due to plasma density variations. The cavity Q also is approximately minimum for this condition. This effect can be used to measure the collision frequency ν (Hirshfield and Brown, 1958).

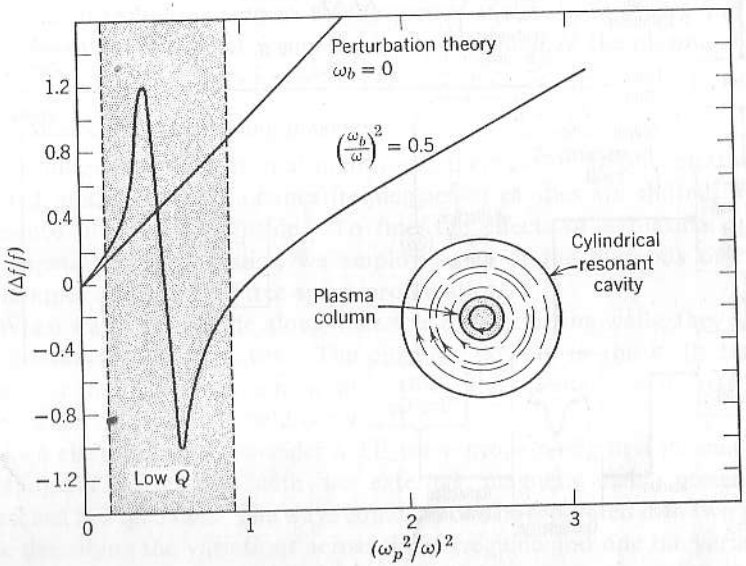

FIG. 5.4 Frequency shift of a TE_{011} mode cavity for high plasma densities, with and without magnetic field applied. (Courtesy S. C. Brown, M.I.T. Research Laboratory for Electronics.)

5.1.3 ***Special cavity modes for high density plasmas.*** The TE_{011} mode is useful for high densities ($\omega_p/\omega > 1$) when no static magnetic field is applied and the electron density gradient is radial (and, thus, perpendicular to the electric field). The circumferential electric fields induce no spacecharge fluctuations in the plasma (Persson, 1957). When a magnetic field is applied, the anisotropy permits radial currents and fields and the frequency-shift relations become complicated, as shown in Fig. 5.4. At very high densities and low collision rates, where the skin depth is much smaller than the cavity diameter, a high mode TE_{01M} cavity may be used, with M as large as perhaps 8 or 10. The smaller the "active" volume of cavity, that

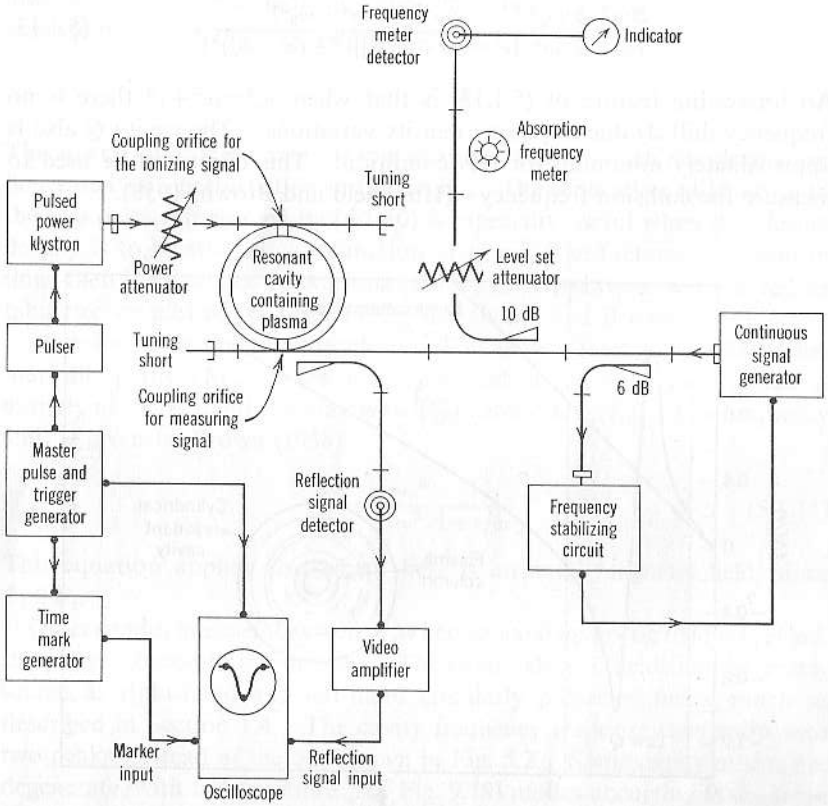

FIG. 5.5 Microwave cavity excitation and measurement system for studies of plasma contained in a resonant cavity. The ionizing signal couples to a different cavity mode, at a different frequency, from the measuring signal. Either the reflected signal (as shown) or VSWR may be observed.

is, that part of the cavity fields perturbed by the plasma, the smaller will be $\Delta\omega/\Delta n$ and the less sensitive will be the measurement. It is important to note that these techniques for high-density plasmas, with the skin depth much less than the plasma diameter, require an independent knowledge of the plasma density (and temperature) profile if anything more than the plasma *surface* properties are desired.

5.1.4 ***Experimental techniques for cavity measurements.*** Often a cavity can be excited in two modes at once, at widely separated frequencies, such that there is no coupling between the two inputs. It is then possible to use one mode to break down a gas and heat the plasma with a high power source, and to use the other mode for diagnostics. A sketch of a typical system is shown in Fig. 5.5. The excitation source may be steady, or it may be pulsed, with the diagnostics done in the afterglow period.

Ordinarily, the frequency of the signal source is swept back and forth over the resonant frequency of the cavity. The reflection coefficient or the standing-wave ratio is observed on an oscilloscope, and the shift in resonance frequency and cavity de-Qing are recorded for various plasma conditions. If the plasma is transient, the timing of the sweep may be delayed to sample various parts of the plasma transient event (Biondi, 1951; Sexton et al., 1959).

A second technique is to fix the frequency of the signal source and wait until the cavity resonance frequency sweeps through, as the plasma density decays (Biondi and Brown, 1949).

5.2 Waveguides containing plasmas

Waveguides also have normal modes and their cut-off frequencies will be shifted, much as the resonance frequencies of cavities are shifted, by the presence of a plasma inside. To find the effects of a plasma on the propagation characteristics, we employ some of the methods of cavity techniques and some of free-space propagation.

When waves propagate along dielectric or conducting walls, they are no longer strictly TEM waves. The currents flowing in the walls lead to components of electromagnetic field along the direction of propagation, even when no magnetic field is present.

As a clean example, consider a TE wave propagating in a plasma-filled rectangular waveguide with no external magnetic field present, as sketched in Fig. 5.6*a*. The wave equation can be separated into two parts, one describing the variations across the waveguide and one the variations along it. The wave equation becomes

$$\nabla^2\mathbf{H} = \nabla_t^2\mathbf{H} + \check{\gamma}^2\mathbf{H} = -\omega^2\mu_0\check{\epsilon}\mathbf{H} = -\frac{\omega^2}{c^2}\check{\kappa}\mathbf{H} \qquad (5.2.1)$$

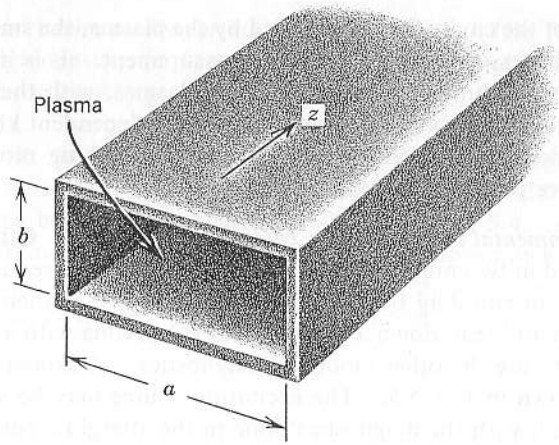

(a)

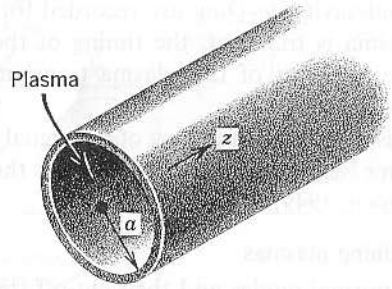

(b)

FIG. 5.6 Plasma-filled waveguides; (*a*) rectangular, (*b*) cylindrical.

where $\check{\epsilon}=\epsilon_0\check{\kappa}$ is the equivalent complex permittivity of the system and $\check{\gamma}$ is the propagation coefficient or complex wave number, which depends on the waveguide mode. In rectangular coordinates, the transverse term (∇_t^2) is

$$\nabla_t^2\mathbf{H}=\frac{\partial^2\mathbf{H}}{\partial x^2}+\frac{\partial^2\mathbf{H}}{\partial y^2}. \tag{5.2.2}$$

For TE waves, no E_z component exists, and it is convenient to solve (5.2.1) for the H_z component

$$H_z=H_0\left(\cos\frac{m\pi}{a}x\right)\left(\cos\frac{n\pi}{b}y\right)\exp(j\omega t-\check{\gamma}z) \tag{5.2.3}$$

where m is the mode number across x (or a) and n is the mode number across y (or b). From (5.2.1), (5.2.2), and (5.2.3),

$$-\left(\frac{m\pi}{a}\right)^2-\left(\frac{n\pi}{b}\right)^2+\check{\gamma}^2=-\beta_c^2+\check{\gamma}^2=-\frac{\omega^2}{c^2}\check{\kappa} \tag{5.2.4}$$

where

$$\left(\frac{m\pi}{a}\right)^2+\left(\frac{n\pi}{b}\right)^2=\beta_c^2=\left(\frac{2\pi}{\lambda_c}\right)^2=\left(\frac{\omega_c}{c}\right)^2$$

β_c = mode cutoff wave number
λ_c = mode cutoff free-space wavelength
ω_c = mode cutoff frequency.

Here we neglect any losses in the waveguide walls. Solving (5.2.4) for the propagation coefficient, we have

$$\check{\gamma}^2=\beta_c^2-\frac{\omega^2}{c^2}\kappa_r+j\frac{\omega^2}{c^2}\kappa_i. \tag{5.2.5}$$

The value of $\check{\kappa}$, calculated in Section 1.3.2 for a Lorentz plasma, is

$$\kappa_r=1-\frac{\omega_p^2}{\omega^2}\frac{1}{1+\nu^2/\omega^2}$$
$$\kappa_i=\frac{\omega_p^2}{\omega^2}\frac{\nu/\omega}{1+\nu^2/\omega^2}. \tag{5.2.6}$$

To obtain the attenuation and phase constants, we take the square root of (5.2.5) as in Section 1.3.3

$$\alpha=\left\{-\frac{1}{2}\left(\beta_c^2-\frac{\omega^2}{c^2}\kappa_r\right)+\frac{1}{2}\left[\left(\beta_c^2-\frac{\omega^2}{c^2}\kappa_r\right)^2+\left(\frac{\omega^2}{c^2}\kappa_i\right)^2\right]^{1/2}\right\}^{1/2}$$

$$=\frac{\omega}{c}\left\{-\frac{1}{2}\left(\frac{\omega_c^2}{\omega^2}-\left(1-\frac{\omega_p^2}{\omega^2+\nu^2}\right)\right)\right. \tag{5.2.7}$$
$$\left.+\frac{1}{2}\left[\left(\frac{\omega_c^2}{\omega^2}-\left(1-\frac{\omega_p^2}{\omega^2+\nu^2}\right)\right)^2+\left(\frac{\omega_p^2}{\omega^2+\nu^2}\frac{\nu}{\omega}\right)^2\right]^{1/2}\right\}^{1/2}$$

$$\beta=\{+\tfrac{1}{2}\ (\text{AS ABOVE})+\tfrac{1}{2}[(\text{AS ABOVE})^2+(\text{AS ABOVE})^2]^{1/2}\}^{1/2} \tag{5.2.8}$$

where $\omega_c=c\beta_c$ is the mode cutoff frequency in absence of plasma. These equations look similar to (1.3.20) and (1.3.21), except for the presence of the mode cutoff wave number β_c. This factor tends to increase the plasma cutoff frequency (now $>\omega_p$) or, at fixed frequency, to cause the transmission to cut off at a lower density than for the free-space case.

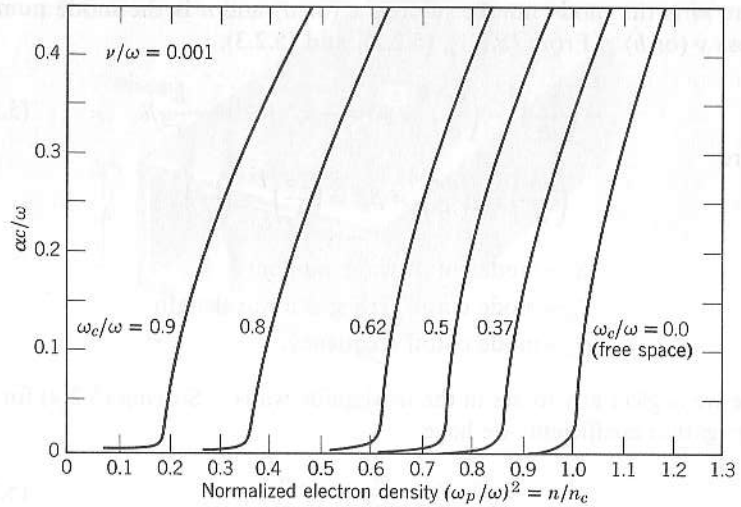

FIG. 5.7 Wave attenuation for a plasma-filled waveguide as a function of plasma density, for various mode cutoff wave numbers. Attenuation in dB is dB$=8.69\alpha$; $\omega_c=$the mode cutoff frequency.

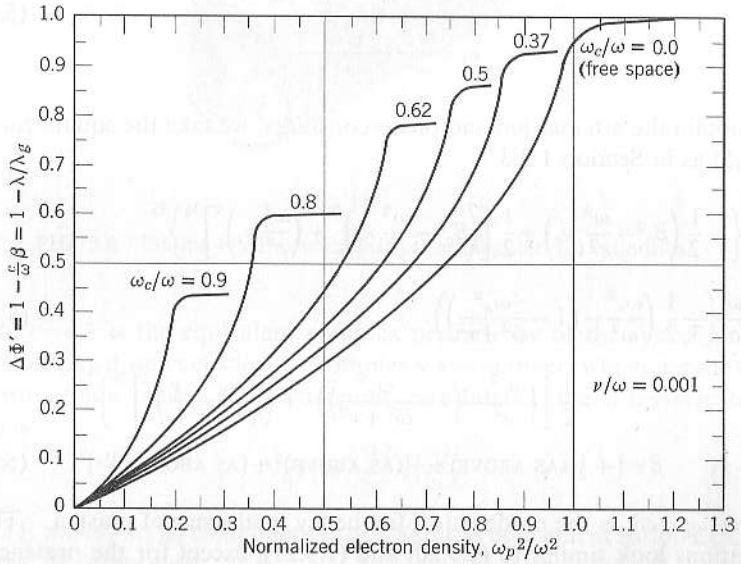

FIG. 5.8 Wave phase shift for a plasma-filled waveguide as a function of plasma density, for various mode cutoff wave numbers; $\omega_c/\omega=0.62$ corresponds to RG-51/U waveguide at 8.5 Gc; $\omega_c/\omega=0.37$ corresponds to PRD 90-ohm ridge guide at 8.5 Gc.

Normalized α and β are plotted in Figs. 5.7 and 5.8, respectively, as a function of electron density.

Since β_c is the cutoff wave number of any mode in which waves happen to be propagating, (5.2.7) and (5.2.8) hold for any uniform, bounded system for which a β_c can be specified. For example, for TE modes in a plasma-filled cylindrical waveguide of radius a (see Fig. 5.6*b*)

$$\beta_c = P'_{mn}/a \quad \text{(TE)} \tag{5.2.9}$$

where P'_{mn} is the nth root of the Bessel function derivative $dJ_m(x)/dx=0$; for example, $P'_{11}=1.841$, $P'_{21}=3.054$, $P'_{01}=3.832$. Cylindrical TE modes have H_z field dependence

$$H_z = H_0 \begin{bmatrix} \sin n\theta \\ \cos n\theta \end{bmatrix} J_m(\beta_c r). \tag{5.2.10}$$

We can handle the TM case as well by substituting E_z for H_z in (5.2.1) to (5.2.4), and we emerge with equivalent results. The difference between the two cases is that for waveguide of given diameter the β_c's for the TM modes and TE modes are different. Cylindrical TM modes have E_z dependence analogous to H_z in (5.2.10) but with

$$\beta_c = P_{mn}/a \quad \text{(TM)} \tag{5.2.11}$$

where P_{mn} is the nth root of $J_m(x)=0$; for example, $P_{01}=2.405$, $P_{11}=3.832$.

As a second simple example, suppose that a very large magnetic field ($\approx$infinite) lies along the z direction of the waveguide. The electrons now are free to travel along z but are unable to move in the x and y directions. The presence of plasma then has no effect on TE modes, but for TM modes (with an E_z component) the propagation coefficient is again given by (5.2.7) and (5.2.8).

When a finite magnetic field is present, Bevc and Everhart (1961) find that both an E_z and an H_z component are present, and thus no purely transverse wave propagates. To solve for the relative magnitudes of the **E** and **H** fields of this mixed wave requires a complete solution of the boundary value problem.

5.3 The ω-β diagram

The propagation coefficient γ or the phase velocity v_ϕ are often plotted another way when the losses are sufficiently low that α may be ignored within the passbands. Then γ equals $j\beta$. These plots are called ω-β or Brillouin diagrams (Watkins, 1958) and are especially useful when the density is fixed and the frequency can be varied.

To have ω the independent variable, (1.3.20) and (5.2.8) may be rewritten

$$\beta \approx \frac{\omega_p}{c}\left(\frac{\omega^2}{\omega_p{}^2}-1\right)^{1/2} \qquad \text{(free space)} \qquad (5.3.1)$$

$$\beta \approx \frac{\omega_p}{c}\left[1+\frac{\omega^2}{\omega_p{}^2}\left(\frac{\omega_c{}^2}{\omega^2}-1\right)\right]^{1/2} \qquad \text{(in waveguide)} \qquad (5.3.2)$$

$$\approx \beta_c\left[1-\frac{\omega^2}{\omega_p{}^2}\frac{\omega_p{}^2}{\omega_c{}^2}\left(1-\frac{\omega_p{}^2}{\omega^2}\right)\right]^{1/2}$$

where $\omega_c = c\beta_c$ is the mode cutoff frequency and the approximation is due to setting $\nu = 0$. The cutoff frequency, ω_{cp}, of a "hot mode" (that is, when plasma is present) is higher than that for a "cold mode," ω_c. From (5.2.8), ω_{cp} is seen to be

$$\omega_{cp} = (\beta_c{}^2 c^2 + \omega_p{}^2)^{1/2}. \qquad (5.3.3)$$

Figures 5.9 and 5.10 show ω-β diagrams normalized in two ways for the plasma slab and for the rectangular waveguide, where the collision frequency ν is very small, the density is uniform, and no magnetic field is present. The slope of the radius vector to each point on the diagram is seen to be proportional to ω/β, which is the wave phase velocity v_ϕ. The slope of the tangent at each point is proportional to $d\omega/d\beta$, which is the wave group velocity v_g.

5.4 Nonuniform plasma in a waveguide

When we considered that the plasma was uniform across the waveguide diameter, we implied that it had no effect on the magnitude of the microwave fields, that is, that **E** and **H** were unperturbed. That, of course, is not true for dense plasmas, when ω_p approaches ω.

Let us take the case for a rectangular waveguide again, in which the plasma has a diffusion-limited density distribution (Brown, 1959)

$$n(x, y) = n_0\left(\cos\frac{\pi}{a}x\right)\left(\cos\frac{\pi}{b}y\right) \qquad (5.4.1)$$

where n_0 is the axial density. The corresponding dielectric constant is

$$\kappa(x, y) = 1-\frac{n_0}{n_c}\left(\cos\frac{\pi}{a}x\right)\left(\cos\frac{\pi}{b}y\right). \qquad (5.4.2)$$

The wave equation must now be written

$$\frac{\partial^2 H_z}{\partial x^2}+\frac{\partial^2 H_z}{\partial y^2}+\left[\tilde{\gamma}^2+\frac{\omega^2}{c^2}\kappa(x, y)\right]H_z = [\kappa(\nabla\kappa^{-1})\times(\nabla\times\mathbf{H})]_z \qquad (5.4.3)$$

in accord with (4.4.7). For sufficiently small gradients, the right-hand side, which cross-couples H_z to H_x and H_y, may be neglected. Even so,

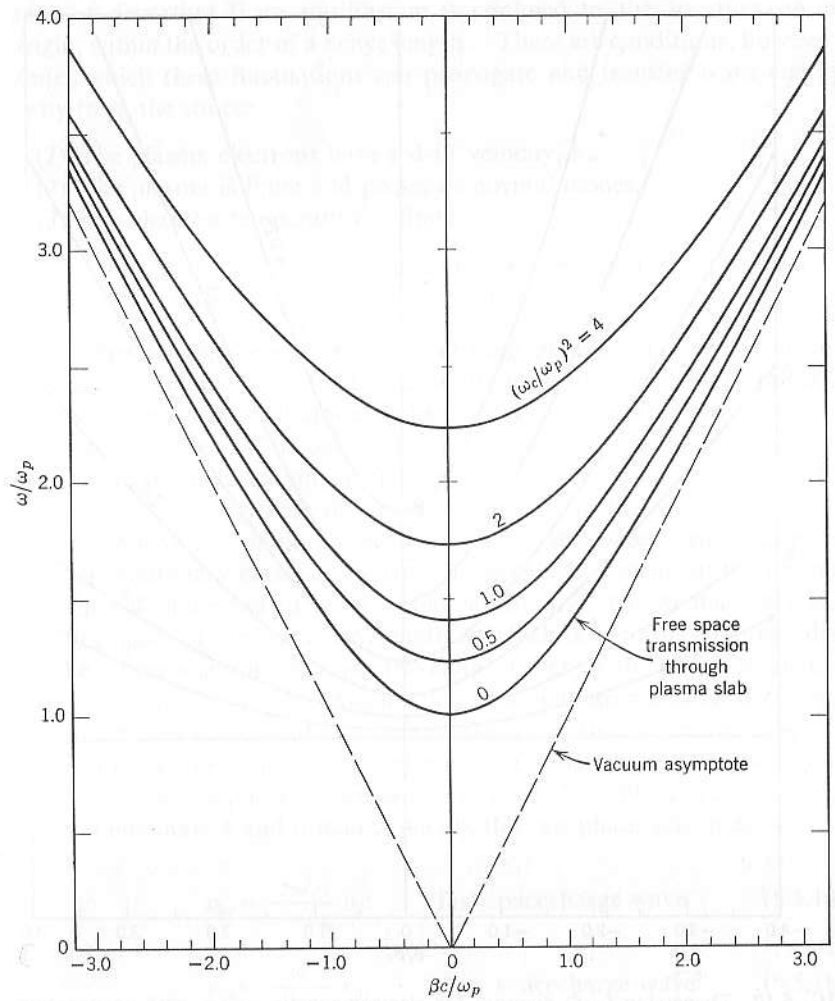

FIG. 5.9 Dispersion (ω-β) diagram, normalized to the plasma frequency ω_p, for a uniform plasma in waveguide; ω_c = cold mode cutoff frequency, $\omega_{cp} = (\omega_c{}^2 + \omega_p{}^2)^{1/2}$ = hot mode cutoff frequency.

the simplified equation is not separable and cannot be solved explicitly for $\tilde{\gamma}$ as before. It resembles Mathieu's equation

$$\frac{d^2 H}{dx^2}+\left(b+c\sin\frac{\pi}{a}x\right)H = 0. \qquad (5.4.4)$$

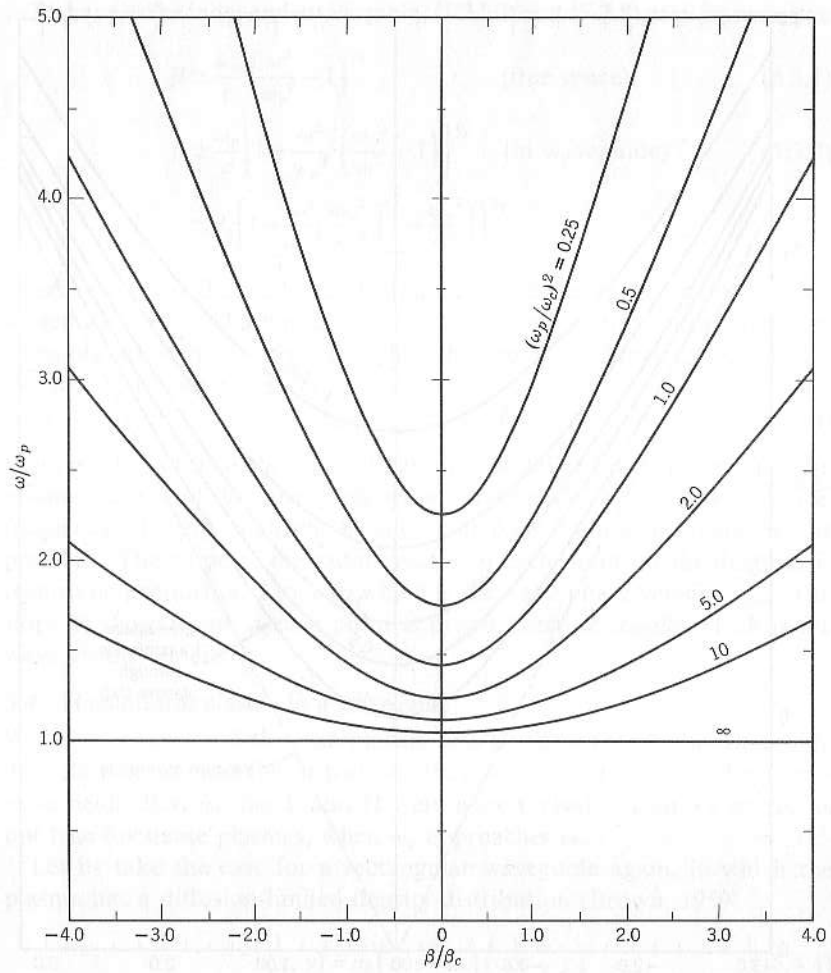

FIG. 5.10 Dispersion (ω-β) diagram for electromagnetic waves, with propagation phase constant normalized to the mode cutoff wave number, for a plasma filling a waveguide; $\omega_c = \beta_c c$ = cold mode cutoff frequency.

Various solutions to (5.4.4) exist, and series and numerical approximations are also possible (Madelung, 1943).

5.5 Spacecharge waves

In Chapter 1, it was pointed out that spacecharge fluctuations in a cold, stationary, infinite, uniform plasma were nonpropagating. Any disturbance or departure from equilibrium is confined to the location of its origin, within the order of a debye length. There are conditions, however, under which these fluctuations *can* propagate and transfer wave energy away from the source.

(*1*) The plasma electrons have a drift velocity, v_0.
(*2*) The plasma is finite and possesses normal modes.
(*3*) The electron temperature is finite.

Let us now consider the characteristics of some of these propagating plasma waves under various plasma conditions.

5.5.1 ***Spacecharge waves in a cold, drifting plasma.*** Let the electrons have a drift velocity v_0. If plasma oscillations (at $\omega \approx \omega_p$) were present, they would be convected along at the drift velocity, and would constitute a convective wave. If no oscillations are present, but rather an externally applied electric field varying at frequency ω is present, we can also excite plasma waves arising from the resulting velocity fluctuations.

First from a naive point of view, we recall that the spacecharge oscillation in a cold stationary plasma, discussed in Section 1.2, occurs at the plasma frequency ω_p independent of its spatial variation. Thus we may choose a standing wave of arbitrary wavelength λ, which in turn may be regarded as the superposition of two traveling waves with phase velocities $v_\phi = \pm \lambda\omega_p/2\pi$. Now if we imagine that this oscillating plasma is moving past our observation point at a steady velocity v_0, the two traveling waves appear to us to have the same wavelength λ, a doppler-shifted frequency ω, and the respective phase velocities $v_\phi = v_0 \pm \lambda\omega_p/2\pi$. But since $\omega\lambda = 2\pi v_\phi$, we may eliminate λ and obtain explicitly the two phase velocities

$$v_{\phi f} = \frac{\omega}{\omega - \omega_p} v_0 \qquad \text{"fast spacecharge wave"} \qquad (5.5.1a)$$

$$v_{\phi s} = \frac{\omega}{\omega + \omega_p} v_0. \qquad \text{"slow spacecharge wave"} \qquad (5.5.1b)$$

Now on a more analytical level, we seek the dispersion relations for these waves under the action of an applied electric field. We rewrite the equation of motion of a Lorentz plasma, (1.4.1), in Eulerian rather than Lagrangian coordinates (that is, we watch the plasma stream flow past our fixed coordinate system, rather than use a coordinate system in which the plasma is at rest); the force equation now is (Marcuvitz, 1958)

$$\frac{\partial \mathbf{v}}{\partial t} + \mathbf{v}\cdot\nabla\mathbf{v} + \nu(\mathbf{v} - \mathbf{v}_0) = -\frac{e}{m}(\mathbf{E} + \mathbf{v}\times\mathbf{B}). \qquad (5.5.2)$$

Let us now assume the following.

(*1*) The drift velocity v_{0z} is constant, in the $+z$ direction.

(*2*) The induced a-c velocity variations are much smaller than the drift velocity.

(*3*) The driving electric field is of the form $E_{1z}\exp(j\omega t-\gamma z)$, that is, a longitudinal wave propagating in the z direction.

(*4*) No magnetic field effect is present ($\mathbf{v}\times\mathbf{B}\to 0$).

(*5*) We neglect collisions ($\nu\to 0$).

The electron velocity is of the form

$$v_z(z,t)=v_{0z}+v_{1z}\exp(j\omega t-\gamma z) \tag{5.5.3}$$

where the subscript 0 represents the steady-state component and the subscript 1 the complex perturbation component.

The second term of (5.5.2) may be evaluated to first order as

$$\mathbf{v}\cdot\nabla\mathbf{v}=v_{0z}\frac{\partial\mathbf{v}}{\partial z}=v_{0z}(-\gamma\mathbf{v}_1) \tag{5.5.4}$$

where $\mathbf{v}_1$ is the perturbation part of (5.5.3), in the z direction. Substituting in (5.5.2) and canceling the phase factor $\exp(j\omega t-\gamma z)$, we obtain

$$(j\omega-\gamma v_0)v_{1z}=-\frac{e}{m}E_{1z}. \tag{5.5.5}$$

In contrast to the case with electromagnetic (transverse) waves, the a-c current density J_{1z} depends on the oscillating spacecharge as well as the oscillating velocity component; thus

$$\begin{aligned}J_z&\equiv J_{0z}+J_{1z}\exp(j\omega t-\gamma z)\\&=-n_0ev_{0z}-e(n_0v_{1z}+n_1v_{0z})\exp(j\omega t-\gamma z),\end{aligned} \tag{5.5.6}$$

neglecting higher than first-order terms. To evaluate the perturbation component n_1 of the electron density,

$$n=n_0+n_1\exp(j\omega t-\gamma z), \tag{5.5.7}$$

we invoke the equation of continuity (3.3.7)

$$\nabla\cdot\mathbf{J}\to\frac{\partial J_z}{\partial z}=e\frac{\partial n}{\partial t} \tag{5.5.8}$$

which becomes

$$-\gamma J_{1z}=j\omega en_1. \tag{5.5.9}$$

Substitution of (5.5.9) in (5.5.6) yields

$$J_{1z}=-e\left(n_0v_{1z}+\frac{j\gamma J_{1z}}{\omega e}v_{0z}\right) \tag{5.5.10}$$

or

$$J_{1z}=-\frac{n_0e}{1+j\gamma v_{0z}/\omega}v_{1z}, \tag{5.5.11}$$

which in turn permits us to use (5.5.5) to find the (complex) conductivity

$$\check{\sigma}_{zz}=\frac{J_{1z}}{E_{1z}}=-j\frac{\epsilon_0\omega{\omega_p}^2}{(\omega+j\gamma v_{0z})^2}. \tag{5.5.12}$$

In problems dealing with waves, it is useful to translate the conductivity into the equivalent dielectric constant

$$\check{\kappa}_{zz}=1-j\frac{\check{\sigma}_{zz}}{\epsilon_0\omega}=1-\frac{{\omega_p}^2}{(\omega+j\gamma v_{0z})^2}. \tag{5.5.13}$$

The presence of the $\mathbf{v}\cdot\nabla\mathbf{v}$ term in (5.5.2) makes the drifting plasma, when viewed from a stationary position, behave like an *anisotropic* electromagnetic medium, and the dispersion equation (A.74) is applicable. Since we are here concerned with longitudinal (spacecharge) waves propagating in the z direction (Trivelpiece, 1958), (A.74) reduces to simply $\kappa_{zz}=0$; from (5.5.13)

$$\omega+j\gamma v_{0z}=\pm\omega_p$$

or

$$\gamma=j\frac{\omega\pm\omega_p}{v_{0z}}. \tag{5.5.14}$$

Since we have assumed no loss mechanism (collisions), the propagation coefficient $\check{\gamma}\equiv\alpha+j\beta$ is pure imaginary (the waves are unattenuated) with the respective phase constants,

$$\beta_f=\frac{\omega-\omega_p}{v_{0z}} \tag{5.5.15a}$$

$$\beta_s=\frac{\omega+\omega_p}{v_{0z}} \tag{5.5.15b}$$

which are consistent with the phase velocities of (5.5.1). These two waves have phase velocities grouped about the electron drift velocity, v_0, and vanish when the drift velocity goes to zero. The waves both have the same group velocity, $v_g=v_0$; that is, the wave energy is all carried by the electron drift motion. When β is normalized, as before in (5.3.2), it is written

$$\beta\frac{c}{\omega_p}=\frac{c}{v_0}\left(\frac{\omega}{\omega_p}\pm 1\right). \tag{5.5.16}$$

The ω/β diagram of (5.5.16) is sketched in Fig. 5.11. That the waves both have the same group velocity, $v_g=v_0$, is seen from Fig. 5.11, since the slopes of all three lines (proportional to $d\omega/d\beta=v_g$) are the same.

We have spoken thus far of the spacecharge waves in neutral drifting plasmas of infinite extent. The same dispersion relations apply to an unneutralized electron beam if only z-direction motion is allowed, for

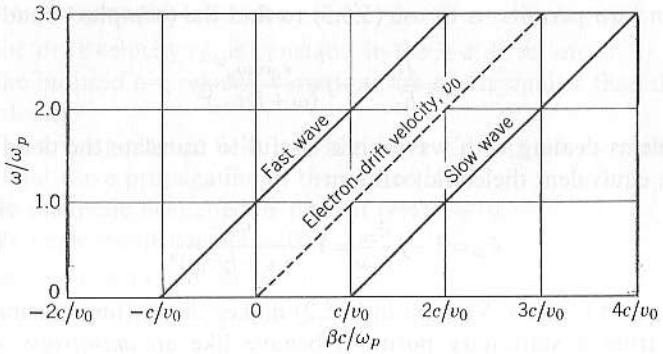

FIG. 5.11 The ω-β diagram for spacecharge "waves," consisting of plasma oscillations or velocity and spacecharge fluctuations carried along by drifting electrons.

example, by having an "infinite" magnetic field present. If the field strength is finite, some radial propagation may occur due to spacecharge blowup of the beam. In this case, gyrofrequency and possibly hydromagnetic effects also would have to be considered, which we shall not do at this point, in the interest of subject continuity.

5.5.2 ***Spacecharge waves in plasma columns of finite radius.*** A plasma column having finite radial extent can have normal modes and, thus,

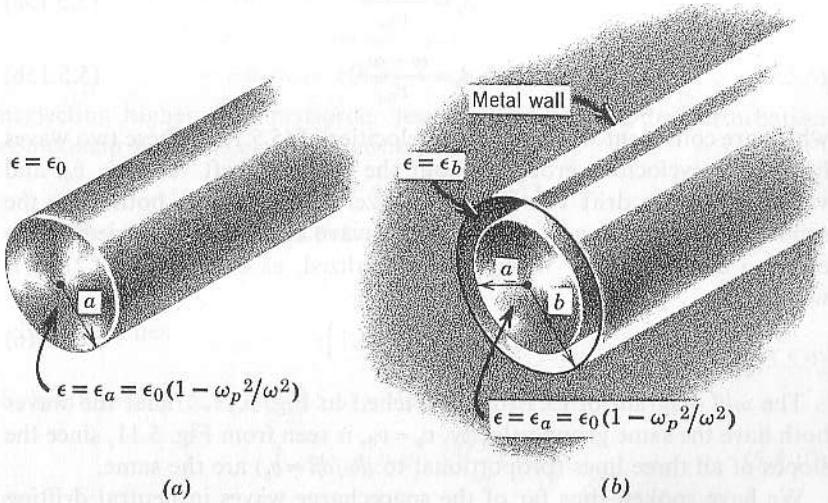

FIG. 5.12 Plasma column (*a*) having a sharp vacuum boundary, and (*b*) surrounded by a dielectric tube inside a metal cylinder.

support spacecharge waves even in the absence of drift motions or finite electron temperature. A column in free space or one surrounded by a dielectric and/or metal wall (such as a discharge tube in a waveguide) has qualitatively similar dispersion relations although the cutoff frequencies are different for the free and bounded cases.

Let us see how the propagation of these *surface waves* (we shall find that the electric fields are confined mainly to the surface) depends upon the plasma density and the frequency. Assume a model having a sharp boundary surrounding a uniform, stationary plasma cylinder, with no magnetic field present, as sketched in Fig. 5.12.

We are concerned here with dielectric effects, the time-varying magnetic field being negligibly small, so that a quasi-static approximation is adequate (Trivelpiece, 1958). The normal component of dielectric displacement is continuous across the boundary and the electric field can be derived from a scalar potential,

$$\nabla \times \mathbf{E}_1 = -j\omega \mathbf{B}_1 \to 0 \tag{5.5.17}$$

$$\nabla \cdot \mathbf{D}_1 = \nabla \cdot \epsilon \mathbf{E}_1 = \epsilon_0 \nabla \cdot \kappa E_1 = \rho \to 0 \tag{5.5.18}$$

$$\mathbf{E}_1 = -\nabla \Phi_1 \tag{5.5.19}$$

where the subscripts 1 denote a-c quantities as before. If ϵ is not a function of position, (5.5.18) may thus be written

$$\nabla \cdot (-\epsilon \nabla \Phi_1) = -\epsilon \nabla^2 \Phi_1 = 0, \tag{5.5.20}$$

which has two solutions:

$$\epsilon = 0 \tag{5.5.21a}$$

$$\nabla^2 \Phi_1 = 0. \tag{5.5.21b}$$

The first solution pertains to nonpropagating fluctuations (plasma oscillations), since it states that the medium is cut off. The second solution describes propagating potential fluctuations.

It is the wave solution that we seek, so let us assume that the potential fluctuation has the form

$$\Phi_1 = \Phi(r) \exp(-jn\theta) \exp(-j\beta z) \exp(j\omega t) \tag{5.5.22}$$

where n is the order of the angular mode number. Writing (5.5.21b) in cylindrical coordinates gives for the radial function Φ

$$\frac{1}{r}\frac{d}{dr}\left(r\frac{d\Phi_1}{dr}\right) - \frac{n^2}{r^2}\Phi_1 - \beta^2 \Phi_1 = 0 \tag{5.5.23}$$

which is Bessel's equation for imaginary argument. The solution for Φ_1 is of the form

$$\Phi_1 = [C\, \mathrm{I}_n(\beta r) + D\, \mathrm{K}_n(\beta r)] \exp j(\omega t - n\theta - \beta z), \tag{5.5.24}$$

where I_n and K_n are the modified Bessel functions of the first and second kinds. We cannot have infinite fields at $r=0$ so the constant D must be zero within the plasma column. The field components within the plasma column ($r<a$) are thus

$$E_{1r} = -C\beta\, I_n'(\beta r) \tag{5.5.25a}$$

$$E_{1\theta} = Cj\frac{n}{r} I_n(\beta r) \tag{5.5.25b}$$

$$E_{1z} = Cj\beta\, I_n(\beta r) \tag{5.5.25c}$$

$$\Big\} \exp j(\omega t - n\theta - \beta z).$$

The permittivities for the two regions (Fig. 5.12) are, using (1.3.5),

$$\begin{aligned} r<a \qquad & \epsilon_a = \epsilon_0(1-\omega_p^2/\omega^2) \\ a<r<b \qquad & \epsilon_b = \epsilon_0\kappa_b. \end{aligned} \tag{5.5.26}$$

The two models shown in Fig. 5.12 may be considered equivalent if $b \to \infty$ and $\epsilon_b = \epsilon_0$. Retaining b as finite (although perhaps very large) permits us to assign a zero-potential boundary condition at $r=b$, which simplifies the solution for the constant C. The tangential electric fields (E_{1z} and $E_{1\theta}$) must also be zero along the conducting wall at $r=b$, but continuous across the boundary at $r=a$.

The potentials inside and outside the plasma column are then found to be

$$r<a \qquad \Phi_a = \frac{I_n(\beta r)}{I_n(\beta a)} = \Phi_{a0}\, I_n(\beta r) \tag{5.5.27}$$

$$a<r<b \qquad \Phi_b = \frac{I_n(\beta r)K_n(\beta b) - I_n(\beta b)K_n(\beta r)}{I_n(\beta a)K_n(\beta b) - I_n(\beta b)K_n(\beta a)} \tag{5.5.28}$$

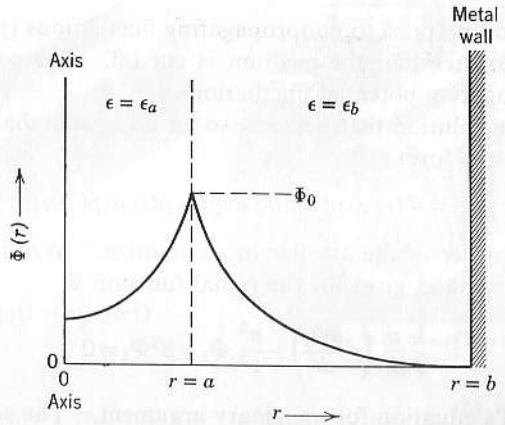

FIG. 5.13 Potential variations in radius for the lowest-order spacecharge surface wave in zero magnetic field.

where the I_n and K_n are again the modified Bessel functions of the first and second kinds.

The potential variation for the lowest order mode ($n=0$) is sketched in Fig. 5.13. It is immediately apparent from Fig. 5.13 that the electric field is indeed confined very near to the surface of the plasma, hence the name surface waves.

Demanding continuity of the normal displacement $D_r = \epsilon E_r$ at $r=a$ leads to the dispersion equation of surface wave propagation, when no magnetic field is present (Trivelpiece, 1958)

$$\frac{1-\omega_p^2/\omega^2}{\kappa_b}\frac{I_n'(\beta a)}{I_n(\beta a)} = \frac{I_n'(\beta a)K_n(\beta b) - I_n(\beta b)K_n'(\beta a)}{I_n(\beta a)K_n(\beta b) - I_n(\beta b)K_n(\beta a)}. \tag{5.5.29}$$

The ω-β diagram for the lowest order mode is shown plotted in Fig. 5.14. Only the $+\beta a$ curves are shown, the diagram being symmetrical about the ω axis for $-\beta a$ (that is, waves traveling in the opposite direction). The difference in curves for $b/a=2$ and $b/a \to \infty$ is seen to be quite small, indicating that the presence of metal walls farther than about one column

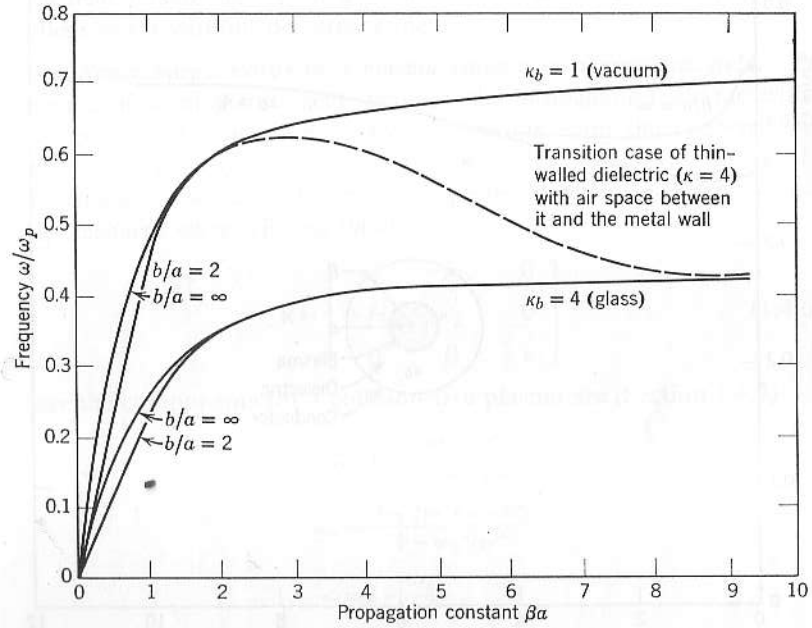

FIG. 5.14 The ω-β diagram for propagation of surface waves on a plasma surrounded by a vacuum interspace ($\epsilon_b = \epsilon_0$) between the column and the wall and for a material of dielectric constant $\kappa = 4$ filling the space (see Fig. 5.12 for geometry).

diameter from the plasma has negligible effect. The propagation extends from zero frequency up to a cutoff frequency of

$$\omega_{co}=\frac{\omega_p}{(1+\kappa_b)^{1/2}} \tag{5.5.30}$$

where κ_b is the dielectric constant of the medium surrounding the plasma.

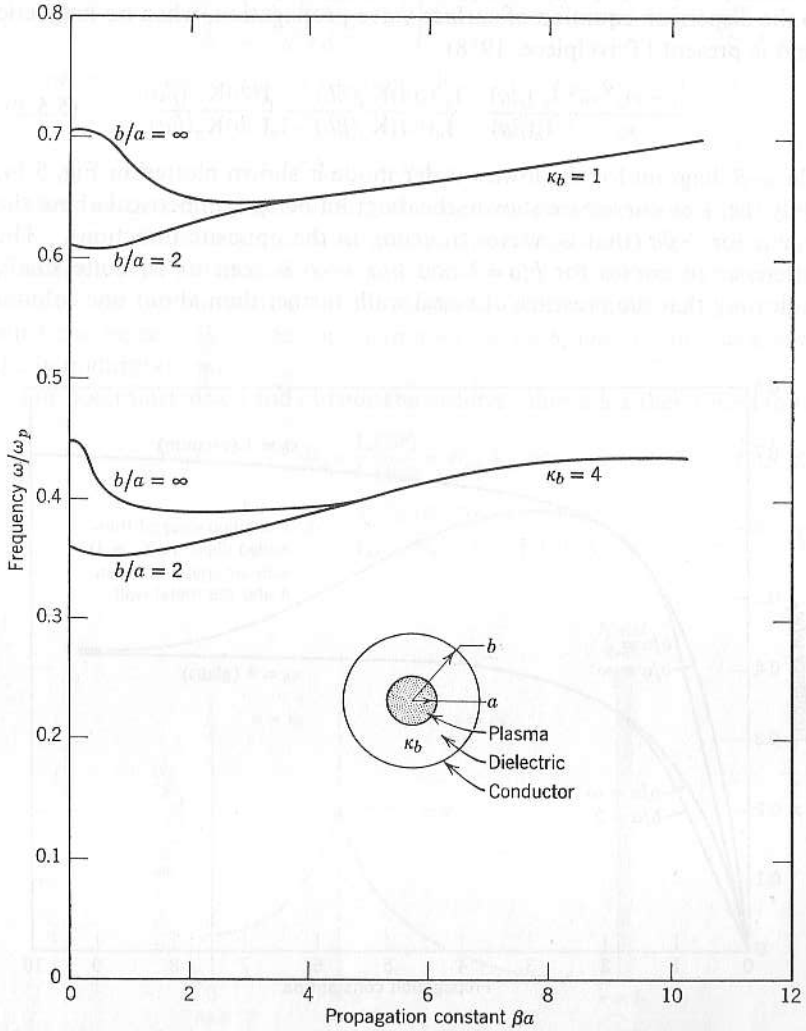

FIG. 5.15 Phase characteristics for a surface wave mode of one angular variation (Trivelpiece, 1958).

In Fig. 5.15 the ω-β diagrams of a higher mode having one angular variation (the corkscrew mode with $n=1$) are shown. This mode does not extend to zero frequency, but has the same upper cutoff frequency as the fundamental mode. In fact, it is found that all of the surface-wave modes have the same cutoff frequency and that it is independent of the column or metal wall diameter, in contrast to the electromagnetic modes. This cutoff frequency, given in (5.5.30), is often referred to as the *dipole* or *column resonant frequency*. The wave velocity, of course, depends on both a and b; for small a, the value of β is large, and the velocity low, especially as $\omega \to \omega_{co}$.

An interesting analogy between the electromagnetic fields and space-charge-wave fields can be drawn. We pointed out that the magnetic component of the surface wave fields can be neglected. But, for a wave to propagate, the energy stored by the electric field must be interchanged with something and, in this case, it is the mass motion of the charges. For this reason, spacecharge waves are sometimes called *electromechanical waves*. The charges move back and forth in such a way that the electric field lines terminate on them, which in part explains the small penetration of the field outside the column and the difficulty of experimentally coupling to these waves without perturbing them.

5.5.3 ***Spacecharge waves in a plasma column in a magnetic field.*** The presence of a magnetic field changes the propagation characteristics considerably. The medium is now anisotropic, and the dielectric permittivity ϵ becomes a tensor, $\epsilon \to \boldsymbol{\varepsilon}=\epsilon_0\mathbf{K}$. The permittivity derived for electromagnetic waves in Chapter 1 is perfectly general and applies also to spacecharge waves (Pines, 1960);

$$\mathbf{K}=\begin{bmatrix} \kappa_\perp & -j\kappa_\times & 0 \\ +j\kappa_\times & \kappa_\perp & 0 \\ 0 & 0 & \kappa_\parallel \end{bmatrix} \tag{1.4.60}$$

where the components for a collision-free plasma are (Section 1.4.7)

$$\kappa_\perp=1-\frac{\omega_p^2/\omega^2}{1-\omega_b^2/\omega^2}$$

$$\kappa_\times=\frac{(\omega_p^2/\omega^2)(\omega_b/\omega)}{1-\omega_b^2/\omega^2}$$

$$\kappa_\parallel=1-\frac{\omega_p^2}{\omega^2}.$$

To find the wave solutions for the magnetic-field case, then, we must rewrite (5.5.18) to include the anisotropic permittivity

$$\nabla\cdot\mathbf{D}_1=\nabla\cdot\boldsymbol{\varepsilon}\cdot\mathbf{E}_1=\epsilon_0\nabla\cdot\mathbf{K}\cdot\mathbf{E}_1=0 \tag{5.5.31}$$

from which (5.5.20) becomes

$$\nabla\cdot\boldsymbol{\varepsilon}\cdot(-\nabla\Phi_1)=\epsilon_0\nabla\cdot\boldsymbol{\kappa}\cdot(-\nabla\Phi_1)=0. \tag{5.5.32}$$

The form of (5.5.32) in cylindrical coordinates is analogous to (5.5.23) but with the permittivities included

$$\frac{1}{r}\frac{d}{dr}\left(r\frac{\partial\Phi_1}{\partial r}\right)-\frac{n^2}{r^2}\Phi_1-\beta^2\frac{\kappa_\parallel}{\kappa_\perp}\Phi_1=0 \tag{5.5.33}$$

and has solutions similar to (5.5.27) and (5.5.28), except that β^2 is now replaced by $\beta^2(\kappa_\parallel/\kappa_\perp)$.

The electric field in the plasma is given by the gradient of the potential Φ. In the z direction, this is

$$\begin{aligned}E_{1z}&=-\frac{\partial\Phi_1}{\partial z}=j\beta\Phi_1\\&=E_{1z}(0)\mathrm{I}_n\left[\beta r\left(\frac{\kappa_\parallel}{\kappa_\perp}\right)^{1/2}\right]\quad\text{for } r<a\end{aligned} \tag{5.5.34}$$

where $E(0)$ is the axial field at $r=0$ and I_n is the modified Bessel function. The radial electric field is

$$\begin{aligned}E_{1r}&=-\frac{\partial\Phi_1}{\partial r}=\frac{j}{\beta}\frac{\partial E_{1z}}{\partial r}\\&=-E_{1z}(0)\left(\frac{\kappa_\parallel}{\kappa_\perp}\right)^{1/2}\mathrm{I}_n'\left[\beta r\left(\frac{\kappa_\parallel}{\kappa_\perp}\right)^{1/2}\right].\end{aligned} \tag{5.5.35}$$

The azimuthal field is similarly obtained

$$\begin{aligned}E_{1\theta}&=-\frac{\partial\Phi_1}{\partial\theta}=\frac{n}{\beta r}\frac{\partial E_{1z}}{\partial r}\\&=E_{1z}(0)\frac{n}{\beta r}\mathrm{I}_n\left[\beta r\left(\frac{\kappa_\parallel}{\kappa_\perp}\right)^{1/2}\right].\end{aligned} \tag{5.5.36}$$

The last three equations are seen to be analogous to (5.5.25). They point out that all electric field quantities are derivable from the axial field.

Trivelpiece (1958) finds a propagation equation similar to (5.5.29), but with the permittivity components included,

$$\frac{(\kappa_\parallel\kappa_\perp)^{1/2}}{\kappa_b}\frac{\mathrm{I}_n'\left[\beta a\left(\frac{\kappa_\parallel}{\kappa_\perp}\right)^{1/2}\right]}{\mathrm{I}_n\left[\beta a\left(\frac{\kappa_\parallel}{\kappa_\perp}\right)^{1/2}\right]}+\frac{n\kappa_\times}{\beta a\kappa_b}=\frac{\mathrm{I}_n'(\beta a)\mathrm{K}_n(\beta b)-\mathrm{I}_n(\beta b)\mathrm{K}_n'(\beta a)}{\mathrm{I}_n(\beta a)\mathrm{K}_n(\beta b)-\mathrm{I}_n(\beta b)\mathrm{K}_n(\beta a)}. \tag{5.5.37}$$

Substituting in the permittivity components of (1.4.60) leads to a complicated expression for the cutoff frequency which involves both ω_b and

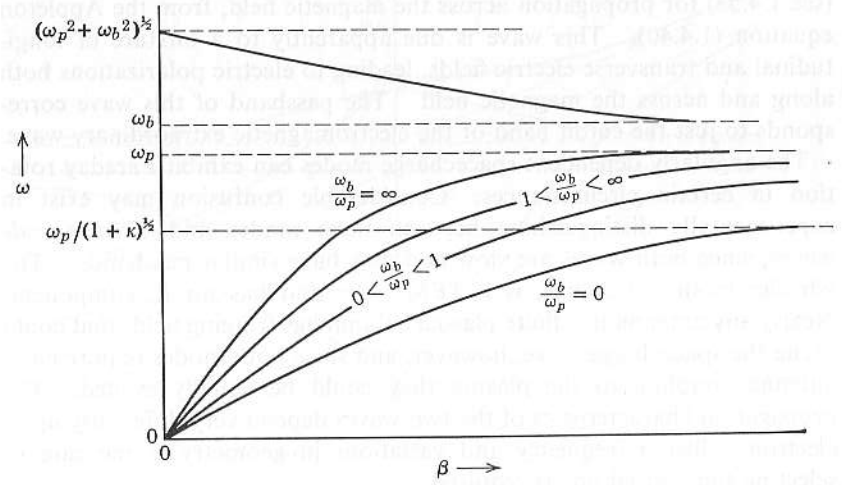

FIG. 5.16 Phase characteristics of spacecharge waves (ω-β diagram) for a plasma column bounded by a dielectric and metal, in an axial magnetic field of various magnitudes.

ω_p. The ω-β diagrams in Fig. 5.16 show the trends for various relationships of ω_b to ω_p. When ω_b is very large, most of the wave energy is carried by charge accumulation within the plasma column, with little surface rippling. These waves are called *body waves*, and have a cutoff frequency approaching ω_p, as do one-dimensional spacecharge waves. Conversely, for $\omega_b\to 0$, the wave energy is carried by surface rippling alone, with little spacecharge bunching within the plasma. The cutoff frequency for these *surface waves* then approaches $\omega_p/(1+\kappa_b)^{1/2}$. The surface waves cannot propagate if the dielectric space (vacuum or material) is absent between the plasma and the metal wall since, then, no charge accumulation can occur. The usual electromagnetic waves can propagate, of course, and a mixing of electromagnetic and spacecharge waves is usually present. For values of ω_b/ω_p between 0 and ∞, and at various values of βa, the wave mechanisms and wave types undergo smooth transitions. At large βa the electric field is almost pure E_z and a mixed electromechanical and TM-type wave ensues. For smaller βa, the wave goes from TM to mixed TE to pure TE (Bevc and Everhart, 1961).

The upper branch shown in Fig. 5.16 is a backward wave whose characteristics are not influenced by the geometry and whose cutoff frequency is $\omega=(\omega_b^2+\omega_p^2)^{1/2}$ (Smullin and Chorney, 1958). This frequency is recognized as the transverse resonance or upper-hybrid frequency ω_{uh}

(see 1.4.53) for propagation across the magnetic field, from the Appleton equation (1.4.40). This wave is due apparently to a mixture of longitudinal and transverse electric fields, leading to electric polarizations both along and across the magnetic field. The passband of this wave corresponds to just the cutoff band of the electromagnetic extraordinary wave.

The angularly dependent spacecharge modes can exhibit Faraday rotation in certain circumstances. Considerable confusion may exist in experimentally distinguishing between these modes and *whistler-mode* waves, since both waves are slow and may have similar passbands. The whistler mode, of course, is a TEM wave and has no E_z component. Nearly any antenna in a finite plasma column has fringing fields that could excite the spacecharge wave, however, and since both modes require close antenna coupling to the plasma they could be equally excited. The propagation characteristics of the two waves depend very differently upon electron collision frequency and variations in geometry; some care in selecting the desired one is required.

5.5.4 ***Surface spacecharge waves on a drifting plasma column.*** The dispersion relations for a finite plasma column drifting along its own axis (z direction) with a velocity v_{0z} are found by applying the nonrelativistic equivalent of a Lorentz transformation to the dispersion relation

$$\omega' = \omega \pm \beta v_0 \tag{5.5.38}$$

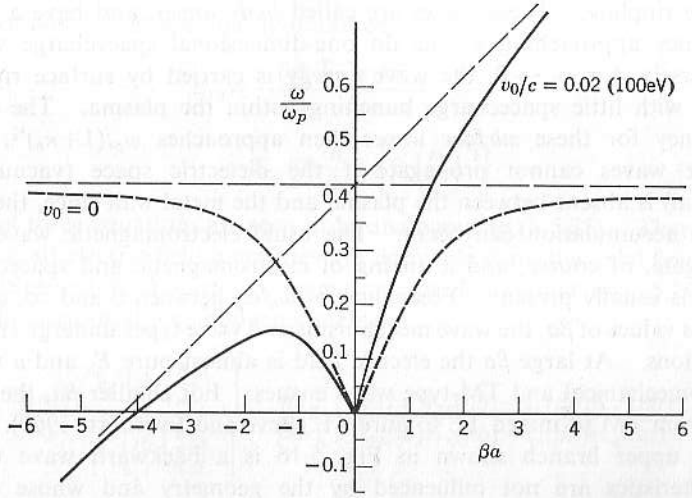

FIG. 5.17 Phase characteristics of surface waves on a drifting plasma column. Example shown is $c/\omega_p a = 5$ (for instance, $\omega_p/2\pi = 1$Gc and $a = 1$ cm).

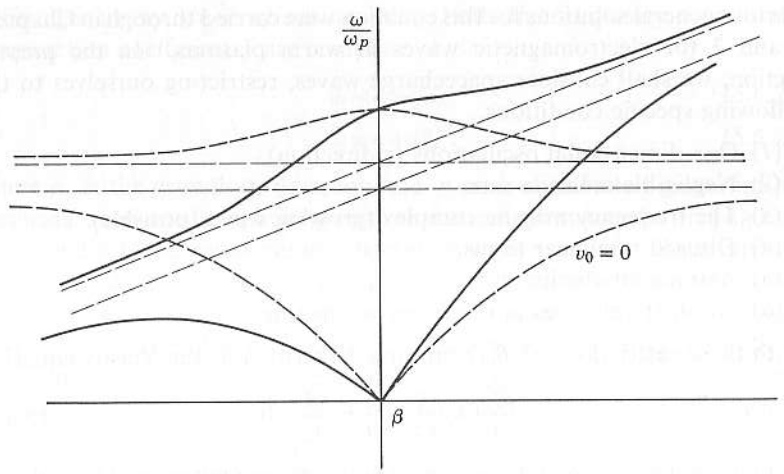

FIG. 5.18 Phase characteristics of spacecharge waves in a magnetic field in a drifting plasma.

where ω' is the frequency in a frame of reference moving at $\pm v_0$. The phase propagation curves (ω-β diagrams) are then tilted, the cutoffs being asymptotic to lines having the slope of v_0. The curves of Fig. 5.14 are replotted for a drift velocity $v_0/c = 0.02$ (100eV electrons) in Fig. 5.17. The phase characteristics of the magnetic-field case (Fig. 5.16) are replotted in Fig. 5.18 for the same drift velocity. We note that, in the laboratory frame, some of the waves that were forward waves are now backward waves and some are stationary. It is simply that the waves are being convected along by the drifting electrons; in the drifting frame of reference the wave characteristics are unchanged.

5.6 Spacecharge waves in a warm plasma

When the plasma temperature is high enough that the thermal electron velocity v_{th} is no longer negligible compared to the wave phase velocity v_ϕ, the dispersion relations must be derived somewhat differently. The kinetic theory method will now be used (Delcroix, 1960; Bernstein, 1958).

5.6.1 ***No magnetic field.*** It is convenient to start with the Boltzmann equation (2.4.4) of the electron velocity distribution function $f(\mathbf{r}, \mathbf{v}, t)$,

$$\frac{\partial f}{\partial t} + \mathbf{v} \cdot \nabla_r f + \mathbf{a} \cdot \nabla_v f = \left(\frac{\partial f}{\partial t}\right)_{coll}. \tag{5.6.1}$$

Various general solutions for this equation were carried through in Chapters 2 and 3 for electromagnetic waves in warm plasmas. In the present section, we shall consider spacecharge waves, restricting ourselves to the following specific conditions.

(*1*) One-dimensional oscillations (z direction).
(*2*) Negligible collision rate.
(*3*) The frequency may be complex (growing waves possible).
(*4*) Discard nonlinear terms.
(*5*) Assume adiabaticity.[1]
(*6*) No drift velocities in the frame of the ions.

With these restrictions, (5.6.1) can now be written as the Vlasov equation

$$\frac{\partial f}{\partial t}+v_z\frac{\partial f}{\partial z}-\frac{e}{m}E\frac{\partial f}{\partial v_z}=0. \tag{5.6.2}$$

Anticipating a wave with $\mathbf{E}\to E_z\exp(j\omega t-\gamma z)$, we may expand the velocity function as

$$f(\mathbf{r},\mathbf{v},t)\to f_0(\mathbf{v})+f_1(\mathbf{v})\exp(j\omega t-\gamma z), \tag{5.6.3}$$

where f_0 is the equilibrium distribution function, and (5.6.2) becomes to first order

$$(j\omega-\gamma v_z)f_1-\frac{e}{m}\frac{\partial f_0}{\partial v_z}E_z=0. \tag{5.6.4}$$

The divergence equation relates the electric field and the charge density,

$$\nabla\cdot\epsilon_0\mathbf{E}=-\epsilon_0\gamma E_z=-ne\int f_1\,d^3\mathbf{v}, \tag{5.6.5}$$

where the uniform positive-ion background has been assumed to cancel the equilibrium electron density. Substituting f_1 from (5.6.4) into (5.6.5) and canceling the arbitrary amplitude E_z, we have

$$-\epsilon_0\gamma=\frac{ne^2}{m}\int\frac{(\partial f_0/\partial v_z)\,dv_x\,dv_y\,dv_z}{j\omega-\gamma v_z}.$$

The integration over the transverse velocity components v_x and v_y may be carried out formally, to yield for the dispersion relation

$$1=\frac{j\omega_p^2}{\gamma}\int\frac{(df_{0z}/dv_z)\,dv_z}{\omega+j\gamma v_z} \tag{5.6.6}$$

where $f_{0z}(v_z)$ is the one-dimensional equilibrium distribution.

[1] The adiabatic assumption allows the gas temperature to fluctuate due to density fluctuations. The neglect of this effect (the isothermal approximation) leads to a factor of 1/3 discrepancy in the thermal term in the final dispersion relation (Bernstein and Trehan, 1960).

For generality we may assume that both the frequency ω and the propagation coefficient γ are complex,

$$\breve{\omega}=\omega+j\alpha_\omega \tag{5.6.7a}$$

$$\breve{\gamma}=\alpha+j\beta, \tag{5.6.7b}$$

where α_ω is the growth or damping rate in time of an initial perturbation, α as usual accounts for spatial growth or damping in space of a propagating wave, and β is the usual phase constant or wave number. Both types of growth or damping may occur in a given situation. Since we ignore collisional damping, we shall neglect α and use explicitly the imaginary part β of the complex propagation coefficient $\breve{\gamma}$. For small growth or damping rates, and for the condition that f_0 vanishes quickly beyond $v_\phi=\omega/\beta$, (5.6.6) can be expressed by a binomial expansion in the form

$$\frac{1}{1-x}=1+x+x^2+\ldots.$$

$$1=\frac{\omega_p^2}{\breve{\omega}\beta}\int\frac{df_{0z}}{dv_z}\left[1+\frac{\beta v_z}{\breve{\omega}}+\left(\frac{\beta v_z}{\breve{\omega}}\right)^2+\ldots\right]dv_z. \tag{5.6.8}$$

An integration by parts can be performed out to $v_z\lesssim\omega/\beta$, at which velocity the integrand has a pole. A contour integration around the negative side of this pole in the complex v_z plane yields the residue (Landau, 1946)

$$j\pi\frac{\omega_p^2}{\beta}\left(\frac{df_{0z}}{dv_z}\right)_{v_{th}}. \tag{5.6.9}$$

The complete integration of (5.6.6) is now

$$1=\frac{\omega_p^2}{\breve{\omega}^2}\left[0+1+3\left(\frac{\beta v_{th}}{\breve{\omega}}\right)^2+0+5\left(\frac{\beta v_{th}}{\breve{\omega}}\right)^4+\ldots\right]+j\pi\frac{\omega_p^2}{\beta^2}\left(\frac{df_{0z}}{dv_z}\right)_{v_{th}} \tag{5.6.10}$$

where v_{th} is the thermal speed. The zeros come from the assumed restriction of no drift motions in the frame of the ions. The third and higher order terms are seen to be negligible for the assumption that v_{th} is small compared to the phase velocity, that is, for low temperatures. The last term of (5.6.10) can represent either wave growth (an instability) or damping (Landau damping) depending on whether the term df_0/dv is positive or negative at v_{th}, that is, on the shape of the tail of the velocity distribution. The magnitude of the damping is roughly proportional to the number of particles moving with the phase velocity of the wave. For further discussion of Landau damping, see Section 3.5 and the references. To find the parameters governing the nonlinear limit of growth of unstable plasma waves, due for example to a bump on the tail of the electron velocity

distribution, one must apply nonlinear theory, for complete rigor retaining the collisional term on the right side of (5.6.1). The treatment then amounts to solving the Boltzmann-Fokker-Planck equation. To good approximation, this solution has been performed by Drummond and Pines (1961) for the quasilinear, collisionless case. The collisional case would be exceedingly complicated.

If the growth term α_ω is not small compared to ω or v_{th} is not small, then higher order terms of (5.6.10) must be retained to represent the total dispersion relation for one-dimensional spacecharge waves in a warm, collisionless plasma. If the growth (or damping) rate is sufficiently slow that an *e*-folding length is several wavelengths, some simplifications can be made to (5.6.10). Let

$$\alpha_\omega \ll \omega$$

$$a = v_{th}/\omega; \quad \frac{\pi\omega_p^2}{\beta^2}\left(\frac{\partial f_0}{\partial v}\right)_{v_{th}} = A_\omega.$$

The dispersion equation then becomes

$$1 = \frac{\omega_p^2}{\breve{\omega}^2}\left[1+3(\beta a)^2\right]+jA_\omega \tag{5.6.11a}$$

or by binomial expansion

$$\breve{\omega} \approx \omega_p\left[1+\frac{3}{2}(\beta a)^2+j\frac{1}{2}\frac{\omega^2}{\omega_p^2}A_\omega\right]. \tag{5.6.11b}$$

Since $\beta v_{th}/\omega$ and A_ω are in general small, the frequency at which wave damping or growth is maximum is only very slightly above ω_p. We note that when $v_{th}^2 = kT_e/m$, that is, for a Maxwellian distribution of electron velocities, then $a \approx \lambda_D$ the debye length, which is $\lambda_D = v_{th}/\omega_p = (\epsilon_0 kT/ne^2)^{1/2}$. The damping is found to increase rapidly at plasma wavelengths ($\lambda = 2\pi/\beta$) shorter than about one debye length, that is, when the phase velocity is about equal to the mean thermal velocity. For the general, non-Maxwellian case, the damping depends on the slope of the distribution function as seen in (5.6.11b). From (5.6.11b) the growth or damping rate in time is

$$\alpha_\omega \approx \tfrac{1}{2}\omega_p A_\omega = \frac{\pi\omega_p^3}{2\beta^2}\left(\frac{df_{0z}}{dv_z}\right)_{v_{th}}. \tag{5.6.12}$$

In terms of space, the corresponding growth or damping rate in (5.6.7b) is

$$\alpha = \frac{\alpha_\omega}{v_g} \approx \frac{\pi\omega_p^2}{2\beta}\left(\frac{df_{0z}}{dv_z}\right)_{v_{th}} \tag{5.6.13}$$

where v_g is the group velocity.

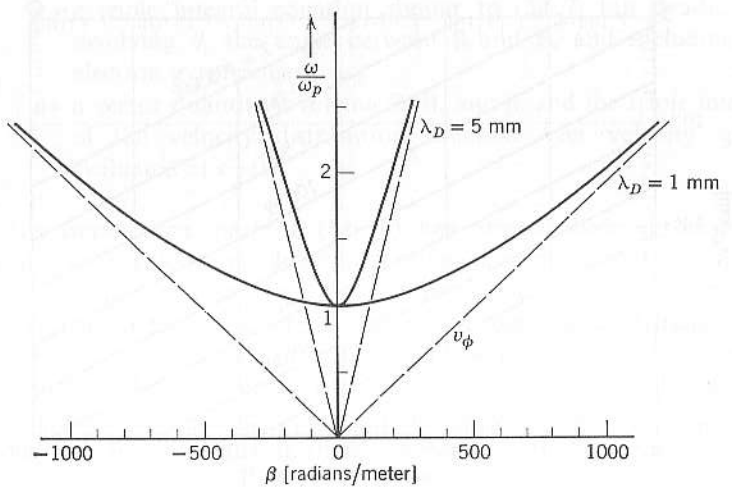

FIG. 5.19 The ω-β diagram for spacecharge waves in a warm, infinite plasma for different values of debye length λ_D.

In the steady-state condition (that is, $df_0/dv = 0$), the damping vanishes, and we recover the form of dispersion relation obtained in Section 3.3,

$$\omega^2 = \omega_p^2[1+3(\beta\lambda_D)^2] = \omega_p^2 + \frac{3kT}{m}\beta^2 \tag{5.6.14a}$$

or

$$\beta^2 = \frac{\omega^2-\omega_p^2}{3v_{th}^2} = (\omega^2-\omega_p^2)\frac{m}{3kT}. \tag{5.6.14b}$$

Equation (5.6.14) is plotted as an ω-β diagram in Fig. 5.19. In certain theoretical cases the damping does not have the exponential dependence shown here, but rather follows an inverse power law, a much weaker dependence (Weitzner, 1963).

In Fig. 5.20, the debye length for various electron temperatures is plotted against plasma density to show the orders of magnitude involved in experiments. Figure 5.19 shows that the propagation phase velocity is very slow for values of debye length typical of many laboratory plasmas. The group velocity, $d\omega/d\beta$, is also slow, tending to zero as $\omega \to \omega_p$. The product of the group and phase velocities for these thermal spacecharge waves is independent of frequency, and equals three times the one-dimensional mean-square thermal velocity,

$$v_\phi v_g = 3v_{th}^2 = \frac{3kT}{m} = 3\omega_p^2\lambda_D^2. \tag{5.6.15}$$

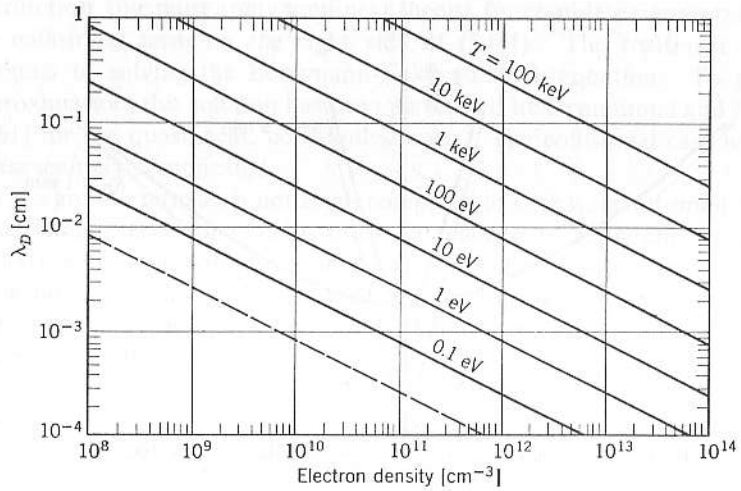

FIG. 5.20 Debye length in a plasma vs. electron density, as a function of electron temperature (see also Fig. 2.5).

5.6.2 ***Spacecharge waves in a warm, magnetized plasma.*** To derive the wave dispersion relation in this case, the Boltzmann equation (5.6.1) again is used but the $\mathbf{v}\times\mathbf{B}$ term must be included in the electric field

$$\frac{\partial f}{\partial t}+\mathbf{v}\cdot\nabla_r f-\frac{e}{m}\,[\mathbf{E}+\mathbf{v}\times\mathbf{B}]\cdot\nabla_v f=\left(\frac{\partial f}{\partial t}\right)_{coll}. \tag{5.6.16}$$

The Vlasov form of (5.6.16) (that is, omitting the collisional term) has been solved (Berstein, 1958) in the small signal case by perturbation analysis, using Laplace transforms. The waves can no longer be treated as one-dimensional because the medium is anisotropic.

Again, as in the discussion in Chapter 1 of electromagnetic waves at arbitrary angles to the magnetic field, we assign vector properties to the propagation coefficient $\breve{\gamma}(\approx j\boldsymbol{\beta})$. The frequency will be complex to allow for wave growth or damping.[2] After the Laplace and Fourier transforms have been applied to the distribution function and Maxwell's equations substituted in, the longitudinal wave part of (5.6.16) becomes

$$-\breve{\omega}^2\boldsymbol{\beta}\cdot\mathbf{E}+\mathbf{E}\cdot\mathbf{Q}\cdot\boldsymbol{\beta}=\boldsymbol{\beta}\cdot\mathbf{a} \tag{5.6.17}$$

where $\breve{\omega}=\omega+j\alpha_\omega$

[2] This linear treatment of course describes only the initial few e-foldings of any growing waves present, and not the final, saturation, equilibrium conditions of wave propagation. The latter would have to be arrived at with a nonlinear treatment (Drummond and Pines, 1961; Sturrock, 1961).

$\mathbf{Q}$ = a triple integral equation similar to (5.6.7) but dyadic and involving θ, the angle between $\boldsymbol{\beta}$ and $\mathbf{B}$, and including the electron gyrofrequency ω_b.

$\mathbf{a}$ = a vector quantity involving $\mathbf{E}$, $\mathbf{B}$, and $\boldsymbol{\beta}$, and the triple integral of the velocity distribution function over velocity space, evaluated at $t=0$.

The transverse wave part of (5.6.16) has already been discussed in Section 3.4, at which point Landau damping was introduced. Solutions of (5.6.17) can be found that yield either wave growth or damping, depending upon the slope of the tail of the distribution function (for example, a double-humped distribution leads to growth). The analogous situation for transverse waves may not occur, that is, the growth modes seem to be absent. The coupling between the longitudinal and transverse waves is, in general, small (Sturrock, 1961; Bevc and Everhart, 1961).

The general solution of (5.6.17) is exceedingly complex. Some simplified cases yield convenient results, however, and we shall discuss these.

For a small magnetic field and a Maxwellian distribution at low temperature, the dispersion relation is found by asymptotic expansion of (5.6.17). For the conditions $\omega^2\gg\omega_b^2$, α_ω^2, $\beta^2v_{th}^2$, the expansion yields, to first order, a dispersion relation similar to (5.6.14) but with an extra term involving the gyrofrequency

$$\omega^2=\omega_p^2+\frac{3kT}{m}\,\beta^2+\omega_b^2\sin^2\theta \tag{5.6.18a}$$

or

$$\beta^2=\frac{\omega^2-\omega_p^2-\omega_b^2\sin^2\theta}{3v_{th}^2}. \tag{5.6.18b}$$

Equation (5.6.18) is plotted in Fig. 5.21 for various values of ω_b/ω_p at an angle of 30°. Since the product $(\omega_b^2/\omega_p^2)\sin^2\theta$ is really the parameter, the curves also apply to other angles such that the products are 0, $\frac{1}{16}$, 1, and 4. The imaginary part of $\breve{\omega}$ gives the damping, analogous to (5.6.12). With $\partial f_0/\partial v$ written explicitly for a Maxwellian distribution, the damping is

$$\alpha_\omega\approx-\left(\frac{\pi}{8}\right)^{1/2}\frac{\omega_p}{\beta^3\lambda_D^3}\exp\left(-\frac{1}{2\beta^2\lambda_D^2}\right)\left[1+\frac{\sin^2\theta\,\omega_b^2}{24\beta^6\lambda_D^6\omega_p^2}\right]. \tag{5.6.19}$$

There is no growth possible for the Maxwellian distribution, since $\partial f_0/\partial v$ is always negative.

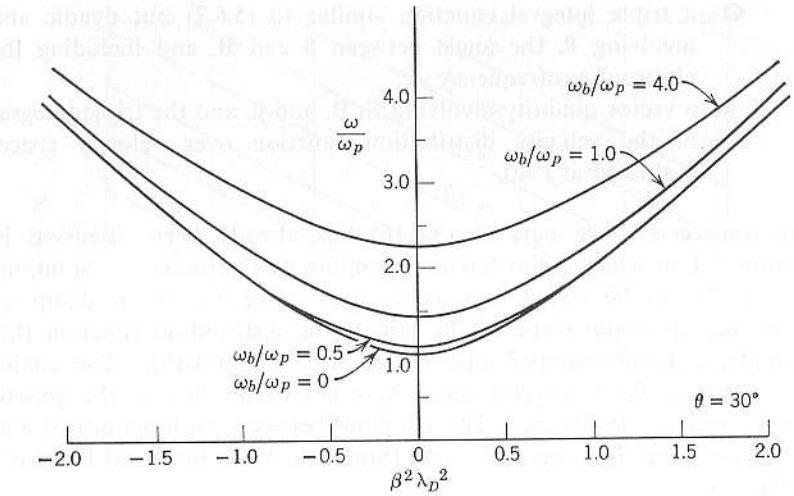

FIG. 5.21 The ω-β diagram for spacecharge waves in a warm, magnetized plasma. The curves are for constant $(\omega_b/\omega_p)\sin\theta$ but are labeled in ω_b/ω_p at $\theta=30°$.

The case of large magnetic field and low temperature (small gyroradius case) also yields uncomplicated results

$$\omega^2=\omega_p^2\cos^2\theta\,[1+3\beta^2\lambda_D^2-\rho_e^2/\lambda_D^2] \tag{5.6.20}$$

$$\alpha_\omega=-\left(\frac{\pi}{8}\right)^{1/2}\frac{\omega_p\cos\theta}{\beta^3\lambda_D^3}\exp\left(-\frac{1}{2\beta^2\lambda_D^2}\right) \tag{5.6.21}$$

where

$$\beta^2\rho_e^2\ll\beta^2\lambda_D^2\ll 1$$

$$\rho_e=(kT/m)^{1/2}\omega_b=\text{electron gyroradius.}$$

The growth or damping rate in space is given by (5.6.13) as before. The small gyroradius causes the plasma to behave as if the electrons moved only along **B**, and to lowest order (5.6.20) is the same as (5.6.14).

Another interesting feature of the finite ρ_e case is that for $\theta\to\pi/2$, that is, propagation across **B**, the Landau damping approaches zero, and within the passbands there is no wave attenuation. There are stopbands, however. For particular values of ω_b and ρ_e there are gaps in the propagation spectrum as $\beta^2\lambda_D^2$ is varied. For $\beta^2\lambda_D^2\ll 1$ the spectrum for longitudinal waves propagating across the B field is given by Bernstein (1958) as

$$\frac{\omega_b^2}{\omega_p^2}=\frac{1-\beta^2\rho_e^2}{(\omega^2/\omega_b^2)-1}+\frac{\beta^2\rho_e^2}{(\omega^2/\omega_b^2)-4}+\sum_{k=3}^{\infty}\frac{k^2}{k!}\left(\frac{\beta^2\rho_e^2}{2}\right)^{k-1}\frac{1}{(\omega^2/\omega_b^2)-k^2}. \tag{5.6.22}$$

Neither growth nor damping of the waves can exist for the assumptions just made. The gaps are also illustrated by writing the dispersion relation

$$\beta^2\lambda_D^2=\exp(-\rho_e^2\beta^2\sin^2\theta)\times\left\{I_0(\rho_e^2\beta^2\sin^2\theta)+\frac{\omega}{\omega_b}\sum_{k=1}^{\infty}I_k(\rho_e^2\beta^2\sin^2\theta)\left[\frac{1}{\left(\frac{\omega}{\omega_b}-k\right)}+\frac{1}{\left(\frac{\omega}{\omega_b}+k\right)}\right]\right\}. \tag{5.6.23}$$

Poles are seen to exist for $\omega=\omega_b$ and its harmonics. A plot of ω/ω_b vs. $\beta^2\lambda_D^2$ is shown in Fig. 5.22. The poles are clearly evident bounding the passbands and stopbands.

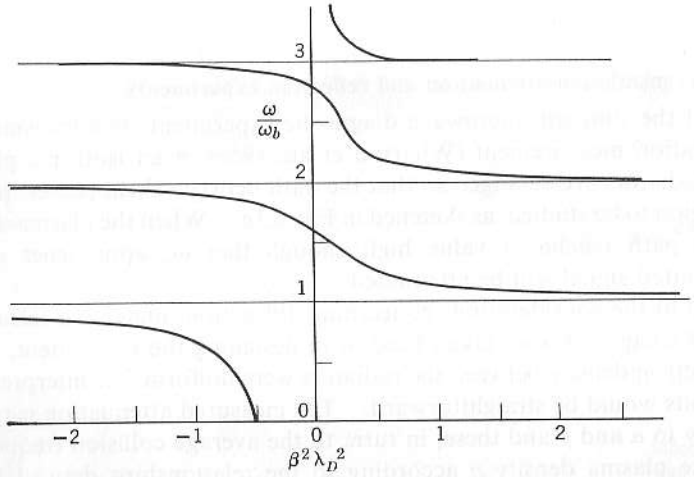

FIG. 5.22 Typical ω-β diagram for spacecharge waves propagating across the magnetic field ($\theta=90°$).

CHAPTER 6

Microwave propagation experiments

6.1 Transmission-attenuation and reflection experiments

One of the simplest microwave diagnostic experiments is a transmission-attenuation measurement (Wharton et al., 1955) in an isotropic plasma. Two radiators are arranged so that the path between them passes through the region to be studied, as sketched in Fig. 6.1*a*. When the plasma density in the path reaches a value high enough that ω_p approaches ω, the transmitted signal will be attenuated.

If all of the considerations concerning diffraction, matching, refraction, etc., of Chapter 4 were taken heed of in designing the experiment, and if the electron density between the radiators were uniform, the interpretation of results would be straightforward. The measured attenuation is related directly to α and β and these, in turn, to the average collision frequency ν and the plasma density n according to the relationships derived in the preceding chapters.

Such an ideal situation will seldom be found in practice, however. Any transmission path will necessarily have density gradients. The total attenuation will thus correspond to an integrated value of transmission coefficient, as pointed out in Sections 4.2 and 4.3. If the gradients are at all steep, compared to wavelength, there will be both external and internal reflections (French et al., 1961; Hain and Tutter, 1961), leading to interference fluctuations on top of the signal. There are plainly "more unknowns than equations" in the simplest experiment, and we must resort to more sophisticated measurements to get meaningful results.

6.1.1 ***Microwave circuits for transmission and reflection measurement.*** The transmission coefficient is related to the surface and internal reflection

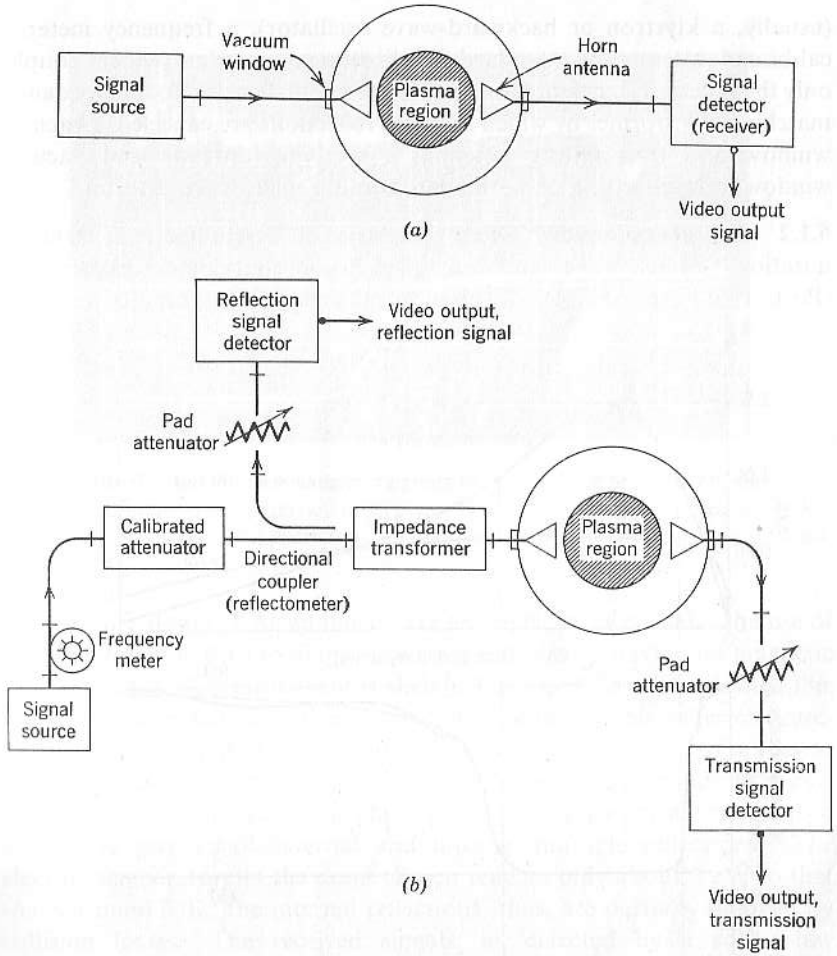

FIG. 6.1 Block diagrams of basic microwave transmission experiments in a plasma. Diagram *b* shows the addition of a directional coupler to permit observing reflections from the plasma.

coefficients. Two additional components added to Fig. 6.1*a* allow us to measure the over-all reflection from the plasma: a directional coupler and an additional detector. A typical composite circuit is sketched in Fig. 6.1*b*.[1] The complete circuit includes a source of microwave power

[1] The microwave components or "hardware" are described in some detail in Chapter 9. At this point, we treat components as blocks having certain properties, in building up the circuits. Readers wishing to familiarize themselves with the waveguide details are referred to Chapter 9 and to the references listed there.

(usually, a klystron or backward-wave oscillator), a frequency meter, a calibrated attenuation standard, a directional coupler (which couples only the reflected signal into the "reflection signal detector"), an impedance-matching transformer by which the fixed reflections are canceled, a vacuum window and transmitting antenna, a receiving antenna and vacuum window, a level-setting pad attenuator, and a microwave detector.

6.1.2 ***Transient plasmas.*** Often the plasma to be studied is of transient duration. Shock waves and controlled-fusion containment experiments (Post, 1958) are examples. The electron density rises rapidly and then

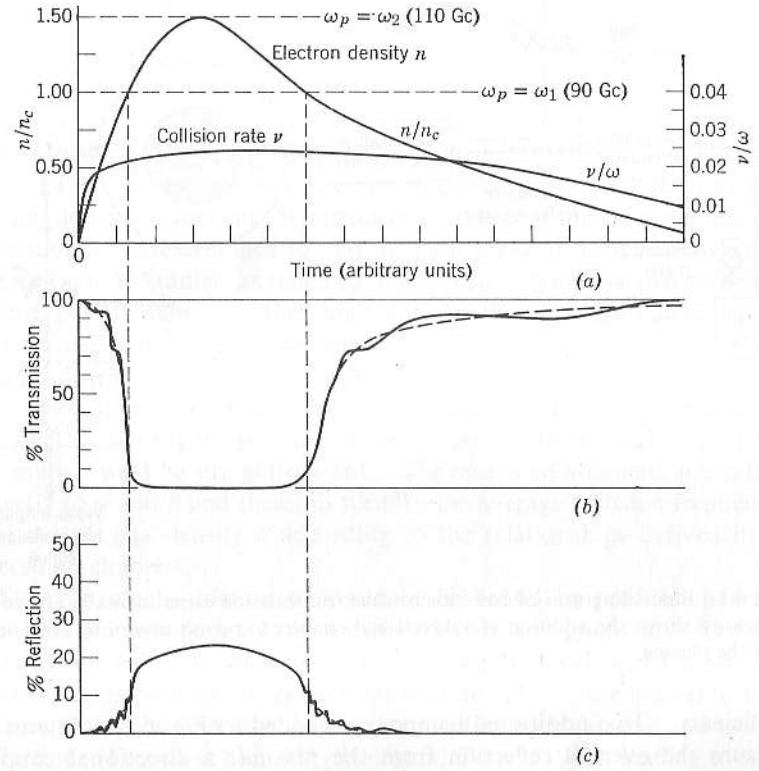

FIG. 6.2 Transient plasma event. The microwave transmission and reflection signals at a frequency of 90 Gc are shown, in relation to assumed density and collision-rate temporal variations (*a*). (*b*) Microwave transmission signal, detected by a silicon diode. Transmission path L through plasma is 6 inches. (*c*) Microwave reflection signal, detected by a silicon diode. The term 100% refers to reflection from a copper cylinder placed at the location of the plasma.

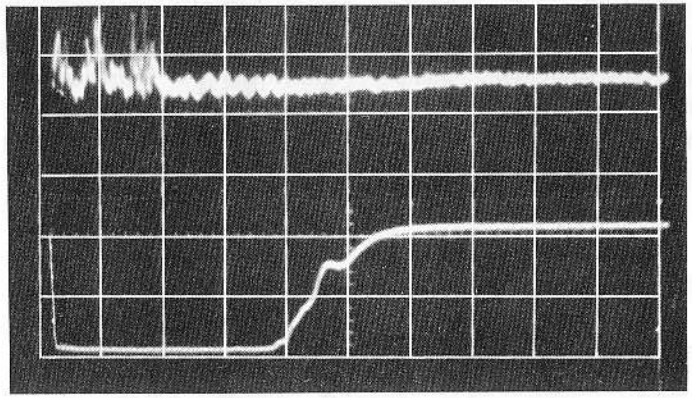

FIG. 6.3 Reflection and transmission signals for microwave propagation through a transient plasma. The frequency is 90 Gc. The amplitude of the reflection spikes corresponds to about 25% reflection. Time scale is 20 microseconds per division.

decays more slowly. As an illustrative example, let us consider the use of the circuit of Fig. 6.1*b* to diagnose a transient plasma having no magnetic field applied.[2] A typical event is sketched in Fig. 6.2*a*. The dashed line represents the density at which $\omega_p = \omega$. We estimate, from other measurements, a cosine spatial distribution of density, 23 wavelengths across at 90 Gc. A peak central density of $1.5 \cdot 10^{14}$ cm^{-3} corresponds to a cutoff frequency of 110 Gc. This plasma column has density gradients steep enough to give small external and internal multiple reflections. The electron temperature in the event chosen reaches only about 2 eV, so that ν/ω is around 0.02; the internal reflections, thus, are partially damped by collision losses. The received signals, as detected by a square-law detector (silicon crystal diode) are sketched in Fig. 6.2*b*. The small fluctuations, due to multiple reflections, are evident.

The reflected signal will depend upon the steepness of the gradient, since the signal must penetrate a lossy layer of plasma to reach the reflecting, cutoff plane and then pass through the layer again after being reflected. The magnitude of the fluctuations, then, gives a qualitative estimate of the steepness of the gradient. A typical reflection signal is sketched in Fig. 6.2*c*, where 100% corresponds to the reflection from a sheet of copper at

[2] The following data were taken by one of us (CBW) at the University of California, Lawrence Radiation Laboratory, on a high-density pulsed plasma experiment (Hester and Reagan, 1960), in the Controlled Fusion Program. We thank the University of California for releasing this unpublished data.

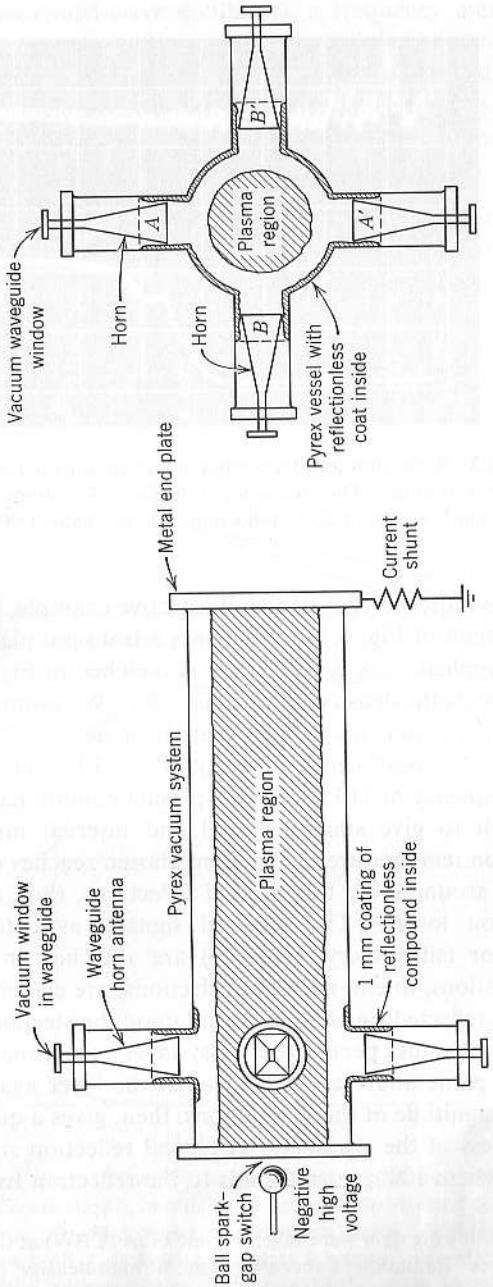

FIG. 6.4a Sketch of the vacuum system for transient plasma studies, showing the microwave diagnostic attachments.

the location of the plasma. The over-all reflection coefficient is seen to be less than 25% for these data. This is typical of many plasma experiments, including some controlled-fusion experiments; the plasma looks either transparent or surprisingly "black." Oscilloscope traces of reflection and transmission are shown in Fig. 6.3. The spikes of reflection correspond to about 25% and, presumably, arise from steep gradients due to turbulence. The rise rate of density is very fast compared to the decay rate.

6.2 Frequency diversity

The simple reflection-transmission experiment, just discussed, gives information only when the electron density is near cutoff, that is, $\omega_p \approx \omega$. Additional temporal information can be gained by using more than one

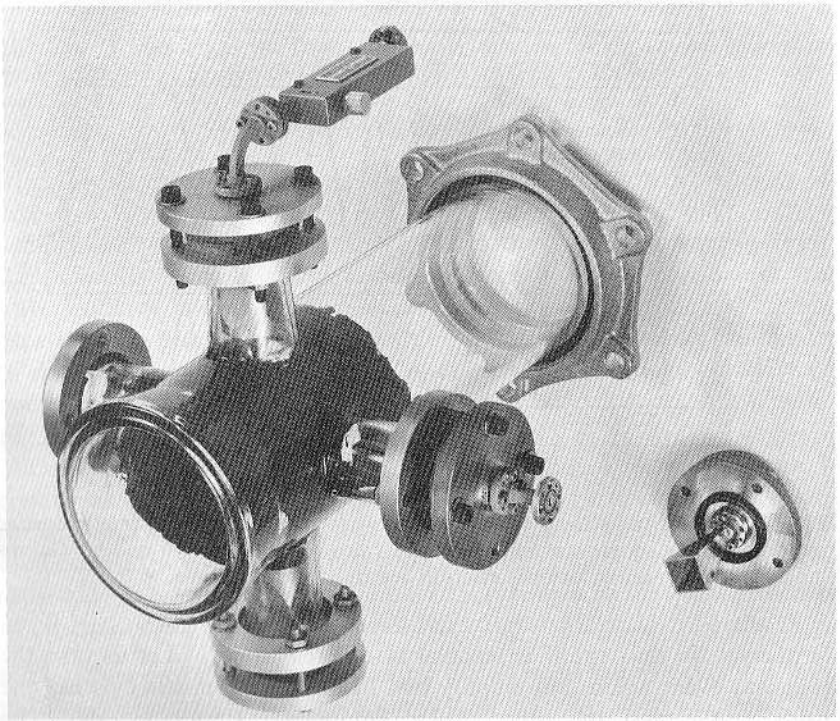

FIG. 6.4b Photograph of discharge chamber. Side arms containing the microwave horns and vacuum windows are shown. The two 70 Gc (4-mm band) horns are mounted in place. One of the 90 Gc (3-mm band) horns is shown removed. The black reflectionless coating inside the chamber can be seen in the vicinity of the horns. The chamber internal diameter is 3 inches. (Photograph courtesy of the University of California Lawrence Radiation Laboratory, Livermore, Calif.)

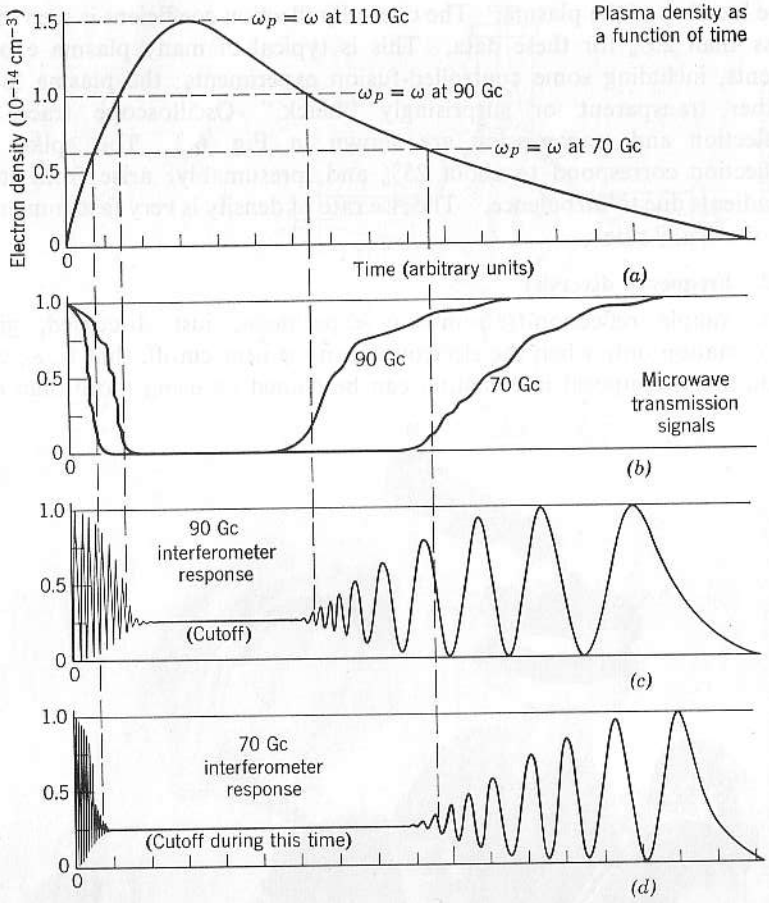

FIG. 6.5 Transient plasma event. Microwave transmission and interferometer responses, using square-law (silicon diode) video detectors, at 70 and 90 Gc are shown in relation to the assumed electron density variation in time.

frequency, so that cutoff is reached at different times. Let us take the transient event again, but employ two identical transmission paths, one using 90-Gc and the other 70-Gc equipment, simultaneously. The arrangement of radiators used is shown in Fig. 6.4*a*.[3] The horn radiators were $\frac{1}{2}$ inch in diameter, separated $3\frac{1}{2}$ inches. The $\frac{1}{2}$-inch dimension, calculated from (4.6.4), avoids Fresnel interference problems but gives poor coupling between the horns. Radiators of 1-inch diameter were

[3] See footnote 2.

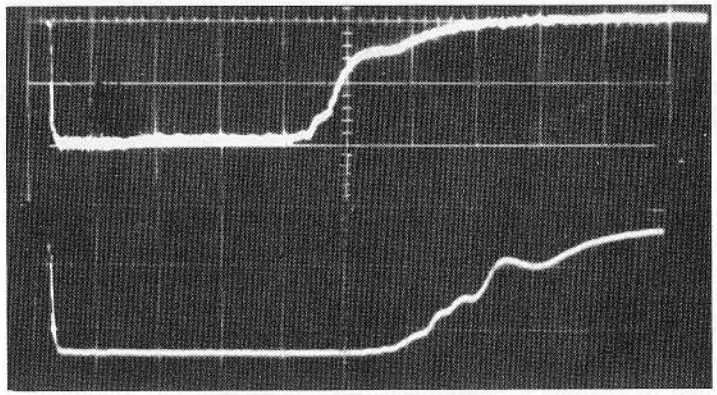

FIG. 6.6 Transmission amplitude signals for microwave propagation through a transient plasma. Frequencies of 90 Gc (top trace) and 70 Gc (bottom trace) were used.

tried, giving much closer coupling, but the Fresnel interferences were excessive.

Since the walls of the chamber are only a few wavelengths away from the transmission path, stray scattering of the diverging portions of the wave leads to spurious interferences. It was found necessary in this experiment to coat the walls of the chamber with a nonreflecting material[4] to eliminate these interferences. A photograph of the chamber, showing one of the vacuum windows and the absorbing coating, appears in Fig. 6.4*b*.

The idealized density variation is sketched in Fig. 6.5*a*, with the cutoff conditions shown by dashed lines. The resulting transmission signals, for square-law detectors, are sketched in Fig. 6.5*b*. Figure 6.6 shows an oscilloscope trace of measurements on a transient plasma event, recorded at 70 and 90 Gc. Small fluctuations ($< 5\%$) are seen on the trace, evidence of internal reflections. The over-all reflection signal is fairly small.

6.2.1 ***Frequency diplexers.*** A feature that is immediately evident is that unless a plasma in the configuration of Fig. 6.4 is symmetrical about the axis (it often is symmetrical) the two transmission paths do not traverse the same thickness of plasma. To ensure the same plasma sample L for both frequencies, the two paths may be incorporated into one pair of antennas by *frequency diplexers*.[5] The two signals are combined into one

[4] See Section 9.6.4 for descriptions of such materials.

[5] See Section 9.2.3.

waveguide, transmitted through the single path and, then, separated to two detectors.

6.2.2 ***Polarization Diplexers.*** *Polarization diplexers*, such as *fin-line couplers*,[6] can also accomplish the function of frequency diplexing, not by using frequency-selective filters but by orienting the two wave polarizations normal to each other. In an isotropic medium, free of nonlinear effects, the waves will not generally couple to each other, and will travel through the same effective path length. In an anisotropic plasma, the two waves of different polarizations will couple to different propagation modes. These effects are discussed in Section 6.5.

6.3 Phase-shift measurements

Without much additional complication, the circuit of Fig. 6.1 can be expanded to become a phase-measuring *interferometer*, analogous to the Mach-Zehnder interferometer used in optics. A *null path* is necessary to provide a phase and amplitude reference with which to compare the transmitted signal (or the reflected signal).

6.3.1 ***Microwave interferometer.*** The *interferometer* or *phase-bridge* circuit (Wharton and Gardner, 1959), sketched in Fig. 6.7, is particularly useful in measurements on transient plasmas. The reference path and transmission path are kept the same electrical length to avoid differential phase changes if the klystron frequency drifts. The circuit shows three detectors. Only the one labeled "phase detector" gives phase-shift information. The "transmission-amplitude detector" plays the role of the detector in Fig. 6.1.

In typical operation with transient plasmas the reference path is adjusted to null with the signal path in the absence of a plasma; the phase shift and amplitude then are observed as the plasma fills and then leaves the test path. The signal levels required depend upon the kind of detectors and video amplifiers used but, ordinarily, are in the microwatt-to-milliwatt range.[7]

An interferometer that is initially nulled will produce a maximum signal when the angle of the aggregate transmission coefficient has shifted 180°, and will return to a null at 360°, repeating indefinitely as the angle rotates through successive values of π and 2π. A square-law detector will yield a sinusoidal variation as the plasma density changes.

[6] See Section 9.2.3 for this and other polarization diplexers.

[7] Commonly, the detectors are silicon diodes. Up to about 100 microwatts, a silicon diode has a fairly faithful square-law response, that is, the output voltage is proportional to input power. The input-output characteristic then begins to straighten out, until at a few milliwatts the characteristic is nearly linear. Most microwave crystals are damaged by power levels in excess of 10 milliwatts.

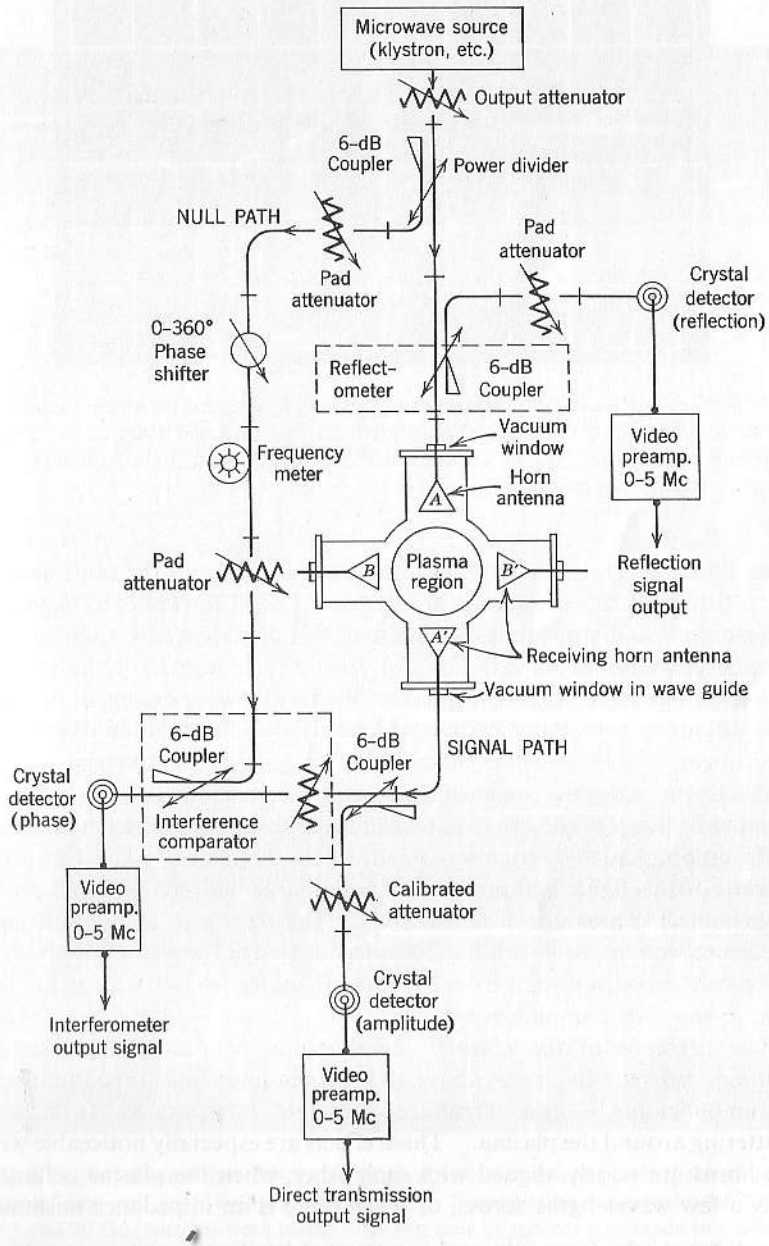

FIG. 6.7 Microwave interferometer and reflectometer for plasma diagnostics.

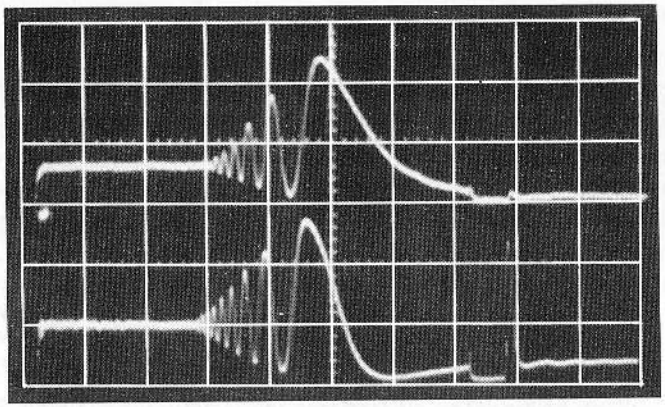

FIG. 6.8a Microwave interferometer responses to a transient plasma. Frequencies of 70 Gc (*top*) and 90 Gc (*bottom*) were used. Sweep time was 100 μsec/cm. Small calibration pulses at 750 μsec indicate that the bridges were slightly off null at the time the traces were made.

Oscilloscope traces of the interferometer responses to the same event as recorded in Fig. 6.6 are shown in Fig. 6.8. Cutoff for the two frequencies is reached at different times as the density falls from maximum to zero. A different number of variations or *fringes*[8] are noted for the two frequencies, due to the different number of effective wavelengths in the path. The attenuation of the signal is evidenced by the amplitude envelope of the fringes. In cases where the collision rate is high, so that signal cutoff is reached at a density somewhat below n_c (see Section 1.4), the observed number of fringes is less than expected for a given path length and density distribution. Such a situation is shown in Fig. 6.8*b*. The top set of records of this figure was made from a discharge between plane electrodes in helium at a pressure of 80 microns. The responses at the bottom of the figure were made by adding 200 microns (partial pressure) of argon, to increase the collision rate from a value of ~ 0.001 to $\sim 0.01\omega$ at the time of $\omega_p = \omega$. The damping is evident.

The presence of the plasma under certain conditions increases the coupling between the horns above the vacuum level (not to be interpreted as amplification!), and introduces multiple interferences from stray scattering around the plasma. These effects are especially noticeable when the horns are poorly aligned with each other, when the plasma column is only a few wavelengths across, or when there is an impedance mismatch.

[8] Analogous to the fringes observed in an optical interference pattern on a Mach-Zehnder or Fabry-Perot interferometer.

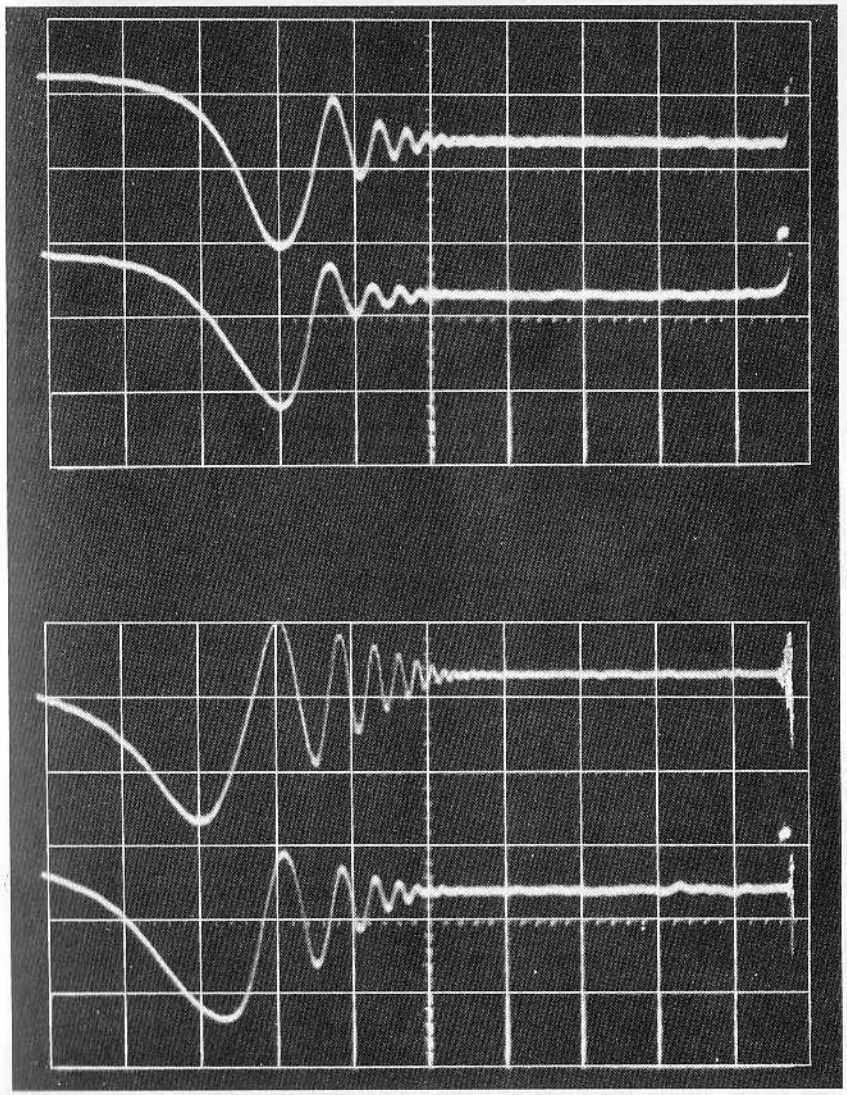

FIG. 6.8b Microwave interferometer responses to a transient plasma, showing the effect of low and high collision frequencies. Transmission frequencies of 70 Gc (*top*) and 90 Gc (*bottom*) were used. The top pair of records was made in a helium discharge at a pressure of 80 microns. The bottom pair was made after 200 microns of argon had been added.

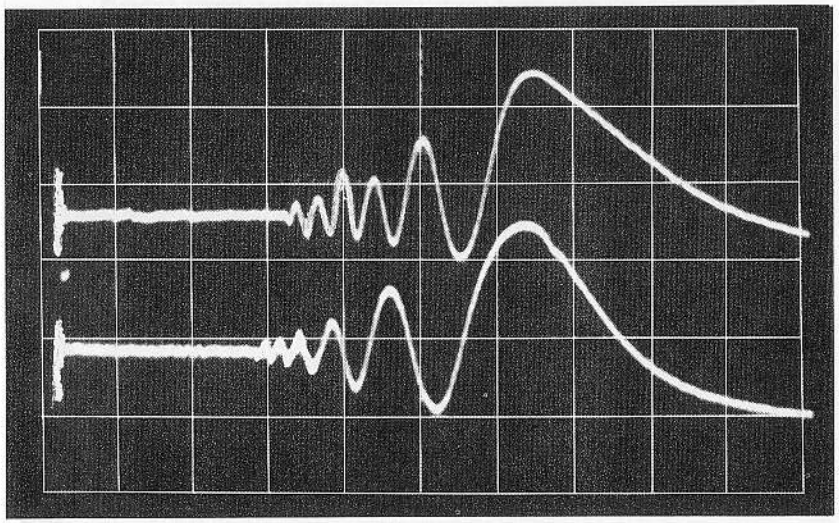

FIG. 6.8c Microwave interferometer response to a transient plasma showing the effect of horn misalignment. The top record was made with the 70-Gc horns misaligned by 20° in a discharge chamber 8 centimeters in diameter. The 90-Gc horns (*bottom record*) were properly aligned.

The effect of misalignment is shown in Fig. 6.8*c* to cause a distortion of the shape of the fringe envelope.

Photographs of a *K*-band (25 Gc) interferometer and a 3-mm band (90 Gc) interferometer are shown in Figs. 6.9 and 6.10. Components are arranged on panels for rack mounting. Coiled lengths of waveguide or flattened copper tubing[9] are mounted behind the panel to compensate the length of the null path (or the plasma path, whichever is longer) to avoid differential phase changes if the klystron frequency drifts.

6.3.2 ***rf Modulation envelope.*** The interferometer circuit of Fig. 6.7 may be used with an rf modulated carrier. The klystron is amplitude modulated, at say 500 kc to 30 Mc, and the amplifiers following the various detectors are tuned to the modulation frequency. The system then resembles a superheterodyne receiver, with the i.f. frequency being that used to modulate the klystron; the name pseudosuperhet is sometimes applied to this system. The i.f. modulation envelope may be demodulated but, for frequencies below about 2 Mc, is better viewed directly on the oscilloscope. The transmission amplitude signal will appear as shown in

[9] See Section 9.1.

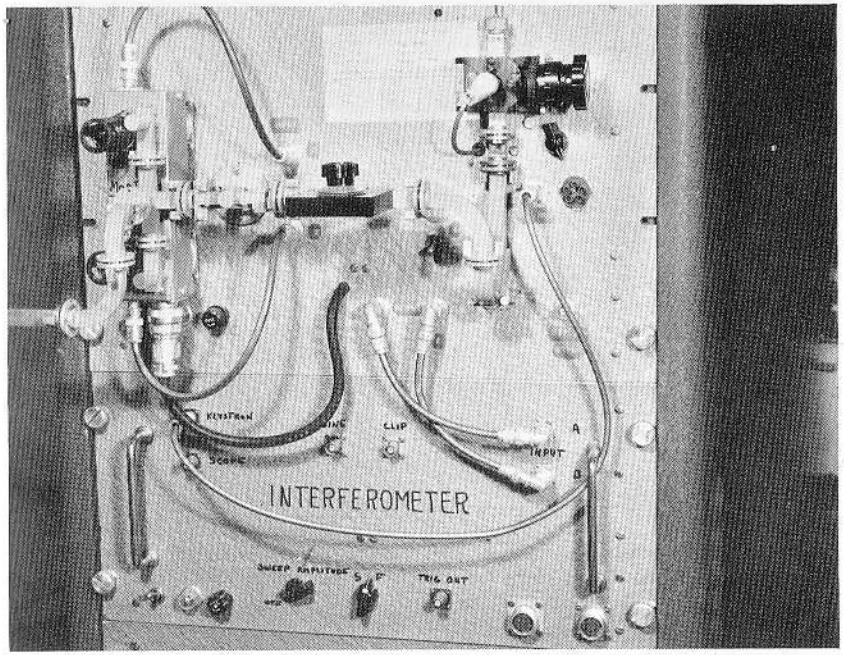

FIG. 6.9. *K*-band (22 to 27 Gc) panel-mounted microwave interferometer for fringe-shift (zebra-stripe) presentation. (Photograph courtesy of the University of California Lawrence Radiation Laboratory, Livermore, Calif.)

Fig. 6.11 (Buser and Buser, 1962). The interference fringes will appear as shown in Fig. 6.12. The Q of the tuned amplifier must not be too high if rapid fluctuations are to be followed. The amplifier band width must be at least $2/\tau_m$ where τ_m is the time from crest to crest of an interferometer fringe. A useful preamplifier circuit is shown in Fig. 9.50. The no-plasma signal level is easy to see with the modulation present, even without d-c amplifiers; this makes a system that is easy to keep in adjustment. If the two arms of the interferometer bridge are approximately the same length, the incidental microwave frequency excursion of the klystron caused by the modulation will not cause problems with differential phase shift.

The modulation envelope will be symmetrical about the base line if the amplifiers are linear. Stray pickup, which sometimes can shock-excite tuned circuits, will be asymmetrical and will cause the base line to bow; pickup is thus easy to distinguish from the real signal.

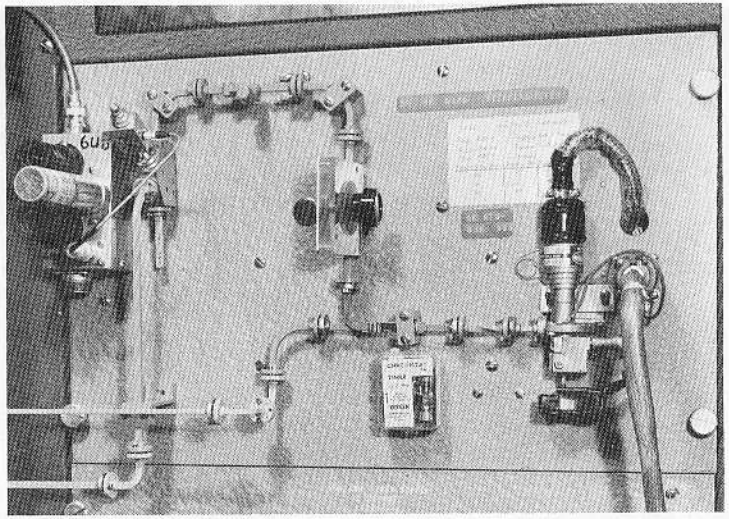

FIG. 6.10 A 3-mm band (89 to 95 Gc) panel-mounted microwave interferometer. (Photograph courtesy of the University of California Lawrence Radiation Laboratory, Livermore, Calif.)

6.3.3 ***Fringe-shift or zebra-stripe interferometer.*** A more sophisticated interferometer is the "fringe-shift" interferometer (Wharton and Gardner, 1959; Heald, 1959c). In this type of data presentation, the phase shift is plotted directly on the oscilloscope, and the effects of amplitude variations

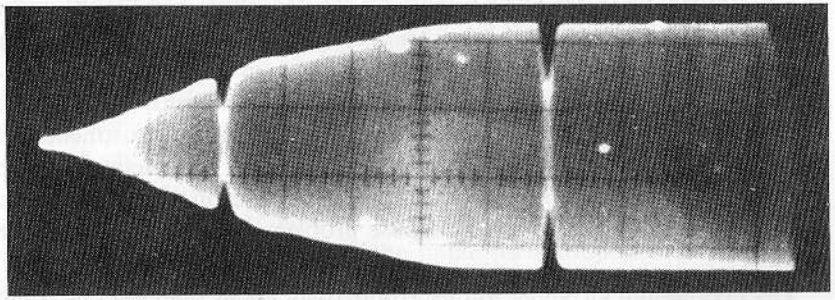

FIG. 6.11 An rf modulation envelope presentation of attenuation due to transmission through a plasma. The notches are time markers. (Photograph courtesy of R. Buser, Ft. Monmouth, N.J.)

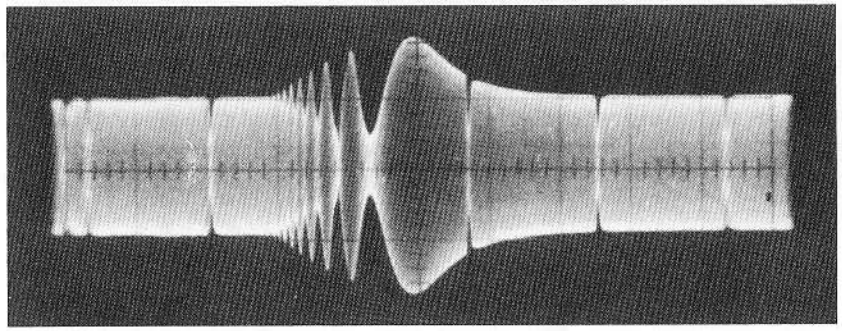

FIG. 6.12 The rf modulation envelope presentation of interferometer fringes for the same plasma event as that in Fig. 6.11. (Photograph courtesy of R. Buser, Ft. Monmouth, N.J.)

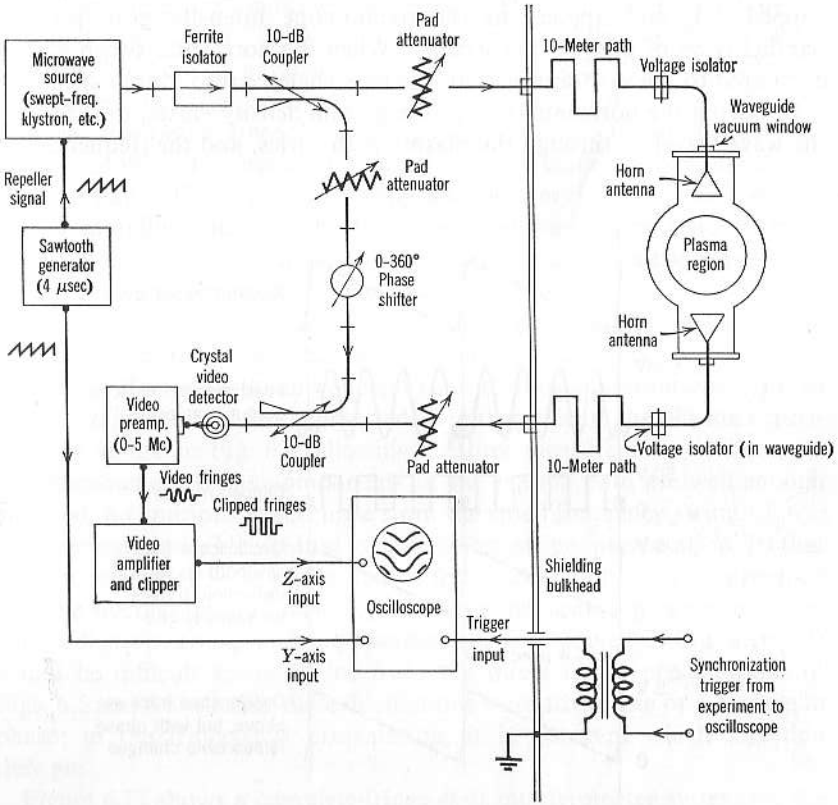

FIG. 6.13 Fringe-shift or zebra-stripe microwave interferometer for plasma diagnostics.

are discriminated against. The circuit of Fig. 6.13 shows the reference or null path to be very much shorter than the plasma path, so that when the frequency of the klystron is swept back and forth, by varying the repeller voltage, the bridge will generate several maxima and minima, the number depending upon the difference in length of the two paths and the frequency excursion. The change in phase in a waveguide of length L, due to a small frequency excursion Δf, is

$$\Delta\Phi=\Delta\beta\, L=2\pi L\,\frac{(\lambda_{g1}-\lambda_{g0})}{\lambda_{g1}\lambda_{g0}}\approx\frac{2\pi L}{\lambda_g}\left(\frac{\lambda_g}{\lambda}\right)^2\frac{\Delta f}{f}. \qquad (6.3.1)$$

The phase change seen by the interferometer, then, is due to the difference in the lengths of the reference path and the plasma path, $\Delta L=L_p-L_{ref}$. The 0 to 360° phase shifter adjusts the position of the fringes on the frequency scale. Figure 6.14 shows how the fringes, when amplified, clipped flat, and applied to the oscilloscope intensity grid, produce parallel rows of bars on the screen. When the horizontal sweep is slow compared to the sawtooth period, the bars coalesce into "zebra stripes."

If, during the horizontal sweep, the plasma density varies, the phase of the wave traveling through the plasma path varies, and the frequencies at

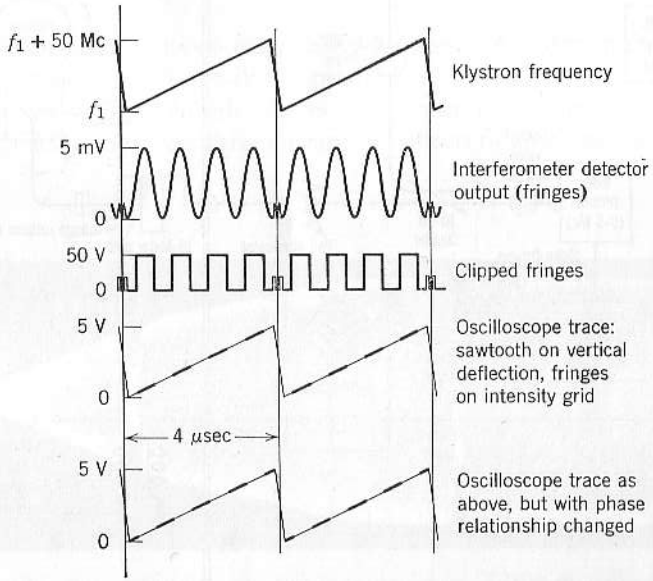

FIG. 6.14 Sawtooth frequency variations and corresponding interference pattern in zebra-stripe interferometer.

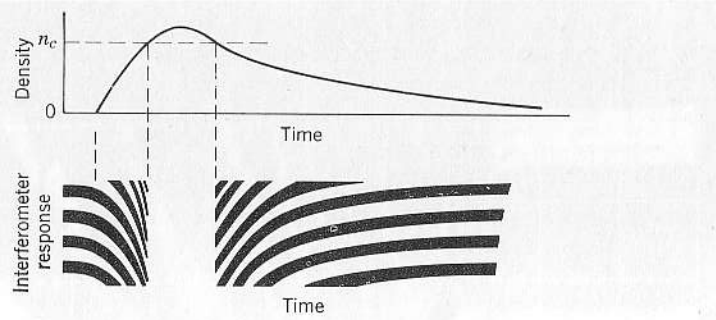

FIG. 6.15 Zebra-stripe fringe shifts in relation to an assumed plasma density variation.

which the fringe maxima occur are shifted. The stripes shift vertically, as indicated in Fig. 6.15. This figure represents the response of the fringe-shift interferometer to a transient plasma as in Fig. 6.2. Four fringe shifts are observed, denoting an effective phase change of $4\times 2\pi$. The deflection is shown downward, since the effective index *decreases* (from one down to zero at cutoff). The horizontal sweep speed is made appropriate to the plasma event. If the plasma density changes very rapidly, the 4-microsecond sampling rate may be too slow, and the fringes tend to blur. Sweep rates faster than about 1 microsecond require very broad-band video systems to handle the fringes (Lisitano, 1962).

Since the fringe-shift method discriminates against amplitude variations, separate phase, reflection, and transmission amplitude measurements must be made. Two directional couplers (one to look at reflections, one to look at transmission) can be inserted on either side of the plasma experiment as before in Fig. 6.7, allowing all three measurements to be made simultaneously. If the components in the plasma path are well enough matched, no spurious effects arise from the small frequency swing.

A second desirable feature of the zebra-stripe presentation is that fluctuations, + or − in phase, can be followed unambiguously, provided that the fluctuations are slow compared to the sawtooth sampling time. An oscilloscope trace, showing fluctuations, is displayed in Fig. 6.16. It would be difficult to determine from the direct fringe presentations of Figs. 6.5 and 6.8 whether these fluctuations were advancing or retarding in phase; in the fringe-shift presentation, it is apparent which direction they go.

Figure 6.17 shows a complete fringe-shift interferometer system for the 4-mm band (68 to 72 Gc) as developed at the plasma physics laboratory of Princeton University. The packaged system is quite flexible and easy to

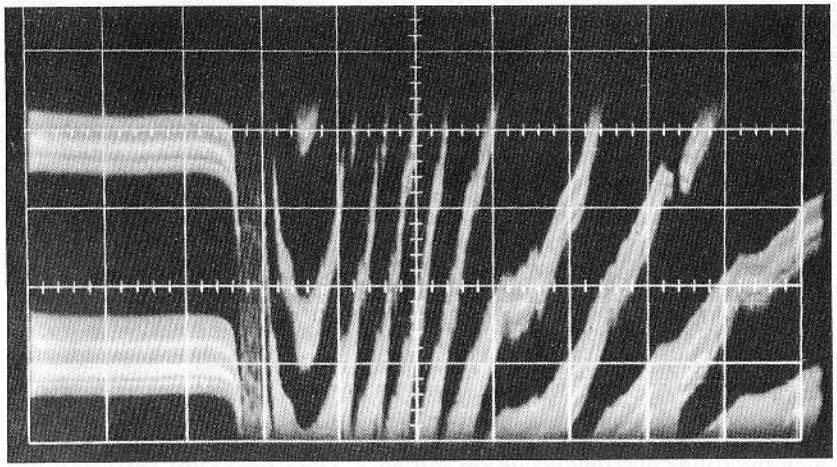

FIG. 6.16 Fringe-shift presentation of interferometer response to the extraordinary wave propagation ($\theta = 90°$, $\mathbf{E} \perp \mathbf{B}$) in a Stellarator plasma at $\omega_p/\omega = 1.008$. Sweep speed is 400 μsec/cm; sampling rate (vertical sawtooth), 4 μsec. (Courtesy of S. P. Schlessinger, Princeton University, Princeton, N.J.)

set up on a variety of plasma experiments. The *K*-band interferometer, shown in Fig. 6.9, can be used for either the direct fringe or zebra-stripe presentation.

6.3.4 ***Polar plot display.*** If the microwave frequency excursion is reduced until only one fringe shift is obtained, and if the preamplifier is tuned to the frequency corresponding to the fringe sweep time (250 kc for the 4 microsecond sawtooth sweep of Fig. 6.14), a sinusoidal output is obtained. The amplitude and phase of the sine wave depend upon the same conditions as just described. To obtain a polar plot of the amplitude and phase changes due to plasma in the path, the circuit of Fig. 6.18 is substituted for the amplifier-clipper of Fig. 6.16 (Lisitano and Tutter, 1961; Osborne, 1962; Lisitano, 1963). The 90° phase difference of the phase-splitter yields a circle on the oscilloscope whose amplitude is proportional to the input signal amplitude. A fiducial mark, obtained from the sweep retrace time, applied to the intensity grid gives a bright spot on the circle at a position depending on the phase. If both the phase and amplitude vary, a spiral is obtained.

Time calibration is difficult with this data display, and it is most appropriate for following variations in steady plasma experiments. Fast transients may be followed, and a time calibration is inherent (although the sense of phase rotation is ambiguous), due to the 4-microsecond spacing

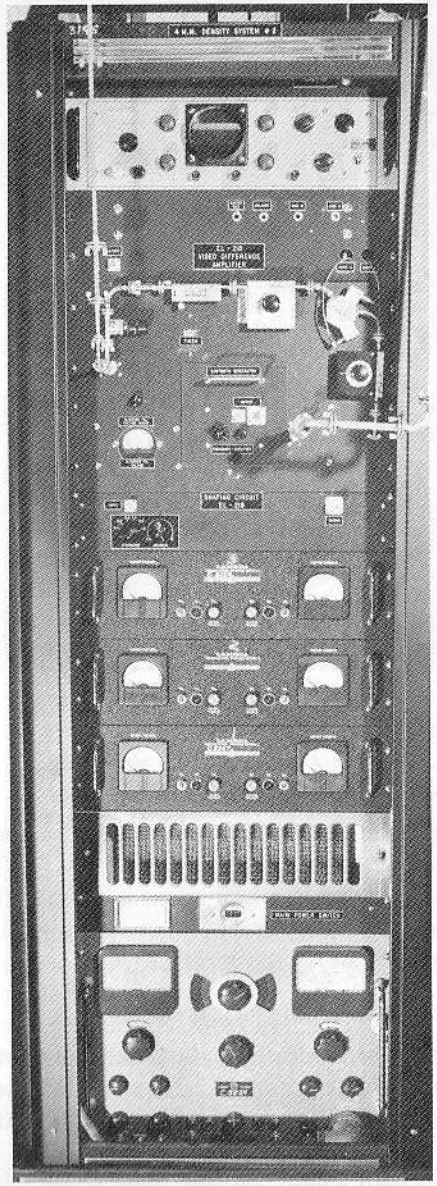

FIG. 6.17 Microwave fringe-shift interferometer system, rack-mounted for convenience. (Photograph courtesy of W. P. Ernst, Plasma Physics Laboratory, Princeton University, Princeton, N.J.)

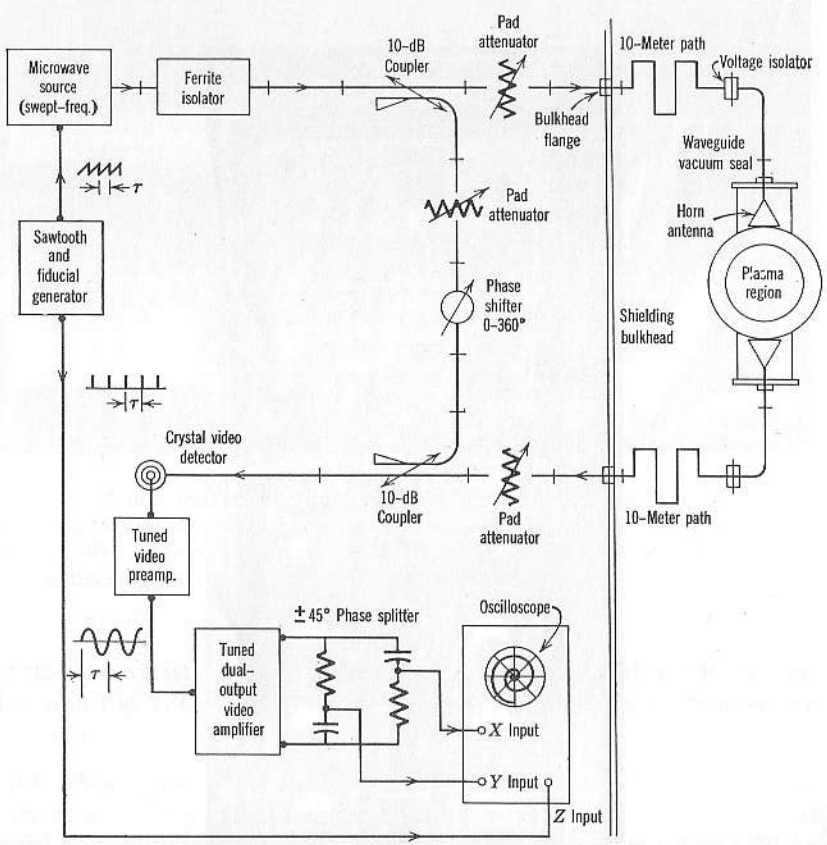

FIG. 6.18 Circuit diagram of microwave interferometer connected to yield data in polar plot form.

(in this example) between intensifying dots. A sample of data display is shown in Fig. 6.19.

6.4 Density distribution: profile measurements

Some techniques for profile determination were discussed in Sections 4.2 and 4.3. The results of integrating (4.2.2) over certain density distribution functions (Wharton and Slager, 1960), in the adiabatic approximation with no magnetic field present, are plotted in Fig. 6.20.

For a given total path length, the aggregate phase change, as the peak density varies from zero to cutoff, is considerably less than if the path were uniformly filled with plasma. For example, the phase change for a cosine distribution is 0.46 that for a uniform density; for a cosine-squared distribution, it is only 0.37. Since different numbers of wavelengths are within the plasma at different frequencies and since the phase shift at a given density is not a linear function of frequency, we have a graphical means of estimating the spatial density distribution.

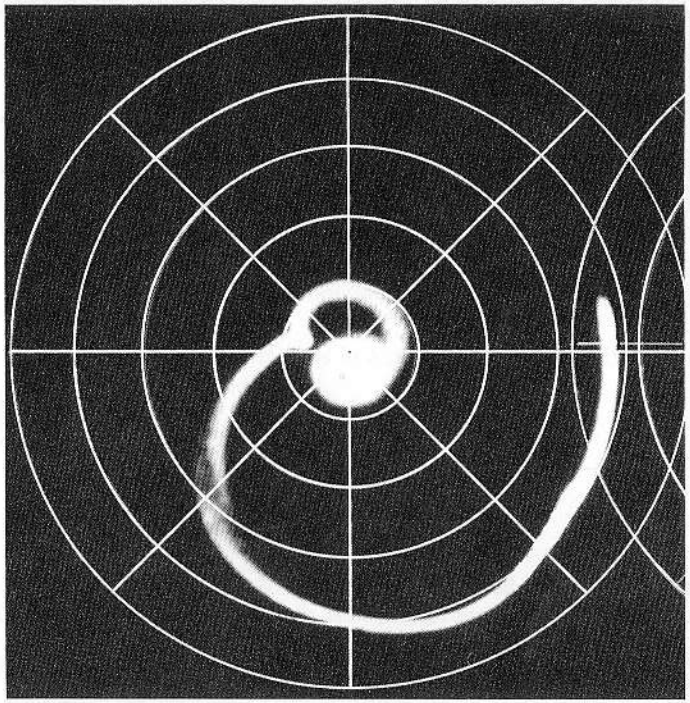

FIG. 6.19 Polar plot display of the phase shift due to a steady-state rf-excited plasma as the density is changed from 10^{10} to 10^{12} cm^{-3}. The transmission frequency was 35 Gc. (Photograph courtesy of G. Lisitano, Max Planck Institute, Munich, Germany.)

To illustrate the technique, the data analysis of a transient plasma experiment will be reproduced. Measurements were made on the Little Pig experiment (Wharton, 1959) at the University of California, Lawrence Radiation Laboratory, at several frequencies simultaneously. Figure 6.21 shows a photograph of the experiment in operation.[10]

[10] P.I.G. type discharge, often called a Penning or reflex discharge, consists of two cathodes, one at either end of a cylindrical anode, all inside a solenoidal magnetic field. The electrons are trapped within a potential well, and are reflexed back and forth between collisions (thus, the name "reflex"). The experiments of F. Chen (1962) and Landauer (1962) are good examples of P.I.G. discharges.

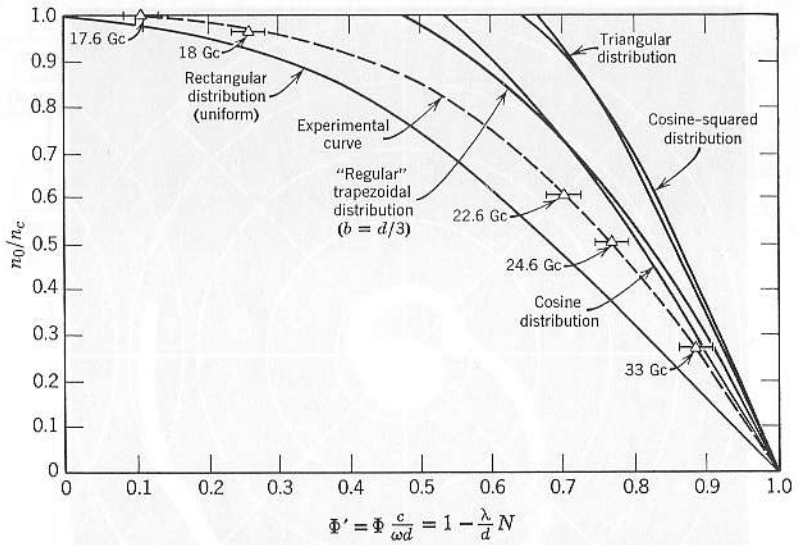

FIG. 6.20 Normalized phase shift as a function of peak plasma density for various spatial distributions. The aggregate phase shift was obtained by integration of (4.2.2) over the distribution. Experimental points (see Table 6.1) were obtained from a P.I.G. (or Penning) type transient discharge. (Wharton and Slager, 1960.)

The plasma conditions were such that the collision rate was small ($\nu \lesssim 0.01\omega$) and the gyrofrequency effects were negligible ($\omega_b \lesssim 0.01\omega$). The radial extent of 4.1 cm (radius) was determined by pushing a movable probe into the chamber until it just began collecting current; data were normalized to that dimension. Results at five frequencies, in all, were recorded. Cutoff occurred at 17.6 Gc, indicating a peak density n_0 of $3.8 \cdot 10^{12}$ cm^{-3}. The data presentation, showing the phase shifts for the four propagation frequencies, 18, 22.6, 24.6, and 33 Gc, appears in Fig. 6.22. Results are calculated from the phase-shift relation (4.2.2), derived in Section 4.2.2,

$$\begin{aligned} \Delta\Phi &= \Phi_0 - \Phi \\ &= \frac{\omega}{c}\left[d - \int_0^d \left[1 - \frac{n(x)}{n_c}\right]^{1/2} dx\right] \\ &= \frac{2\pi}{\lambda}\int_0^d 1 - \left[1 - \frac{n(x)}{n_c}\right]^{1/2} dx. \end{aligned} \tag{6.4.1}$$

The dimensionless phase shift, in terms of the number of fringe shifts N is

$$\Delta\Phi' = \frac{c}{\omega d}\Delta\Phi = \frac{\lambda}{d} N = 1 - \Phi'. \tag{6.4.2}$$

These values are tabulated in Table 6.1 and plotted in Fig. 6.20. The plot of a trapezoidal distribution with $b = d/6$ fits within the experimental points, and probably represents a good approximation to the true distribution. A rough check with Langmuir probes showed the profiles to be flat-topped, giving further correlative evidence with the microwave data.

Profile information from plasmas in a magnetic field may be obtained by methods discussed in Section 6.5.1.

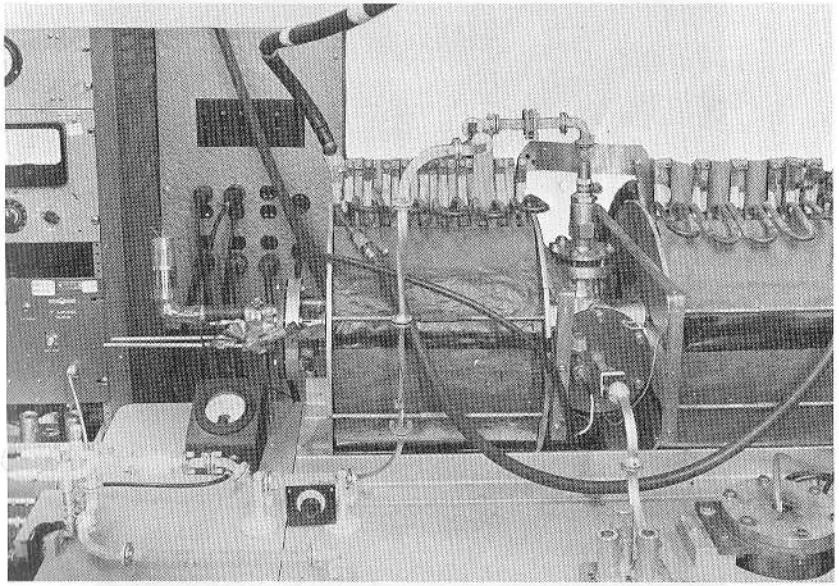

FIG. 6.21 Photograph of the Little Pig diagnostics correlation experiment. At the left is a 24 Gc (*K*-band) radiometer; right is a crystal video receiver for the interferometer. The vacuum flange on the left end carries one of the cathodes and an ion gauge. The front flange has a waveguide vacuum window, a voltage isolation section, and a Langmuir probe. The top flange contains a movable (Wilson) vacuum seal to permit the radiation-receiving antenna to be moved in and out of the plasma chamber. (Photograph courtesy of the University of California Lawrence Radiation Laboratory, Livermore, Calif.)

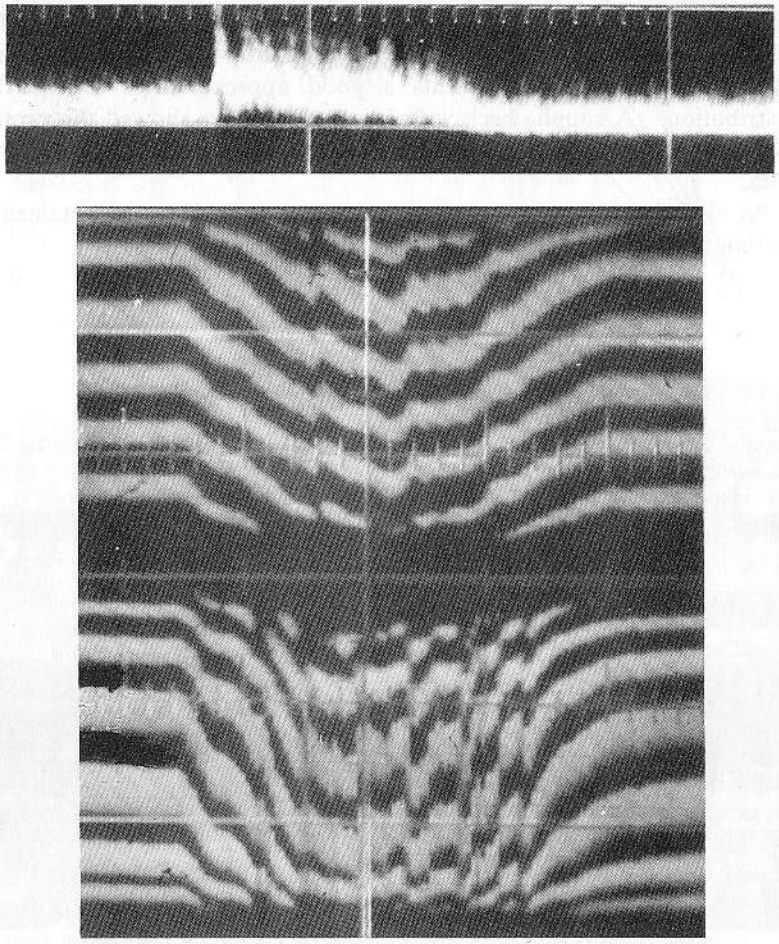

FIG. 6.22 Zebra-stripe data display of a transient plasma at four frequencies simultaneously. The frequencies are: 18 Gc, *lower left*; 22.6 Gc, *upper left*; 24.6 Gc, *lower right*; and 33 Gc, *upper right*. At *top right* is the anode current trace, one

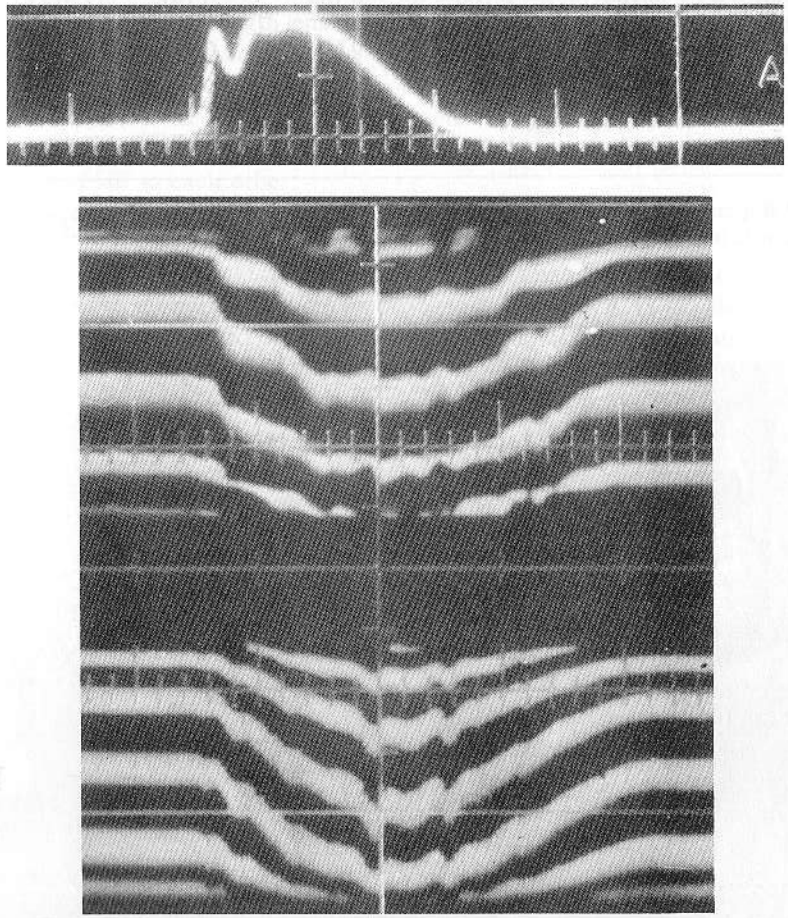

ampere maximum. At *top left* is the plasma radiation display, as received with a 24-Gc superheterodyne receiver. Time scale is 1 millisecond per major division. Phase-shift data at $t = 3$ msec is given in Table 6.1 and plotted in Fig. 6.20.

TABLE 6.1 TABULATION OF DATA FROM A PLASMA SAMPLE AT FIVE FREQUENCIES*

f[Gc]	17.6	18.0	22.6	24.6	33
λ/d	0.200	0.206	0.164	0.151	0.112
n_0/n_c	1.00	0.96	0.61	0.51	0.28
N	4.2	3.6	1.8	1.5	1.0
Φ'	0.11	0.26	0.70	0.77	0.89

* Repeatability of measuring N is $\pm\frac{1}{8}$ fringe. The values of N are taken from Fig. 6.22 at $t=3$ milliseconds. Plasma diameter $d=8.1$ cm.

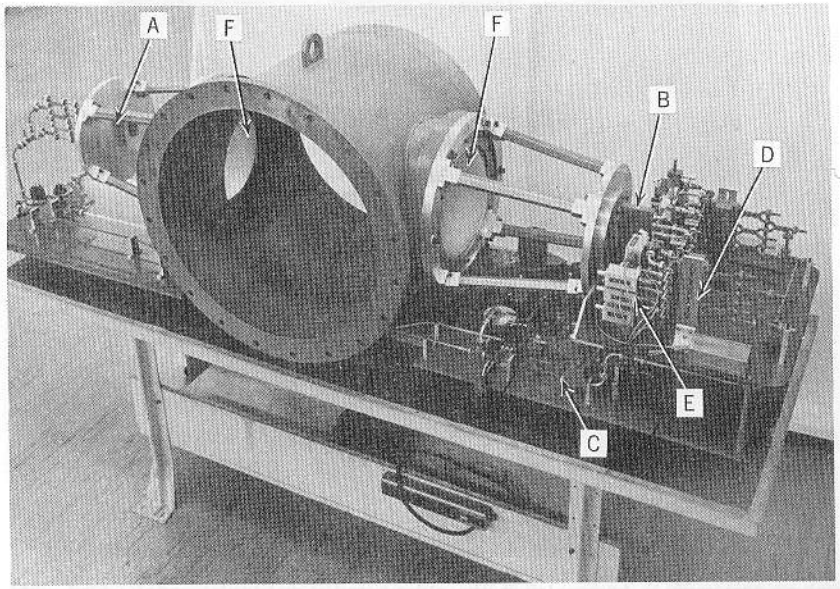

FIG. 6.23 A seven-beam, 70-Gc focused probing system. Seven transmitting horns (A), fed by dividing the power from a single klystron, are focused on the plasma by a lens (F). The seven receiving antennas (B) and split reference paths (C) feed signals to the waveguide junctions (D), which in turn supply the video detectors and preamplifiers (E). The on-axis vertical resolution of each beam is ~1 cm. (Photograph courtesy of R. I. Primich, General Motors Defense Research Laboratory, Santa Barbara, Calif.)

Geometrical scanning can be used to obtain profiles if the microwave beam can be focused to a diameter considerably smaller than that of the plasma. Either Abel integration or trapezoidal approximations of the transverse variations in depth of plasma can be used.

A multiradiator system, developed by Primich and Hayami (1963), provides focusing in the transverse plane by feeding a common 10-inch diameter, long focal length lens with seven horns. The resolution obtained on axis (−10 dB beamwidths) of each beam was 0.5 inch at 35 Gc and 0.25 inch at 70 Gc. A photograph of the apparatus is shown in Fig. 6.23. The multiple horns and the interferometer couplers appear at the right. The resolution is improved by having E-field polarizations of adjacent beams at 90° to each other.

6.5 Magnetic field effects

When a magnetic field is present in the plasma, there are additional quantities to measure. When we propagate a wave across the field lines ($\theta=90°$), we are able to couple to either the ordinary or the extraordinary wave. By using a square horn and waveguide and separating the two waveguide waves (E-fields at right angles with each other) with a polarization diplexer, we can transmit both waves simultaneously and make observations on a dual beam scope.

When we propagate along the field lines ($\theta=0°$), we can measure the Faraday rotation (Section 1.4.2) either by rotating the receiving horn or, again, by using the fin-line coupler to compare the relative magnitudes of the two (x and y) components. When the phase shift and Faraday rotation are combined, the bridge output shows amplitude fluctuations superimposed on the phase fringes. A 180° phase reversal also occurs with each half rotation. Losses in the plasma affect the two wave types differently, leading to ellipticity. An accurate measurement of Faraday rotation is thus difficult, since both the relative and absolute amplitudes of the x and y components are changing. When one of the circular polarizations is attenuated to cutoff, the Faraday rotation ceases, and both the x and y components behave alike, since there is only one wave remaining. If circularly polarized antennas are used to study these waves, the two counterrotating waves can be studied independently.

If the walls of the discharge chamber are close to the plasma, so that currents can flow on them, some ellipticity will result and true right-hand and left-hand waves do not exist. Also, when density and magnetic-field gradients are present, the modes are no longer clean. We observed in Fig. 1.19 that at $\omega=\omega_p$, when θ is not quite 0° and the collision rate is very low (Section 1.4.10), the left-hand wave jumps down to become the right-hand one (which is then cut off) and the right-hand wave jumps up

out of cutoff to become the left-hand one. We must, therefore, use caution, as pointed out in Section 1.4.4, when labeling waves as "left-hand" and "right-hand."

6.5.1 ***Ordinary and extraordinary waves: density profiles.*** The ability to propagate two wave types at the same frequency over the same path allows us to obtain considerable additional data. For particular experimental conditions, the appropriate frequency (or frequencies) is obtained by reference to Figs. 1.2 and 1.13. The values of refractive index vs. plasma density and magnetic field for the ordinary and extraordinary waves are given in Figs. 1.6 and 1.15, respectively. These values, of course, apply only at one particular location within the plasma; if density and/or magnetic field gradients are present (as they invariably are in real experiments), the aggregate transmission properties must be obtained by the methods discussed in Sections 4.2, 4.3, and 4.4.

In the large-plasma case, where the variations of density are gradual in the space of a wavelength in plasma, the adiabatic analysis applies to the total integrated transmission coefficient of the extraordinary wave as well as to the ordinary wave (Section 6.4). If the collision rate is low enough to be ignored, the phase shift for the extraordinary wave in a plasma path of extent d, may be approximated by

$$\Delta\Phi=\frac{2\pi}{\lambda}\int_0^d [1-\mu(x)]\,dx \tag{6.5.1}$$

where, from (1.4.50)

$$\mu\approx\left[1-\frac{\omega_p^2/\omega^2(1-\omega_p^2/\omega^2)}{1-\omega_p^2/\omega^2-\omega_b^2/\omega^2}\right]^{1/2}. \tag{6.5.2}$$

If, in addition, we are content to operate in the range in which $\omega_b/\omega<1$ and $\omega_p/\omega<1-\omega_b/\omega$, we may write the phase shift in the form of (4.2.2)

$$\Delta\Phi\approx\frac{-2\pi}{\lambda}\int_0^d\left(\left[1-\frac{n(x)}{n_c}\right]^{1/2}-1\right)dx \tag{6.5.3}$$

in which the cutoff n_c is no longer specified by $\omega_p^2/\omega^2\to 1$, but rather, on account of (1.4.52), by $\omega_p^2/\omega^2\to 1\pm\omega_b/\omega$. The same data analysis as used for the ordinary waves in Section 6.4 then may be applied and profile information obtained to a fair approximation. A limitation is that the shapes of the index curves for ordinary and extraordinary waves are not exactly the same, the maximum discrepancy leading to errors in calculated density as large as 25% for waves at 90° to **B**, but no error for waves at 0° (along **B**) (see Section 1.4.9). The advantage of using the two polarizations is that two points on the Φ' curve of Fig. 6.20 are obtained for each frequency, instead of one as before. The main limitation of the method is

that the magnetic field must be known and uniform in both space and time for (6.5.3) to be applied unambiguously.

Outside the ranges $\omega_p/\omega<1-\omega_b/\omega$ and $\omega_b/\omega<1$ the phase shift, due to plasma, must be obtained by an integration of (1.4.50) over the diameter

$$\Delta\Phi=\frac{2\pi}{\lambda}\left[\int_0^d\mu(x)\,dx-d\right]. \tag{6.5.4}$$

This integral is, in general, very difficult to evaluate, and is best done by machine or numerical calculation. Motley and Heald (1959) performed these calculations for a regular trapezoidal distribution and analyzed data

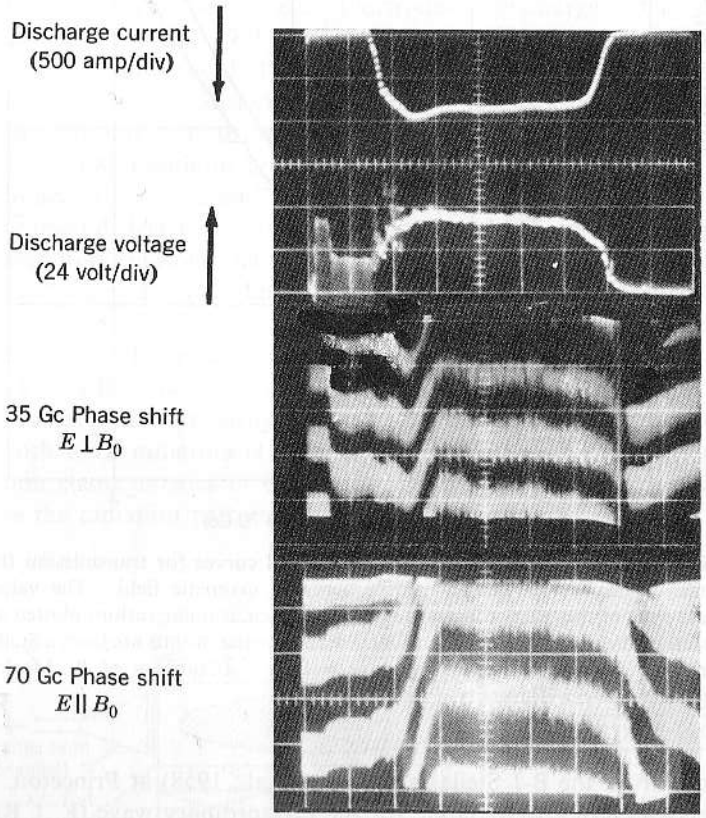

FIG. 6.24 Composite experimental data for crossed-polarizations measurement of plasma density profile in a Stellarator discharge. The magnetic field was 15.6 kilogauss ±10% during the current pulse. (Motley and Heald, 1959.)

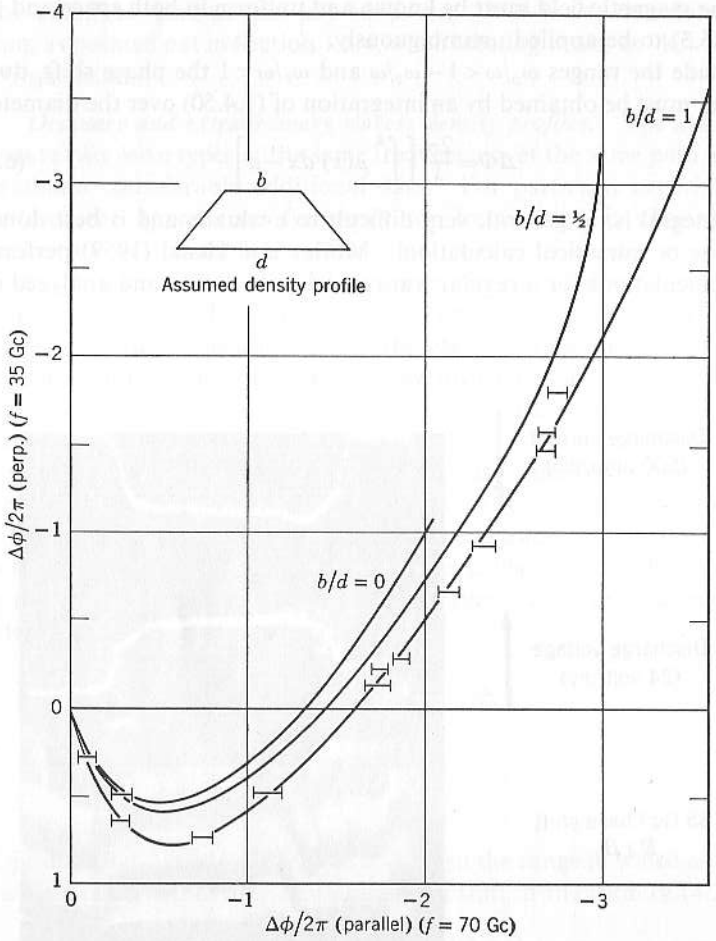

FIG. 6.25 Phase-shift data plotted on theoretical curves for transmission through a plasma of trapezoidal density profile across a magnetic field. The values are for phase shift of the extraordinary wave (perpendicular polarization) plotted against phase shift of the ordinary wave (parallel). Experimental points are from a Stellarator discharge at Princeton University; $\omega_b/\omega = 1.25$. (Courtesy of R. Motley and M. Heald, Princeton University, Princeton, N.J.)

obtained from the B-1 Stellarator (Coor et al., 1958) at Princeton. The frequencies chosen were 35 Gc for the extraordinary wave ($\mathbf{E} \perp \mathbf{B}$), and 70 Gc for the ordinary ($\mathbf{E} \parallel \mathbf{B}$), to optimize the sensitivity and measurable density range. The magnetic field intensity, and thus ω_b, were known very accurately. The fringe-shift (zebra stripe) interferometer presentations are shown in Fig. 6.24. The phase reversal as the refractive index goes through unity is apparent in the 35 Gc trace at 1200 μsec. No phase reversal is seen in the 70 Gc trace, since the index for the ordinary wave is always less than unity. Plots of the calculated phase shift for the two waves at various values of b/d, together with experimental points, are shown in Fig. 6.25. The points are seen to follow the plots of $b/d=1$ (uniform distribution) very closely. This is a reasonable conclusion for the Stellarator, since the plasma is defined by orifice plates at the diameter d to which these data were normalized.

6.5.2 ***Faraday rotation.*** When the ends of a magnetized plasma column are available so that antennas can be mounted with their radiation patterns looking along field lines as shown in Fig. 6.26, the circularly polarized waves can be studied. Electrodeless discharges (rf or pulsed) (Lisitano and Tutter, 1961) and plasma compression or confinement experiments (Consoli et al., 1961) usually lend themselves to such arrangements. Occasionally, discharge experiments are of a configuration that permits small radiators to be inserted directly in the discharge electrodes (Mahaffey, 1963) without upsetting the plasma uniformity.

If no access from the ends can be arranged, it is sometimes possible to insert curved dielectric rod antennas from the sides, as shown in Fig. 6.27. In low-collision plasmas, having small electron orbit sizes, the rods cast a "shadow" along the field lines, but in dense plasmas, or plasmas whose ions or electrons have gyroradii larger than the probe diameter, the rods seem to give little perturbation. Rods made of boron nitride or glass-bonded mica have low loss and low vapor pressure, are highly directive, are refractory, and are easily machined. An example of the use of such rods with horn radiators is shown in Fig. 6.27. The propagation and radiation characteristics of dielectric rods are given in Section 9.3. To confine the radiation pattern to the desired volume, the curvature of the

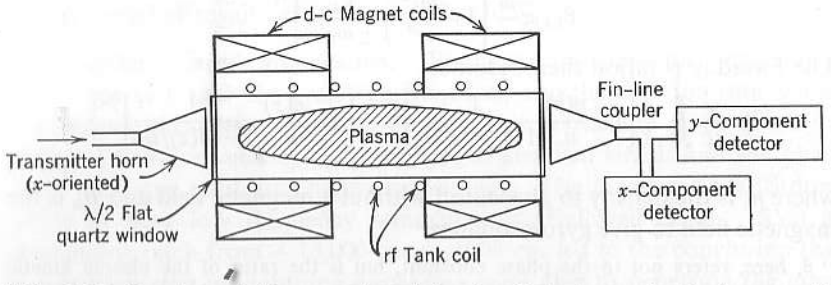

FIG. 6.26 Faraday rotation experiment in rf-excited plasma in steady magnetic field.

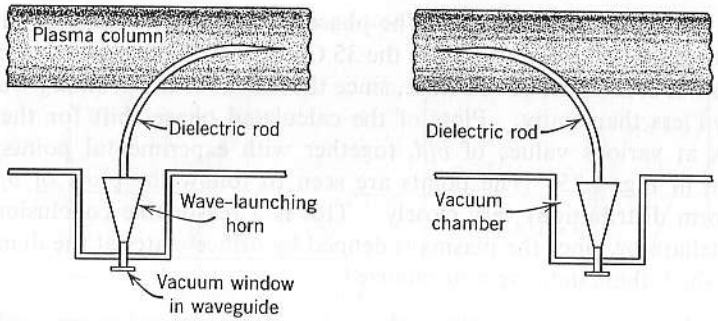

FIG. 6.27 Curved dielectric rods used to launch waves along the magnetic field (or at an angle to it) in a plasma.

bend must be gradual, and the diameter must be held large enough that most of the fields are within the rod until the taper at the end begins. Some photographs of curved dielectric radiators are shown in Fig. 9.37.

Because the waves transmitted through the plasma seldom emerge with purely circular polarization, it is difficult to make quantitative measurements of Faraday rotation. Nevertheless, when differential attenuation of the two counterrotating waves is not excessive, a measurement of the total rotation gives information about the plasma density in a path along the experiment axis.

If the magnetic field is known as a function of position, such as in low β plasmas[11] confined by external fields, the spatial distribution along the axis may be estimated by techniques similar to those described in Sections 4.2, 6.4, and 6.5.1. The total rotation is obtained by integrating (1.4.24).

$$\Psi=\frac{1}{2}\int_0^d \beta_l(z)\,dz-\frac{1}{2}\int_0^d \beta_r(z)\,dz. \tag{6.5.5}$$

In the case of low-collision-frequency plasmas the approximation of the phase constant β given in (1.4.20) can be used

$$\beta_{l,r}\approx\frac{\omega}{c}\left[1-\frac{\omega_p^2}{\omega^2}\frac{1}{1\pm\omega_b/\omega}\right]^{1/2}. \tag{6.5.6}$$

The Faraday rotation then becomes

$$\Psi=\frac{\omega}{2c}\int_0^d\left\{\left[1-\frac{n(z)}{n_c}\frac{1}{1+B(z)/B_R}\right]^{1/2}-\left[1-\frac{n(z)}{n_c}\frac{1}{1-B(z)/B_R}\right]^{1/2}\right\}dz \tag{6.5.7}$$

where n_c is the density to give cutoff without a magnetic field and B_R is the magnetic field to give gyroresonance.

[11] β, here, refers not to the phase constant, but is the ratio of the plasma kinetic pressure to magnetic pressure, $\beta\equiv nkT/(B^2/2\mu_0)$, a notation commonly used in controlled-fusion research.

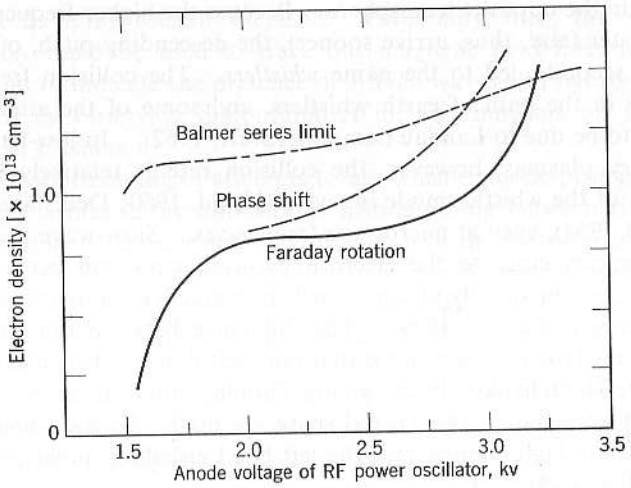

FIG. 6.28 Electron density in rf discharge, measured by three methods, as functions of rf level. (Compiled from data presented in Lisitano and Tutter (1961) and von Gierke et al. (1961).)

Equation (6.5.7) is difficult to integrate, but if B is constant or may be approximated by a stairstep function or a trapezoid, the same concept of an effective cutoff density as explained in Section 6.5.1 may be used for $\omega_p/\omega<1$ and $\omega_b/\omega<1$. In addition, reference to Fig. 1.11 shows that over a considerable range of densities the linear approximation of (1.4.20) may be used.

Using this approach in the data analysis of the experiment sketched in Fig. 6.26, Tutter (in von Gierke et al., 1961) obtained values of peak density and spatial distribution in reasonable agreement with optical and probe data (Schlüter, 1961) as well as with microwave phase-shift measurements across the plasma column (Lisitano and Tutter, 1961). Some compiled results are shown in Fig. 6.28.

6.5.3 ***Whistler mode propagation.*** When the transmission frequency is below but very near the cyclotron frequency and the collision rate is low, the plasma refractive index may be very high, especially if the density is high. The wave velocity and wavelength are then small, and the phase term β is large (and also highly dispersive). The investigations (Storey, 1953) of very low frequency atmospherics (Helliwell et al., 1956) of descending pitch from ~15,000 cps to 1000 cps led to the conclusion that waves generated by lightning discharges were able to penetrate the ionosphere and travel along the earth's magnetic field lines, being ducted back

to earth in the opposite hemisphere. Because the higher-frequency waves travel faster (and, thus, arrive sooner), the descending pitch, of duration about 2 seconds, led to the name *whistlers*. The collision frequency is very low in the path of earth whistlers, and some of the attenuation is thought to be due to Landau damping (Scarf, 1962). In low-temperature laboratory plasmas, however, the collision rate is relatively high, and damping of the whistler mode is severe (Heald, 1960; Dellis and Weaver, 1962 and 1964), even at microwave frequencies. Slow-wave propagation at frequencies close to the electron gyrofrequency can occur in high-temperature, low-density plasmas, such as in magnetic-mirror compression experiments (Wharton, 1959). The difference between this low-density case and the true whistler case is that both left-hand and right-hand waves propagate (Ichtchenko, 1962), giving Faraday rotation, unless circularly polarized antennas in the desired sense are used. In the whistler mode the density is high enough that the left-hand circularly polarized wave is cut off (Fig. 1.25).

An experiment at *S* band (3000 Mc) (Gallet et al., 1960) in ZETA, a large toroidal high-density pinch experiment at Harwell, England (Thonemann et al., 1958), demonstrated that waves appear to be confined to channels or ducts, only a millimeter or so in diameter, if the launching probe is small. The geometry is sketched in Fig. 6.29. The data obtained from this experiment indicated a maximum refractive index of about 12,

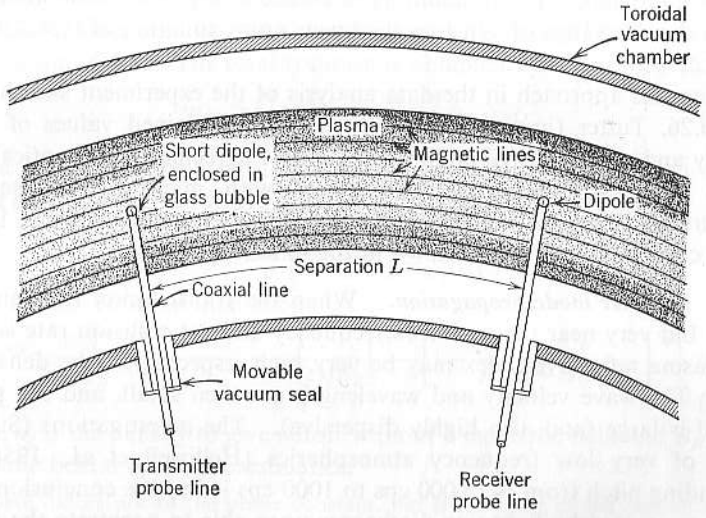

FIG. 6.29 Whistler mode experiment in ZETA (Gallet et al., 1960).

before the damping became excessive. Potentially, then, this mode of propagation could be used to trace out magnetic field lines in high-β plasmas and to indicate the presence of Alfvén waves and hydromagnetic instabilities by observing discontinuities in, and motions of, magnetic field lines in plasmas.

A serious shortcoming of attempts to use whistler-mode propagation in laboratory plasmas is the difficulty of distinguishing between this transverse electromagnetic wave and longitudinal or mixed spacecharge modes; they all have some similarities in dispersion characteristics and may all be excited by a dipole antenna in or near a plasma. Further discussion of spacecharge waves in magnetized plasmas can be found in Sections 5.5 and 5.6.

6.5.4 ***Propagation at angle θ to the magnetic field.*** Ionospheric observations of wave polarizations and dispersion as a function of reflection angle demonstrate that there is a measurable dependence on θ. In laboratory plasmas, however, it is difficult to see the effect. The difficulty is due mainly to the presence of wall reflections and stray scattering masking the signals. Figures 1.19 and 1.20 show resonances occurring at densities and magnetic fields that are clearly functions of angle. Unfortunately, as pointed out previously, these resonating regions occur in the interior of the plasma, and are surrounded by lower-density, cutoff regions. In the ionosphere, where stray scattering is no problem and where mode conversion can generate propagating "bridges" across the cutoff region, the effects are clearly seen.

A wave, by refraction in certain spatially varying magnetic fields, may be able to traverse a resonance region. For example, the propagation through a short magnetic mirror where both density and field gradients existed, was found, in unpublished work by Hill, Martin, and Wharton in 1957 at the Lawrence Radiation Laboratory, to have different resonance frequencies for $\theta=0°$, $\theta\approx30°$, and $\theta=90°$. The geometry is sketched in Fig. 6.30, where the dashed lines indicate the wave paths. The most interesting path is that at 30°. The wave enters the plasma at low density, but at $\omega_b/\omega>1$ (see Figs. 1.25 to 1.28). Both the density and magnetic field increase, at first, but then the field falls to the value at the center of the chamber. The angle θ has been changing slightly along the path due to field curvature. At the center, θ is the smallest although the density is (usually) high, so that resonance will be achieved here first as the density rises and last as the density falls. The paths at $\theta=0°$ and 90° yielded resonances at $\omega_b/\omega=1$ in their respective regions; the $\theta=30°$ path gave a resonance at a lower field strength.

The foregoing experiment was far from a clean, quantitative one.

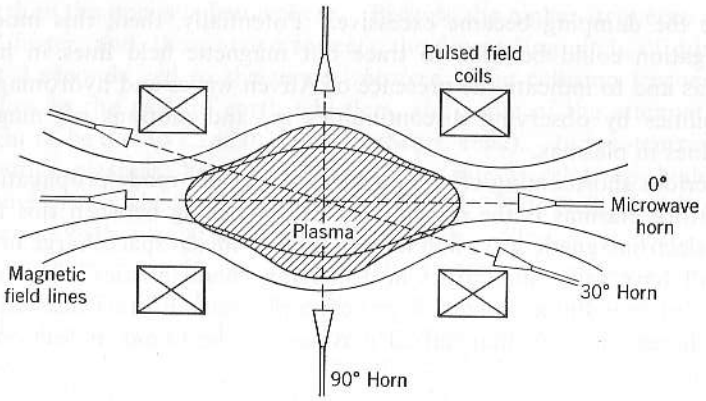

FIG. 6.30 Propagation at angle to the magnetic field lines in a mirror-compression experiment.

Nevertheless, the principles involved may be applied to certain classes of experiments where the parameters are under more precise control of the experimenter, in which case the results will be meaningful.

Coupling to the ordinary resonance of Figs. 1.27 and 1.28 can occur only through wave coupling or by "tunneling" of evanescent waves through cutoff regions. The resonance in either case would be quite small and easily masked by other spurious fluctuations. If it could be detected, however, the measurement of its position in frequency would extend the measurable plasma density a factor of 4 or 5 at angles near 60°.

6.5.5 ***Doppler-shifted gyrofrequency in drifting plasmas.*** When the electrons in a plasma are drifting along magnetic field lines, the electron gyrofrequency is doppler-shifted in the laboratory frame of reference. A circularly polarized wave, directed along the field lines, will then have a different transmission coefficient in one direction than in the other, especially noticeable if the frequency is near the electron gyrofrequency. The coupling rods shown in Fig. 6.27 allow transmission from left to right or from right to left. If the plasma being studied is drifting in either direction, the measurement of transmission coefficient will be non-reciprocal. The amount of nonreciprocity will depend upon the derivative of the curve of refractive index vs. frequency,[12] the maximum effect occurring at frequencies slightly below gyroresonance.

The effect, which is somewhat analogous to the Fizeau effect, is not an easy one to measure in practice unless the magnetic field and frequency are

[12] For example, see Fig. 1.9, obtained from (1.4.17).

well known and constant during the measurement. The change in wavelength in the moving medium is

$$\Delta\lambda = \pm \lambda\mu v_0/c \tag{6.5.8}$$

where λ is wavelength, and μ is the refractive index, and v_0 the drift velocity. The phase velocity in the moving frame is then

$$v_\phi = \frac{c}{\mu} - \frac{c}{\mu^2}\frac{d\mu}{d\lambda}\Delta\lambda = \frac{c}{\mu} \pm \frac{c\lambda}{\mu}\frac{d\mu}{d\lambda}\frac{v_0}{c}. \tag{6.5.9}$$

The phase shift observed in path length L from the left or right sense is thus

$$\Phi = \frac{2\pi L\mu}{\lambda}\frac{1}{\left(1 \pm \lambda\dfrac{d\mu}{d\lambda}\dfrac{v_0}{c}\right)} \text{ radians.} \tag{6.5.10}$$

As an example, consider that the plasma electrons are drifting with 10 eV of directed velocity ($v_0 = 2 \cdot 10^8$ cm/sec). Near gyroresonance, $\lambda\, d\mu/d\lambda$ may be between 10 and 100, and μ may be between 2 and 10, respectively. The differential phase shift for a given path length L/λ may, thus, be between 0.07 ($2\pi L/\lambda$) and 23 ($2\pi L/\lambda$) for the example chosen.

6.6 Propagation through fluctuating plasmas

A plasma whose electron density is fluctuating periodically may phase-modulate and amplitude-modulate an electromagnetic wave propagating through it. These effects are in addition to the Luxembourg effect (due to temperature fluctuations), discussed in Section 2.6. For example, an examination of the frequency spectrum of a signal transmitted through an rf-excited plasma invariably reveals side bands at frequencies displaced by the rf-excitation frequency and its harmonics (von Gierke et al., 1961). Figure 6.31 sketches such a spectrum, where f_m is the rf driving frequency. The harmonics, if present, presumably arise from nonlinearities (Dreicer, 1961).

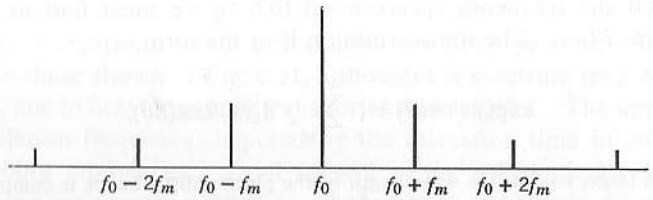

FIG. 6.31 Frequency spectrum of wave propagated through a plasma fluctuating at frequency f_m.

Suppose that the electron density is fluctuating sinusoidally with a small amplitude a, at frequency $\omega_m/2\pi$

$$n(t)=n_0(1+a\cos\omega_m t)=n_0+n_1(t), \quad \text{where } a\ll 1. \tag{6.6.1}$$

Ignoring damping, for the moment, the refractive index is then

$$\mu^2(t)=1-\frac{e^2 n(t)}{m\epsilon_0\omega^2}=1-\frac{\omega_{p0}^2}{\omega^2}-\frac{e^2}{m\epsilon_0\omega^2}\,n_1(t)=\mu_0{}^2-\mu_1{}^2(t) \tag{6.6.2}$$

where the subscript 0 represents steady-state quantities and the 1 represents first-order perturbation quantities. If the frequency of fluctuation ω_m is slow, the wavelength of the disturbance in the plasma will be large, and the electromagnetic wave as a whole will be equally affected.[13] There is not the limitation on modulation frequency here as we found in the Luxembourg effect, since here we do not have a relaxation time to consider. For $|\mu_1|$ smaller than about $0.2\mu_0$, the time-varying index may be approximated by expansion

$$\begin{aligned}\mu(t)&=[\mu_0{}^2-\mu_1{}^2(t)]^{1/2}\approx\mu_0[1-\tfrac{1}{2}\mu_1{}^2(t)/\mu_0{}^2]\\ &\approx\mu_0\left(1-\frac{1}{2}\frac{n_1(t)}{n_0}\right)\\ &\approx\mu_0(1-\tfrac{1}{2}a\cos\omega_m t).\end{aligned} \tag{6.6.3}$$

The perturbed electric field is then obtained from a perturbation solution of the wave equation,

$$E(t)=E_0\exp\left[-j\frac{2\pi L\mu_0}{\lambda}\right]\exp\left[j\omega_0 t+\frac{\pi L\mu_0}{\lambda}\,a\cos\omega_m t\right]. \tag{6.6.4}$$

If a (or n_1) is not small, these linearizations are not valid and the calculation must begin with substitution of n_1 into the Maxwell equations, either in terms of a fluctuating conductivity or a fluctuating dielectric constant. The Poynting flux calculated from solutions of Maxwell's equations then will give the frequency spectrum and the component magnitudes.

To find the frequency spectrum of (6.6.4), we must find its Fourier transform, $E(\omega)$. The transformation is of the form

$$\exp(jx\cos\theta)=\sum_{n=-\infty}^{\infty} j^n J_n(x)\cos(n\theta). \tag{6.6.5}$$

[13] If ω_m is large, so that the wavelength of the plasma disturbance is comparable to the electromagnetic wavelength and to the extent of the region being probed by the microwave beam, the present analysis will not be valid. The reader is referred to Sections 6.7.1 and 6.7.2 for the latter case.

Expanding (6.6.4) according to (6.6.5) and taking the real part (since we are interested in the transmitted power) yields

$$\begin{aligned}E(\omega)=E_0\exp\left(-j\frac{2\pi L\mu_0}{\lambda}\right)\Big\{&J_0\left(\frac{\pi L\mu_0}{\lambda}\,a\right)\cos\omega_0 t\\ &-J_1\left(\frac{\pi L\mu_0}{\lambda}\,a\right)[\sin(\omega_0+\omega_m)t+\sin(\omega_0-\omega_m)t]\\ &+J_2\left(\frac{\pi L\mu_0}{\lambda}\,a\right)[\cos(\omega_0+2\omega_m)t-\cos(\omega_0-2\omega_m)t]\\ &+J_3\left(\frac{\pi L\mu_0}{\lambda}\,a\right)[\sin(\omega_0+3\omega_m)t+\sin(\omega_0-3\omega_m)t]\\ &+\cdots\Big\}.\end{aligned} \tag{6.6.6}$$

Equation (6.6.6) is seen to have a frequency spectrum such as that sketched in Fig. 6.31, with the amplitudes of the side bands given by the Bessel coefficients.

An examination of (6.6.6) shows that the fundamental frequency component vanishes if the argument of J_0 is such that $J_0\to 0$; that is, $\pi L\mu_0 a/\lambda$ equals 2.40; 5.52; $8.65+n\pi$. Likewise, the first side band vanishes for the J_1 zeros, etc. In fact, however, since we have used a perturbation analysis, tacitly assuming that E remains essentially unchanged, the Bessel arguments must remain much smaller than unity. For larger arguments, the spectral appearance will be qualitatively similar but the relative magnitudes of the side bands will not be correctly given by (6.6.6).

In warm plasmas a collisionless Luxembourg effect (see Section 2.6.3) may occur, when a wave suffering Landau damping propagates through a fluctuating plasma. If the fluctuations are in density, as in (6.6.1), we see from (3.5.6) that changes in ω_p influence the attenuation exponentially, leading to possibly large amplitude modulation for small density changes. If it is the slope of the velocity distribution, $\partial f_0/\partial v$, that is fluctuating, due to some nonthermal effect for example, the attenuation again is affected exponentially, as shown by (5.6.13). The amplitude modulation introduced by fluctuations in the collisionless damping produces sidebands similar to those shown in Fig. 6.31, although the spectrum may be asymmetrical, due to heavier damping at shorter wavelengths. The upper limit in modulation frequency, imposed by the relaxation time in collisional Luxembourg modulation, is not present in the collisionless case, since there is no analogous relaxation phenomenon. A wave propagating through a fluctuating plasma then can suffer both amplitude and phase modulation simultaneously.

Collisionless damping occurs for spacecharge waves as well, so that all of the above effects apply qualitatively to spacecharge wave propagation. One might expect, for example, to see an electron spacecharge wave modulated by a low frequency ion wave.

If the fluctuations are at random frequencies (that is, noise fluctuations), the side bands will tend to run together into a continuous noise spectrum. The phase sense of the transmitted wave then becomes ambiguous. The ambiguity becomes worse for μ_1/μ_0 increasing, which occurs as the density approaches cutoff. This effect often is called *phase-sense scrambling*, but should be distinguished from *phase mixing*, associated with Landau damping (Section 3.5).

6.7 Microwave scattering experiments

The foregoing section has discussed a subject that could also be handled by treating the transmission as coherent forward scattering. Although scattering cross sections for free electrons are in general very small, in the case of a scattering angle $\theta=0$ the phases of all the scattered wavelets are the same, and the properties of the scattered wave are identical to those discussed up to this point in terms of propagation through plasmas (Ratcliffe, 1959).

For angles other than $\theta=0$, however, we must specify the scattering cross sections and sum up all the wavelet components to find the scattered intensity in a given solid angle $d\Omega$. The total intensities are generally small, and stray reflections from walls and obstacles, as well as plasma radiation, may contribute as much (or more) power to the detector as the plasma scattering, unless great care is taken. Typically, the background must be down by at least 90 dB and often 120 dB to be able to detect the scattered signal with a good, broad-band superheterodyne receiver. If coherent detection is used,[14] the background level can be considerably higher before the scattered signal becomes undetectable. With coherent detection, of course, the response time is necessarily long, which may be a disadvantage.

6.7.1 ***Incoherent scattering.*** The scattering from individual charged particles, namely, electrons, is called *Thomson scattering*. The total Thomson cross section is

$$q_t=\frac{8\pi}{3}r_0^2=0.66\cdot10^{-28}\ \mathrm{m}^2 \tag{6.7.1}$$

[14] The scatterer is modulated at a low frequency, for instance, 1000 cps, and a phase-sensitive detector compares the received signal with a sample of the modulating signal. Further elaboration is given in Section 9.5.

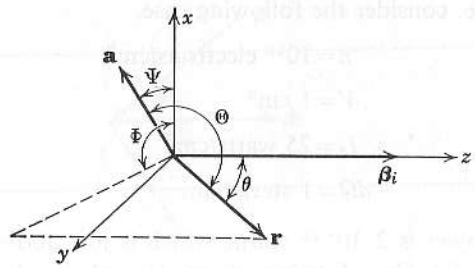

FIG. 6.32 Coordinate system for microwave scattering.

where $r_0=e^2/4\pi\epsilon_0 mc^2=2.8\cdot10^{-15}$ meter, the classical electron radius. The differential cross section is defined as

$$q_\Omega=\frac{dq}{d\Omega}=\frac{\text{energy scattered/unit solid angle-unit time}}{\text{incident energy flux/unit area-unit time}}$$
$$=r_0^2\sin^2\Theta \tag{6.7.2}$$

where Θ is the angle between the electron acceleration **a** and the direction of observation **r**, as shown in Fig. 6.32. In the absence of an external magnetic field (isotropic medium) the electron acceleration will be along **E**; in an anisotropic medium, this may not be the case. The angular distribution is given by (Jackson, 1962):

$$\sin^2\Theta=1-\sin^2\theta\cos^2(\Phi-\Psi). \tag{6.7.3a}$$

If the incident radiation is randomly polarized, the distribution is obtained by averaging over θ

$$\sin^2\Theta=\tfrac{1}{2}(1+\cos^2\theta). \tag{6.7.3b}$$

The rate of incoherent reradiation (scattering) per unit solid angle, $d\Omega$, assuming that the electron displacement is small compared to wavelength, for s electrons and $d\Omega$ solid angle is (Fejer, 1960)

$$P_\Omega=sI_0\,dq/d\Omega=nVI_0\,dq/d\Omega$$
$$=\tfrac{1}{2}nVI_0r_0^2\sin^2\Theta \tag{6.7.4}$$

where V is the scattering volume

I_0 is the incident intensity (watts/m^2),

n is the electron density in V.

If the incident radiation is randomly polarized, the scattered power received is one half that given in (6.7.4).

As an example, consider the following case.

$$n = 10^{12} \text{ electrons/cm}^3$$
$$V = 1 \text{ cm}^3$$
$$I_0 = 25 \text{ watts/cm}^2$$
$$d\Omega = 1 \text{ steradian.}$$

The scattered power is $2 \cdot 10^{-12}$ watts, which is just above the detectable threshold at $f = 90$ Gc. Further discussion of incoherent scattering appears in Section 2.6.5.

6.7.2 ***Scattering from plasma fluctuations of any wavelength.*** Two kinds of fluctuation scattering can be observed, both due to collective electron interactions. In both cases, the scattering cross sections are considerably enhanced over the Thomson cross section by the degree of coherency. For complete coherency, the scattered-signal intensity would be proportional to n^2 instead of n, as shown in (6.7.4).

The first type that we consider is incoherent backscattering; it has a cross section that is roughly proportional to the potential energy associated with plasma waves of any wavelength; the scattered frequency is doppler-broadened in proportion to the ion velocities (Rosenbluth and Rostoker, 1962).

The second type (Drummond and Pines, 1961) also has a scattering cross section proportional to the potential energy of plasma waves, but is sensitive to angle and has scattered-frequency components in side bands spaced at multiples of the frequency of the plasma oscillations giving the scattering, similar to the case discussed in Section 6.6. In a given experiment, both kinds of scattering may occur at once, the scattered side bands being broadened by the doppler shift.

The plasma fluctuations may be driven by an external frequency source, in which case the plasma column may oscillate in the dipole resonant mode as well (see Section 5.5). Or the oscillations may be due to an electrostatic instability, in which case the amplitude will be a function of position. Nonlinear effects can lead to the generation of harmonics of both the fundamental frequency and of the side bands.

The scattered intensity is a function of angle and of frequency. The probing frequency to be scattered should be much higher than the frequency of plasma oscillations, perhaps an order of magnitude or so.

For instability waves arising from electrons streaming through a plasma, the density fluctuations due to the plasma spacecharge waves are traveling essentially with the electron drift velocity, $\mathbf{v}_0$. The wave numbers (phase constants) of the incident wave, spacecharge wave, and scattered wave will

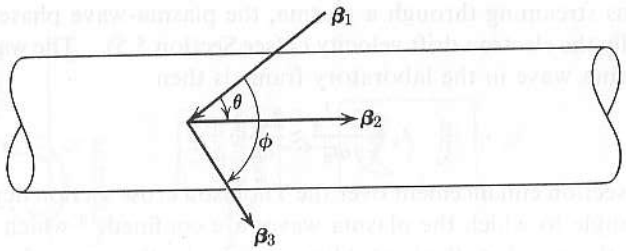

FIG. 6.33 Wave-number vectors for scattering from fluctuations in a plasma column.

be related vectorially by the Bragg relationship, as sketched in Fig. 6.33

$$\boldsymbol{\beta}_1 + \boldsymbol{\beta}_2 = \boldsymbol{\beta}_3 \tag{6.7.5}$$

where $\boldsymbol{\beta}_1$ = incident wave number,

$\boldsymbol{\beta}_2 = \omega_2 \mathbf{v}_0 / v_0^2$ = fluctuation wave number,

$\boldsymbol{\beta}_3$ = final (scattered) wave number.

For a wave vector incident at angle θ to the plasma wave, the scattering angle ϕ is given by

$$\beta_3 \cos(\phi - \theta) = \beta_2 - \beta_1 \cos\theta \tag{6.7.6a}$$

or, since $|\beta_3| = |\beta_1|$

$$\cos\phi \cos\theta + \sin\phi \sin\theta = \frac{\beta_2}{\beta_1} - \cos\theta. \tag{6.7.6b}$$

In a plasma that is only weakly unstable—that is, the e-folding growth coefficient is only slightly larger than the damping coefficient—the plasma wave amplitude will be essentially constant over several wavelengths of the electromagnetic scattering wave.

The scattered waves will contain side bands, much as in the case described in Section 6.6, the frequencies being ω_1 and $\omega_1 \pm \omega_m$. If the plasma wave amplitude is large or the scattering is large, higher harmonics of ω_m will also be present.

Plasma instability waves, obeying the Bohm dispersion relation, are well understood; the dispersion is expressed by

$$\omega_m^2 = \omega_2^2 = \omega_p^2 + \beta_2^2 \, 3kT_e/m_e. \tag{6.7.7}$$

The frequency of oscillation of such waves is near ω_p, and lies between ω_p and $\sqrt{2}\,\omega_p$, depending on the density distribution, temperature, and magnetic field. If the instability is due to counterstreaming flows, such

as electrons streaming through a plasma, the plasma-wave phase velocity is essentially the electron drift velocity v_0 (see Section 5.5). The wavelength of the plasma wave in the laboratory frame is then

$$\lambda_2 = \frac{2\pi v_\phi}{\omega_2} \approx \frac{2\pi v_0}{\omega_p}. \tag{6.7.8}$$

The cross section enhancement over the Thomson cross section depends on the solid angle to which the plasma waves are confined,[15] which is determined by the number R of e-folding lengths in the case of instability waves. The enhancement factor is given by Drummond and Pines (1961) as

$$\mathcal{B} = \frac{8\pi^2 R}{(\beta_2 \lambda_D)^5} \left(\frac{\alpha_\omega}{\omega_p}\right) n\lambda_D{}^3 \tag{6.7.9}$$

where α_ω is the wave growth rate in time.

Let us consider a typical example and compute the scattering properties when a plasma wave is present. Assuming

$$n = 10^{10} \text{ electrons/cm}^3$$
$$T = 10 \text{ eV}$$
$$v_0 = 10^7 \text{ m/sec (275 eV drift velocity)}$$
$$\omega_1/2\pi = 35 \text{ Gc},$$

we obtain

$$\lambda_D = 2.2 \text{ mm}$$
$$\omega_p/2\pi = 894 \text{ Mc}$$
$$\omega_1/\omega_2 \approx \omega_1/\omega_p = 39$$
$$\lambda_1 = 2\pi c/\omega_1 = 8.6 \text{ mm}$$
$$\lambda_2 \approx \lambda_p = 2\pi v_0/\omega_p = 1.12 \text{ cm}$$
$$\beta_1 = \omega_1/c = 730 \text{ radians/m}$$
$$\beta_2 = \omega_2/c = 560 \text{ radians/m}.$$

Typically, $\alpha_\omega/\omega_p \approx 10^{-2}$, $R \approx 5$, so that $\mathcal{B}$ is from 10^7 to 10^9. The scattered wave intensity would, thus, be many orders of magnitude above the detectable threshold, even for weak instabilities. Further, since the wave scattered from the plasma contains side bands at $\omega_1 \pm \omega_2$, $\omega_1 \pm 2\omega_2$, etc., and the wave scattered from walls and other passive objects is at the fundamental frequency, the plasma-scattered component can be selected with filters. Stray background, thus, gives little trouble as long as it is down by 20 dB or so from the desired signal, and thus does not block the detector.

[15] Plasma waves in thermodynamic equilibrium are spread uniformly over a debye sphere of volume $\approx (4\pi/3)\lambda_D{}^3$, where λ_D is the debye length.

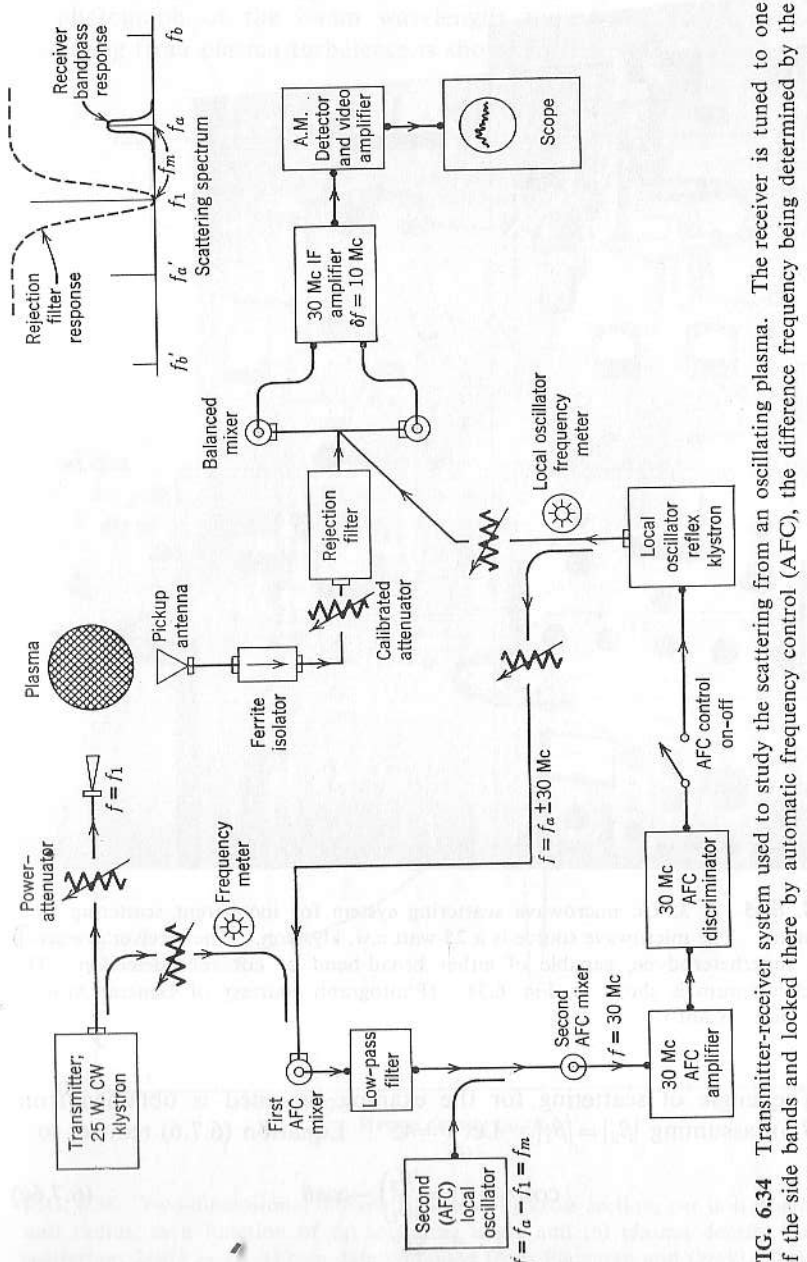

FIG. 6.34 Transmitter-receiver system used to study the scattering from an oscillating plasma. The receiver is tuned to one of the side bands and locked there by automatic frequency control (AFC), the difference frequency being determined by the second local oscillator.

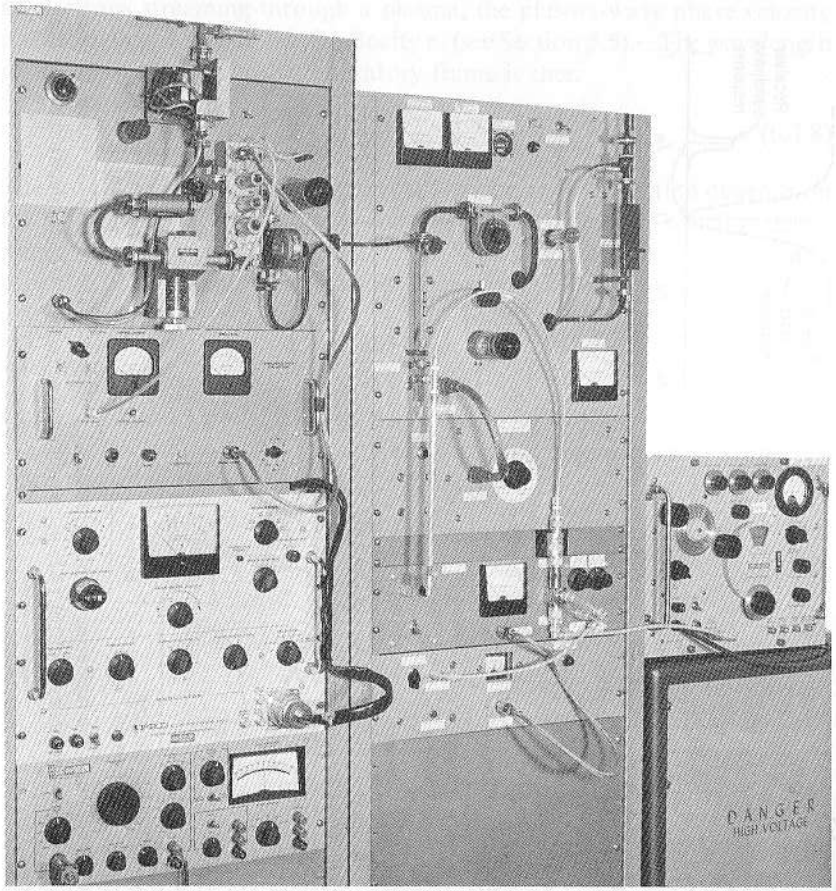

FIG. 6.35 A 35-Gc microwave scattering system for incoherent scattering from plasmas. The microwave source is a 25-watt c.w. klystron. The receiver is a sensitive superheterodyne, capable of either broad-band or coherent detection. The block diagram is shown in Fig. 6.34. (Photograph courtesy of General Atomic, San Diego, Calif.)

The angle of scattering for the example assumed is obtained from (6.7.6), assuming $|\beta_3| = |\beta_1|$. Let $\theta = 45°$. Equation (6.7.6) reduces to

$$\cos(\phi - \theta) = \left(\frac{\beta_2}{\beta_1}\right) - \cos\theta \qquad (6.7.6c)$$

$$\phi - \theta = 86°$$

$$\phi = 131°.$$

A block diagram of a typical scattering experiment is shown in Fig. 6.34. A photograph of the 8-mm wavelength equipment used to observe scattering from plasma turbulence is shown in Fig. 6.35.

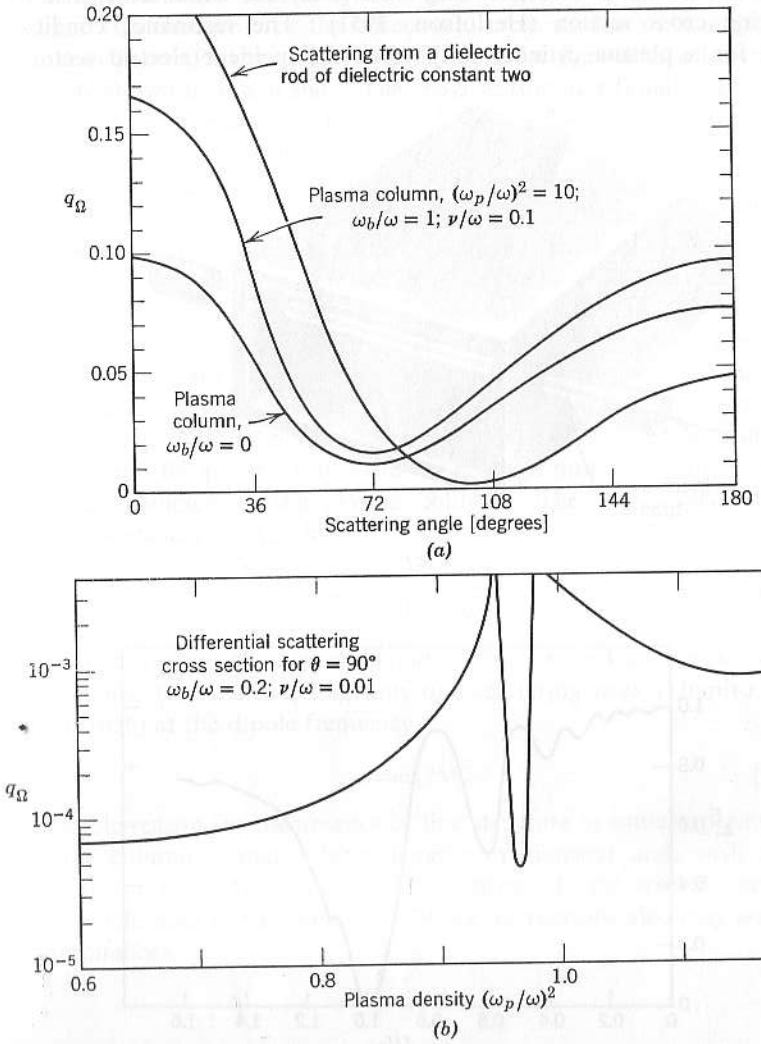

FIG. 6.36 Two-dimensional differential scattering cross section, per unit length and unit radius, as a function of (*a*) scattering angle and (*b*) plasma density for 90° scattering; $2\pi a/\lambda = 1$. (From data compiled from Platzman and Ozaki, 1960, and Smythe, 1950).

6.7.3 ***Scattering from small plasma columns.*** When the scattering plasma has a diameter comparable to a free-space wavelength, it may have a scattering cross section that is highly frequency-sensitive. Under certain circumstances, a resonance condition between plasma waves and external waves may occur, leading to a manyfold enhancement of the scattering cross section (Herlofson, 1951). The resonance condition occurs for a plasma cylinder only when the incident electric vector is

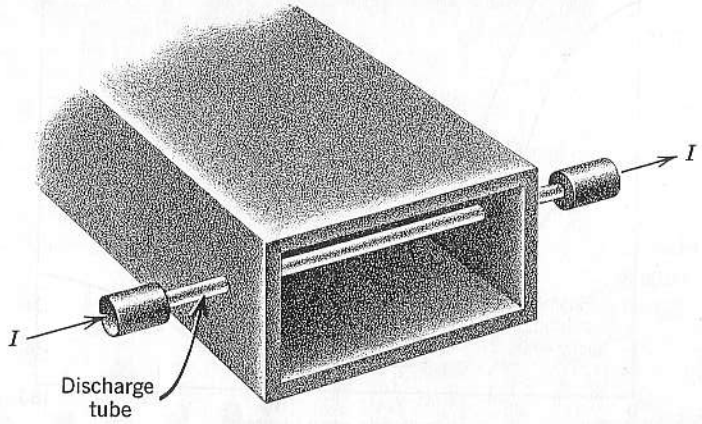

(*a*)

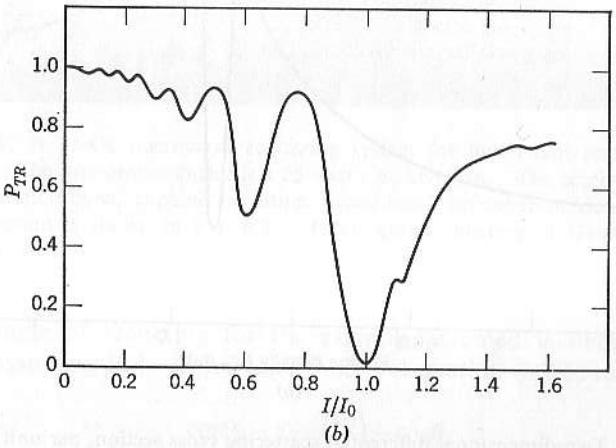

(*b*)

FIG. 6.37 Microwave scattering from a resonant plasma column. (*a*) The small discharge tube mounted across an *S*-band waveguide. (*b*) Relative power transmitted through the waveguide vs. normalized plasma current (Dattner, 1957).

perpendicular to the axis of the cylinder z, in which case the electric field couples to the dipole resonance mode and the scattered magnetic vector **H** lies entirely in the z plane (Smythe, 1950; Boley, 1958).

The scattering cross section as a function of angle between the incident wave vector and the plasma cylinder axis may also exhibit maxima and minima. Calculations for the differential cross section of a magnetized plasma cylinder (Platzman and Ozaki, 1960) for $\beta_0 a=1$ as a function of angle are shown in Fig. 6.36*a*. The cross section as a function of plasma density for "perpendicular resonance" $\omega=(\omega_p{}^2+\omega_b{}^2)^{1/2}$ is sketched in Fig. 6.36*b*. The maximum and minimum shown are due to interferences of the electromagnetic wave, matched to the boundaries.

Even when the plasma column is very small compared to a wavelength, maxima and minima are observed, in some cases having multiple peaks (Romell, 1951). An example of the transmission vs. plasma density, through a discharge tube mounted in the waveguide is shown in Fig. 6.37 (Dattner, 1957). Multiple peaks of reflection (scattering) also are found. An explanation for the multiple peaks is that the dipole resonance of plasma waves gives enhanced scattering whenever a particular plasma wave mode is excited (Battocletti, 1963; Hershberger, 1960; Crawford et al., 1963). Since the plasma waves are very slow, a number of modes can fit into the diameter of the plasma column. The mode spectrum, for normal incidence, is given by

$$\frac{2N}{2N+1}=\left[1-\frac{\omega_p{}^2}{\omega^2}\right]^{1/2}. \tag{6.7.10}$$

Other investigators have been unable to find the multiple peaks in their experiments, but, instead, find only one scattering peak (Shapiro, 1957; Keitel, 1956) at the dipole frequency

$$\omega=\omega_p/\sqrt{2}. \tag{6.7.11}$$

A possible reason for the absence of fine structure in some experiments is that the column is many debye lengths in diameter and, with density gradients or collisions present, the resulting closely spaced resonance peaks would tend to run together. Noise fluctuations also may wash out the resonances.

CHAPTER 7

Microwave radiation from plasma

7.1 Introduction

We can, in general, distinguish between incoherent and coherent radiation from a plasma. The former arises from uncorrelated radiation processes of single particles and can be interpreted statistically in terms of a "radiation temperature." The latter arises from collective motions of a large number of individual particles and has little or no connection with such statistical concepts as temperature. From a diagnostic point of view, the measurement of thermal (incoherent) radiation provides information on the *electron temperature* of the plasma, while observation of non-thermal (coherent) radiation indicates the presence of instabilities and other *cooperative processes.* The interest in thermal radiation at microwave frequencies, specifically, arises because of the availability of microwave superhet receivers which are sensitive, have a well-defined band width, and can easily be built to have fast transient response for use with pulsed discharges. Furthermore, a plasma most closely approximates a blackbody at low frequencies and especially near the plasma and cyclotron frequencies. The question of radiation necessarily involves two problems: (*1*) the mechanism by which the plasma generates electromagnetic waves; and (*2*) the transport of such waves through the plasma and across the boundary (Bekefi and Brown, 1961a).

7.2 Strict blackbody radiation

The energy density (joules/m^3) of radiation in thermodynamic equilibrium with matter at temperature T, in the frequency band between ω and $\omega+d\omega$, is (Planck, 1914; Richtmyer et al., 1955)

$$U_\omega\, d\omega=\frac{\hbar\omega^3}{\pi^2c^3}\frac{1}{\exp(\hbar\omega/kT)-1}\,d\omega, \tag{7.2.1}$$

where $\hbar=h/2\pi$, $h=$Planck's constant. This energy density represents an isotropic flux of electromagnetic energy flowing at velocity c. Thus, the radiation intensity (watts/m^2) into the solid angle $d\Omega$ is

$$cU_\omega(d\Omega/4\pi)\,d\omega,$$

and,

$${}^2B_\omega(\omega, T)=\frac{cU_\omega}{4\pi}=\frac{\hbar\omega^3}{4\pi^3c^2}\frac{1}{\exp(\hbar\omega/kT)-1}, \tag{7.2.2}$$

the so-called *Planck function*, is the intensity per unit solid angle per unit radian frequency interval. In the Rayleigh-Jeans limit ($\hbar\omega\ll kT$), which is generally appropriate for microwaves, (7.2.2) reduces to

$${}^2B_\omega(\omega, T)\approx\frac{kT\omega^2}{4\pi^3c^2}. \tag{7.2.3}$$

The prescript 2 denotes that two polarizations are included. The intensity in one of the two available polarizations is

$${}^1B_\omega=\tfrac{1}{2}\,{}^2B_\omega. \tag{7.2.4}$$

Meanwhile, the directive properties of a transmitting antenna (in the far field) are specified in terms of a gain function

$$G(\theta, \phi)=\frac{d\Psi/d\Omega}{\Psi/4\pi} \tag{7.2.5}$$

where $d\Psi$ is the power radiated into the solid angle $d\Omega$ in the direction (θ, ϕ) from the antenna and Ψ is the total power radiated. The angles θ and ϕ are those of a conventional spherical coordinate system with origin at some convenient point within the antenna and, as usual, $d\Omega=\sin\theta\, d\theta\, d\phi$. By definition

$$\left(\frac{1}{4\pi}\right)\oint G(\theta, \phi)\,d\Omega=\oint\frac{d\Psi}{\Psi}=1. \tag{7.2.6}$$

By reciprocity, the angular response of a receiving antenna can be specified in terms of the same gain function. The effective area of a receiving antenna for wavelength λ is given by (Schelkunoff and Friis, 1952, pp. 43–44 and Chapter 6)

$$S(\theta, \phi)=G(\theta, \phi)\frac{\lambda^2}{4\pi}. \tag{7.2.7}$$

Assuming that the antenna is sensitive to only one polarization, we obtain for the total received blackbody power

$$\begin{aligned}P_\omega\, d\omega&=\oint_\Omega {}^1B_\omega\, S(\theta, \phi)\,d\Omega\, d\omega\\&=kT\frac{d\omega}{2\pi},\end{aligned} \tag{7.2.8}$$

a well-known result, valid whenever a receiver is matched to a blackbody noise source (Nyquist, 1928; Knol, 1951).[1]

If the absolute power is measured with a receiver of known band width, the temperature of the emitter is readily obtained, according to (7.2.8). However, a number of conditions must be satisfied if this simple analysis is to be applicable. First, the emitted radiation must be in radiation equilibrium with the emitting medium; that is, the body must be truly "black" at the frequency band in question. To ensure this, the following conditions must be met.

(*1*) The depth of the medium must be large with respect to the absorption length α^{-1}. A partially transparent medium is often referred to as a "gray body," although in some usage this term also carries the implication that the optical thickness is independent of frequency.

(*2*) The radiation must be able to escape freely from the medium and dissipate itself in the detector. If the nature of the medium is such that significant reflection occurs at the boundary, we may speak of a "silvery body."

These considerations are implicit in the absorptivity or emissivity coefficient of Kirchhoff's law in radiation theory. In the case of a plasma for which the collision frequency is much less than the plasma frequency ($\nu^2 \ll \omega_p^2$), these conditions are often hard to meet. This question is considered further in Section 7.5.

Second, there are conditions on the receiving antenna. With the notation

R = distance from surface of blackbody to antenna

A = linear dimension of the antenna aperture

D = transverse dimension of the blackbody

we have three additional requirements.

(*3*) The antenna must be beyond the induction field of the blackbody[2]

$$R \gtrsim \lambda. \tag{7.2.9}$$

(*4*) The blackbody must be in the far (Fraunhofer) field of the antenna

$$R \gtrsim A^2/\lambda. \tag{7.2.10}$$

[1] It is important to note the distinction between the specific intensity (per unit solid angle) of blackbody radiation (7.2.3), which is proportional to ω^2, and the power received by an antenna (7.2.8), which is independent of frequency because of the λ^2 term in (7.2.7). The fact that the gain function G is, in general, frequency dependent is of no consequence because of the normalization (7.2.6).

[2] Under other conditions, we may wish to sample fields of modes that are trapped inside the plasma and have no radiation field (Dawson and Oberman, 1959).

(*5*) The antenna must "see" only the blackbody

$$(2\lambda/A)R \lesssim D, \tag{7.2.11}$$

where $2\lambda/A$ is a measure of the angular width of the antenna pattern. Thus, there is a bound on R,

$$\left.\begin{matrix}\lambda \\ A^2/\lambda\end{matrix}\right\} \lesssim R \lesssim \frac{AD}{2\lambda}, \tag{7.2.12}$$

which may be difficult to meet in practice.

The five conditions listed above are equivalent to saying, in electrical engineer's terminology, that the plasma must be matched to the detector. In the common situation where all the conditions cannot be met, we must employ experimental tests and calibration procedures to relate received noise power to emitter temperature. This subject is discussed in Section 7.5.3 and Chapter 8.

An alternative analysis for calculating the radiation from the positive column of a glow-discharge is to consider explicitly the fluctuations of the d-c current due to the statistics of the individual electron motions between collisions. The plasma is looked upon as a resistor for which the Johnson noise is explicitly calculated. When such a discharge plasma is matched to a microwave receiver (that is, when the conditions for blackbody emission are met), the available noise power is $kT\,d\omega/2\pi$, as (7.2.8), plus a small frequency-dependent term involving the geometry and the d-c power dissipated in the discharge (Parzen and Goldstein, 1951). The latter effect arises because of the distortion of the electron velocity distribution produced by the static electric field maintaining the discharge.

7.3 Bremsstrahlung in a transparent medium

The opposite limit to that of blackbody radiation is the case where the thickness of the plasma is small compared to the absorption length α^{-1} for a wave propagating through the plasma. The acceleration of electrons deflected in the field of positive ions produces radiation known as *bremsstrahlung* which, from a quantum-mechanical viewpoint, corresponds to transitions between the unquantized energy states of the free electrons ("free-free" transitions). If the plasma is sufficiently dilute, the radiation produced by individual electron-ion encounters passes out of the plasma without absorption or reflection. The observable external radiation intensity is simply the sum of the uncorrelated contributions of the individual encounters.

7.3.1 ***Radiation by a single electron.*** According to classical electrodynamics,[3] an accelerated electron, moving in a nondissipative medium of refractive index μ, radiates electromagnetic energy at the rate

$$\frac{dW}{dt}=\frac{e^2a^2\mu}{6\pi\epsilon_0c^3} \tag{7.3.1}$$

where a is the acceleration. The total energy emitted as the electron passes by the ion is

$$W=\int_{-\infty}^{\infty}\frac{dW}{dt}\,dt=\frac{e^2\mu}{6\pi\epsilon_0c^3}\int_{-\infty}^{\infty}[a(t)]^2\,dt. \tag{7.3.2}$$

Since we are interested in the frequency spectrum of the emitted radiation, it is necessary to Fourier-analyze the acceleration and use Parseval's formula:

$$a(t)=\int_0^{\infty}a_\omega(\omega)\exp(j\omega t)\,d\omega \tag{7.3.3}$$

$$a_\omega(\omega)=\frac{1}{\pi}\int_{-\infty}^{\infty}a(t)\exp(-j\omega t)\,dt \tag{7.3.4}$$

$$\int_{-\infty}^{\infty}[a(t)]^2\,dt=\pi\int_0^{\infty}|a_\omega(\omega)|^2\,d\omega \tag{7.3.5}$$

The total energy emitted in the encounter in the frequency band ω to $\omega+d\omega$ is thus

$$W_\omega(\omega)\,d\omega=\frac{e^2\mu}{6\pi\epsilon_0c^3}\,\pi|a_\omega(\omega)|^2\,d\omega. \tag{7.3.6}$$

For an electron in the coulomb field of an ion of charge Z, the acceleration is in general

$$a(t)=\frac{F(t)}{m}=\frac{Ze^2}{4\pi\epsilon_0m}\frac{1}{[r(t)]^2}. \tag{7.3.7}$$

The dominant contribution to low-frequency radiation involves distant encounters with small deflections. In this limit we may approximate the acceleration by transverse and longitudinal components in the form

$$\begin{aligned}a_\perp(t)&=\frac{Ze^2}{4\pi\epsilon_0m}\frac{b}{[b^2+(vt)^2]^{3/2}}\\ a_\parallel(t)&=\frac{Ze^2}{4\pi\epsilon_0m}\frac{vt}{[b^2+(vt)^2]^{3/2}}\end{aligned} \tag{7.3.8}$$

[3] Quantum mechanical effects can be neglected when $\hbar\omega\ll\frac{1}{2}mv^2\lesssim R_y=13.6$ eV; relativistic effects, when $\frac{1}{2}mv^2\ll mc^2=510$ keV.

where b is the impact parameter and the time of closest approach is taken as $t=0$. The Fourier transforms (7.3.4) are

$$\begin{aligned}a_{\omega\perp}&=\frac{1}{\pi}\frac{Ze^2b}{4\pi\epsilon_0mv^3}\int_{-\infty}^{\infty}\frac{\exp(-j\omega t)\,dt}{[(b/v)^2+t^2]^{3/2}}\\ &=\frac{Ze^2}{4\pi\epsilon_0m}\frac{2\omega}{\pi v^2}\,\mathrm{K}_1\!\left(\frac{\omega b}{v}\right)\\ a_{\omega\parallel}&=\frac{1}{\pi}\frac{Ze^2b}{4\pi\epsilon_0mv^2}\int_{-\infty}^{\infty}\frac{t\exp(-j\omega t)\,dt}{[(b/v)^2+t^2]^{3/2}}\\ &=\frac{Ze^2}{4\pi\epsilon_0m}\frac{2\omega}{\pi v^2}j\mathrm{K}_0\!\left(\frac{\omega b}{v}\right)\end{aligned} \tag{7.3.9}$$

where the K's are modified Bessel functions of the second kind.[4] The spectrum is

$$\begin{aligned}W_\omega(\omega,b,v)&=\frac{2}{3}\left(\frac{e^2}{4\pi\epsilon_0c}\right)^3\frac{Z^2\mu}{m^2}\frac{4\omega^2}{\pi v^4}\left[\mathrm{K}_1{}^2\!\left(\frac{\omega b}{v}\right)+\mathrm{K}_0{}^2\!\left(\frac{\omega b}{v}\right)\right]\\ &\xrightarrow[\omega\ll v/b]{}\frac{2}{3}\left(\frac{e^2}{4\pi\epsilon_0c}\right)^3\frac{Z^2\mu}{m^2}\frac{4}{\pi b^2v^2}.\end{aligned} \tag{7.3.10}$$

As a given electron passes through the plasma, the number of ions per second lying with impact parameters between b and $b+db$ is $n_iv2\pi b\,db$; the total power emitted per electron at frequency ω, assumed small, is

$$\begin{aligned}{}^2P_\omega(v)\,d\omega&=n_iv\int_{b_{min}}^{b_{max}}W_\omega(b,v)\,2\pi b\,db\,d\omega\\ &=\frac{16\pi}{3\sqrt{3}}\left(\frac{e^2}{4\pi\epsilon_0c}\right)^3\frac{n_iZ^2}{m^2v}\left[\mu\frac{\sqrt{3}}{\pi}\ln\frac{b_{max}}{b_{min}}\right]d\omega.\end{aligned} \tag{7.3.11}$$

Thus, the result of this simplified theory contains the same divergent factor, $\ln(b_{max}/b_{min})$, as was obtained in the theory of coulomb collisions, Section 2.5. It is necessary to invoke physical arguments to provide appropriate cutoffs on the maximum and minimum impact parameters. We return to this point in Section 7.3.5.

[4] $\mathrm{K}_n(x)=(\pi/2)j^{n+1}\mathrm{H}_n^{(1)}(jx)$ where $\mathrm{H}_n^{(1)}$ is the (first) Hankel function (Jahnke and Emde, 1945, pp. 133–36, 236–42).

$$\lim_{x\to0}\mathrm{K}_0(x)=\ln(2/\gamma x)\qquad\gamma=1.78$$

$$\lim_{x\to0}\mathrm{K}_n(x)=\frac{(n-1)!}{2}\left(\frac{2}{x}\right)^n\qquad n>0$$

$$\lim_{x\to\infty}\mathrm{K}_n(x)=\left(\frac{\pi}{2x}\right)^{1/2}\exp(-x)\qquad n\geqslant0.$$

Meanwhile, the number of electrons per unit volume having speed v is $n_e f(v) 4\pi v^2\, dv$; the total power emitted per unit volume at low frequencies is

$$
\begin{aligned}
{}^2\rho_\omega(T)\, d\omega &= n_e \int_0^\infty {}^2W_\omega(v)\, f(v, T)\, 4\pi v^2\, dv\, d\omega \\
&= \frac{16\pi}{3\sqrt{3}} \left(\frac{e^2}{4\pi\epsilon_0 c}\right)^3 \frac{n_e n_i Z^2}{m^2} \int_0^\infty \left[\mu \frac{\sqrt{3}}{\pi} \ln \frac{b_{max}}{b_{min}}\right] f(v, T)\, 4\pi v\, dv\, d\omega \\
&\xrightarrow[\text{distribution}]{\text{Maxwellian}} \frac{16}{3} \left(\frac{2\pi}{3}\right)^{1/2} \left(\frac{e^2}{4\pi\epsilon_0 c}\right)^3 \frac{n_e n_i Z^2}{m^{3/2}(kT)^{1/2}} \left[\mu \frac{\sqrt{3}}{\pi} \ln \frac{b_{max}}{b_{min}}\right] d\omega.
\end{aligned}
\tag{7.3.12}
$$

7.3.2 ***The Gaunt factor.*** The calculation of free-electron bremsstrahlung was originally undertaken by Kramers (1923), using a classical analysis similar to the above. However, he was principally concerned with higher frequencies, the dominant contribution to which comes from close encounters (large electron deflections). In a limit of moderate frequencies and low initial electron velocities (parabolic orbits), one obtains results identical to (7.3.11) and (7.3.12), except for the absence of the quantity in square brackets. This is a "white" spectrum, independent of frequency. It is possible, then, for arbitrary frequency and velocity (temperature), to write the results of any calculation in the forms:

Power radiated per electron of velocity v:

$${}^2P_\omega(\omega, v)\, d\omega = \frac{16\pi}{3\sqrt{3}} \left(\frac{e^2}{4\pi\epsilon_0 c}\right)^3 \frac{n_i Z^2}{m^2 v}\, \mu\, \mathfrak{G}(\omega, v)\, d\omega \tag{7.3.13}$$

Power radiated per unit volume by Maxwellian electron distribution:[5]

$${}^2\rho_\omega(\omega, T)\, d\omega = \frac{16}{3} \left(\frac{2\pi}{3}\right)^{1/2} \left(\frac{e^2}{4\pi\epsilon_0 c}\right)^3 \frac{n_e n_i Z^2}{m^{3/2}(kT)^{1/2}}\, \mu\, \bar{\mathfrak{G}}(\omega, T)\, d\omega \tag{7.3.14}$$

The refractive index μ represents the effect of coherent motions of neighboring electrons (Westfold, 1950). Although introduced by Kramers (1923), the correction factors $\mathfrak{G}$ and $\bar{\mathfrak{G}}$ are known as Gaunt factors (Gaunt, 1930). Kramers obtained, on the basis of calculations using the exact (7.3.7) in place of approximations such as (7.3.8) (Landau and Lifshitz, 1962, §70),

$$\mathfrak{G}(\omega, v) = \frac{\pi\sqrt{3}}{4}\, j\Omega\, \mathrm{H}^{(1)}_{j\Omega}(j\Omega) \left[\frac{d\mathrm{H}^{(1)}_{j\Omega}(u)}{du}\right]_{u=j\Omega} \tag{7.3.15}$$

$$\xrightarrow[\omega \ll v/b_{90}]{} \frac{\sqrt{3}}{\pi} \ln\left(\frac{8\pi\epsilon_0 m v^3}{\gamma Z e^2 \omega}\right) = \frac{\sqrt{3}}{\pi} \ln\left(\frac{2v}{\gamma b_{90}\omega}\right) \tag{7.3.16}$$

[5] We here distinguish between electron and ion densities, instead of making the usual simplification $n = n_e = Z n_i$, in order to permit calculation of partial contributions to the total radiation when several species of ions of various charge numbers Z are present.

where $\mathrm{H}^{(1)}_{j\Omega}$ is the first Hankel function (of imaginary order and argument), $\Omega = \omega b_{90}/v$, $b_{90} = Ze^2/4\pi\epsilon_0 m v^2$ is the impact parameter for a 90° deflection, and $\gamma = \exp C = 1.781$ is Euler's constant. The integration over velocity for a Maxwellian distribution yields in the important low-frequency case (Oster, 1961b; Scheuer, 1960)

$$
\begin{aligned}
\bar{\mathfrak{G}}_0(\omega, T) &\xrightarrow[\omega \ll v_{th}/b_{90}]{} \frac{\sqrt{3}}{\pi} \ln\left[\frac{1}{3}\left(\frac{2}{\gamma}\right)^{5/2} \frac{v_{th}}{\bar{b}_{90}\omega}\right] \\
&= \frac{\sqrt{3}}{\pi} \ln \Lambda_0
\end{aligned}
\tag{7.3.17}
$$

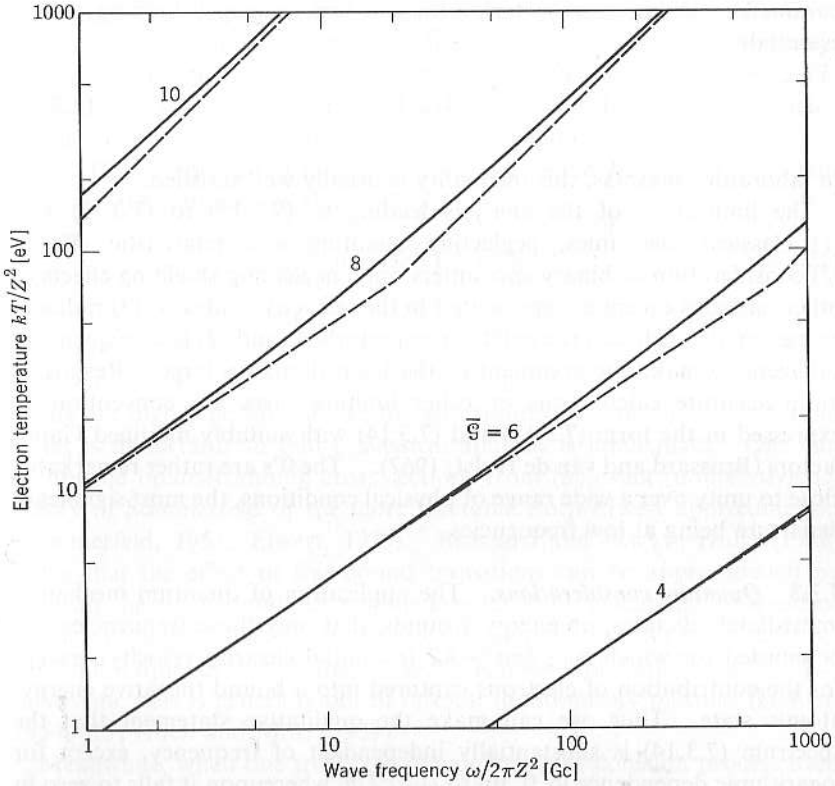

FIG. 7.1 The high-frequency (unshielded), velocity-averaged Gaunt factor $\bar{\mathfrak{G}}$, for ions of charge Z. The solid curves include the temperature-dependent quantum correction of Fig. 7.2. The dashed lines are the asymptotic forms (7.3.17) and (7.3.23). The shielding correction must be obtained from Fig. 7.2.

where $v_{th}=(kT/m)^{1/2}$, $\bar{b}_{90}=Ze^2/4\pi\epsilon_0 3kT$, and the parameter Λ_0, already defined in (2.5.30), is

$$\Lambda_0=\left(\frac{2}{\gamma}\right)^{5/2}\frac{4\pi\epsilon_0(kT)^{3/2}}{Ze^2m^{1/2}\omega}=\frac{4}{\gamma^{5/2}}\frac{kT}{\hbar\omega}\left(\frac{kT}{Z^2R_y}\right)^{1/2}$$

$$=6.2\cdot10^4\frac{(kT[\mathrm{eV}])^{3/2}}{Z\,\omega/2\pi[\mathrm{Gc}]}. \tag{7.3.18}$$

Numerical values of $\bar{\mathfrak{G}}_0$ are given in Fig. 7.1. It is to be noted that (7.3.15) to (7.3.17) follow directly from the exact classical dynamics without the necessity for imposing physical cutoffs on the impact parameter. A necessary criterion for this low-frequency limiting case is essentially

$$\Lambda_0\gg1. \tag{7.3.19}$$

In laboratory plasmas, this inequality is usually well satisfied.

The limitations of the analysis leading to (7.3.15) to (7.3.17) are: (*1*) classical mechanics, neglecting quantum and relativistic effects; (*2*) consideration of binary encounters only, neglecting shielding effects of other particles except as represented in the refractive index μ; (*3*) radiated energy small, such that the orbit is not perturbed; and (*4*) low frequencies, sufficient to make the argument of the logarithm very large. Results of more accurate calculations or other limiting cases are conventionally expressed in the form (7.3.13) and (7.3.14) with suitably modified Gaunt factors (Brussard and van de Hulst, 1962). The $\mathfrak{G}$'s are rather remarkably close to unity over a wide range of physical conditions, the most significant departure being at low frequencies.

7.3.3 ***Quantum considerations.*** The application of quantum mechanics immediately dictates, on energy grounds, that only those frequencies will be emitted for which $\hbar\omega\lesssim\frac{1}{2}mv^2\sim kT$ (v=initial electron velocity), except for the contribution of electrons captured into a bound (negative energy) atomic state. Thus, we can make the qualitative statement that the spectrum (7.3.14) is substantially independent of frequency, except for logarithmic dependence in $\mathfrak{G}$, up to $\omega\sim kT/\hbar$, whereupon it falls to zero in a manner the details of which depend upon specific atomic processes (Kramers, 1923). This consideration implies that the velocity-averaged formula (7.3.14) may be improved by performing the integration from a minimum velocity v_{min}, such that $\frac{1}{2}mv_{min}^2=\hbar\omega$, rather than from zero.

Since the velocity integration was of the form [neglecting here the logarithmic velocity dependence of the Gaunt factor $\mathfrak{G}(v)$]

$$2\lambda\int_0^\infty\exp(-\lambda v^2)\,v\,dv=1,$$

the modified integral is

$$2\lambda\int_{v_{min}}^\infty\exp(-\lambda v^2)\,v\,dv=2\lambda\int_0^\infty\exp(-\lambda v^2)\,v\,dv-2\lambda\int_0^{v_{min}}\exp(-\lambda v^2)\,v\,dv$$

$$=1-[1-\exp(-\hbar\omega/kT)]$$

$$=\exp(-\hbar\omega/kT). \tag{7.3.20}$$

That is, the general expression (7.3.14) is to be multiplied by $\exp(-\hbar\omega/kT)$ [note also (7.4.28)]. It is customary to write this factor explicitly in (7.3.14), rather than including it within the Gaunt factor $\bar{\mathfrak{G}}(\omega,T)$. We anticipate, then, that the remaining $\bar{\mathfrak{G}}$ is rather insensitive to frequency, even when quantum-mechanical effects are considered, so long as $\hbar\omega\lesssim kT$. Radiation, according to formula (7.3.14), including the exponential factor (7.3.20), is sometimes termed *Cillie radiation* (Cillie, 1932).

The Cillie exponential factor is negligible in the *Rayleigh-Jeans limit*, $\hbar\omega\ll kT$. Quantitatively, this limit is

$$\frac{\omega}{2\pi}[\mathrm{Gc}]\ll2.4\cdot10^5\,kT[\mathrm{eV}]. \tag{7.3.21}$$

This inequality is usually well satisfied for microwave frequencies in laboratory plasmas.

Parenthetically, for the case of high frequencies $\hbar\omega\gtrsim kT$, the electron orbits are highly perturbed and the contribution of transitions to bound states is important, so that a classical analysis is inadequate. One can obtain the bremsstrahlung cross sections from the exact (nonrelativistic) theory of Sommerfeld or the more tractable Born-Elwert approximation (Sommerfeld, 1951; Elwert, 1939). Brussard and van de Hulst (1962) argue that the effect of free-bound transitions can be approximated by omitting the exponential factor while keeping the $\bar{\mathfrak{G}}$ calculated for free-free transitions alone. Extensive numerical computations have been made for the high-frequency case (Greene, 1959; Karzas and Latter, 1961). The relativistic case is generally not of interest in laboratory plasmas (Heitler, 1954, §25; Koch and Motz, 1959).

Meanwhile, when one treats the dynamics of the collision process itself by quantum mechanics, in analogy to Section 7.3.1, one obtains in the low-frequency limit (Gaunt, 1930)

$$\mathfrak{G}(\omega,v)\xrightarrow[\hbar\omega\ll\frac{1}{2}mv^2]{}\frac{\sqrt{3}}{\pi}\ln\left[\frac{4(\frac{1}{2}mv^2)}{\hbar\omega}\right]. \tag{7.3.22}$$

This result is most readily obtained by a calculation using the Born approximation, which is valid in the limit of high temperatures and low frequencies (Sauter, 1933). Comparison with (7.3.16) indicates that the impact parameter b_{90} has been replaced by $\lambda\!\!\!^{-}/\gamma$ where $\lambda\!\!\!^{-}=\hbar/mv$ is the reduced de Broglie wavelength. Velocity averaging of (7.3.22) gives

$$\bar{\mathcal{G}}(\omega, T) \xrightarrow[\hbar\omega \ll kT]{} \frac{\sqrt{3}}{\pi} \ln\left(\frac{4kT}{\gamma\hbar\omega}\right). \tag{7.3.23}$$

The quantum mechanical result can be expected to apply when $\lambda\!\!\!^{-} \gtrsim \bar{b}_{90}$ (a relation depending only on temperature and atomic number), since then the deflection caused by diffraction of the electron wave is greater than that of the classical collision process (Marshak, 1940). The crossover from the classical to quantum form can be estimated from the condition for equality between (7.3.17) and (7.3.23); we obtain

$$kT \approx \gamma^3 Z^2 R_y = (77 \text{ eV})\, Z^2 = (890{,}000\ ^\circ\text{K})\, Z^2, \tag{7.3.24}$$

where $R_y = 13.6$ eV is the Rydberg energy constant. Note that the criterion may be stated in terms of the relation between kT ($\sim$electron energy) and the ionization potential for the (fully stripped) ion. Note further that the criterion (7.3.24) for the applicability of classical vs. quantum mechanics is of a different form from the Rayleigh-Jeans criterion (7.3.21). Thus, a purely classical analysis is justified only for temperatures such that

$$\hbar\omega \ll kT \ll \gamma^3 Z^2 R_y. \tag{7.3.25}$$

7.3.4 ***Electron shielding.*** A second important correction to the Kramers theory concerns the proximity of other particles when the plasma is not infinitely dilute. At frequencies of the order of ω_p and below, the electron cloud is able to adjust itself so as to shield the scattering ion (Chang, 1962a). The radiating electron no longer "sees" ions farther away than the debye length λ_D. Qualitatively, we may say that the radiation contributions from individual scattering ions are no longer independent and uncorrelated. The result of this effect appears only in the argument of the logarithm of (7.3.17), which is then multiplied by a factor of approximately ω/ω_p at frequencies less than ω_p (Burkhardt, Elwert, and Unsöld, 1948; DeWitt, 1958; Oster, 1964).

Consideration of shielding requires that we amend the use of the term "low frequency" as used in the important limiting case given by (7.3.17). To avoid shielding but satisfy $\omega \ll v_{th}/\bar{b}_{90}$,

$$1 \ll \omega/\omega_p \ll \Lambda_{Sp} = \lambda_D/\bar{b}_{90}. \tag{7.3.26}$$

As noted in Section 2.5.2, Spitzer's ratio Λ_{Sp} is approximately the number

of electrons in a sphere of radius equal to the debye length, and is normally quite large ($\sim 10^4$) in common laboratory situations.

7.3.5 ***The Gaunt factor and*** $\ln\Lambda$. The simple bremsstrahlung theory given in Section 7.3.1 led to results, (7.3.11) and (7.3.12), containing a term of the form $\ln(b_{max}/b_{min})$. A term of this same form arose in the theory of the electrical conductivity of an electron-ion plasma discussed in Section 2.5, where the generic notation $\ln\Lambda$ was used. These two theories have rather different points of view. Bremsstrahlung is concerned with incoherent radiation by a (thermal) electron, accelerated in the field of an ion. The conductivity theory is concerned with the loss of directed (wave-induced) momentum by the electron, in being deflected by the ion. However, the two effects are very closely related (Theimer, 1963). The quantitative connection, invoking the principle of detailed balance, is made in Section 7.4.4. Comparing (7.3.11) and (7.3.12) with (7.3.13) and (7.3.14), we may make the identification

$$\mathcal{G} \equiv \frac{\sqrt{3}}{\pi} \ln\Lambda \tag{7.3.27}$$

where the Gaunt factor $\mathcal{G}$ and the $\ln\Lambda$ term may be thought of as equivalent

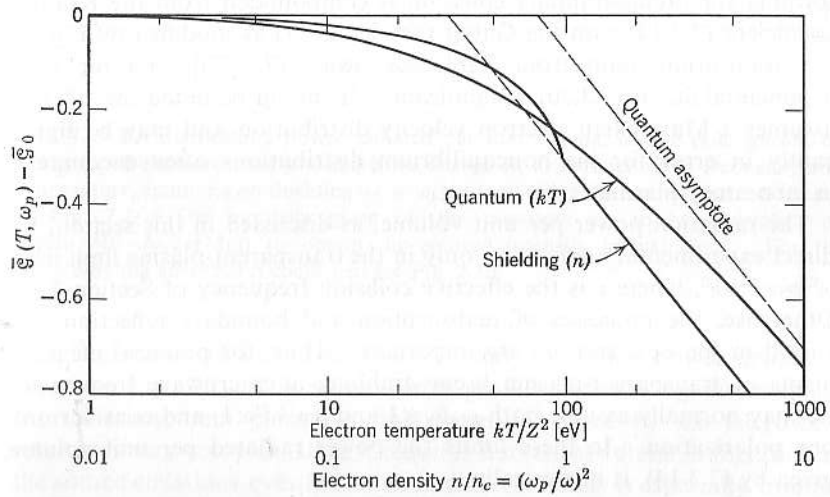

FIG. 7.2 Corrections to the unshielded, classical Gaunt factor $\bar{\mathcal{G}}_0$ of (7.3.17) to take account of quantum and shielding effects. The two corrections are independent and are to be applied simultaneously. This figure represents the same data as Fig. 2.9.

correction factors (slowly varying functions of plasma parameters) arising in the bremsstrahlung and conductivity theories, respectively.

In Section 2.5.4, we discussed at length the form of the impact parameter ratio $\Lambda = b_{max}/b_{min}$ appropriate for various regimes of electron density and temperature. The same arguments and calculations apply here. For convenience, Fig. 7.2 reproduces Fig. 2.9 (Greene, 1959; Dawson and Oberman, 1962), labeling the scales as corrections to the high-frequency, low-temperature Gaunt factor (7.3.17). The two corrections are independent of each other in the Rayleigh-Jeans limit ($\hbar\omega \ll kT$) (Oster, 1963a). The analytic form of the Gaunt factor in various limiting cases of electron density and temperature may be obtained from Table 2.3, using (7.3.27).

7.3.6 ***Summary of microwave bremsstrahlung.*** To summarize the theoretical results for bremsstrahlung emission, we first recognize that three independent variables are involved: frequency, electron density (plasma frequency), and electron temperature. These may most conveniently be packaged in the following normalized parameters: $\hbar\omega/kT$, which measures the importance of bound atomic states and the validity of the Rayleigh-Jeans approximation; ω_p/ω, which measures the importance of shielding; and kT/R_y, which determines the applicability of classical vs. quantum mechanics.[6] For microwave frequencies, where $\hbar\omega/kT \ll 1$, the formula for bremsstrahlung emission is compounded from the Kramers coefficient (7.3.14) with the Gaunt factor (7.3.17) as modified by Fig. 7.2 [or appropriate limit from Table 2.3, using (7.3.27)], and the Cillie exponential factor (7.3.20) if significant. It should be noted that (7.3.17) assumes a Maxwellian electron velocity distribution and may be significantly in error for the nonequilibrium distributions often encountered in laboratory plasmas.

The radiation power per unit volume, as discussed in this section, has direct experimental application only in the transparent-plasma limit when $\omega^2 \gg \omega_p{}^2 \gg \nu^2$, where ν is the effective collision frequency of Section 2.4.3. Otherwise, the processes of reabsorption and boundary reflection, discussed in the next section, are important. Thus, for practical measurements of transparent-plasma bremsstrahlung at microwave frequencies, we may normally assume both $\omega_p/\omega \ll 1$ and $\hbar\omega/kT \ll 1$, and consider only one polarization. In these limits the power radiated per unit volume, given by (7.3.14), is numerically

$$ {}^1\rho_\omega \, d\omega = 3.2 \cdot 10^{-41} \, \bar{\mathfrak{G}} \, \frac{Z \, (n[\mathrm{cm}^{-3}])^2}{(kT[\mathrm{eV}])^{1/2}} \, \frac{d\omega}{2\pi}[\mathrm{Mc}] \, \frac{\mathrm{watt}}{\mathrm{cm}^3}, \qquad (7.3.28) $$

[6] We assume that $kT/mc^2 \ll 1$ so that relativistic effects may be ignored.

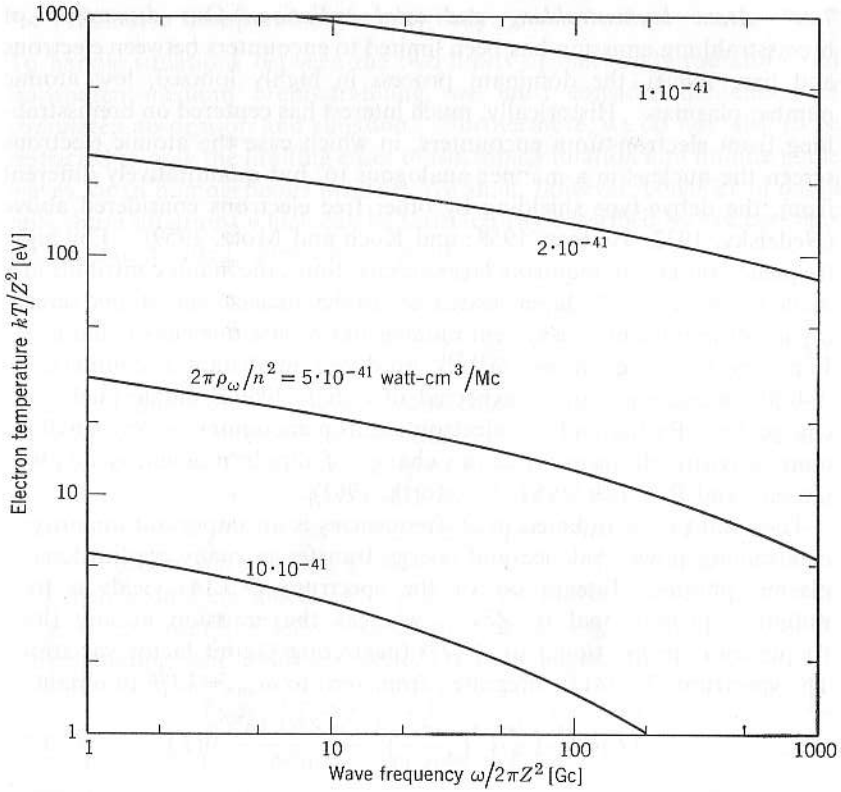

FIG. 7.3 Bremsstrahlung power radiated per unit volume in one polarization by a plasma of electron density n and ionic charge Z, as a function of frequency and temperature, assuming no shielding ($\omega \gg \omega_p$) but including the temperature correction of Fig. 7.2. The numbers given on the contours are to be multiplied by $\{(n[\mathrm{cm}^{-3}])^2 \cdot d\omega/2\pi[\mathrm{Mc}]\}$ to obtain the emitted intensity in watts/cm^3. For the corresponding absorption coefficient see Fig. 2.10.

with $\bar{\mathfrak{G}}$ given by (7.3.17) and Figs. 7.1 and 7.2. This power density is shown in Fig. 7.3. The experimental problem of relating the emission from a transparent plasma to the power measured by the microwave receiver is very complex, since it requires numerical volume integration of the source emissions over the antenna pattern. This is especially troublesome when nearby apparatus provides danger of reflection of radiation into the antenna as well as resonance or interference effects. It is to be noted that, at a given microwave frequency, the emission goes *down* with increasing temperature.

7.3.7 ***Atom bremsstrahlung and total radiation.*** Our discussion of bremsstrahlung emission has been limited to encounters between electrons and bare nuclei, the dominant process in highly ionized, low atomic number plasmas. Historically, much interest has centered on bremsstrahlung from electron-atom encounters, in which case the atomic electrons screen the nucleus in a manner analogous to, but quantitatively different from, the debye-type shielding by other free electrons considered above (Nedelsky, 1932; Hettner, 1958; and Koch and Motz, 1959). For high-frequency radiation, requiring large accelerations, the major contribution is made by electrons which penetrate close to the nucleus, and atomic screening is not important; the system radiates like a bare nucleus of charge Ze. For very low frequencies, mainly produced in distant encounters, an X-fold ionized ion can be expected to radiate like a simple nucleus of charge Xe. Radiation from electron-electron encounters is very small for nonrelativistic electrons, since no change of dipole moment is involved (Joseph and Rohrlich, 1958; Stickforth, 1961).

The total power radiated in all frequencies is an important quantity in determining power balance and energy transfer in many applications of plasma physics. Integration of the spectrum (7.3.14) yields a total radiation proportional to $Z^2T^{1/2}$, whereas the emission at any (low) frequency is proportional to $Z^2/T^{1/2}$ (neglecting Gaunt factor variation). The spectrum (7.3.14) is integrated from zero to $\omega_{max}=kT/\hbar$ to obtain

$$^2\rho(T)=\frac{16}{3}\left(\frac{2\pi}{3}\right)^{1/2}\left(\frac{e^2}{4\pi\epsilon_0 c}\right)^3\frac{n_e n_i Z^2(kT)^{1/2}}{m^{3/2}\hbar}\,\bar{\bar{\mathfrak{G}}}(T) \tag{7.3.29}$$

where $\bar{\bar{\mathfrak{G}}}(T)\sim 1$ is the Gaunt factor averaged over both electron velocity and frequency (Greene, 1959). The plasma is assumed transparent throughout, ignoring self-absorption and nonpropagation at low frequencies. For interesting temperatures, frequencies well above the microwave region contribute most of the radiated power. For moderate temperatures where the high-Z impurities are only partially ionized (X-fold, for instance) they contribute approximately as Z^2 to the total bremsstrahlung but only as X^2 to the microwave bremsstrahlung. It follows, then, that the total power loss is sensitive to relatively small concentrations of high-Z impurities in a low-Z plasma. Furthermore, the presence of bound electrons permits enhanced radiation at the frequencies of the positive-ion's discrete spectrum, which may greatly increase the total radiation power loss but does not greatly affect the microwave radiation (Post, 1961). Likewise, the presence of a magnetic field introduces cyclotron radiation or "magnetic bremsstrahlung," which can be the dominant radiative loss mechanism for a hot plasma. This point is discussed further in Section 7.6.

7.4 Radiation transport and the gray body

To handle situations between the two limits of blackbody radiation and transparent-medium bremsstrahlung, we must consider the effects of stimulated absorption and emission. Furthermore, we do not wish to be restricted to only the limiting cases of isotropic radiation and infinite plane waves, or to homogeneous media. We shall, however, consider in detail only those situations which can be satisfactorily described by ray concepts rather than detailed diffraction analysis.

7.4.1 ***Energy flow in an inhomogeneous medium.*** Let

$$I_\omega(\theta,\phi)\,d\omega\,d\Omega \tag{7.4.1}$$

be the radiation power per unit perpendicular area flowing into the element of solid angle $d\Omega$ in the (θ,ϕ) direction, in the angular frequency band ω to $\omega+d\omega$. I_ω is known as the *spectral specific intensity*, or *radiance*, which we hereafter often abbreviate as *intensity* (Milne, 1930; Nicodemus, 1963).[7] The specific intensity has the property that in a homogeneous lossless medium it is constant along a ray path. At the boundary between two slightly different media, as in Fig. 7.4, the power reaching an element of area dA from the left must equal that leaving to the right in the corresponding solid angle if reflection may be neglected;

$$I_\omega\,d\omega\,d\Omega\cos\theta\,dA=I_\omega'\,d\omega\,d\Omega'\cos\theta'\,dA. \tag{7.4.2}$$

But using Snell's law, $\mu\sin\theta=\mu'\sin\theta'$, we find $d\Omega'/d\Omega=(\mu/\mu')^2(\cos\theta/\cos\theta')$, whereupon

$$I_\omega/\mu^2=I_\omega'/\mu'^2. \tag{7.4.3}$$

Thus, in general, the quantity I_ω/μ^2 is constant along a ray path in a slowly varying inhomogeneous transparent medium and, using partial derivatives to signify the neglect of all other mechanisms for the change of intensity,

$$\frac{\partial}{\partial s}\left(\frac{I_\omega}{\mu^2}\right)=\frac{1}{\mu^2}\frac{\partial I_\omega}{\partial s}-\frac{2I_\omega}{\mu^3}\frac{d\mu}{ds}, \tag{7.4.4}$$

where s is the spatial coordinate measured along the ray path in the direction of energy flow. If the total spontaneous emission power per unit volume[8] is $^2\rho_\omega\,d\omega$, assumed isotropic, and the net space-dependent

[7] A monochromatic plane wave is an idealized limiting case. Relations for the total intensity I (watts/m^2) of a monochromatic plane wave may be obtained from relations given for specific intensity by the formal substitution $I_\omega\,d\omega\to I$. However, relation (7.4.3) is no longer valid for a plane wave.

[8] Many texts use the notation $j_\omega=\rho_\omega/4\pi$ for the emission power per unit volume *per unit solid angle*. See Section 7.6.

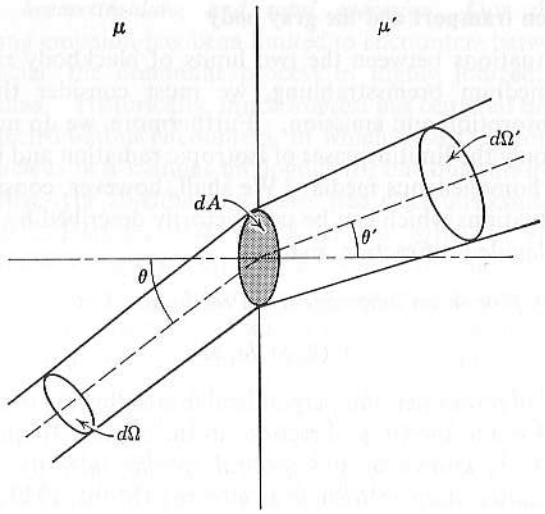

FIG. 7.4 Refraction of a pencil at an interface.

amplitude attenuation coefficient is $\alpha(s)$, the change in intensity along a ray path from all effects (except reflection at a discontinuity) is

$$\frac{dI_\omega}{ds}=\frac{\partial I_\omega}{\partial s}+\frac{{}^2\rho_\omega}{4\pi}-2\alpha I_\omega. \tag{7.4.5}$$

Using (7.4.4), we obtain finally

$$\mu^2\frac{d}{ds}\left(\frac{I_\omega}{\mu^2}\right)=\frac{{}^2\rho_\omega}{4\pi}-2\alpha I_\omega. \tag{7.4.6}$$

It is convenient to introduce a new distance coordinate, the *optical depth*

$$\tau(s_0)=\int_{s_0}^{observer}2\alpha(s)\,ds, \tag{7.4.7}$$

where s_0 is the origin of s, that is, the position of the source. Note that τ may be thought of as being measured positively away from the observer toward the source and, hence, in the opposite direction to the coordinate s. Equation (7.4.6) then becomes

$$\frac{d}{d\tau}\left(\frac{I_\omega}{\mu^2}\right)=\frac{I_\omega}{\mu^2}-\frac{{}^2\rho_\omega}{8\pi\alpha\mu^2}, \tag{7.4.8}$$

the solution of which is

$$\left(\frac{I_\omega}{\mu^2}\right)_{obs}=\left(\frac{I_\omega}{\mu^2}\right)_1\exp(-\tau)+\int_{obs}^{\tau}\frac{{}^2\rho_\omega}{8\pi\alpha\mu^2}\exp(-\tau)\,d\tau. \tag{7.4.9}$$

The first term on the right represents the contribution from the intensity

existing at the depth τ, the second term the net contribution from emission between depth τ and the observer. The emission parameter ${}^2\rho_\omega/8\pi\alpha\mu^2$, discussed below, has been called the *ergiebigkeit* of a medium (Smerd and Westfold, 1949). For an optically thick body, it may be seen that most of the observed intensity originates in the region $0<\tau\lesssim 1$. This type of analysis has been found useful in solar astronomy (Woolley and Stibbs, 1953).

7.4.2 ***The Einstein coefficients.*** We now investigate general relationships between the spontaneous emission ${}^2\rho_\omega$ and the attenuation coefficient α. The problem may be approached through the Einstein coefficients of elementary quantum radiation theory (Condon and Shortley, 1951; Smerd and Westfold, 1949). Consider two particular energy levels of a physical system (for example, a free electron in the field of a nucleus) with energies W_2 and W_1 ($W_2>W_1$). Emission of a photon of energy $\hbar\omega=W_2-W_1$ is associated with a transition from level 2 to level 1, where $\hbar=h/2\pi=1.05\cdot 10^{-34}$ joule-sec is the reduced Planck's constant. The probability per unit time per unit solid angle that a system in level 2 will undergo a *spontaneous* transition to level 1 is denoted by A_{21}. If the number of systems per unit volume in level 2 is n_2, the total radiated power per unit volume is

$$4\pi n_2 A_{21}\hbar\omega; \tag{7.4.10}$$

this is the emission considered in Section 7.3.[9] However, the presence of radiation of frequency ω will cause *induced* or *stimulated* emission and absorption. We assume that the probabilities of these induced processes are proportional to the intensity of the ambient radiation at the proper frequency. The probabilities (per unit time–volume–solid angle) for induced emission and absorption may then be written $B_{21}I_\omega$ and $B_{12}I_\omega$, respectively. The A and B coefficients represent the detailed interaction processes of the physical system with the radiation field and have the same value whether or not there is thermal, or even kinetic, equilibrium. However, for the special case of matter and radiation in thermodynamic equilibrium, we can make the following assumptions.

(*1*) The relative population of the two states is given by the Maxwell-Boltzmann distribution

$$\frac{n_2}{n_1}=\frac{G_2\exp(-W_2/kT)}{G_1\exp(-W_1/kT)}=\frac{G_2}{G_1}\exp(-\hbar\omega/kT) \tag{7.4.11}$$

where G_1 and G_2 are the statistical weights or degeneracies of the respective energy levels, relevant only when dealing with bound atomic states.

[9] In the case of the continuous energy levels of interest in free-free transitions, we consider frequencies in the band ω to $\omega+d\omega$. The coefficients A and B then contain implicitly the frequency interval $d\omega$.

(2) The specific intensity is given by the Planck function (7.2.2), generalized by the theorem (7.4.3) (Oster, 1963b),

$$I_\omega = \mu^2\, {}^2B_\omega(\omega, T) = \frac{\hbar\omega^3\mu^2}{4\pi^3c^2}\frac{1}{\exp(\hbar\omega/kT)-1}, \tag{7.4.12}$$

where μ is the index of refraction of the medium.

(3) The net emission is zero since, in equilibrium, equal numbers of transitions occur in the two directions (the principle of *detailed balancing*); thus

$$n_2[A_{21}+B_{21}I_\omega]-n_1B_{12}I_\omega=0. \tag{7.4.13}$$

When (7.4.11)–(7.4.12) are substituted into (7.4.13), we obtain

$$A_{21}-\frac{G_1}{G_2}B_{12}\frac{\hbar\omega^3\mu^2}{4\pi^3c^2}=\left(A_{21}-B_{21}\frac{\hbar\omega^3\mu^2}{4\pi^3c^2}\right)\exp(-\hbar\omega/kT). \tag{7.4.14}$$

But, since the A and B coefficients may or may not depend upon temperature, while the equation must hold for all temperatures, it follows that both sides of (7.4.14) may be equated to zero, with the result

$$A_{21}=\frac{\hbar\omega^3\mu^2}{4\pi^3c^2}B_{21}, \qquad B_{12}=\frac{G_2}{G_1}B_{21}. \tag{7.4.15}$$

In the case where the material system is itself in kinetic equilibrium, described by temperature T, but not in thermal equilibrium with the radiation field, we may use the general relations to obtain for the net emission power density (watts/m^3)

$$4\pi n_2\left\{1-\frac{4\pi^3c^2}{\hbar\omega^3\mu^2}[\exp(\hbar\omega/kT)-1]\,I_\omega\right\}A_{21}\hbar\omega = 4\pi n_2\left[1-\frac{I_\omega}{\mu^2\,{}^2B_\omega(\omega,T)}\right]A_{21}\hbar\omega, \tag{7.4.16}$$

where the specific intensity I_ω is no longer restricted to the Planck distribution (7.2.2) but is assumed unpolarized. Comparison of (7.4.10) and (7.4.16) shows that the effect of induced transitions is a net absorption.[10] Expression (7.4.16) establishes, in principle, the connection between the transparent-medium case of Section 7.3, for which I_ω is effectively zero, and the blackbody case of Section 7.2, for which I_ω has the Planck value (7.4.12). However, it remains to be found how to evaluate I_ω in the intermediate case.

[10] On the contrary, a net emission is obtained in a nonequilibrium situation such that the level populations are inverted ($n_2 > n_1$), which may be described by a negative temperature in (7.4.11). This is the basic principle of the maser and laser.

7.4.3 ***The partially transparent plasma.*** We wish first to relate phenomenological Einstein A and B coefficients to the specific processes for a highly ionized gas. In Section 7.3, we calculated the emission power density from bremsstrahlung; (7.3.13) and (7.4.10) may be identified as the same quantity,

$$n_2\,{}^2P_\omega\,d\omega = 4\pi\hbar\omega n_2A_{21}. \tag{7.4.17}$$

The summation over all available initial (upper) states corresponds to integrating over the Maxwellian electron velocity distribution; we obtain

$${}^2\rho_\omega\,d\omega = 4\pi\hbar\omega n\bar{A}_{21} \tag{7.4.18}$$

where $\bar{A}_{21}=\int A_{21}f(\mathbf{v})\,d^3\mathbf{v}$. Meanwhile, under conditions where the spontaneous emission may be neglected (for example, an externally generated signal propagated through a relatively transparent plasma), the observable amplitude attenuation constant α, defined by (see footnote 7)

$$\frac{dI_\omega}{ds}=-2\alpha I_\omega, \tag{7.4.19}$$

is related to the Einstein B coefficients by[11]

$$\begin{aligned}2\alpha I_\omega\,d\omega &= \hbar\omega n I_\omega\int\left[B_{12}\exp\left(\frac{\hbar\omega}{kT}\right)-B_{21}\right]f(\mathbf{v})\,d^3\mathbf{v}\\ &= \hbar\omega n I_\omega\left[\exp\left(\frac{\hbar\omega}{kT}\right)-1\right]\frac{4\pi^3c^2}{\hbar\omega^3\mu^2}\,\bar{A}_{21}\\ &= \hbar\omega n\,\frac{I_\omega}{\mu^2\,{}^2B_\omega}\,\bar{A}_{21}.\end{aligned} \tag{7.4.20}$$

Canceling out I_ω and using (7.4.18), we find that the ergiebigkeit parameter appearing in (7.4.8) and (7.4.9), has the value[12]

$$\frac{{}^2\rho_\omega}{8\pi\alpha\mu^2}={}^2B_\omega(\omega,T), \tag{7.4.21}$$

the Planck function (7.2.2). Thus, under all conditions in which the matter is in local kinetic equilibrium (not necessarily in equilibrium with the radiation), (7.4.9) can be written as

$$\left(\frac{I_\omega}{\mu^2}\right)_{obs}=\left(\frac{I_\omega}{\mu^2}\right)_\tau\exp(-\tau)+\int_{obs}^{\tau}{}^2B_\omega[T(\tau)]\exp(-\tau)\,d\tau. \tag{7.4.22}$$

[11] The velocity integrations in (7.4.18) and (7.4.20) are both written in terms of the upper-state density n_2, so that they are fully comparable.

[12] Closer examination reveals that this general relation is only valid for relatively low-loss media, such that $\chi^2 \ll \mu^2$ (Rytov, 1953).

If the electron distribution function of the matter is not Maxwellian, the $\exp(\hbar\omega/kT)$ term in (7.4.20), from (7.4.11), is not valid, and the value of the ergiebigkeit parameter must be calculated explicitly. For instance, it may be evaluated for a Druyvesteyn distribution (Davies and Cowcher, 1955). As an application of (7.4.22), consider a sample of uniform temperature T_1, but unspecified geometry. If the sample is illuminated from the rear with blackbody radiation of temperature T_2, the observable radiation emerging from the sample will be independent of the optical thickness of the plasma when $T_1 = T_2$. This feature has been exploited as a diagnostic technique under conditions where the density profile of a plasma is unknown and not easily measurable (Bekefi and Brown, 1961b). It is equivalent to the classical line-reversal technique of optical pyrometry.

7.4.4 ***Correlation of emission and conductivity theories.*** We may now compare the value of $\bar{A}_{21}$ computed by alternative theoretical models for the specific case of a highly ionized gas (coulomb collisions only) (Martyn, 1948; Westfold, 1950; Yamada, 1962; and Theimer, 1963). From the Kramers free-free bremsstrahlung theory of Section 7.3, using (7.3.14) and (7.4.18), we obtain

$$\bar{A}_{21} = \frac{{}^2\rho_\omega\, d\omega}{4\pi\hbar\omega n} = \frac{4}{3}\left(\frac{2}{3\pi}\right)^{1/2}\left(\frac{e^2}{4\pi\epsilon_0 c}\right)^3 \frac{nZ\mu\bar{\mathfrak{G}}}{m^{3/2}(kT)^{1/2}\hbar\omega}\, d\omega \tag{7.4.23}$$

where $\bar{\mathfrak{G}}$ is the Gaunt factor averaged over the electron velocity distribution. From the Lorentz theory of a-c conductivity of Section 1.3.4 in the limit $\nu^2 \ll \omega_p{}^2 < \omega^2$, using (1.3.30) and (A.47),

$$\alpha = \frac{\omega_p{}^2\nu}{2\omega^2 c\mu} = \frac{8\pi(2\pi)^{1/2}}{3}\left(\frac{e^2}{4\pi\epsilon_0}\right)^3 \frac{n^2 Z \ln\Lambda}{(mkT)^{3/2} c\omega^2\mu} \tag{7.4.24}$$

where the appropriate electron-ion collision frequency ν is obtained from the Margenau-Spitzer theory of Section 2.5.3, equation (2.5.23). Accordingly, (7.4.20) yields in the classical (Rayleigh-Jeans) limit $\hbar\omega \ll kT$

$$\bar{A}_{21} = \frac{\mu^2\omega kT\alpha\, d\omega}{2\pi^3 c^2\hbar n} = \frac{4}{3\pi}\left(\frac{2}{\pi}\right)^{1/2}\left(\frac{e^2}{4\pi\epsilon_0 c}\right)^3 \frac{nZ\mu\ln\Lambda}{m^{3/2}(kT)^{1/2}\hbar\omega}\, d\omega. \tag{7.4.25}$$

Comparison of (7.4.23) and (7.4.25) shows that the two theoretical models lead to identical results except for the respective correction factors

$$\bar{\mathfrak{G}} = \frac{\sqrt{3}}{\pi}\ln\Lambda. \tag{7.4.26}$$

Indeed, as already shown in Section 7.3.1, the simple classical "straight-line" model yields a $\mathfrak{G}$ of precisely the form $(\sqrt{3}/\pi)\ln\Lambda$, where Λ is a

ratio of impact parameters. The evaluation of these factors, for various regimes of frequency, electron density, and temperature, has been discussed at length in Sections 2.5.4 and 7.3.5.

The Einstein-coefficients argument enables us to infer the emission and absorption for high frequencies at which the Rayleigh-Jeans approximation breaks down. We obtain

$${}^2\rho_\omega\, d\omega = \frac{16}{3}\left(\frac{2\pi}{3}\right)^{1/2}\left(\frac{e^2}{4\pi\epsilon_0}\right)^3 \frac{n^2 Z}{m^{3/2}c^3(kT)^{1/2}}\,\mu\,\bar{\mathfrak{G}}\exp\left(-\frac{\hbar\omega}{kT}\right) d\omega \tag{7.4.27}$$

$$2\alpha = \frac{16\pi^2}{3}\left(\frac{2\pi}{3}\right)^{1/2}\left(\frac{e^2}{4\pi\epsilon_0}\right)^3 \frac{n^2 Z}{m^{3/2}ch(kT)^{1/2}\omega^3}\,\frac{\bar{\mathfrak{G}}}{\mu}\left[1-\exp\left(-\frac{\hbar\omega}{kT}\right)\right] \tag{7.4.28}$$

The exponential in (7.4.27) is simply the Cillie term (7.3.20). The bracketed term in (7.4.28) measures the competition between induced absorption and emission. The Gaunt factor $\bar{\mathfrak{G}}(\omega, \omega_p, T)$, for this case, must usually be obtained by numerical calculations (Greene, 1959; Karzas and Latter, 1961; and Brussard and van de Hulst, 1962).

7.5 Radiation from a slab and Kirchhoff's law

As an introduction to the thermal radiation transport problem, we restrict ourselves to the case of a dilute plasma having the propagation properties of free space; that is, we assume $\omega^2 \gg \omega_p{}^2 \gtrsim \nu^2$.

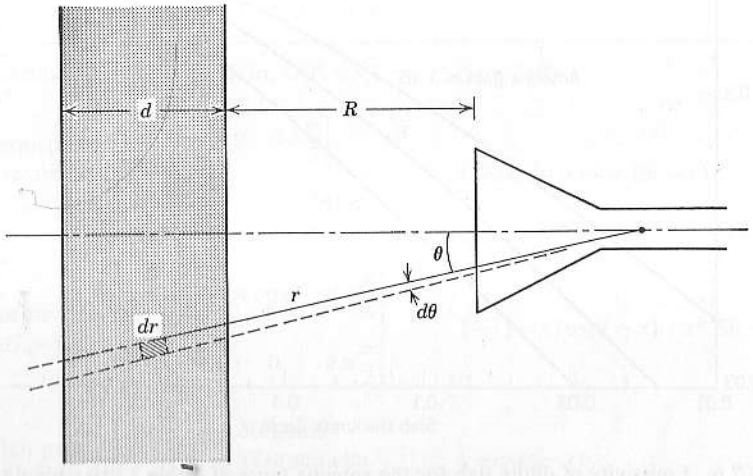

FIG. 7.5 Geometry of slab radiation.

7.5.1 ***Effect of antenna gain.*** Consider an infinite homogeneous slab of plasma of thickness d and uniform kinetic temperature (Allen and Hindmarsh, 1955). We wish to calculate the intensity of thermal radiation received by an external antenna. The radiation emitted in a unit volume per unit solid angle by spontaneous transitions is ${}^2\rho_\omega(\omega, T)\, d\omega/4\pi$ [watts/m^3-sterad], given by (7.3.14). As it passes a distance Δx, through the plasma, the intensity is attenuated by the factor $\exp(-2\alpha\,\Delta x)$, where the connection between α and ${}^2\rho_\omega$ is given by (7.4.21). Therefore, we may compute the power entering a polarized antenna according to the geometry of Fig. 7.5 by integrating the quantity

$$\left(\frac{{}^1\rho_\omega\, d\omega}{4\pi}\right)(r^2 \sin\theta\, d\theta\, d\phi)\{\exp[-2\alpha(r - R\sec\theta)]\}\left[\frac{S(\theta,\phi)}{r^2}\right] \qquad (7.5.1)$$

over the volume of the plasma. The factors represent, respectively, the polarized emission power density per unit solid angle, volume element, attenuation factor, and solid angle subtended by the antenna using the effective-area formalism of (7.2.5) and (7.2.7). The integration over r, between the limits $R\sec\theta$ and $(R+d)\sec\theta$, yields

$${}^1B_\omega(\omega, T)[1-\exp(-2\alpha d\sec\theta)]S(\theta,\phi)\sin\theta\, d\theta\, d\phi, \qquad (7.5.2)$$

where ${}^1B_\omega = \frac{1}{2}{}^2B_\omega$ is the polarized Planck function (7.2.2). The antenna distance R drops out, although we must assume that the plasma lies in the

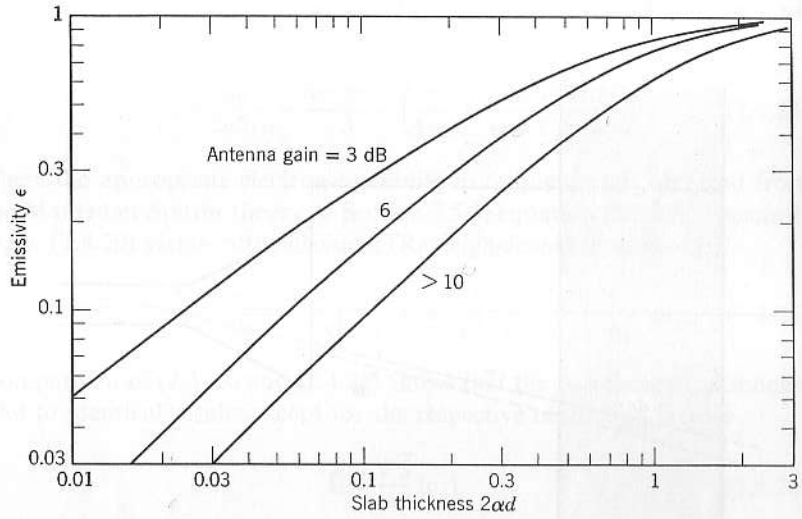

FIG. 7.6 Emissivity of dilute slab for the antenna types of Table 7.1; α = amplitude absorption coefficient, d = slab thickness; $\omega^2 \gg \omega_p{}^2 > \nu^2$.

far field of the antenna ($R \gtrsim S_{max}/\lambda$). To proceed further, analytically, we must make some assumption as to the antenna pattern, the effective area $S(\theta, \phi)$ being proportional to the gain function $G(\theta, \phi)$ according to (7.2.7). Three representative samples are given in Table 7.1.[13] In any case, the integration of (7.5.2) over angles yields for the received power in one polarization

$$P_\omega\, d\omega = \epsilon(2\alpha d, G)\,\frac{\hbar\omega\, d\omega/2\pi}{1-\exp(-\hbar\omega/kT)} \qquad (7.5.3)$$

where the *emissivity* ϵ is a function of the optical thickness parameter $2\alpha d$, and the antenna pattern $G(\theta, \phi)$. The emissivity represents simply the actual radiation intensity normalized to that of a blackbody at the same temperature. The emissivities for our specific cases are given in Table 7.1 and Fig. 7.6. In the Rayleigh-Jeans limit ($\hbar\omega \ll kT$) (7.5.3) becomes

$$P_\omega\, d\omega = \epsilon(2\alpha d, G)\, kT\,\frac{d\omega}{2\pi}, \qquad (7.5.4)$$

which may be compared with (7.2.8). For most practical purposes, the dependence on antenna properties is small. The thickness parameter $2\alpha d$

[13] The cosine case gives the conventional emissivity for the total intensity (watts/m^2) radiated into the hemispheric solid angle on one side of the slab.

TABLE 7.1 EMISSIVITY ϵ OF A DILUTE PLASMA SLAB FOR REPRESENTATIVE ANTENNA TYPES

Antenna	Gain, $G(\theta, \phi)$	$\epsilon(x = 2\alpha d)$
Hemispheric isotropic $G_0 = 3$ dB	$\begin{cases} 2 & \theta < \frac{\pi}{2} \\ 0 & \theta > \frac{\pi}{2} \end{cases}$	$1-\exp(-x)-x\,\mathrm{Ei}(-x)$
Cosine pattern $G_0 = 6$ dB	$\begin{cases} 4\cos\theta & \theta < \frac{\pi}{2} \\ 0 & \theta > \frac{\pi}{2} \end{cases}$	$1-(1-x)\exp(-x)+x^2\,\mathrm{Ei}(-x)$
High gain $G_0 \gtrsim 10$ dB	$2\,\delta(\theta)/\sin\theta$ (Dirac delta function)	$1-\exp(-x)$

can be easily measured in an auxiliary transmission experiment. Since $\alpha \propto 1/\omega^2$ for low frequencies, according to (7.4.24), there will exist a critical frequency ω_0 for which $2\,\alpha(\omega=\omega_0,\ \mu=1)\,d=1$; that is,

$$\frac{\omega_0^2}{\omega_p^2}=2\left(\frac{2\pi}{3}\right)^{3/2}\left(\frac{e^2}{4\pi\epsilon_0}\right)^2\frac{\overline{\mathcal{G}}Znd}{m^{1/2}c(kT)^{3/2}}=\frac{(2\pi)^{3/2}}{\sqrt{3}}\frac{\overline{\mathcal{G}}}{\Lambda_{Sp}}\frac{\omega_p d}{2\pi c}$$

$$=1.76\cdot10^{-16}\,\frac{\overline{\mathcal{G}}Z\ n[\mathrm{cm}^{-3}]\ d[\mathrm{cm}]}{(kT[\mathrm{eV}])^{3/2}} \tag{7.5.5}$$

where $\Lambda_{Sp}=\lambda_D/\bar{b}_{90}$ is Spitzer's coulomb cutoff parameter (2.5.18). Below ω_0 the slab radiation approaches blackbody and above, transparent-medium Cillie radiation. However, it must be recalled that the above analysis, neglecting refractive effects, is valid only for frequencies well above the plasma frequency. The criterion that this critical frequency be above the plasma frequency is

$$d\gg\frac{\Lambda_{Sp}}{60}\left(\frac{2\pi c}{\omega_p}\right), \tag{7.5.6}$$

where the numerical coefficient assumes an average value (~ 7) for the Gaunt factor, and the final quantity is the wavelength of a free-space wave at the plasma frequency. Since Λ_{Sp} is very large ($\sim 10^4$, see Fig. 2.5) in most situations of practical interest in plasma physics, condition (7.5.6) is usually not fulfilled by laboratory plasmas. In general, therefore, a laboratory plasma will not radiate as a blackbody under circumstances uncomplicated by refractive effects (Wort, 1962).[14]

7.5.2 ***Surface reflection.*** To account for the discontinuity in propagation characteristics for frequencies near the plasma frequency, we may make the following simplified analysis. Assume, again, a uniform, semiinfinite-slab plasma, as in Fig. 7.5, of thickness d. We consider only the high-gain antenna case and, hence, radiation flowing perpendicular to the slab (coordinate x). The spontaneous emission power per unit volume per unit solid angle is ${}^2\rho_\omega\, d\omega/4\pi$. Let the existing specific intensity [see (7.4.1)] in the $+x$ direction be $I_\omega(x)$. The change in intensity within the plasma is then

$$\frac{dI_\omega}{dx}=\frac{{}^2\rho_\omega}{4\pi}-2\alpha I_\omega, \tag{7.5.7}$$

the solution of which is, using (7.4.21),

$$I_\omega(x)=I_\omega(0)\exp(-2\alpha x)+\mu^2\,{}^2B_\omega\,[1-\exp(-2\alpha x)], \tag{7.5.8}$$

[14] We refer here to the low-pressure, highly ionized plasmas generally characteristic of "plasma physics." Higher-pressure, low-ionization gas discharges are, of course, well-known as microwave blackbody noise standards (Knol, 1951; Mumford, 1949).

which may be recognized as a special case of (7.4.22). We assume a power reflection coefficient r at each plasma-free-space interface and, therefore, a power transmission coefficient $t=1-r$. Let us neglect interference effects here by considering the reflections at the two boundaries to be incoherent.[15] We obtain a self-consistent solution by considering radiation flowing in both directions within the plasma such that

$$I_\omega(0)=r\,I_\omega(d) \tag{7.5.9}$$

and the external intensity

$$I_\omega(\text{external})=(1-r)\,\frac{I_\omega(d)}{\mu^2} \tag{7.5.10}$$

in which the index of refraction μ accounts for refraction of the element of solid angle according to (7.4.3). The result for the radiation intensity per unit solid angle normal to the slab is

$$I_\omega(\text{external})=\frac{(1-r)[1-\exp(-2\alpha d)]}{[1-r\exp(-2\alpha d)]}\,{}^2B_\omega$$

$$=\epsilon(r,\,2\alpha d)\,{}^2B_\omega. \tag{7.5.11}$$

In analogy with (7.2.8), the power received by a high-gain polarized antenna is given by (7.5.3) and (7.5.4) with

$$\epsilon(r,\,2\alpha d)=\frac{1-r}{1-r\exp(-2\alpha d)}\,[1-\exp(-2\alpha d)], \tag{7.5.12}$$

which reduces to the high-gain case of Table 7.1 for $r\to 0$.

For a low-loss ($\nu^2\ll\omega_p^2$), moderately thick ($d\gg c/2\omega_p$) plasma, we have

	r	$2\alpha d$
$\omega<\omega_p$	1	$(2\omega_p d/c\gg 1)$
$\omega>\omega_p$	$\left(\frac{1-\mu}{1+\mu}\right)^2$	$\frac{1}{\mu}\left(\frac{\omega_0}{\omega}\right)^2$

where the refractive index is $\mu=[1-(\omega_p/\omega)^2]^{1/2}$ and the critical frequency $\omega_0(d,\,\omega_p,\,T)$ is defined by (7.5.5). The thermal radiation spectrum of a plasma slab may be presented in two formats, shown in Fig. 7.7. The

[15] This approximation is valid for a plasma which is nearly optically thick, $d\gtrsim 1/2\alpha$, or when a wide enough frequency band $\Delta\omega$ is accepted to average out the resonances, $d\gtrsim 2\pi c/\mu\,\Delta\omega$. It may also be reasonable when the change in propagation characteristics at the boundary, is "smeared out" or "bloomed" over an appreciable fraction of a wavelength, instead of being perfectly sharp, but then r is considerably reduced. Otherwise, our result will give only an average result which suppresses resonances (Bekefi and Brown, 1961a).

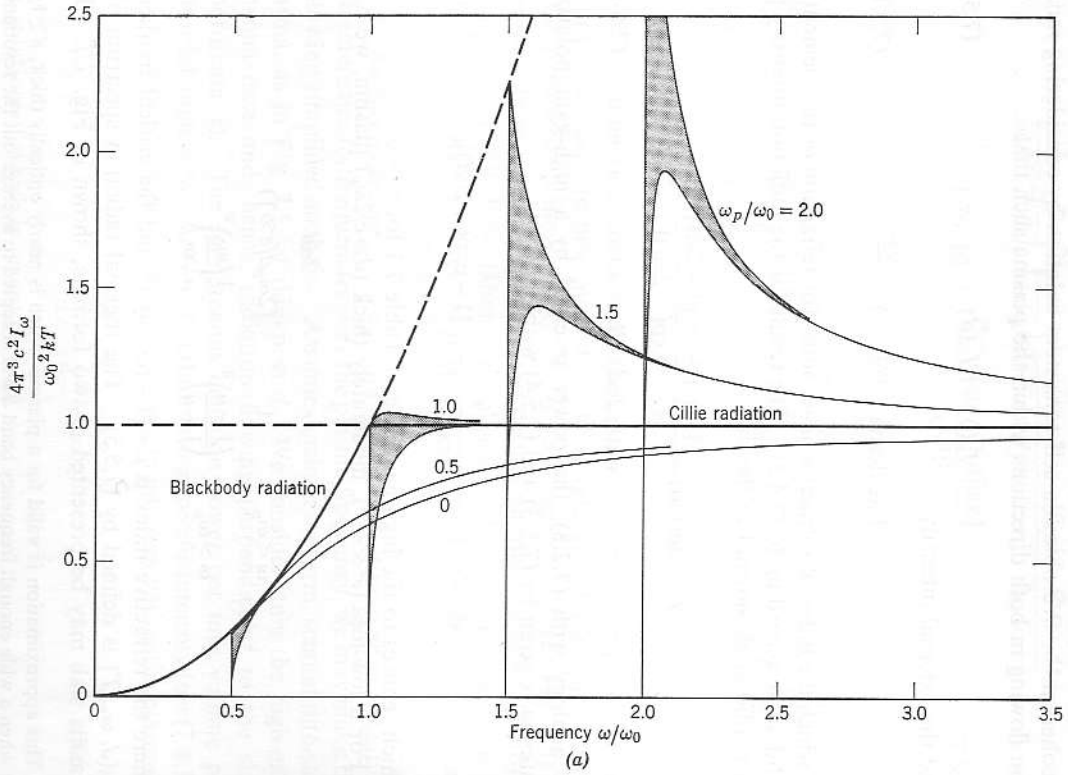

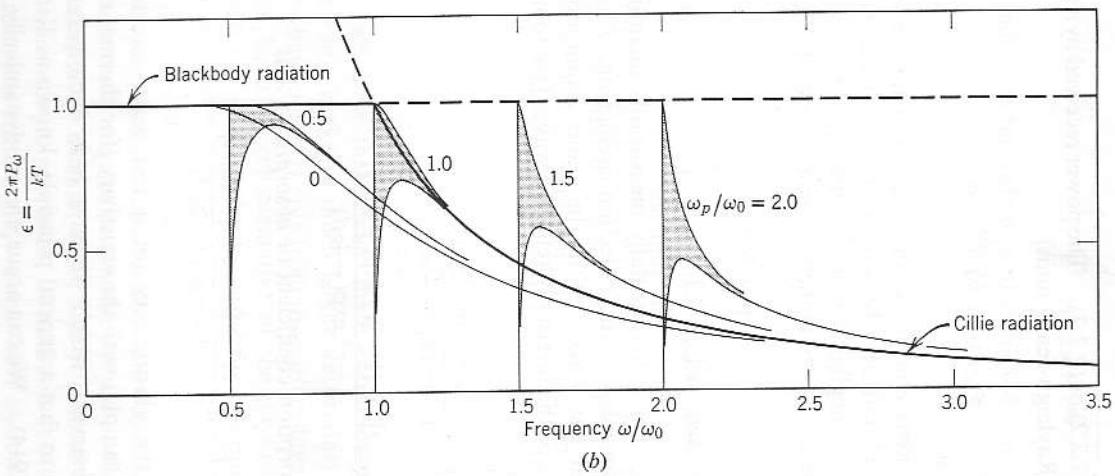

FIG. 7.7 Emission spectrum of plasma slab of low loss ($\nu^2 \ll \omega_p^2$) and of thickness $d \gg c/\omega_p$. (*a*) Specific intensity normal to slab. (*b*) Power received by high-gain antenna. The curves forming the lower limits of the shaded areas assume a sharp plasma boundary, according to (7.5.12). The upper limits assume a diffuse boundary, according to (7.5.15). The critical frequency ω_0 is defined in (7.5.5).

specific intensity normal to the slab is then (Dellis, 1957; Bekefi and Brown, 1961a; and French et al., 1961)

$$I_\omega = \epsilon\, {}^2B_\omega. \tag{7.5.13}$$

where ${}^2B_\omega$ is given by (7.2.2) or (7.2.3). The power received by a polarized, high-gain antenna is (Rayleigh-Jeans limit)

$$P_\omega\, d\omega = \epsilon\, kT \frac{d\omega}{2\pi}. \tag{7.5.14}$$

In both cases, the emissivity ϵ measures the fraction of the corresponding blackbody radiation level emitted. By way of contrast, it may be assumed that surface reflection is negligible (that is, the gradual boundary of Section 4.2). Then the emissivity is the high-gain case of Table 7.1

$$\epsilon = 1 - \exp(-2\alpha d). \tag{7.5.15}$$

This condition is also shown in Fig. 7.7.

7.5.3 ***Kirchhoff's law.*** The experimentally measurable quantities for a slab are the (power) transmission and reflection coefficients, T and R, for an externally generated test wave. With the same assumptions made above as to incoherency of the internally reflected waves (see footnote 15), we obtain (Section 4.3)

$$T = \frac{(1-r)^2 \exp(-2\alpha d)}{1 - r^2 \exp(-4\alpha d)} \tag{7.5.16}$$

$$R = \frac{r[1 + (1-2r)\exp(-4\alpha d)]}{1 - r^2 \exp(-4\alpha d)}. \tag{7.5.17}$$

The corresponding absorption coefficient or *absorptivity* A is

$$A = 1 - T - R = \frac{(1-r)[1-\exp(-2\alpha d)]}{1 - r\exp(-2\alpha d)} = \epsilon. \tag{7.5.18}$$

This identification of the absorptivity (of a test wave directed from observer to the plasma sample) with the emissivity (for thermal radiation from the sample to observer), which we have here demonstrated in a highly idealized case, is in fact a general principle, known as Kirchhoff's radiation law (Planck, 1914). We can argue, thermodynamically, that the fraction of a test wave directed at the plasma that is absorbed in the sample is equal to the emissivity, independent of details of propagation characteristics and plasma geometry, so long as the propagation characteristics are

fully reciprocal. The formal statement may be made by identifying the emissivity with the quantity

$$\epsilon \to A = \frac{\int_V \mathrm{Re}(\mathbf{J}\cdot\mathbf{E}^*)\, dV}{\int_S \mathrm{Re}(\mathbf{E}_0 \times \mathbf{H}_0^*)\, dS} \tag{7.5.19}$$

where V and S are the volume and projected area of the sample, $\mathbf{J}$ and $\mathbf{E}$ are the a-c current and electric field existing inside the sample, and $\mathbf{E}_0$ and $\mathbf{H}_0$ are the test wave fields in the absence of the sample (Levin, 1957; Bekefi, Hirshfield, and Brown, 1959; and Bekefi and Brown, 1961a). Note that $\mathbf{J}$ may be related to $\mathbf{E}$ by the well-established conductivity theory. This formulation holds generally for homogeneous isotropic samples; caution must be used in extending it further. An important feature is that it is valid for boundary-value problems, so that we no longer need demand that ray optics be applicable. Thus, experimentally, we can establish a power balance whereby we measure R and T directly, in an auxiliary calibration experiment, and infer $\epsilon = A = 1 - R - T$ therefrom. While this technique automatically accounts for internal reflections and diffraction effects within the plasma, in practical situations other than infinite plane slabs it is often difficult to measure dependably all nonabsorbed power, because of scattering, refraction, and diffraction. In many cases where the interface reflection coefficient r and the optical thickness $2\alpha d$ are simultaneously large, as for instance for $\omega < \omega_p$, it is possible to approximate the emissivity by (Bekefi, Hirshfield, and Brown, 1959; Hirshfield and Brown, 1961)

$$\epsilon \approx 1 - r \ll 1. \tag{7.5.20}$$

However, we note that under these conditions a small experimental uncertainty in r makes a much larger uncertainty in ϵ. Also, since the received radiation comes only from the surface layer of the plasma sample, it may not be at all representative of the physical state of the interior. Wort (1964) has given a simple model for computing the emissivity of a turbulent plasma.

In the presence of a magnetic field, which we have thus far ignored, the anisotropic propagation characteristics and opportunity for mode coupling and nonreciprocity require caution in the use of Kirchhoff's law (Martyn, 1948; Rytov, 1953; Bunkin, 1957; and Hirshfield and Brown, 1961). In terms of microscopic processes, in addition to ordinary bremsstrahlung from electron-ion encounters, we also have cyclotron radiation, which we discuss in Section 7.6. In the case of non-Maxwellian electron velocity distributions, the Kirchhoff radiation law must be suitably reinterpreted (Bekefi, Hirshfield, and Brown, 1961a; Fields, Bekefi, and Brown, 1963).

7.6 Cyclotron radiation

When a plasma is immersed in a steady magnetic field, the individual charged particles execute orbits which are in general helical. The particles are accelerated and radiate electromagnetic energy at the cyclotron frequency. Relativistic effects cause radiation at harmonics of the cyclotron frequency; this extension is often called *synchrotron radiation* (Schwinger, 1949; di Francia, 1959). The total cyclotron radiation is also known as *magnetic bremsstrahlung* (Trubnikov and Kudryavtsev, 1958). We note that ordinary bremsstrahlung occurs only during collisions, whereas cyclotron radiation occurs during the time interval between collisions.

7.6.1 ***Total radiation.*** The relativistic equivalent to (7.3.1) for the power radiated by an accelerated charge is (Panofsky and Phillips, 1962)

$$P=\frac{e^2a^2}{6\pi\epsilon_0c^3(1-\beta^2)^2} \tag{7.6.1}$$

where $\beta=v/c$ and the index of refraction of the surrounding medium is assumed to be unity. The acceleration of an electron resulting from the Lorentz (magnetic) force is

$$a=\frac{e|\mathbf{v}\times\mathbf{B}|}{m}=\frac{ev_\perp B}{m}=\omega_b v_\perp(1-\beta^2)^{1/2}, \tag{7.6.2}$$

where

$$\omega_b=\frac{eB}{m_0} \tag{7.6.3}$$

is the cyclotron frequency defined for the electron rest mass m_0. The total rate of radiation for one electron is then

$$P=\frac{e^2\omega_b{}^2v_\perp{}^2}{6\pi\epsilon_0c^3(1-\beta^2)}. \tag{7.6.4}$$

If the electron velocity distribution is isotropic and Maxwellian, the total power radiated per unit volume is

$${}^2\rho(T,\omega_b)=\frac{ne^2\omega_b{}^2}{3\pi\epsilon_0c}\left(\frac{kT}{mc^2}\right)\left[1+\frac{5}{2}\left(\frac{kT}{mc^2}\right)+\dots\right]. \tag{7.6.5}$$

The prescript 2 signifies that the receiving antenna is assumed unpolarized. The total power from ordinary and magnetic bremsstrahlung may be compared; from (7.3.29) and the leading term of (7.6.5),

$$\frac{{}^2\rho_{brem}}{{}^2\rho_{cycl}}=\frac{2}{(3\pi)^{1/2}}\left(\frac{\omega_p}{\omega_b}\right)^2\left(\frac{Z^2R_y}{kT}\right)^{1/2}\bar{\bar{\mathcal{G}}}(T) \tag{7.6.6}$$

where R_y, the Rydberg energy constant, equals 13.6 eV and $\bar{\bar{\mathcal{G}}}\sim1$ is the averaged Gaunt factor. In many practical situations the magnetic field ($\propto\omega_b$) and the particle pressure ($\sim nkT\propto\omega_p{}^2kT$) are correlated by confinement considerations such that $\omega_p{}^2/\omega_b{}^2\lesssim mc^2/4kT$ (Glasstone and Lovberg, 1960, pp. 50–54). Under this condition the cyclotron radiation is dominant above a crossover temperature which may be as high as 5 keV; in many cases of experimental interest, the crossover temperature may be as low as a few electron volts. Thus, cyclotron radiation represents an important energy loss from a hot plasma, and is of serious concern in connection with the power balance of thermonuclear reactors (Drummond and Rosenbluth, 1963). Cyclotron radiation, often from a nonequilibrium electron distribution, is of astrophysical interest in connection with radiation from radio stars and galaxies, the disturbed sun, and the so-called "dawn chorus" (Shklovsky, 1960). We note from (7.6.3) and (7.6.5) that cyclotron radiation by ions is smaller by the cube of the mass ratio (assuming equal electron and ion temperatures) and may usually be neglected.

In two ways cyclotron radiation is very different from ordinary bremsstrahlung. First, it is emitted and propagated anisotropically, so that the intensity depends upon the direction of observation (with respect to the magnetic field) and upon the state of polarization received. Second, in contrast to ordinary bremsstrahlung, the magnetic case represents a *line spectrum*, so that the question of line broadening is central to the determination of the detailed spectrum (unless the broadening is so large as to smear out the individual harmonics).

7.6.2 ***Radiation anisotropy (nonrelativistic).*** A nonrelativistic gyrating electron may be regarded as a superposition of two oscillating dipoles, each having the familiar $\sin^2$ intensity distribution. Thus, the power per unit volume radiated into the solid angle $d\Omega$ from a Maxwellian distribution is

$${}^2j\,d\Omega=\frac{ne^2\omega_b{}^2}{16\pi^2\epsilon_0c}\left(\frac{kT}{mc^2}\right)(1+\cos^2\theta)\,d\Omega \tag{7.6.7}$$

where θ is the angle between the directions of observation and the magnetic field. The radiation in the direction of the field ($\theta=0$) is right-hand circularly polarized; the radiation across the field ($\theta=\pi/2$) is linearly polarized transverse to the field. At intermediate angles the radiation has a well-defined elliptical polarization. If the radiation is received by a linearly polarized antenna, the angular variation is

$$\begin{aligned}{}^1j_\parallel&\sim\cos^2\theta\\ {}^1j_\perp&\sim1\end{aligned} \tag{7.6.8}$$

where the subscripts $\parallel$ and $\perp$ identify the polarization of the wave with respect to the magnetic field.

7.6.3 ***Line shape (nonrelativistic).*** In the nonrelativistic limit the radiation from a given electron velocity distribution is a single line broadened by several effects.

(*1*) Collisions interrupt the phase of gyration, limiting the length of the coherent wave train. This *collisional* broadening is equivalent to the well-known phenomenon of pressure broadening of atomic spectral lines. The net result is that (7.6.7) is multiplied by the Lorentz shape factor

$$\frac{\nu/\pi}{(\omega-\omega_b)^2+\nu^2}\,d\omega \tag{7.6.9}$$

where ν is the effective collision rate. This result may be obtained either from a single-particle analysis or from the macroscopic absorption coefficient invoking Kirchhoff's law (Oster, 1960; Hirshfield and Brown, 1961). The full width at half maximum is

$$\delta\omega=2\nu. \tag{7.6.10}$$

The factor (7.6.9) assumes ν independent of velocity. By the use of macroscopic arguments, it follows that the formalism of Section 2.4.3, involving the correction factors g and h, can be used when $\nu=\nu(v)$ (Kelly, Margenau, and Brown, 1957). In the case of highly ionized plasmas, the effect of electron-electron collisions must be included in the correction factors (Hwa, 1958).

(*2*) If the gyrating electrons stream rapidly through the sensitive region of the antenna pattern in a time τ, the length of the received coherent wave train is again limited. This effect may be termed *transit-time* broadening, and is significant when $\tau<1/\nu$. The line is again Lorentz-shaped, as (7.6.9) with ν replaced by $1/\tau$.

(*3*) The component of motion of the electron parallel to the field produces a doppler shift which, of course, depends upon the direction of observation;

$$\omega_b \rightarrow \frac{\omega_b}{1-(v_\parallel/c)\cos\theta}. \tag{7.6.11}$$

For a Maxwellian distribution, the resulting *doppler* broadening is given by (7.6.7) multiplied by the gaussian shape factor

$$\left(\frac{mc^2}{2\pi kT}\right)^{1/2}\frac{1}{\omega_b\cos\theta}\exp\left[-\left(\frac{mc^2}{2kT}\right)\frac{(\omega-\omega_b)^2}{\omega_b^2\cos^2\theta}\right]d\omega. \tag{7.6.12}$$

The full width at half maximum is

$$\delta\omega=\left[\frac{8(\ln 2)kT}{mc^2}\right]^{1/2}\cos\theta\;\omega_b. \tag{7.6.13}$$

Doppler broadening dominates that due to electron-ion collisions when

$$\frac{(kT[\mathrm{eV}])^2\,B[\mathrm{kG}]\cos\theta}{Z\,n[\mathrm{cm}^{-3}]}\gtrsim 10^{-11}. \tag{7.6.14}$$

Doppler broadening, when obtained from the macroscopic absorption coefficient via Kirchhoff's law, is the result of the noncollisional (Landau) absorption process of Section 3.5 (Hirshfield and Brown, 1961; Rukhadze and Silin, 1962). Combined doppler and collisional broadening leads to a Voight line shape (Aller, 1953; Posener, 1959).

(*4*) When the magnetic field is not uniform, the line is *inhomogeneity*-broadened.

(*5*) Dense, high-temperature plasmas (high β, in the language of controlled fusion research) can produce cyclotron radiation at frequencies somewhat below the expected frequency because of diamagnetism. The field depression, which may be quite large, generally is not uniform in space and time, so that this *diamagnetic* shifting and broadening is large and variable. The effect can be used to measure nkT and, since n is measurable independently, leads to a determination of T.

7.6.4 ***Radiation by a single relativistic electron.*** If the electron velocity is relativistic, the instantaneous radiation intensity is peaked in the direction of the electron's motion (Panofsky and Phillips, 1962). Qualitatively, this "headlight effect" concentrates the radiation in the direction perpendicular to the field and produces harmonics of the fundamental gyration frequency. Quantitatively, if the electron has no motion along the field, one obtains for the power radiated into solid angle $d\Omega$ by a single electron of velocity $\beta=v/c$ (Schott, 1912; Schwinger, 1949; and Landau and Lifshitz, 1962, §74)

$${}^2P_{\Omega s}\,d\Omega=\frac{e^2s^2\omega_b{}^2(1-\beta^2)}{8\pi^2\epsilon_0 c}\left[\beta^2\mathrm{J}_s'^2(\xi)+\cot^2\theta\;\mathrm{J}_s{}^2(\xi)\right]$$
$$\xi=s\beta\sin\theta. \tag{7.6.15}$$

where $s=1, 2, 3, \ldots$ is the harmonic number of the radiation (fundamental is $s=1$) and J_s and J_s' are the ordinary Bessel function and its derivative. If the electron has velocity components both parallel and perpendicular to the field, $\beta_\parallel=v_\parallel/c$ and $\beta_\perp=v_\perp/c$, with $\beta^2=\beta_\parallel{}^2+\beta_\perp{}^2$, the generalization of (7.6.15) to include the resulting doppler shift is (Trubnikov, 1958)

$${}^2P_{\Omega s}\,d\Omega=\frac{e^2s^2\omega_b{}^2(1-\beta^2)}{8\pi^2\epsilon_0 c(1-\beta_\parallel\cos\theta)^2}\left[\beta_\perp{}^2\mathrm{J}_s'^2(\xi)+\left(\frac{\cos\theta-\beta_\parallel}{\sin\theta}\right)^2\mathrm{J}_s{}^2(\xi)\right]d\Omega$$
$$\xi=\frac{s\beta_\perp\sin\theta}{1-\beta_\parallel\cos\theta}. \tag{7.6.16}$$

In the special case of observation across the field ($\theta=\pi/2$), the term in J_s' gives the intensity in the extraordinary polarization ($\mathbf{E}_{rf} \perp \mathbf{B}$), which is dominant, while the term in J_s gives the intensity in the ordinary polarization ($\mathbf{E}_{rf} \parallel \mathbf{B}$). Along the field ($\theta=0$), only the first harmonic remains, and the radiation is circularly polarized.

The intensity ratio of successive harmonics may be obtained from (7.6.16) by expansion of the Bessel functions for the limit $\xi \ll 1$, valid in the barely relativistic case, $\beta_\perp \ll 1$. We obtain

$$\frac{{}^2P_s}{{}^2P_{s-1}}=\frac{1}{4}\left(\frac{s}{s-1}\right)^{2s}\xi^2=\frac{1}{4}\left(\frac{s}{s-1}\right)^{2s}\frac{\beta_\perp{}^2\sin^2\theta}{(1-\beta_\parallel\cos\theta)^2}, \tag{7.6.17}$$

which, by hypothesis, is very small; the intensity decreases monotonically with increasing order. In particular, the ratio of second harmonic to fundamental, observed perpendicular to the field, is

$$\frac{P_2}{P_1}=4\beta_\perp{}^2. \tag{7.6.18}$$

For high harmonics ($s \gg 1$) in this weakly relativistic limit the envelope of the harmonic intensities may be seen from (7.6.17) to fall off exponentially, at $20\log_{10}(2/e\xi)$ decibels per harmonic ($e=2.718$). In the highly relativistic case, on the other hand, the intensity increases somewhat with harmonic number up to a broad maximum near $s\sim(1-\beta^2)^{-3/2}$ (Landau and Lifshitz, 1962, §74). The radiation of a single relativistic electron consists of the series of harmonics

$$\omega_s=\frac{s\omega_b(1-\beta^2)^{1/2}}{1-\beta_\parallel\cos\theta} \tag{7.6.19}$$

where $s=1, 2, 3, \ldots$ is the harmonic number.

7.6.5 ***Spectrum (relativistic).*** For a group of electrons, with some assumed velocity distribution, the spectrum is a series of shifted, broadened lines. The shift is produced by the relativistic mass-increase (time-dilation) factor $(1-\beta^2)^{1/2}$ and, for a Maxwellian distribution, amounts to

$$\Delta\omega_{shift}=-\frac{1}{2}\left(\frac{kT}{mc^2}\right)s\omega_b. \tag{7.6.20}$$

The broadening arises from the same effects mentioned in the nonrelativistic case, plus the dispersion of the velocity distribution in the relativistic shift. The shape factor for the latter effect alone is approximately

$$\frac{2}{\sqrt{\pi}}\left(\frac{mc^2}{kT}\right)^{3/2}y^{1/2}\exp\left(-\frac{mc^2}{kT}y\right)dy \tag{7.6.21}$$

where $y=1-(\omega/s\omega_b)>0$; the full width at half maximum is

$$\delta\omega=1.8\left(\frac{kT}{mc^2}\right)s\omega_b. \tag{7.6.22}$$

This is normally much smaller than the doppler width (7.6.13) except very close to perpendicular observation. To obtain the complete spectrum in the relativistic case it is necessary to integrate (7.6.16) over the electron velocity distribution $f(\boldsymbol{\beta})$. This integration, which is very complicated in the general case, may be stated formally as

$$j_{\omega s}(\omega, T)\,d\omega\,d\Omega=n\int_{\boldsymbol{\beta}}P_{\Omega s}(\boldsymbol{\beta})\,\delta\left[\omega-\frac{s\omega_b(1-\beta^2)^{1/2}}{1-\beta_\parallel\cos\theta}\right]f(\boldsymbol{\beta}, T)\,d^3\boldsymbol{\beta}\,d\omega\,d\Omega \tag{7.6.23}$$

where $j_{\omega s}$ is the power radiated per unit volume, solid angle, and frequency interval in the sth harmonic, $\boldsymbol{\beta}=\mathbf{v}/c$, and $\delta(x)$, the Dirac delta-function, is simply a formal way of stating the resonance condition between ω, $\boldsymbol{\beta}$, and θ.[16] The total radiation spectrum is then obtained by summing over harmonics

$$j_\omega(\omega, T)\,d\omega=\sum_s j_{\omega s}(\omega, T)\,d\omega, \tag{7.6.24}$$

and the total power radiated (per unit volume and solid angle) by integrating over frequency

$$j(T)=\int j_\omega(\omega, T)\,d\omega. \tag{7.6.25}$$

The integration (7.6.23) may be carried out numerically or in certain limiting cases analytically (Hirshfield, Baldwin, and Brown, 1961; Motley, Lustig, and Sanders, 1961; Beard and Baker, 1962; and Trubnikov and Yakubov, 1963). Figure 7.8 shows an example of such a spectrum. Cyclotron radiation may also be calculated from the macroscopic absorption coefficient, invoking Kirchhoff's law in analogy to the bremsstrahlung

[16] The Dirac delta-function is defined by the properties (Dirac, 1947)

$$\delta(x)\begin{cases}=0 & x\neq 0,\\ \to\infty & x=0,\end{cases}$$

$$\int\delta(x)\,dx=1,$$

$$\int F(x)\,\delta(x-a)\,dx=F(a)$$

where $F(x)$ is an arbitrary function and the limits of integration extend over the entire range of the variable x. It is somewhat analogous to the Kronecker delta defined by

$$\delta_{lm}\begin{cases}=0 & l\neq m\\ =1 & l=m\end{cases}$$

where l and m are integral indices.

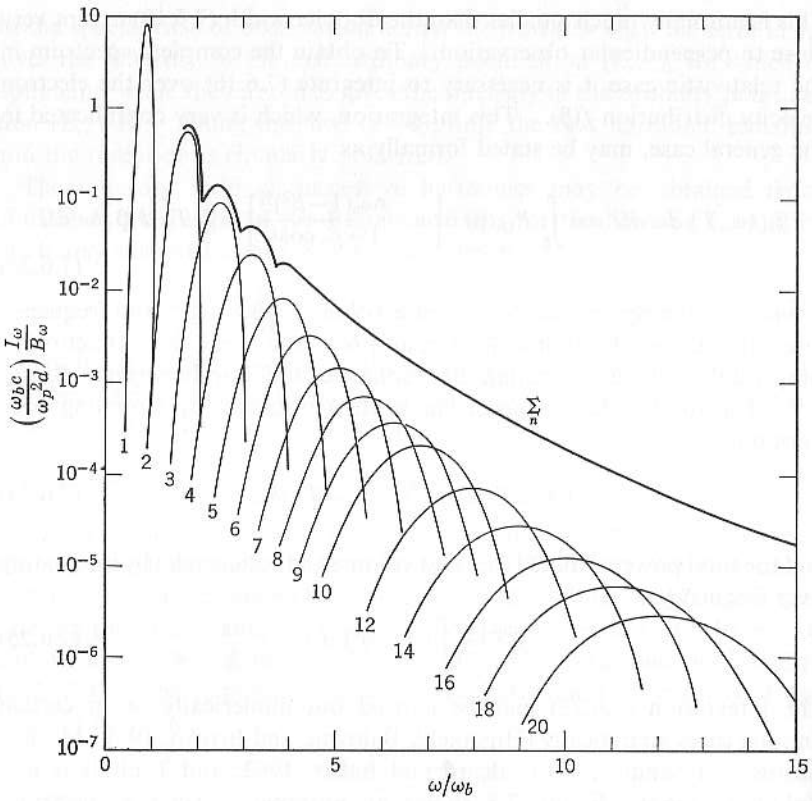

FIG. 7.8 Cyclotron emission spectrum from transparent plasma slab of temperature $kT = 50$ keV, and thickness d, integrated over angles. The emission intensity I_ω is modified by reabsorption and other effects when the condition $I_\omega \ll B_\omega$ (the blackbody intensity level) is violated. (Figure reproduced by courtesy of the *American Journal of Physics*; Bekefi and Brown, 1961a.)

treatment of Sections 7.4.4 and 7.5.3 (Beard, 1959). An important practical problem is radiation from plasmas with non-Maxwellian electron velocity distributions (Oster, 1961a; Bekefi, Hirshfield, and Brown, 1961b).

7.6.6 ***Effect of collective electron motion.*** Except for the mention of collisional broadening and diamagnetic shifting and broadening, we have thus far assumed that individual electrons radiate independently of each other. When a significant electron density is present, any existing cyclotron radiation exerts a synchronous force on neighboring electrons (Chang, 1962b; Oberman and Shure, 1963). The result is to displace the

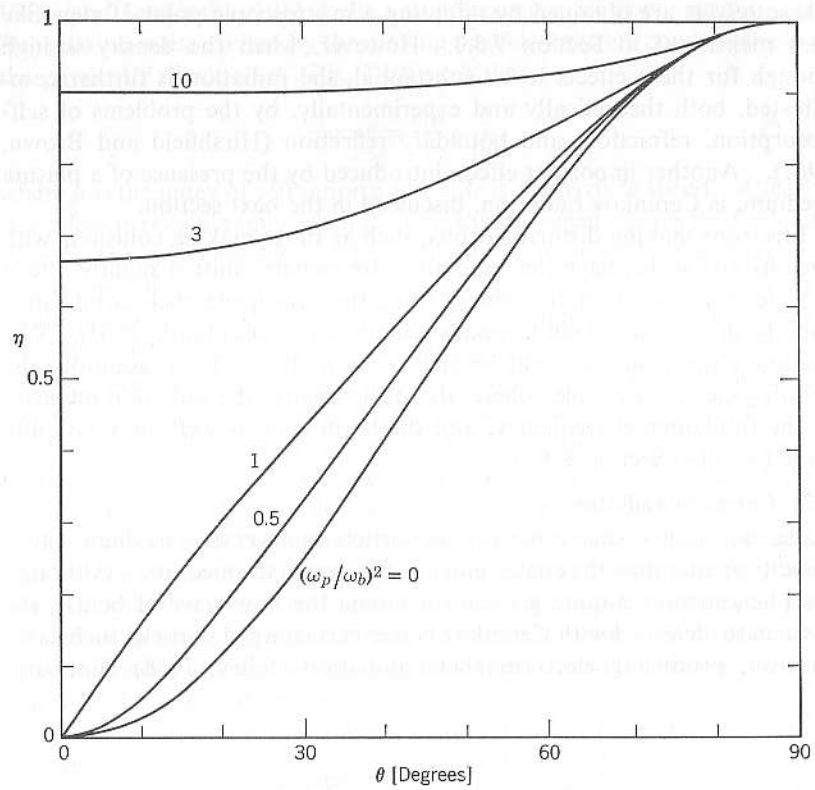

FIG. 7.9 Coefficient measuring displacement of cyclotron resonance for finite electron density but negligible collision rate, as a function of propagation direction. Resonant frequency is $(\omega_b^2 + \eta\omega_p^2)^{1/2}$.

resonance line, to an extent depending upon the direction and polarization of the wave considered (and also to broaden it if the plasma density is inhomogeneous). Specifically, for the right-handed–extraordinary wave the resonance frequency, from (1.4.81) with $\mu^2 \to \infty$, may be written in the form

$$\omega_b'^2 = \omega_b^2 + \eta\omega_p^2 \tag{7.6.26}$$

where the coefficient η is given as a function of ω_p and θ in Fig. 7.9. The coherent motion of neighboring electrons also broadens the line asymmetrically toward the cutoff frequency

$$\omega_2 = \frac{\omega_b}{2} + \left[\left(\frac{\omega_b}{2}\right)^2 + \omega_p^2\right]^{1/2}. \tag{7.6.27}$$

These results are obtained by adopting a macroscopic point of view like that mentioned in Section 7.5.3. However, when the density is high enough for these effects to be substantial, the radiation is further complicated, both theoretically and experimentally, by the problems of self-absorption, refraction, and boundary reflection (Hirshfield and Brown, 1961). Another important effect, introduced by the presence of a plasma medium, is Cerenkov radiation, discussed in the next section.

Electrons making distorted orbits, such as those making collisions with sheaths and walls, have their radiation frequencies shifted slightly above the electron cyclotron frequency, since they complete their orbits in a slightly shorter time than normally (Simon and Rosenbluth, 1963). The radiation spectrum also will be rich in harmonics. If, in addition, the orbiting electrons couple coherently to the sheath, the radiation intensity at the fundamental frequency, and the harmonics as well, may be quite large (see also Section 8.4.2).

7.7 Cerenkov radiation

Radiation occurs when a perturbing particle transverses a medium with a velocity greater than the phase velocity of a wave in the medium. Although the phenomenon is quite general (including the bow wave of boats), the usual case identified with Cerenkov concerns a charged particle, such as an electron, producing electromagnetic radiation (Jelley, 1958; Ginzburg,

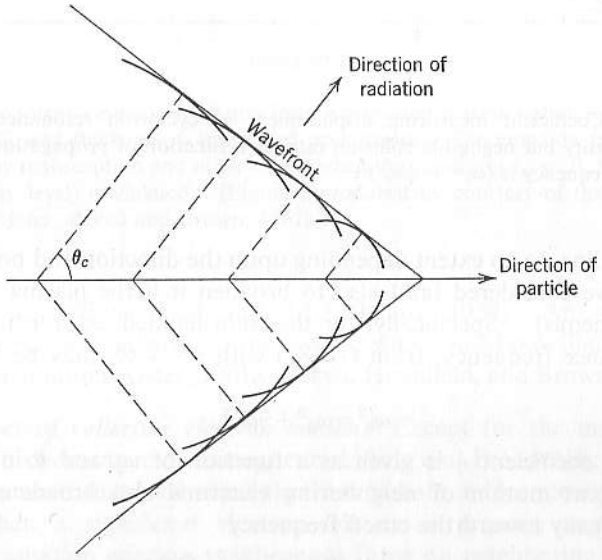

FIG. 7.10 Geometry of Cerenkov radiation.

1960; and Lashinsky, 1961). In a nondispersive, isotropic medium, the Huygens wavelets excited by the moving particle interfere constructively in the particular direction θ_c (Fig. 7.10) such that

$$\cos\theta_c=\frac{c/\mu}{v}=\frac{1}{\beta\mu} \tag{7.7.1}$$

where μ is the index of refraction and $v=\beta c$ is the particle speed. Clearly, this effect is possible only when $\beta>1/\mu$; that is, when the particle velocity exceeds the wave velocity. The radiation is emitted in the directions which form the elements of a cone of half-angle θ_c. The radiation from a single particle is received as a short pulse (delta-function) with, consequently, a broad-band frequency spectrum.

When the medium is dispersive, so that $\mu=\mu(\omega)$, the condition for constructive interference involves the phase velocity and (7.7.1) remains valid, with the characteristic angle θ_c depending on frequency as well as particle speed. The pulse radiated by a single particle is of finite duration. The frequency spectrum is dependent on the particular variation of $\mu(\omega)$. When the medium is further complicated by anisotropy, so that μ depends also on the direction of propagation, the radiation pattern is no longer conical, except in the special case of particle motion along the optic axis.

In the absence of a magnetic field, the refractive index of a plasma for electromagnetic waves is less than unity; Cerenkov radiation cannot occur. When a field is present, the index is greater than unity for certain frequency bands. We shall consider only the special case in which the electron motion is parallel to the magnetic field. Thus, the Cerenkov angle θ_c coincides with the angle θ of propagation (with respect to the field) and (7.7.1) becomes

$$\cos\theta=\frac{1}{\beta\,\mu(\theta,\,\omega)}. \tag{7.7.2}$$

For low plasma temperatures, the index is given by the Appleton formula (1.4.40), so that the Cerenkov condition is (neglecting collisions)

$$\frac{1}{\beta^2\cos^2\theta}=\mu^2=1-\frac{\omega_p^2/\omega^2}{1-\frac{\frac{1}{2}\omega_b^2\sin^2\theta}{\omega^2-\omega_p^2}\pm\left[\left(\frac{\frac{1}{2}\omega_b^2\sin^2\theta}{\omega^2-\omega_p^2}\right)^2+\frac{\omega_b^2\cos^2\theta}{\omega^2}\right]^{1/2}}. \tag{7.7.3}$$

This relation may be solved for $\cos^2\theta$, yielding (Kolomenski, 1956; McKensie, 1963)

$$\cos^2\theta=\frac{\omega^2}{2\beta^2\{(\omega^2-\omega_p^2)^3\beta^2-\omega^2\omega_b^2[\omega^2\beta^2+(1-\beta^2)\omega_p^2]\}\times\{2(\omega^2-\omega_p^2)^2\beta^2-\omega_b^2[2\omega^2\beta^2+(1-\beta^2)\omega_p^2]\pm\omega_p^2\omega_b[4(\omega^2-\omega_p^2)\beta^2+\omega_b^2(1-\beta^2)^2]^{1/2}\}}. \tag{7.7.4}$$

Insight into this relation for low (nonrelativistic) velocities may be obtained from (1.4.81) subject to the condition that $\mu^2 \to \infty$ (cyclotron resonance); Cerenkov radiation can thus occur near the angles given by

$$\tan^2\theta = -\frac{\kappa_\parallel}{\kappa_\perp} = -\frac{\left[1-\left(\frac{\omega_p}{\omega}\right)^2\right]\left[1-\left(\frac{\omega_b}{\omega}\right)^2\right]}{1-\left(\frac{\omega_p}{\omega}\right)^2-\left(\frac{\omega_b}{\omega}\right)^2}. \tag{7.7.5}$$

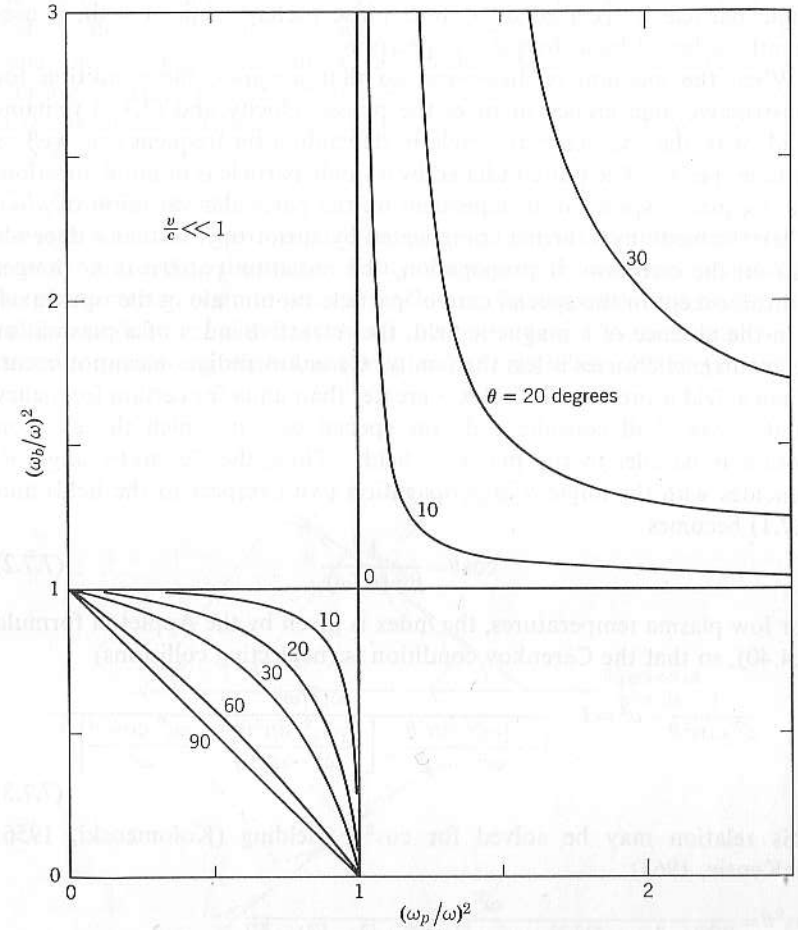

FIG. 7.11 Cerenkov angles for an electron moving parallel to the magnetic field; (*a*) nonrelativistic, (*b*) $v/c = 0.5$, (*c*) $v/c = 0.707$.

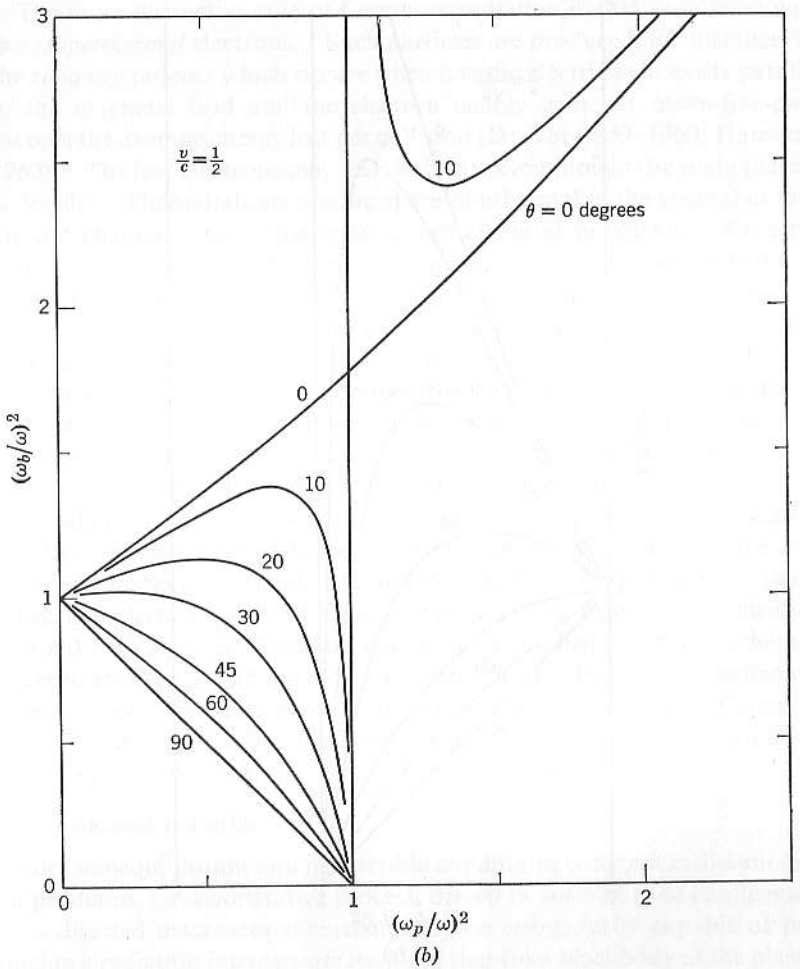

FIG. 7.11 (*continued*)

Figure 7.11*a* shows this condition. The relativistic case is far more complicated; numerical illustrations are shown in Figs. 7.11*b* and 7.11*c*. It should be noted that for all cases the radiation has one or the other of the two states of polarization, characteristic of propagation in the given direction.

When the radiating electron is a representative member of the thermal distribution, other electrons of similar velocity are present to support the inverse absorption process, which may be recognized as the Landau damping of Section 3.5. Hence, the emission of Cerenkov radiation

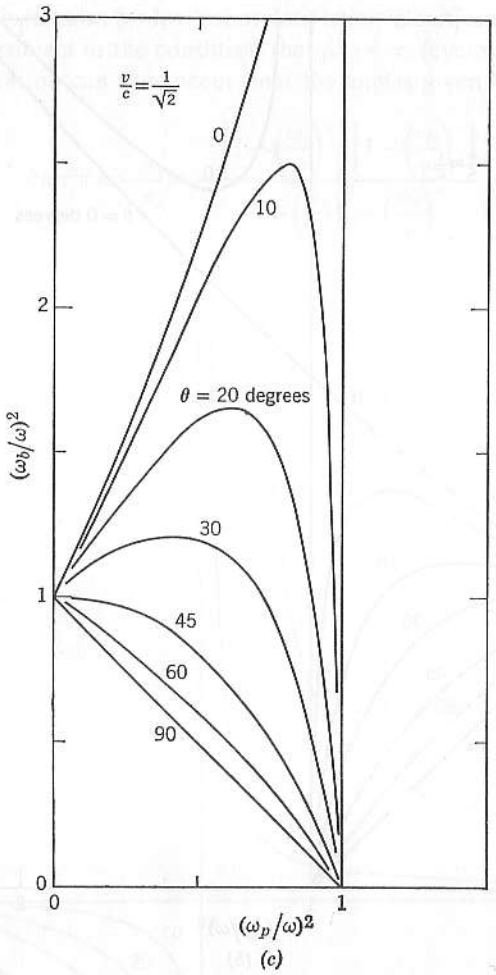

FIG. 7.11 (*concluded*)

cannot exceed the blackbody limit. Also the relation (7.7.5) shows that the conditions for Cerenkov radiation by nonrelativistic electrons are precisely those for cyclotron radiation. Thus, the processes of cyclotron, Cerenkov, and inverse Landau radiation are largely indistinguishable, if not synonymous, in a nonrelativistic, thermal (that is, approximately Maxwellian) plasma (Kihara et al., 1961; Pakhomov et al., 1962). Together they determine the plasma emissivity in the vicinity of the cyclotron frequency. There are even close relations to collisional bremsstrahlung (Lawson, 1954; Butler and Buckingham, 1962).

The more distinctive role of Cerenkov radiation is that associated with fast, *superthermal* electrons. Such particles are produced, for instance, by the *runaway* process which occurs when a static electric field exists parallel to the magnetic field and the electron energy gain per mean-free-path exceeds the average energy lost per collision (Dreicer, 1959–1960; Harrison, 1960). The fast electrons may be relativistic even though the main plasma is "cold." The radiations produced are nonthermal in the sense that they are not characteristic of the temperature of the main plasma. Since the coulomb cross sections decrease with increasing velocity, heat transfer to the thermal component of the plasma and collisional bremsstrahlung are not important energy loss mechanisms for these fast electrons. The more significant radiative losses are synchrotron and Cerenkov radiation. The former is most dependent on the velocity component transverse to the magnetic field; the latter, by contrast, on the longitudinal component. The spectrum and the energy loss rate have been calculated by Eidman (1958). Johnson (1962) gives a brief numerical example.

Another form of Cerenkov-like radiation in a plasma is the generation of electrostatic or spacecharge waves (plasma oscillations) of the sort discussed in Sections 3.4.4, 5.5, and 5.6 (Cohen, 1961; Eidman, 1962). Since the phase velocity of these waves is of the order of the electron thermal velocity, the Cerenkov condition is fulfilled for a superthermal electron even in the absence of a magnetic field. In many experimental situations involving a magnetic field and superthermal electrons, Cerenkov radiation and excitation of plasma oscillations are the dominant known processes by which the fast electrons are degraded.

7.8 Coherent radiation

Under nonequilibrium and irreversible conditions, coherent radiation may be produced. A cooperative process, driven by instability of confinement or a directed macroscopic current, may be energetically capable of producing a radiation intensity greater than that for a blackbody at the plasma temperature. Such processes are intrinsically complex and difficult to study, both experimentally and theoretically. Conversely, it is notoriously difficult to produce a plasma in the laboratory that is not subject to some instability or nonequilibrium process, known or unknown. The most tractable simple theoretical model is that of a high-speed electron stream, or *beam*, traversing an equilibrium plasma (Sumi, 1959; Stepanov and Kitsenko, 1961). Such streams may be injected from outside the plasma or produced within the plasma by the *runaway* phenomenon mentioned in the preceding section. If the beam density is large enough, beam *bunching* may occur, as in a klystron, so that beam electrons interact coherently and therefore vastly more efficiently than as individual particles. Alternatively,

the theoretical model may assume interpenetrating plasmas or a "double-humped" velocity distribution (Rukhadze, 1962; Ichimaru, 1962). Further discussion is given in Section 8.4.

Since longitudinal plasma oscillations become slow traveling electrostatic waves, either in the finite temperature case or for a bounded plasma, a relatively fast electron stream can synchronize with the wave in a manner closely related to Cerenkov radiation and to the conventional traveling-wave tube (Kompfner, 1952). This process can be an important energy loss from the beam. The theory and relevant experiments have been discussed by Boyd, Gould, and Field (1961) and Emeleus and Mahaffey (1961). Other experiments have been described by Kharchenko et al. (1960) and Targ and Levine (1961).

The longitudinal electrostatic waves generated in a plasma do not couple efficiently to electromagnetic waves external to the plasma. Several coupling mechanisms have been studied, such as the presence of a magnetic field and of density gradients or boundaries (Field, 1956; Wyld, 1960; Oberman, 1961; Majumdar, 1961; and Tidman and Boyd, 1962). Electromagnetic radiation, which may be due to plasma oscillations, has been observed from astronomical objects such as the sun and Jupiter (Kuiper, 1953; Field, 1959), from the aurora (Forsyth et al., 1950), and from Stellarators in the presence of runaway electrons (Bernstein et al., 1958; Heald, 1956). A common feature of the experimental observations is the occurrence of the radiation in short intense bursts. It also appears that two colliding spacecharge waves can produce electromagnetic dipole radiation at $\omega=2\omega_p$, the oscillating currents being maintained by momentum conservation (Aamodt and Drummond, 1963) The conversion efficiency is small, but still the radiation intensities can be very much larger than blackbody levels.

Microwave amplification by a nonequilibrium plasma has been proposed (Bekefi, Hirshfield, and Brown, 1961a). Amplification at frequencies other than those near the cyclotron and plasma frequencies has been postulated on the basis of a parametric amplification theory with the beam-driven plasma oscillation serving as pump (Coor, 1961; Kino, 1960).

CHAPTER 8

Plasma radiation experiments

8.1 Radiation from dense plasmas: blackbody radiation

When a plasma is in thermal equilibrium, or at least in radiative equilibrium, the radiation spectrum is determined by the absorption spectrum (Rytov, 1953). The radiation should be maximum when the plasma is "black." A meaningful radiation experiment, therefore, must be coupled with an absorption measurement and, perhaps, also a density determination. The absorptivity A can be calculated from (7.5.19) for complicated geometries, or from (7.5.18) for plane plasma configurations. For small power reflection coefficients r, such as achieved with diffuse boundaries, A can be identified with ϵ, the emissivity, shown graphically in Fig. 7.7*b*. In addition, for a high-gain antenna and a uniform plasma of depth d, approximating a one-dimensional case, A reduces to

$$A=\epsilon=1-\exp(-2\alpha d). \tag{8.1.1}$$

The radiation power in the frequency interval $d\omega$, radiated from an equilibrium plasma, is given by Kirchhoff's law when the absorptivity is large

$$P_\omega\, d\omega=kT_e\,\frac{d\omega}{2\pi}\,\frac{S}{\lambda^2}\,A \tag{8.1.2}$$

where S is the radiating surface area, and λ is the wavelength. The power received by a high-gain antenna is given by (7.5.4), or in terms of (8.1.1)

$$P_\omega\, d\omega=kT_e\,\frac{d\omega}{2\pi}\,[1-\exp(-2\alpha d)]. \tag{8.1.3}$$

For incomplete opacity, wall reflections become troublesome and must be eliminated (see Section 9.6.4 for absorbers). For complicated geometries

an integration over the plasma volume must be performed, taking account of wall reflections, if present (Wort, 1964).

A quantitative determination of the radiation temperature of a dense plasma can be made with the radiometer circuit of Fig. 9.44, together with the transmission circuit of Fig. 6.7 (or that of Fig. 6.13). A microwave

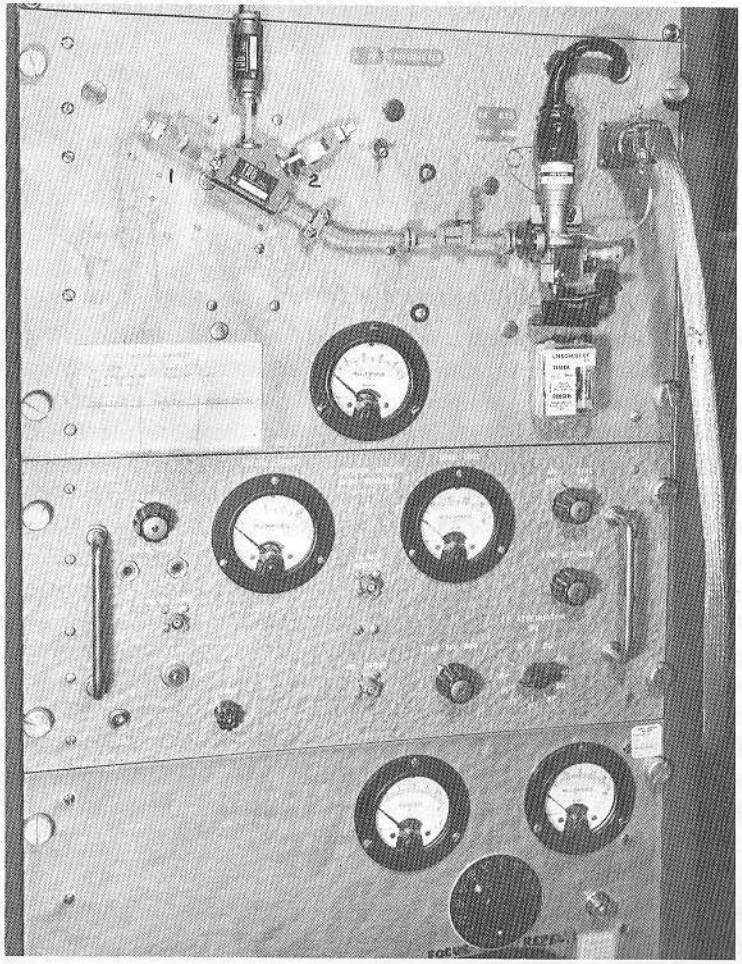

FIG. 8.1 A 3-mm (90-Gc) radiometer, including the klystron local oscillator, the power supply and the 30-Mc i.f. circuit. The i.f. circuit can be operated with direct detection video output or with coherent detection and d-c output. (Photograph courtesy of the University of California Lawrence Radiation Laboratory, Livermore, Calif.)

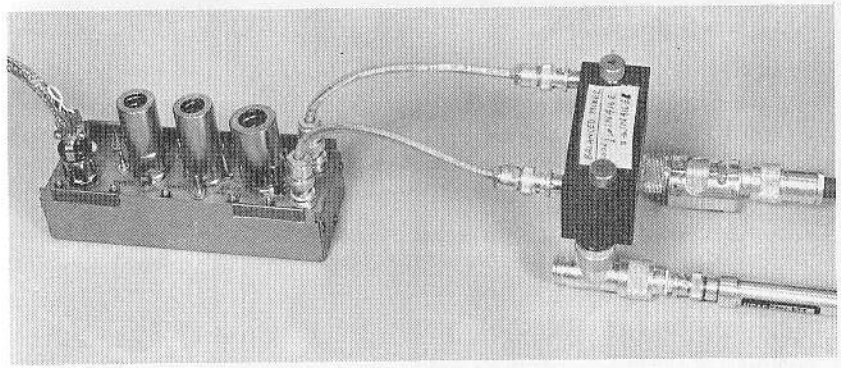

FIG. 8.2 A coaxial line, UHF swept radiometer, for use with an octave bandwidth, swept-frequency local oscillator. A band-pass filter in the signal input line is required, since otherwise the coaxial line passes extraneous noise and signals. (Photograph courtesy of General Atomic, San Diego, Calif.)

system is pictured in Fig. 6.21 having only one klystron source; part of the signal provides local oscillator drive for the radiometer and part of the signal is used for the interferometer. No cross coupling between the two circuits exists, since the radiometer receiver is tuned to a frequency displaced by the i.f. frequency from the interferometer. Also the horns are cross-polarized, giving 20 dB of geometrical decoupling.

A 3-mm radiometer (90 Gc) is shown in Fig. 8.1, including a 30-Mc i.f. amplifier and second detector that permits either direct video output or coherent detection with a long averaging time (see Section 9.5.5).

A coaxial-line, swept-frequency radiometer, operating in the uhf bands with a swept-frequency local oscillator, is shown in Fig. 8.2. A band-pass filter is required in the signal input line to reject spurious signals, since a coaxial line does not have a lower cut-off frequency like a waveguide. Further discussion of radiometers and the associated hardware can be found in Section 9.5.

Figure 8.3 demonstrates the relationship between opacity and radiation intensity. The lower trace is the transmission attenuation signal (the same event as recorded in Figs. 6.3 and 6.6) at 90 Gc. The upper trace shows the detected noise output from the radiometer of Fig. 8.1. Enhanced noise is seen to occur early in time, just as the hot, central core of the plasma is reaching cutoff, and later, just as it is coming out of cutoff. The noise level is low in intermediate times, since the cut-off, radiating shell is at a large radius, where the plasma is relatively cold. Also, when $\omega_p \gg \omega$, the plasma is no longer "black" but "shiny" (see Sections 7.2 and 7.5).

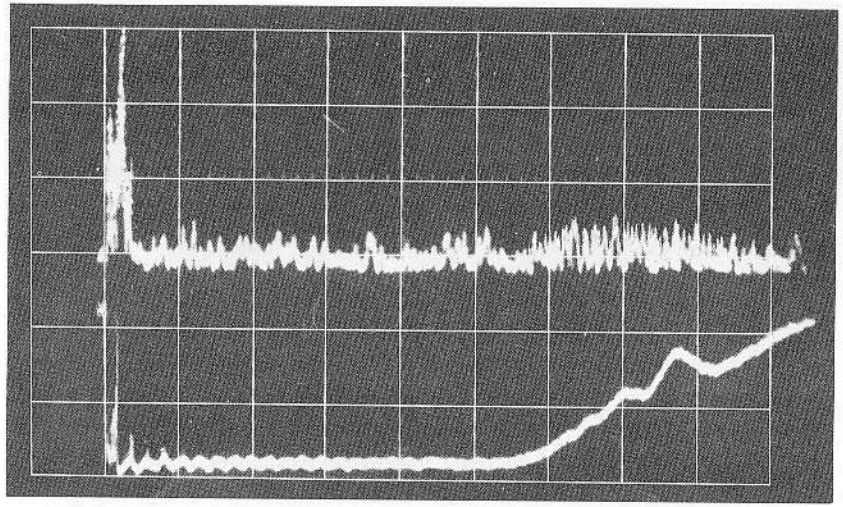

FIG. 8.3 Plasma radiation intensity correlated with opacity. In the top trace the 90-Gc radiometer shows radiation signals during the times that the attenuation measurement in the bottom trace indicates $\omega_p \approx \omega$. The radiometer of Fig. 8.1 was used.

Similar evidence is presented in Fig. 8.4, where the cutoff is indicated by the vanishing of the interference fringes (see also Wharton, 1961, p. 326). Three events are recorded, of consecutively higher-peak densities from top to bottom, all showing the increase in noise near cutoff. The data were made with the apparatus shown in Fig. 6.21, at 24 Gc. The peak amplitudes correspond to blackbody temperatures of 2 to 5 eV.

A signal compression is inherent in superhet radiometers, since the output signal is proportional to the input *voltage* and thus to the square root of the *noise temperature* T_N. The vertical scope deflection then is $D \propto (T_N)^{1/2}$. The peak noise signal of Fig. 8.3 thus corresponds to a blackbody (electron) temperature of ~ 10 eV, which agreed within a factor of 2 to the value obtained spectroscopically.[1]

In general, noise temperature (blackbody radiation) measurements made in dense, high-collision-rate plasmas yield electron temperatures in good agreement with those obtained by Langmuir probes (Knol, 1951; Easley and Mumford, 1951) or spectroscopically (Harding et al., 1958). Even in high-temperature plasmas, where the collision rates are too low to provide the thermalizing mechanism for electrons, nevertheless the electrons often are found to have a Maxwellian distribution (Gabor et al.,

[1] Unpublished data of C. B. Wharton, J. E. Katz, and D. Reagan, University of California, Lawrence Radiation Laboratory, Livermore, Calif., 1961.

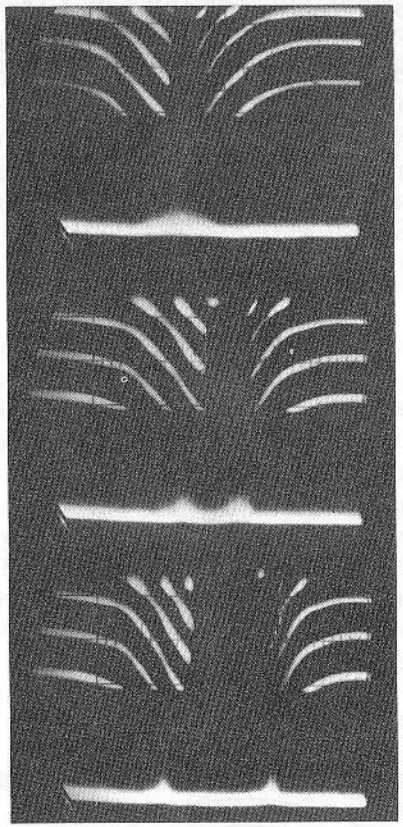

FIG. 8.4 Plasma radiation intensity correlated with opacity. The radiometer response is maximum just before the plasma goes to cutoff, as indicated by the disappearance of the interferometer fringes. The apparatus of Fig. 6.21 was used.

1955), and in many cases the electron temperatures inferred from microwave radiation intensities compare favorably with temperatures measured by other methods (Dellis, 1958; also see Section 8.2.1).

Occasionally, however, some obviously *nonthermal radiation* is observed, emanating from plasmas. Evidence for this type of radiation was reported in Section 7.8, and further discussion is given in Section 8.4.

8.2 Radiation from a plasma in a magnetic field

An electron spiraling about a magnetic field line will radiate, due to its acceleration, as demonstrated in Section 7.6, where radiation intensities and frequency spectra were calculated. In transparent plasmas, the

maximum radiation intensity was found to be in the plane of the orbits. In dense plasmas having radial density gradients (as real plasmas do), however, the cyclotron radiation is inhibited from escaping radially across the magnetic field, since it eventually reaches a cut-off region as the density falls toward zero at the edge (see Section 4.2.3). But, if the cut-off region is not extensive, some of the radiation generated in the hot interior can "tunnel" out and escape the plasma. Experimental evidence of this tunneling has been reported (Wharton, 1959; Motley et al., 1961).

8.2.1 ***Magnetic mirror radiation experiments.*** Cyclotron radiation emitted along the field lines is often observed. This can be explained in terms of Kirchhoff's law. The trapped magnetic bremsstrahlung is strongly absorbed at the QL resonance frequency (see Section 1.4.10) so that the plasma reaches an anisotropic radiative equilibrium (Beard, 1961). The radiation is able to diffuse along the magnetic lines or in directions in which the field increases in the appropriate manner to avoid the cut-off condition as the density decreases. The radiation escaping directly along magnetic field lines should be right-hand circularly polarized, since that is the wave that exhibits the large absorption. Measurements made on magnetic mirror machines at Livermore, Calif. (Wharton, 1958, 1959, and 1961), however, failed to show this polarization effect, presumably because of polarization coupling or wall reflections.

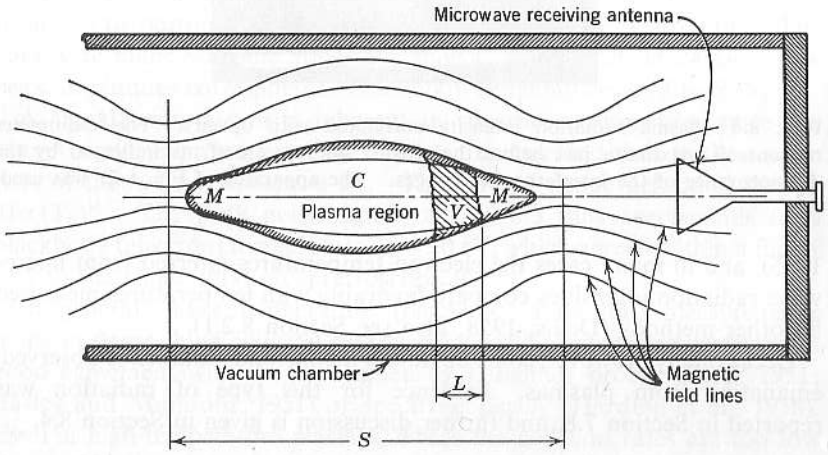

FIG. 8.5 Geometry for observing radiation from the end of a magnetic mirror plasma experiment. L is the radiation absorption length of the volume V. The region to the left of V is cut off, that to the right is transparent. C is the central region, M the mirror regions. S is the mirror separation.

The radiation geometry for mirror or cusp experiments is sketched in Fig. 8.5. The radiation absorption length L denotes the distance in which radiation is effectively absorbed and reradiated in random phases. It is important that L be smaller than or comparable to the dimensions of the plasma for at least two reasons: (*1*) to establish quasi-blackbody conditions, and (*2*) to quench any coherent radiation by *phase scrambling* during the absorption-reradiation process. The phase scrambling[2] is enhanced by a magnetic field gradient, such as found in a magnetic mirror, with a resulting action much like that of a magnetic beach (Stix, 1962). Absorption lengths typical of many controlled fusion experiments are from 0.5 to 5 cm. If the plasma extends for some distance into the magnetic mirror regions, M, it is this part of the plasma and not that in region C that will be sampled at a frequency giving cyclotron resonance in M. Region C can be probed by a second receiver, tuned to the lower frequency corresponding to the cyclotron frequency of that location. Waves can propagate in regions having higher magnetic fields, allowing the radiation from region C to pass unimpeded out through M.

8.2.2 ***Absorption-radiation experiment in a pulsed mirror machine.*** Many magnetic mirror experiments have pulsed fields to provide magnetic compression and heating of the plasma (Post, 1958). Fixed-frequency radiation receivers thus can be in tune with the cyclotron frequency twice each pulse, once during the rise and once during decay. Even though the intrinsic cyclotron resonance may be sharp (Drummond, 1958; Hayakawa et al., 1958), the received signals tend to be broadened by the magnetic field fluctuations and gradients. Typical variations of the fields in the Tabletop II experiment at Livermore (Post et al., 1960) with time are sketched in Fig. 8.6. The upper curve pertains to the field strength in the mirror region M, the lower curve to the field strength in the central region C. The low-β plasma, of course, is confined in the region within the mirrors, that is, between the curves of Fig. 8.6. The Tabletop II experiment had a chamber 15 cm in diameter and 1.5 meters long, with a mirror separation S of 50 cm (see Fig. 8.5). The peak pulsed field was programmable up to 50,000 gauss. The plasma was provided by injection from titanium hydride sources into the evacuated chamber (Coensgen et al., 1958), the peak injected density before magnetic compression rising to about 10^{12} electrons/cm^3.

To determine the plasma opacity, an absorption experiment also was performed. The equipment is shown in Fig. 8.7. The receiver is a

[2] To be distinguished from the *phase mixing* of Landau damping, which may also contribute to the establishment of radiative equilibrium, but not radiation, except through the inverse process, Cerenkov radiation (see Sections 6.6 and 7.7).

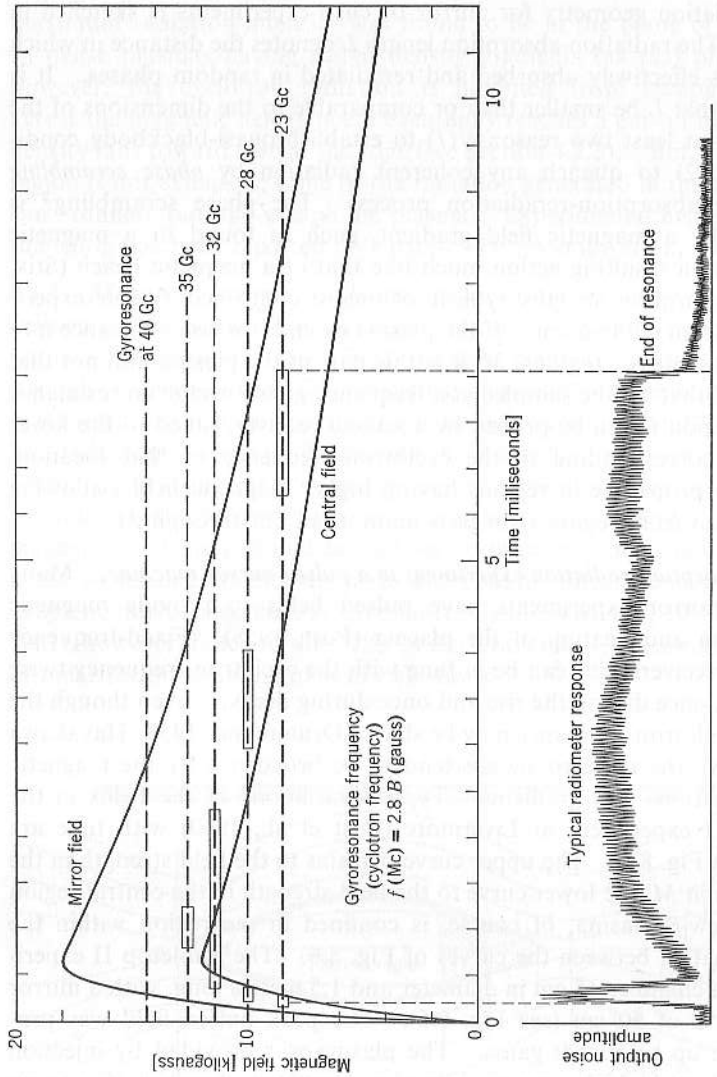

FIG. 8.6 Pulsed magnetic field strengths in the mirror and central regions of the Tabletop II controlled fusion experiment at Livermore, showing microwave radiometer response times at various frequencies. At bottom is sketched a typical reponse of a radiometer at 23 Gc.

superhet, having a 10 Mc band width and 0.1 micro-microwatt threshold sensitivity, with detected noise viewed directly on an oscilloscope. Amplitude and geometry calibration were made by moving a standard 15.2 dB thermal noise source (with a small horn radiator attached) about inside the experiment chamber before it was evacuated (see Section 9.5.6).

The transmitter klystron is modulated by random noise to produce a microwave spectrum some 200 Mc wide. The effects of high-order

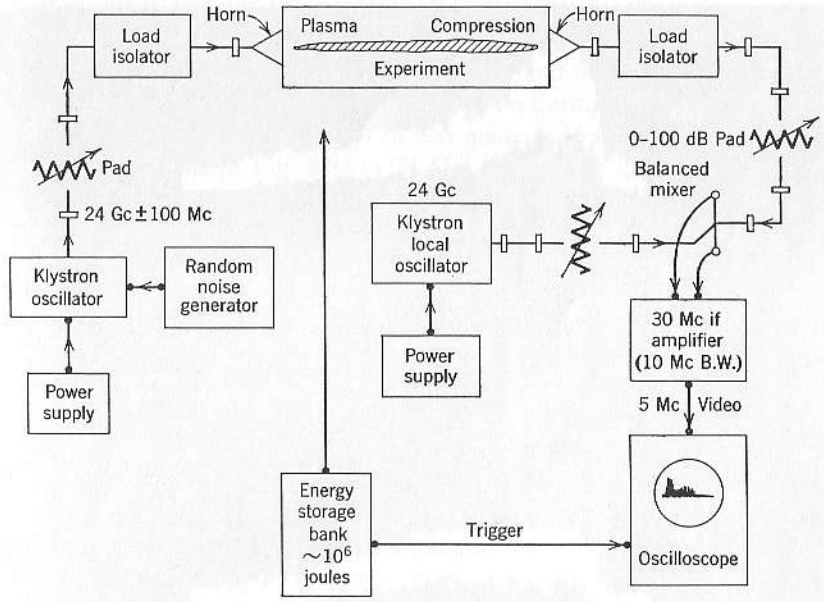

FIG. 8.7 Microwave equipment used for a 24-Gc microwave gyroresonance absorption-radiation experiment on a pulsed magnetic mirror machine. (See Figs. 8.6 and 8.8 for experimental results.)

waveguide modes and reflections in the vacuum chamber are thus minimized. The frequency stability of the receiver and transmitter are good enough that no AFC system is required. The transmitter power level is a few milliwatts; the receiver output is set to a steady arbitrary signal level by adjusting the 0 to 100 dB attenuator in the input. Two such systems were used simultaneously, one in the *K*-band (23 to 28 Gc) and one in the 8-mm band (32 to 40 Gc).

All plasma radiation (of order 10^{-11} watts maximum) is masked by the transmission signal (of the order of 10^{-3} watts). A *K*-band reflection experiment at the transmitter end was performed, showing plasma reflection coefficients less than 1% under all conditions, when the plasma was both opaque and transparent. Absorption lengths are of the order of a centimeter or two (many plasma wavelengths, at resonance).

When the radiation was to be viewed, the transmitters were turned off and the input attenuators turned to zero. The plasma experiment was operated again, exactly as before, but now the receivers viewed the plasma radiation. Typical receiver output responses are shown in Fig. 8.8. The times of resonance are also shown on the field plots of Fig. 8.6,

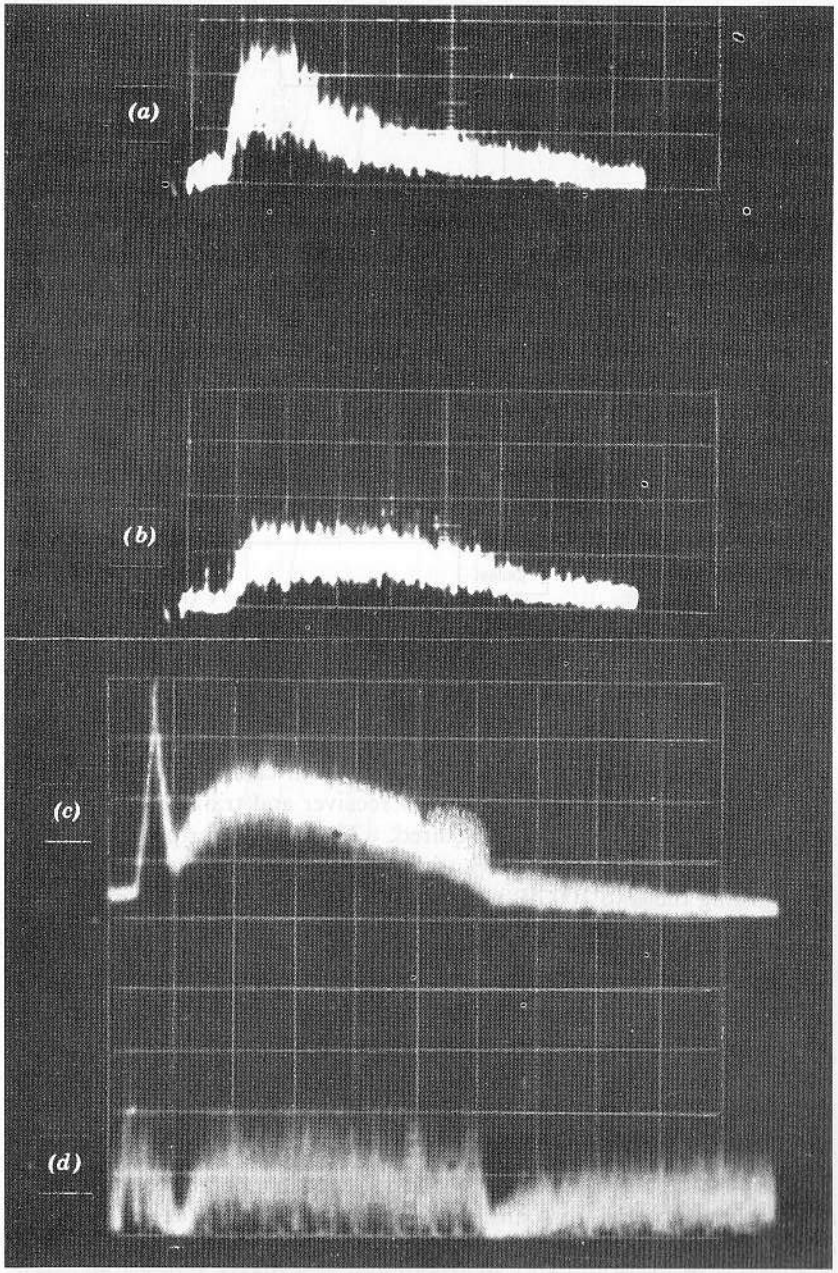

FIG. 8.8 Plasma microwave radiation data. Responses of radiometers to the cyclotron radiation from a magnetic mirror machine, (*a*) at $f=35$ Gc, (*b*) at $f=32$ Gc, and (*c*) at $f=24$ Gc. Trace (*d*) is the absorption response, with a 24 Gc noise-modulated transmitter propagating through the plasma. The response times are shown in Fig. 8.6. (See the circuit of Fig. 8.7.)

together with a sketch of the receiver response to indicate the interpretation of the results. The received radiation is seen in this experiment to correspond to radiating regions between the central and mirror portions of the chamber, somewhat closer to the central region during times of maximum compression. The trace in Fig. 8.8*a* was made at 35 Gc, that in Fig. 8.8*b* at 32 Gc, and that in Fig. 8.8*c* at 24 Gc. The trace in Fig. 8.8*d* is the attenuation response with the noise-modulated transmitter on (at 24 Gc), showing sharp absorption at the same times that radiation resonances occurred. During times between resonances ($B > B_c$), the transmission signal strength is seen to be twice as high as for the vacuum case, indicating enhanced coupling when the cyclotron frequency is above resonance, as would be expected for ducted cyclotron wave propagation (low-density case of whistler-mode propagation). It is highly unlikely that the enhancement is due to any kind of wave growth or amplification.

The amplitudes of the first radiation peaks (at $t \approx 400$ μsec), in many of the events, corresponded to blackbody temperatures of 15 keV (170 million degrees Kelvin). A direct energy analysis of escaping electrons (Ellis and Parker, 1958), assuming adiabatic trapping, yielded an average plasma electron energy of 17 keV at that time. The velocity distribution was not distinguishable from Maxwellian. The ions did not have a Maxwellian distribution, but their average energy was estimated at between 500 and 1000 eV. The average energy of escaping X-rays was within the range 10 to 100 keV, as estimated from absorber measurements.

8.2.3 ***Absorption-radiation measurements in a waveguide or cavity.*** The interactions between plane waves and plasma slabs can be simulated under certain conditions by enclosing the plasma in waveguides or resonant cavities (Buchsbaum et al., 1960). The boundary conditions can be satisfied, but the plasma ordinarily does not look "optically thick," so that local equilibrium is not established, except in the cases of high collision rates or strong resonances. Also, the sharp boundaries may permit charge separation, with attendant coupling between spacecharge and electromagnetic waves, or may allow wave tunneling through otherwise cut-off regions.

For two cases, the radiation from bounded plasmas can be studied by applying corrections to the free-space relationships (Hirshfield and Brown, 1961): (*1*) weakly absorbing, tenous plasmas, utilizing a perturbation analysis, and (*2*) highly absorbing plasmas, such that the absorption length is much smaller than the plasma dimensions. In case *1* the plasma critical frequencies are shifted by the mode cutoffs (see Section 5.2) and the total wave absorption is decreased by the increase in guide wavelength. In case *2*, when the absorption is large, the effects of boundaries

are small, and the resonance occurs at the free-space frequency given by (1.4.111)

$$\omega_R^2=\frac{\omega_b^2(1-\omega_p^2\cos^2\theta)}{1-\omega_p^2} \tag{8.2.1}$$

where θ is the angle in respect to the magnetic field. It is usually not convenient in waveguide experiments to observe radiation at angles very far from $\theta=0°$ (along **B**) or $\theta=90°$ (across **B**). Solenoidal magnetic fields can be made very uniform, so that ω_b is well defined. If the density along the plasma column is also uniform, ω_p and the transverse resonant frequency, $\omega_R=(\omega_p^2+\omega_b^2)^{1/2}$, are also well defined.

The presence of the reflecting walls may increase the effective emissivity by multiple internal reflections, very much as in an optical hohlraum or integrating sphere (Wort, 1964). The total radiation transmission coefficient T_{rad} analogous to (4.3.13), is obtained by summing over all of the S single-interface reflection coefficients r, for a system of dimension d

$$\begin{aligned}T_{rad}&=(1-r)^2\sum_{S=1}^{\infty}(r)^{S-1}\exp(-2S\alpha d)\\&=(1-r)^2\frac{\exp(-2\alpha d)}{1-r^2\exp(-4\alpha d)}.\end{aligned} \tag{8.2.2}$$

The total radiated power, compared to the blackbody power, is

$$P=P_{BB}\frac{(1-r)[1-\exp(-2\alpha d)]}{1-r\exp(-2\alpha d)}. \tag{8.2.3}$$

If αd is small, the reflection coefficient is important; if αd is large, the reflection enters only in determining the effective emissivity of the sampling orifice.

In the waveguide experiments of Hirschfield and Brown (1961), a time-integrating S-band Dicke radiometer, similar to the one shown in Fig. 9.44 and having a sensitivity of 10^{-17} watts, permitted measurements on tenuous plasmas to be made. Cyclotron resonance line profiles were made under various conditions of gas pressure. If the broadening of the line were to be explained as due to collisions, of constant ν, then the line half-width would be

$$\delta\omega_{1/2}=\nu. \tag{8.2.4}$$

If the broadening were pure doppler broadening, the half-width would be

$$\delta\omega_{1/2}=\omega_b\left(\frac{2kT_e}{mc^2}\ln 2\right)^{1/2}. \tag{8.2.5}$$

A combination would lead to a Voigt profile. The results obtained in this experiment showed much greater broadening in helium than would be

expected by either of these effects, with also slight shifts toward higher frequencies than ω_b for the known magnetic field. The conclusion was that either the magnetic field was not as uniform as they thought (0.5%), the electron temperature exceeded 4 eV, or some additional mechanism was contributing. The radiation intensities for blackbody radiation at densities from 10^{10} to 10^{12} cm^{-3} and for cyclotron radiation for densities between 10^9 and 10^{10} gave a noise temperature of 2 eV. At low densities (10^9 down to 10^7 electrons/cm^3), the noise temperatures for cyclotron radiation rose to 7 or 8 eV. The data were all obtained at a fixed frequency by sweeping the magnetic field and the electron density.

8.3 Swept-frequency radiometers

In some experiments the plasma conditions change radically as either the magnetic field or electron density are varied. The swept-frequency radiometer pictured in Fig. 8.2 avoids some of the difficulties by providing a voltage-tunable octave band. Both side bands are received, since it would be difficult to sweep a tunable rejection filter in exact synchronism with the local oscillator. The balanced mixer must be carefully matched over the band to achieve optimum performance. A coaxial-line ferrite isolator and a band-pass filter in the input minimize the spurious responses. If single-sideband reception is required then the band-pass filter must be tunable and tracked with the local oscillator.

If an integrating detection radiometer is used, the frequency sweep rate must be slow enough that the response can follow. Typical response times of Dicke radiometers are from 0.1 to 10 seconds.

A swept intermediate frequency also can be used to scan over a spectrum. This permits a fixed-frequency local oscillator, with a high-Q cavity to stabilize it and remove much of its noise contribution to the mixer circuit. Single-ended mixers can then be used, instead of the more critical and expensive balanced mixers. For narrow frequency scanning, such as looking at resonance line profiles, the i.f. amplifier can be a conventional low-noise i.f. strip, followed by either a second mixer and swept local oscillator or a sweeping filter (Long and Butterworth, 1963). For wide frequency scanning, a low-noise traveling-wave tube or distributed amplifier, in conjunction with a swept-frequency tuned amplifier, can be used (Cohn et al., 1963). These techniques are particularly useful at millimeter wavelengths, where mixers are critical, especially if harmonic mixing is required (see Section 9.5).

8.4 Radiation of nonthermal origin

It is often difficult to distinguish nonthermal from thermal radiation. True, when the radiation is observed in intense bursts or has an abnormally

high harmonic content, the generation is clearly not of purely thermal origin. But the radiation emanating from a plasma having a non-Maxwellian velocity distribution or containing plasma waves or electrostatic instabilities may not *appear* abnormal. It is important to understand the basic radiation processes, then, to be able to attach much importance to various features of the emission.

8.4.1 ***Instability-generated radiation.*** Among early observations of nonthermal radiation were bursts in the VHF bands of fairly short-duration emanations from the sun, presumably associated with plasma oscillations in solar prominences (Kuiper, 1953).

Similar large bursts at 8 mm wavelength have been observed in Stellarators (Heald, 1956), presumably due to instabilities driven by runaway electrons. The intense "generation" of waves by the Stellarators was of sufficiently high power to endanger crystal detectors in microwave interferometers used for diagnostics.

An electron beam-plasma interaction experiment was set up at Livermore in 1959 to simulate the runaway electron interaction, but with controlled electrons from a gun. The gun was pulsed with 5 to 20 μsec pulses 30 times per second, firing into the steady-state P-4 plasma (Hall and Gardner, 1961) as shown in Fig. 8.9. Radiation pulses, of microwatt intensity (that is, about 10^6 times the blackbody level) were detected during the electron pulses, in a narrow frequency band centered about the plasma frequency, at 34 to 36 Gc,[3] depending on the electron density at the location of the beam. The radiation intensity varied smoothly with variation of the pulse current, the detectable threshhold occurring when the peak current was about 5 to 10 milliamperes. Two orientations were used for the pickup horns, as shown in Fig. 8.9, both using square cross-section horns and fin-line couplers to resolve the two polarizations. With the horn looking along the column (actually looking up at the plasma with a 20° angle from the axis), the radiation intensity was found to be about 5 times as large from up stream (radiation coming from the gun end) as from down stream. With the horn looking at 90° to the plasma, the radiation polarized along the direction of the beam was 6 times as intense as that polarized across the beam. The intensities measured at three ports along the column were essentially the same, although the frequencies varied by about 10%. The signals from two ports detected simultaneously with two wide-band 8-mm radiometers were uncorrelated, when fed into a coincidence circuit (< 2% coincidence over 10 seconds).

[3] Here, the word "radiation" is used in the strictest sense, that is, far-field, electromagnetic reception, as distinguished from "noise," which may be picked up by a probe or antenna immersed in a plasma, and subject to near-field induction or spacecharge field fluctuations.

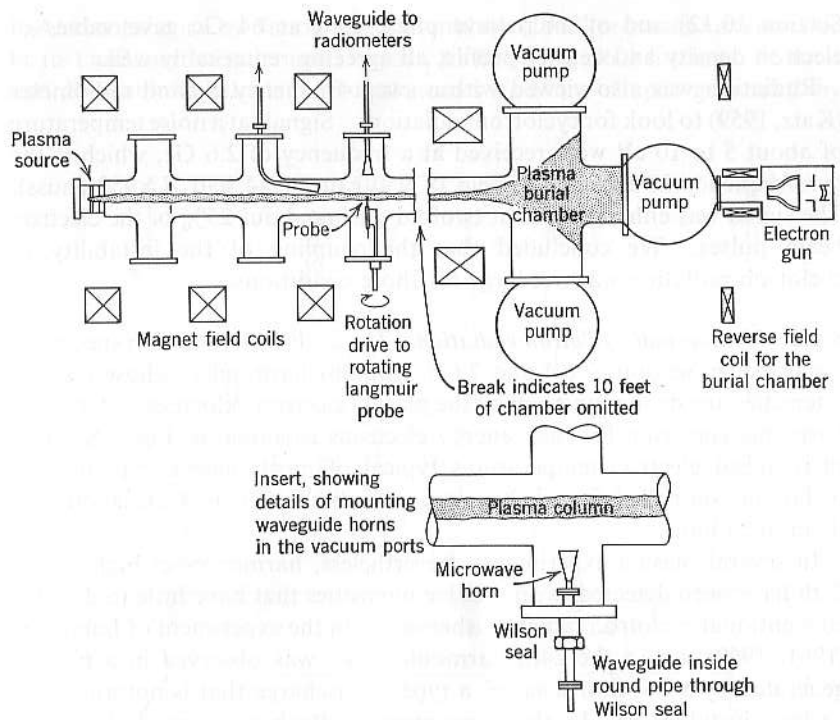

FIG. 8.9 Electron beam–plasma interaction experiment. The electron gun injects 20 μsec, 1-amp pulses of 25 keV electrons into the steady P-4 plasma column. The P-4 plasma was 99% ionized, with 10^{13} electrons/cm^3 at 10 to 20 eV temperature. (From unpublished data of C. B. Wharton and A. L. Gardner, University of California, Lawrence Radiation Laboratory, Livermore, Calif.)

When a Langmuir probe was inserted in the plasma in the space in front of the horn, the radiation power increased a hundredfold, and the frequency emitted became a function of the radial position of the probe.[4] Presumably, the enhancement was due to conversion of some of the space-charge wave energy into currents on the probe which, in turn, radiated electromagnetic waves as a dipole. Since the beam-induced plasma oscillations are very nearly at the plasma frequency (Stepanov and Kitsenko, 1961; also see Section 5.5), a measurement of the radiation frequency gives a measurement of the local electron density. Correlative measurements of saturated ion current of the Langmuir probe (see

[4] Actually, the probe was swept through the plasma with a 15% duty cycle to prevent its burning up (Gardner et al., 1961), so that the radial positioning was actually done by timing the firing of the electron beam pulse with a variable delay.

Section 10.12) and of microwave phase shift at 64 Gc gave values of electron density and density profile, all agreeing remarkably well.

Radiation was also viewed with a swept-frequency *S*-band radiometer (Katz, 1959) to look for cyclotron radiation. Signals at a noise temperature of about 5 to 10 eV were received at a frequency of 2.6 Gc, which is the gyrofrequency in a magnetic field of 930 gauss (P-4 had $B \approx 950$ gauss). The signal was enhanced about twofold during about 25% of the electron beam pulses. We concluded that the coupling of the instability to cyclotron radiation was not large for those conditions.

8.4.2 ***Nonthermal cyclotron radiation.*** The cyclotron radiation spectrum, discussed in Sections 7.6.4 and 7.6.5, contains harmonics, whose relative intensities are strong functions of the plasma electron velocities. A typical harmonic spectrum for high energy electrons is shown in Fig. 7.8. For thermalized electron temperatures typical of most plasma experiments, including controlled fusion, harmonic numbers of 3 or 4 are about the theoretical limit.

In several plasma experiments, nevertheless, harmonics as high as the 24th have been detected, with relative intensities that have little to do with conventional cyclotron radiation theories. In the experiment of Landauer (1961, 1962), up to the 24th harmonic of ω_b was observed in a plasma generated by a P.I.G. discharge, a type of discharge that is notorious for various instabilities. In the experiment of Bazhanova et al. (1961), a spectrum of 10 harmonics of the ion-gyrofrequency were detected in the Ogra machine (Artsimovich, 1958; Golovin, 1959) having a high-energy plasma of density about 10^8 ions/cm^3. The observations of 8 or 10 harmonics of ω_b by Fields et al. (1963) and Bekefi et al. (1962) were made in the positive column of a hot cathode arc discharge having $\omega_p \approx \omega$. All of these observations were made by holding the frequency of the receiver constant and varying the magnetic field. Landauer used two frequencies at once, 34 Gc and 10 Gc, and found that in all cases the peaks occurred at slightly higher frequencies than multiples of ω_b, rather than being shifted downward as given by (7.6.19). A typical spectrum is shown in Fig. 8.10*a*, in which it is seen that the intensities of the first 18 peaks are essentially the same. Observations made with the antenna oriented with E along the magnetic field even showed several harmonics, but with reduced amplitude. Landauer (1962) offers several qualitative explanations, involving "quasirelativistic" electrons and high, nonlinear refractive index, that partially explains the observed effects.

A theory given by Pistunovich and Shafranov (1961), also involving a very large refractive index due to resonance, partly explains Landauer's and also Bazhanova's results on Ogra.

A recent theory by Simon and Rosenbluth (1963) provides a reasonable fit to Landauer's results and, in part, to Bekefi's (1962) findings. Simon and Rosenbluth calculate the harmonics and line shapes generated by

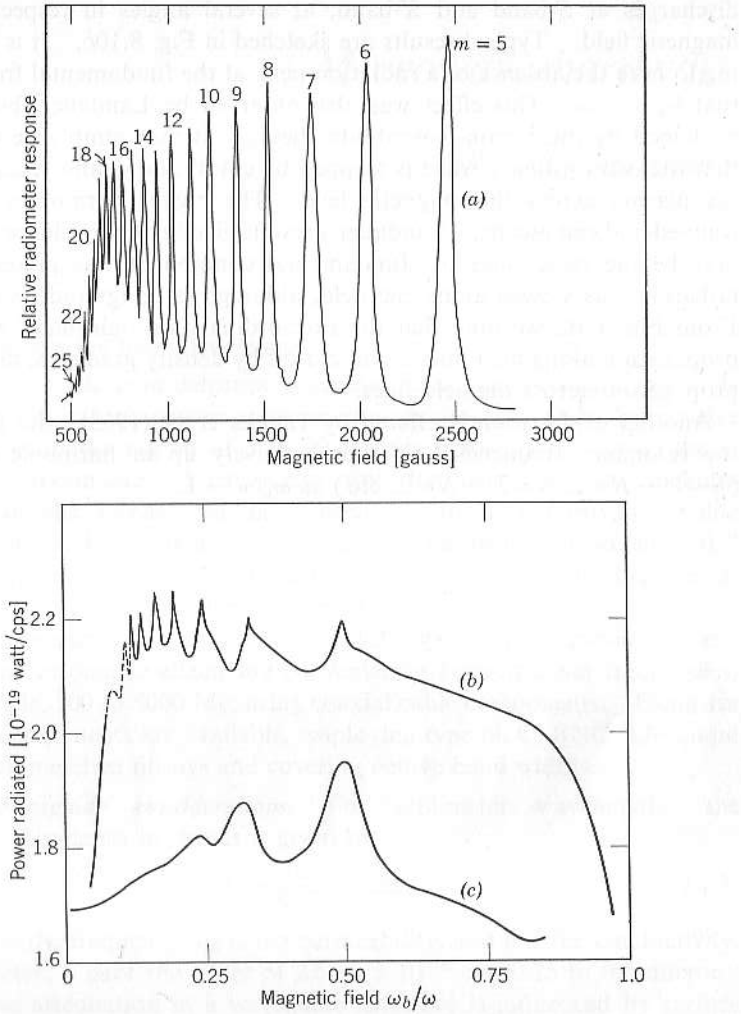

FIG. 8.10 Cyclotron harmonic radiation spectra for nonthermal radiation. (*a*) Some results of Landauer (1962); pressure $= 1.5 \cdot 10^{-2}$ torr.; m is the harmonic number. (*b*) and (*c*) Some results of Bekefi et al. (1962), showing the effect of pressure. In (*b*) the pressure was $5.4 \cdot 10^{-3}$ torr; in (*c*), 0.6 torr. The peak intensities are orders of magnitude above blackbody.

particles making cyclotron orbits and collisions with walls and sheaths simultaneously. The broadening and shifting of the low harmonic number peaks and the variations with plasma frequency agree well with Landauer's data.

The observations by Bekefi (1962) were made in argon and mercury discharges at *S*-band and *X*-band, at several angles in respect to the magnetic field. Typical results are sketched in Fig. 8.10*b*. It is interesting to note the absence of a radiation peak at the fundamental frequency, that is, $\omega_b = \omega$. This effect was also observed by Landauer, but is not explained by the Simon-Rosenbluth theory. It may simply be evidence that the extraordinary wave is trapped by cutoff and cannot escape from the plasma across the magnetic field. The higher harmonics are not trapped and can escape. Landauer's results give further evidence that this may be the case, since the fundamental component was present when radiation was viewed along the field, although its magnitude was small. From Fig. 1.10, we note that the extraordinary or right-hand wave for propagation along field lines is not cut off by density gradients, as it is for propagation across the field lines.

Another explanation is offered by Tanaka et al. (1963), who find that the resonance frequencies shift progressively up in harmonic number ($N=1 \rightarrow N=2$, $N=2 \rightarrow N=3$, etc.) as $\omega_p/\omega \rightarrow 1$.

CHAPTER 9

Microwave hardware and techniques

9.1 Transmission lines and fittings

The ranges of electron densities, magnetic fields, and plasma dimensions of many laboratory plasma experiments require the use of microwave frequencies in the region of 3 to 90 Gc for free-space (beamed) transmission experiments. Fortunately, this frequency interval includes several of the bands that have been developed extensively. Some experiments call for higher frequencies, the hardware for which is still largely experimental. Table 9.1 lists some of the bands and the present standard waveguides and flanges of each.

Plasma experiments involving spacecharge wave transmission and hybrid ion resonance effects are conveniently done at lower frequencies, for example, 500 to 5000 Mc, using coaxial cable components. Extensive lines of components are available, employing type N, C, BNC, TNC, and other well-matched fittings and covering octave band widths.

9.1.1 ***Waveguide considerations.*** For millimeter wavelengths, the nominal skin-depth in metals is given by

$$\delta = \frac{1}{\sqrt{\pi f \mu_0 \sigma}} \text{ meters}, \tag{9.1.1}$$

where f is the frequency, μ_0 is the permeability, and σ is the conductivity, mhos/meter; δ is of the order of 2.5 to $5 \cdot 10^{-5}$ cm (0.25 to 0.5 micron). The wave attenuation in a waveguide therefore is influenced by surface roughness, oxidation and chemical deposits, and work-hardening (Thorp, 1954). A quantity that describes the surface condition is the surface resistivity,

$$R_s = \frac{1}{\sigma\delta} = \sqrt{\frac{\pi f \mu_0}{\sigma}} \text{ ohms/unit square}. \tag{9.1.2}$$

TABLE 9.1 STANDARD WAVEGUIDE BANDS

Frequency range, Gc	Band-center wavelength	Designations	Waveguide		Flanges
			JAN	EIA	
2.6–3.95	10 cm	*S*	RG-48	WR 284	UG 53, 54A
8.2–12.4	3 cm	*X, Xs*	RG-52	WR 90	UG 39, 40A
12.4–18	20 mm	*Ku, P*	RG-91	WR 62	UG419, 541
18–26.5	12 mm	*K*	RG-53	WR 42	UG425, 595, 596
26.5–40	8.6 mm	*Ka, R, U, V*	RG-96	WR 28	UG381, 599, 600
33–50	6.8 mm	*Q*	RG-97	WR 22	UG383
50–75	4.3 mm	*M, V, W*	RG-98	WR 15	UG385
60–90	3 mm	*E*	RG-99	WR 12	UG387
75–110	3 mm	—	—	WR 10	EIA standard flanges*
90–140	2.2 mm	*F*	RG-138	WR 8	
110–170	2 mm	—	RG-136	WR 7	
140–220	1.5 mm	*G*	RG-135	WR 5	
170–260	1.2 mm	—	RG-137	WR 4	
220–325	1 mm	—	RG-139	WR 3	

* A U.N. commission, the International Electro-Technical Commission, is currently studying waveguide standards problems and is making recommendations for standard flanges in the millimeter bands. These will become EIA standard flanges.

R_s has the same value as the d-c resistivity of a plane conductor of thickness δ and conductivity σ. Surface roughness and porosity increase R_s. For example, a microscopic roughness of depth and spacing equal to 2δ will increase R_s about 50% (Lending, 1955; Morgan, 1949). High-conductivity, nonoxidizing materials commonly are used for waveguide fabrication, including pure copper, coin silver (90% silver, 10% copper) and pure silver laminated on copper or bronze. At the shorter wavelengths, gold, chromium, or iridium often are plated on exposed surfaces to impede oxidation. Figure 9.1 shows skin depths for several materials at various frequencies.

Waveguide attenuation is dependent on the frequency, the dimensions of the waveguide, and the type of transmission mode. For example, the attenuation due to wall losses for the TE_{10} mode in rectangular waveguide of width a, height b is

$$\alpha_{dB}=\frac{8.686R_s(\epsilon_0/\mu_0)^{1/2}}{b\left[1-\left(\frac{\lambda}{2a}\right)^2\right]^{1/2}}\left[1+\frac{2b}{a}\left(\frac{\lambda}{2a}\right)^2\right] \text{ dB/meter} \qquad (9.1.3)$$

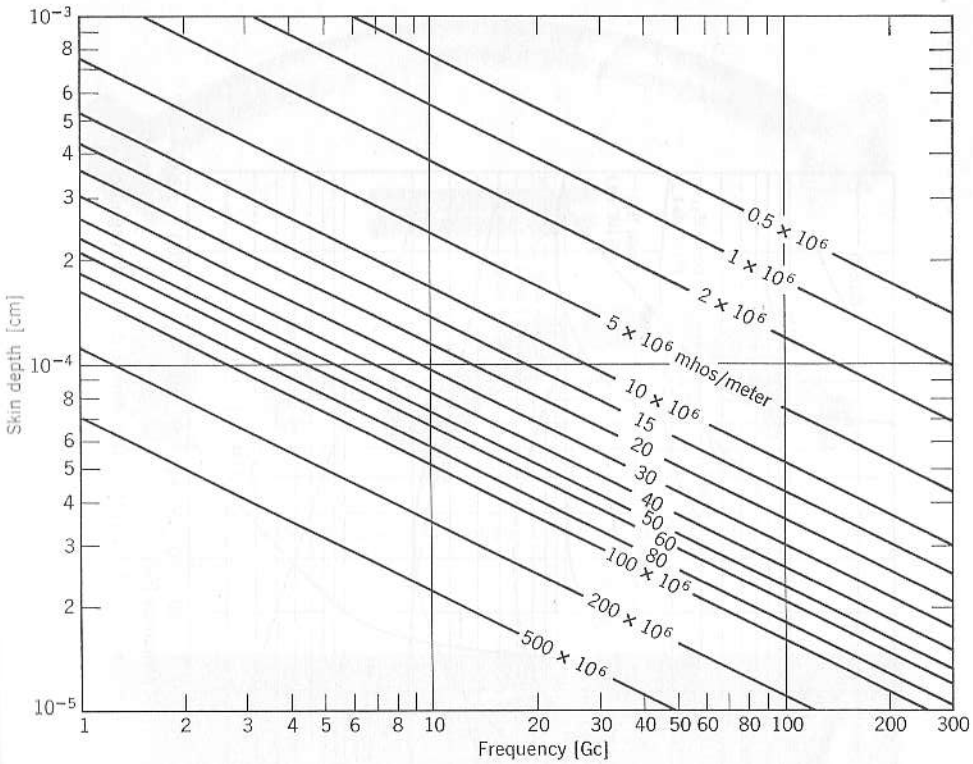

FIG. 9.1 Skin depth in metals of various conductivities as a function of frequency. d-c Conductivities of common metals in units of 10^6 mhos/meter: silver 64; copper 59; gold 41; chromium 38; aluminum 35; magnesium 22; iridium 16; brass 15; platinum 9; soft solder 7; mercury 1.1.

where λ is the free-space wavelength. The attenuations of the common RG-type waveguides in the TE_{10} mode are shown in Fig. 9.2. In addition, the values for some high-mode waveguides are shown, including some RG waveguides of extreme oversize (Valenzuala, 1963). In oversize or high-mode waveguides, mode purity is sometimes difficult to maintain (Lewin, 1959). Usually, bends, junctions, or obstructions lead to mode conversion, with attendant frequency sensitivity and attenuation. A common practice is to use conventional-waveguide-size components for circuits, short runs, sharp bends, etc., and taper up to the oversize or high-mode guide with a long, electroformed transition for long straight runs, where excessive attenuation in the conventional waveguide would normally occur. Round copper tubing that has been slightly flattened

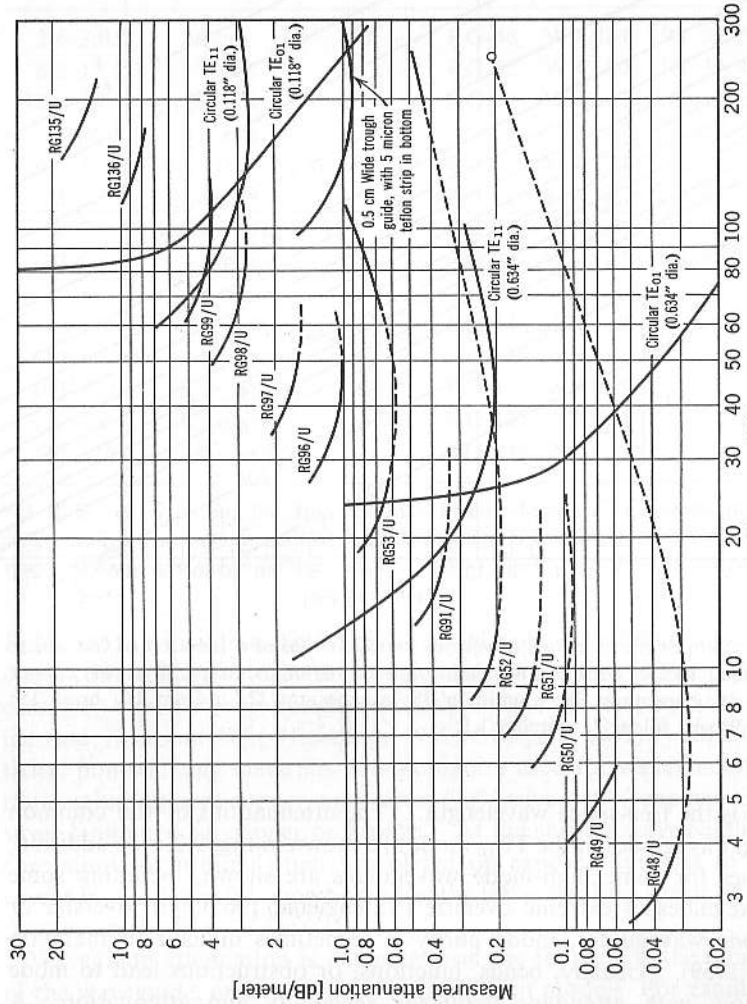

FIG. 9.2 Waveguide attenuation as a function of frequency for standard RG waveguides and for some special waveguides.

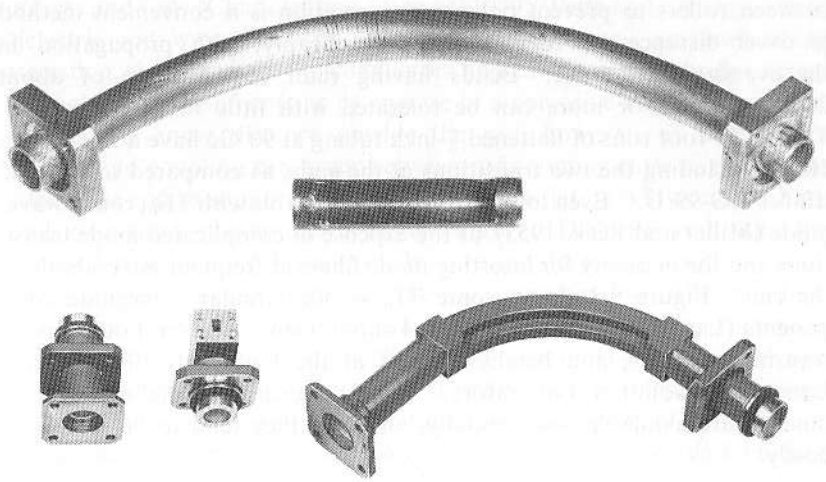

FIG. 9.3 TE_{01}-mode circular waveguide components. (Courtesy Microwave Associates, Inc.)

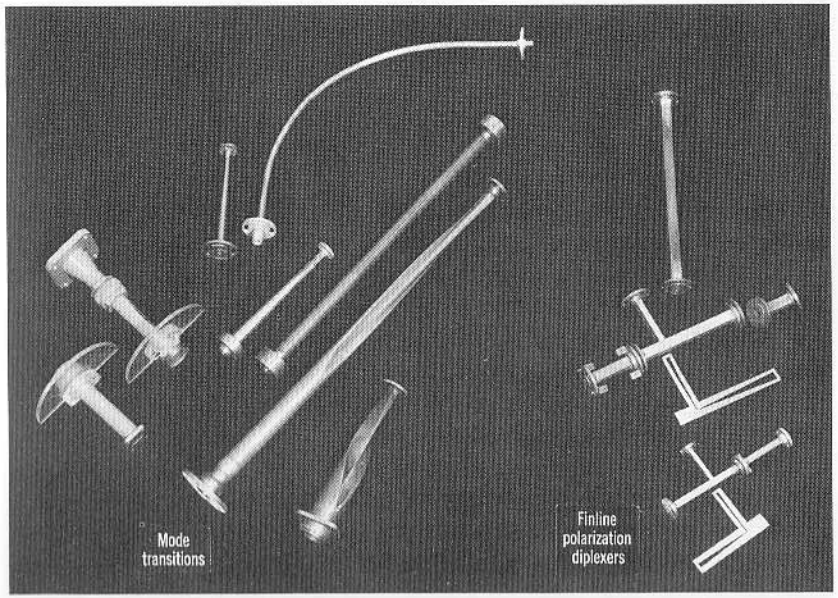

FIG. 9.4 Photograph of several mode transitions and polarization diplexers for wave launching or analyzing. (Courtesy of University of California, Lawrence Radiation Laboratory, Livermore, Calif.)

between rollers to prevent polarization rotation is a convenient method to cover distances up to about 50 feet, cheaply, with propagation in the oversize TE_{11} mode. Bends having radii of curvature of about 20 wavelengths or more can be tolerated with little mode conversion. Typical 50-foot runs of flattened $\frac{5}{8}$-inch tubing at 90 Gc have a loss of 7 to 10 dB, including the two transitions at the ends, as compared to 70 to 80 dB for RG-99/U. Even lower losses are obtainable with TE_{01} round waveguide (Miller and Beck, 1953), at the expense of complicated mode transitions and the necessity for inserting mode filters at frequent intervals along the run. Figure 9.3 shows some TE_{01}-mode circular waveguide components (Lanciani, 1954). Figure 9.4 shows views of several other mode transitions, filters, and bends, as used at the University of California Lawrence Radiation Laboratory. Highly-oversize, special-mode components are available commercially, although they tend to be somewhat costly.

9.1.2 ***Open waveguide transmission lines.*** Other interesting types of wave-guiding structures utilize surface waves on metallic (Sobel et al., 1961), dielectric-coated metallic (Diament et al., 1961), or purely dielectric

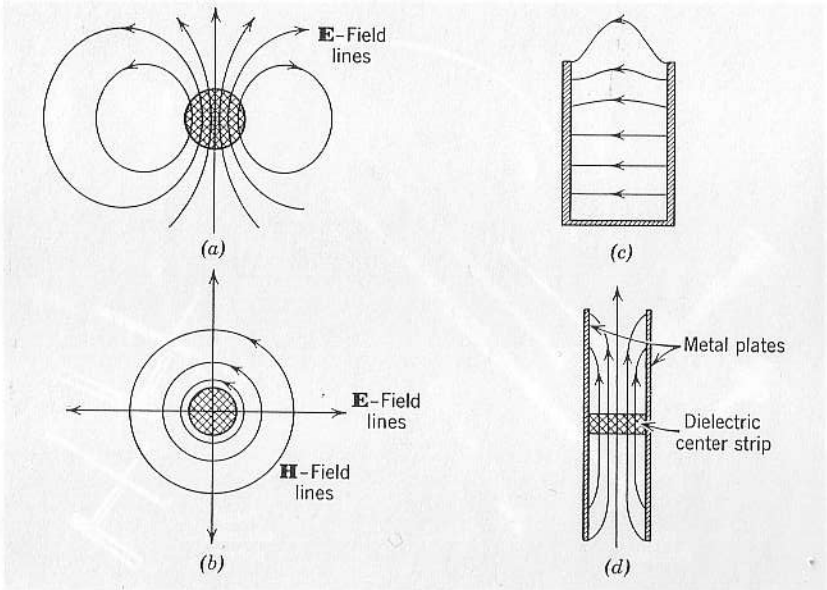

FIG. 9.5 Sketches of field patterns of open waveguide transmission lines. The fields are seen to fringe some distance outside the line. (*a*) Dielectric rod, HE_{11} dipole mode. (*b*) Dielectric rod, TM_{01} mode. (*c*) Trough. (*d*) *H*-Guide.

surfaces and rods (Chandler and Elsasser, 1949; Weiss and Gyorgy, 1954). Dielectric rod waveguides of teflon, polystyrene, etc., are particularly interesting, since they are nonconductors and can be used to bridge across high voltage environments or to operate in a corrosive atmosphere. The fields extend some distance outside the rod, however, as sketched in Fig. 9.5, and coupling can occur between rods coming close to each other or from the rod to support structures. Also, radiation will occur at sharp bends or regions of nonuniform cross sections. Dielectric rod radiators, discussed in Section 9.3.3, are made by tapering the end of a rod.

Various open waveguide or surface-wave propagation structures have been devised. Among the more useful ones are H-line, V-line, trough-line (Tischer, 1956, 1958), and dielectric-coated wire or G-line (Goubau and Schwering, 1961). The attenuation at millimeter wavelengths of these lines can be several orders of magnitude lower than that of conventional waveguide, the attenuation decreasing with frequency. Wave launching

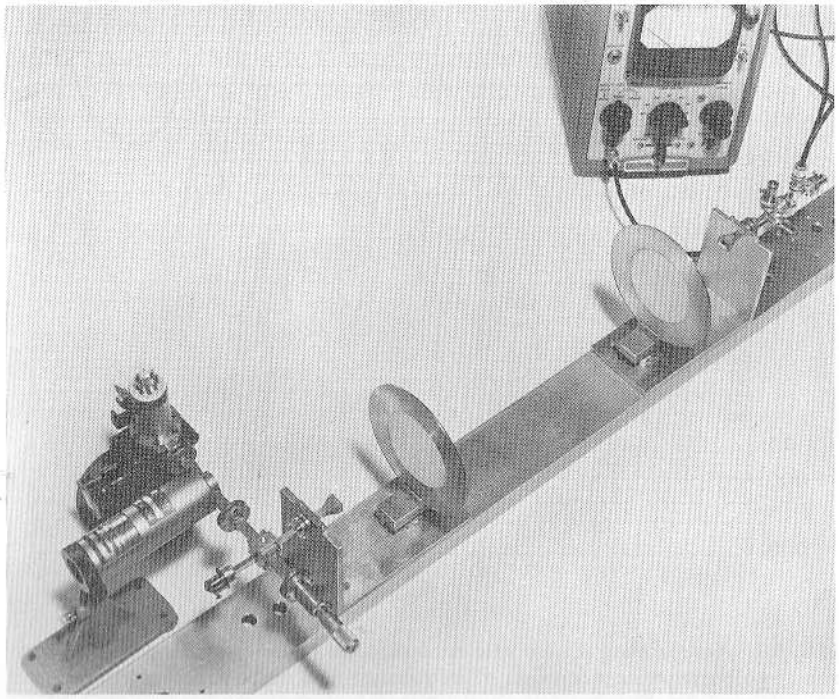

FIG. 9.6 Free space transmission path utilizing dielectric lenses. Path length of 4 feet has a loss of 1 dB at 70 Gc. (Courtesy TRG, Inc.)

is generally difficult and the structure tolerances are often extreme. They are useful for very long runs, but have little advantage for short ones.

9.1.3 ***Free-space radiation.*** Free-space radiation links are possible at millimeter wavelengths because large-aperture antennas (in wavelengths) are easily realizable. The minimum insertion loss is limited in practice by diffraction and interference conditions, as pointed out in Section 4.9. Large apertures can be obtained with lenses, Fresnel zone plates (van Buskirk and Hendrix, 1961) and parabolic reflectors. An example of a transmission link using lenses is shown in Fig. 9.6. Transmission over distances of 15 to 20 meters between zone-plate radiators with attenuation as low as 10 dB at 140 Gc is obtainable. Even lower loss is obtained if the cross-sectional phase distribution is corrected at periodic intervals (Goubau and Schwering, 1961) by inserting long-focal-length lenses in the transmission path. Attenuations as low as 2 dB over path lengths of a kilometer have been achieved.

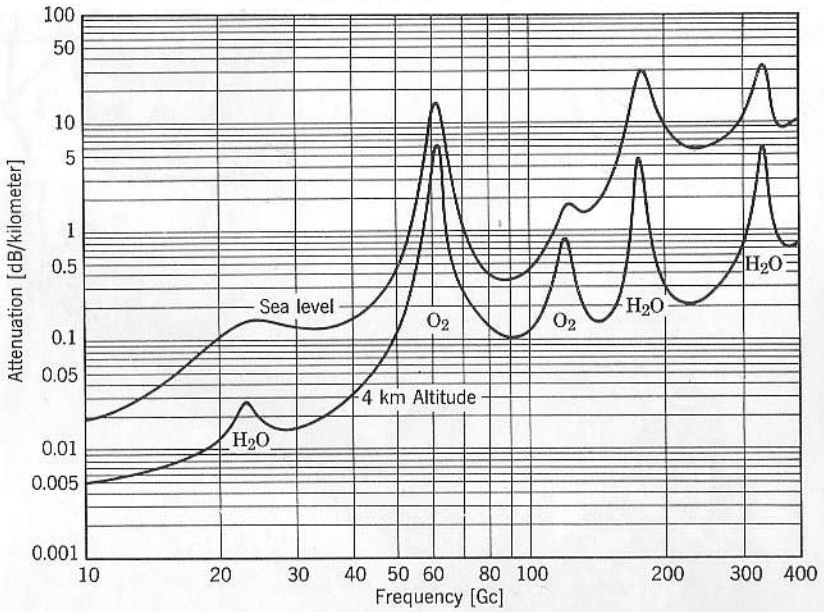

FIG. 9.7 Approximate atmospheric attenuation of electromagnetic waves for horizontal propagation as a function of frequency. The water vapor density was 7.5 grams/meter^3 for the upper curve and 1.0 gram/meter^3 for the lower curve. (Compiled from data of Straiton and Tolberg, 1960; Dicke et al., 1946; and Theissing and Caplan, 1956.)

In free-space transmission, atmospheric attenuation becomes important. Except over very long paths, however, the air attenuation is practically negligible. Figure 9.7 shows the attenuation due to molecular resonances and the atmospheric "windows" between (Dicke et al., 1946; Theissing and Caplan, 1956; Straiton and Tolbert, 1960).

9.2 Special components

Many techniques and component designs can be carried over from the highly perfected waveguide bands into millimeter wavelengths by simple scaling laws. There are, of course, some problems:

(*1*) Dimensional tolerances become exacting.
(*2*) Losses increase, due to small skin depth and small component size.
(*3*) Oscillators and amplifiers become less efficient (and more expensive) because of greater beam density and heat dissipation requirements.
(*4*) Crystal detectors become less efficient because of increased internal impedance, and have lower power handling capabilities.

The cost of waveguide systems, in general, increases with frequency in a nearly linear fashion above *K*-band. For example, a 4-mm interferometer costs about twice as much as an 8-mm one, and a 2-mm interferometer

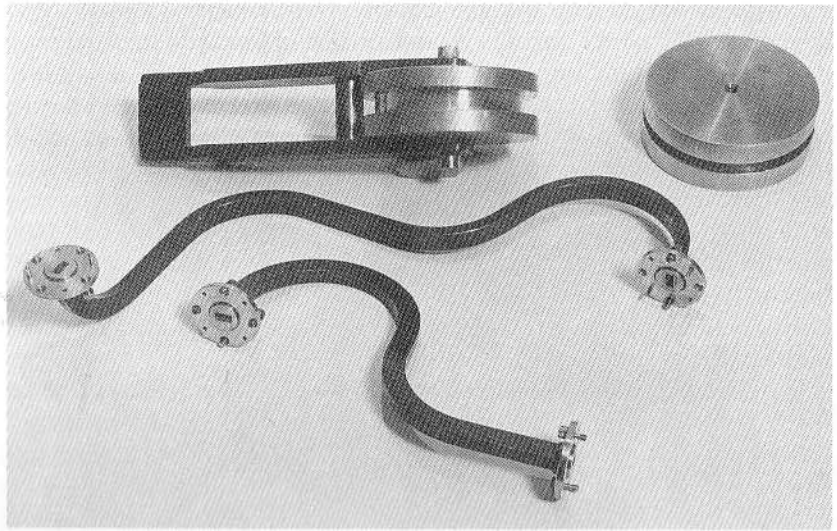

FIG. 9.8 Simple waveguide bending tool and samples of some elbows fabricated in RG-96/U waveguide. (Courtesy General Atomic, San Diego, Calif.)

about twice as much again. The choice of the frequency at which to do diagnostics, then, clearly contains an economic factor as well as physical factors. Nearly always, some kind of compromise is necessary. Often, the budget can be eased by fabrication of components, both waveguide and electronic, within the laboratory shops. Elbows, twists, phase shifters, terminations, etc., are particularly easy and inexpensive to make.

As an example, a simple waveguide bending tool and some elaborate bends made in RG-96/U waveguide are shown in Fig. 9.8. No reflections or attenuation due to these bends were measurable in the systems where they were employed. The flange faces were finished off in a lathe after soldering. The same techniques have been used successfully up to 90 Gc.

9.2.1 ***Phase shifters.*** Waveguide phase shifters change the electrical length of a section of waveguide, either physically (as with a line stretcher) or by varying the cut-off frequency and thus the phase velocity. Commonly, phase shifters are made with a dielectric vane oriented in the E-plane and either lowered through a slot in the top wall or moved back and forth across the broad dimension of the guide. Both of these types must be used with considerable caution. The first type tends to radiate badly, unless the vane is well shielded and, even then, may introduce standing waves. Both types can support higher modes when the vanes are well in, or when the frequency is near the top of the band; frequency

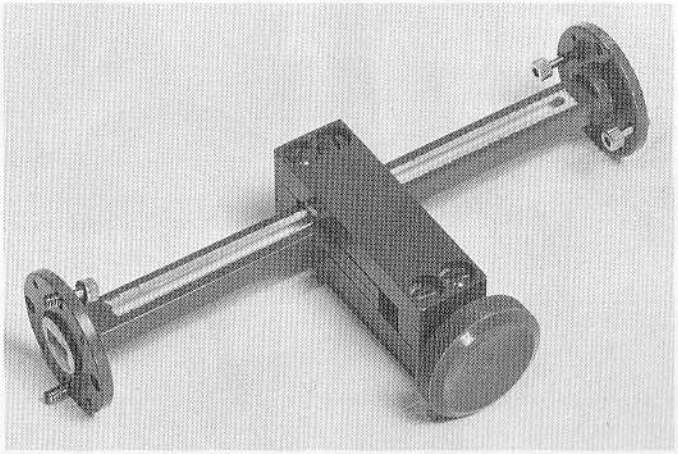

FIG. 9.9 Squeeze-section phase shifter in RG-96/U waveguide. Maximum phase shift $\approx 360°$ at 35 Gc. (Courtesy General Atomic, San Diego, Calif.)

sensitivity and standing waves then result, leading to significant errors in phase measurements.

A phase shifter whose cut-off frequency is *decreased* by operation (no higher modes are then possible) is the squeeze section. A longitudinal slot is cut through both top and bottom walls of the waveguide along the center line for about ten guide wavelengths. A captive screw is then soldered to one side wall, and a manipulator attached that can both spread and squeeze together the slit. Phase shifts of 2π to 4π are easily obtained, with essentially no radiation or reflections. A squeeze-section phase shifter is shown in Fig. 9.9.

A more elegant type of phase shifter is formed by rotating a half-wave plate, in circular waveguide carrying a circularly polarized wave, between two quarter-wave plates that transform from circular to linear polarization (Fox, 1947). The phase is shifted 2π with each rotation. If the center section is rotated at constant velocity with a motor, a frequency adder (or single-side-band modulator) thus results. The rotation velocity can be made very large if it is performed electrically by means of a ferrite section driven by a varying or rotating magnetic field (Cacheris, 1954; and Fox et al., 1954). Such devices are useful for serrodyne detection systems.

The line-stretcher types of phase shifters include a short-slot hybrid with ganged shorting plungers (Barnett, 1955) and a circulator with a shorting plunger.

9.2.2 ***Hybrid junctions.*** Hybrid junctions are used as power dividers, phase comparators, and in balanced mixers (Jones, 1961). The matching posts and irises used in the conventional "magic tee" at frequencies up to *K*-band become difficult to fabricate in the millimeter range. The hybrid ring or "rat-race" is often used, since no matching is required. It may be milled, dye-cast or electroformed, even in small waveguide sizes. Typical band width, determined by the geometry of the ring, is about 6%. The basic design, shown in Fig. 9.10, is straightforward. The isolation is obtained by arranging the coupling arms $\lambda/4$ apart, so that a signal entering arm 1 divides equally between arms 2 and 4, the waves that travel around the ring in opposite directions reinforcing. The waves reaching arm 3 just cancel. The junction ports are reciprocal, of course. Isolation between opposite arms is usually about 20 dB within the 6% band.

Short-slot hybrids and multihole directional couplers having 3 dB coupling can also be used as hybrid junctions over fairly wide band widths, although directional couplers tend to be somewhat larger and not as well balanced as rat-races (Riblet, 1952). Fin-line couplers and turnstile junctions (Sections 9.2.3 and 9.2.5) also are useful for hybrid junctions and balanced mixers (Loth, 1956).

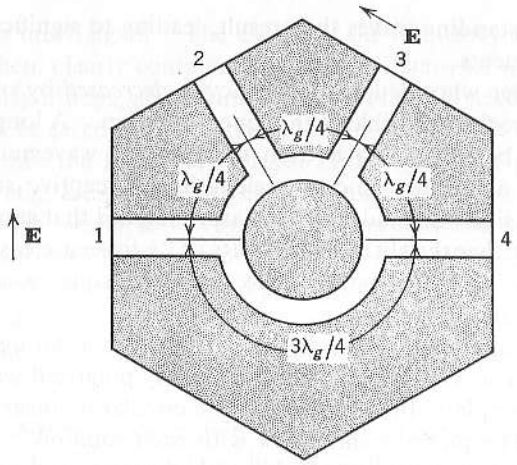

FIG. 9.10 Plan of rat-race hybrid junction, showing the lengths of the ring segments. The E-plane dimension of the ring groove is typically $1/\sqrt{2}$ that of the side arm grooves.

Coaxial-line hybrid junctions use hybrid rings, $\lambda/4$ couplers, etc., and may have octave band width.

9.2.3 ***Polarization and frequency diplexers.*** A simple and useful polarization diplexer is the *fin-line coupler* (Robertson, 1956), sketched in Fig. 9.11 and shown in Fig. 9.4. By installing two side arms at 45° on either side of the plane of symmetry in the cylindrical form, a 3-dB coupler is obtained. Two arms, installed at 90° to each other, make a *polarization diplexer*, with the arms decoupled from each other. By properly phasing the drive to the two arms, a circularly polarized wave results.

A square-cross-section coupler is made either by electroforming walls around a copper plate that has had a slot etched in it (see Fig. 9.4) or by machining and soldering. One way of fabrication is to mill off the top walls of two pieces of waveguide, fit them together with the fins sandwiched between and with the side arm positioned by a jig. The assembly is then soldered.

The cross-coupling between two waves having their electric vectors oriented at 90° to one another in either type of fin-line coupler is typically down by 20 to 40 dB. The coupling loss to each of the polarizations is typically 0.5 to 1.5 dB, most of the loss being in reflections and in excitation of resonances in the structure. Resonances also lead to cross-coupling. Fin-line couplers are useful at frequencies between about 3 and 70 Gc.

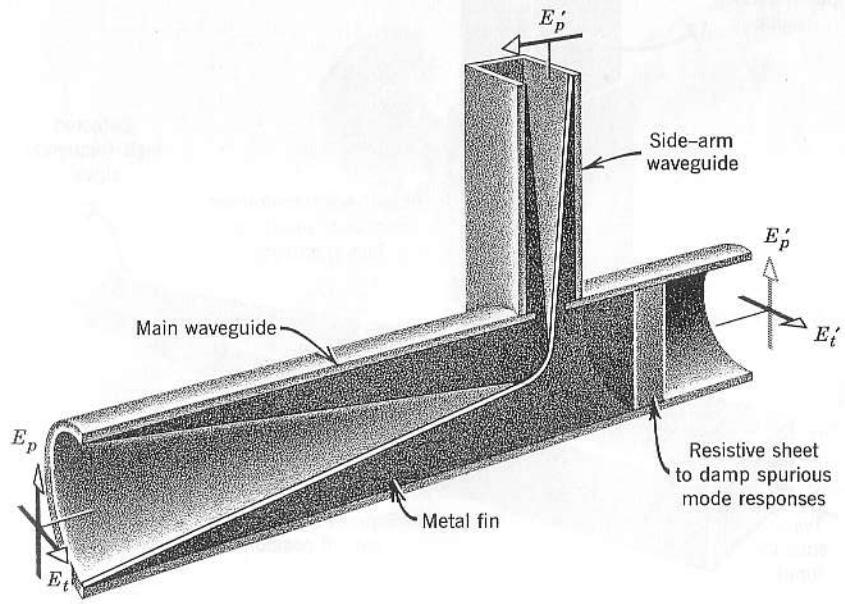

FIG. 9.11 Sketch of a fin-line coupler in cylindrical waveguide in a cut-away view, to show the internal construction of the coupling vanes or fins and the resistive mode suppressor.

The fin-line coupler can also be used as a frequency diplexer if the frequencies are not too widely spaced. For example, a 25-Gc wave can be propagated in one polarization and a 35-Gc wave in the other, with little cross-talk. An electroformed waveguide having a square cross section for carrying the two polarizations is also shown in Fig. 9.4. A square-cross-section vacuum window and horn antenna complete the dual-polarization system. Some measurements utilizing such a system are described in Section 6.5.

Frequency diplexers or multiplexers ordinarily use filters to separate the channels. A waveguide itself is a high-pass filter; a squeeze section of waveguide then becomes a variable-cutoff high-pass filter. A simple diplexer can be made using a series tee junction, containing a squeeze section in one arm for the high frequency signal and a phase shifter and low-pass filter or an impedance transformer in the other arm for the low frequency wave. The phase shifter and squeeze section are adjusted for matching at the junction at the frequencies in use. Isolation in excess of

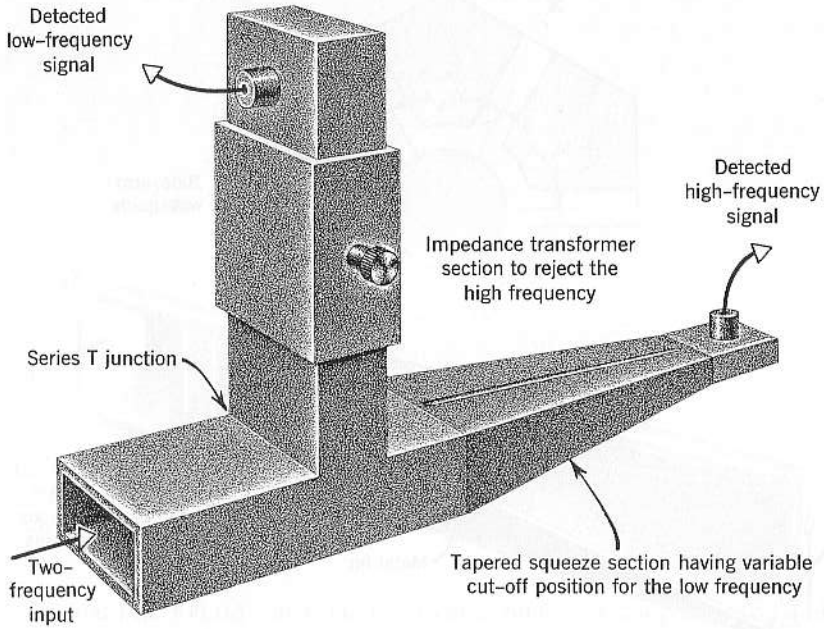

FIG. 9.12 Dual frequency diplexer-detector for frequencies 30% to 80% apart.

30 dB between 25 Gc and 35 Gc signals propagating in RG-96/U, with little signal loss and reflection, have been obtained with such a diplexer.

An advantage of this type of diplexer over that using fixed-frequency filters is that it is easy to adjust for changes in operating frequency, and not very sensitive to incidental frequency changes. The unit is sketched in Fig. 9.12.

9.2.4 ***Filters.*** Waveguide filters commonly are made up of inductive or capacitive iris-coupled sections. The susceptance of the iris and the spacing between them determines the cutoff characteristics (Cohn, 1957). Low-pass, high-pass, and band-pass configurations can be made, the design following standard transmission line theory (Guillemin, 1948). Typical six-section filters have an increase in insertion loss beyond cutoff of 36 dB per octave. High-Q cavity filters of the band-pass or band-rejection type may have a 30-dB change for a 1% frequency change (Riblet, 1958b). For example, the band-rejection filter used with the scattering experiment described in Section 6.7, consisting of two orifice-coupled tunable waveguide cavities, has an insertion attenuation of ~ 50 dB over a 20-Mc band and >20 dB over a 50-Mc band, but falls to 1.5 dB outside

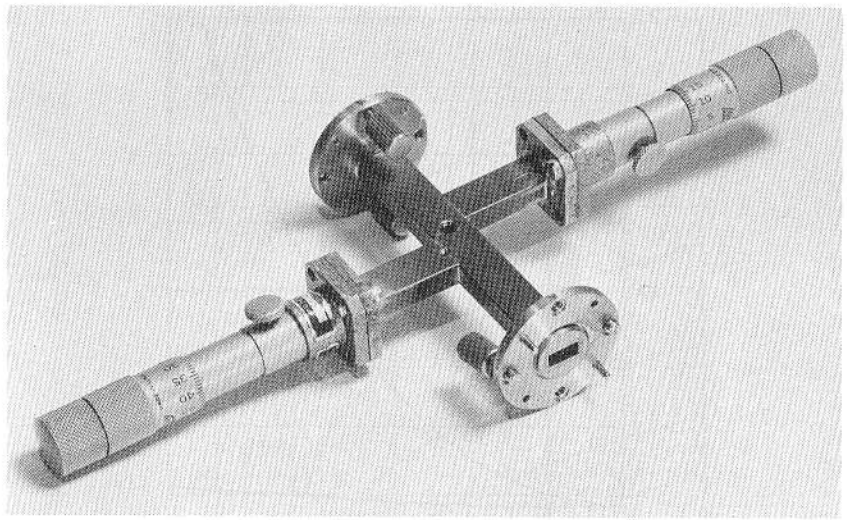

FIG. 9.13 Band rejection filter. Two-section orifice-coupled cavity filter, tunable between 30 and 40 Gc with peak rejection $\gtrsim 50$ dB. (Courtesy General Atomic, San Diego, Calif.)

$f_0 \pm 100$ Mc. A photograph of the filter is shown in Fig. 9.13. The orifice-coupled waveguides are $\lambda_g/2$ cavities, tuned by conventional shorting plungers.

Low-pass filters find application in rejecting harmonics from mixers and from magnetrons or klystrons. Band-pass and high-pass filters remove unwanted noise or image frequencies in superhet receivers. High-Q, band-pass filters are usually a transmission cavity, that is, two waveguides orifice-coupled through a resonant cavity. Minimum insertion loss is usually at least 2 to 6 dB.

A common construction method for iris-coupled waveguide filters is to saw thin slots part way through the waveguide, insert copper shim stock to the depth giving desired performance, and solder the shims in place. Alternatively, the iris vanes (shim stock) may be inserted in slots in an aluminum mandrel and the walls then electroformed around them. Either method gives satisfactory performance, using graphical design data to obtain the spacings (see *Microwave Engineers Handbook* and Cohn, 1957).

9.2.5 ***Circular polarizers.*** A basic arrangement for transforming between linear and circular polarization is a quarter-wave plate oriented at 45° with respect to the linear polarization. In waveguide terms, a quarter-

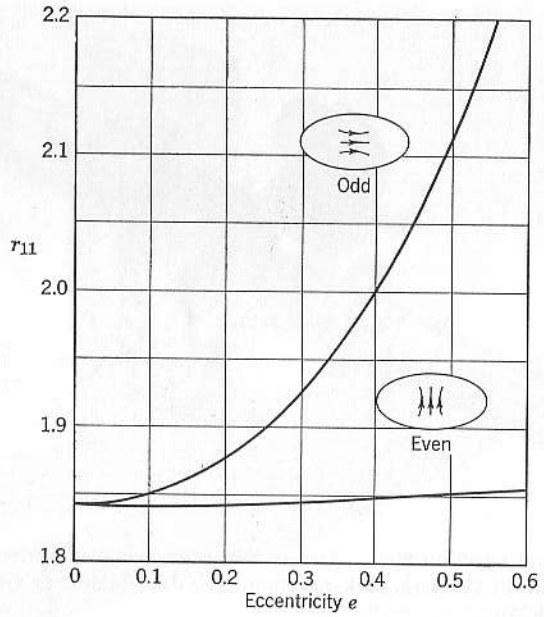

FIG 9.14 Mathieu-function roots for TE_{11}-like modes in elliptical waveguide, as functions of eccentricity.

wave plate is a section of waveguide capable of supporting two orthogonal modes having different phase velocities such that the respective electrical lengths differ by one-quarter wavelength. A simple technique is to deform circular waveguide (TE_{11} mode) into an elliptical cross section. The cut-off wavelength in elliptical waveguide is given by

$$(\lambda_c)_{lm}=\frac{2\pi a}{r_{lm}} \tag{9.2.1}$$

where a is the semimajor axis and r_{lm} is a Mathieu function root. These roots are given for TE_{11}-like modes in Fig. 9.14 as functions of eccentricity. The length of a quarter-wave section is given in Fig. 9.15 as a function of wavelength, perimeter, and eccentricity (Blau and Heald, 1959). In practice, quarter-wave sections of this type can be made by electroforming on a precut mandrel or by mechanically deforming a section of circular waveguide, with gradually tapered transitions from circular to elliptical cross section to suppress reflections. End effects from the transitions usually require a final empirical adjustment by further deformation. The useful frequency band width is about 4%.

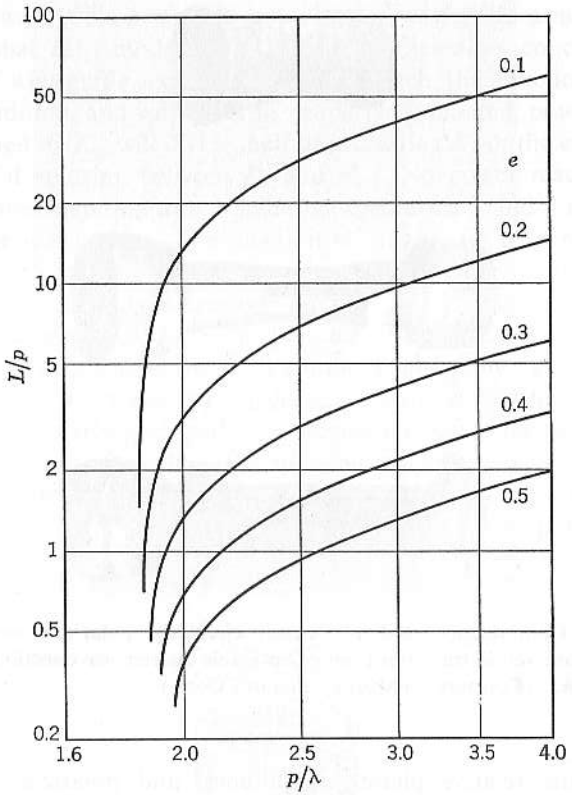

FIG. 9.15 Dependence of length L on wavelength λ for waveguide quarter-wave sections in elliptic waveguide of eccentricity e and perimeter p.

Waveguide quarter-wave plates may also be made by dielectric or ferrite loading. Wide-band designs have been developed (Ayres et al., 1957), as well as designs in which the quarter-wave plate can be rotated 45° to provide the option of circular or linear polarization. Such a polarizer, used as a horn feed, is shown in Fig. 9.16.

A system for transmitting simultaneously in the two counterrotating circular polarizations can be made by using a polarization diplexer with the quarter-wave section. Figure 9.17 illustrates such a system in which both modes are fed from a single power source. The transmitting antenna launches a linearly polarized wave which is equivalent to two counter-rotating circularly polarized waves of equal amplitude. The receiving antenna analyzes the effect of the plasma region between the horns in

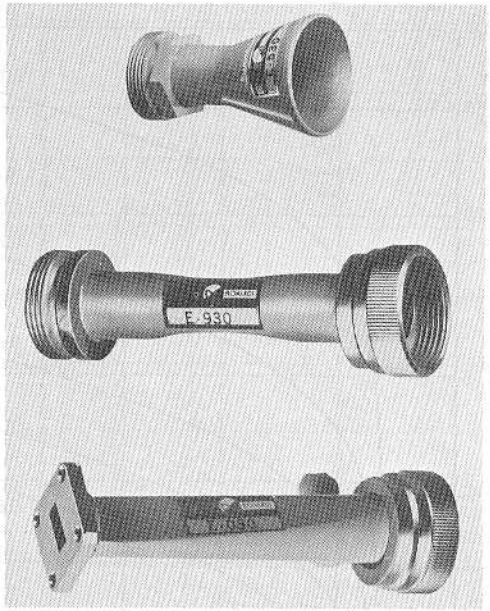

FIG. 9.16 Components used to launch circularly polarized waves. *Bottom*, rectangular to circular transition; *center*, rotatable quarter-wave section; *top*, circular horn antenna. (Courtesy DeMornay-Bonardi Corp.)

changing the relative phases, amplitudes, and polarizations of these waves.

Another interesting circular polarizer is the turnstile junction (Montgomery et al., 1948; Meyer and Goldberg, 1955). The basic junction, sketched in Fig. 9.18*a*, is a six-terminal network, consisting of four

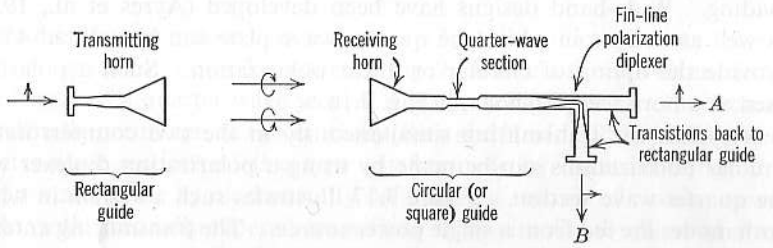

FIG. 9.17 System for diplexing circularly polarized waves from a common source, using a polarizer and fin-line coupler.

rectangular waveguide arms and one circular waveguide arm excited in two orthogonal TE_{11} modes. Two pins in the junction, concentric with the circular waveguide axis, are used to match the junction. In the matched condition, and with all arms properly terminated, power entering arm 1, denoted by E_1, will divide, half of it creating E_A in the circular arm and half of it splitting between E_3 and E_4. No power reaches arm 2. Likewise, power entering arm 3 splits between arms 1 and 2 and creates E_B in the circular guide. The junction is thus useful as a polarization diplexer, as well as for a number of other applications; we shall discuss, here, its use as a circular-polarization analyzer. To generate a right-hand circularly polarized wave, we short-circuit arms 3 and 4 at $5\lambda_g/8$ and $7\lambda_g/8$, respectively, and drive the junction from input 1, as shown in Fig. 9.18*b*. The wave emitted will have a clockwise rotation sense. As a receiver, a circularly polarized wave having a counterclockwise rotation sense will be coupled into the side arm 2 and one having a clockwise sense into arm 1. If matched detectors are put on the two arms, we now have a direct measurement of an elliptically polarized wave entering the junction.

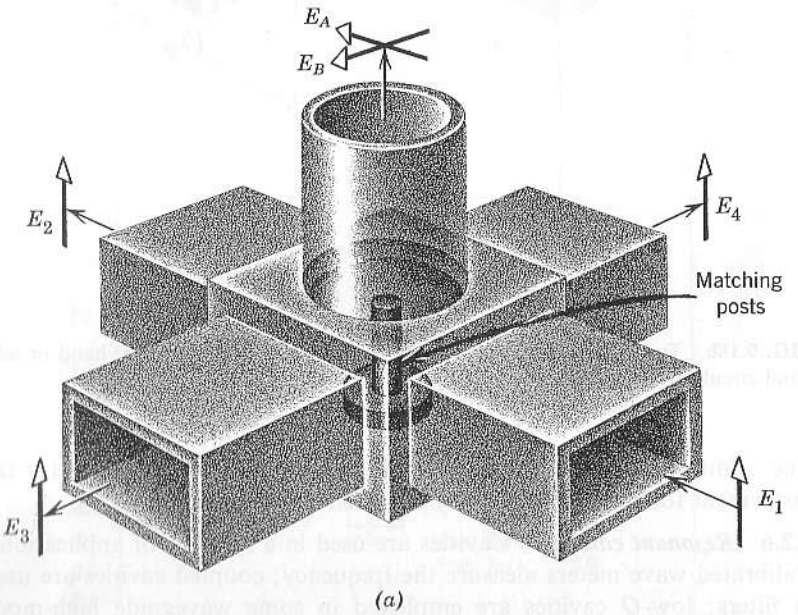

FIG. 9.18a Basic turnstile junction, showing the four rectangular waveguide arms and the circular waveguide. The matching post is used to isolate opposite arms and to match impedances.

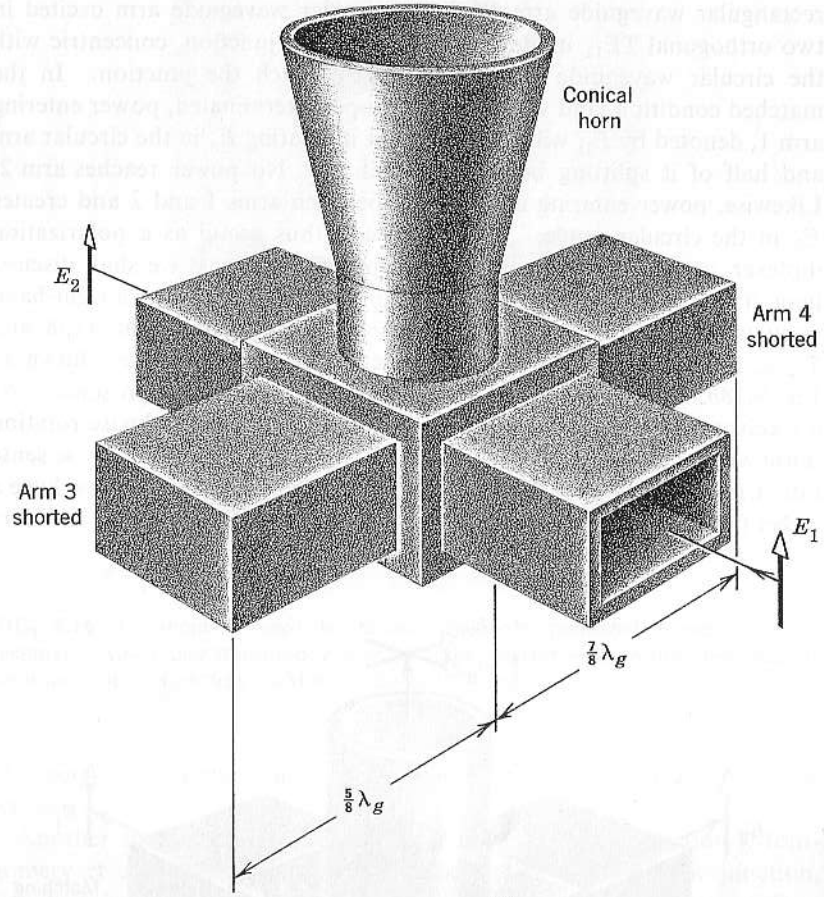

FIG. 9.18b Turnstile junction connected to transmit or receive right-hand or left-hand circularly polarized waves.

The addition of a conical horn to the circular junction completes the instrument for polarization analysis (Allen and Tompkins, 1959).

9.2.6 ***Resonant cavities.*** Cavities are used in a number of applications. Calibrated wave meters measure the frequency; coupled cavities are used in filters; low-Q cavities are employed in some waveguide high-mode couplers; and evacuated resonant cavities are used to heat and measure density of plasmas, as discussed in Section 5.1.

A common configuration is the right circular cylinder, sketched in

Fig. 9.19. The wavelength of the resonance frequency for TM modes is (Moreno, 1948)

$$\lambda_0 = \frac{2h}{[S^2 + (h/a)^2 (P_{mn}/\pi)^2]^{1/2}} \tag{9.2.2}$$

where h is the height, a the radius,

S is the integral number of nodes along h,

P_{mn} is the nth root of $J_m(P)=0$,

m is the number of circumferential maxima, and

n is the number of radial maxima.

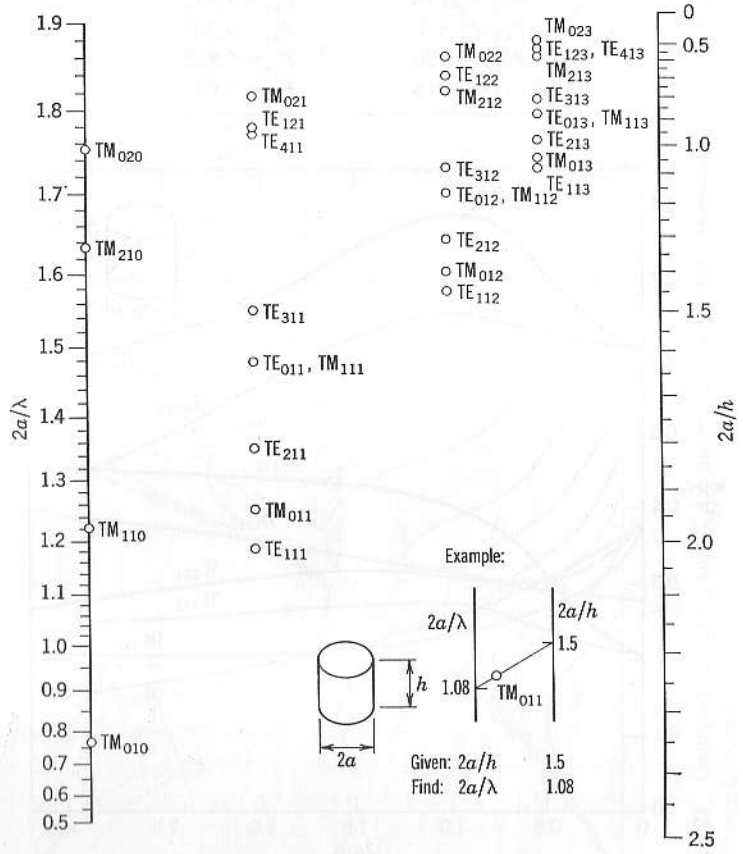

FIG. 9.19 Mode chart for resonant cavity modes in a right circular cylinder. (Courtesy R. N. Bracewell, Stanford University, Stanford, Calif.)

For TE modes, the resonance wavelength is given by (9.2.2) if P_{mn} is replaced by P'_{mn}, the nth root of $dJ_m(P)/dP=0$. Some of the roots are tabulated in Table 9.2. Other roots can be found in Wilson et al. (1946–1947). A mode chart, showing the resonance wavelengths and frequencies for several modes as a function of h and a, is shown in Fig. 9.19.

TABLE 9.2 ROOTS OF THE BESSEL FUNCTIONS J_{mn} AND J'_{mn}, USED IN RESONANT CAVITY DESIGN

TM	TE
$P_{01}=2.405$	$P'_{11}=1.841$
$P_{11}=3.832$	$P'_{21}=3.054$
$P_{21}=5.136$	$P'_{01}=3.832$
$P_{02}=5.520$	$P'_{31}=4.201$
$P_{31}=6.380$	$P'_{12}=5.332$
$P_{12}=7.016$	$P'_{02}=7.016$

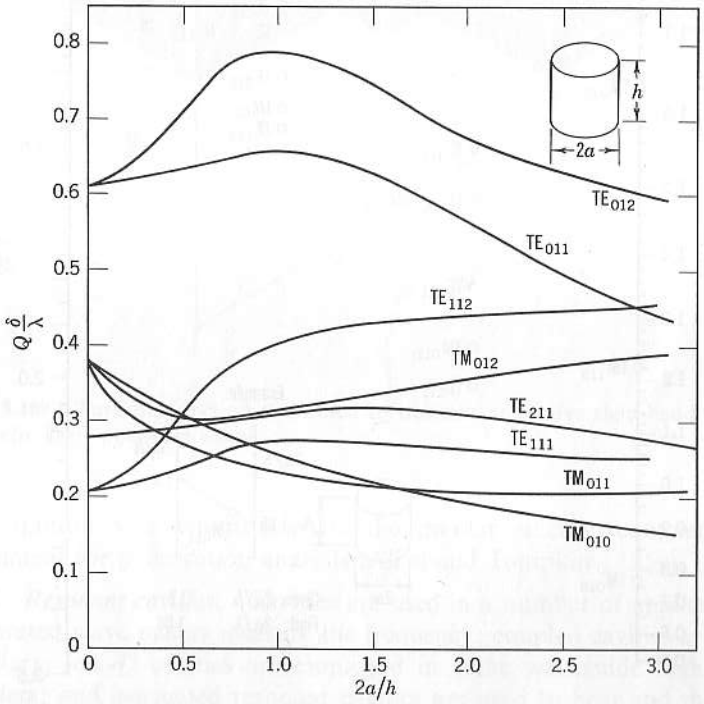

FIG. 9.20 Q chart for right circular cylinder resonant cavities. Various oscillation modes are shown.

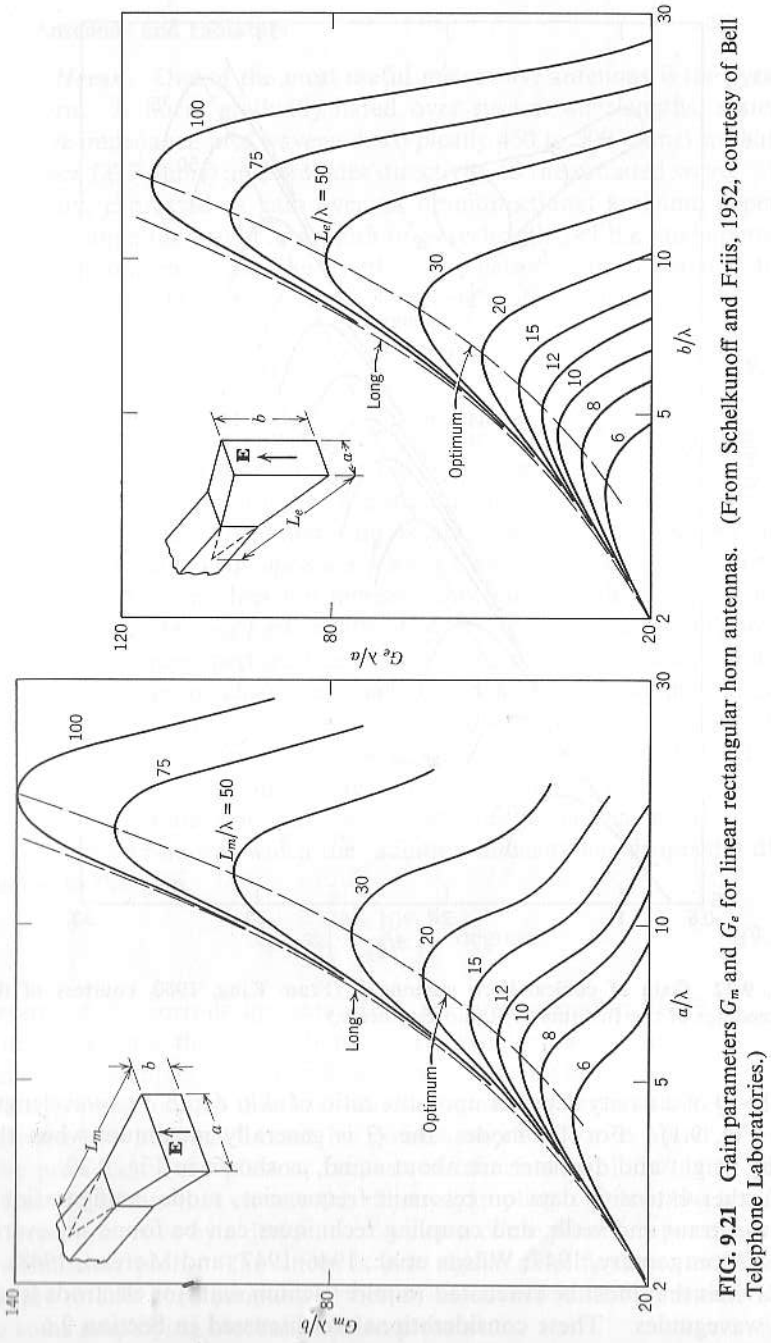

FIG. 9.21 Gain parameters G_m and G_e for linear rectangular horn antennas. (From Schelkunoff and Friis, 1952, courtesy of Bell Telephone Laboratories.)

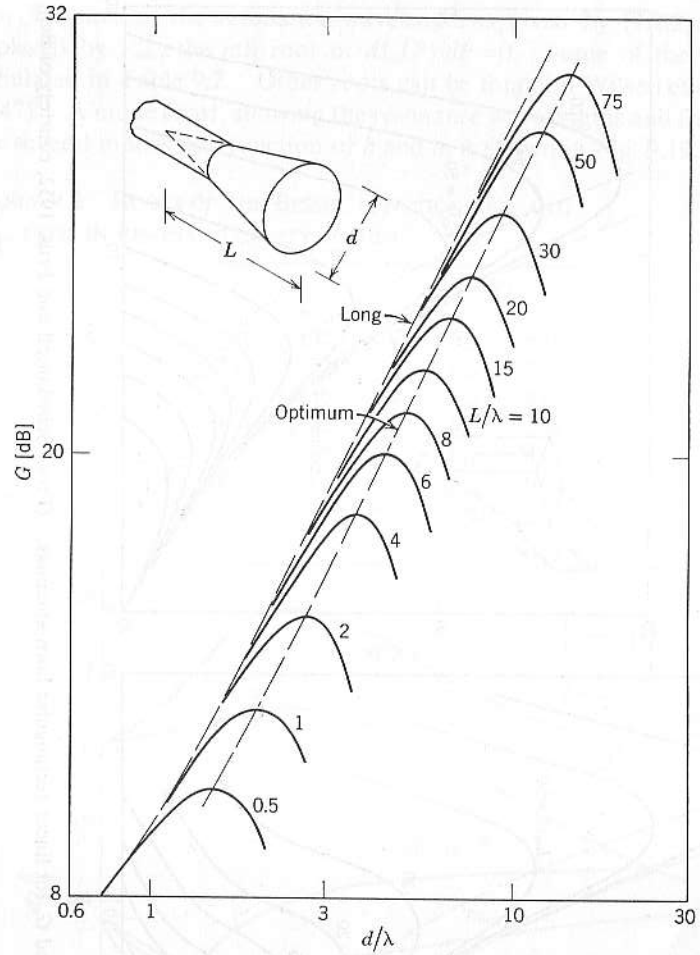

FIG. 9.22 Gain of conical horn antennas. (From King, 1950, courtesy of the Proceedings of the Institute of Radio Engineers.)

The Q of a cavity depends upon the ratio of skin depth δ to wavelength (see Fig. 9.1). For TE modes, the Q is generally maximum when the cavity height and diameter are about equal, as shown in Fig. 9.20.

Further extensive data on resonant frequencies, mode configurations, Q, re-entrant end walls, and coupling techniques can be found in several texts (Montgomery, 1947; Wilson et al., 1946–1947; and Moreno, 1948).

Cavities that must be evacuated require vacuum seals for electrode leads and waveguides. These considerations are discussed in Section 9.6.

9.3 Antennas and radiators

9.3.1 ***Horns.*** One of the most useful microwave antennas is the pyramidal horn. A horn, gradually flared over several wavelengths, matches the wave impedance of a waveguide (typically 450 to 500 ohms) to that of free space (377 ohms) and provides directivity to the radiated wave. The directivity, expressed as gain over an omnidirectional antenna, depends primarily upon the height and width (in wavelengths) of the final aperture, but also secondarily upon the length. The gain of a horn flared in both the **E**-plane and **H**-plane is given as (Schelkunoff and Friis, 1952)

$$G=\frac{\pi}{32}\frac{G_m\lambda}{b}\frac{G_e\lambda}{a} \tag{9.3.1}$$

where G_m and G_e are gain factors given in Fig. 9.21. Gain data for circular (conical) horns are given in Fig. 9.22 (King, 1950).

For both types of horns, at a particular length, there is a particular aperture for which maximum gain is achieved. A horn having these dimensions is called an *optimum horn*. Conversely, for given aperture dimensions, the gain does not increase appreciably with increasing axial length beyond the *long horn* length of ab/λ. In most plasma diagnostics experiments, where aperture diameters must be restricted, the long horn is preferred in order to achieve reasonably good gain and minimum radiation field curvature. The curvature can be further corrected by using a lens in front of the horn (see Section 4.9). The long horn also has a larger effective area for radiation, the area S being about 80% of the geometrical area. The optimum horn has S about 50% the geometrical area.

The angle off-axis at which the radiation intensity has dropped 3 dB is related to the gain

$$\theta_{3dB}\approx\left(\frac{3\times10^4}{G}\right)^{1/2}\text{ degrees.} \tag{9.3.2}$$

Several of the horn-design parameters are summarized in Fig. 9.23. We note in passing that, at millimeter wavelengths, horns having modest gains (for example, 10 to 15 dB) are not physically large.

As pointed out in Section 4.9, the maximum permissible coupling between two horns is limited by Fresnel interferences to about -6 dB. The presence of the plasma, because of its refractive index, may cause refraction effects that change the effective coupling. Often, the coupling is seen to improve by a decibel or so when a dilute plasma is present in the transmission path. The effect is not signal amplification, but is due simply to enhanced coupling or better impedance matching, unless there be some amplifying mechanism also present.

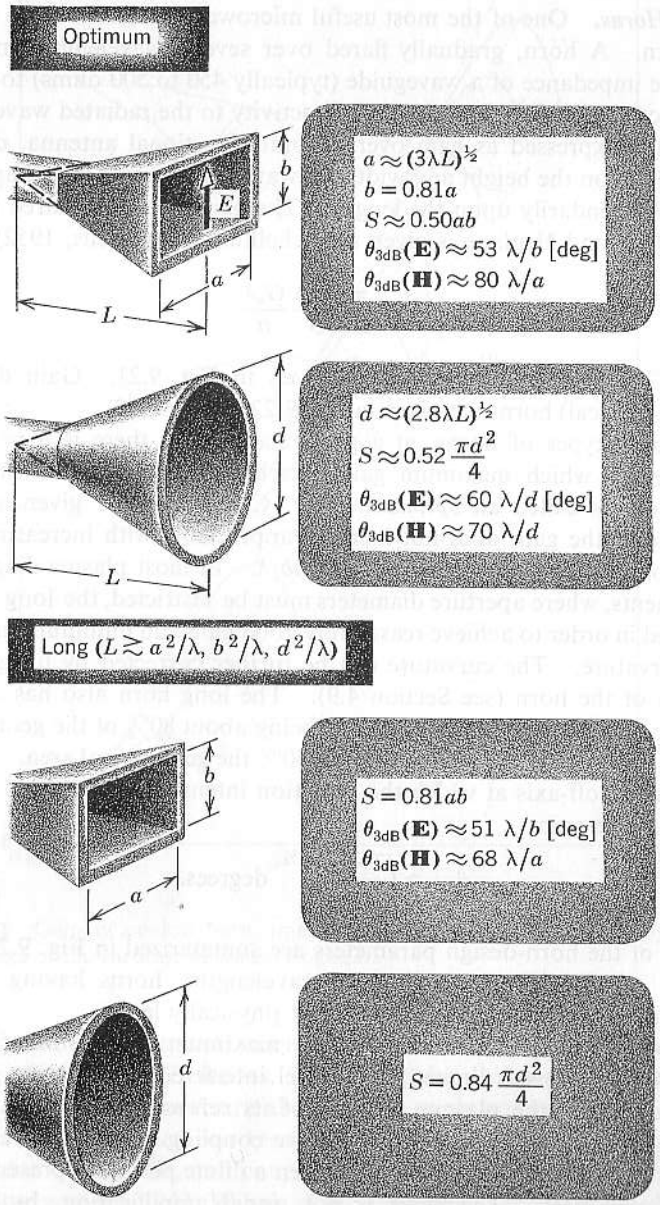

FIG. 9.23 Summary of horn-design parameters.

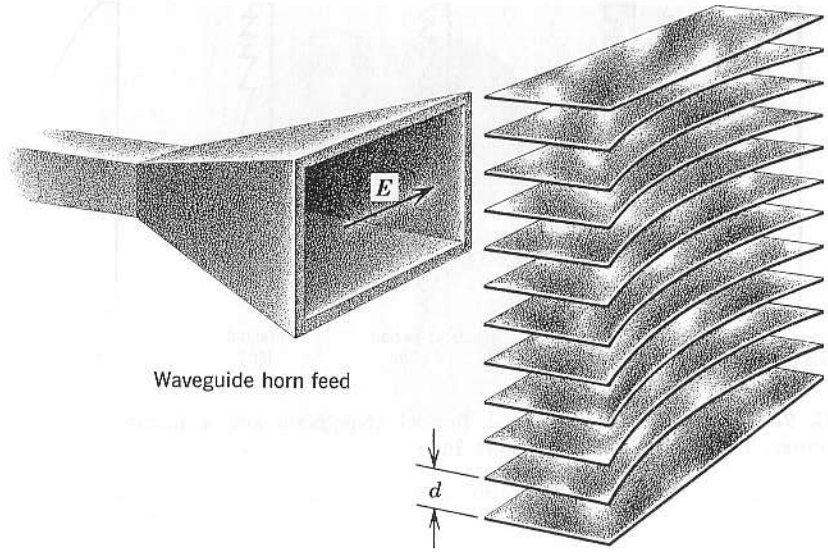

FIG. 9.24 Metal plate (artificial dielectric) microwave lens. The electric field is parallel to the metal plates.

9.3.2 ***Lenses.*** Two modified forms of the ordinary horn find applications in many experiments: the horn-lens and the horn-fed dielectric rod. Microwave lenses are classed as dielectric, artificial-dielectric, or metal-plate.

The metal-plate or "venetian-blind" lenses are made of parallel strips of metal of varying width, supported parallel to the incident electric field, as shown in Fig. 9.24. The phase velocity of the wave between the plates is greater than c (equivalent refractive index less than unity), so that a concave lens focuses (Kunz, 1954). Short-focal-length, stigmatic lenses that bring the waves to a line focus on the axis of a plasma column are straightforward to make by this method. The properties, including focal length, are frequency-sensitive, since it is the plate spacing that determines the equivalent refractive index (Brown, 1953).

Dielectric lenses may be simply convex, as the common optical lens, or made up of zones (van Buskirk and Hendrix, 1961). The relation between a lens and Fresnel zone plates is shown in Fig. 9.25. The simple zone plate rejects half of the incident power because alternate zones are clear and opaque, as shown in Fig. 9.26. The phase-reversing zone plate is made by arranging the thickness of dielectric material in adjacent zones to give a phase difference of π. The full transmission then results.

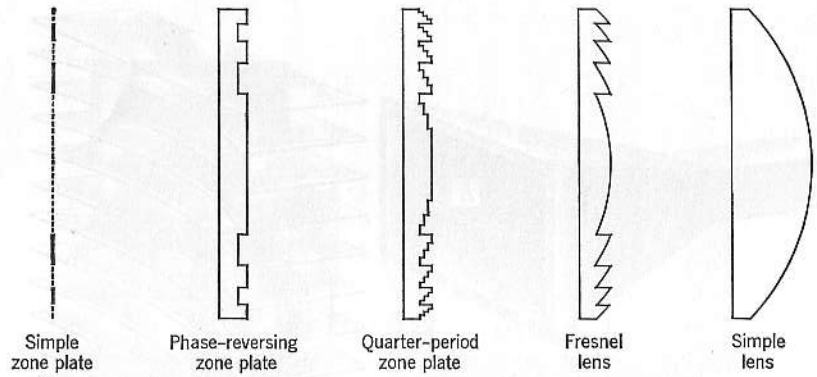

FIG. 9.25 Relationship between a Fresnel zone plate and a microwave lens. (Courtesy Electronic Communications, Inc.)

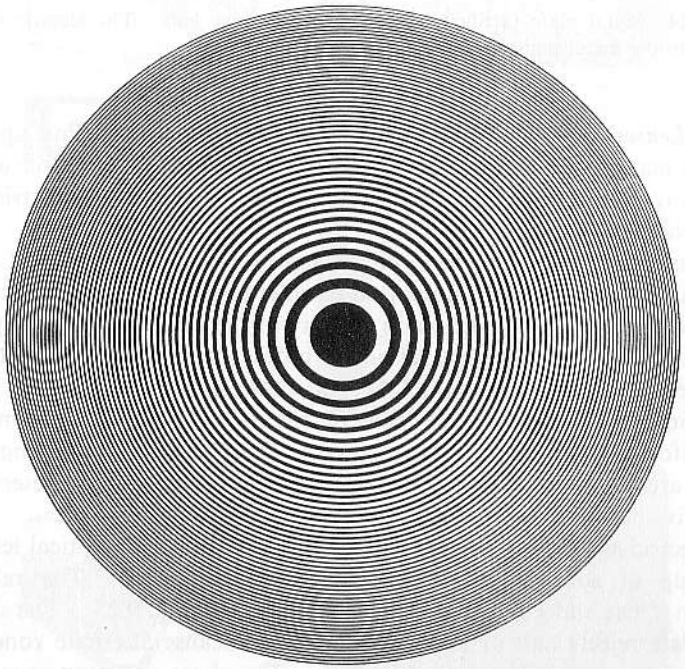

FIG. 9.26 Fresnel zone plate for use as a microwave lens. (Courtesy Electronic Communications, Inc.)

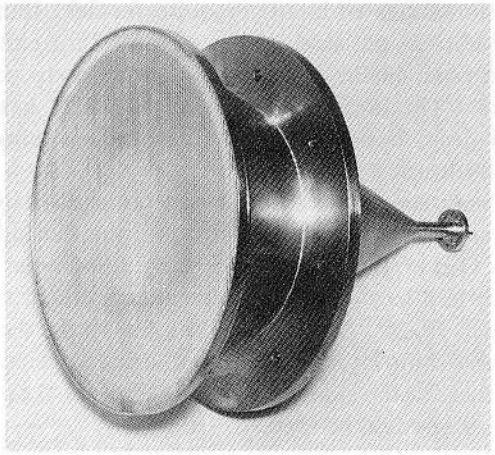

FIG. 9.27 Dielectric microwave lens, using impedance matching grooves. (Courtesy TRG, Inc.)

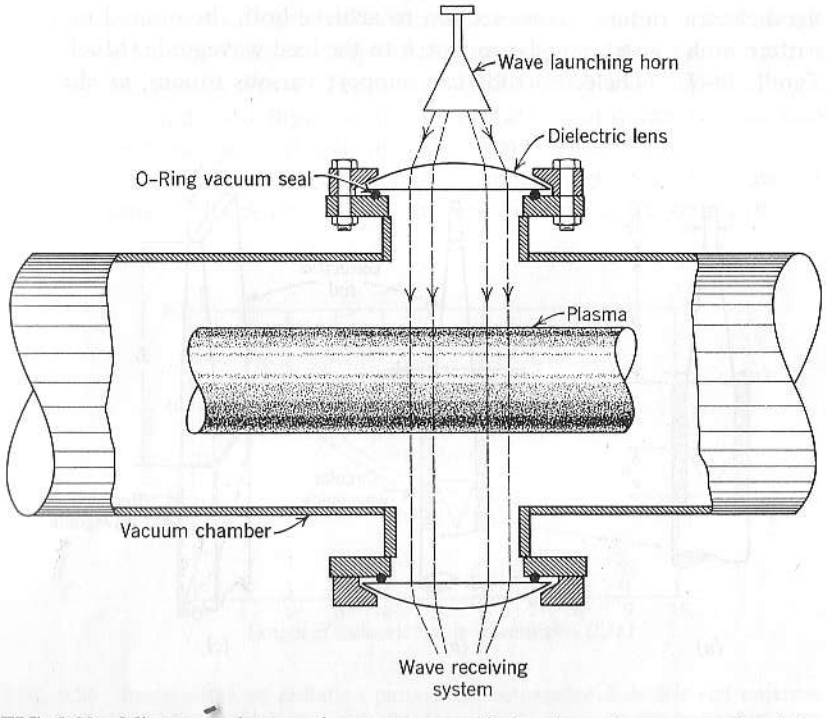

FIG. 9.28 Microwave lens used as a vacuum window in a plasma experiment (see also Fig. 6.23). (Gardner, 1962.)

Horn-lens combinations ordinarily require far-field illumination, or at least as long a horn as possible. They are useful for either focussing the waves at some point in the plasma experiment, or to correct for wavefront curvature. The horn-lens shown in Fig. 9.27 has lineal grooves, which are $\lambda/4$ deep, but evenly spaced, to reduce reflections from the surface of the dielectric convex lens.

The lenses may serve as vacuum seals, as shown in Fig. 9.28. In vacuum systems that do not require baking, the flat side of the lens is sealed with an O-ring, the convex side being illuminated by a horn. At 4 mm wavelength, a lens of 4 inches diameter is found to be quite satisfactory (Gardner, 1962). Some reflections, due to the dielectric interface, are present; a matching layer (analogous to coated optics) could be added to correct for these at the expense of band width, or the grooves shown in the lens of Fig. 9.27 could be used.

9.3.3 ***Dielectric rod antennas.*** The waves propagating in a dielectric rod (see Section 9.1.2) tend to excite radiation fields when discontinuities are present in the line. To intentionally make a radiator, then, one shapes the dielectric radiator cross section to achieve both the desired radiation pattern and a good impedance match to the feed waveguide (Mueller and Tyrell, 1947). Dielectric rods can support various modes, as shown in

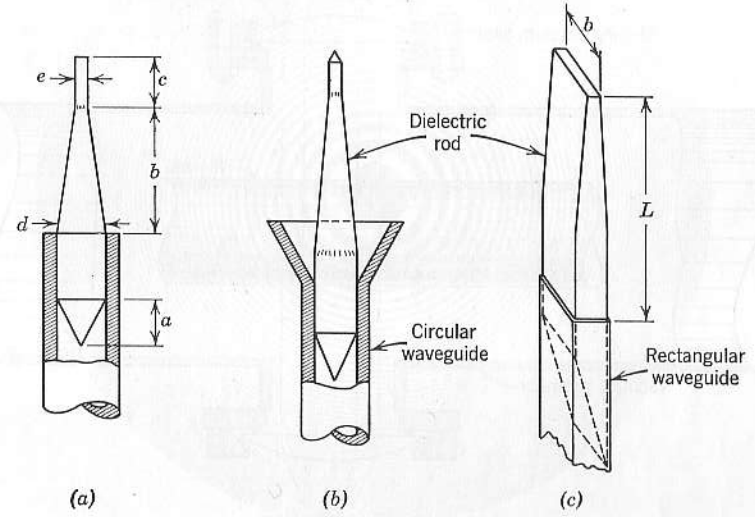

FIG. 9.29 Dielectric rod antennas, showing launching mechanisms. Dimensions are discussed in the text in Section 9.3.3.

Fig. 9.5. One mode that closely approaches the circular TE_{11} waveguide mode is the dipole or HE_{11} mode (Brown and Spector, 1957). The mode may be launched by simply inserting a tapered dielectric rod into an open waveguide (Harvey, 1963), as shown in Fig. 9.29*a*. A circularly polarized wave at 35 Gc, launched by a teflon rod having $a=1.0$ inch, $b=1.0$ inch, $c=1.125$ inch, $d=0.328$ inch, and $e=0.125$ inch, produced a nearly symmetrical radiation pattern having **E**- and **H**-plane widths of 25°. A slightly better impedance match is obtained by flaring the waveguide into a small horn, as sketched in Fig. 9.29*b* (Elsasser, 1949).

Rectangular cross-section rods can be excited by inserting them into a rectangular TE_{10} mode waveguide, as shown in Fig. 9.29*c*. The taper is not very critical in determining beam width, but does affect the impedance match. An average rod thickness between 0.2λ and 0.4λ seems to give optimum results (Watson and Horton, 1948). A curve of beam half-widths as a function of rod length is shown in Fig. 9.30. The curve also applies reasonably well to rods of circular cross section.

Part of the radiation field arises directly from the launching structure, part from the end of the rod, and part from the sides along the rod. Tapered rods of low dielectric constant material, longer than about 2 wavelengths, fed from a horn that is not more than a wavelength in diameter, are usually free of side lobes. If the feed horn is too broad, the dielectric constant too high, or the taper too abrupt, the pattern may develop side lobes or even split into two major lobes. Long rods (6 to 18 wavelengths) of low dielectric constant material produce the cleanest, narrow beams. The beam width is not very sensitive to frequency (that is,

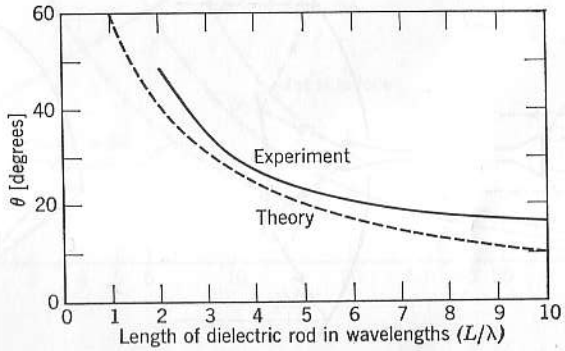

FIG. 9.30 Beam width of radiation pattern of rectangular dielectric-rod antennas. θ is the half width at which the radiation intensity is down 10 dB from that at the center.

the radiator is broad-band), the dependence of long rods being approximately (Watson and Horton, 1948)

$$\theta \approx 60(\lambda/L)^{1/2} \text{ degrees} \qquad (9.3.3)$$

where L is the length. Typical rod antennas are useful over a 2-to-1 frequency range.

Narrow beams are obtained also by feeding the rod from double-ridge guide. The rod is inserted between the double ridges, filling the guide in the H-plane. Beam widths as narrow as 12° have been obtained by such an antenna rod 20 wavelengths long, tapered to a point at the end (Parker and Anderson, 1957).

A rod, of course, is an insulator and can be inserted into some plasmas with little perturbation. Plasma measurements, utilizing this feature, were described in Section 6.5. Fused quartz, boron nitride, teflon, and sapphire are particularly good for such applications. Boron nitride is easily machinable, and retains its dielectric properties up to high temperatures.

9.3.4 ***Reflecting antennas.*** The gain and, thus, directivity of an antenna system can be increased greatly by adding a reflector of appropriate shape. For example, a 90° corner reflector placed $\lambda/2$ from a half-wave dipole increases the dipole's gain by 10 dB (Harris, 1953; Cottony and Wilson, 1958).

Parabolic reflectors, fed from the focal point, in theory generate strictly plane waves. At microwave frequencies, however, where the wavelength

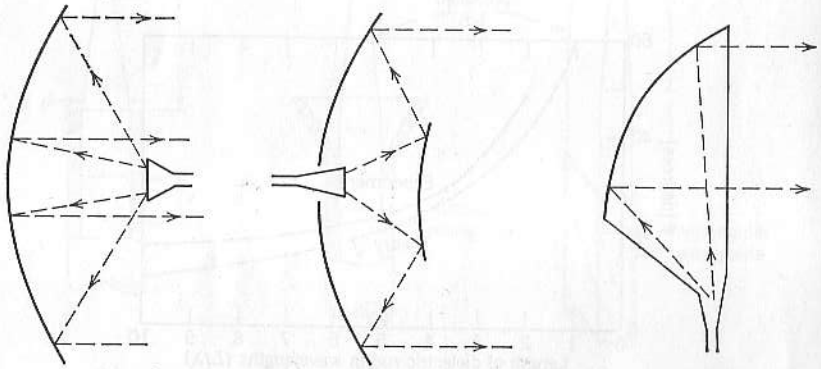

FIG. 9.31 Some common feed systems for parabolic reflectors. (*a*) Horn-feed. (*b*) Cassegrain. (*c*) Hog-horn.

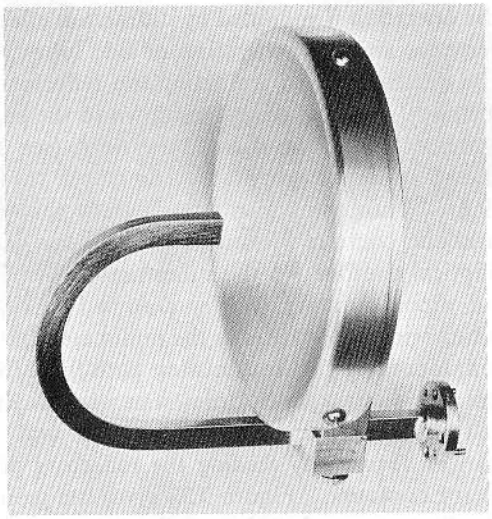

FIG. 9.32 Small paraboloidal reflector fed by a horn, for operation in the 4-mm band, 68 to 75 Gc. (Courtesy of TRG, Inc.)

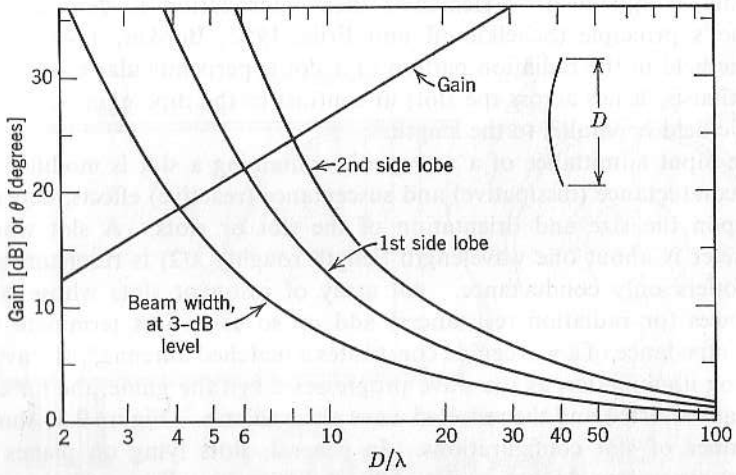

FIG. 9.33 Gain over a dipole for paraboloidal reflectors as a function of diameter, D/λ. The gain figures assume a 55% aperture efficiency (RETMA standard). The beam width is at the half-power (−3 dB) level. The first and second side-lobe curves are at the peaks.

is appreciable, the operation is modified by diffraction effects, with subsequent beam divergence and the generation of side lobes. The side-lobe intensities may be decreased by illuminating the reflector nonuniformly, the usual taper being 10 dB from the center down to the edge (Crompton, 1954). Feed systems include the dipole, the horn (see Fig. 9.32), the Cassegrain, and the offset or hog-horn. Some of these systems are sketched in Fig. 9.31. The Cassegrain or double-reflector system (Hannan, 1961) uses a parabolic contour for the main reflector or "dish" and a hyperbolic or elliptical contour for the subreflector. The subreflector is fed by a horn or dipole primary feed as sketched in Fig. 9.31*b*. The Cassegrain is finding wide application in the millimeter and submillimeter wavelength region, especially for transmission path links (Section 9.1.3).

A full paraboloid produces a pencil beam; a parabolic cylinder produces a fan beam. Extreme fan beams, cosecant beams, and other specially shaped beams can be formed by feeding the reflectors off focus, or by shaping the reflector contours. Figure 9.33 gives the gain over a dipole for paraboloidal reflectors as a function of diameter.

9.3.5 ***Slot radiators.*** A slot cut in a conducting sheet illuminated by an electromagnetic wave can radiate. The radiation fields are derivable from the scattered magnetic induction, much as the radiation fields from a dipole are derived from its driving electric field. The slot and dipole are thus complementary elements; their interrelation is described by Babinet's principle (Schelkunoff and Friis, 1952; Booker, 1946). The electric field in the radiation pattern of a slot is perpendicular to the long axis (that is, **E** lies across the slot) in contrast to the dipole, in which the electric field is parallel to the length.

The input admittance of a waveguide containing a slot is modified by both conductance (dissipative) and susceptance (reactive) effects, depending upon the size and orientation of the slot or slots. A slot whose perimeter is about one wavelength (length roughly $\lambda/2$) is resonant, and thus offers only conductance. An array of resonant slots whose conductances (or radiation resistances) add up so as to just terminate the wave impedance of a waveguide constitutes a matched antenna. To avoid tapering illumination as the wave progresses down the guide, the far end is usually shorted and the reflected wave also radiates. Figure 9.34 shows a number of slot configurations. In general, slots lying on planes of current symmetry do not radiate; the radiative coupling, and thus the waveguide loading, increases with asymmetry in a complicated manner (Oliner, 1957).

The radiation patterns of slot arrays depend upon several factors (Stevenson, 1948). The wavelength in the waveguide invariably is longer

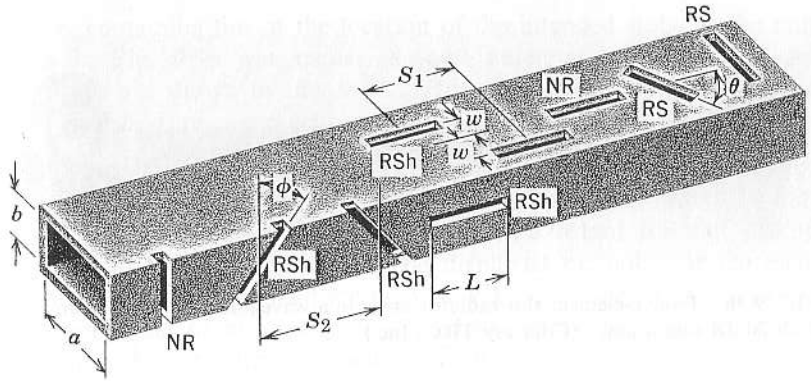

FIG. 9.34 Radiation and nonradiating slots in rectangular waveguide, propagating the TE_{10} mode. NR indicates nonradiating; RSh, radiating shunt slots; and RS, radiating series slots.

than the free-space wavelength, unless the guide is filled with dielectric material. In order to drive the slots in phase, then, they must be spaced more than a free-space half-wavelength apart, leading to possible diffraction effects. Aside from these effects, the design criteria for ordinary dipole radiator arrays may be applied directly to the complementary structure, the slot, with the interchange of the **E** and **H** fields.

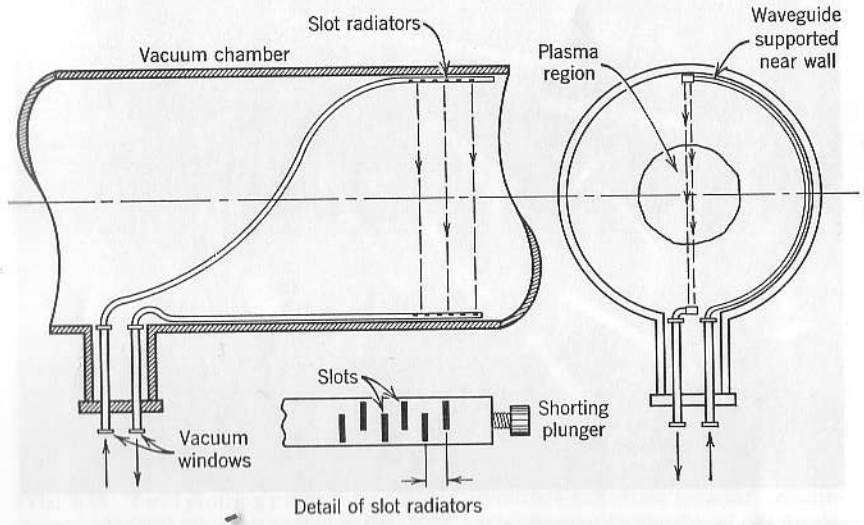

FIG. 9.35 Slot antennas installed in a plasma experiment chamber.

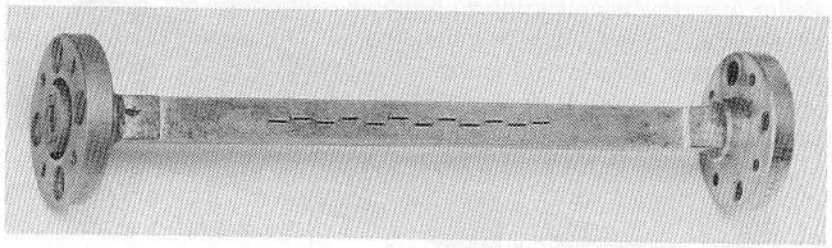

FIG. 9.36 Twelve-element slot-radiator array in a waveguide, giving 7° beam width with 20-dB side lobes. (Courtesy TRG, Inc.)

Slot arrays are particularly useful for antennas in cramped quarters, such as inside a vacuum system accessible only from the end, as shown in Fig. 9.35. Photographs of some slotted waveguide antennas are shown in Figs. 9.36 and 9.37. Several waveguides, each containing slots, may even be stacked up in a curved broadside array to give focussing, analogous to a lens.

Slot arrays may be fabricated by milling, by drilling and sawing the slots in a waveguide, or by electroforming the waveguide around a

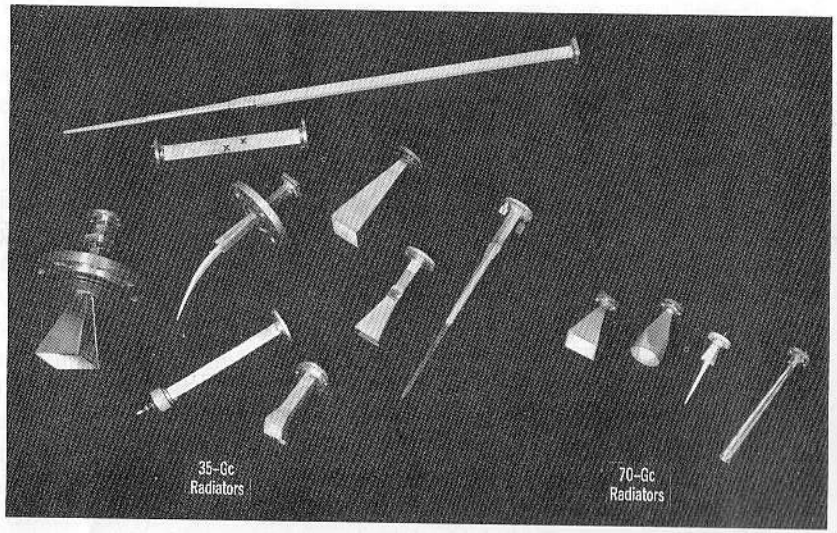

FIG. 9.37 Several microwave radiators useful for plasma experiments. (Courtesy of University of California, Lawrence Radiation Laboratory, Livermore, Calif.)

mandrel containing fins at the location of the intended slots, as the unit shown in Fig. 9.36 was made. Several antennas useful for plasma diagnostics are shown in Fig. 9.37. Thin-wall, stainless steel horns are useful in pulsed magnetic field systems.

9.3.6 ***Antenna pattern measurements.*** *Antenna radiation patterns* (that is, far-field measurements) are usually plotted by rotating the radiator about an axis and recording the intensity measured by a distant, isolated, pickup antenna. Radiation patterns may be displayed on polar or cartesian coordinate paper. The field strength may be calibrated relative to the maximum signal or absolutely by a field-strength meter or comparison against a known standard antenna (Lawson, 1948).

Often, it is inconvenient to monitor the radiation at the large distances required for far-field measurements. Measurements made within the Fresnel zone can be related to the far fields if the radiator can be refocussed (Woonton and Carruthers, 1950). Indeed, it may be the Fresnel zone or even the near-field zone fields that are of interest in the case of radiators used in plasma experiments. Often the field configurations of the antennas *in situ* (that is, mounted in the same position as they are to be

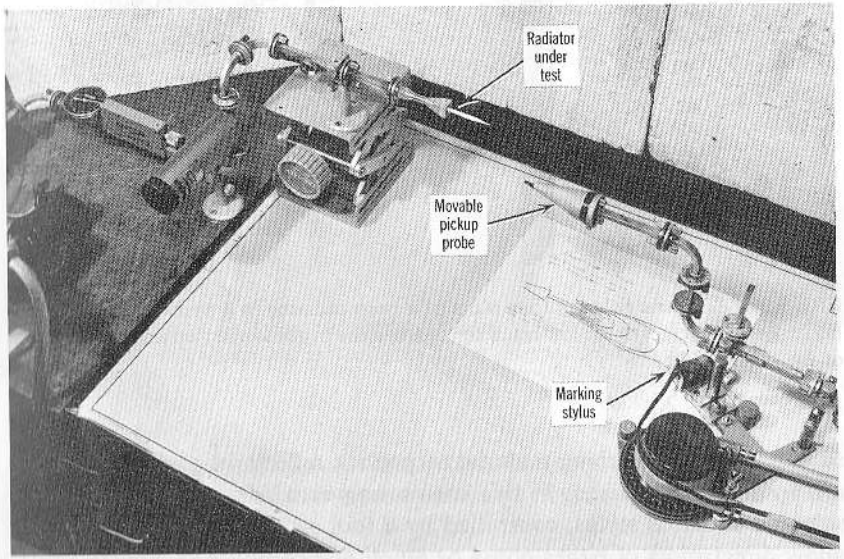

FIG. 9.38 Field plotting probe for near-field amplitude and phase contour measurements. Typical plots are shown in Fig. 9.39. (Courtesy of University of California, Lawrence Radiation Laboratory, Livermore, Calif.)

used) are desired, to determine the effects of walls, magnet coils, and other diagnostic apparatus. The radiator is then fixed in place, and the fields probed either by a scatterer or a small receiving probe (Richmond and Tice, 1955; Buser and Buser, 1962).

An example of a field plotter, using a small pickup probe, is shown in Fig. 9.38. The probe, shown at the right of center, is a section of undersize waveguide, electroformed around a dielectric rod. The probe is

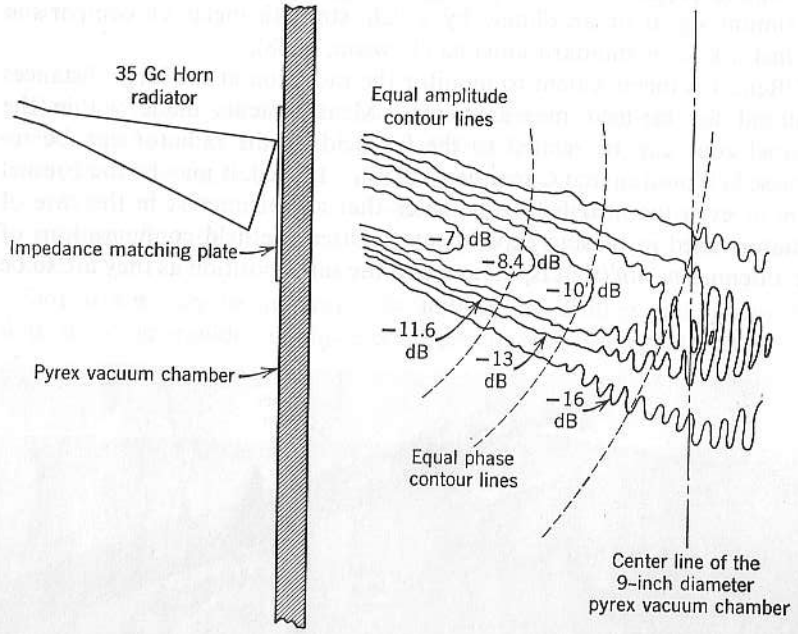

FIG. 9.39a Electric field contour plots of a horn radiator in a pyrex vacuum chamber. Zero dB refers to the indicated signal when the probe is inserted inside the throat of the horn radiator.

surrounded by absorbing material to prevent reflections and mounted on an x-y motion carriage, in this case a converted drafting machine. A solenoid-actuated stylus, controlled by a foot switch, marks the paper to allow direct plots of either phase or amplitude contours (Klapper, 1962). The probe shown is rather large, and can cause serious perturbations in enclosed systems. Very small probes, made by electroforming thin walls around high dielectric constant cores, reduce the perturbation but cause

large signal loss. The small probes have 90° wide radiation patterns (at −3 dB), and thus introduce little angular error in most measurements.

The scattering technique ordinarily employs a small rotating dielectric or resistive rod, mounted on a large x-y positioning frame. The rod is motor-driven to produce modulation in the scattered signal (Buser and Buser, 1962). Some systems use a semiconductor diode, supported by slightly conducting thread (silk painted with Aquadag), through which an

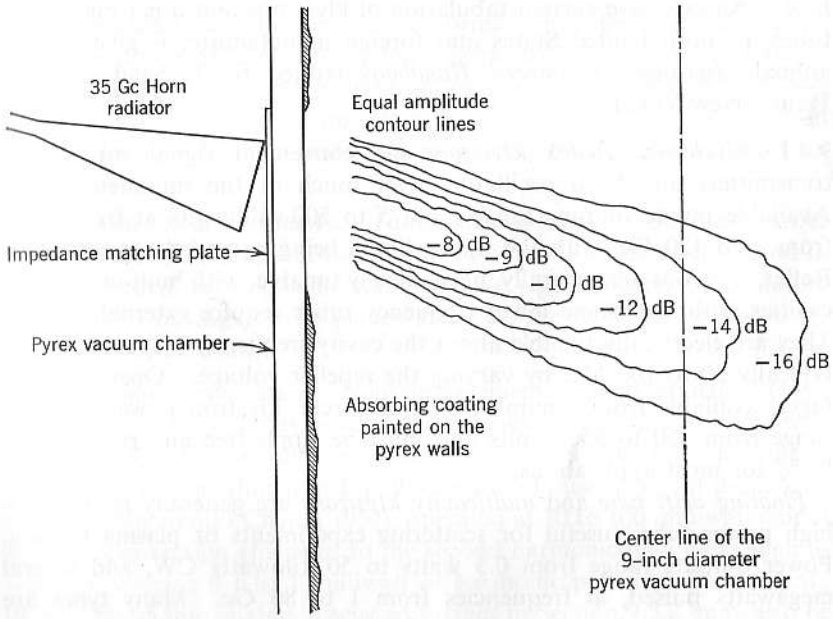

FIG. 9.39b Electric field contour plots of a horn radiator in a vacuum chamber of pyrex, coated with absorbing materials to damp internal reflections.

audio current is passed to modulate the conductivity of the diode. These systems require complicated servo-systems to indicate the position of the scatterer.

Some sample field contour patterns of a 35-Gc horn radiator, made with a pickup probe inside a 9-inch diameter pyrex vacuum chamber, are shown in Fig. 9.39. In Fig. 9.39*a*, the chamber walls were bare glass; multiple internal reflections are very apparent in the ridges of the contour

lines. In Fig. 9.39*b*, the glass had been coated with a special Sauereisen-base absorber (Section 9.6.4); the internal reflections are hardly discernible.

9.4 Signal sources

A variety of signal sources are available, at prices that are steeply ascending functions of frequency. To study a time-varying plasma requires either a CW source or a pulsed source having a very rapid repetition rate. Powers of a few milliwatts or more are usually necessary to provide adequate signal-to-noise ratios in the systems normally employed. Millimeter and submillimeter-source development is currently an active field. An extensive current tabulation of klystrons and other microwave tubes, of both United States and foreign manufacture, is given in the annual *Microwave Engineers' Handbook* (edited by T. Saad, Horizon House, New York).

9.4.1 ***Klystrons.*** *Reflex klystrons* are convenient signal sources for transmitters and local oscillators over much of the millimeter band. Available power outputs range from 5 to 500 milliwatts at frequencies from 2 to 120 Gc, with the upper limits being extended year by year. Reflex klystrons are generally mechanically tunable, with built-in resonant cavities, although some lower frequency tubes require external cavities. They are electrically tunable about the cavity frequency by about $\frac{1}{4}\%$, or typically 50 to 100 Mc, by varying the repeller voltage. Operating voltages, available from a number of commercial klystron power supplies, range from 350 to 3500 volts and must be ripple-free and regulated to 0.1% for most applications.

Floating drift tube and *multicavity klystrons* are generally medium-to-high power tubes, useful for scattering experiments or plasma heating. Power outputs range from 0.5 watts to 50 kilowatts CW, and several megawatts pulsed, at frequencies from 1 to 80 Gc. Many types are mechanically tunable over a 5 to 10% frequency band and electrically tunable over 10 to 50 Mc.

9.4.2 ***Traveling-wave oscillators and amplifiers.*** *Backward-wave oscillators* (BWO) are another class of voltage-tunable tubes, many of them having output over a full frequency octave (2:1). BWO's, also known as *Carcinotrons*, are not mechanically tuned. Power outputs range from a milliwatt to a few watts at frequencies from 0.5 to 220 Gc. These tubes tend to be more expensive than klystrons, require fancier and more expensive power supplies, and are quite heavy, due to their focusing magnets. However, if there is need for their performance, then the choice is clear. Many types have a control grid to permit power leveling or amplitude modulation.

In this class may be included the *M-type* or cross-field oscillators (as distinguished from lineal beam or *O-type*), although often they are referred to as *voltage-tunable magnetrons.* Aside from slightly higher noise content, their performance is comparable to that of the *O*-type BWO's.

Traveling-wave amplifiers of both *O*-type and *M*-type can be used to increase the available power from a transmitter or to serve as a pre-amplifier in a receiver. They are broad-band, some covering an octave and, at frequencies up to *X*-band, many *O*-types have low noise figures rivaling superheterodyne receivers.

9.4.3 ***Magnetrons.*** Magnetrons are normally intended for high-power, pulsed operation, at levels up to a few megawatts from 500 Mc to 100 Gc. They are useful for plasma heating, scattering, or transmitting over long distances, such as for studying plasmas in the upper atmosphere or in space. Voltages from 5 to 60 kV in pulses from 0.1 to 10 μsec are required.

9.4.4 ***Tunnel diode oscillators.*** Tunnel diodes (Esaki, 1958) are negative resistance elements and will oscillate at low power levels when placed in resonant structures. All-solid-state, tunable signal sources of miniature construction, having fair frequency stability, are available at the lower microwave frequencies.

9.4.5 ***Harmonic generators.*** Nonlinear elements, such as semiconductors, ferrites, and electron tubes, produce harmonics when driven at high levels (Page, 1958). Commercial harmonic generators for CW millimeter waves, such as that shown in Fig. 9.6, ordinarily use a crystal diode or a varactor (Bloom and Chang, 1957), operated at 10 to 100 milliwatts input power. Conversion efficiency to the second harmonic may be as high as -20 dB, yielding 0.1 to 1 milliwatt of harmonic power (Johnson et al., 1954). Harmonic mixing, discussed further in Section 9.5.2, may also be accomplished with the unit shown in Fig. 9.6.

Ferrite harmonic generators must be operated at kilowatt levels and, thus, are pulsed at a low-duty rate to permit cooling. Conversion efficiencies of -10 dB at 20 kilowatts input level yield pulsed output powers as high as 50 watts at 150 Gc (Ayres et al., 1957).

Gas discharges, field-emission rectifiers, arcs and relativistic electron beams have also yielded harmonic output (Coleman and Becker, 1959).

Microwave tubes, such as klystrons, BWO's and especially magnetrons, may contain usable harmonic content in their outputs, especially if the operating conditions are optimized. Frequency-multiplier klystrons and carcinotrons are available commercially; in these tubes the harmonic content is extracted directly from the electron beam and excites a resonator.

9.5 Signal detection

The detector is one of the most critical parts of the transmission-reception system. At the millimeter wavelengths, especially, where the transmitted power is small, the receiver sensitivity must be good, while the band width must be kept large enough to allow the output to follow the rapid fluctuations imposed by the plasma variations. Generally, point-contact crystal diodes are used for the detector; the crystal material may be silicon, germanium, gallium arsenide, indium antimonide, etc. (Smith, 1959; Torrey and Whitmer, 1948). Thermal detectors, such as calorimeters, Golay cells, and bolometers (Byrne and Cook, 1963) may be made to have great sensitivity, but have very slow response time, typically a second or more.

9.5.1 ***Video crystal detectors.*** A diode that rectifies the microwave current, producing a video output proportional to the impressed wave envelope, is the simplest form of receiver. The limit of sensitivity is governed by the *Johnson noise*, due to temperature-induced field fluctuations in the junction (Johnson, 1928), or to *shot noise*, due to current fluctuations if the junction is biased (Petritz, 1952). The shot noise and *flicker noise* are, ordinarily, the most serious for video detectors operating at low modulation frequencies, since the noise in the output is proportional to $1/f$ (van der Ziel, 1950). It is well to avoid bias (that is, allowing direct current to pass through the junction) if possible, for this reason. A justification for using bias is that most diodes have nearly square-law response at low power levels (10^{-7} to 10^{-4} watts); the application of a forward current of 10 to 100 microamperes both lowers the internal impedance (Staniforth and Craven, 1960) (thus reducing the output RC time constant and improving the video frequency response) and raises the operating point to a steeper slope region on the I-V curve. Unless the load resistance is decreased, however, the increase in noise, due to the current flicker offsets the increase in current sensitivity, and no improvement in *signal-to-noise ratio* results. A second and perhaps more vital reason to avoid using externally introduced bias is that unwanted stray pickup (see Section 9.7) may enter the circuit in this low-level part of the receiver.

The sensitivity and video impedance of millimeter crystals vary widely with type and particular sample; typical sensitivities are 300 microvolts/microwatt, and impedances are 1000 to 10,000 ohms at a level of 5 microwatts. Short-circuit current sensitivity is between 0.2 and 10 microamperes per microwatt (Richardson and Riley, 1957). The *threshold sensitivity* of a crystal video microwave receiver is expressed in detectable power below 1 milliwatt, or $-dBm$. Figure 9.40 gives curves of threshold

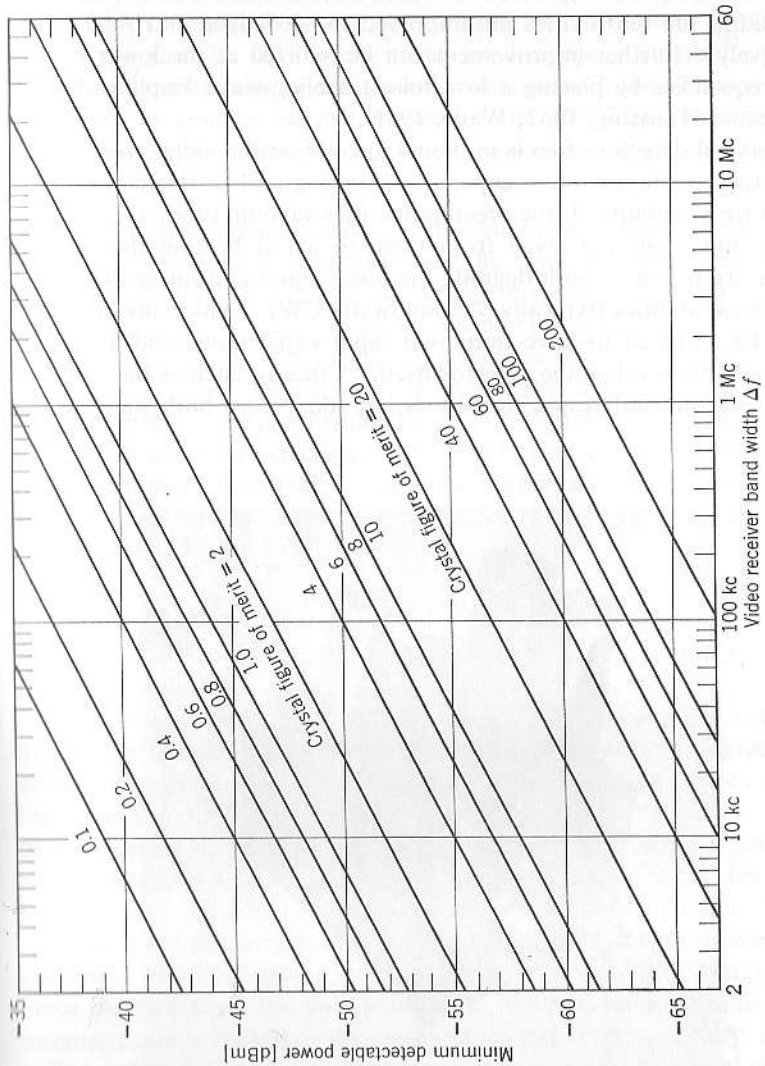

FIG. 9.40 Minimum detectable signal (threshold) of crystal video receivers, expressed in decibels below one milliwatt (−dBm), as a function of video band width, and crystal figure of merit. (Courtesy of *Microwave Engineers Handbook*, Random House, New York, 1964.)

sensitivity vs. receiver band width for various crystal *figure-of-merit* values. The figure of merit (FM) is obtainable from the manufacturer. Typical sensitivities vary from −57 dBm at 2.5 Gc (FM=200) to −40 dBm at 300 Gc (FM=4), for 10 Mc video band width. For 100-kc video band width, the sensitivities are improved to −67 dBm and −50 dBm, respectively. Further improvement can be realized at the lower microwave frequencies by placing a low-noise traveling-wave amplifier before the detector (Taussing, 1962; Wade, 1961).

The crystal detector often is mounted directly on the video preamplifier chassis to provide minimum capacitive shunting and to lessen the likelihood of stray pickup. If the preamplifier uses vacuum tubes, the detector must be mounted well away from them to avoid heating the crystal; temperature increases both degrade the noise figure and lower the power handling capabilities (typically $\lesssim 5$ milliwatts CW). Video preamplifiers should be designed to have minimum input capacitance and a smaller noise contribution than the detector itself. Circuits, such as the cascode, both for vacuum tubes and transistors, are ideal from both standpoints.

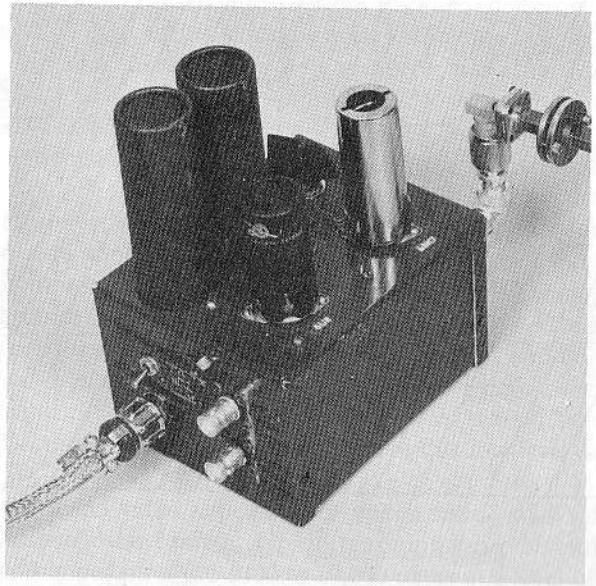

FIG. 9.41 Crystal video detector and video preamplifier. Amplifier voltage gain is 400 over a broad video band of 100 cps to 2 Mc or 1000 to 2000 over narrow, tuned bands at 10 kc, 100 kc, and 1 Mc (see circuit diagram in Fig. 9.49). (Photograph courtesy of General Atomic, San Diego, Calif.)

D-c heaters for vacuum tubes, and ripple-free, well-regulated power supplies are necessary, since the signals being amplified are as small as a microvolt. An example of a *crystal video receiver* is shown in Fig. 9.41. The cascode triodes, followed by a pentode and a cathode follower, have an over-all voltage gain of 400, over a band from 100 cps to 2 Mc. The output can then be fed directly to an oscilloscope. To obtain the full video band width, the crystal detector may have to be shunted with a 5000-ohm or smaller resistor to reduce the *RC* time constant. This compromises the figure of merit, but improves the relative response above a megacycle or so.

9.5.2 ***Superheterodyne receivers.*** The microwave *superheterodyne* has considerably increased sensitivity over the simple crystal video detector (Harvey, 1963). The threshhold signal magnitude is related to the *noise figure* of the receiver, as shown in the curves of Fig. 9.42. Typical noise figures for *balanced mixers* at centimeter to millimeter wavelengths lie between 10 and 18 dB, yielding sensitivities of −90 dBm to −100 dBm for usual video band widths, and −120 dBm for very narrow band widths and coherent detection (Smith, 1951; also see Section 9.5.5).

The minimum detectable signal power may also be expressed as an equivalent *noise temperature* T_n of the receiver, the conversion factor being derived from (7.2.8)

$$T_n = \frac{P_{min}}{k\,\Delta f}. \tag{9.5.1}$$

For $P_{min}=1$ picowatt (−90 dBm) and $\Delta f=10$ Mc band width, the equivalent noise temperature is $T_n=7250\ ^\circ\mathrm{K}=0.625$ eV.

The greater sensitivity of the superhet over the simple video detector is due mainly to its higher intermediate frequency. Since, for a given video band width, the shot noise is roughly proportional to $1/f$, the choice of a high intermediate frequency reduces the over-all noise figure. I.f. amplifiers, however, have worsening performance above 20 Mc or so, requiring a compromise in intermediate frequency; the optimum value, for normal band widths from 2 to 10 Mc, is between 30 and 60 Mc (Rennie, 1957).

The over-all receiver noise figure depends also on the mixer conversion efficiency, which improves with higher crystal current (Pound, 1948). Since the shot noise becomes worse with higher crystal currents, a compromise again is required; the optimum crystal current, usually, is found to lie between 0.2 and 0.6 milliamperes, corresponding to a local oscillator power of about a milliwatt for a balanced mixer (2 crystals).

The current flowing in mixer crystals raises their operating point on the *I-V* characteristic curve well out of the square-law region. For small signals, the output voltage is thus nearly linear with input signal, rather

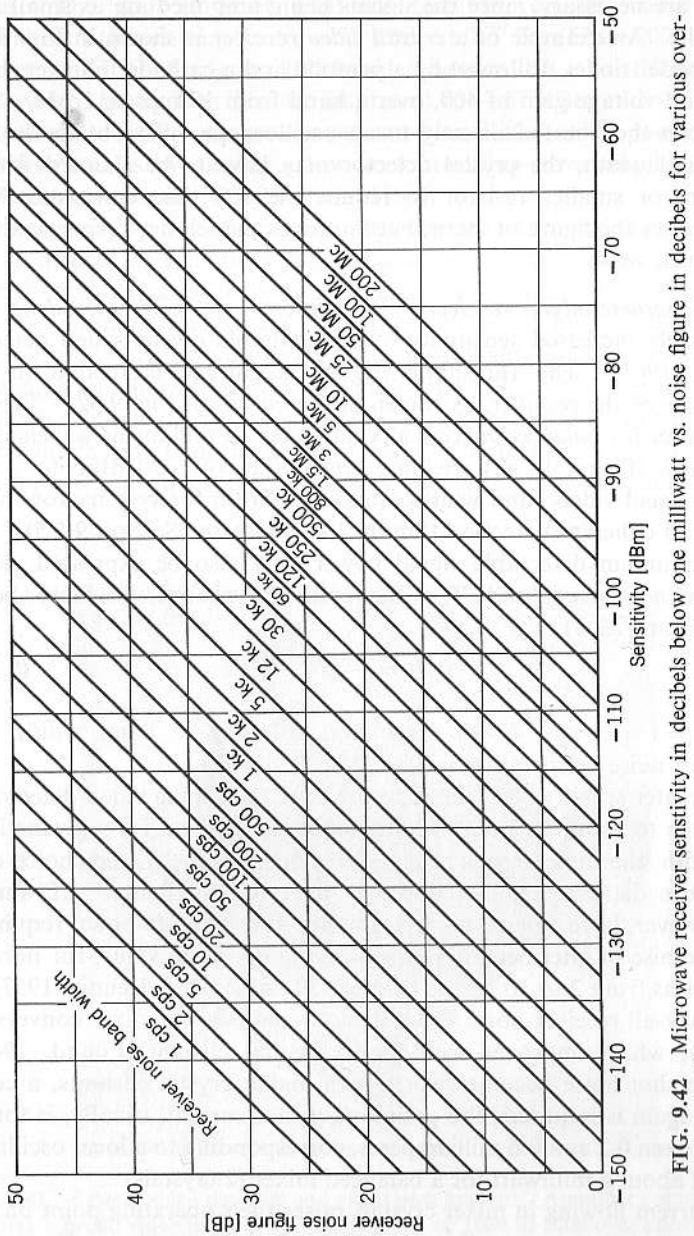

FIG. 9.42 Microwave receiver senstivity in decibels below one milliwatt vs. noise figure in decibels for various over-all band widths.

than quadratic as in direct video detection. For this reason, superheterodyne systems have much greater dynamic range than crystal video systems, besides having considerably better sensitivity (Taub and Giordano, 1954).

Harmonic mixing provides a useful detection method for millimeter wavelengths where local oscillators are not available. The local oscillator is operated at a subharmonic of the frequency at which detection is desired. The pulses in the rectified crystal current contain harmonics that mix with the incoming signal to produce beats at the intermediate frequency (Johnson, 1954). Silicon and gallium arsenide crystals seem to give best results, yielding over-all noise figures intermediate between straight superhet receivers and crystal video receivers. Harmonics as high as the fifth and sixth give useful mixing action.

The superhet has some disadvantages, however, the chief one being the need for a local oscillator. For transmission and scattering experiments, in order to keep the receiver tuned to the transmitter, it is usually necessary to provide *automatic frequency control* or AFC (Jenks, 1947), requiring still further circuit and operational complication. The reflex klystron is a convenient local oscillator for use with AFC because it is voltage-tunable over a small band. Changing the transmitter frequency over a large excursion requires retuning the local oscillator. A backward-wave oscillator is voltage-tunable over a wide range and, with proper adjustment, can be made to track a transmitter over its entire tuning range. Ordinarily, the mixer assembly requires peaking for each particular frequency, although some mixers retain low noise figures over a 6% band. A swept-frequency superhet can be made by sweeping the local oscillator electrically or mechanically. A well-matched, broad-band mixer, such as a short-slot hybrid or rat-race, is necessary for this type of service. An application requiring a swept receiver was mentioned in Section 8.3 for examining the electron gyro-frequency harmonics.

9.5.3 ***Parametric mixer-amplifiers.*** The parametric amplifier (Bloom and Chang, 1957), in some respects, resembles a superheterodyne receiver; the *pump* is analogous to the local oscillator, and the nonlinear reactive element is analogous to the mixer. The *idler frequency* appears at the sum and difference frequencies, for down-mixing, just as does the intermediate frequency of a superhet. In its component form, the microwave parametric amplifier uses a nonlinear capacitor, often a silicon *p-n* junction *varactor* with reverse bias so that it forms a voltage-variable, capacitive depletion layer, but draws no current. The resistive component of the "mixer" is thus practically absent, and the shot and Johnson noise contributions are very small (van der Ziel, 1959). Equivalent noise temperatures of units operated under ambient conditions may be as low as 300 °K

and, when cooled to liquid nitrogen temperature (77 °K), the noise temperature may be reduced to about 80 °K. In addition, since the nonlinear element has little loss, the over-all conductance can be made negative by proper choice of operating conditions. Instead of "conversion loss," as in a diode mixer superhet, the unit then exhibits "conversion gain" over a narrow frequency spectrum. The varactor usually is mounted in a resonant structure, which makes tuning difficult. A typical *X*-band parametric amplifier, pumped at 10.15 Gc, exhibited a gain of 50 dB over a band width of 2.4 Mc at an input frequency of 8.5 Gc, with an equivalent noise temperature of 600 °K (Bossard et al., 1960). Generally speaking, parametric amplifiers, including traveling-wave and distributed-line units (Mount and Begg, 1960), have the widest application at the UHF and low microwave frequencies in fixed-tuned operation. Typical output powers are between 1 and 500 milliwatts. As components and techniques improve, the upper cut-off frequencies are being raised, and amplification at frequencies as high as *K*-band or the 8-mm band (35 Gc) has now become possible (de Loach, 1960).

Other nonlinear reactive elements, such as ferrites, electron beams, garnets, and various solid-state, crystalline substances, are also finding application (Mount and Begg, 1960).

9.5.4 ***Miscellaneous receiver systems.*** Quantum-mechanical amplifiers or *masers* are useful for very low-level amplification at particular frequencies corresponding to the energy gaps in the molecules of various solids, liquids, and gases. To allow the levels to be populated to high enough concentrations to give spontaneous emission, the element must be cooled, often to liquid helium temperatures. In principle, at 0 °K, the maser should be capable of detecting individual microwave photons (Weber, 1959). To achieve level-splitting or paramagnetic resonance, a magnetic field is required. The maser, thus, is not a simple amplifier to operate but, for some critical applications, such as radio astronomy, it provides amplification at noise temperatures of a few degrees Kelvin and frequency stability unmatched by other devices (Gordon et al., 1955).

Tunnel diodes (Esaki, 1958) will oscillate if placed across a tuned circuit because they possess negative resistance. When isolated by nonreciprocal elements, such as a circulator, however, they act as amplifiers, having noise figures as low as 7 dB. Gallium arsenide diodes have been used as Esaki amplifiers as high as 26 Gc (Holonyak and Lesk, 1960). The diodes are low-power elements, operating at levels up to a milliwatt or so.

Thermionic diodes are useful as low-level detectors up to about *S*-band (3 Gc) before transit-time effects degrade the efficiency. At higher power levels (100 watts to 100 kW pulsed power), coaxial diodes, in which the

thermionic cathode is the center conductor, have been constructed with waveguide inputs for frequencies from 3 to 35 Gc (Hawkins et al., 1958). Commercially available units have large enough voltage outputs to deflect a cathode ray tube directly, with 0.1 microsecond response times and, thus, may be used directly for power oscillator monitoring.

9.5.5 ***Microwave radiometers.*** Receivers intended for reception of thermal or quasithermal radiation in the microwave spectrum are called radiometers (Harris, 1960). The received signals have the characteristics of noise, generally over a broad frequency band, leading to the name *white noise*. The signals may be steady, slowly fluctuating, or transient.

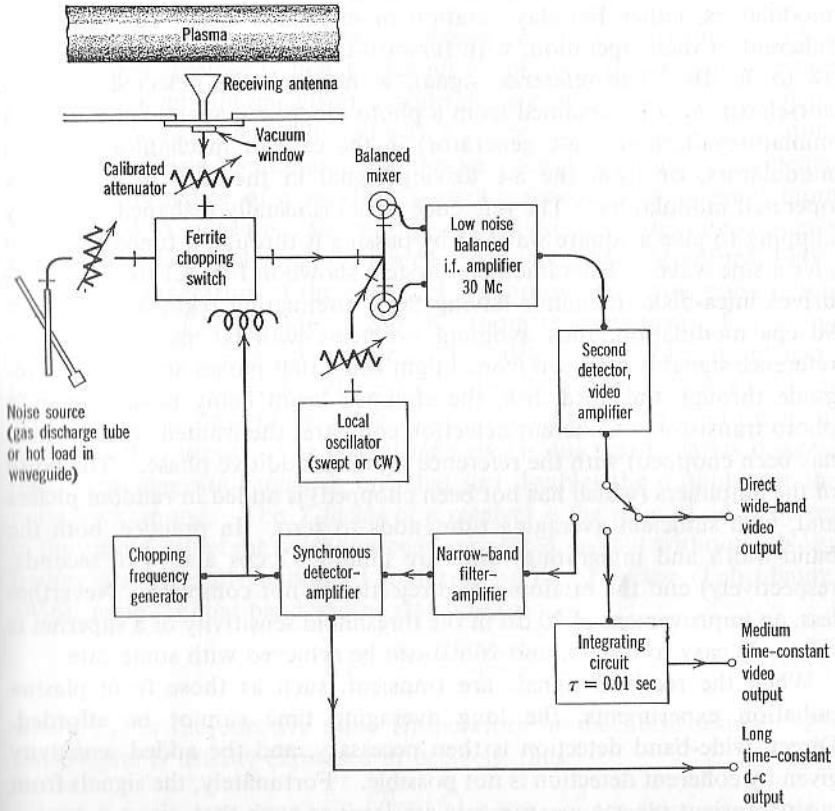

FIG. 9.43 Microwave radiometer with coherent detection. The input is switched between the signal and a noise standard either mechanically or electrically. The detected, chopped signal is correlated with the reference. Uncorrelated signals average to zero. Without chopping, a direct, wide-band signal is obtained.

The steady or slowly fluctuating noise signals can be measured by the use of coherent detection (Dicke, 1946) with narrow band widths and long averaging times. The block diagram of a typical coherent-detection radiometer (also called phase-sensitive detection) is shown in Fig. 9.43. The signal modulator may be a motor-driven attenuator or phase shifter (see Section 9.2.1) or a ferrite modulator. Or the radiating source itself may be modulated at a low frequency and the detected signal compared with the modulating signal, in the coherent detector. Crystal and plasma modulators ordinarily have too high noise temperatures to be useful for low-level modulation. An isolator must be mounted between the modulator and the mixer; local oscillator leakage back up the input line may be reflected back into the input and appear as a false signal. Ferrite modulators, either Faraday rotation or circulator types, have isolation inherent in their operation, with forward-to-reverse attenuation ratios of 18 to 30 dB. The reference signal, with which the detected signal is correlated, may be obtained from a photo diode, a magnetic pickup, or a miniature alternator (a-c generator) in the case of mechanically driven modulators, or from the a-c driving signal in the case of electrically operated modulators. The reference signal is usually reshaped, either by clipping to give a square wave or by passing it through a tuned circuit to give a sine wave. The radiometer system shown in Fig. 8.1 uses a motor-driven mica-disk attenuator having three attenuating regions to produce 90 cps modulation, thus avoiding problems with 60-cps pickup. The reference signal is obtained from a light beam that passes across the waveguide through the mica disk, the chopped beam being picked up by a photo transistor. Coherent detection compares the wanted signal (which has been chopped) with the reference signal in additive phase. The noise of the amplifiers (which has not been chopped) is added in random phases and, with sufficient averaging time, adds to zero. In practice, both the band-width and integrating times are finite ($\sim$2 cps and $\sim$10 seconds, respectively) and the random noise rejection is not complete. Nevertheless, an improvement of 20 dB in the threshhold sensitivity of a superhet is relatively easy to obtain, and 26 dB can be achieved with some care.

When the received signals are transient, such as those from plasma radiation experiments, the long averaging time cannot be afforded. Direct, wide-band detection is then necessary, and the added sensitivity given by coherent detection is not possible. Fortunately, the signals from most transient plasma experiments are large enough that direct detection with a sensitive superhet receiver is possible, and the detected video signal can be displayed directly on an oscilloscope.

Some transient plasma experiments operate at a fast repetition rate (for example, 60 pulses/sec). If the radiation intensity is reproducible

from pulse to pulse, the time-average noise temperature can be obtained by switching the radiometer input back and forth between the radiation input and a standard noise source with a fast-operating ferrite switch, as shown in Fig. 9.43 (Bekefi et al., 1960). The amplitude variation in time during the radiation pulse can be measured by making the sampling pulse width much shorter than the radiation pulse width and varying the sampling delay back and forth over the duration of the radiation pulse. The noise temperature may be obtained either by calibrating the output against a known noise standard (White and Greene, 1956) or by reading a calibrated attenuator in the input as it is varied to achieve a null in the output signal. Signal sensitivities equivalent to a Dicke-type radiometer are obtainable, even with a transient discharge, by this technique.

9.5.6 ***Measurement of receiver performance.*** The performance of a crystal video receiver is best evaluated by plotting the output response against the input, obtained from a calibrated signal generator or a klystron whose output has been calibrated with a power meter. The receiver input is ordinarily fairly broad-band, and not very sensitive to any adjustments.

The performance of a sensitive superhet receiver is somewhat more complicated to measure. Ordinarily, some kind of white noise source is used, often a gas discharge tube inserted in a waveguide (Mumford, 1949). The noise temperature of these sources is expressed as excess noise power above that of a blackbody at 290 °K (room temperature). For argon discharge tubes, the excess is typically 15.2 dB (10,100 °K) and, for neon tubes, 18 dB (18,600 °K). The *noise figure* of the receiver (see Fig. 9.42) is defined as the ratio of available signal-to-noise power ratio at the input to that at the output. The *threshhold signal* is one that is barely discernible. The *tangential signal* is one that just doubles the output over the noise background. The *Y-factor* of a receiver is the ratio of noise power in the output, when the noise source is connected, to that without. Noise figures are generally expressed in terms of the Y-factor (Lebenbaum, 1956), assuming that band widths are constant

$$NF=\frac{(T_{NS}/290)-1}{Y-1} \tag{9.5.2}$$

where T_{NS} is the effective noise temperature of the noise source. The noise figure is usually expressed in decibels, thus,

$$NF_{dB}=10\log_{10}\left(\frac{T_{NS}}{290}-1\right)-10\log_{10}(Y-1). \tag{9.5.3}$$

The Y-factor is obtained directly from a calibrated attenuator inserted between the noise source and the receiver. The attenuator is increased until the effect on the output signal of turning the source on and off just

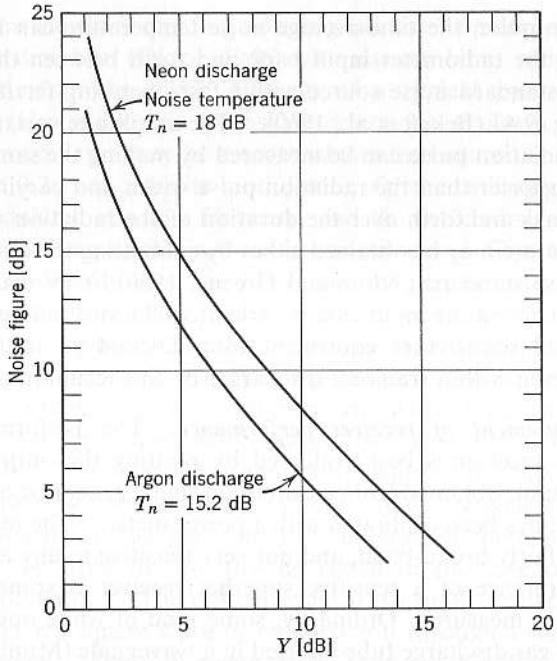

FIG. 9.44 Receiver noise figure vs. measured Y-factor for argon and neon gas-discharge noise sources.

vanishes; this setting is Y, expressed in decibels. A graph of noise figure vs. Y factor is given in Fig. 9.44.

9.6 Vacuum system considerations

The vacuum system is a necessary part of a plasma experiment; still, the vacuum walls impose some difficult problems in making diagnostic measurements. Microwave radiators and probes must be inserted through vacuum seals, often buried deep inside a maze of magnet coils, outgassing heater windings, pulsed electrodes, water, air, and liquid nitrogen lines, and all the rest of the control and diagnostics connections. In many experiments the radiators and probes must be movable or, at least, removable.

9.6.1 ***Vacuum materials.*** Many materials commonly used in waveguide components are completely unsatisfactory in a vacuum environment. Most organic materials have a high vapor pressure (Dushman, 1962), and deteriorate under plasma bombardment. Materials that are fibrous or contain voids usually trap air or moisture and take excessively long to

pump out. Screws tapped into blind holes are exceedingly bad in this respect; all threaded members should be slotted, drilled, or filed to allow rapid pump-out. In general, metals, ceramics, glasses, some synthetic rubbers, and some plastics, such as teflon, polyvinyl chloride, PTFE, etc., are useful in systems having ultimate vacuums down to 5×10^{-7} torr (Kohl, 1960). To go below that level, most systems must be baked, perhaps to 400 °C, and then the troubles begin. Plastics and rubber are out of the question, and even metal alloys that contain low-melting temperature components, such as brass, most solders, and sealing compounds, can be used only with care (Strong, 1938).

9.6.2 ***Transmission-line windows.*** In glass vacuum systems it is possible to mount horn antennas outside the glass and couple to the plasma region inside (see Fig. 9.39). Unless the glass is $\lambda/2$ thick, or its mismatch can be matched at both surfaces, however, its presence in the near field may distort the radiation pattern or lead to frequency sensitivity due to multiple internal reflections. For reliable measurements, it is usually best to mount the antennas inside the vacuum and run the waveguides out to some convenient point before sealing them (Benderly and Kilduff, 1962).

Waveguide and coaxial-line windows for continuously pumped, non-bakable vacuum systems present no special problems. In regions where magnetic materials are permissible, commercially produced kovar-sealed windows may be attached by soft solder, epoxy, or silver chloride, or by clamping against an O-ring. Such windows are available in waveguide sizes down to about WR 28 (RG-96/U). At higher frequencies, it is usually necessary to "do it yourself." A simple window may be made by clamping a thin (~0.001 inch) teflon, mylar, or mica sheet against an O-ring between a choke-and-cover flange assembly. If insulating screws (such as nylon) are used, the window section serves also as an insulation break to suppress ground-current loops. Such a window is somewhat risky for long-term operation, and an improvement is to cement a 0.001-inch thick mica disc on either a choke flange or in a recessed area cut with a lathe in a contact flange, as shown in Fig. 9.45. Windows for waveguides as small as WR 12 (RG-99/U), having standing-wave ratios smaller than 1.2 and losses of 0.5 dB, can be made by this technique. Some examples are shown in Fig. 6.4 for operating frequencies of 70 and 90 Gc. Square cross-section waveguide windows are made by the same techniques, allowing polarization diplexing (see Sections 9.2.3 and 6.2.2) or simply changing from one polarization to the other without opening the vacuum system.

The simple O-ring and cemented seals, mentioned above, are not suitable for *ultrahigh-vacuum* systems, operating at base pressures perhaps as low

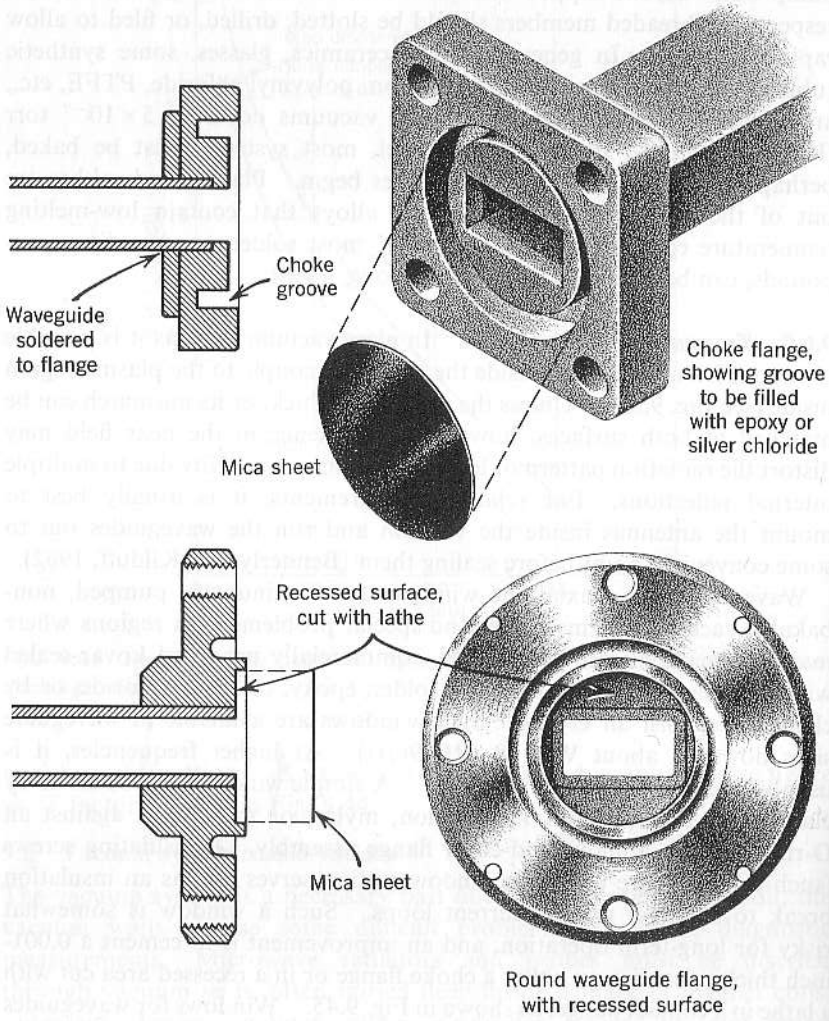

FIG. 9.45 Waveguide vacuum windows for use on nonbakable vacuum systems. The windows are cemented in place with a low-vapor-pressure epoxy, vacuum wax, or silver chloride.

as 10^{-10} torr. To attain such low pressures, it is necessary to exclude all high vapor-pressure materials and bake out the entire vacuum system to temperatures as high as 400 to 450 °C. Transmission-line windows for these conditions follow standard practice for microwave tube output

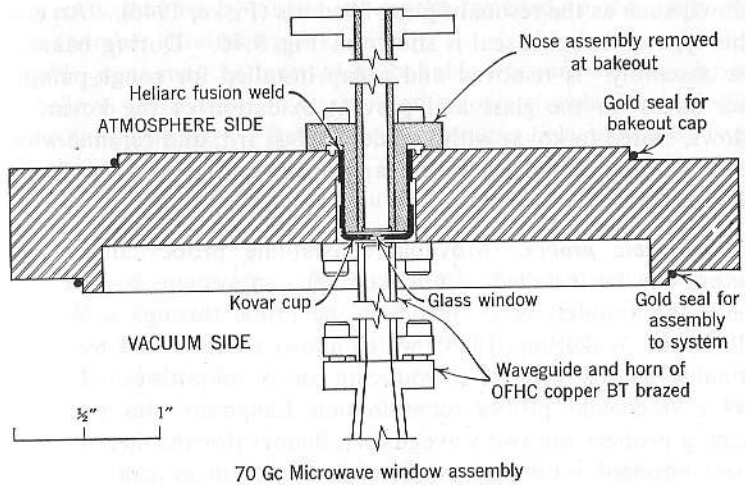

70 Gc Microwave window assembly

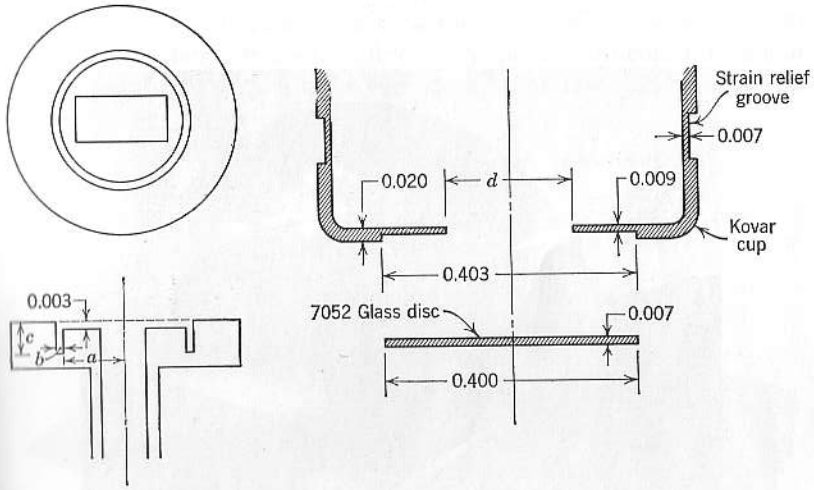

Rectangular waveguide inside dimensions	Design frequency	*a* rad.	*b*	*c*	*d* dia.
0.280 × 0.140 (RG-96/U)	35 Gc	0.160	0.026	0.089	0.203
0.280 × 0.280	35	0.203	0.032	0.086	0.345
0.148 × 0.074 (RG-98/U)	70	0.086	0.012	0.044	0.109
0.080 × 0.040 (RG-138/U)	140	0.076	0.020	0.023	0.047

FIG. 9.46 Bakable vacuum window assembly for millimeter waveguide systems. Insets show details of metal-glass window seal and choke grooves used on each side of windows (all dimensions in inches). (Courtesy of W. P. Ernst and D. Grove, Princeton University, Plasma Physics Laboratory, Princeton, N.J.)

windows, such as the resonant glass-filled iris (Fiske, 1946). An example of this type of bakable seal is shown in Fig. 9.46. During bakeout the "nose assembly" is removed and a cap installed for rough-pumping to reduce stress on the glass and prevent oxidation of the kovar. Mica windows, sealed to kovar with powdered glass frit, and ceramic windows, sealed by ultrasonic soldering or evaporative plating, may also be used at high temperatures.

9.6.3 ***Movable probes.*** Movable coaxial-line probes and waveguide radiators can be installed in unbaked vacuum systems in several ways. Perhaps the simplest is to introduce the probe through a Wilson seal (Guthrie and Wakerling, 1949), which allows rotation and translation at reasonable speeds without introducing air or impurities. Figure 9.47 shows two coaxial probes (combination Langmuir and plasma wave launching probes) and two waveguide radiators (for incoherent scattering studies) mounted in tubing that passes through Wilson seals. The probes

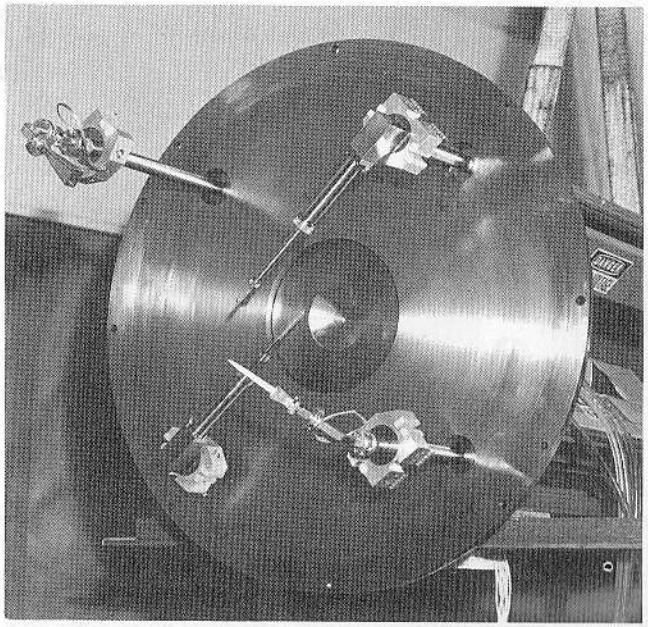

FIG. 9.47 Probe and waveguide assemblies mounted in tubing introduced through a vacuum wall with Wilson seals. The probe carts move on rails inside the vacuum system, allowing accurate positioning. (Courtesy of General Atomic, San Diego, Calif.)

ride on carts, carried by alignment tracks fastened to the walls of the vacuum chamber (Malmberg et al., 1963).

Movable parts may be inserted in bakable vacuum systems by using metal bellows (sylphons). This method allows translation and tilting, but not rotation directly. Rotational motion can be achieved by complicated linkages inside the vacuum. The bellows usually require support against the air pressure; double nuts on threaded rods permit stable positioning.

9.6.4 ***Microwave absorbers.*** Nearly all microwave propagation experiments benefit from having nonreflecting surfaces surrounding the sampled region. In some experiments it is absolutely necessary.[1] For example, the experimental chamber shown in Fig. 6.4 produced such severe standing waves that interferometer fringes were practically unintelligible, before the absorbing coating was added.

A wide variety of microwave absorbers, suitable for antenna testing and anechoic rooms, is commercially available (Harvey, 1963). Practically all of these materials either have too high vapor pressure to permit their use in vacuum or contain ferromagnetic constituents that disturb the magnetic fields of plasma experiments. The few suitable absorbers tend to be quite expensive.

[1] See Fig. 9.39 for a comparison of coated and uncoated wall conditions.

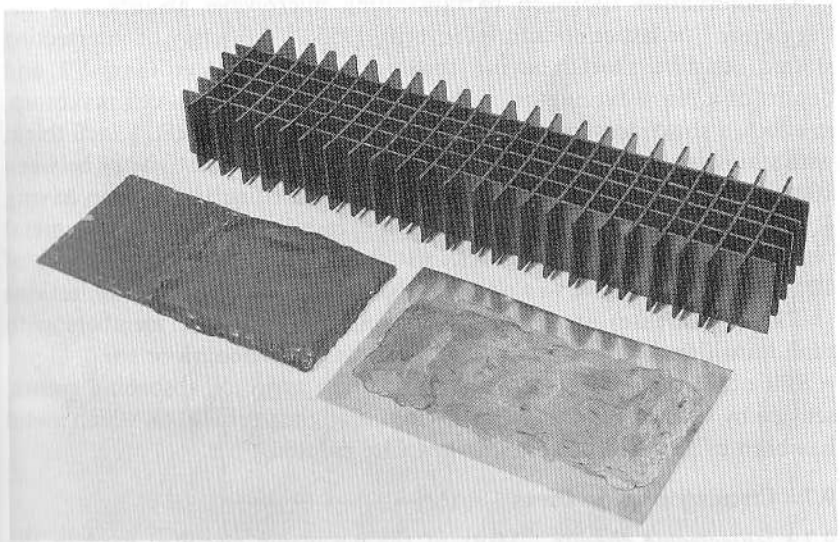

FIG. 9.48 Microwave absorbers useful inside a vacuum chamber. (Courtesy of General Atomic, San Diego, Calif.)

It is possible, however, to make satisfactory absorbing materials in the laboratory. Absorbers for noncritical vacuum systems, that is, pressures down to about 5×10^{-7} torr, are made by adding carbon powder and silicon carbide or boron carbide to ceramic enamel or epoxy. Sauereisen or its equivalent is particularly suitable, since it can withstand the high temperatures of bakeout and does not tend to deteriorate with modest plasma bombardment. It does absorb moisture and must be baked out overnight after it is first applied. A mixture (by weight) of 75% Sauereisen No. 1 paste, 15% boron carbide powder, 10% carbon powder, and enough thinner to make a smooth paste has been found to cure to a hard, crack-free surface. Three coats, each about a millimeter thick after drying, on stainless steel reduces the reflection coefficient at 4 mm wavelength by 18 dB at any angle and that at 8 mm wavelength by more than 12 dB. Similar preparations, using epoxy or other potting compounds as the bulk material, usually give satisfactory performance and pump down rapidly, but may not stand up under plasma bombardment. Some samples are shown in Fig. 9.48.

In applications where slightly magnetic materials are permissible, a small amount of ferrite powder may be added to increase the magnetic permeability. Increasing the relative permeability in equal proportion to the dielectric constant keeps the wave impedance the same as that of free space and reduces the interface reflections.

An alternative approach to fabricating microwave absorbers is the "egg crate" or lattice structure (Severin, 1956). An array of intersecting slotted resistive sheets, having spacings slightly greater than $\lambda/2$ and depths of a few wavelengths, is shown in Fig. 9.48. Each cell makes up, in effect, a short, lossy waveguide. Polyvinyl chloride sheet, $\frac{1}{8}$ inch thick, with stainless steel evaporated on both sides to give a resistivity of between 100 and 200 ohms per square and made into a lattice 1 inch deep having $\frac{1}{2}$ inch spacing, gave more than 18 dB decrease in reflection from a metal plate over the band 32 to 40 Gc. Its presence in a vacuum system of 10^{-7} torr base pressure was not distinguishable. Even smaller reflections (>22 dB decrease) are obtained by making the lattice members with random widths or by letting points protrude a wavelength or so.

Still other types of absorbers consist of an array of absorbing spears, set side by side, or bundles of short lengths of glass tubing, on which metal has been evaporated or colloidal graphite painted.

9.7 Circuitry considerations

9.7.1 ***Electronic circuits.*** Most of the electronic circuitry used in the transmitters, receivers, control and timing chassis, and power supplies required for microwave diagnostics are more or less standard. Power

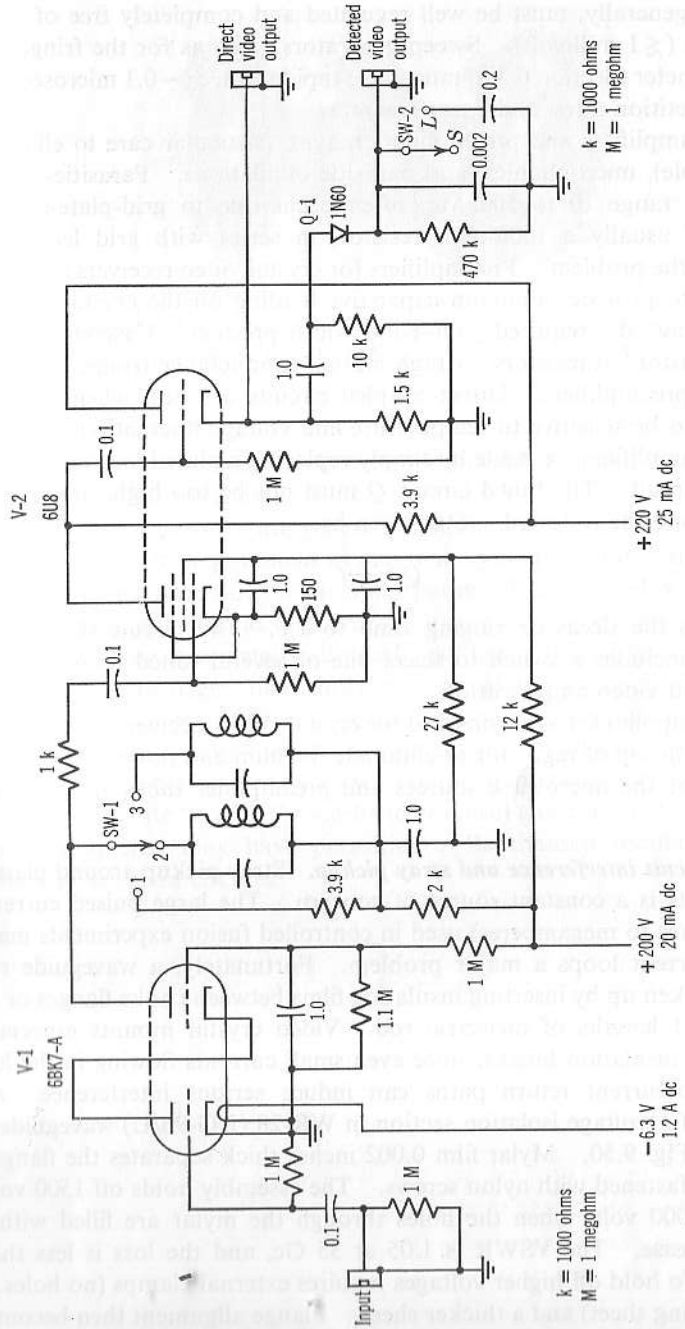

FIG. 9.49 Video preamplifier circuit for broad-band or tuned amplification. Voltage gain = 400 over video band 100 cps to 2 Mc. Maximum hum and noise in output, 1 millivolt. Maximum undistorted output signal voltage, 5 volts.

supplies, generally, must be well regulated and completely free of ripple and noise ($\lesssim 1$ millivolt). Sweep generators, such as for the fringe-shift interferometer (Section 6.3.3) must have rapid retrace (~ 0.1 microsecond), stable repetition rates, and linear rise rates.

Video amplifiers and preamplifiers require particular care to eliminate hum (ripple), microphonics, and parasitic oscillations. Parasitics, in the frequency range 10 to 500 Mc, often occur due to grid-plate-cathode feedback; usually a 1000-ohm resistor, in series with grid leads, will eliminate the problem. Preamplifiers for crystal video receivers should be designed to provide minimum capacitive loading on the crystal detector and yet have the required gain–band width product. Cascode circuits, using nuvistors, transistors, or high mutual-conductance triodes, are ideal for such preamplifiers. Direct-coupled circuits are best when possible, but tend to be sensitive to temperature and voltage fluctuations. Tuned video preamplifiers are made by simply replacing a plate load resistor with a tuned circuit. The tuned circuit Q must not be too high, or transient events cannot be followed. Q is given by

$$Q \approx \tau \pi f \tag{9.7.1}$$

where τ is the decay or ringing time to $1/e$. The circuit sketched in Fig. 9.49 includes a switch to select one of several tuned frequencies or broad-band video amplification.

Power supplies for klystrons and for crystal video receivers often require regulator on top of regulator to eliminate the hum and noise. D-c heater supplies for the microwave sources and preamplifier tubes are generally desirable.

9.7.2 ***Circuit interference and stray pickup.*** Stray pickup around plasma experiments is a constant source of concern. The large pulsed currents (kiloamperes to megamperes) used in controlled fusion experiments make ground-current loops a major problem. Fortunately, a waveguide run can be broken up by inserting insulating films between choke flanges or by using short lengths of dielectric rod. Video crystal mounts especially must have insulation breaks, since even small currents flowing in the low level video-current return paths can induce serious interference. An example of a voltage isolation section in WR-28 (RG-96/U) waveguide is shown in Fig. 9.50. Mylar film 0.002 inches thick separates the flanges, which are fastened with nylon screws. The assembly holds off 1500 volts dry and 3000 volts when the holes through the mylar are filled with a silicone grease. The VSWR is 1.05 at 35 Gc, and the loss is less than 0.5 dB. To hold off higher voltages requires external clamps (no holes in the insulating sheet) and a thicker sheet. Flange alignment then becomes

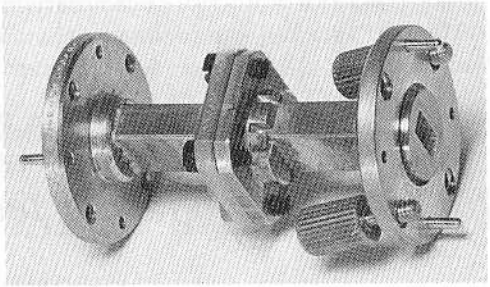

FIG. 9.50 Waveguide voltage isolation section. Loss is 0.5 dB and VSWR is 1.05 at 35 Gc. Hold-off voltage is 1500 V. (Courtesy of General Atomic, San Diego, Calif.)

a problem and with sheets thicker than about 0.005 inches there is some leakage as well as reflection.

Screen-cage enclosures are generally helpful for the diagnostics system although the main requirement to eliminate pickup is simply to make all ground returns have low inductance paths. Running all waveguides, trigger cables, etc., so that they are well grounded as they pass through a large metal sheet or a metal wall usually suffices. In addition, the power lines, oscilloscope trigger lines, and timing signal lines may need decoupling filter networks or transformers. Coordination with the other diagnostic instrument leads is also necessary. Direct radio-frequency interference by electromagnetic radiation is seldom encountered, but occasionally spark gaps radiate "hash" (broad-band rf noise) and power tubes used in modulators, etc., may have parasitic or Barkhausen oscillations that radiate to sensitive circuits.

CHAPTER 10

General plasma diagnostic techniques

10.1 Tabulation of some useful diagnostic techniques

Several diagnostic techniques yield information similar to that obtained by microwaves, that is, the plasma electron properties. Many of the same experimental requirements also apply, such as shielding against stray pickup, multiple-channel simultaneous measurements, and the need for simplified, automatic data presentation. Some measurements involve internal probing, such as Langmuir and magnetic probes, which may perturb the plasma, while other external measurements, such as optical diagnostics, are nonperturbing. Some techniques are useful only in dense plasmas or plasmas containing a strong magnetic field. To sort out the measurements useful for a given kind of determination, brief tabulations of several techniques, grouped according to applications, will be helpful. Techniques useful for ion diagnostics and other plasma measurements are also included. The ranges of applicability shown are not necessarily exclusive, but are intended only as qualitative guides. Elaboration on a few of the techniques will be given in subsequent sections. A much more extensive discussion may be found in Huddlestone and Leonard, ed., *Plasma Diagnostic Techniques* (Academic Press, New York, 1965).

ELECTRON DENSITY AND DISTRIBUTION

(*a*) Microwave interferometer; $10^{10} < n_e < 10^{14}$ cm^{-3}.
(*b*) Microwave cavity perturbation; $10^{8} < n_e < 10^{12}$ cm^{-3}.
(*c*) Rf-conductivity probes; $10^{8} < n_e < 10^{15}$ cm^{-3}; for high collision rates.
(*d*) Microwave scattering; $10^{12} < n_e < 10^{14}$ cm^{-3}; sensitive to instabilities.

(*e*) Optical interferometer; $10^{14} < n_e < 10^{19}$ cm^{-3}.
(*f*) Optical Faraday rotation; $n_e > 10^{16}$ cm^{-3} for 10,000 gauss.
(*g*) Optical spectroscopic intensities; $n_e > 10^{13}$ cm^{-3}; equilibrium plasmas.
(*h*) Optical scattering; $10^{14} < n_e < 10^{19}$ cm^{-3}.
(*i*) Optical Balmer series limit; $10^{13} < n_e < 10^{15}$ cm^{-3}.
(*j*) Particle collectors; $10^{-6} < J_e < 1$ amp/cm^2; yields product qn_ev.
(*k*) Electron or ion beam scattering; sensitive to potential fluctuations.

ELECTRON TEMPERATURE

(*a*) Microwave radiation intensities; $T_e \gtrsim 0.1$ eV; stable plasmas.
(*b*) Doppler broadening of cyclotron radiation line; $T_e \gtrsim 50$ eV.
(*c*) Infrared and optical intensities; $T_e \gtrsim 10$ eV; equilibrium plasmas.
(*d*) X-ray intensities; $T_e \gtrsim 6$ keV; wall problems.
(*e*) Relative intensities of spectral lines; $1 < T_e < 50$ eV.
(*f*) Relative intensities of bremsstrahlung and recombination radiation.
(*g*) Doppler broadening of optical (Thomson) scattering; $T_e \gtrsim 5$ eV.
(*h*) Langmuir probes; $0.1 < T_e < 1000$ eV; moderate densities.

ION DENSITY AND DISTRIBUTION

(*a*) Stark broadening of spectral lines; $n_i \gtrsim 10^{15}$ cm^{-3}.
(*b*) Langmuir probes, single and double.
(*c*) Electron, ion, neutral atom, or neutron beam probes; $n_i \gtrsim 10^{14}$ cm^{-3}.
(*d*) Diamagnetic effect (requires knowledge of temperature).
(*e*) Alfven and sound wave propagation; dense plasmas.
(*f*) Calorimetry (requires knowledge of temperature).
(*g*) Radioactive gas tracers and collimated detectors.
(*h*) Charge-exchange neutral detectors.

ION TEMPERATURE AND ENERGY

(*a*) Calorimetry; total energy and momentum.
(*b*) Doppler broadening of spectral lines; $T_i > 5$ eV.
(*c*) External energy–momentum analyzer; samples escaping ions.
(*d*) Time-of-flight; gives particle or shock front velocity.
(*e*) Diamagnetic effect; use magnetic probes inside and outside plasma.

NEUTRAL DENSITY, DISTRIBUTION AND IDENTITY

(*a*) Shielded ionization gauge.
(*b*) Ion or neutral atom beam scattering.
(*c*) Rayleigh scattering and resonance absorption of infrared and light photons by bound electrons.
(*d*) Schlieren and Mach-Zehnder photography.

(e) Charge-exchange detectors; fast neutrals.
(f) Molecular resonance spectroscopy; rf and infrared.
(g) Reionization by delayed ionizing pulses.

DRIFT VELOCITY, SHOCK VELOCITY, ROTATION, AND THRUST

(a) Doppler frequency of reflected microwaves.
(b) Doppler shift of synchrotron radiation.
(c) Doppler shift of spectral lines.
(d) Ballistics and calorimetry.
(e) Time-of-flight; probes, light, and microwave sampling.
(f) Nonreciprocity of phase shift for spacecharge and electromagnetic wave propagation.

INSTABILITIES AND TURBULENCE

(a) Electron and ion energy–momentum analysis; external measurement.
(b) Microwave radiation (nonthermal effects).
(c) Microwave scattering from turbulence.
(d) Electron and ion beam scattering.
(e) Fast photography, time-resolved spectroscopy and total light; high densities.
(f) Magnetic probes and Rogowsky loops.
(g) Langmuir and rf probes.
(h) External voltage–current measurements.
(i) X-rays (if high energy electrons are generated).
(j) Neutron energy analysis (if high energy ions are present).

SHEATH REGIONS

(a) Langmuir probes.
(b) Rf probes (sheath oscillations and spacecharge waves).
(c) Electron and ion beam probes.
(d) Microwave scattering from sheath oscillations.

CONSTITUENT IDENTITY (PURITY)

(a) Optical and atomic-resonance spectroscopy.
(b) Ion cyclotron resonance absorption; e/m ratio.
(c) Magnetic analyzer; escaping ions.
(d) Mass spectrometer; neutral gas.

10.2 Optical and infrared probing

Probing by means of light beams is, in principle, very similar to microwave probing, and the bulk of the theory developed in previous chapters applies with the addition that the increase in refractive index due to the neutral

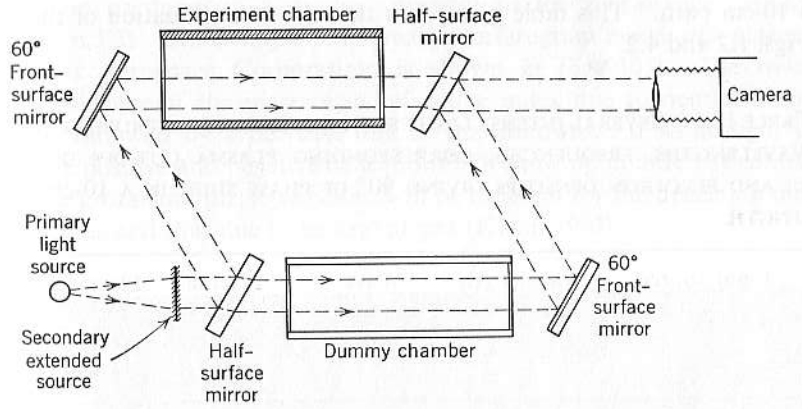

FIG. 10.1 Mach-Zehnder interferometer used for studies of plasma refractive index.

background gas in high density plasmas must also be accounted for. The techniques differ somewhat, but numerous parallels can be drawn (Alpher and White, 1959; Ascoli-Bartoli et al., 1960).

Optical interferometers that are direct analogs of the microwave interferometer are useful for dense plasma measurements. The Mach-Zehnder interferometer sketched in Fig. 10.1 is an example (Ascoli-Bartoli et al., 1963). A monochromatic light source is required; the smaller the wavelength spread, the sharper the interferences. Optical masers, or lasers (Schawlow and Townes, 1958; Javan et al., 1961; Lengyel, 1962), intrinsically are excellent monochromatic sources but, for transient events, it is difficult to achieve accurate timing without elaborate triggering arrangements. The giant pulse technique is a method to achieve fast triggering. A number of pulsed and CW lasers are now available commercially (Serchuk, 1962), covering wavelength ranges from 6900 to 72,000 Å (7.2μ). Spark and arc light sources, followed by a filter (Billings, 1951) or monochromator, are also useful for interferometers of medium resolution. Metal electrode spark sources can produce microsecond pulses of intense light, having jitter times of only a few nanoseconds. A filter accepts the desired line, rejecting the others, as well as plasma-generated light. The light from the source must be much more intense than that from the plasma, of course, at the wavelength of interest.

A tabulation of some useful intense monochromatic light sources is given in Table 10.1, together with wavelengths of peak outputs. Also shown are the oscillation frequencies, the corresponding plasma cut-off densities, and the electron densities required to give 90° of phase shift in

a 10-cm path. This table gives data that are a continuation of those in Figs. 1.2 and 4.2.

TABLE 10.1 SEVERAL INTENSE LIGHT SOURCES FOR OPTICAL PROBING, GIVING WAVELENGTHS, FREQUENCIES, CORRESPONDING PLASMA CUT-OFF DENSITIES n_c, AND ELECTRON DENSITIES GIVING 90° OF PHASE SHIFT IN A 10-cm PATH LENGTH

Light source	Wavelength (microns)	Wave frequency (cps)	Plasma cut-off density (cm^{-3})	Plasma density for $\Delta\Phi = 90°$ in $L = 10$ cm (cm^{-3})
Mg spark	0.3838	7.83×10^{14}	7.73×10^{21}	1.48×10^{16}
Hg^{198} arc	0.4358	6.89	5.89	
Ruby/Cr^3 laser	0.6943	4.33	2.32	8.05×10^{15}
Rb^{85} flash lamp	0.7800	3.85	1.835	7.16
	0.7948	3.78	1.77	7.04
Xenon flash lamp	0.8200	3.66	1.66	6.8
GaAs junction	0.90	3.34	1.38	6.2
$CaWO_4/Nd^3$ laser	1.06	2.83	9.9×10^{20}	5.25
He-Ne gas laser	1.153	2.60	8.40	4.85
	1.207	2.48	7.61	4.6
CaF_2/U^3 laser	2.6	1.15	1.64	2.13
Cs vapor laser	3.20	9.37×10^{13}	1.09	1.74
	7.18	4.18	2.17×10^{19}	7.78×10^{14}
Microwave ($\lambda = 1$ mm)	1000	3.33×10^{11}	1.35×10^{15}	1.5×10^{12}

A 0.1-μsec recording of the interferences obtained looking along the axis in the Scylla experiment at Los Alamos (Elmore et al., 1958), made with a giant pulse laser source, is shown in Fig. 10.2*a*. The high-density compressed plasma shows up plainly in the center. Figure 10.2*b* shows a recording of another event, in which flute instabilities were evident. The camera field of view was 8 cm in diameter, and the chamber length about 70 cm. The mirrors were aligned slightly tilted so that the background field contains several parallel interference fringes, with those due to the plasma superimposed.

Continuous time resolution of a one-dimensional slice of an experiment can be made by scanning with a slit and rotating mirror as a transient plasma event is occurring in the chamber to obtain a *streak interferogram* (Bennet et al., 1960; Ramsden and McLean, 1962). The fringes will be

shifted up or down in a display identical to the zebra-stripe display (Section 6.3.3). An example of a streak interferogram made on a plasma source at Aerospace Corporation, is shown in Fig. 10.3. The trace shows evidence of the increase in refractive index due to neutral atom density, followed by a decrease due to the electrons. If white light is used, the positive and negative deflections will show up in different colors, since the group and phase velocities will be different for the deflection due to electrons and that due to neutral atoms (Klein, 1963).

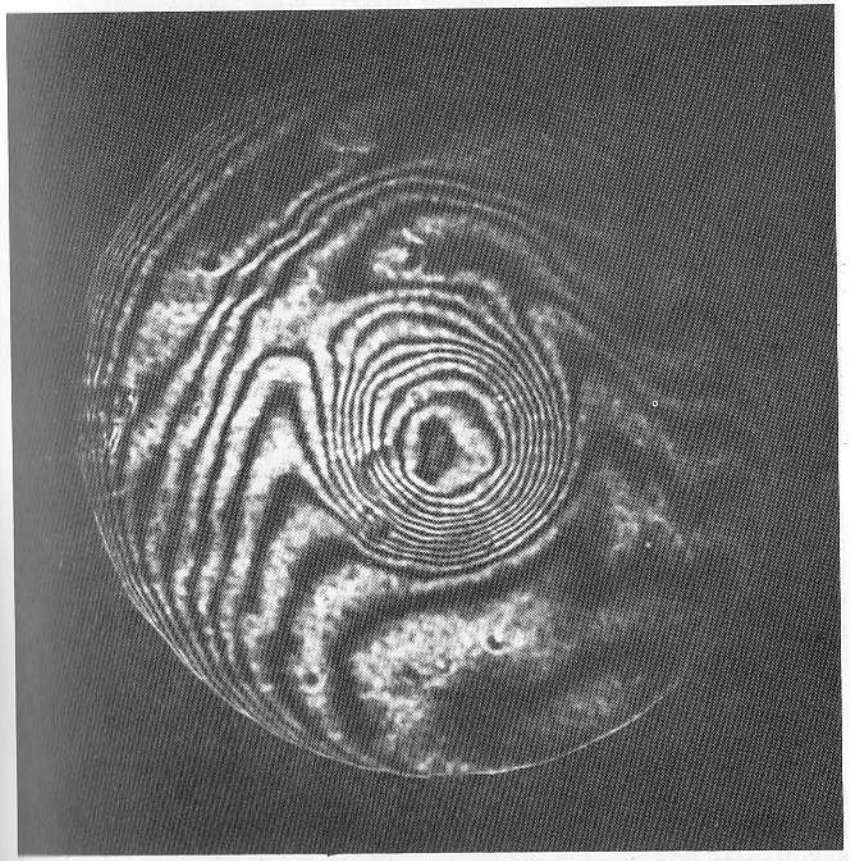

FIG. 10.2a Mach-Zehnder interferometer presentation of the refractive index in a cross section of the Scylla IV controlled fusion experiment. The 0.1 μsec exposure was made near the peak of the compression time, showing the high-density central core. The exposure was made by triggering a giant-pulse laser with a Kerr cell and light polarization prism. (Courtesy of W. E. Quinn, G. A. Sawyer, and F. L. Ribe, Los Alamos Scientific Laboratory, University of California, Los Alamos, N.M.)

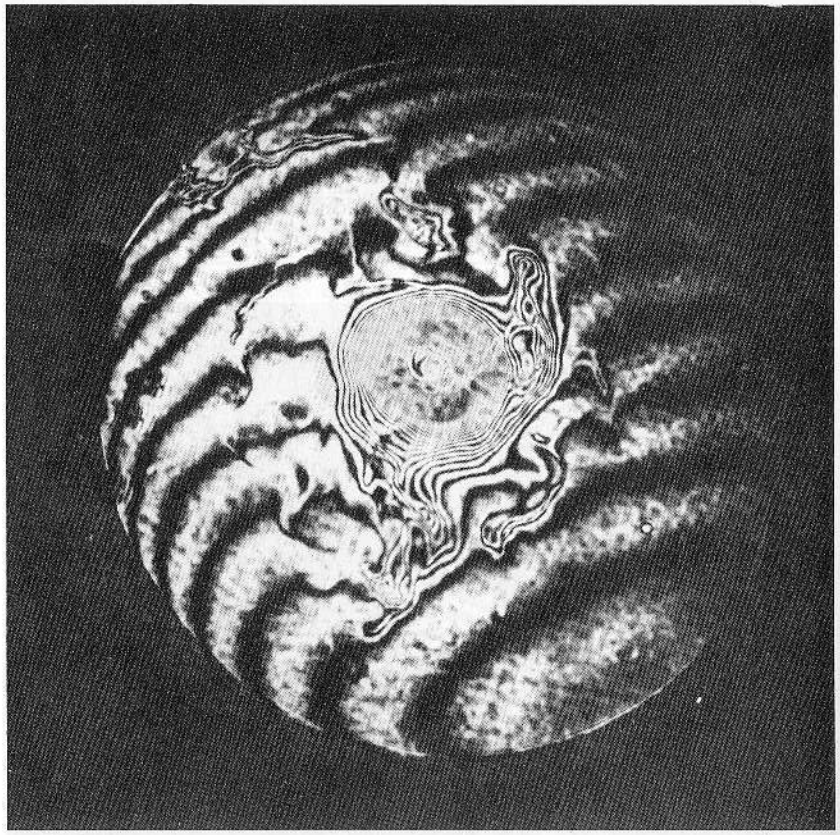

FIG. 10.2b Mach-Zehnder interferometer presentation as in Fig. 10.2*a*, but showing the turbulence due to a flute instability, developing at high compression ratios. (Courtesy of W. E. Quinn, G. A. Sawyer, and F. L. Ribe, Los Alamos Scientific Laboratory, University of California, Los Alamos, N.M.)

A similar optical arrangement is used for Schlieren photography, except that changes in refractive index are recorded as modulations of light intensity, rather than interference fringes. An experimental arrangement for studying shock waves is shown in Fig. 10.4 (Lovberg, 1963). The light source is a spark between tungsten electrodes in nitrogen. The accurate timing necessary to follow the fast front is obtained by a Kerr-cell light shutter. A typical photograph is shown in Fig. 10.5, showing the sharp electron density gradient in the "snow plow" front.

From Table 10.1, it is apparent that greater sensitivity for plasmas of medium density is obtained in the far infrared. Golay cell and bolometer

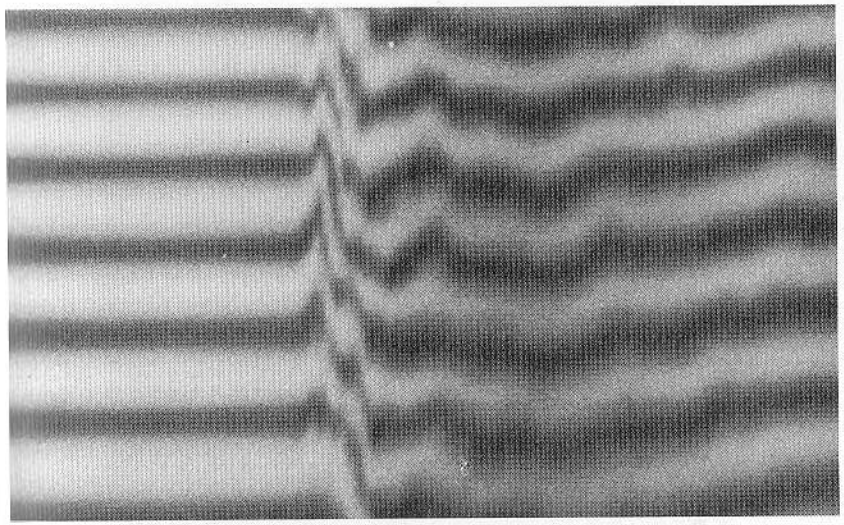

FIG. 10.3 Streak interferogram of the refractive index changes vs. time in an electromagnetic shock tube. The plasma is generated by a conical pinch driver (Scott and Josephson, 1957) in hydrogen at 2 torr. The Mach number was 20, at 18 inches down stream from the driver. The initial positive deflection of fringes ($+\Delta\mu$) is due to an increase in neutral density by compression and dissociation, followed by the negative deflection ($-\Delta\mu$) due to the electrons in the plasma. Peak electron density was 5.7×10^{16} cm^{-3}. (Courtesy of A. F. Klein, Aerospace Corp., Los Angeles, Calif.)

detectors are useful at wavelengths all the way across the infrared to the microwave band, although their response times are of the order of a second. Nevertheless, some plasma experiments have been done at infrared wavelengths (Brown, 1962; Harding et al., 1961) with results that compare favorably with microwave results.

Optical Faraday rotation can be used to study dense plasmas in strong magnetic fields (Dougal, 1963). The total rotation is given by (6.5.7), where the collisionless linear approximation is easily justified for these frequencies. Equation (6.5.7) then reduces to

$$\psi = 180^\circ \frac{L}{\lambda}\frac{n}{n_c}\frac{B/B_R}{1-B^2/B_R{}^2} \tag{10.2.1}$$

where B is the magnetic field and B_R is the magnetic field necessary to give gyroresonance, $B_R=\omega m/e$. As an example, the plasma density in a 10-cm path with 20 kilogauss applied, necessary to give 90° of rotation at $\lambda=2.6$ microns is 4.36×10^{18} cm^{-3}. The sensitivity increases in direct

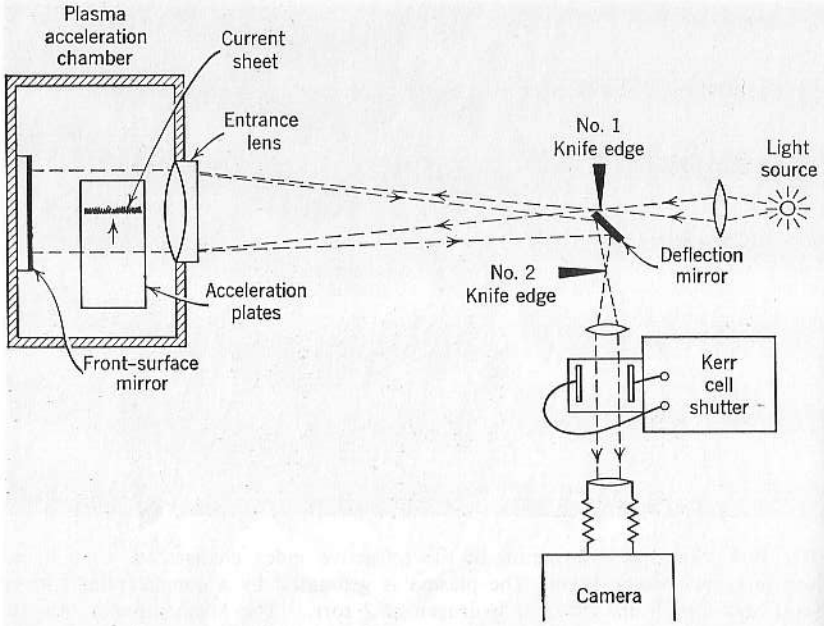

FIG. 10.4 Experimental arrangement for studying fast current sheets in a parallel-plate plasma accelerator by Schlieren photography. (Courtesy of R. Lovberg, General Atomic, San Diego, Calif.)

proportion to the density, the path length, and the magnetic field applied. Crossed polarization plates, sensitive to rotations as small as 5°, are experimentally feasible.

10.3 Conductivity probes

Plasmas having high collision rates have appreciable real components of conductivity, as can be seen from (1.3.14). A small rf coil immersed in such a plasma will induce currents in the plasma. The current is complex, the real part extracting power, and the imaginary part changing the coil's effective inductance by diamagnetic effects. Figure 10.6 shows two methods to measure the effect of the plasma on the coil. In Fig. 10.6*a*, the voltage across the coil is a measure of its impedance, and the phase angle in respect to the input voltage gives the relative magnitudes of J_i to J_r. In Fig. 10.6*b*, the unloaded coil is resonated at the drive frequency f_0. The plasma current then both detunes and de-Q's the circuit, much as in the resonant cavity cases in Section 5.1. Equation (5.1.2) may be used to calculate the loading as a function of conductivity. When

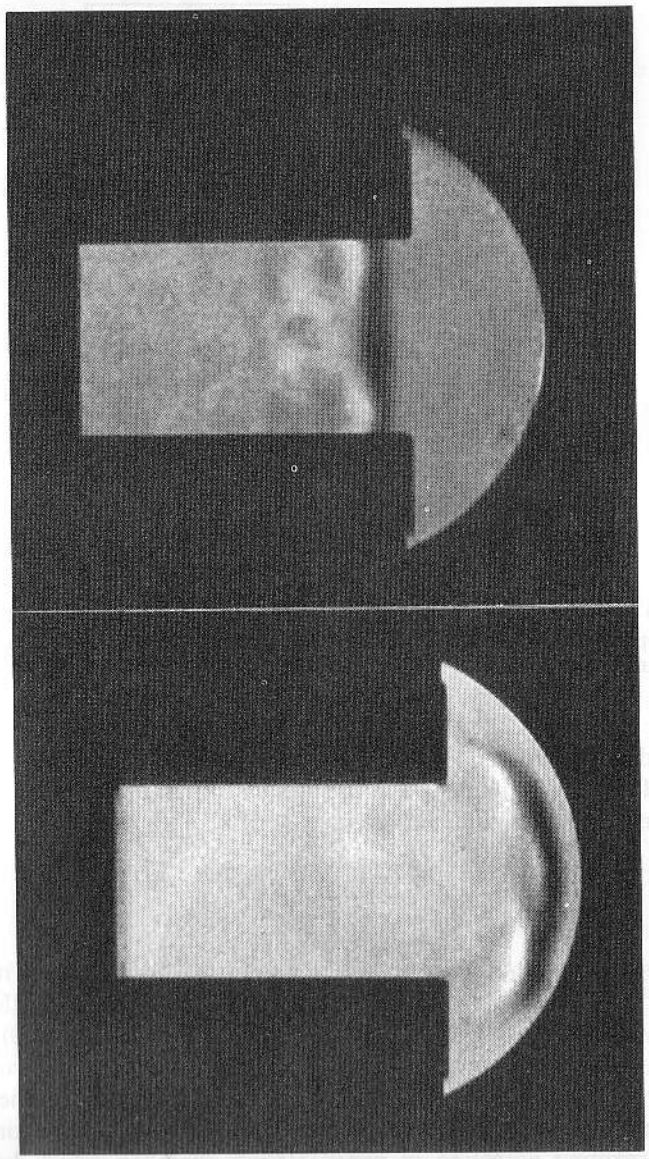

FIG. 10.5 Schlieren photographs of a current sheet, traveling at 7 cm/μsec between parallel plates in a plasma accelerator. (Courtesy of R. Lovberg, General Atomic, San Diego, Calif.)

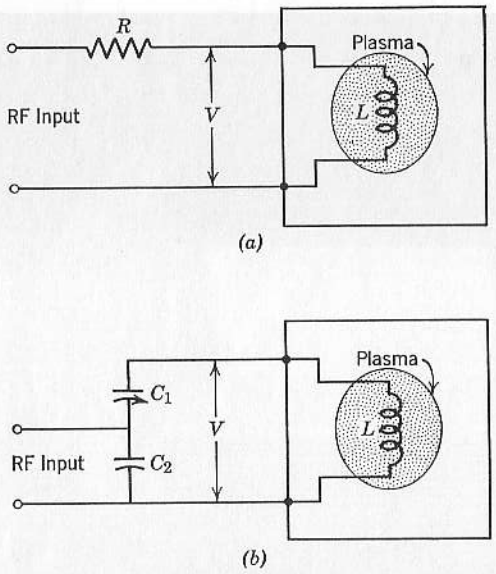

FIG. 10.6 Conductivity probes for high collision rate plasmas. In (*a*) the changes in coil impedance are measured. In (*b*) the changes in Q and f_0 of a resonant circuit are measured. $C_2 > 10C_1$; $R \approx \omega L$.

$\nu \gg \omega$ and $\omega_p \gg \omega$, the major effect of the plasma on the coil is in lowering its Q. If the coil is immersed in the plasma so that σ is uniform in space, (5.1.2) may be approximated as

$$\frac{1}{Q_1(t)} - \frac{1}{Q_0} = \frac{\sigma_r(t)}{\epsilon_0 \omega}. \tag{10.3.1}$$

In most experiments, however, σ is not uniform, since the coil is mounted on a form or otherwise obstructs the plasma. Calibration is then conveniently carried out with ionic solutions (van der Pol, 1920), whose conductivities can be measured directly with a platinum electrode conductivity cell. For example, the data of Fig. 10.7 were obtained in an experiment at Livermore, Calif. (Wharton and Hawke, 1962) from a coil wrapped around a section of pyrex plasma chamber, which had been removed and filled with a conducting solution. The Q was measured by observing the width δf at half-height of the frequency response, where

$$Q = \frac{f}{\delta f}. \tag{10.3.2}$$

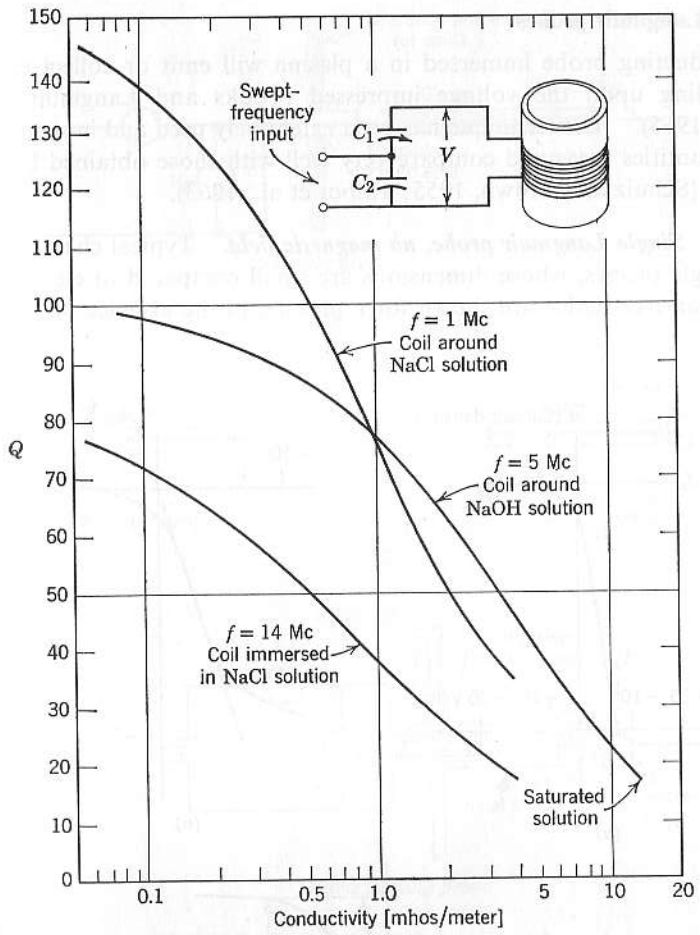

FIG. 10.7 Typical rf conductivity probe calibration data. The changes of Q of resonant circuits due to the conductivity of enclosed ionic solutions, for frequencies of 1, 5, and 14 Mc are shown. (After Wharton and Hawke, 1962.)

The center frequency f_0 was held constant by trimming C_1 slightly as the conductivity was varied. Q_0 was 105 for the 5-Mc coil and 85 for the 14-Mc coil, with distilled water in the chamber. A Faraday screen inside the coil helped reduce electrostatic effects between the coil and the solution, and the coil and the plasma, when later the assembly was used to study high density plasmas.

10.4 Langmuir probes

A conducting probe immersed in a plasma will emit or collect current, depending upon the voltage impressed (Tonks and Langmuir, 1929; Chen, 1965). The technique has been extensively used and in many cases the quantities measured compare very well with those obtained by other means (Schulz and Brown, 1955; Talbot et al., 1963).

10.4.1 ***Single Langmuir probe, no magnetic field.*** Typical characteristics for single probes, whose dimensions are small compared to electron and ion mean-free-paths, are shown for a plasma, in the absence of magnetic

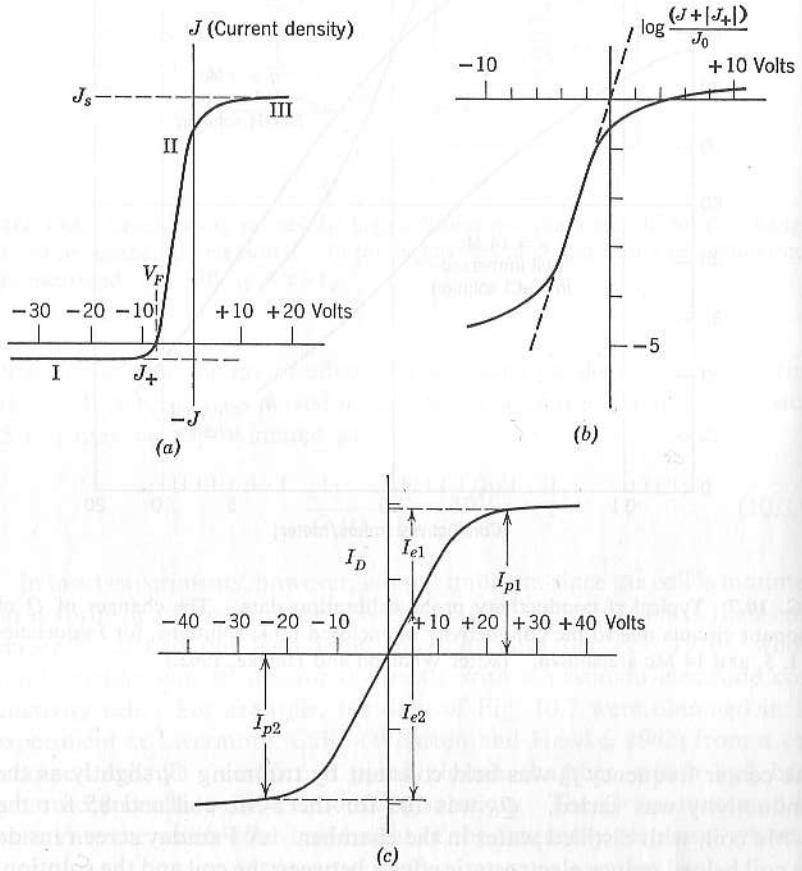

FIG. 10.8 Langmuir probe *V-I* characteristics. (*a*) Linear characteristic. (*b*) Logarithmic characteristic. (*c*) Double floating probe characteristic.

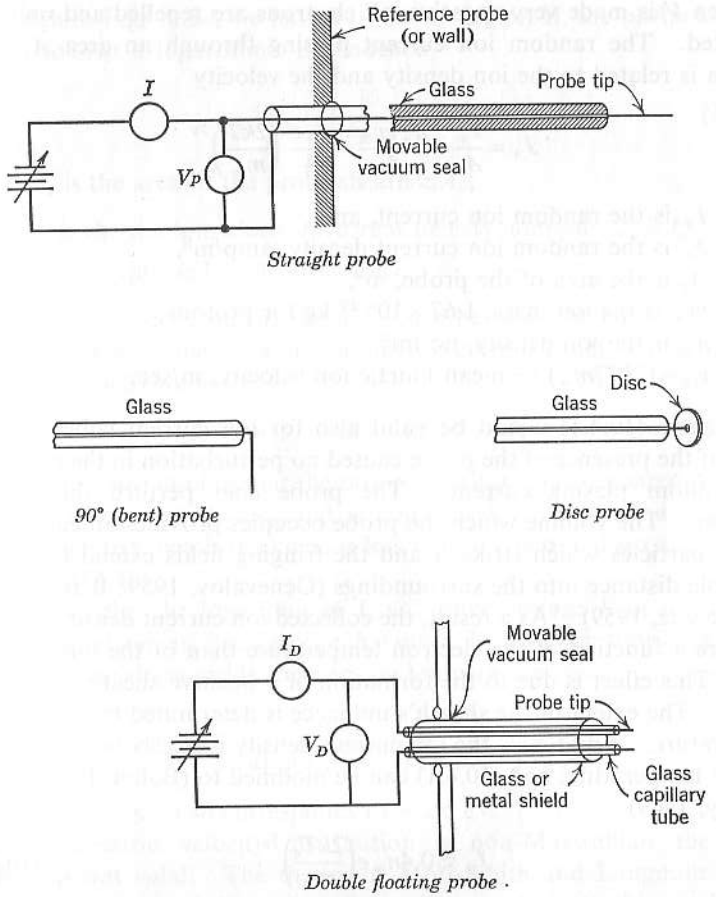

FIG. 10.9 Some typical Langmuir probes.

field, in Fig. 10.8. Sketches of some typical probes and their geometry are given in Fig. 10.9.

The probe potential is measured in respect to some convenient, fixed-potential point, such as the anode or walls of a discharge tube or a floating "wall probe," which has an area at least 50 times as large as the probe itself. The requirement that the potential difference between the plasma and the reference point remain fixed often excludes the use of the anode or chamber walls for this purpose because of current fluctuations. We shall presume, for our purposes, that the probe potential can be specified in respect to the plasma potential, and potential V refers to that value.

When V is made very negative, all electrons are repelled and only ions collected. The random ion current passing through an area A in the plasma is related to the ion density and the velocity

$$J_+ = \frac{I_+}{A_p} = \frac{n_+ e v_{th}}{4} = \frac{n_+ e}{4}\left(\frac{2kT}{m_+}\right)^{1/2} \tag{10.4.1}$$

where I_+ is the random ion current, amp,
J_+ is the random ion current density, amp/m^2,
A_p is the area of the probe, m^2,
m_+ is the ion mass, 1.67×10^{-27} kg for protons,
n_+ is the ion density, no./m^3,
$v_{th} = (2kT/m_+)^{1/2}$ = mean kinetic ion velocity, m/sec.

Equation (10.4.1) would be valid also for ion current collected by a probe if the presence of the probe caused no perturbation in the surrounding random plasma currents. The probe *does* perturb the plasma, however. The volume which the probe occupies provides an energy sink for all particles which strike it and the fringing fields extend for a considerable distance into the surroundings (Genevalov, 1959; Bernstein and Rabinowitz, 1959). As a result, the collected ion current density seems to be more a function of the electron temperature than of the ion temperature. This effect is due to the formation of a positive sheath around the probe. The extent of the sheath's influence is determined by the electron temperature. For $T_i \lesssim T_e$ the ion current density is nearly independent of the ion temperature, and (10.4.1) can be modified to (Bohm, Burhop, and Massey, 1949)

$$J_+ \approx 0.4 n_+ e\left(\frac{2kT_e}{m_+}\right)^{1/2}. \tag{10.4.2}$$

Secondary electrons emitted by the collected ions also give a positive current indistinguishable from the ion current. Various tests for secondaries, such as changing the work function or temperature of the probes, should be made to ascertain the magnitude of this error.

When the probe potential, V, is made less negative, a few of the high energy electrons are collected, partially canceling the positive ion current. As the potential is changed further in the positive direction, the random ion and electron currents collected just cancel. This probe-plasma potential, V_F in Fig. 10.8*a*, is the *floating potential*. For a thermalized plasma, this voltage is approximately $\frac{1}{2}kT_e$ (expressed in electron volts).

Increasing V beyond V_F results in a steep rise in electron current, in region II. This current eventually saturates at the *space potential* value, V_s, due to spacecharge limitation in current collection. According to

the sketch in Fig. 10.8*a*, we have $V_s = 0$. In region II, the probe electron current follows a logarithmic dependence

$$\ln I_e = +\frac{V}{kT_e} + \ln A_s J_0 \tag{10.4.3}$$

where A_s is the area of the probe sheath $\approx A_p$,

J_0 is the random electron current density, amp/m^2; $J_0 = J_s + |J_+|$,

kT_e is expressed in electron volts.

The total probe current is the difference between the electron current and ion current. Since it is the total probe current I that is measured, to find I_e in (10.4.3) we write

$$I_e = I + |I_+| \quad \text{and} \quad J_e = J + |J_+|. \tag{10.4.4}$$

Equation (10.4.4) implies that the probe sheath is thin compared to probe dimensions, so that $A_s \approx A_p$ and is constant in size. In many plasma experiments, the sheath thickness is less than 0.1 mm and we are justified in using (10.4.4).

When we plot the logarithm of J_e vs. probe voltage V or display the current signal on an oscilloscope having a logarithmic amplifier, as in Fig. 10.10, the slope yields the electron temperature

$$kT_e[\text{eV}] = \frac{dV}{d[\ln(J + |J_+|)]} \approx \frac{\Delta V}{\Delta[\ln(J + |J_+|)]}. \tag{10.4.5}$$

The slope of Fig. 10.8*b* corresponds to ~ 1.5 eV.

If the electron velocity distribution is non-Maxwellian, the above analysis is not valid. The theory of Mott-Smith and Langmuir (1926) in relating the second derivative of current by voltage to the distribution function applies, however. Practical techniques for extracting and displaying the second derivative have been developed by Medicus (1956) and Boyd and Twiddy (1959).

Unless a discharge is exceptionally quiet, it is difficult to hold all conditions constant long enough to plot out the V-I characteristic using milliammeters and voltmeters. The ability to swing the voltage rapidly and to record it and the resulting current on an oscilloscope are to be desired, even for steady-state plasmas, and are essential for transient discharges. A compromise must be struck. If the sweep rate is too slow, the plasma properties will change during the sweep. If the sweep rate is too fast the probe sheath will not have time to come to equilibrium, and the collected current will be in error. Also, too fast a sweep rate leads to displacement currents due to the capacitance of the probe and shielded leads running to

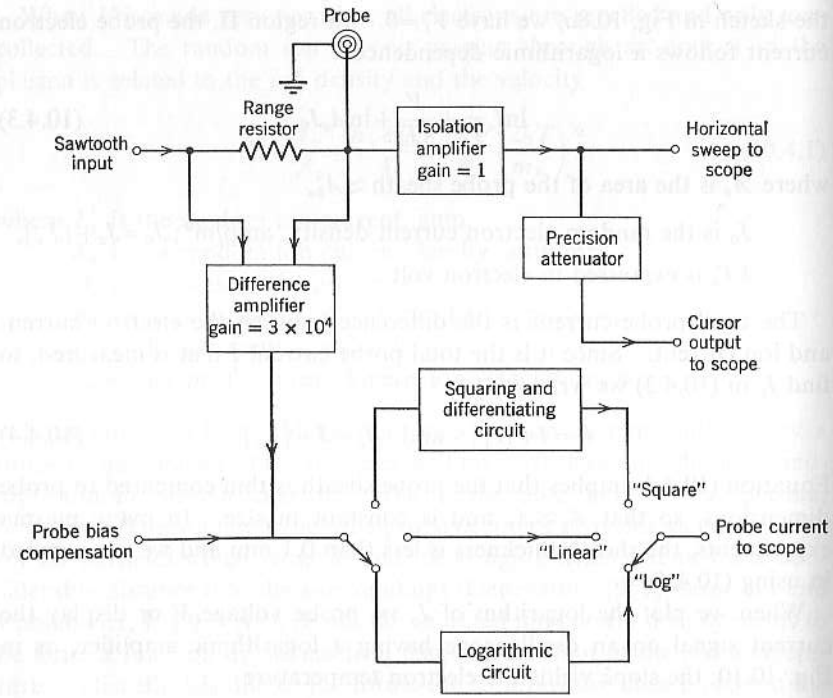

FIG. 10.10 Langmuir probe sweeper. In "Log" or "Square" position, the precision attenuator is adjusted to produce a cursor line having the same slope as the desired portion of the probe current trace. The reading on the multiturn potentiometer is calibrated directly in electron temperature or ion density. (After Harp, 1963.)

it. Sweeps rates of 1 to 10 volts per microsecond are commonly used, the main limitation in rate being caused by displacement currents and not sheath formation, which occurs typically in a fraction of a microsecond. An instrument that permits a direct reading of T_e, by sweeping the probe voltage and observing the logarithm of the current, is sketched in Fig. 10.10 (Harp, 1963).

Increasing the probe voltage beyond V_s does not cause J to rise much higher than J_s, due to spacecharge. The spacecharge saturation current is

$$I_s = J_s A_s \approx J_0 A_s = \frac{n_e e A_s}{4}\left(\frac{2kT_e}{m_e}\right)^{1/2}. \tag{10.4.6}$$

Comparing (10.4.6) with (10.4.2), we note that

$$\frac{J_s}{J_+} \approx \left(\frac{m_+}{2m_e}\right)^{1/2}. \tag{10.4.7}$$

The electron density is determinable from (10.4.6) and the ion density from (10.4.2). In many plasmas the two are essentially the same, giving us a cross check on the measurement of n.

In region III of the curve (Fig. 10.8*a*) the stray electric field in the plasma due to the probe may be very large, and considerable perturbation occurs. For example, the density decay time in afterglow measurements and in controlled-fusion containment experiments may be considerably shortened by the presence of only a 0.5-mm diameter probe. In discharges maintained by fairly small cathode currents, such as P.I.G. or reflex types, the character or mode of discharge may be completely altered as the probe voltage is swung from V_F to V_S.

10.4.2 ***Single probe with a magnetic field.*** When a magnetic field is present, of such strength that the electron cyclotron radii are comparable to the probe dimensions, the situation is drastically altered. Since the effective mean-free-paths also are now comparable to probe dimensions, the electron spacecharge saturation current is considerably reduced. It is only the mobility transverse to the field which is impaired, however, and electrons may flow along the lines essentially unimpeded, so that the probe may actually be sampling the conditions in the plasma some distance away. There may also be a "short-circuiting" effect if magnetic lines connect the probe with metallic surfaces, so that current can flow in the metal across the field lines.

Since the ion gyroradius is much bigger than that of electrons, the ion saturation current J_+ is not much affected until the field strength is fairly large.

By orienting the axis of the probe either along or across the field lines, the collection of electrons across and along field lines, respectively, may

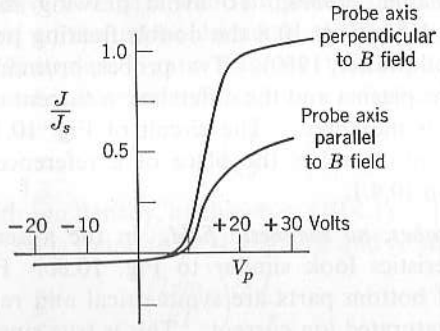

FIG. 10.11 Typical langmuir probe characteristics with probe oriented along and across magnetic field lines.

be observed. The qualitative comparison is shown in Fig. 10.11, indicating the large reduction in J_s/J_+ for collection across the field. The slopes at low current values are seen to be essentially the same and, at moderate field strengths, the logarithmic plot still yields valid electron temperatures (Bohm et al., 1949).

10.4.3 ***Single probe: miscellaneous effects.*** Besides the perturbations which the probe produces in the plasma, there are certain plasma perturbations upon the probe. The most serious of these is destruction, either partial or complete. A probe, immersed in plasma, suffers continual bombardment, which evaporates away metal, and plates it on surrounding surfaces, including the insulating probe support. This may either decrease the current-collecting area or increase it, depending upon whether the metal gets away or is plated onto the insulating support adjacent to the probe tip. If the latter occurs, the collecting area may suddenly increase a hundredfold over an hour's time.

In high-temperature plasmas, the probe may be bombarded so violently that it glows red hot and evaporates at a fast rate. In the extreme, for example in controlled fusion work, the probe may have vanished after a few minutes' operation.

The presence of metastable ions near the probe may lead to abnormal current collection, when the ions strike the probe and lose electrons. Incident uv light and X-rays also lead to abnormal currents due to photo emission, and high energy ions striking the probe may give secondary emission.

In transient plasma measurements, if the reference point is the anode or chamber wall, the plasma–anode or plasma–wall potential may fluctuate considerably. The apparent floating potential, V_F, then fluctuates and, again, the collected current is wild.

10.4.4 ***Double floating probes.*** To avoid drawing the large electron currents of region III in Fig. 10.8 the double floating probe technique is useful (Johnson and Malter, 1950). Two probes, ordinarily of equal area, are inserted into the plasma and the difference in current due to an applied voltage difference is measured. The circuit of Fig. 10.10 may be used, where the second probe takes the place of a reference wall probe, as discussed in Section 10.4.1.

10.4.5 ***Double probes, no magnetic field.*** In the absence of magnetic field, the characteristics look similar to Fig. 10.8*c*. For equal probe areas, the top and bottom parts are symmetrical and represent only the magnitude of the saturated ion current. This is true since the sum of the probe currents must be zero and, when the negative probe reaches ion saturation, the current of the positive probe must also saturate. The

saturation value is again given by (10.4.2) if the electron temperature is known. Since a plasma is grossly neutral, we may usually presume that $n_e = n_+$.

To find the electron temperature, we may use (10.4.3) again. It will be convenient to rewrite it in the notation used in Fig. 10.8*c*. We shall be very general and presume that the probe areas are not equal and therefore $I_{p1} \neq I_{p2}$.

Since the net current to the system must be zero,

$$I_{p1}+I_{p2}=\sum I_p=I_{e1}+I_{e2}=A_1J_0\exp(\phi V)+A_2J_0\exp(\phi V) \qquad (10.4.8)$$

where $A_{1,2}$ are the areas of the respective probes,

J_0 is the random electron space current density,

$V_{1,2}$ are the plasma-to-probe potentials,

$V_D = V_2 - V_1$,

$I_D = I_{p1} - I_{e1} = I_{e2} - I_{p2}$,

$$\phi = \frac{e}{kT_e} = \frac{1}{T_e[\text{eV}]} = \frac{11{,}600}{T_e[^\circ\text{K}]}.$$

The logarithm of (10.4.8) is

$$\ln\left[\frac{\sum I_p}{I_{e2}} - 1\right] = -\phi V_D + \ln\frac{A_1}{A_2}. \qquad (10.4.9)$$

The slope of (10.4.9) plotted against V_D yields the electron temperature, just as in Section 10.4.1.

10.4.6 ***Double probes in a magnetic field.*** Double probes are not influenced as much by magnetic fields as single probes. The collected current is governed by ion mobility, and it is not until the magnetic field strength is very large (several thousand gauss) that the ion gyroradius is as small as the probe size.

When the negative voltage is sufficiently large that the sheath thickness is large compared to the probe diameter, the theory of Langmuir and Mott-Smith (1924) applies, even in magnetic fields up to several thousand gauss. The current-voltage relationship then follows a square law

$$J = J_+ \frac{2}{\pi}\left(\frac{eV}{kT}+1\right)^{1/2}. \qquad (10.4.10)$$

J_+ is linear with ion density, as shown in (10.4.1). The ion density, far out in region I, then is found to be (Langmuir and Mott-Smith, 1924)

$$n_+ = \left(\frac{2\pi m_+}{kT_+}\right)^{1/2}\frac{J_+}{e} \qquad (10.4.11a)$$

$$= 3.32\times 10^{11}\frac{S^{1/2}}{A}\left(\frac{m_+}{m_e}\right)^{1/2} \qquad (10.4.11b)$$

where S is the slope of I^2 vs. V expressed in amperes and volts, and A is the effective collecting area of the probe sheath. Gardner (1962) expresses the relationship in terms of current density, not specifying A, but assuming that it remains constant as V varies

$$n_+^2 = -\frac{d(J_+^2)}{dV}\frac{\pi^2 m_+}{2e^3}. \tag{10.4.12}$$

The circuit of Fig. 10.10, in the switch position marked "Square," gives direct readings of n_+^2, when the cursor slope has been calibrated.

10.4.7 ***Double probes: miscellaneous effects.*** Although floating probes represent less of a perturbation than a single probe in an equilibrium discharge, when the ion temperature is well above the neutral gas temperature any kind of an object in the plasma leads to severe energy loss. The probe element suffers from bombardment and, even though it floats, it possesses capacitance, which tends to hold its potential fixed long enough to expose it to arcing, which of course melts the elements away.

10.5 Plasma wave and resonant probes

When plasma waves or oscillations are present, they may be detected with probes. Spacecharge waves may also be launched with probes, but this method of launching tends to excite all modes. Langmuir-type probes, having coaxial shields brought up near the collecting surface, are adequate for many measurements up to frequencies of 1000 Mc (Bailey and Emeleus, 1955). A pair of small disc probes has been used successfully to measure ω_p in dilute plasmas (Yeung and Sayers, 1957) and, in fact, wire and disc probes were used in experiments that probably were the first microwave diagnostic measurements (van der Pol, 1920).

When a current-collecting probe simultaneously has a large rf voltage applied to it, the nonlinear sheath characteristics cause rectification of the rf signal. The d-c current is thus altered a small amount. The rf electric field around the probe is maximum at a frequency near the plasma frequency, leading to an increase in the rectified direct current as the applied frequency is swept through the local plasma frequency (Takayama et al., 1960; Ikegami and Takayama, 1963). The probe, of course, perturbs the plasma and thus the frequency measured is slightly below the true plasma frequency.

Resonant probes, fed by transmission lines (Levitskii and Shashurin, 1961), permit measurement of the plasma impedance, plasma density, and guide wavelength (see Sections 5.5 and 5.6). Probes loosely coupled to a tunable filter, such as a motor-driven coaxial resonator (Malmberg et al., 1963), permit rapid analysis of the frequency spectrum of oscillations picked up in the plasma, or as a means to filter received signals. The movable probes shown in Fig. 9.47 were used for these purposes.

10.6 Magnetic probes

Small inductive probes immersed in the plasma will have voltages induced in them by changes in the local magnetic field, dB/dt (Glasstone and Lovberg, 1960; Colgate et al., 1958). Field sensitive elements, such as Hall current probes, measure the instantaneous magnitude of the magnetic field B. Magnetic probes may be made as small as 1 mm in diameter and grouped in x-y-z arrays to measure three-dimensional field configurations (Pollock et al., 1960). Current density contours and the presence of hydromagnetic instabilities in dense plasmas are measured by a linear array across current channels. The data can be displayed by rapid sampling. The output voltage of the coil-type probe may be integrated to yield the magnitude of field. The resulting signals are very small (depending on the integration time), and care must be used to avoid stray pickup. Hall probes have outputs of a volt or so, response times up into the megacycles, and are easily calibrated with a standard magnet. They are somewhat temperature sensitive.

Another kind of coil assembly that measures rates of change in enclosed current channels is the Rogowsky loop or girdle (Golovin et al., 1958; Cooper, 1963). The assembly consists of two sets of coils, one around the entire experimental region and the other around only the current channel or a part of it. The difference in induced voltage represents the currents not enclosed, such as wall currents. The coils may be segmented, with leads brought out separately, to indicate current profiles.

Low inductance coils can also be used to pick up high frequency fluctuations, such as those associated with ion-wave instabilities or ion-cyclotron-frequency instabilities. These frequencies are typically from 10 kc to 10 Mc.

10.7 Ballistic probes

The measurement of thrust, shock intensity, and momentum transfer by plasmas is possible by using ballistic probes (Marshall, 1958). Considerable care is required to avoid electrostatic force deflections and thermal shock deflections. Piezo-electric transducers (Stern and Dacus, 1961) are particularly useful, since they can be driven by insulated pickup probes and produce an output voltage having very fast time response. These transducers are also sensitive to thermal shock produced by intense light pulses (for example, laser beams) or microwave pulses (White, 1962).

10.8 Optical spectroscopy

Spectroscopy is a very large subject in itself, having wide and well-developed applications to nearly all categories of plasma research. At best, we can only hope to give a few of the highlights in this section, indicating where fuller treatments of the various spectroscopic techniques may be found.

10.8.1 ***Constituent identity and state.*** Identification of radiating species has been studied perhaps longer than any other of the spectroscopic techniques, and numerous tables of line wavelengths, intensities, and related information exist (*Chemical Rubber Handbook*, 1962; M.I.T Tables, 1955; Kelly, 1959; and *A.I.P. Handbook*, 1963). A photographic plate exposed in a calibrated spectrograph can reveal immediately a great deal of qualitative information about the degree of ionization, whether molecular dissociation is occurring, what impurities are present, and even some knowledge of the electron temperature by observing the highest ionization potentials excited. The one-dimensional extent of the various species is obtained from the lengths of the lines. The presence of a continuum between the lines indicates the presence of recombination or bremsstrahlung. A quantitative examination of the lines, such as with a line splitter (Scott et al., 1962) or microdensitometer, then reveals detailed information about plasma properties (Wulff, 1959).

Of the three types of line broadening, only the Stark and Doppler broadening give measurable effects in most normal plasmas. Collisional or pressure broadening is generally a very small effect. Zeeman splitting of lines, if observable in laboratory plasmas, gives information on the local magnetic field strength. Field strengths of 50 to 100 kilogauss are required to be able to see the effect at all, in most cases.

10.8.2 ***Stark broadening.*** In high-density, low-temperature plasmas ($n \gtrsim 10^{15}\text{cm}^{-3}$, $T_e \lesssim 4$ eV) the spectral lines are shifted and broadened by the electric fields due to ions and electrons. In the Holtsmark theory (Griem, 1960), the line profile is described by a slowly varying function $S(\alpha)$

$$\int_{-\infty}^{\infty} S(\alpha)\, d\alpha = 1 \tag{10.8.1}$$

where $\alpha = \Delta\lambda / F_0$

$F_0 = 2.61\, en^{2/3}$ = the Holtsmark normal field strength

n = electron and ion density, number/cm^3

$\Delta\lambda$ = displacement from unperturbed line, Å

e = electron charge

$S(\alpha)$ is a complicated function, and it is convenient to use either approximations or tabulated values (Griem, Kolb, and Shen, 1959; Underhill and Waddell, 1959). Several modifications to the Holtsmark theory have been made to account for correlations among ions (Margenau, 1932, 1951) and for nonadiabatic effects. The density dependence, nevertheless, does not depart much from the $n^{2/3}$, especially in the wings of the Balmer and Lyman series lines. Some lines exhibit linear Stark effect and others quadratic effects; the total broadening is calculated by summing over all of the Stark coefficients.

Typical measurements of *Stark broadening* range from a fraction of an angstrom for the N IV 3479 Å line due to a 5% N_2 impurity in a 10^{17} cm^{-3} D^+ plasma (Lukyanov and Sinitsin, 1958) to tens of angstroms in dense H_2 plasmas having $n \approx 10^{16}$ cm^{-3} (Wilcox et al., 1961). The *Stark shift*, which is generally quite small, has a slight temperature dependence and a density dependence $\sim n_e^{1.22}$ (Margenau, 1951).

10.8.3 ***Doppler broadening.*** The relative velocity, v, of a radiating atom in respect to the observer leads to a doppler shift of the radiation frequency

$$\Delta\nu = \nu - \nu_0 = \nu_0\, v/c. \tag{10.8.2}$$

If the emitting atoms are in kinetic equilibrium, this leads to a gaussian line shape for the doppler broadening

$$S_D(\nu) = \frac{\pi^{-1/2}}{\delta\nu_D} \exp\left[-\left(\frac{\nu-\nu_0}{\delta\nu_D}\right)^2\right]. \tag{10.8.3}$$

The doppler half-width in frequency or wavelength is

$$\frac{\delta\nu_D}{(\ln 2)^{1/2}\nu_0} = \frac{\delta\lambda_D}{(\ln 2)^{1/2}\lambda_0} = (\ln 2)^{1/2}\left(\frac{2kT_i}{Mc^2}\right)^{1/2} \tag{10.8.4}$$

where M is the ion mass. For example, the doppler broadening of the Balmer H_β line is approximately

$$\frac{\delta\lambda_D}{\lambda_0} \approx 4 \cdot 10^{-5}\, (T_{H^+}[\text{eV}])^{1/2}. \tag{10.8.5}$$

In terms of the intensity at the line center, I_0, the intensity $I(\nu)$ is

$$I(\nu) = I_0 \exp\left[-\frac{Mc^2}{2kT}\left(\frac{\nu-\nu_0}{\nu_0}\right)^2\right]. \tag{10.8.6}$$

Typical line half-widths are between 0.3 to 30 Å for hydrogen ion temperatures between 10^5 to 10^9 °K.

Transient plasmas often are not reproducible from pulse to pulse, and it is desirable to observe the line profile completely with each shot. A line

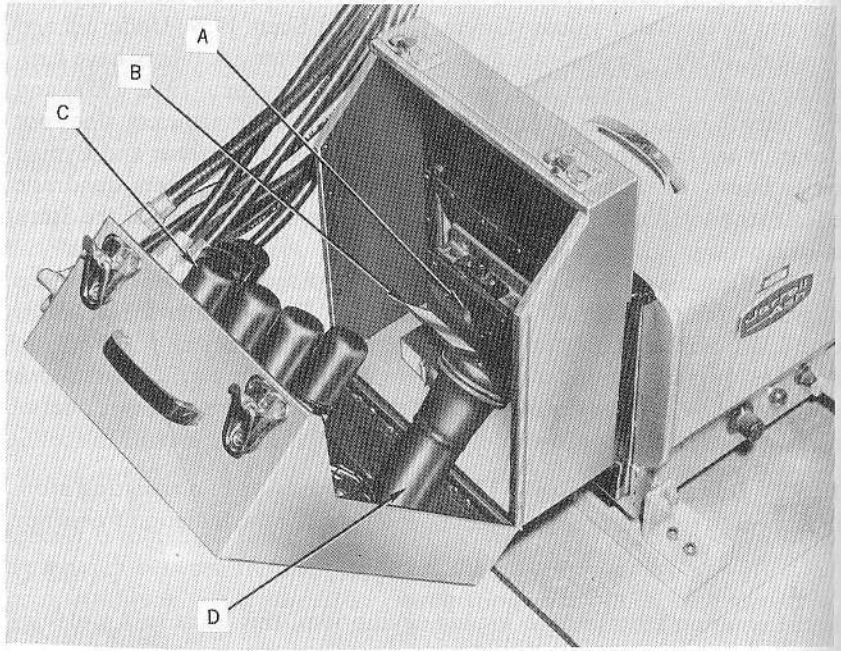

FIG. 10.12 Optical line splitter assembly, showing the exit slit with the cylindrical lens *A*, the deflection mirror *B*, the photomultiplier array *C*, and the light-tight entrance tube *D*. (Courtesy of F. R. Scott, General Atomic, San Diego, Calif.)

splitter (Scott et al., 1962) permits a sampling of a broadened line at six intervals over a narrow wavelength band. A cylindrical lens, attached to a 250μ-wide slit on a 500-mm JACO monochromator, allows a variation in the dispersed band from 0.04 Å/mm to 18 Å/mm. Seven 1P21 photomultipliers are used as detectors. The instrument is shown in Fig. 10.12. Besides giving the profile shape, if the detector outputs are observed for signal time correlation, one can determine if the broadening is true doppler (thermal) broadening or due to mass motions in the plasma.

10.8.4 ***Doppler shift.*** If the plasma as a whole is moving (mass motion), the emission lines will be shifted in wavelength. In a rotating plasma, the spectral lines originating in that part of the plasma moving toward the observer will be shifted to shorter wavelengths and *vice versa*. If the entrance slit to the spectrometer spans the plasma diameter, the lines will be tilted, leading to the *slant effect* (Dickerman and Morris, 1961).

10.9 Bremsstrahlung and recombination continuum

The radiation from free-free and free-bound transitions (see Section 7.3) also may be analyzed in the X-ray, ultraviolet, optical, or infrared wavelengths as a diagnostic technique. In the optical spectrum, this radiation appears as a continuum between the emission lines. The continuum is made up of bremsstrahlung radiation (due to the acceleration of electrons during collisions), from high, overlapping harmonics of synchrotron radiation (due to acceleration of electrons between collisions), and from recombination radiation (due to the radiative capture of electrons into the bound states of atoms). The contributions of these three depend, in different manners, on the electron density and temperature and on the wavelength at which observations are made. For example, in equilibrium hydrogen plasmas (electrons having a Maxwellian velocity distribution), the difference in background intensities of the Balmer continuum (that is, the background intensity between Balmer series lines) and that just beyond the series limit ($\lambda < 3642$ Å) is strongly dependent on the electron temperature, but not very sensitive to density (McWhirter, 1965). The absolute intensity of the continuum, however, is proportional to $n_e n_i$, with a square-root dependence on temperature. At short wavelengths, then, where effects of impurity radiation are not too serious, the electron density can be measured by absolute intensity measurements of the continuum (Glasstone and Lovberg, 1960; McWhirter et al., 1959).

The frequency dependence of the continuum intensity (that is, the shape of the spectral intensity curve) is a strong function of temperature in other portions of the spectrum away from the Balmer series limit as well, especially if there is self absorption. For example, in the far infrared the bremsstrahlung continuum merges into blackbody radiation. In experiments at Harwell, England, by Harding and Roberts (1961), the gap between optical and microwave radiation was bridged by the use of a special far infrared spectrometer, covering wavelengths of 0.1 to 2.0 mm. The radiation intensities were found to follow blackbody curves quite well up to about the plasma frequency and then to saturate, becoming insensitive to further changes in frequency. The experimental curves had the general shape of Fig. 7.7*a*.

APPENDIX A

Review of electromagnetic wave propagation

The purpose of this appendix is to review the well-known arguments of electromagnetism leading to the concepts of complex conductivity and dielectric constant and to wave propagation in a general lossy medium. The final sections consider microscopic fields and the Lorentz-term paradox, and propagation in anisotropic media. For a more extensive discussion of these matters, see von Hippel's *Dielectrics and Waves* (Technology Press/Wiley, New York, 1954), and also the standard treatises on electromagnetism by Panofsky and Phillips, Jackson, Stratton, and others.

A.1 Basic relations for a linear medium

Maxwell's equations for a macroscopic medium are, in rationalized mks units,

$$\nabla \cdot \mathbf{D} = \rho \tag{A.1}$$

$$\nabla \cdot \mathbf{B} = 0 \tag{A.2}$$

$$\nabla \times \mathbf{E} = -\frac{\partial \mathbf{B}}{\partial t} \tag{A.3}$$

$$\nabla \times \mathbf{H} = \mathbf{J} + \frac{\partial \mathbf{D}}{\partial t} \tag{A.4}$$

where ρ is the volume density of free charge and $\mathbf{J}$ the explicit current density. The field vectors $\mathbf{E}$, $\mathbf{D}$, $\mathbf{B}$, and $\mathbf{H}$ are related by the constituitive relations

$$\mathbf{D} = \epsilon_0 \mathbf{E} + \mathbf{P} \tag{A.5}$$

$$\mathbf{H} = \frac{\mathbf{B}}{\mu_0} - \mathbf{M} \tag{A.6}$$

where $\mathbf{P}$ and $\mathbf{M}$ are the *polarization* and *magnetization* (net dipole moments per unit volume) and ϵ_0, μ_0 are the usual dimensional constants of mks units.[1] In the case of a *linear, isotropic* medium

$$\mathbf{P} = \Psi_e \epsilon_0 \mathbf{E} \tag{A.7}$$

$$\mathbf{M} = \Psi_m \mathbf{H} \tag{A.8}$$

where Ψ_e and Ψ_m, the electric and magnetic *susceptibilities*, are constants characteristic of the medium.[2] For this linear case, the constituitive relations (A.5) and (A.6) reduce to

$$\mathbf{D} = \epsilon \mathbf{E} = \kappa \epsilon_0 \mathbf{E} \tag{A.9}$$

$$\mathbf{H} = \frac{\mathbf{B}}{\mu} = \frac{\mathbf{B}}{\kappa_m \mu_0} \tag{A.10}$$

where ϵ and μ are the *permittivity* and *permeability* of the medium and

$$\kappa = 1 + \Psi_e \tag{A.11}$$

$$\kappa_m = 1 + \Psi_m \tag{A.12}$$

are the *dielectric constant* (or *relative permittivity*) and *relative permeability*. Likewise a linear, isotropic medium obeys Ohm's law,

$$\mathbf{J} = \sigma \mathbf{E} \tag{A.13}$$

where σ is the *conductivity*.[3] Thus the electromagnetic properties of a linear, isotropic medium are specified by the three independent constants κ, κ_m, and σ.

[1] The mks units of these various quantities are

$\mathbf{E}$	volt/meter
$\mathbf{D}$, $\mathbf{P}$	coulomb/meter^2
$\mathbf{B}$	weber/meter^2 $= 10^4$ gauss
$\mathbf{H}$, $\mathbf{M}$	ampere/meter
ρ	coulomb/meter^3
$\mathbf{J}$	ampere/meter^2

$1/4\pi\epsilon_0 = 10^{-7}c^2 \approx 9 \cdot 10^9$ meter/farad (c = velocity of light)

$\mu_0/4\pi = 10^{-7}$ henry/meter.

[2] We follow convention here in writing $\mathbf{M}$ proportional to $\mathbf{H}$, rather than to the average microscopic field $\mathbf{B}$.

[3] Many authors use *mobility*, defined as the ratio of average electron velocity to electric field, rather than conductivity in discussing ionized gases. Thus, mobility equals σ/ne. If more than one species of charged particle contributes to the current, the conductivity is $\sigma = \sum_k \sigma_k = \sum_k n_k q_k \mathcal{M}_k$, where n_k, q_k, and $\mathcal{M}_k$ are the density, charge, and mobility of the kth species.

From an energy point of view, the constants κ and κ_m measure energy *stored* in the "stretching" or alignment of electric and magnetic dipoles by the respective fields. The conductivity σ measures energy *dissipated* by collisions or other relaxation processes. Thus, κ and κ_m measure the *reactive* properties of the medium, while σ measures the *resistive* properties.

A.1.1 ***Complex dielectric constant or conductivity.*** Consider oscillatory fields with time dependence

$$\exp j\omega t. \tag{A.14}$$

Faraday's and Ampere's laws (A.3) and (A.4) become

$$\nabla\times\mathbf{E}=(-j\omega\kappa_m\mu_0)\mathbf{H} \tag{A.15}$$

$$\nabla\times\mathbf{H}=(\sigma+j\omega\kappa\epsilon_0)\mathbf{E}. \tag{A.16}$$

If the medium exhibits dispersion, σ, κ, and κ_m are functions of frequency. The form of (A.16) makes it convenient to incorporate *one* of the two constants σ, κ in the *other* by means of complex notation. This technique is directly analogous to the familiar representation of the resistive and reactive processes of circuit theory by a complex impedance.

In the case of ordinary dielectrics and wave propagation, it is customary to define a complex dielectric constant such that

$$\sigma+j\omega\kappa\epsilon_0 \rightarrow j\omega\breve{\kappa}\epsilon_0 \tag{A.17}$$

or

$$\breve{\kappa}\equiv\kappa_r-j\kappa_i=\kappa-j\frac{\sigma}{\omega\epsilon_0}, \tag{A.18}$$

where we use the symbol $\cup$ to denote a complex quantity and the subscripts r and i to indicate real and imaginary parts.[4] The a-c κ_i may include hidden dissipative currents (such as dielectric hysteresis loss) in addition to currents resulting from ohmic conductivity. Some texts refer to $\kappa_i=\sigma/\epsilon_0\omega$ as the *loss factor* of the medium. The ratio of conduction current to displacement current is often called the *loss tangent*,

$$\tan\delta=\frac{\sigma}{\omega\epsilon_0\kappa}=\frac{\kappa_i}{\kappa_r}. \tag{A.19}$$

The *power factor* of the medium is $\sin\delta$ which, for small losses, is nearly equal to $\tan\delta$. Some of these quantities, for various common dielectric materials, are listed in Table A.1, for comparison with plasma characteristics.

[4] Note the choice of sign such that $\kappa_i>0$ in dissipative media.

TABLE A.1 DIELECTRIC CONSTANT AND LOSS TANGENT FOR COMMON MATERIALS AT 25°C AND 25 Gc

Material	κ_r	$\tan\delta$
Glass, Kovar sealing 7052	4.85	0.011
Neoprene	4	0.03
Paraffin wax	2.2	<0.001
Polyethylene	2.26	<0.001
Teflon	2.08	<0.001
Water	34	0.26
Wood	~ 1.7	~ 0.02

In the case of ionized gases, it is customary to employ a complex conductivity such that

$$\sigma+j\omega\kappa\epsilon_0 \rightarrow \breve{\sigma}+j\omega\epsilon_0 \tag{A.20}$$

or

$$\breve{\sigma}\equiv\sigma_r+j\sigma_i=\sigma+j\omega(\kappa-1)\epsilon_0=\sigma+j\omega\Psi_e\epsilon_0, \tag{A.21}$$

where Ψ_e is the susceptibility from (A.7). It is to be noted that (A.18) and (A.21) are alternative, equivalent formalisms, which are not to be used simultaneously.[5] The interrelations are

$$\breve{\kappa}\equiv\kappa_r-j\kappa_i=1-j\frac{\breve{\sigma}}{\omega\epsilon_0}=\left(1+\frac{\sigma_i}{\omega\epsilon_0}\right)-j\left(\frac{\sigma_r}{\omega\epsilon_0}\right) \tag{A.22}$$

$$\breve{\sigma}\equiv\sigma_r+j\sigma_i=j\omega\epsilon_0(\breve{\kappa}-1)=[\kappa_i+j(\kappa_r-1)]\omega\epsilon_0 \tag{A.23}$$

Other authors make use of a complex susceptibility or a complex mobility.

The complex dielectric constant formalism (A.18) eliminates σ and, hence, the explicit current density $\mathbf{J}$ in Ampere's law (A.4). It also automatically eliminates the explicit charge density ρ in Gauss's law (A.1), which may be seen by considering the equation of continuity of charge

$$\nabla\cdot\mathbf{J}=-\frac{\partial\rho}{\partial t}. \tag{A.24}$$

[5] Depending upon the microscopic models used, it is sometimes useful to ascribe complex properties simultaneously to two or three of the constants, σ, κ, and κ_m, where each represents a different physical effect. For instance, $\breve{\sigma}$ might describe the in-phase and out-of-phase components of explicit currents, while the imaginary parts of $\breve{\kappa}$ and $\breve{\kappa}_m$ describe dipole hysteresis loss not counted in σ_r. We shall not have occasion to use this more detailed formalism.

For our assumptions in (A.13) and (A.14), (A.24) becomes

$$\nabla\cdot\sigma\mathbf{E}=-j\omega\rho. \tag{A.25}$$

Using (A.9) and (A.25), (A.1) becomes

$$\nabla\cdot\kappa\epsilon_0\mathbf{E}=\nabla\cdot j\frac{\sigma}{\omega}\mathbf{E}$$

or

$$\nabla\cdot\left(\kappa\epsilon_0-j\frac{\sigma}{\omega}\right)\mathbf{E}=\nabla\cdot\check{\kappa}\epsilon_0\mathbf{E}=0. \tag{A.26}$$

Thus, formally, the charge density ρ is zero.

A.1.2 ***Complex propagation constants.*** The formalism of a complex dielectric constant $\check{\kappa}$ absorbs the explicit charge and current densities so that Maxwell's equations become:

$$\nabla\cdot\check{\kappa}\epsilon_0\mathbf{E}=0 \tag{A.27}$$

$$\nabla\cdot\kappa_m\mu_0\mathbf{H}=0 \tag{A.28}$$

$$\nabla\times\mathbf{E}=-\kappa_m\mu_0\frac{\partial\mathbf{H}}{\partial t} \tag{A.29}$$

$$\nabla\times\mathbf{H}=\check{\kappa}\epsilon_0\frac{\partial\mathbf{E}}{\partial t} \tag{A.30}$$

Taking the curl of (A.29) and the time derivative of (A.30) to eliminate $\mathbf{H}$, we obtain the generalized wave equation

$$\nabla\times\nabla\times\mathbf{E}=\nabla\nabla\cdot\mathbf{E}-\nabla^2\mathbf{E}=-\frac{\check{\kappa}\kappa_m}{c^2}\frac{\partial^2\mathbf{E}}{\partial t^2}, \tag{A.31}$$

where $c=(\epsilon_0\mu_0)^{-1/2}$ is the velocity of light in vacuum. For a *homogeneous* medium ($\check{\kappa}$ independent of position), (A.27) reduces (A.31) to the usual wave equation

$$\nabla^2\mathbf{E}=\frac{\check{\kappa}\kappa_m}{c^2}\frac{\partial^2\mathbf{E}}{\partial t^2}. \tag{A.32}$$

An analogous argument yields the same equation for $\mathbf{H}$. These wave equations may be solved in a variety of coordinate systems, provided it is remembered that (A.32) is, in fact, three scalar equations for the components of $\mathbf{E}$ expressed in *cartesian* (*rectangular*) coordinates.

Our primary interest is in plane waves propagating in an infinite, uniform medium. We assume then that a wave traveling in the x direction has the phase factor

$$\exp(j\omega t-\check{\gamma}x) \tag{A.33}$$

where $\check{\gamma}$ is the *propagation coefficient*, and[6]

$$\check{\gamma}\equiv\alpha+j\beta \tag{A.34}$$

where α=*attenuation coefficient* (nepers/meter)
β=*phase coefficient* (radians/meter).

Substituting in (A.29) and (A.30), and following the procedure leading to (A.32), we obtain

$$\check{\gamma}^2=-\check{\kappa}\kappa_m\frac{\omega^2}{c^2} \tag{A.35}$$

and hence

$$\check{\gamma}\equiv\alpha+j\beta=j(\check{\kappa}\kappa_m)^{1/2}\frac{\omega}{c}. \tag{A.36}$$

The sign of the square root is to be chosen such that $\beta=\mathrm{Im}(\check{\gamma})$ is positive.

The reciprocal of the attenuation coefficient α is the *attenuation length* δ, the distance in which field amplitudes diminish by a factor of e. The phase coefficient β is related to the *wavelength* λ and *phase velocity* v_ϕ by

$$\beta=\frac{2\pi}{\lambda}=\frac{\omega}{v_\phi}. \tag{A.37}$$

The refractive index μ is conventionally defined as the ratio of the vacuum velocity of light c to the phase velocity in the medium;

$$\mu=\frac{c}{v_\phi}=\beta\frac{c}{\omega}. \tag{A.38}$$

[6] While our notation is that commonly found in electrical engineering literature, most theoretical physics authors use the complex *angular wave number* $\check{k}=-j\check{\gamma}$. Often these authors put $\check{k}=\alpha+j\beta$, in which case the definitions of α and β are *interchanged* with respect to our notation! A second common variation is the choice of sign in the phase factor; although arbitrary, this choice controls the sign of the imaginary parts of $\check{\sigma}$, $\check{\kappa}$, $\check{\gamma}$, etc. Often, but not always, these two notational conventions are signaled by the use of i or j for $\sqrt{-1}$. Thus, the notations $\exp(j\omega t-\check{\gamma}x)$ and $\exp i(\check{k}x-\omega t)$ are most common.

Accordingly, it is useful to define a *complex refractive index* $\check{\mu}$, or normalized propagation coefficient,[7]

$$\check{\mu} \equiv \mu - j\chi = -j\check{\gamma}\frac{c}{\omega} = (\check{\kappa}\kappa_m)^{1/2}, \tag{A.39}$$

where $\mu = (real)$ *refractive index*

$\chi =$ *attenuation index*,

and the sign of the square root is taken such that μ is positive. Thus

$$\alpha = \chi\frac{\omega}{c} \tag{A.40}$$

$$\beta = \mu\frac{\omega}{c}. \tag{A.41}$$

If $\check{\mu}$ varies with frequency, the medium is said to exhibit *dispersion*. The *group velocity* of a wave packet in a loss-free dispersive medium is

$$v_g = \frac{d\omega}{d\beta}. \tag{A.42}$$

[7] Note that some authors use the form

$$\check{\mu} = \mu(1 - j\xi)$$

where $\xi = \chi/\mu$ is called the *extinction coefficient*.

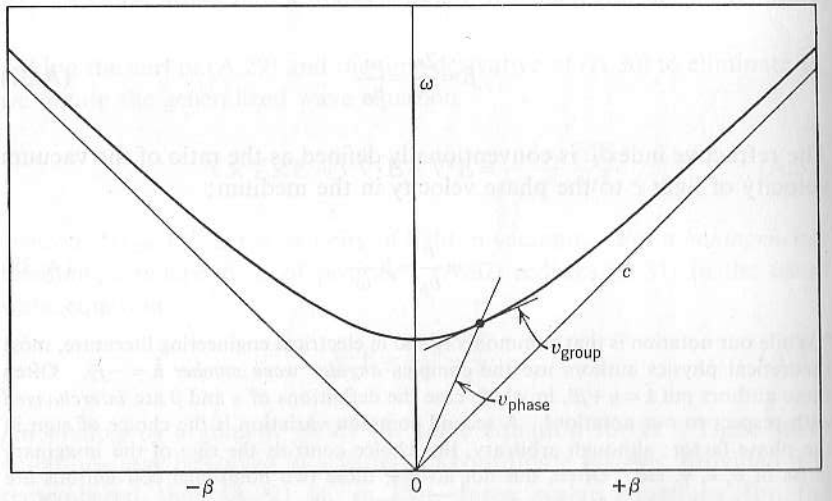

FIG. A.1 Example of an ω–β diagram. See also Fig. 1.5, and Section 5.3.

The dispersion relation between frequency and wavelength may be shown graphically (Fig. A.1) as an ω-β or *Brillouin diagram*. The phase and group velocities appear as total and marginal slopes, as indicated in the figure. Considerable use of ω-β diagrams is made in Chapter 5.

In most cases of practical interest in plasma physics, the relative permeability κ_m is unity.[8] With this simplification we have

$$\check{\mu} = \mu - j\chi = \check{\kappa}^{1/2} = (\kappa_r - j\kappa_i)^{1/2}. \tag{A.43}$$

Squaring and equating real and imaginary parts, we obtain

$$\mu^2 - \chi^2 = \kappa_r \tag{A.44}$$

$$2\mu\chi = \kappa_i \tag{A.45}$$

from which

$$\mu = \left[\frac{\kappa_r + (\kappa_r^2 + \kappa_i^2)^{1/2}}{2}\right]^{1/2} = \frac{\kappa_i}{2\chi} \tag{A.46}$$

$$\chi = \left[\frac{-\kappa_r + (\kappa_r^2 + \kappa_i^2)^{1/2}}{2}\right]^{1/2} = \frac{\kappa_i}{2\mu}. \tag{A.47}$$

The coefficients α and β are readily obtained from (A.40) and (A.41).

A number of approximations of (A.46) and (A.47) are useful:

$\kappa_r \ll \kappa_i$ (ohmic conductor)

$$\mu \to \left(\frac{\kappa_i}{2}\right)^{1/2}\left(1 + \frac{\kappa_r}{2\kappa_i}\right) \tag{A.48}$$

$$\chi \to \left(\frac{\kappa_i}{2}\right)^{1/2}\left(1 - \frac{\kappa_r}{2\kappa_i}\right) \tag{A.49}$$

$\kappa_r^2 \gg \kappa_i^2$; $\kappa_r > 0$ (low-loss dielectric)

$$\mu \to \kappa_r^{1/2}\left(1 + \frac{\kappa_i^2}{8\kappa_r^2}\right) \tag{A.50}$$

$$\chi \to \kappa_r^{1/2}\left(\frac{\kappa_i}{2\kappa_r}\right) \tag{A.51}$$

$\kappa_r^2 \gg \kappa_i^2$; $\kappa_r < 0$ (cut-off low-pressure plasma)

$$\mu \to (-\kappa_r)^{1/2}\left(-\frac{\kappa_i}{2\kappa_r}\right) \tag{A.52}$$

$$\chi \to (-\kappa_r)^{1/2}\left(1 + \frac{\kappa_i^2}{8\kappa_r^2}\right). \tag{A.53}$$

[8] In Section 3.2 we make use of the permeability to approximate high-temperature effects in a plasma.

From (A.35) and (A.36), it follows that the *wave impedance* $\check{\eta}$, defined as the ratio of E to H, is

$$\check{\eta}=\frac{E}{H}=\left(\frac{\kappa_m\mu_0}{\check{\kappa}\epsilon_0}\right)^{1/2}. \tag{A.54}$$

Thus, E and H are in phase in a dielectric ($\check{\kappa}$ real), 45° out of phase in a conductor ($\check{\kappa}$ imaginary). In vacuum $\eta=(\mu_0/\epsilon_0)^{1/2}\approx 377$ ohms.

By applying electromagnetic boundary conditions at the interface between two homogeneous regions, one can discuss reflection and transmission of waves at discontinuities. The combination of incident and reflected waves represents a *standing wave* in the first medium. The depth of penetration of the wave into the second medium is known as the *skin depth*, equal to the attenuation length $\delta=1/\alpha$. There is no reflection when the wave impedances of the two media are equal. These questions are considered in more detail in Chapters 4 and 9.

A.2 Microscopic relations

The preceding discussion has been concerned with macroscopic fields, averaged over dimensions large compared to the mean interparticle separation $1/n^{1/3}$. Clearly, the local, microscopic fields vary violently in the neighborhood of particles which carry net charge or possess a dipole moment. In order to relate the macroscopic constants to atomic properties, one must investigate the relation between the macroscopic fields and the effective average microscopic field experienced, for instance, by a free electron or polarizable molecule (VanVleck, 1932; Rosenfeld, 1951).[9]

It is shown in most modern electromagnetism texts that **E** and **B** are the macroscopic space averages of the microscopic electric and magnetic fields, respectively, inside a uniform medium. **H** is the space-average magnetic field which would exist if all (true) atomic magnetization currents were replaced by (fictitious) magnetic dipoles. A similar direct visualization for **D** is more awkward, since it requires replacing the (true) electric dipoles by (fictitious) magnetic currents consisting of circulating poles. However, for the special case of free electric charge imbedded in a uniform medium, **D** is the electric field which would exist if the polarization (bound) charge were simply ignored. A familiar operational specification for the fields is given by Kelvin's arguments involving needle- and disc-shaped cavities cut in the medium.

[9] The references cited in this appendix are included in the cumulative reference list on pp. 412–438.

A.2.1 ***The microscopic field in a dielectric.*** To relate the macroscopic dielectric constant $\kappa=D/\epsilon_0E$ or susceptibility $\Psi_e=P/\epsilon_0E$ to molecular properties, one proceeds to calculate the effective field at the molecule $\mathbf{E}_{eff}$ by decomposing it into three component fields.

(*1*) The externally applied field, identical with the macroscopic field **E**.
(*2*) The average field $\mathbf{E}_1$ of nearby molecules, treated as individuals.
(*3*) The average field $\mathbf{E}_2$ of more distant molecules, treated as a continuum.

The distinction between nearby and distant molecules is made formally by imagining a spherical boundary of radius large compared to intermolecular distances but small on a macroscopic scale. By symmetry arguments, one can show that in most cases $\mathbf{E}_1=0$. The polarization charge appearing at the surface of the spherical cavity yields, in a simple calculation, $\mathbf{E}_2=\mathbf{P}/3\epsilon_0$, which is often called the *Lorentz polarization term* (Lorentz, 1915). Thus

$$\mathbf{E}_{eff}=\mathbf{E}+\mathbf{E}_1+\mathbf{E}_2=\mathbf{E}+\frac{\mathbf{P}}{3\epsilon_0}. \tag{A.55}$$

An equivalent argument is to say that the effective field experienced by a molecule is the uniform macroscopic field **E** diminished by the molecule's own field $\mathbf{E}_{mol}$. The field of a dipole averaged over a sphere of volume $1/n$ is $\mathbf{E}_{mol}=-\mathbf{P}/3\epsilon_0$, from which (A.55) follows.

If the dipole moment **p** of a molecule is directly proportional to $\mathbf{E}_{eff}$ by the constant *polarizability* a, then the polarization **P** resulting from n molecules per unit volume is given by

$$\mathbf{P}=n\mathbf{p}=na\epsilon_0\mathbf{E}_{eff}=na\left(\epsilon_0\mathbf{E}+\frac{\mathbf{P}}{3}\right), \tag{A.56}$$

whereupon

$$\Psi_e=\frac{P}{\epsilon_0E}=\frac{na}{1-\frac{1}{3}na} \tag{A.57}$$

$$\kappa=\frac{D}{\epsilon_0E}=1+\Psi_e=\frac{1+\frac{2}{3}na}{1-\frac{1}{3}na} \tag{A.58}$$

$$\frac{3(\kappa-1)}{\kappa+2}=na. \tag{A.59}$$

Relation (A.59), which says that the quantity $(\kappa-1)/(\kappa+2)$ is directly proportional to molecule density, is known variously as the Clausius-Mossotti or the Lorentz-Lorenz formula, and has been verified experimentally for polarizable gases over a wide range of pressures (Boudouris, 1963).

A.2.2 ***The microscopic field in a plasma.*** To derive the electromagnetic properties of an ionized gas, we consider directly the dynamics of the electrons (and positive ions, also, if significant). At high frequencies, it is well known that a plasma behaves macroscopically like a dielectric. The question then arises as to what effective local electric field should appear in the force equation for the electron's motion. The answer is that the effective field in the case of unbound charge is simply the applied field **E**, and the Lorentz polarization term $\mathbf{P}/3\epsilon_0$ is omitted from (A.55). Thereupon (A.57) to (A.59) take the simpler form

$$\Psi_e = na \tag{A.60}$$

$$\kappa = 1 + na \tag{A.61}$$

$$\kappa - 1 = na, \tag{A.62}$$

the latter relation being known as the Sellmeier formula. The difference between (A.59) and (A.62) is of practical interest only when κ differs significantly from unity, but this is an important case in plasma physics.

Extensive controversy has surrounded this apparent paradox whereby the formal treatment for free electrons (in a plasma) differs from that for bound electrons (in polarizable molecules), even though both media may be described macroscopically by a dielectric constant (Ratcliffe, 1959, Chapter 15). Indeed, the basic relation for high-frequency propagation in a magnetized plasma, commonly known as the Appleton-Hartree formula, was derived by Appleton and by Hartree on models which omitted and included the Lorentz term, respectively. Hartree's version does not permit the low-frequency "whistler" mode, for example, in contradiction with experiment (Storey, 1953; Jackson, 1954; and Buchsbaum and Brown, 1962).

The distinction between the bound and free electron cases is most clear when the plasma is represented by the electron gas approximation, with the ions treated as a smeared-out, continuous background charge (a Lorentz plasma). Then it is clear from the isotropy of the electron's monopole field (in contrast to the polarized molecule's dipole field) that no modification to the effective local field arises. Further, if we look into the meaning of the polarization **P** in this case, we see that within a uniform medium there is no unique definition of the origin of **P** since a displacement of the electrons yields a new situation indistinguishable from the old. (Nevertheless, the time variation of **P** is well defined in terms of the electron velocity, $\partial\mathbf{P}/\partial t = -ne\mathbf{v}$, and it is this variation which appears in Maxwell's equations.) An additional distinction is that the molecular dipoles store potential energy in the stretched bonds, whereas the free electrons do not.

The problem becomes more subtle when the discreteness of the positive ions is included. Even though the ions and electrons are energetically dissociated, it is not obvious that there are no statistical correlations between them which would give more direct meaning to the polarization. The dilemma can be posed more concretely by using the classical model of an electron elastically bound in a massive molecule with one or more natural (resonant) frequencies ω_0, characteristic of the molecule (Slater and Frank, 1947). This model fits ordinary dielectrics well when the Lorentz polarization term is included in the analysis. But now the free-electron case corresponds formally to the limit $\omega_0 \to 0$, and it is not clear at what point in the limiting process the Lorentz term is dropped (Unz, 1963). Theoretical explanations of the distinction between the two cases have been sought in terms of the amplitude of the electron motions and of the dynamics of electron-ion collisions (Booker and Berkner, 1938; Darwin, 1943; and Theimer and Taylor, 1961). An interesting application of these theories is to the case of propagation through shock waves in dense gases, in which both dielectric polarization of neutrals (and positive ions) and the dynamic polarization of free electrons contribute simultaneously to the observed dielectric constant (Alpher and White, 1959; Ascoli-Bartoli et al., 1960; see also Fig. 10.3).

By way of summary, we note that the fundamental approach for treating wave propagation in an ionized gas is to consider all particle motions explicitly, expressing the results in terms of the conductivity or mobility coefficients. The formalism of dielectric polarization and susceptibility coefficient is often useful (and that of magnetization, occasionally), on a macroscopic level. However, these macroscopic concepts are treacherous when dealing with questions of local field and energy storage in the medium.

A.3 Propagation in an anisotropic medium

The electromagnetic properties of an *anisotropic* medium depend upon the orientation of the fields with respect to the medium. A plasma in a magnetostatic field is anisotropic, as are many crystals and ferrites. Currents are not, in general, parallel to the applied electric field. Likewise, the polarization **P** and magnetization **M** are not necessarily parallel to the applied **E** and **B**. Formally, this situation is handled by treating the constants σ, κ, κ_m as tensors (see Appendix B). From (A.9), (A.10), and (A.13),

$$\mathbf{J} = \boldsymbol{\sigma} \cdot \mathbf{E} \tag{A.63}$$

$$\mathbf{D} = \epsilon_0 \boldsymbol{\kappa} \cdot \mathbf{E} \tag{A.64}$$

$$\mathbf{B} = \mu_0 \boldsymbol{\kappa}_m \cdot \mathbf{H}. \tag{A.65}$$

We shall have no need for the tensor permeability $\boldsymbol{\kappa}_m$ and, henceforth, we shall neglect it. The same arguments used in Section A.1.1 permit us to make use of a complex conductivity tensor $\check{\boldsymbol{\sigma}}$ *or* a complex dielectric constant tensor $\check{\boldsymbol{\kappa}}$, with

$$\check{\boldsymbol{\kappa}}=\mathbf{1}-j\frac{\check{\boldsymbol{\sigma}}}{\epsilon_0\omega} \tag{A.66}$$

where $\mathbf{1}$ is the unit tensor.

Assume a plane wave traveling in the $\check{\gamma}$ direction with the phase factor

$$\exp(j\omega t-\check{\gamma}\cdot\mathbf{r}), \tag{A.67}$$

where $\mathbf{r}$ is the three-dimensional space coordinate vector (x, y, z) and $\check{\gamma}$ is the usual propagation coefficient to which we now ascribe vector properties. Substituting in Maxwell's equations (A.27) to (A.30) with $\check{\kappa}$ as a tensor (and $\kappa_m=1$), and assuming a homogeneous medium, we obtain:

$$\check{\gamma}\cdot\epsilon_0\check{\boldsymbol{\kappa}}\cdot\mathbf{E}=0 \tag{A.68}$$

$$\check{\gamma}\cdot\mu_0\mathbf{H}=0 \tag{A.69}$$

$$\check{\gamma}\times\mathbf{E}=j\omega\mu_0\mathbf{H} \tag{A.70}$$

$$\check{\gamma}\times\mathbf{H}=-j\omega\epsilon_0\check{\boldsymbol{\kappa}}\cdot\mathbf{E} \tag{A.71}$$

Comparison of the vector properties of (A.69) and (A.71) shows that the vectors $\mathbf{D}=\epsilon_0\check{\boldsymbol{\kappa}}\cdot\mathbf{E}$, $\mathbf{H}=\mathbf{B}/\mu_0$, and $\check{\gamma}$ form a mutually perpendicular right-handed set. However, $\mathbf{E}$ may have a longitudinal component.

By crossing $\check{\gamma}$ into (A.70) and using (A.71), we obtain the wave equation for an anisotropic medium,

$$\check{\gamma}\times(\check{\gamma}\times\mathbf{E})-\frac{\omega^2}{c^2}\check{\boldsymbol{\kappa}}\cdot\mathbf{E}=0 \tag{A.72}$$

or, in terms of the complex vector refractive index $\check{\boldsymbol{\mu}}=-j\check{\gamma}c/\omega$ from (A.39),

$$\check{\boldsymbol{\mu}}\times(\check{\boldsymbol{\mu}}\times\mathbf{E})+\check{\boldsymbol{\kappa}}\cdot\mathbf{E}=0. \tag{A.73}$$

Equation (A.73) is a set of three linear homogeneous equations for the field components (E_x, E_y, E_z). A nonzero solution exists only if the determinant of the coefficients vanishes:

$$\begin{vmatrix} \check{\kappa}_{xx}-\check{\mu}_y{}^2-\check{\mu}_z{}^2 & \check{\kappa}_{xy}+\check{\mu}_x\check{\mu}_y & \check{\kappa}_{xz}+\check{\mu}_x\check{\mu}_z \\ \check{\kappa}_{yx}+\check{\mu}_y\check{\mu}_x & \check{\kappa}_{yy}-\check{\mu}_z{}^2-\check{\mu}_x{}^2 & \check{\kappa}_{yz}+\check{\mu}_y\check{\mu}_z \\ \check{\kappa}_{zx}+\check{\mu}_z\check{\mu}_x & \check{\kappa}_{zy}+\check{\mu}_z\check{\mu}_y & \check{\kappa}_{zz}-\check{\mu}_x{}^2-\check{\mu}_y{}^2 \end{vmatrix}=0. \tag{A.74}$$

To apply the *dispersion equation* (A.74), one specifies the direction of propagation, which fixes the direction cosines of $\check{\boldsymbol{\mu}}=(\check{\mu}_x, \check{\mu}_y, \check{\mu}_z)$. The determinantal equation then becomes, formally, a quadratic in $\check{\mu}^2=\check{\mu}_x{}^2+\check{\mu}_y{}^2+\check{\mu}_z{}^2$ with coefficients which are functions of the elements $\check{\kappa}_{ij}$ of the dielectric constant tensor. However, in some cases (for example, a warm plasma), these elements are themselves implicit functions of the refractive index $\check{\boldsymbol{\mu}}$, a phenomenon known as *spatial dispersion*. The dispersion equation (A.74) is applied to waves in plasmas in Chapters 1 and 3. Additional details are given by Allis, Buchsbaum, and Bers (1963).

APPENDIX B

Tensor and matrix algebra

This appendix gives a very brief review of the tensor manipulations that are used in this book. An excellent presentation of the physical and mathematical properties of tensors is given in Symon's *Mechanics*, 2nd ed., Chapter 10. For more extensive discussion of matrix theory, see, for instance, the texts by Schwartz, Heading, and Aris.[1]

B.1 Vectors, tensors, and matrices

A *vector* is a physical quantity possessing *direction* as well as *magnitude*. In a physical sense, its meaning is independent of any coordinate system. However, for convenience, it is often expressed in terms of its *components* in a particular coordinate system. In a mathematical sense, a vector is defined entirely in terms of its components, but with rules which permit transformation to any other acceptable coordinate system. In this way, the physicist's generality (independence of any one particular coordinate system) is recovered.

The product of a scalar with a vector produces a new vector with altered magnitude but unchanged direction. A *tensor* is a linear operator that operates on (multiplies) a vector to yield a new vector with changed direction as well as magnitude. Many physical relations are of this form as, for example, the relation between angular velocity and angular momentum in rigid-body mechanics and Ohm's law for an anisotropic

[1] K. R. Symon, *Mechanics*, 2nd ed., Addison-Wesley, Reading, Mass., 1960; J. T. Schwartz, *Introduction to Matrices and Vectors*, McGraw-Hill, New York, 1961; J. Heading, *Matrix Theory for Physicists*, Longmans, Green, London, 1958, see especially Chapter V; and R. Aris, *Vectors, Tensors, and the Basic Equations of Fluid Mechanics*, Prentice-Hall, Englewood Cliffs, N.J., 1962.

conductor. As in the case of a vector, it is usually convenient to express a tensor in terms of its *elements* in some particular coordinate system. Thus, the tensor Ohm's law equation

$$\mathbf{J}=\check{\boldsymbol{\sigma}}\cdot\mathbf{E} \tag{B.1}$$

is an abbreviation for the three scalar equations relating the vector components

$$\begin{aligned} J_x&=\sigma_{xx}E_x+\sigma_{xy}E_y+\sigma_{xz}E_z\\ J_y&=\sigma_{yx}E_x+\sigma_{yy}E_y+\sigma_{yz}E_z\\ J_z&=\sigma_{zx}E_x+\sigma_{zy}E_y+\sigma_{zz}E_z \end{aligned} \tag{B.2}$$

where $\sigma_{xx}, \sigma_{xy}, \ldots$ are the elements of the tensor $\check{\boldsymbol{\sigma}}$, expressed in a particular set of cartesian coordinates. The tensor equation may also be written in the symbolic form

$$J_i=\sum_{j=x,y,z}\sigma_{ij}E_j \qquad (i=x, y, z) \tag{B.3}$$

where J_x, J_y, J_z are the components of $\mathbf{J}$ in the chosen coordinate system. Finally, the equation may be written in *matrix form*

$$\begin{bmatrix} J_x\\ J_y\\ J_z \end{bmatrix}=\begin{bmatrix} \sigma_{xx} & \sigma_{xy} & \sigma_{xz}\\ \sigma_{yx} & \sigma_{yy} & \sigma_{yz}\\ \sigma_{zx} & \sigma_{zy} & \sigma_{zz} \end{bmatrix}\begin{bmatrix} E_x\\ E_y\\ E_z \end{bmatrix} \tag{B.4}$$

in which $\mathbf{J}$ and $\mathbf{E}$ are written as column matrices and the tensor $\check{\boldsymbol{\sigma}}$ as a 3-by-3 matrix.

There are two distinct uses of tensors in physical problems. One is to relate two different physical quantities that are proportional in magnitude but not parallel, as in the conductivity example used above and throughout Chapters 1 and 3. The other use is to perform the transformation whereby the components *in one coordinate system* of a particular vector are converted to the components *in a second coordinate system* of the same vector; that is, the physical meaning of the vector is unchanged. This second application appears in Section 1.4.8.

In most physical problems, symmetry conditions demand that only six of the nine tensor elements be independent. In particular, the following are important special types of tensors:

Symmetric	$A_{ij}=A_{ji}$
Antisymmetric	$A_{ij}=-A_{ji}$
Hermitian	$A_{ij}=A_{ji}^*$

where A_{ij} is the ijth element of the tensor $\mathbf{A}$, and the symbol * signifies complex conjugate.

B.2 Addition, multiplication, and inversion of tensors

Just as vectors are added algebraically by summing respective components, the addition rule for tensors may be stated in terms of a representative element:

$$\begin{aligned} &\text{If} && \mathbf{C}=\mathbf{A}+\mathbf{B}, \\ &\text{then} && C_{ij}=A_{ij}+B_{ij}, \end{aligned} \tag{B.5}$$

where A_{ij} is the ijth element of the tensor $\mathbf{A}$, etc. Multiplication of a tensor into a vector yields a new vector according to the rule:

$$\begin{aligned} &\text{If} && \mathbf{Q}=\mathbf{A}\cdot\mathbf{P} \\ &\text{then} && Q_i=\sum_{j=1}^{3} A_{ij}P_j. \end{aligned} \tag{B.6}$$

The (inner or scalar) product of one tensor into a second is a new tensor:

$$\begin{aligned} &\text{If} && \mathbf{C}=\mathbf{A}\cdot\mathbf{B} \\ &\text{then} && C_{ij}=\sum_{k=1}^{3} A_{ik}B_{kj}, \end{aligned} \tag{B.7}$$

which is the basic rule for multiplying matrices. Multiplication of tensors is distributive and associative but not commutative; that is, in general

$$\mathbf{A}\cdot\mathbf{B}\neq\mathbf{B}\cdot\mathbf{A}. \tag{B.8}$$

The tensor $\mathbf{A}^{-1}$ is the *inverse* or *reciprocal* of the tensor $\mathbf{A}$ such that

$$\mathbf{A}^{-1}\cdot\mathbf{A}=\mathbf{A}\cdot\mathbf{A}^{-1}=\mathbf{1} \tag{B.9}$$

where $\mathbf{1}$ is the *unit tensor*

$$\mathbf{1}=\begin{bmatrix}1 & 0 & 0\\ 0 & 1 & 0\\ 0 & 0 & 1\end{bmatrix}. \tag{B.10}$$

Note that the multiplication of the unit tensor by any vector or tensor leaves the quantity unchanged,

$$\begin{aligned} &\mathbf{1}\cdot\mathbf{P}=\mathbf{P}\cdot\mathbf{1}=\mathbf{P} \\ &\mathbf{1}\cdot\mathbf{A}=\mathbf{A}\cdot\mathbf{1}=\mathbf{A}. \end{aligned} \tag{B.11}$$

Given the 3-by-3 square matrix representing the tensor $\mathbf{A}$, one finds its inverse by the following prescription.

(*1*) Regard the matrix as a determinant, and compute its value $\det(\mathbf{A})$. If the determinant is zero, the matrix is called *singular*, and no reciprocal exists.

(*2*) Still regarding the matrix as a determinant, compute the *cofactor* ${}^{ij}A$ of each element A_{ij}. The cofactor is $(-1)^{i+j}$ times the *minor* which, in turn, is the value of the 2-by-2 determinant obtained by striking out the ith row and jth column.

(*3*) The jith element of the reciprocal matrix is then the ijth cofactor divided by the determinant; that is,

$$(A^{-1})_{ji}=\frac{{}^{ij}A}{\det(\mathbf{A})}. \tag{B.12}$$

A very important problem in tensor relationships is to find the coordinate system for which the tensor is *diagonal*; that is, $A_{ij}=0$ unless $i=j$. We do this in Section 1.4.7, but without making use of a general procedure.

References

GENERAL REFERENCES

Electromagnetic wave propagation in plasmas

Allis, W. P., S. J. Buchsbaum, and A. Bers (1963). *Waves in Anistropic Plasmas.* M.I.T. Press, Cambridge, Mass.

Brandstatter, J. J. (1963). *An Introduction to Waves, Rays and Radiation in Plasma Media.* McGraw-Hill, New York.

Denisse, J. F., and J. L. Delcroix (1963). *Plasma Waves*, translated by M. Weinrich and D. J. Ben Daniel. Interscience, New York.

Shkarofsky, I. P., T. W. Johnston, and M. P. Bachynski (1965). *Particle Kinetics of Plasma.* Addison-Wesley, Reading, Mass.

Stix, T. H. (1962). *The Theory of Plasma Waves.* McGraw-Hill, New York.

Waves in the context of ionospheric propagation

Budden, K. G. (1961). *Radio Waves in the Ionosphere.* University Press, Cambridge.

Ginzburg, V. L. (1964). *Propagation of Electromagnetic Waves in Plasmas*, translated by J. B. Sykes and R. J. Tayler. Pergamon, New York.

Ratcliffe, J. A. (1959). *The Magneto-Ionic Theory and Its Application to the Ionosphere.* University Press, Cambridge.

Processes in classical gas discharges

Brown, S. C. (1959). *Basic Data of Plasma Physics.* Technology Press (M.I.T.) and Wiley, New York.

Francis, G. (1960). *Ionization Phenomena in Gases.* Academic Press, New York.

McDaniel, E. W. (1964). *Collision Phenomena in Ionized Gases.* Wiley, New York.

Introductions to plasma physics

Alfvén, H., and C. G. Fälthammar (1963). *Cosmical Electrodynamics*, 2nd ed. Clarendon Press, Oxford.

Cambel, A. B. (1963). *Plasma Physics and Magnetofluidmechanics.* McGraw-Hill, New York.

Chandrasekhar, S., and S. K. Trehan (1960). *Plasma Physics.* University of Chicago Press, Chicago.

Delcroix, J. L. (1960). *Introduction to the Theory of Ionized Gases*, translated by M. Clark et al. Interscience, New York.
Longmire, C. L. (1963). *Elementary Plasma Physics*. Interscience, New York.
Montgomery, D. C., and D. A. Tidman (1964). *Plasma Kinetic Theory*. McGraw-Hill, New York.
Spitzer, L., Jr. (1962). *Physics of Fully Ionized Gases*, 2nd ed. Interscience, New York.
Thompson, W. B. (1962). *An Introduction to Plasma Physics*. Pergamon, New York.
Uman, M. A. (1964). *Introduction to Plasma Physics*. McGraw-Hill, New York.

Controlled fusion

Glasstone, S., and R. H. Lovberg (1960). *Controlled Thermonuclear Reactions*. Van Nostrand, Princeton, N.J.
Rose, D. J., and M. Clark, Jr. (1961). *Plasmas and Controlled Fusion*. M.I.T. Press and Wiley, New York.

Compilations of tutorial research-level papers

Drummond, J. E., ed. (1961). *Plasma Physics*. McGraw-Hill, New York.
Huddlestone, R., and S. L. Leonard, ed. (1965). *Plasma Diagnostic Techniques*. Academic Press, New York.
Kunkel, W., ed. (1965). *Plasma Physics, in Theory and Application*. McGraw-Hill, New York.
Landshoff, R., ed. (1958). *The Plasma in a Magnetic Field*. Stanford University Press, Stanford, Cal.
Mitchner, M., ed. (1961). *Radiation and Waves in Plasmas*. Stanford University Press, Stanford, Cal.

Microwave techniques and hardware

Harvey, A. F. (1963). *Microwave Engineering*. Academic Press, New York.
M.I.T. Radiation Laboratory (1948). Series of 32 volumes, especially Vols. 8–12. McGraw-Hill, New York.
Moreno, T. (1948). *Microwave Transmission Design Data*. Dover, New York.
Saad, T., ed. (1964). *The Microwave Engineer's Handbook*. Horizon House, New York.

CUMULATIVE REFERENCE LIST FOR PREFACE, CHAPTERS 1–8, AND APPENDICES

The numbers appearing in brackets after an item indicate the pages on which that item is cited in the text. The corresponding reference lists for Chapters 9 and 10, dealing with somewhat different material, are given separately below. These listings serve as an author index, although cross-referencing of co-authors has been omitted for brevity.

Aamodt, R. E., and W. E. Drummond (1963). Nonlinear coupling of plasma oscillations to transverse waves. *Plasma Phys.* (*J. Nuclear Energy* C) **6**, 147. [286]

Albini, F. A., and R. G. Jahn (1961). Reflection and transmission of electromagnetic waves at electron density gradients. *J. Appl. Phys.* **32**, 75. [135, 136]
Allen, J. E., and W. R. Hindmarsh (1955). The bremsstrahlung radiation from ionized hydrogen. Rept. A.E.R.E. GP/R-1761, U.K. Atomic Energy Authority. [264]
Aller, L. H. (1953). *Astrophysics: Atmospheres of the Sun and Stars*. Ronald Press, New York. Pages 251–256. [275]
Allis, W. P. (1956). Motions of ions and electrons. *Handbuch der Physik* **21**, 383 (Springer-Verlag, Berlin); preprinted as M.I.T. Tech Rept. 299 (1956). [60, 67, 68, 71, 81, 83]
Allis, W. P., S. J. Buchsbaum, and A. Bers (1963). *Waves in Anisotropic Plasmas*. M.I.T. Press, Cambridge, Mass. [*x*, 26, 45, 51, 56, 81, 95, 99, 105, 405]
Alpher, R. A., and D. R. White (1959). Optical refractivity of high-temperature gases. *Phys. Fluids* **2**, 153, 162. [403]
Anderson, J. M., and L. Goldstein (1955). Interaction of electromagnetic waves of radio-frequency in isothermal plasmas: collision cross section of helium atoms and ions for electrons. *Phys. Rev.* **100**, 1037. [83, 92]
Andrews, C. L. (1947). Diffraction pattern of a circular aperture at short distances. *Phys. Rev.* **71**, 777. [144, 145]
Andrews, C. L. (1950). Diffraction pattern in a circular aperture measured in the microwave region. *J. Appl. Phys.* **21**, 761. [145]
Andrews, C. L. (1960). *Optics of the Electromagnetic Spectrum*. Prentice-Hall, Englewood Cliffs, N.J. Chapter II. [142]
Appleton, E. V. (1932). Wireless studies of the ionosphere. *J. Inst. Elec. Engrs.* (*London*) **71**, 642. [*vii*, 24]
Appleton, E. V., and F. W. Chapman (1932). The collisional friction experienced by vibrating electrons in ionised air. *Proc. Phys. Soc.* (*London*) **44**, 246. [64]
Artsimovich, L. A. (1958). Research into controlled thermonuclear reactions in the U.S.S.R. *Proc. 2nd U.N. Conf. Peaceful Uses of Atomic Energy* (Geneva) **31**, 6. [302]
Ascoli-Bartoli, U., A. De Angelis, and S. Martellucci (1960). Wavelength dependence of the refractive index of a plasma in the optical region. *Nuovo cimento* **18**, 1116. [403]
Åström, E. (1950). On waves in an ionized gas. *Arkiv Fysik* **2**, 443. [31, 51]
Åström, E. (1958). Waves in a hot ionized gas in a magnetic field. In B. Lehnert, ed., *Electromagnetic Phenomena in Cosmical Physics*. University Press, Cambridge. Page 81. [96]
Auer, P. L., H. Hurwitz Jr., and R. D. Miller (1958). Collective oscillations in a cold plasma. *Phys. Fluids* **1**, 501. [53]
Bachynski, M. P. (1960). Nature of electromagnetic waves in nonhomogeneous, anisotropic plasmas. Rept. 7-801,7, RCA Victor Research Laboratories, Montreal. [133, 134]
Bailey, V. A., and D. F. Martyn (1934). The influence of electric waves on the ionosphere. *Phil. Mag.* **18**, 369. [92]
Baird, J. R., and P. D. Coleman (1961). Frequency conversion in a microwave discharge. *Proc. I.R.E.* **49**, 1890. [93]
Baranger, M., and B. Mozer (1961). Light as a plasma probe. *Phys. Rev.* **123**, 25. [92]
Battocletti, J. H., and W. D. Hershberger (1962). Resonances in the positive column of a low-pressure arc discharge. *J. Appl. Phys.* **33**, 2618. [241]

Bazhanova, A. E., V. T. Karpukhin, A. N. Karkhov, and V. I. Pistunovich (1961). Cyclotron and thermal radiations of plasma in Ogra. *Nuclear Fusion 1962 Supplement* (Salzburg Conf.), Part 1, 227. [302]

Beard, C. I., T. H. Kays, and V. Twersky (1962). Mid-field forward scattering. *J. Appl. Phys.* **33**, 2851. [141]

Beard, D. B. (1959). Cyclotron radiation from magnetically confined plasmas. *Phys. Fluids* **2**, 379. [116, 278]

Beard, D. B. (1961). Optical properties and emission of relativistic plasmas at cyclotron resonance. *Plasma Phys. (J. Nuclear Energy* C) **2**, 94. [292]

Beard, D. B., and J. C. Baker (1962). Synchrotron radiation losses from energetic plasmas. *Phys. Fluids* **5**, 1113. [277]

Bekefi, G. (1957). Studies in microwave optics. Eaton Electronics Research Lab. Tech. Rept. 38, McGill Univ., Montreal. Chapter 3. [150]

Bekefi, G., and S. C. Brown (1961*a*). Emission of radio-frequency waves from plasmas. *Am. J. Phys.* **29**, 404. [242, 267, 270, 271, 278]

Bekefi, G., and S. C. Brown (1961*b*). Microwave measurements of the radiation temperature of plasmas. *J. Appl. Phys.* **32**, 25. [262]

Bekefi, G., J. L. Hirshfield, and S. C. Brown (1959). Incoherent microwave radiation from plasmas. *Phys. Rev.* **116**, 1051. [271]

Bekefi, G., J. L. Hirshfield, and S. C. Brown (1961*a*). Kirchhoff's radiation law for plasmas with non-Maxwellian distributions. *Phys. Fluids* **4**, 173. [271, 286]

Bekefi, G., J. L. Hirshfield, and S. C. Brown (1961*b*). Cyclotron emission from plasmas with non-Maxwellian distributions. *Phys. Rev.* **122**, 1037. [278]

Bekefi, G., J. D. Coccoli, and E. B. Hooper (1962). Microwave emission and absorption at cyclotron harmonics of a warm plasma. *Phys. Rev. Letters* **9**, 6. [302, 303]

Bernstein, I. B. (1958). Waves in a plasma in a magnetic field. *Phys. Rev.* **109**, 10. [104, 105, 106, 112, 113, 183, 188, 190]

Bernstein, I. B., and S. K. Trehan (1960). Plasma oscillations. *Nuclear Fusion* **1**, 3. [67, 81, 100, 184]

Bernstein, W., F. F. Chen, M. A. Heald, and A. Z. Kranz (1958). "Runaway" electrons and cooperative phenomena in B-1 Stellarator discharges. *Phys. Fluids* **1**, 430. [286]

Bevc, V., and T. E. Everhart (1962). Fast waves in plasma-filled waveguides. Electronics Research Lab. Rept. Series 60, No. 362, University of California, Berkeley, Calif. Condensed version in *J. Electron. Control* **13**, 185. [167, 181, 189]

Biondi, M. A., and S. C. Brown (1949). Measurements of ambipolar diffusion in helium. *Phys. Rev.* **75**, 1700. [*vii*, 163]

Biondi, M. A. (1951). Measurement of the electron density in ionized gases by microwave techniques. *Rev. Sci. Instr.* **22**, 500. [163]

Bohm, D. (1951). *Quantum Mechanics.* Prentice-Hall, Engelwood Cliffs, N.J. Chapter 12. [119]

Bohm, D., and E. P. Gross (1949). Theory of plasma oscillations. *Phys. Rev.* **75**, 1851, 1864. [95, 103, 115]

Boley, F. J. (1958). Scattering of microwave radiation by a plasma column. *Nature* **182**, 790. [241]

Booker, H. G. (1935). The application of the magneto-ionic theory to the ionosphere. *Proc. Roy. Soc. (London)* **A150**, 267. [38]

Booker, H. G., and L. V. Berkner (1938). An ionospheric investigation concerning the Lorentz polarization correction. *Terrest. Magn. Atmos. Elect.* **43**, 427. [403]

Boudouris, G. (1963). On the index of refraction of air, the absorption and dispersion of centimeter waves by gases. *J. Research Natl. Bur. Standards* **67D**, 631. [401]

Bowles, K. L. (1961). Incoherent scattering by free electrons as a technique for studying the ionosphere and exosphere: some observations and theoretical considerations. *J. Research Natl. Bur. Standards* **65D**, 1. [94]

Bowles, K. L., G. R. Ochs, and J. L. Green (1962). On the absolute intensity of incoherent scatter echoes from the ionosphere. *J. Research Natl. Bur. Standards* **66D**, 395. [94]

Boyd, F. E. (1950). Converging lens dielectric antennas. Rept. 3780, U.S. Naval Research Laboratory, Washington, D.C. [150]

Boyd, G. D., R. W. Gould, and L. M. Field (1961). Interaction of a modulated electron beam with a plasma. *Proc. I.R.E.* **49**, 1906. [286]

Branch, G. M., and T. G. Mihran (1955). Plasma frequency reduction factors in electron beams. *I.R.E. Trans.* **ED-2**(*2*), 3. [130]

Brandstatter, J. J. (1963). *An Introduction to Waves, Rays and Radiation in Plasma Media.* McGraw-Hill, New York. [48]

Brown, S. C. (1956). Breakdown in gases: alternating and high-frequency fields. *Handbuch der Physik* **22**, 531 (Springer-Verlag, Berlin); preprinted as M.I.T. Tech. Rept. 301 (1955). [91]

Brown, S. C. (1958). Microwave studies of gas discharge plasmas. *Proc. 2nd Intl. Conf. Peaceful Uses of Atomic Energy* (Geneva) **32**, 394. [160, 331]

Brown, S. C. (1959). *Basic Data of Plasma Physics.* Technology Press, M.I.T., and Wiley, New York. [59, 62, 64, 168]

Brussard, P. J., and H. C. van de Hulst (1962). Approximation formulas for non-relativistic bremsstrahlung and average Gaunt factors for a Maxwellian electron gas. *Revs. Modern Phys.* **34**, 507. [250, 251, 263]

Buchsbaum, S. J. (1960). Resonance in a plasma with two ion species. *Phys. Fluids* **3**, 418. [56]

Buchsbaum, S. J., and S. C. Brown (1957). Microwave measurements of high electron densities. *Phys. Rev.* **106**, 196. [132, 159, 160]

Buchsbaum, S. J., and S. C. Brown (1962). The dielectric coefficient of a plasma. *J. Electron. Control* **13**, 573. [402]

Buchsbaum, S. J., L. Mower, and S. C. Brown (1960). Interaction between cold plasmas and guided electromagnetic waves. *Phys. Fluids* **3**, 806. [297]

Budden, K. G. (1961). *Radio Waves in the Ionosphere.* University Press, Cambridge. [45, 48]

Bunkin, F. V. (1957). Thermal radiation from an anisotropic medium. *Soviet Phys.—JETP* **5**, 665. [271]

Burkhardt, G., G. Elwert, and A. Unsöld (1948). Über das langwellige Ende des kontinuierlichen Röntgenspektrums und die Theorie der Radiofrequenzstrahlung der Milchstrasse und der Sonne. *Z. Astrophys.* **25**, 310. [252]

Burnett, D. (1931). The propagation of radio waves in an ionized atmosphere. *Proc. Cambridge Phil. Soc.* **27**, 578. [69]

Buser, R., and W. Buser (1962). Determination of plasma properties by free-space microwave techniques. *J. Appl. Phys.* **33**, 2275. [205]

Butler, S. T., and M. J. Buckingham (1962). Energy loss of a fast ion in a plasma. *Phys. Rev.* **126**, 1. [284]

Chandrasekhar, S. (1943). Stochastic problems in physics and astronomy. *Revs. Modern Phys.* **15**, 1. [81]
Chang, D. B. (1962*a*). Bremsstrahlung from a plasma. *Phys. Fluids* **5**, 1558. [252]
Chang, D. B. (1962*b*). Plasma correction to single-particle cyclotron radiation. *Phys. Fluids* **5**, 1564. [278]
Chapman, S., and T. G. Cowling (1952). *The Mathematical Theory of Non-Uniform Gases*, 2nd ed. University Press, Cambridge. Chapter 7. [68]
Chen, F. F. (1962). Radial electric field in a reflex discharge. *Phys. Rev. Letters* **8**, 234. [213]
Chen, K-M. (1962). Interaction of a high-intensity EM field with a low-density plasma. *I.R.E. Trans.* **AP-10**, 31. Nonlinear electrical conductivity of a fully ionized gas. *I.R.E. Trans.* **AP-10**, 43. [92]
Christian, J. R., and G. Goubau (1961). Experimental studies on a beam waveguide for millimeter waves. *I.R.E. Trans.* **AP-9**, 256. [150]
Cillie, G. (1932). The hydrogen emission in gaseous nebulae. *Mon. Not. Roy. Astron. Soc.* **92**, 820. [251]
Clemmow, P. C., and R. F. Mullaly (1955). The dependence of the refractive index in magneto-ionic theory on the direction of the wave normal. In *The Physics of the Ionosphere*. Physical Society, London. Page 340. [45]
Coensgen, F. H., F. C. Ford, and R. E. Ellis (1958). Pyrotron plasma heating experiments. *Proc. 2nd U.N. Conf. Peaceful Uses of Atomic Energy* (Geneva) **32**, 266. [293]
Cohen, M. H. (1961). Radiation in a plasma: Cerenkov effect. *Phys. Rev.* **123**, 711. [285]
Cohen, R. S., L. Spitzer Jr., and P. M. Routly (1950). The electrical conductivity of an ionized gas. *Phys. Rev.* **80**, 230. [80, 81, 83, 84]
Cohn, M., F. E. Wentworth, and J. C. Wiltse (1963). High-sensitivity 100 to 300 Gc radiometers. *Proc. I.E.E.E.* **51**, 1227. [299]
Condon, E. V., and G. H. Shortley (1951). *Theory of Atomic Spectra*. University Press, Cambridge. Chapter 4. [259]
Consoli, T., R. Legardeur, and L. Slama (1961). Interaction d'ondes electromagnetiques à polarisation circulaire avec un plasma. Saclay Rept. 1995, Commissariat à l'Energie Atomique, Paris. [25, 223]
Coor, T., S. Cunningham, R. Ellis, M. Heald, and A. Kranz (1958). Experiments on the ohmic heating and confinement of plasma in a Stellarator. *Phys. Fluids* **1**, 411. [222]
Coor, T. (1961). Plasma diffusion in Stellarators. *Plasma Phys. (J. Nuclear Energy* C) **2**, 81. [286]
Crawford, F. H. (1949). Jacobian methods in thermodynamics. *Am. J. Phys.* **17**, 1. [47]
Crawford, F. W., G. S. Kino, and A. B. Cannara (1963). Dipole resonances of a plasma in a magnetic field. *J. Appl. Phys.* **34**, 3168. [130, 241]
Cullen, A. L. (1960). Propagation of microwaves through a magneto-plasma, and a possible method for determining the electron velocity distribution. *J. Research Natl. Bur. Standards* **64D**, 509. [114]
Darwin, C. G. (1943). The refractive index of an ionized medium. *Proc. Roy. Soc. (London)* **A182**, 152. [403]
Dattner, A. (1957). The plasma resonator. *Ericsson Technics* **13**, 309. [240, 241]
Davies, L. W., and E. Cowcher (1955). Microwave and meter wave radiation from the positive column of a gas discharge. *Australian J. Phys.* **8**, 108. [262]

Dawson, J. (1959). Nonlinear electron oscillations in a cold plasma. *Phys. Rev.* **113**, 383. [4]
Dawson, J. (1961). On Landau damping. *Phys. Fluids* **4**, 869. [114]
Dawson, J., and C. Oberman (1959). Oscillations of a finite cold plasma in a strong magnetic field. *Phys. Fluids* **2**, 103. [130, 244]
Dawson, J., and C. Oberman (1962). High-frequency conductivity and the emission and absorption coefficients of a fully ionized plasma. *Phys. Fluids* **5**, 517. See also Oster (1964) and A. Ron and N. Tzoar, *Phys. Rev.* **131**, 12 (1963). [86, 87, 89, 254]
Dawson, J., and C. Oberman (1963). Effect of ion correlations on high-frequency plasma conductivity. *Phys. Fluids* **6**, 394. See also C. Oberman, A. Ron, and J. Dawson, *Phys. Fluids* **5**, 1514 (1962). [77, 86]
Debye, P., and E. Hückel (1923). Zur Theorie der Elektrolyte. *Physik Z.* **24**, 185. English translation in *The Collected Papers of Peter J. W. Debye*. Interscience, New York, 1954. Page 217. [77]
Delcroix, J. L. (1960). *Introduction to the Theory of Ionized Gases*, translated by M. Clark et al. Interscience, New York. [66, 183]
Dellis, A. N. (1957). The measurement of electron temperatures by microwave methods. Rept. A.E.R.E. GP/R2265, U.K. Atomic Energy Authority. [270, 291]
Dellis, A. N., and J. M. Weaver (1964). Whistler-mode propagation in a laboratory plasma. *Proc. Phys. Soc. (London)* **83**, 473. See also *Nature* **193**, 1274 (1962). [226]
Denisov, N. G. (1958). Resonance absorption of electromagnetic waves by an inhomogeneous plasma. *Soviet Phys.—JETP* **7**, 364. [126]
Desloge, E. (1963). Fokker-Planck equation. *Am. J. Phys.* **31**, 237. [81]
Desloge, E. and S. W. Matthysse (1960). Collision term in the Boltzmann transport equation. *Am. J. Phys.* **28**, 1. [81]
De Witt, H. (1958). The free-free absorption coefficient in ionized gases. Lawrence Radiation Lab. Rept. UCRL-5377, Univ. of California, Livermore, Calif. [85, 252]
di Francia, G. T. (1959). Introduction to the theory of synchrotron radiation. In *Solar Radioastronomy*, Varenna Summer School (Zanichelli, Bologna), page 414. [272]
Dingle, R. B., D. Arndt, and S. K. Roy (1957). The integrals $\mathfrak{E}_p(x)$ and $\mathfrak{F}_p(x)$ and their tabulation. *Appl. Sci. Research* **6B**, 245. [76]
Dirac, P. A. M. (1947). *The Principles of Quantum Mechanics*, 3rd ed. Clarendon Press, Oxford. Section 15. [277]
Dnestrovskii, Yu. N., and D. P. Kostomarov (1961). Dispersion equation for an ordinary wave moving in a plasma perpendicular to an external magnetic field. *Soviet Phys.—JETP* **13**, 986. [111]
Dreicer, H. (1959–1960). Electron and ion runaway in a fully ionized gas. *Phys. Rev.* **115**, 238 and **117**, 329. [229, 285]
Dreicer, H. (1961). Incoherent scattering of microwaves by plasma vibrations. *Nuclear Fusion 1962 Supplement* (Salzburg Conf.), Part 3, 1141. [229]
Drummond, J. E. (1958). Basic microwave properties of hot magnetoplasmas. *Phys. Rev.* **110**, 293. See also *Phys. Rev.* **112**, 1460 (1958). [96, 105, 111, 293]
Drummond, J. E., R. A. Gerwin, and B. G. Springer (1961). The concept of conductivity. *Plasma Phys. (J. Nuclear Energy* C) **2**, 98. [96, 132]
Drummond, W. E. (1962). Microwave scattering from unstable plasma waves. *Phys. Fluids* **5**, 1133. [94]

Drummond, W. E., and D. Pines (1961). Non-linear stability of plasma oscillations. *Nuclear Fusion 1962 Supplement* (Salzburg Conf.), Part 3, 1049. [115, 186, 188, 234, 236]

Drummond, W. E., and M. N. Rosenbluth (1963). Cyclotron radiation from a hot plasma. *Phys. Fluids* **6**, 276. [273]

Easley, M. A., and W. W. Mumford (1951). Electron temperature vs. noise temperature in a low pressure Hg-A discharge. *J. Appl. Phys.* **22**, 846. [290]

Eidman, V. Ya. (1958). Investigation of the radiation of an electron moving in a magnetoactive medium. *Soviet Phys.—JETP* **7**, 91. Note corrections in *Soviet Phys.—JETP* **9**, 947 (1959). [285]

Eidman, V. Ya. (1962). Radiation of a plasma wave by a charge moving in a magnetoactive plasma. *Soviet Phys.—JETP* **14**, 1401. [285]

Eleonskii, V. M., P. S. Zyryanov, and V. P. Silin (1962). Collision integral for charged particles in a magnetic field. *Soviet Phys.—JETP* **15**, 619. [89]

Ellis, R. E., and N. L. Parker (1958). Electron energy distribution. Lawrence Radiation Lab. Rept. UCRL-5117, Univ. of California, Livermore, Calif. [297]

Elwert, G. (1939). Verschärfte Berechnung von Intensität und Polarisation im kontinuierlichen Röntgenspektrum. *Ann. Physik* **34**, 178. [251]

Emeleus, K. G., and D. W. Mahaffey (1961). Plasma oscillations. *Plasma Phys. (J. Nuclear Energy* C) **2**, 117. [286]

Epstein, M. (1960). Nonlinear behavior of the electrical conductivity of a slightly ionized gas. *Phys. Fluids* **3**, 1016. [92]

Epstein, M. (1962). Electromagnetic-wave propagation in a plasma with nonlinear electrical conductivity. *Phys. Fluids* **5**, 492. [92]

Farley, D. T., J. P. Dougherty, and D. W. Barron (1961). A theory of incoherent scattering of radio waves by a plasma. *Proc. Roy. Soc. (London)* **A263**, 238. [93]

Farnell, G. W. (1958). Measured phase distribution in the image space of a microwave lens. *Can. J. Phys.* **36**, 935. See also G. W. Farnell, "Phase distribution in the image space of a microwave lens system," Eaton Electronics Research Lab. Tech. Rept. 39 (1958), McGill Univ., Montreal. [145, 150]

Fejer, J. A. (1960). Radio-wave scattering by an ionized gas in thermal equilibrium. *J. Geophys. Research* **65**, 2635. [93]

Field, G. B. (1956). Radiation by plasma oscillations. *Astrophys. J.* **124**, 555. [286]

Field, G. B. (1959). The source of radiation from Jupiter at decimeter wavelengths. *J. Geophys. Research* **64**, 1169. [286]

Fields, H., G. Bekefi, and S. C. Brown (1963). Microwave emission from non-Maxwellian plasmas. *Phys. Rev.* **129**, 506. [271, 302]

Forsyth, P. A., W. Petrie, and B. W. Currie (1950). On the origin of ten centimeter radiation from the polar aurora. *Can. J. Research* **A28**, 324. [286]

Francis, G. (1960). *Ionization Phenomena in Gases.* Academic Press, New York. [62, 91]

French, I. P., G. G. Cloutier, and M. P. Bachynski (1961). The absorptivity spectrum of a uniform anisotropic plasma slab. *Can. J. Phys.* **39**, 1273. [130, 192, 270]

Fried, B. D., and S. D. Conte (1961). *The Plasma Dispersion Function.* Academic Press, New York. [105]

Gabor, D., E. A. Ash, and D. Dracott (1955). Langmuir's paradox. *Nature* **176**, 916. [290]

Gallet, R., J. M. Richardson, B. Wieder, G. D. Ward, and G. N. Harding (1960). Microwave whistler mode propagation in a dense laboratory plasma. *Phys. Rev. Letters* **4**, 347. [226]

Gardner, A. L., W. L. Barr, R. L. Kelly, and N. L. Oleson (1961). Diagnostic measurements on the P-4 steady-state plasma. Lawrence Radiation Lab. Rept. UCRL-6562, Univ. of California, Livermore, Calif. [301]

Gaunt, J. A. (1930). Continuous absorption. *Phil. Trans. Roy. Soc. London* **A229**, 163. [248, 251]

Gershman, B. N. (1960). Nonresonance absorption of electromagnetic waves in a magnetoactive plasma. *Soviet Phys.—JETP* **10**, 497. Gyromagnetic absorption of electromagnetic waves in a plasma. *Soviet Phys.—JETP* **11**, 657. [114]

Ginzburg, V. L. (1944). On the absorption of radio waves and the number of collisions in the ionosphere. *J. Phys. (U.S.S.R.)* **8**, 253. [83]

Ginzburg, V. L. (1959). Nonlinear interaction of radio waves propagating in a plasma. *Soviet Phys.—JETP* **8**, 1100. [93]

Ginzburg, V. L. (1960). Certain theoretical aspects of radiation due to superluminal motion in a medium. *Soviet Phys.—Uspekhi* **2**, 874. [280]

Ginzburg, V. L., and A. V. Gurevich (1960). Nonlinear phenomena in a plasma located in an alternating electromagnetic field. *Soviet Phys.—Uspekhi* **3**, 115, 175. [89]

Glasstone, S., and R. H. Lovberg (1960). *Controlled Thermonuclear Reactions.* Van Nostrand, Princeton, N.J. [97, 273]

Goldstein, L. (1958). Nonreciprocal electromagnetic wave propagation in ionized gaseous media. *I.R.E. Trans.* **MTT-6**, 19. [20]

Golovin, I. N. (1959). Studies of trapping fast charged particles in a constant magnetic field, conducted in the U.S.S.R. according to the program of controlled thermonuclear reactions. Atomic Energy Institute Rept. 23, U.S.S.R. Academy of Sciences, Moscow. Reprinted in *Proc. Inst. Elect. Engrs.* **106**, Pt. A, Suppl. No. 2, p. 95 (1959). [302]

Graben, H. W. (1963). Relativistic corrections to microwave interferometry in plasmas. *Phys. Fluids* **6**, 1659. [115]

Graf, K., and M. P. Bachynski (1961). Transmission and reflection of electromagnetic waves at a plasma boundary for arbitrary angles of incidence. *Can. J. Phys.* **39**, 1544. See also *Can. J. Phys.* **36**, 456 (1958). [130]

Greene, J. (1959). Bremsstrahlung from a Maxwellian gas. *Astrophys. J.* **130**, 693 (Fig. 3 is in error; corrected data appears in our Figs. 2.9 and 7.2). An additional appendix is included in U.S. Atomic Energy Comm. Rept. NYO-7905 (1958). [86, 87, 89, 251, 254, 256, 263]

Gross, E. P. (1951). Plasma oscillations in a static magnetic field. *Phys. Rev.* **82**, 232. [104]

Gurevich, A. V. (1956). On the effect of radio waves on the properties of plasma (ionosphere). *Soviet Phys.—JETP* **3**, 895. [76]

Hain, K., and M. Tutter (1962). Durchgang von Mikrowellen durch ebene Plasmaschichten. *Z. Naturforsch.* **17a**, 59. [136, 192]

Hall, L. S., and A. L. Gardner (1961). P-4, a steady-state plasma system. Lawrence Radiation Lab. Rept. UCRL-6561, Univ. of California, Livermore, Calif. [300]

Harding, G., A. Dellis, A. Gibson, B. Jones, D. Lees, R. McWhirter, S. Ramsden, and S. Ward (1958). Diagnostic techniques used in controlled thermonuclear research at Harwell. *Proc. 2nd U.N. Conf. Peaceful Uses of Atomic Energy* (Geneva) **32**, 365. [290]

Harrison, E. R. (1960). Runaway and suprathermal particles. *Plasma Phys. (J. Nuclear Energy* C) **1**, 105. [285]
Hayakawa, S., N. Hokkyō, Y. Terashima, and T. Tsuneto (1958). Cyclotron radiation from a magnetized plasma. *Proc. 2nd U.N. Conf. Peaceful Uses of Atomic Energy* (Geneva) **32**, 385. [293]
Heald, M. A. (1956). Microwave generation in B-1 Stellarator. U.S. Atomic Energy Commission Rept. TID-7520, Vol. 1, 202. [*vii*, 286, 300]
Heald, M. A. (1958). Microwave measurements in controlled fusion research. *I.R.E. Natl. Conv. Record*, Part 9, 14.
Heald, M. A. (1959*a*). The application of microwave techniques to Stellarator research. U.S. Atomic Energy Commission Rept. MATT-17. [137, 148]
Heald, M. A. (1959*b*). Experimental measurements in controlled fusion research. *I.R.E. Trans.* **NS-6**(*3*), 33.
Heald, M. A. (1959*c*). Engineering design of microwave electron density measuring systems. Project Matterhorn Tech. Memo 78, Princeton Univ., Princeton, N.J. [206]
Heald, M. A. (1960). An attempt of observe whistler mode propagation in Stellarators. Project Matterhorn Tech. Memo. 109, Princeton Univ., Princeton, N.J. [226]
Heitler, W. (1954). *Quantum Theory of Radiation*, 3rd ed. University Press, Oxford. [93, 251]
Helliwell, R. A., J. H. Crary, J. H. Pope, and R. L. Smith (1956). The nose whistler—a new high-latitude phenomenon. *J. Geophys. Research* **61**, 139. [225]
Helliwell, R. A., and M. G. Morgan (1959). Atmospheric whistlers. *Proc. I.R.E.* **47**, 200. [19, 49, 225]
Herlofson, N. (1951). Plasma resonance in ionospheric irregularities. *Arkiv Fysik* **3**, 247. [240]
Hershberger, W. D. (1960). Absorption and reflection spectrum of a plasma. *J. Appl. Phys.* **31**, 417. [241]
Hester, R., and D. Reagan (1960). Hose instability beam experiment. Lawrence Radiation Lab. Rept. UCID-4192, Univ. of California, Livermore, Calif. [195]
Hettner, G. (1958). Zur Theorie der Bremsstrahlung in Plasmen hoher Temperatur. *Z. Physik* **150**, 182. [256]
Hines, C. O. (1951). Wave packets, the Poynting vector, and energy flow. *J. Geophys. Research* **56**, 63, 197, 207, 535. [45]
Hirshfield, J. L., D. E. Baldwin, and S. C. Brown (1961). Cyclotron radiation from a hot plasma. *Phys. Fluids* **4**, 198. [277]
Hirshfield, J. L., and S. C. Brown (1958). Microwave method for measuring the probability of elastic collision of electrons in a gas. *J. Appl. Phys.* **29**, 1749. [161]
Hirshfield, J. L., and S. C. Brown (1961). Incoherent microwave radiation from a plasma in a magnetic field. *Phys. Rev.* **122**, 719. [271, 274, 275, 280, 297, 298]
Hu, M-K. (1961). Fresnel region fields of circular aperture antennas. *J. Research Natl. Bur. Standards* **65D**, 137. [146]
Hwa, R. C. (1958). Effects of electron-electron interactions on cyclotron resonances in gaseous plasmas. *Phys. Rev.* **110**, 307. [84, 274]
Iams, H. (1950). A method of simulating propagation problems. *Proc. I.R.E.* **38**, 543. [151]
Ichimaru, S. (1962). Wave properties of a plasma with a doubly humped velocity distribution. *Phys. Fluids* **5**, 1264. [286]

Ichtchenko, G. (1962). Propagation d'une onde electromagnetiques parallelement à un champ magnetique dans un gas ionise. Thesis, Faculte des Sciences, Universite de Paris. [226]
Imre, K. (1962). Oscillations in a relativistic plasma. *Phys. Fluids* **5**, 459. [116]
Jackson, J. D. (1962). *Classical Electrodynamics.* Wiley, New York. [233]
Jackson, J. E. (1954). Measurements in the *E*-layer with the navy Viking rocket. *J. Geophys. Research* **59**, 377. [402]
Jahn, R. G. (1962). Microwave probing of ionized-gas flows. *Phys. Fluids* **5**, 678. [150]
Jahnke, E., and F. Emde (1945). *Tables of Functions*, 4th ed. Dover, New York. [72, 247]
Jancel, R., and R. Kahan (1955). Examen critique de la théorie des plasmas basée sur le libré parcours moyen, à la lumiére de la méthode fondée sur la fonction de distribution solution de l'équation de Boltzmann. *J. phys. radium* **16**, 824. [66]
Jelley, J. V. (1958). *Cerenkov Radiation.* Pergamon Press, New York. [280]
Johnson, P. S. (1962). Cerenkov radiation spectra for a cold magnetoactive plasma. *Phys. Fluids* **5**, 118. [285]
Johnson, R. C. (1959). Design of linear double tapers in rectangular waveguides. *I.R.E. Trans.* **MTT-7**, 374. [136]
Johnston, T. W. (1962). Waves in warm quiescent plasmas. *Can. J. Phys.* **40**, 1208. [105, 116]
Joseph, J., and F. Rohrlich (1958). Pair production and bremsstrahlung in the field of free and bound electrons. *Revs. Modern Phys.* **30**, 354. [256]
Karzas, W. J., and R. Latter (1961). Electron radiative transitions in a Coulomb field. *Astrophys. J., Supplement Series* **6**, 167. [251, 263]
Katz, J. E. (1959). Instabilities excitation experiment diagnostics. Electronics Dept. Rept. LE-319, Lawrence Radiation Lab., Univ. of California, Livermore, Calif. [302]
Keitel, G. H. (1956). On the dipole resonant mode of an ionized gas column. *Australian J. Phys.* **9**, 144. [241]
Kelly, D. C. (1960). Microwave conductivity of a plasma in a magnetic field. *Phys. Rev.* **119**, 27. [84]
Kelly, D. C., H. Margenau, and S. C. Brown (1957). Cyclotron resonance: method for determining collision cross sections for low-energy electrons. *Phys. Rev.* **108**, 1367. [274]
Kerker, M., and E. Matijević (1961). Scattering of electromagnetic waves from concentric infinite cylinders. *J. Opt. Soc. Am.* **51**, 506. [137]
Kerns, D. M., and E. S. Dayhoff (1961). Theory of diffraction in microwave interferometry. *J. Research Natl. Bur. Standards* **64B**, 1. [130]
Kharchenko, I., Ya. Fainberg, R. Nikolaev, E. Kornilov, E. Lutsenko, and N. Pedenko (1960). Interaction of an electron beam with a plasma. *Soviet Phys.—JETP* **11**, 493. [286]
Kihara, T., and O. Aono (1963). Unified theory of relaxations in plasmas: basic theorem. *J. Phys. Soc. Japan* **18**, 837. [86]
Kihara, T., O. Aono, and R. Sugihara (1961). Theory of Cerenkov and cyclotron radiations in plasma. *Nuclear Fusion* **1**, 181. [284]
Kihara, T., M. H. Taylor, and J. O. Hirschfelder (1960). Transport properties for gases assuming inverse power intermolecular potentials. *Phys. Fluids* **3**, 715. [62]
Kildal, A. (1961). Energy absorption in a longitudinal wave in collisionless, magnetized plasma. *Plasma Phys. (J. Nuclear Energy* C) **3**, 256. [115]

King, R. W. P., and T. T. Wu (1959). *The Scattering and Diffraction of Waves.* Harvard Univ. Press, Cambridge, Mass. [137]

Kino, G. S. (1960). Parametric amplifier theory for plasmas and electron beams. *J. Appl. Phys.* **31**, 1449. [286]

Kino, G. S., and M. A. Allen (1961). The effects of fluctuations on propagation through a plasma medium. *Proc. 5th Intl. Conf. Ionization Phenomena in Gases* (Munich), 602 (North Holland Publ. Co., Amsterdam, 1962). [94]

Kittel, C. (1958). *Elementary Statistical Physics.* Wiley, New York. Section 44. [115]

Klein, M., H. Greyber, J. King, and K. Brueckner (1961). Interaction of a non-uniform plasma with microwave radiation. *Planetary and Space Sci.* **6**, 105. [136]

Knol, K. S. (1951). Determination of the electron temperature in gas discharges by noise measurements. *Phillips Research Rept.* **6**, 288. [244, 266, 290]

Koch, H. W., and J. W. Motz (1959). Bremsstrahlung cross-section formulas and related data. *Revs. Modern Phys.* **31**, 920. [251, 256]

Kolomenskii, A. A. (1956). Radiation from a plasma electron in uniform motion in a magnetic field. *Soviet Phys.—Doklady* **1**, 133. [281]

Kompfner, R. (1952). Travelling-wave tubes. *Repts. Progr. Phys.* **15**, 275. [286]

Kramers, H. A. (1923). On the theory of x-ray absorption and of the continuous x-ray spectrum. *Phil. Mag.* **46**, 836. [248, 250]

Kuiper, G. P., ed. (1953). *The Sun.* Univ. of Chicago Press, Chicago. Chapter 7. [286, 300]

Landau, L. D. (1946). On the vibrations of the electronic plasma. *J. Phys. (U.S.S.R.)* **10**, 25. [115, 185]

Landau, L. D., and E. Lifshitz (1962). *Classical Theory of Fields*, 2nd ed., translated by M. Hamermesh. Addison-Wesley, Reading, Mass. [248, 275, 276]

Landauer, G. (1961). Magnetfeldabhängige Mikrowellenstrahlung aus einer He-Gasentladung. *Proc. 5th Intl. Conf. Ionization Phenomena in Gases* (Munich), 389 (North-Holland Publ. Co., Amsterdam, 1962). [302]

Landauer, G. (1962). Generation of harmonics of the electron-gyrofrequency in a Penning discharge. *Plasma Phys. (J. Nuclear Energy C)* **4**, 395. [213, 302, 303]

Lashinsky, H. (1961). Cerenkov radiation at microwave frequencies. *Advances Electronics and Electron Phys.* **14**, 265. [281]

Lashinsky, H. (1963). Analogous propagation modes in inhomogeneous plasma and tapered waveguides. Plasma Physics Lab. Tech. Memo 177, Princeton Univ., Princeton, N.J. [151]

Lawson, J. D. (1954). On the relation between Cerenkov radiation and bremsstrahlung. *Phil. Mag.* **45**, 748. [284]

Lenard, A. (1959). Adiabatic invariance to all orders. *Ann. Phys.* **6**, 261. [97]

Leontovich, M. (1961). Generalization of the Kramers-Kronig formulas to media with spatial dispersion. *Soviet Phys.—JETP* **13**, 634. See also V. L. Ginzburg and N. N. Meiman, *Soviet Phys.—JETP* **19**, 169 (1964). [115]

Levin, M. L. (1957). Thermal radiation of good conductors. *Soviet Phys.—JETP* **4**, 225. [271]

Lewis, R. M., and J. B. Keller (1962). Conductivity tensor and dispersion equation for a plasma. *Phys. Fluids* **5**, 1248. [105]

Lin, S.-C., E. L. Resler, and A. Kantrowitz (1955). Electrical conductivity of highly ionized argon produced by shock waves. *J. Appl. Phys.* **26**, 95. [83]

Linfoot, E. H., and E. Wolf (1956). Phase distribution near focus in an aberration-free diffraction image. *Proc. Phys. Soc. (London)* **B69**, 823. [145, 150]

Lisitano, G. (1962). Mikrowellen Interferometer mit 1μs Zeitablösung. Report IPP 2/15, Institut für Plasmaphysik, Garching b. München, Germany. [209]

Lisitano, G. (1963). The application of the sinusoidal interference method in the design of a reflectometer and polarimeter in the range of millimetric waves. *Nachr. tech. Z-CJ*, No. 3, 103. English version of *Nachr. tech. Z.* **15**, 446 (1962). [210]

Lisitano, G., and M. Tutter (1961). Mikrowellenmessungen an einer hochfrequenzerregten Gasentladung. *Z. Naturforsch.* **16a**, 692. [210, 223, 225]

Long, M. W., and J. C. Butterworth (1963). New technique for microwave radiometry. *IEEE Trans.* **MTT-11**, 389. [299]

Lorentz, H. A. (1915). *The Theory of Electrons*, 2nd ed. Dover, New York, 1952. Sections 117–19. [401]

Madelung, E. (1943). *Die Mathematischen Hilfsmittel des Physikers*, 3rd ed. Dover, New York. [170]

Maecker, H., T. Peters, and H. Schenk (1955). Ionen und Atomquerschnitte im Plasma verschiedener Gase. *Z. Physik* **140**, 119. [84]

Mahaffey, D. W. (1963). Microwave propagation through a plasma in a magnetic field. *Phys. Rev.* **129**, 1481. [108, 223]

Majumdar, S. K. (1961). Radiation by charged particles passing through an electron plasma in an external magnetic field. *Proc. Phys. Soc. (London)* **77**, 1109. [286]

Marcuvitz, N. (1958). General electronic waveguides. *Proc. Symp. Electronic Waveguides*, 63 (Polytechnic Inst. of Brooklyn). [171]

Margenau, H. (1946). Conduction and dispersion of ionized gases at high frequencies. *Phys. Rev.* **69**, 508. [*vii*, 69]

Margenau, H. (1958). Conductivity of plasmas to microwaves. *Phys. Rev.* **109**, 6. [69]

Marshak, R. E. (1940). The internal temperature of white dwarf stars. *Astrophys. J.* **92**, 321. [86, 252]

Martyn, D. F. (1948). Solar radiation in the radio spectrum. *Proc. Roy. Soc. (London)* **A193**, 44. [86, 262, 271]

Massey, H. S. W., and E. H. S. Burhop (1952). *Electronic and Ionic Impact Phenomena.* Clarendon Press, Oxford. [61, 63]

McKensie, J. F. (1963). Cerenkov radiation in a magneto-ionic medium. *Phil. Trans. Roy. Soc. London* **A255**, 585. See also H. S. Tuan and S. R. Seshadri, *IEEE Trans.* **MTT-11**, 462. [281]

Milne, E. A. (1930). Thermodynamics of the stars. *Handbuch der Astrophys.* **3**(*I*), 65 (Springer, Berlin). [257]

Mitra, S. K. (1952). *The Upper Atmosphere*, 2nd ed., The Asiatic Soc., Calcutta. [*vii*]

Molmud, P. (1959). Langevin equation and the a.c. conductivity of non-Maxwellian plasmas. *Phys. Rev.* **114**, 29. [73, 76]

Montgomery, C. G., ed. (1947). *Technique of Microwave Measurements*, M.I.T. Radiation Lab. Series Vol. 11. McGraw-Hill, New York. Chapter 15. [146, 148]

Motley, R., and M. A. Heald (1959). Use of multiple polarizations for electron density profile measurements in high-temperature plasmas. *Proc. Symp. Millimeter Waves*, 141 (Polytechnic Inst. of Brooklyn). See also Project Matterhorn Tech. Memo 83 (1959), Princeton Univ. [125, 221]

Motley, R., C. D. Lustig, and S. Sanders (1961). Synchrotron radiation from runaway electrons in the Stellarator. *Plasma Phys. (J. Nuclear Energy C)* **3**, 17. [277, 292]

Mott, N. F., and H. S. W. Massey (1949). *The Theory of Atomic Collisions*, 2nd ed. Clarendon Press, Oxford. [61, 63]

Mott-Smith, H. M. (1960). Collision trajectories for inverse power intermolecular potentials. *Phys. Fluids* **3**, 721. [62]

Mower, L. (1956). Propagation of plane waves in an electrically anisotropic medium. Rept. MPL-1, Sylvania Microwave Physics Laboratory, Mountain View, Calif. [35]

Mower, L. (1959). Conductivity of a warm plasma. *Phys. Rev.* **116**, 16. [105]

Mumford, W. W. (1949). A broadband microwave noise source. *Bell System Tech. J.* **28**, 608. [266]

Nedelsky, L. (1932). Radiation from slow electrons. *Phys. Rev.* **42**, 641. [256]

Neufeld, J. (1961). Space dispersive properties of plasma. *Phys. Rev.* **123**, 1. [100]

Neufeld, J. (1963). Constitutive equations for a plasma-like medium. *J. Appl. Phys.* **34**, 2549. [96]

Nicodemus, F. E. (1963). Radiance. *Am. J. Phys.* **31**, 368. [257]

Nyquist, H. (1928). Thermal agitation of electric charge in conductors. *Phys. Rev.* **32**, 110. [244]

Oberman, C. (1961). On the radiation from co-operative phenomena in plasmas. *Plasma Phys. (J. Nuclear Energy* C) **2**, 154. [286]

Oberman, C., and F. Shure (1963). High-frequency plasma conductivity in a magnetic field. *Phys. Fluids* **6**, 834. See also C. Oberman and A. Ron, *Phys. Rev.* **130**, 1291 (1963). [89, 278]

Osborne, F. J. F. (1962). A multiple-probe microwave system for plasma studies. *Can. J. Phys.* **40**, 1620. [210]

Oskam, H. J. (1957). Microwave investigation of disintegrating gaseous discharge plasmas. Thesis, Univ. of Utrecht, Holland. [160]

Oster, L. (1960). Effects of collisions on the cyclotron radiation from relativistic particles. *Phys. Rev.* **119**, 1444. [274]

Oster, L. (1961*a*). Cyclotron radiation from relativistic particles with an arbitrary velocity distribution. *Phys. Rev.* **121**, 961. [278]

Oster, L. (1961*b*). Emission, absorption, and conductivity of a fully ionized gas at radio frequencies. *Revs. Modern Phys.* **33**, 525. [86, 249]

Oster, L. (1963*a*). Note on thermal radio radiation. *Astrophys. J.* **137**, 332. [86, 87, 254]

Oster, L. (1963*b*). Radiative transfer in dispersive media. *Astrophys. J.* **138**, 761. See also R. P. Mercier, *Proc. Phys. Soc. (London)* **83**, 811 (1964). [260]

Oster, L. (1964). Bremsstrahlung cross sections in the neighborhood of the plasma frequency. *Phys. Fluids* **7**, 263. See also R. P. Mercier, *Proc. Phys. Soc. (London)* **83**, 819 (1964). [252]

Osterberg, H. (1958). Propagation of plane electromagnetic waves in inhomogeneous media. *J. Opt. Soc. Am.* **48**, 513. [133]

Pakhomov, V. I., V. F. Aleksin, and K. N. Stepanov (1962). The radiation from an electron moving in a spiral in a magnetoactive plasma. *Soviet Phys.—Tech. Phys.* **6**, 856. [284]

Panofsky, W. K. H., and M. Phillips (1962). *Classical Electricity and Magnetism*, 2nd ed. Addison-Wesley, Reading, Mass. Chapter 20. [272, 275]

Papoular, R., and J. Wegrowe (1961). Utilisation de lentilles focalisantes pour le diagnostic micro-onde des plasmas. *Proc. 5th Intl. Conf. Ionization Phenomena in Gases* (Munich), 1456 (North-Holland Publ. Co., Amsterdam, 1962). [150]

Parzen, P., and L. Goldstein (1951). Current fluctuations in the direct current gas discharge plasma. *Phys. Rev.* **82**, 724. [245]

Persson, K. B. (1957). Limitations of the microwave cavity method of measuring electron densities in a plasma. *Phys. Rev.* **106**, 191. [162]

Phelps, A. V. (1960). Propagation constants for electromagnetic waves in weakly ionized, dry air. *J. Appl. Phys.* **31**, 1723. [73]

Pines, D. (1960). Plasma oscillations of electron gases. *Proc. Intl. Congress Many-Particle Problems* (Utrecht). [179]

Pistunovich, V. I., and V. D. Shafranov (1961). Cyclotron radiation by ions in cold plasma. *Nuclear Fusion* **1**, 189. [302]

Planck, M. (1914). *Theory of Heat Radiation.* Dover, New York, 1959. [242, 270]

Platzman, P. M., and S. J. Buchsbaum (1961). Effect of collisions on the Landau damping of plasma oscillations. *Phys. Fluids* **4**, 1288. [109, 115]

Platzman, P. M., and S. J. Buchsbaum (1962). Wave propagation along a magnetic field in a warm plasma. *Phys. Rev.* **128**, 1004. [108, 114]

Platzman, P. M., and S. J. Buchsbaum (1963). Transmission of electromagnetic waves through plasma slabs. *Phys. Rev.* **132**, 2. [108, 114]

Platzman, P. M., and H. T. Ozaki (1960). Scattering of electromagnetic waves from an infinitely long magnetized cylindrical plasma. *J. Appl. Phys.* **31**, 1597. [130, 239, 241]

Posener, D. W. (1959). The shape of spectral lines: tables of the Voigt profile. *Australian J. Phys.* **12**, 184. [275]

Post, R. F. (1958). Summary of UCRL Pyrotron (mirror machine) program. *Proc. 2nd U.N. Conf. Peaceful Uses of Atomic Energy* (Geneva) **32**, 245. [194, 293]

Post, R. F. (1961). Impurity radiation losses from a high temperature plasma. *Plasma Phys. (J. Nuclear Energy* C) **3**, 273. [256]

Post, R. F., R. E. Ellis, F. C. Ford, and M. N. Rosenbluth (1960). Stable confinement of a high temperature plasma. *Phys. Rev. Letters* **4**, 166. [293]

Pradhan, T. (1962). Causality and the dispersion formulas for waves in a plasma. *Ann. Phys.* **17**, 418. See also B. Gourary, *J. Appl. Phys.* **28**, 283 (1957). [115]

Primich, R. I., and R. A. Hayami (1963). Millimeter wavelength focussed probes and focussed resonant probes for use in studying ionized wakes behind hypersonic velocity projectiles. *Proc. Millimeter and Submillimeter Conf. of the IEEE* (Orlando, Fla.). See also General Motors Defense Research Lab. Report TR63-2176 (ARPA Order No. 347-63), Santa Barbara, Calif., and *IEEE Trans.* **MTT-12**, 33 (1964). [219]

Ramachandran, G. N., and S. Ramaseshan (1961). Crystal optics. *Handbuch der Physik* **25/1**, 1 (Springer-Verlag, Berlin). See also A. Sommerfeld, *Optics*, Academic Press, New York, 1954, Chapter 4; and M. Born and E. Wolf, *Principles of Optics*, Pergamon Press, New York, 1959, Chapter 14. [48]

Ramo, S., and J. R. Whinnery (1953). *Fields and Waves in Modern Radio*, 2nd ed. Wiley, New York. Chapters 1 and 7. [157]

Rao, K. V. N., J. T. Verdeyen, and L. Goldstein (1961). Interaction of microwaves in gaseous plasmas immersed in magnetic fields. *Proc. I.R.E.* **49**, 1877. [92]

Rao, M. S. V. G., and H. G. Booker (1963). Guiding of electromagnetic waves along a magnetic field in a plasma. *J. Geophys. Research* **68**, 387. [49]

Ratcliffe, J. A. (1959). *The Magneto-Ionic Theory and Its Applications to the Ionosphere.* University Press, Cambridge. [24, 45, 93, 127, 402]

Redheffer, R. M. (1949). Microwave antennas and dielectric surfaces. *J. Appl. Phys.* **20**, 397. [130, 150]

Renau, J., J. Camnitz, and W. Flood (1961). The spectrum and total intensity of electromagnetic waves scattered from an ionized gas in thermal equilibrium in the presence of a static quasi-uniform magnetic field. *J. Geophys. Research* **66**, 2703. [93]

Richtmyer, F. K., E. H. Kennard, and T. Lauritsen (1955). *Introduction to Modern Physics*, 5th ed. McGraw-Hill, New York. Chapter 4. [242]

Romell, D. (1951). Radio reflexions from a column of ionized gas. *Nature* **167**, 243. [241]

Rose, D. J., and S. C. Brown (1952). Measurement of discharge admittance and electron density. *J. Appl. Phys.* **23**, 719, 1028. [158]

Rose, D. J., and M. Clark, Jr. (1961). *Plasmas and Controlled Fusion.* Wiley, New York. Chapter 3. [64]

Rosen, B. B. (1959). The "inverted universe" plasma analog for microwaves. Project Matterhorn Tech. Memo 85, Princeton Univ., Princeton, N.J. [151, 152, 154]

Rosen, P. (1960). Scattering of electromagnetic waves by longitudinal plasma waves. *Phys. Fluids* **3**, 416. [92]

Rosen, P. (1961). Generation of the third harmonic by an electromagnetic signal in a plasma. *Phys. Fluids* **4**, 341. [92]

Rosenbluth, M. N., and C. L. Longmire (1957). Stability of plasmas confined by magnetic fields. *Ann. Phys.* **1**, 120. [66]

Rosenbluth, M. N., and N. Rostoker (1962). Scattering of electromagnetic waves by a non-equilibrium plasma. *Phys. Fluids* **5**, 776. [234]

Rosenfeld, L. (1951). *Theory of Electrons.* Interscience, New York. [400]

Rukhadze, A. A. (1962). Electromagnetic waves in interpenetrating plasmas. *Soviet Phys.—Tech. Phys.* **6**, 900. [286]

Rukhadze, A. A., and V. P. Silin (1962). Line shape of cyclotron resonance absorption in a plasma. *Soviet Phys.—Tech. Phys.* **7**, 307. [275]

Rytov, S. M. (1953). *Theory of Electric Fluctuations and Thermal Radiation.* Translation TR-59-162. Air Force Cambridge Research Center, Bedford, Mass., 1959. [261, 271, 287]

Sagdeyev, R. S., and V. D. Shafranov (1958). Absorption of high-frequency electromagnetic energy in a high-temperature plasma. *Proc. 2nd U.N. Conf. Peaceful Uses of Atomic Energy* (Geneva) **31**, 118. [114]

Salpeter, E. E. (1963). Density fluctuations in a nonequilibrium plasma. *J. Geophys. Research* **68**, 1321. [94]

Sampson, D. H. (1959). The opacity at high temperatures due to Compton scattering. *Astrophys. J.* **129**, 734. [93]

Sampson, D. H., and J. Enoch (1963). Electron distribution function and electrical conductivity of a slightly ionized gas. *Phys. Fluids* **6**, 28. [69]

Sauter, F. (1933). Zur unrelativistischen Theorie des kontinuierlichen Röntgenspektrums. *Ann. Physik* **18**, 486. See also *Ann. Physik* **20**, 404 (1934). [252]

Scarf, F. L. (1962). Landau damping and the attenuation of whistlers. *Phys. Fluids* **5**, 6. [114, 226]

Schelkunoff, S. A., and H. T. Friis (1952). *Antennas: Theory and Practice.* Wiley, New York. [143, 144, 243]

Scheuer, P. A. G. (1960). The absorption coefficient of a plasma at radio frequencies. *Mon. Not. Roy. Astron. Soc.* **120**, 231. [87, 249]

Schiff, L. I. (1955). *Quantum Mechanics*, 2nd ed. McGraw-Hill, New York. Section 28. [125]

Schlüter, H. (1961). Untersuchungen an Balmer-Spektren bei einer Hochfrequenzentladung. *Z. Naturforsch.* **16a**, 972. [225]

Schott, G. A. (1912). *Electromagnetic Radiation.* University Press, Cambridge. Page 109. [275]

Schwinger, J. (1949). On the classical radiation of accelerated electrons. *Phys. Rev.* **75**, 1212. [272, 275]

Sears, F. W. (1953). *Thermodynamics, the Kinetic Theory of Gases, and Statistical Mechanics*, 2nd ed. Addison-Wesley, Reading, Mass. [47, 74]

Sen, H. K., and A. A. Wyller (1960). On the generalization of the Appleton-Hartree magneto-ionic formulas. *J. Geophys. Research* **65**, 3931. [76]

Sexton, M. C., J. J. Lennon and M. J. Mulcahy (1959). Mircowave method of investigating the afterglows of pulsed gaseous discharges. *Brit. J. Appl. Phys.* **10**, 356. [163]

Shapiro, H. (1957). Electromagnetic scattering properties of a resonant plasma. Ph.D. Thesis, California Inst. of Technology, Pasadena, Calif. [241]

Sherman, J. W. (1962). Properties of focused apertures in the Fresnel region. *I.R.E. Trans.* **AP-10**, 399. [147]

Shkarofsky, I. P. (1961). Values of the transport coefficients in a plasma for any degree of ionization based on a Maxwellian distribution. *Can. J. Phys.* **39**, 1619. [75, 76, 83, 84]

Shkarofsky, I. P., I. B. Bernstein, and B. B. Robinson (1963). Condensed presentation of transport coefficients in a fully ionized plasma. *Phys. Fluids* **6**, 40. [75]

Shklovsky, I. S. (1960). *Cosmic Radio Waves*, translated by Rodman and Varsavsky. Harvard Univ. Press, Cambridge, Mass. [273]

Shmoys, J. (1961). Proposed diagnostic method for cylindrical plasmas. *J. Appl. Phys.* **32**, 689. [137]

Silin, V. P. (1960). Kinetic equation for rapidly varying processes. *Soviet Phys.—JETP* **11**, 1277. [86]

Silin, V. P. (1960–1962). Electromagnetic properties of a relativistic plasma. *Soviet Phys.—JETP* **11**, 1136 (1960); **13**, 430 (1961); **14**, 115 (1962). [115]

Silin, V. P. (1962). High-frequency dielectric constant of a plasma. *Soviet Phys.—JETP* **14**, 617. [89]

Silver, S. (1949). *Microwave Antenna Theory and Design*, M.I.T. Radiation Lab. Series, Vol. 12. McGraw-Hill, New York. [143]

Simon, A., and M. N. Rosenbluth (1963). Single particle cyclotron radiation near walls and sheaths. *Phys. Fluids* **6**, 1566. [280, 303]

Sitenko, A. G., and K. N. Stepanov (1957). On the oscillations of an electron plasma in a magnetic field. *Soviet Phys.—JETP* **4**, 512. [105, 107]

Slater, J. C. (1946). Microwave electronics. *Revs. Modern Phys.* **18**, 441. [156, 157]

Slater, J. C., and N. H. Frank (1947). *Electromagnetism.* McGraw-Hill, New York. Chapter IX. [403]

Smerd, S. F., and K. C. Westfold (1949). The characteristics of radio-frequency radiation in an ionized gas, with applications to the transfer of radiation in the solar atmosphere. *Phil. Mag.* **40**, 831. [259]

Smullin, L. D., and P. Chorney (1958). Properties of ion filled waveguides. *Proc. I.R.E.* **46**, 360. [181]

Smyth, W. R. (1950). *Static and Dynamic Electricity.* McGraw-Hill, New York. Chapter 14. [239, 241]

Snyder, W., and R. A. Helliwell (1952). Universal wave-polarization chart for the magneto-ionic theory. *J. Geophys. Research* **57**, 73. [25]

Sodha, M. S., and C. J. Palumbo (1963). Nonlinear propagation of electromagnetic waves in magnetoplasmas. *Can. J. Phys.* **41**, 2155. See also *Can. J. Phys.* **42**, 349 (1964). [92]

Sommerfeld, A. (1951). *Atombau und Spektrallinien*, Vol. II (*Wellenmechanik*). Frederick Ungar, New York. Chapter 7. [251]

Southworth, G. C. (1959). Using the Smith diagram. *Microwave J.* **2**(*1*), 25 and **2**(*2*), 24. [158]

Spitzer, L., Jr. (1940). The stability of isolated clusters. *Mon. Not. Roy. Astron. Soc.* **100**, 396. [92]

Spitzer, L., Jr. (1962). *Physics of Fully Ionized Gases*, 2nd ed. Interscience, New York. [56, 67, 78, 80, 81, 84, 98, 99]

Spitzer, L., Jr., and R. Härm (1953). Transport phenomena in a completely ionized gas. *Phys. Rev.* **89**, 977. [84]

Stepanov, K. N., and A. B. Kitsenko (1961). Excitation of electromagnetic waves in a magnetoactive plasma by a beam of charged particles. *Soviet Phys.—Tech. Phys.* **6**, 120. [285, 301]

Stickforth, J. (1961). Zur Theorie der Bremsstrahlung in Plasmen hoher Temperatur. *Z. Physik* **164**, 1. [256]

Stix, T. H. (1958). Generation and thermalization of plasma waves. *Phys. Fluids* **1**, 308. [127]

Stix, T. H. (1960). Absorption of plasma waves. *Phys. Fluids* **3**, 19. [126, 127]

Stix, T. H. (1962). *The Theory of Plasma Waves*. McGraw-Hill, New York. [45, 47, 48, 51, 56, 105, 108, 127, 293]

Storey, L. R. O. (1953). An investigation of whistling atmospherics. *Phil. Trans. Roy. Soc. London* **A246**, 113. [225, 402]

Stratton, J. A. (1941). *Electromagnetic Theory*. McGraw-Hill, New York. Sections 9.10–9.12. [129]

Sturrock, P. A. (1957). Non-linear effects in electron plasmas. *Proc. Roy. Soc. (London)* **A242**, 277. See also *Plasma Phys. (J. Nuclear Energy* C) **2**, 158 (1961). [188, 189]

Sumi, M. (1959). Theory of spatially growing plasma waves. *J. Phys. Soc. Japan* **14**, 653. [285]

Sweet, P. A. (1959). Coulomb scattering in a magnetic field. *Phil. Mag.* **4**, 1155. [88]

Symon, K. R. (1960). *Mechanics*, 2nd ed. Addison-Wesley, Reading, Mass. [60, 62]

Tanaka, S., K. Mitani and H. Kubo (1963). Microwave radiation from a plasma in a magnetic field. Institute of Plasma Physics Rept. IPPJ-13, Nagoya University, Nagoya, Japan. [304]

Targ, R., and L. P. Levine (1961). Backward-wave microwave oscillations in a system composed of an electron beam and a hydrogen gas plasma. *J. Appl. Phys.* **32**, 731. [286]

Taylor, L. S. (1961). Electromagnetic propagation in an exponential ionization density. *I.R.E. Trans.* **AP-9**, 483. [136]

Theimer, O. (1963). Collective aspects of bremsstrahlung emission and electrical conductivity in a plasma. *Ann. Phys.* **22**, 102. [85, 253, 262]

Theimer, O., and L. S. Taylor (1961). On the index of refraction in the ionosphere. *J. Geophys. Research* **66**, 3157. [403]

Thonemann, P. C. et al. (1958). Controlled release of thermonuclear energy. *Nature* **181**, 217. [226]

Tidman, D. A., and J. M. Boyd (1962). Radiation by plasma oscillations incident on a density discontinuity. *Phys. Fluids* **5**, 213. [286]

Tonks, L., and I. Langmuir (1929). Oscillations in ionized gases. *Phys. Rev.* **33**, 195, 990. [*vii*, 2]

Trivelpiece, A. W. (1958). Slow wave propagation in plasma waveguides. Tech. Rept. 7, California Inst. of Technology, Pasadena, Calif. [173, 175, 177, 178, 180]

Trubnikov, B. A. (1958). Plasma radiation in a magnetic field. *Soviet Phys.—Doklady* **3**, 136. [275]

Trubnikov, B. A., and V. S. Kudryavtsev (1958). Plasma radiation in a magnetic field. *Proc. 2nd U.N. Conf. Peaceful Uses of Atomic Energy* (Geneva) **31**, 93. [272]

Trubnikov, B. A., and V. B. Yakubov (1963). Cyclotron radiation of electrons having a two-dimensional Maxwellian distribution. *Plasma Phys. (J. Nuclear Energy* C) **5**, 7. [277]

Turner, C. H. M. (1954). Birefringence in crystals and in the ionosphere. *Can. J. Phys.* **32**, 16. [31, 33]

Unz, H. (1963). The magneto-ionic theory for bound electrons. *J. Atmosph. Terr. Phys.* **25**, 281. [403]

Vachaspati (1962). Harmonics in the scattering of light by free electrons. *Phys. Rev.* **128**, 664. [93]

van der Pol, B. (1920). De invloed van een geioniseerd gas op het voortschrijden van electromagnetische golven. Thesis, Univ. of Utrecht. Reprinted in van der Pol, *Selected Scientific Papers*, Vol. I (North-Holland Publ. Co., Amsterdam, 1960). [*vi*]

Van Vleck, J. H. (1932). *The Theory of Electric and Magnetic Susceptibilities*. University Press, Oxford. [400]

Vlasov, A. A. (1938). Theory of vibrational properties of an electron gas and its applications. *J. Exptl. Theoret. Phys. (U.S.S.R.)* **8**, 291. See also *J. Phys. (U.S.S.R.)* **9**, 25, 130 (1945). [67]

Vogt, E., and G. H. Wannier (1954). Scattering of ions by polarization forces. *Phys. Rev.* **95**, 1190. [63]

von Gierke, G., L. Lisitano, G. Müller, H. Schlüter, M. Tutter, and H. Wulff (1961). Vergleich spektrosckopische Untersuchen mit Mikrowellen- und Sonden, Messungen. *Proc. 5th Intl. Conf. Ionization Phenomena in Gases* (Munich)-380 (North-Holland Publ. Co., Amsterdam, 1962). [225, 229]

Warder, R., M. Brodwin, and A. B. Cambel (1962). Sources of error in the microwave diagnostics of plasmas. *J. Appl. Phys.* **33**, 2868. [151]

Watkins, D. A. (1958). *Topics in Electromagnetic Theory*. Wiley, New York. [167]

Weitzner, H. (1963). Plasma oscillations and Landau damping. *Phys. Fluids* **6**, 1123. [187]

Westfold, K. C. (1950). Refractive index and classical radiative processes in an ionized gas. *Phil. Mag.* **41**, 509. [248, 262]

Wetzel, L. (1961). Wave interaction in plasma inhomogeneities. *J. Appl. Phys.* **32**, 327. [93]

Wharton, C. B. (1957). Microwave diagnostics for controlled fusion research. Lawrence Radiation Lab. Rept. UCRL-4836(Rev.), Univ. of California, Livermore, Calif.

Wharton, C. B. (1959). Microwave radiation measurements of very hot plasmas. *Proc. 4th Intl. Conf. Ionization Phenomena in Gases* (Uppsala), 737 (North-Holland Publ. Co., Amsterdam, 1960). [213, 226, 292]

Wharton, C. B. (1961). Microwave diagnostics for controlled fusion research. In J. E. Drummond, ed., *Plasma Physics*. McGraw-Hill, New York. Chapter 12. [290, 292]

Wharton, C. B., and A. L. Gardner (1959). Microwave circuits and horns for plasma measurements. U.S. Patent No. 2,971,153. [200, 206]

Wharton, C. B., R. F. Post, and T. Prosser (1955). Microwave diagnostics in arc research. Lawrence Radiation Lab. Rept. UCRL-4477, Univ. of California, Livermore, Calif. [*vii*, 192]

Wharton, C. B., and D. M. Slager (1960). Microwave determination of plasma density profiles. *J. Appl. Phys.* **31**, 428. [125, 212, 214]

Whitehead, J. D. (1952). The quasi-transverse (QT) approximation to Appleton's magneto-ionic equation. *J. Atmos. Terrest. Phys.* **2**, 361. [38]

Whitmer, R. F., and E. B. Barrett (1961, 1962). Nonlinear interaction of an electromagnetic wave with a plasma layer in the presence of a static magnetic field. *Phys. Rev.* **121**, 661 (1961); **125**, 1478 (1962). [93]

Willett, J. E. (1962). Effects of electron random motion on microwave propagation through a plasma parallel to a magnetic field. *J. Appl. Phys.* **33**, 898. [108, 109, 114]

Woolley, R. R., and D. W. N. Stibbs (1953). *The Outer Layers of a Star*. Clarendon Press, Oxford. Chapter 11. [259]

Wort, D. J. H. (1962). The emission of microwave noise by plasma. *Plasma Phys. (J. Nuclear Energy* C) **4**, 353. [136, 266]

Wort, D. J. H. (1963). Refraction of microwaves by a plasma cylinder. Rept. CLM-R27, U.K. Atomic Energy Authority. [137]

Wort, D. J. H. (1964). The microwave emissivity of turbulent plasma. *Plasma Phys. (J. Nuclear Energy* C) **6**, 237. [271, 288, 298]

Wyld, H. W., Jr. (1960). Radiation by plasma oscillations in a bounded plasma in a magnetic field. *Phys. Fluids* **3**, 408. [286]

Yamada, K. (1962). General expressions of absorption coefficient and radiation intensity in plasma and Kirchhoff's law. *Progr. Theoret. Phys. (Kyoto)* **28**, 599. [262]

Yoshikawa, S. (1962). Electrical conductivity of a turbulent plasma. *Phys. Fluids* **5**, 1272. [94]

REFERENCES FOR CHAPTER 9

Allen, P. J., and R. D. Tompkins (1959). An instantaneous microwave polarimeter. *Proc. I.R.E.* **47**, 1231. [324]

Ayres, W. P., P. H. Vartanian, and J. L. Melchor (1957). Frequency doubling in ferrites. *J. Appl. Phys.* **27**, 188. [321, 345]

Barnett, E. F. (1955). A new precision X-band phase-shifter. *Trans. 4th Conf. on High Frequency Measurements, IRE, AIEE, NBS and URSI* (Washington, D.C.), 150. [315]

Bekefi, G., J. C. Ingraham, and J. J. McCarthy (1962). A transient microwave radiation pyrometer. *Research Lab. of Electronics Quarterly Report* (March), M.I.T., Cambridge, Mass. [355]

Benderly, A. A., and T. J. Kilduff (1962). A teflon microwave window. *Microwave J.* **4**(*3*), 101. [357]

Blau, R., and M. A. Heald (1959). Mathieu function roots for TE_{11} modes in elliptic waveguide. Project Matterhorn Tech. Memo 79, Princeton Univ., Princeton, N.J. [320]

Bloom, S., and K. K. N. Chang (1957). Theory of parametric amplification using non-linear reactances. *R.C.A. Rev.* **18**, 578. [345, 351]

Booker, H. G. (1946). Slot aerials and their relation to complementary wire aerials. *J. Inst. Elec. Engrs. (London)* **93**, Part IIIA, 620. [338]

Bossard, B. B., E. Frost, and W. Fishbein (1960). X-band super-regenerative parametric mixer. *Proc. I.R.E.* **48**, 1329. [352]

Brown, J. (1953). Artificial dielectrics having refractive indices less than unity. *Proc. Inst. Elec. Engrs. (London)* **100**, Part IV, 51. [331]

Brown, J., and J. O. Spector (1957). The radiating properties of end-fire aerials. *Proc. Inst. Elec. Engrs. (London)* **104B**, 27. [335]

Buser, R., and W. Buser (1962). Determination of plasma properties by free-space microwave techniques. *J. Appl. Phys.* **33**, 2275. [205, 342, 343]

Byrne, J. F., and C. F. Cook (1963). Microwave type bolometer for submillimeter wave measurements. *IEEE Trans.* **MTT-11**, 379. [346]

Cacheris, J. (1954). Microwave single-sideband modulator using ferrites. *Proc. I.R.E.* **42**, 1242. [315]

Chandler, C. H. (1949). An investigation of dielectric rod as waveguide. *J. Appl. Phys.* **20**, 1188. [311]

Cohn, S. B. (1957). Direct-coupled resonator filters. *Proc. I.R.E.* **45**, 187. [318, 319]

Coleman, P. D., and R. C. Becker (1959). Present state of the millimeter wave generation and technique art. *I.R.E. Trans.* **MTT-7**, 42. [345]

Cottony, H. V., and A. C. Wilson (1958). Gains of finite-size corner reflector antennas. *I.R.E. Trans.* **AP-6**, 366. [336]

Crompton, J. W. (1954). On the optimum illumination taper for the objective of a microwave aerial. *Proc. Inst. Elec. Engrs. (London)* **101**, Part III, 371. [338]

Diament, P., S. P. Schlesinger, and A. Vigants (1961). A dielectric surface wave structure: the V-line. *I.R.E. Trans.* **MTT-9**, 322. [310]

Dicke, R. H. (1946). The measurement of thermal radiation at microwave frequencies. *Rev. Sci. Instr.* **17**, 268. [354]

Dicke, R. H., R. Beringer, R. L. Kyhl, and A. B. Vane (1946). Atmospheric absorption measurements with a microwave radiometer. *Phys. Rev.* **70**, 340. [312, 313]

Dushman, S. (1962). *Scientific Foundations of Vacuum Technique*, 2nd ed. Wiley, New York. [356]

Elsasser, W. M. (1949). Attenuation in a dielectric circular rod. *J. Appl. Phys.* **20**, 1193. [335]

Esaki, L. (1958). New phenomenon in narrow Ge *p–n* junctions. *Phys. Rev.* **109**, 603. [352]

Fiske, M. D. (1946). Resonant windows for vacuum seals in rectangular waveguides. *Rev. Sci. Instr.* **17**, 478. [360]

Fox, A. G. (1947). An adjustable waveguide phase changer. *Proc. I.R.E.* **35**, 1489. [315]

Fox, A. G., S. E. Miller, and M. T. Weiss (1954). Behavior and applications of ferrites in the microwave region. *Bell System Tech. J.* **34**, 5. [315]

Gardner, A. L. (1962). Diagnostic measurements of a highly ionized, steady-state plasma. In *Engineering Aspects of Magnetohydrodynamics*, C. Mannal and N. Mather ed., Columbia University Press, p. 438 [333, 334, 386]

Gordon, J. P., H. J. Zeiger, and C. H. Townes (1955). The maser—new type of microwave amplifier, frequency standard and spectrometer. *Phys. Rev.* **99**, 1264. [352]

Goubau, G., and F. Schwering (1961). On the guided propagation of electromagnetic wave beams. *I.R.E. Trans.* **AP-9**, 248. [311, 312]

Guillemin, E. A. (1948). *Communication Networks*. Wiley, New York. [318]

Guthrie, A., and R. K. Wakerling (1949). *Vacuum Equipment and Techniques*. McGraw-Hill, New York. [360]

Hannan, P. W. (1961). Microwave antennas derived from the cassegrain telescope. *I.R.E. Trans.* **AP-9**, 140. [338]

Harris, D. B. (1960). Microwave radiometry. *Microwave J.* **3**(*4*), 41 and **3**(*5*), 47. [353]

Harris, E. F. (1953). An experimental investigation on the corner reflector antenna. *Proc. I.R.E.* **41**, 645. [336]

Harvey, A. F. (1963). *Microwave Engineering*. Academic Press, New York. [349, 361]

Hawkins, P. O., H. J. Curnow, and R. Redstone (1958). The coaxial-line diode: a rectifier of microwaves. *Proc. Inst. Elec. Engrs. (London)* **105B**, Sup. No. 12, 886. [353]

Holonyak, N., and I. A. Lesk (1960). Gallium arsenide tunnel diodes. *Proc. I.R.E.* **48**, 1405. [352]

Jasik, Henry, ed. (1961). *Antenna Engineering Handbook*. McGraw-Hill, New York. [329]

Jenks, F. A. (1947). Simplified microwave A.F.C. *Electronics* **20**(*11*), 120, and **20**(*12*), 132. [351]

Johnson, C. M. (1954). Superheterodyne receiver for the 100 to 150 kMc region. *I.R.E. Trans.* **MTT-2**(*3*), 27. [351]

Johnson, C. M., D. M. Slager, and D. D. King (1954). Millimeter waves from harmonic generators. *Rev. Sci. Instr.* **25**, 213. [345]

Johnson, J. B. (1928). Thermal agitation of electricity in conductors. *Phys. Rev.* **32**, 97. [346]

Jones, C. W. (1961). Concerning hybrids. *Microwave J.* **4**(*10*), 98. [315]

King, A. P. (1950). The radiation characteristics of conical horn antennas. *Proc. I.R.E.* **38**, 249. [328, 329]

Klapper, H. (1962). Microwave field plotter. Electronics Dept. Rept. LER 579, Lawrence Radiation Lab., Univ. of California, Livermore, Calif. [342]

Kohl, W. H. (1960). *Materials and Techniques for Electron Tubes*. Reinhold, New York. [357]

Kunz, K. S. (1954). Propagation of microwaves between parallel doubly curved conducting surfaces. *J. Appl. Phys.* **25**, 642. [331]

Lanciani, D. A. (1954). HO_1 mode circular waveguide components. *I.R.E. Trans.* **MTT-2**(*3*), 45. [310]

Lawson, J. D. (1948). Some methods of determining the power gain of microwave aerials. *J. Inst. Elec. Engrs. (London)* **95**, Part III, 205. [341]

Lebenbaum, M. (1956). Measurement of noise figure. Chapter XI in *Handbook of Electronic Measurements*. Polytechnic Institute of Brooklyn Press, Brooklyn, N.Y. [355]

Lending, R. D. (1955). New criteria for microwave component surfaces. *Proc. Nat. Electronics Conf.* **11**, 391. [306]

Lewin, L. (1959). A note on quasi optical methods at millimeter wavelengths. *Proc. of Symp. on Millimeter Waves*, Polytechnic Institute of Brooklyn Press, Brooklyn, N.Y. [307]

de Loach, B. C. (1960). 17 and 30 kMc parametric amplifiers. *Proc. I.R.E.* **48**, 1323. [352]

Loth, P. A. (1956). Recent advances in waveguide hybrid junctions. *I.R.E. Trans.* **MTT-4**, 268. [315]

Malmberg, J., N. W. Carlson, C. B. Wharton, and W. E. Drummond (1963). A collisionless plasma for wave propagation studies. *Proc. 6th Intl. Conf. on Ionization Phenomena in Gases* (Paris) **4**, 229. [361]

Meyer, M. A., and H. B. Goldberg (1955). Applications of the turnstile junction. *I.R.E. Trans.* **MTT-3**(*6*), 40. [322]

Miller, S. E., and A. C. Beck (1953). Low-loss waveguide transmission. *Proc. I.R.E.* **41**, 348. [310]

Montgomery, C. G. (1947). *Technique of Microwave Measurements*. M.I.T. Radiation Lab. Series, Vol. 11. McGraw-Hill, New York. [328]

Montgomery, C. G., R. H. Dicke, and E. M. Purcell (1948). *Principles of Microwave Circuits*. M.I.T. Radiation Lab. Series, Vol. 8. McGraw-Hill, New York. [322, 328]

Moreno, T. (1948). *Microwave Transmission Design Data*. Dover, New York. [325, 328]

Morgan, S. P. (1949). Effect of a surface roughness on eddy current losses at microwave frequencies. *J. Appl. Phys.* **20**, 352. [306]

Mount, E., and B. Begg (1960). Parametric devices and masers: an annotated bibliography. *I.R.E. Trans.* **MTT-8**, 222. [352]

Mueller, G. E., and W. A. Tyrrell (1947). Polyrod antennas. *Bell System Tech. J.* **26**, 837. [334]

Mumford, W. W. (1949). A broadband microwave noise source. *Bell System Tech. J.* **28**, 608. [355]

Oliner, A. A. (1957). The impedance properties of narrow radiating slots in the broad face of rectangular waveguides. *I.R.E. Trans.* **AP-5**, 4, 12. [338]

Page, C. H. (1958). Harmonic generation with ideal rectifiers. *Proc. I.R.E.* **46**, 1738. [345]

Parker, C. F., and R. J. Anderson (1957). Constant beamwidth broadband antennas. *I.R.E. National Convention Record*, Vol. **5**, Part I, 87. [336]

Petritz, R. L. (1952). On the theory of noise in *p–n* junctions and related devices. *Proc. I.R.E.* **40**, 1440. [346]

Pound, R. V. (1948). *Microwave Mixers*. M.I.T. Radiation Laboratory Series, Vol. 16. McGraw-Hill, New York. [349]

Rennie, J. C. (1957). Design considerations in a wideband microwave mixer and i.f. preamplifier. *I.R.E. Trans.* **CS-5**, 221. [349]

Riblet, H. J. (1952*a*). The short-slot hybrid junction. *Proc. I.R.E.* **40**, 180. [315]

Riblet, H. J. (1952*b*). Synthesis of narrow band direct-coupled filters. *Proc. I.R.E.* **40**, 1219. [318]

Riblet, H. J. (1958). A unified discussion of high-Q waveguide filter design theory. *I.R.E. Trans.* **MTT-6**, 359. [318]

Richardson, J. M., and K. B. Riley (1957). Performance of 3-mm harmonic generators and crystal detectors. *I.R.E. Trans.* **MTT-5**, 131. [346]

Richmond, J. H., and T. E. Tice (1955). Probes for microwave nearfield measurements. *I.R.E. Trans.* **MTT-3**(*3*), 32. [342]

Robertson, S. D. (1956). Recent advances in finline circuits. *I.R.E. Trans.* **MTT-4**, 263. See also The ultra-bandwidth finline coupler, *Proc. I.R.E.* **43**, 739 (1955). [316]

Schelkunoff, S. A., and H. T. Friis (1952). *Antennas: Theory and Practice*. Wiley, New York. [327, 329, 338]

Severin, H. (1956). Nonreflecting absorbers for microwave radiation. *I.R.E. Trans.* **AP-4**, 385. [362]

Smith, R. A. (1951). The relative advantages of coherent and incoherent detectors. *Proc. Inst. Elec. Engrs. (London)* **98**, Part IV, 43. [349]

Smith, R. A. (1959). *Semiconductors*. University Press, Cambridge. [346]

Sobel, F., F. L. Wentworth, and J. C. Wiltse (1961). Quasi-optical surface waveguide and other components for the 100 to 300 Gc region. *I.R.E. Trans.* **MTT-9** 512. [310]

Staniforth, A., and J. H. Craven (1960). Improvement in square law operation of crystals. *I.R.E. Trans.* **MTT-8**, 111. [346]

Stevenson, A. F. (1948). Theory of slots in rectangular waveguides. *J. Appl. Phys.* **19**, 24. [338]

Straiton, A. W., and C. W. Tolbert (1960). Anomalies in the absorption of radio waves by atmospheric gases. *Proc. I.R.E.* **48**, 898. [312, 313]

Strong, J. (1938). *Procedures in Experimental Physics*. Prentice-Hall, Englewood Cliffs, N.J. [357]

Taub, J., and P. J. Giordano (1954). Use of crystals in balanced mixers. *I.R.E. Trans.* **MTT-2**(*2*), 26. [351]

Taussing, N. W. (1962). Some design factors affecting pulse and CW sensitivity of crystal video receivers employing RF amplification. *Microwave J.* **5**(*2*), 94. [348]

Theissing, H. H., and P. J. Caplan (1956). Atmospheric attenuation of solar millimeter wave radiation. *J. Appl. Phys.* **27**, 538. [312, 313]

Thorp, J. S. (1954). Rf conductivity in copper at 8 mm wavelength. *Proc. Inst. Elec. Engrs. (London)* **101**, Part III, 357. [305]

Tischer, F. J. (1956). The H-guide, a waveguide for microwaves. *I.R.E. National Convention Record*, Part V, 44. [311]

Tischer, F. J. (1958). Properties of H-guide at microwaves and millimeter waves. *I.R.E. Wescon Convention Record*, Part I, 4. [311]

Torrey, H. C., and C. A. Whitmer (1948). *Crystal Rectifiers*. M.I.T. Radiation Lab. Series, Vol. 15. McGraw-Hill, New York. [346]

van Buskirk, L. F., and C. E. Hendrix (1961). The zone plate as a radio frequency focusing element. *I.R.E. Trans.* **AP-9**, 319. [312, 331]

van der Ziel, A. (1950). On the noise spectra of semiconductor noise and of flicker effect. *Physica* **16**, 359. [346]

van der Ziel, A. (1954). *Noise*. Prentice Hall, Englewood Cliffs, N.J. [346]

van der Ziel, A. (1959). Noise figure of reactance converters and parametric amplifiers. *J. Appl. Phys.* **30**, 1449. [351]

Valenzuela, G. R. (1963). Millimeter transmission by oversize and shielded-beam waveguides. *IEEE Trans.* **MTT-11**, 429. [307]

Wade, G. (1961). Low noise amplifiers for centimeter and shorter wavelengths. *Proc. I.R.E.* **49**, 880. [348]

Watson, R. B., and C. W. Horton (1948). The radiation patterns of dielectric rods—experiment and theory. *J. Appl. Phys.* **19**, 661. [335, 336]

Weber, J. (1959). Masers. *Revs. Modern Phys.* **31**, 681. [352]

White, W. D., and J. G. Greene (1956). On the effective noise temperature of gas discharge noise generators. *Proc. I.R.E.* **44**, 939. [355]

Wilson, I. G., C. W. Schramm, and J. P, Kinzer (1946–1947). High Q resonant cavities for microwave testing. *Bell System Tech. J.* **25**, 408 (1946), and **26**, 31, 410 (1947). Reprinted in *Radar Systems and Components* (Van Nostrand, New York, 1949), pp. 909–1020. [326, 328]

Woonton, G. A., and J. A. Carruthers (1950). Indoor measurements of microwave antenna radiation patterns by means of a metal lens. *J. Appl. Phys.* **21**, 428. [341]

REFERENCES FOR CHAPTER 10

Alpher, R., and D. White (1959). Optical refractivity of high temperature gases. *Phys. Fluids* **2**, 153, 162. [369]

Ascoli-Bartoli, U., and A. de Angelis (1963). Interferometric study of a rf discharge. *Proc. 6th Intl. Conf. on Ionization Phenomena in Gases* (Paris) **2**, 475. [369]

Ascoli-Bartoli, U., A. de Angelis, and S. Martellucci (1960). Wavelength dependence of a plasma in the optical region. *Nuovo cimento* **18**, 1116. [369]

Bailey, R. A., and K. G. Emeleus (1955). Plasma electron oscillations. *Proc. Roy. Irish Acad.* **57A**, 53. [386]

Bennett, F., D. Shear, and H. Burden (1960). Streak interferometry. *J. Opt. Soc. Am.* **50**, 212. [370]

Bernstein, I. B., and I. N. Rabinowitz (1959). Theory of electrostatic probes in a low-density plasma. *Phys. Fluids* **2**, 112. [380]

Billings, B. H. (1951). Narrow band optical interference filters. *Phot. Eng.* **2**(*2*), 45. [369]

Bohm, D., E. H. S. Burhop, and H. S. W. Massey (1949). Use of probes for plasma exploration. In *The Characteristics of Electrical Discharges in Magnetic Fields*, edited by A. Guthrie and R. K. Wakerling, McGraw-Hill, New York, Chapter 2. [380, 384]

Boyd, R. L. F., and N. D. Twiddy (1959). Electron energy distribution in plasmas. *Proc. Roy. Soc. (London)* **A250**, 53. [381]

Brown, S. C. (1963). Far infrared studies of high density plasmas. *Bull. Am. Phys. Soc.* **8**, 174. See also S. C. Brown, G. Bekefi, and R. E. Whitney, *J. Opt. Soc. Am.* **53**, 448 (1963). [373]

Chen, F. F. (1965). Electrostatic probes. In *Plasma Diagnostic Techniques*, edited by R. Huddleston and S. Leonard, Academic Press, New York. Chapter 4. [378]

Colgate, S., J. Ferguson, and H. Furth (1958). A toroidal stabilized pinch. *Proc. 2nd U.N. Conf. on Peaceful Uses of Atomic Energy* (Geneva) **32**, 129, 140. [387]

Cooper, J. (1963). On the high-frequency response of a Rogowsky coil. *Plasma Phys. (J. Nuclear Energy* C) **5**, 285. [387]

Dickerman, P. J., and J. C. Morris (1961). Experimental studies of the temperature in a field-free plasma. In *Optical Spectroscopic Measurements of High Temperatures*, P. J. Dickerman, ed. Univ. of Chicago Press, p. 170. [390]

Dougal, A. A. (1963). Optical maser probing theory for magnetoplasma diagnostics. *Proc. 4th Symposium on Engineering Aspects of Magnetohydrodynamics* (Berkeley), p. 1. [373]

Elmore, W. C., E. M. Little, and W. E. Quinn (1958). Neutrons from plasma compressed by an axial magnetic field (Scylla). *Proc. 2nd U.N. Conf. on Peaceful uses of Atomic Energy* (Geneva) **32**, 337. [370]

Gardner, A. (1962). Diagnostic measurements of a highly ionized, steady-stage plasma. In *Engineering Aspects of Magnetohydrodynamics*, C. Mannal and N. Mather, ed., Columbia University Press, New York, p. 438. [386, 333, 334]

Generalov, N. P. (1959). The theory of probes. *Plasma Phys. (J. Nuclear Energy* C) **9**, 148. [380]

Glasstone, S., and R. H. Lovberg (1960). *Controlled Thermonuclear Reactions*. Van Nostrand, Princeton, N.J. [387, 391]

Golovin, I. N., D. P. Ivanov, V. D. Kirilov, D. P. Petrov, K. A. Razumova, and N. A. Yaulinsky (1958). Stable plasma column in longitudinal magnetic field. *Proc. 2nd U.N. Conf. on Peaceful Uses of Atomic Energy* (Geneva) **32**, 72. [387]

Griem, H. R. (1960). Stark broadening of higher hydrogen and hydrogenlike lines by electrons and ions. *Astrophys. J.* **132**, 883. [388]

Griem, H. R., and A. C. Kolb (1959). Advances in the theory of Stark broadening. *Proc. 4th Intl. Conf. on Ionization Phenomena in Gases* (Uppsala), North-Holland Publishing Co., Amsterdam, p. 808. [389]

Griem, H. R., A. C. Kolb, and K. Y. Shen (1959). Stark broadening of hydrogen lines in plasma. *Phys. Rev.* **116**, 4. [389]

Harding, G., and V. Roberts (1961). Spectroscopic investigation of plasma in the wavelength range 0.1 to 2.0 mm. *Proc. 5th Intl. Conf. on Ionization Phenomena in Gases* (Munich), p. 1977. [391]

Harding, G. N., M. F. Kimmitt, J. H. Ludlow, P. Porteous, A. C. Prior, and V. Roberts (1961). Emission of sub-millimetre electromagnetic radiation from hot plasma in ZETA. *Proc. Phys. Soc. (London)* **77**, 1069. [373, 391]

Harp, R. S. (1963). Circuit for display of Langmuir probe characteristics. *Rev. Sci. Instr.* **34**, 416. [382]

Ikegami, H., and K. Takayama (1963). Resonance probe. Institute of Plasma Physics Report *IPPJ-10*, Nagoya University, Japan. [386]

Javan, A., W. R. Bennett, Jr., and D. R. Herriott (1961). Inversion and continuous optical maser oscillation in a gas discharge containing a He–Ne mixture. *Phys. Rev. Letters* **6**, 106. [369]

Johnson, E. O., and L. Malter (1950). A floating double probe method for measurements in gas discharges. *Phys. Rev.* **80**, 58. [384]

Kelly, R. L. (1959). Vacuum ultraviolet emission lines. Lawrence Radiation Lab. Rept. UCRL 5612, Univ. of California, Livermore, Calif. [388]

Klein, A. (1963). Some results using optical interferometry for plasma diagnostics. *Phys. Fluids* **6**, 310. [371]

Langmuir, I., and H. Mott-Smith (1924). Studies of electric discharges in gases at low pressures. *Gen. Elec. Rev.* **27**, 449, 538, 616, 762, and 810. [385]

Lengyel, B. A. (1962). *Lasers*. Wiley, New York. [369]

Levitskii, S. M., and I. P. Shashurin (1961). Resonant microwave probe for measuring charge density in a plasma. *Soviet Phys.—Tech. Phys.* **6**, 315. [386]

Lovberg, R. H. (1963). Acceleration of plasma by displacement currents resulting from ionization. *Proc. 6th Intl. Conf. on Ionization Phenomena in Gases* (Paris) **4**, 235. [372]

Lovberg, R. H. (1964). Measurement of plasma density in a rail accelerator by means of Schlieren photography. *IEEE Trans.* **NS-11**(*1*), 187. [372]

Lukyanov, S. Yu., and V. I. Sinitsin (1958). Spectroscopic research of high temperature plasmas. *Proc. of 2nd U.N. Conf. on Peaceful Uses of Atomic Energy* (Geneva) **32**, 358. [389]

McWhirter, R. W. P. (1965). Spectral intensities. In *Plasma Diagnostic Techniques*, edited by R. Huddlestone and S. Leonard, Academic Press, New York. Chapter 5. [391]

McWhirter, R. W. P., W. G. Griffin, and T. J. L. Jones (1959). The interpretation, in terms of atomic collision processes, of a measurement of the absolute intensities of some of the Balmer spectral lines, as emitted by a deuterium discharge in ZETA. *Proc. 4th Intl. Conf. on Ionization Phenomena in Gases* (Uppsala), North-Holland Publ. Co., Amsterdam, p. 833. [391]

Malmberg, J. H., N. W. Carlson, C. B. Wharton, and W. E. Drummond (1963). A collisionless plasma for wave propagation studies. *Proc. 6th Intl. Conf. on Ionization Phenomena in Gases* (Paris) **4**, 229. [386]

Margenau, H. (1932). Theory of pressure effects of foreign gases on spectral lines. *Phys. Rev.* **40**, 387. See also *Phys. Rev.* **48**, 755 (1935). [389]

Margenau, H. (1951). Statistical theory of pressure broadening. *Phys. Rev.* **82**, 156. [389]

Marshall, J. (1958). Acceleration of plasma into vacuum. *Proc. of 2nd U.N. Conf. on Peaceful Uses of Atomic Energy* (Geneva) **31**, 341. [387]

Medicus, G. (1956). Simple way to obtain the velocity distribution of the electrons in gas discharge plasmas from probe curves. *J. Appl. Phys.* **27**, 1242. [381]

Mott-Smith, H., and I. Langmuir (1926). Theory of collectors in gaseous discharges. *Phys. Rev.* **28**, 727. [381]

Pollock, H., L. Goldman, and W. Westendorp (1960). Multiple magnetic probe measurements in compressed deuterium plasma. *Bull. Am. Phys. Soc.* **5**, 337. [387]

Ramsden, S., and E. McLean (1952). Optical refractivity of free electrons. *Nature* **194**, 761. [370]

Schawlow, A. L., and C. H. Townes (1958). Infrared and optical masers. *Phys. Rev.* **112**, 1940. [369]

Schulz, G. J., and S. C. Brown (1955). Microwave study of positive ion collection by probes. *Phys. Rev.* **98**, 1642. [378]

Scott, F. R., and V. Josephson (1957). Apparatus for producing high velocity shock waves and gases. U.S. Patent No. 2,923,852 (appl. October, 1957, granted February, 1960). [373]

Scott, F. R., E. Dacus, and R. G. Tuckfield (1962). Optical emission line profile analyzer. *Rev. Sci. Instr.* **33**, 1001. [388, 390]

Serchuk, A. (1962). Commercially available optical masers. *Microwaves* **1**, 54. [369]

Stern, M. O., and E. Dacus (1961). Piezoelectric probe for plasma research. *Rev. Sci. Instr.* **32**, 140. [387]

Takayama, K., H. Ikemagi, and S. Miyasaki (1960). Plasma resonance in a radio-frequency probe. *Phys. Rev. Letters* **5**, 238. [386]

Talbot, L., J. Katz, and M. Brundin (1963). Comparison between Langmuir probe and microwave electron density measurements in an arc-heated low-density wind tunnel. *Phys. Fluids* **6**, 559. [378]

Tonks, L., and I. Langmuir (1929). Theory of the arc plasma. *Phys. Rev.* **34**, 876. [378]

Underhill, A., and W. Waddell (1959). Optical wavelength tables. Natl. Bur. of Standards Circulars No. 603 and 604 (U.S. Govt. Printing Office). [389]

van der Pol, B. (1920). De invloed van een geioniseerd gas op het voortschrijden van electromagnetische golven. Thesis, Utrecht University, Holland. Reprinted in van der Pol, *Selected Scientific Papers*, Vol. I (North-Holland Publ. Co., Amsterdam, 1960). [376, 386]

Wharton, C. B., and R. Hawke (1962). Calibration of rf conductivity probes by immersion in ionic solutions. Lawrence Radiation Lab. Electronics Engineering Report LEL, Univ. of California, Livermore, Calif. [376]

White, R. M. (1962). Elastic wave production by electromagnetic wave absorption or particle bombardment. General Electric TWT Rept. TIS-R62EIM232, Palo Alto, Calif. [387]

Wilcox, J. M., A. W. De Silva, W. S. Cooper, and F. I. Boley (1961). Experiments on Alfven-wave propagation. In *Radiation and Waves in Plasmas*, edited by M. Mitchner, Stanford Univ. Press, Stanford, Calif., p. 138. [389]

Wulff, H. (1959). Plasma diagnostics by spectroscopical means. *Nuclear Instr. and Methods*, **4**, 352. [388].

Yeung, T. H. Y., and J. Sayers (1957). An rf probe technique for the measurement of plasma electron concentrations in the presence of negative ions. *Proc. Phys. Soc. (London)* **70**, 663. [386]

Subject index

Absorbers, microwave, 196, 197, 343, 361
Absorption coefficients, 129, 130, 131, 270; *see also* Absorptivity; Attenuation coefficient
Absorption length, 244, 293, 297, 298; *see also* Attenuation length
Absorptivity, radiation, 270, 287
  relation to emissivity, 270, 287, 289
Accelerated charge, radiation by, 246, 272
Adiabatic analysis, 120, 123, 133, 220
Admittance, transmission line, 157
  measurement of, 158
  plasma equivalent, 156, 158
Amplification, *see* Growth
Amplifiers, i.f., 295, 299, 349, 353
  maser, 352
  parametric, 351
  video, 201, 205, 346, 363
Anisotropic medium, 45, 160, 179, 403
Antennas, calibration of, 294, 342
  Cassegrain, 336
  circularly polarized, 223, 226, 322
  dielectric rod, 224, 309, 334, 340, 360
  effective area of, 243
  far field of, 146, 341
  for free-space beams, 141, 311
  for spacecharge waves, 182, 360, 386
  Fresnel zone, 332
  gain of, 243, 264, 265
  horn, 143, 197, 204, 224, 237, 292, 322, 329, 333, 360
Antennas, lens, 146, 150, 218, 311, 331, 333
  measurement of field pattern, 145, 341
  near field of, 341
  optimization of, 148
  parabolic reflector, 336, 337
  phase anomalies of, 145, 150
  slotted waveguide, 223, 338
Appleton (-Hartree) equation, 23, 24, 31
  including ion motions, 56
  "$\tan^2\theta$" form, 31, 32
Area of antenna, effective, 243
Atmosphere, wave attenuation in, 226, 312
Attenuation, atmospheric, 226, 312
  by internal reflections, 128, 140, 141
  by refraction, 137, 140
  collisional, 115, 121, 140, 141, 202, 226
  collisionless, 113, 186, 226
  in finite plasma, 129
  in plasma-filled waveguide, 163, 166
  measurement of, 122, 192, 200, 210, 287, 293
  waveguide, 306, 308
Attenuation coefficient, 5, 397; *see also* Transmission coefficient
  for electron-ion collisions, 90, 263
  for incoherent scattering, 93
  for Landau (collisionless) damping, 114, 186, 190
Attenuation index, 7, 165, 398

Attenuation index, for cyclotron wave, 16, 18, 115
for extraordinary wave, 27, 28
for ordinary wave, 11
in warm plasma, 114
Attenuation length, 8, 10, 195, 307, 397; *see also* Skin depth; Absorption length
Automatic frequency control (AFC), 237, 295, 351
Averages, collision frequency, 64, 73
electron density, 120, 125, 160, 221
velocity, 74, 261

Backward-wave oscillator, 289, 299, 344; *see also* Microwave sources
Beam, free-space microwave, 117, 141
Beam-plasma interactions, 185, 188, 285, 300; *see also* Instability
Bessel functions, 113, 176, 180, 247, 275
Beta (β), of magnetically confined plasma, 97, 224, 275
Blackbody radiation, 242, 266, 269, 287, 297
conditions for, 244
see also Radiation
Boltzmann (Maxwell-Boltzmann) distribution, 259
Boltzmann equation, 67, 105
collision term, 67, 188
in deriving spacecharge wave propagation, 112, 183, 188
Boltzmann theory of conductivity, 69
Boundaries, cutoff regions due to, 125, 191, 292, 297, 304
diffuse, 120, 297
effects on spacecharge waves of, 155, 174
finite gradient, 130, 134, 136
internal reflections from, 129, 131
ramp profile, 135
refraction by, 137
sharp interface, 127; *see also* Inhomogeneous plasmas
Breakdown, 91, 163
Bremsstrahlung, 245
correlation of theory with conductivity theories, 262
Bremsstrahlung, from atoms, 256
magnetic, 256, 272
power radiated as, 248, 254, 255, 263, 268, 272
summary of, 254
total, 256, 391
Bridge, microwave, 119, 200; *see also* Interferometer
Brillouin (ω-β) diagram, 10, 11, 102, 167, 177, 187, 398, 399
Broadening, collisional, 274, 298
doppler, 274, 298, 367, 389
due to collective effects, 279, 304
due to inhomogeneity, 275, 293, 299
of cyclotron radiation, 274, 279, 298, 303
Stark, 367, 388

Calorimetric viewpoint, 90, 92
Cavities, coupling coefficient of, 158
frequency of, 325
frequency shift due to perturbation in, 159, 297
high mode number, 162
measurements using, 163
modes of, 155, 159, 325
plasmas in, 155, 158, 297
Q of, 156, 326
reflection coefficient of, 157
Cerenkov radiation, 96, 114, 280, 282, 286, 293; *see also* Landau damping; Cyclotron radiation
Chapman-Enskog technique, 68
Characteristic velocities, 73
Characteristic waves, 24, 38; *see also* Principal waves
Charge separation in a plasma, 78
Cillie radiation, 251, 263, 266, 269
Circularly polarized waves, 12, 40, 108, 160, 223, 292
handedness, 14, 15, 40
see also Elliptically polarized waves
Classical electron radius, 93, 233
Clausius-Mossotti formula, 401
Coherent detection, 232, 298, 353; *see also* Detectors; Radiometer
Coherent radiation, 242, 285; *see also* Collective interactions
Cold plasma, 1, 57, 171

Collective interactions, 235, 242, 278, 285, 299
Collimation of microwave beam, 147, 219, 331, 336
Collisional broadening, 274, 298; *see also* Broadening
Collisional damping, 6, 64, 121, 140, 141, 203, 226; *see also* Damping
Collision frequency, 6, 57, 66
average, 64, 73
coulomb, 82, 87, 90
dependence on velocity, 63, 92
effective, 71, 72, 73, 82, 83, 90
measurement of, 161, 192, 203, 374
momentum transfer, 60, 64, 65
total, 59
Collisionless (Landau) damping, in fluctuating plasma, 231
of electromagnetic waves, 96, 114, 226, 231, 275, 283, 293
of spacecharge waves, 185, 190, 232
Collisions, attenuation by, 121, 140, 141
coulomb, 62, 79, 81, 87, 110
elastic, 60
electron-electron, 76, 84, 85, 256
electron-ion, 62, 76, 79, 82, 90, 110
electron-molecule, 61, 63
energy lost in, 60, 91
hard sphere, 61
inelastic, 62
ionization by, 62, 91
of electrons with sheaths, 280, 304
Collision term in Boltzmann equation, 67
Complex conductivity, *see* Conductivity
Complex dielectric constant, *see* Dielectric constant
Complex refractive index, *see* Refractive index
Components, laboratory fabrication of, 313–328
Compton effect, 93
Conductivity, 393
complex, 70, 71, 395
d-c, 83, 94
Lorentz, 6, 71
measurement of, 374, 378, 387
of metals, 307
Conductivity, summary of computation, 76
tensor, *see* Conductivity tensor
warm plasma, 96, 105
Conductivity probes, 374, 386
calibration of, 377
Conductivity tensor, 30, 71, 75, 101, 105, 404
including ion motions, 51
in rotating coordinates, 32, 34, 106
Conductivity theory, correlation with bremsstrahlung theory, 262
Continuity, equation of, 67, 99, 395
Cooperative processes, 235, 242, 285, 299
Coordinate systems, for propagation in magnetic field, 20
rotating, 13, 31
Correction factors, g and h, 74, 75, 85, 274
γ_E, 84
Correlation, between microwave and other diagnostic techniques, 216, 225, 290, 297, 373, 378
of instability-generated radiation, 299, 300
Cotton-Mouton effect, 29
Coulomb collision frequency, 82, 87, 90; *see also* Collision frequency
Coulomb collisions, 62, 79, 81, 87, 110
Coulomb cross section, 62; *see also* Cross section
Coulomb force, 63
Coulomb logarithm, *see* ln Λ
Couplers, directional, 193, 201, 315, 322
fin-line, 200, 219, 223, 300, 316, 322
Coupling, between antennas, 148, 198, 218, 329
mode, 182, 227, 307, 309
resonant cavity, 158, 318
spacecharge wave to radiation field, 189, 286, 300
wave-type, 103, 127, 181, 189
Critical angle, 45
Critical electron density, 12, 118; *see also* Cutoff conditions
Cross modulation, *see* Modulation

Cross section, coulomb, 62
dependence on velocity, 62, 63
differential, 59
momentum transfer, 60
Thomson, 232
total, 59
Cutoff conditions, 18, 28, 34–39, 44, 53–56, 125, 179
Cutoff density, 118, 220, 224; *see also* Critical electron density
Cutoff regions, 125, 191, 292, 304; *see also* Tunneling
Cutoffs on impact parameter, 85
Cyclotron damping, 114, 225; *see also* Cyclotron wave; Damping
Cyclotron frequency, 15, 52, 189, 224, 226, 272, 292
shift of, 228, 304
spatial variation of, 228, 292, 293
Cyclotron radiation, 272, 284
anisotropy, 273
at harmonics of ω_b, 191, 304
effects of collective motion, 278, 279
line shape, 274, 278, 298
power radiated as, 272
relativistic, *see* Synchrotron radiation
Cyclotron resonance, 18, 84, 91, 92, 110, 279
Cyclotron wave, attenuation of, 16, 114
Faraday rotation of, 19, 224
in warm plasma, 102, 108, 116
refractive index for, 15, 35, 47, 109
spacecharge mode, 181, 183, 191
whistler mode of, 19, 48, 54, 182, 225, 297
Cylindrical plasma, inhomogeneous, 136, 174, 179, 212, 222
sharply bounded, 130, 137, 138, 175
see also Boundaries

Damping, collisional, 6, 64, 91, 121, 140, 141, 203, 226
collisionless (Landau), 96, 114, 185, 190, 226, 231, 275, 283, 293
cyclotron, 114, 225
of spacecharge waves, 185, 190, 232
deBroglie wavelength, 63, 85, 252
Debye length, 78, 80, 86, 93, 186, 188, 236
Debye shielding, 76, 82, 256, 380
Debye sphere, 79, 80, 236
Delta functions, 265, 277
Density, *see* Electron density
Detailed balance, principle of, 260
Detectors, bolometer, 372
coherent, 232, 298, 353
crystal-video, 195, 200, 218, 346, 348
diode, 200, 346, 352
noise in, 346, 349
sensitivity of, 346, 350
Golay cell, 372
mixers, 349
harmonic, 351
parametric, 351
performance of, 355
square-law, 198, 200
superheterodyne, 204, 232, 295, 349, 353
Diagnostic techniques, catalog of, 366–368
phase shift, 200–223
radiation as, 287–299, 391
resonant cavity, 155–163
Diamagnetism of plasma, 96, 275
measurement of, 275, 374
Dielectric constant, 393, 395
complex, 5, 70, 176, 179, 394
d-c, 56
Lorentz, 6, 71
summary of computation of, 76
Dielectric constant tensor, 30, 71, 101, 106, 179, 404
including ion motions, 52
in rotating coordinates, 32
Differential cross section, 59
Diffraction theory, 142
Diffuse boundaries, plasma with, 120, 297; *see also* Boundaries
Diplexer (Duplexer), frequency, 199, 316, 318
polarization, 200, 219, 223, 315, 316, 322, 324
see also Filters; Polarization
Dipole resonance, 178, 181, 235, 240, 386
D-c conductivity, 83, 94
D-c dielectric constant, 56
Dispersion, 46, 281, 398
spatial, 100, 405

Dispersion equation, 46, 47, 168, 225, 404
Bohm, 103, 186, 187, 235
for spacecharge wave, 177, 180, 184, 186, 189, 190
Disturbing wave 91, 229
Doppler effect, broadening by, 274, 298, 367, 389
frequency shift due to, 110, 114, 119, 228, 274, 275, 390
in drifting plasmas, 171, 182, 228
shift of cyclotron frequency by, 228, 299
Druyvesteyn distribution, 262

Effective collision frequency, 71, 72, 73, 82, 90
Einstein A and B coefficients, 86, 259, 261
Elastic collisions, 60
Electroacoustical waves, *see* Plasma waves; Spacecharge waves
Electron density, average, 121, 160, 222
catalog of measuring techniques for, 366
critical, or cutoff, 12, 118, 194, 198, 214
errors in determination, 212, 214, 218, 222
fluctuations of, 229
measurement by phase shift, 200, 214, 225
measurement by probes, 376, 380, 385, 386
measurement by resonant cavities, 155, 162
measurement by spectroscopy, 225, 388
range of measurable, 121, 122, 370
spatial distribution of, 123, 161, 212, 214, 218, 222
special, 35, 53
wave propagation as function of, 11, 28, 35, 37, 47–50, 56, 194, 214, 225
see also Ion density
Electron-electron collisions, 84, 85, 256
Electron energy, analysis of, 297
average, 74
Electron energy, distribution of, 68, 114, 184, 189
measurements of, 297
related to noise temperature, 290, 302
see also Velocity; Electron temperature
Electron-ion collisions, 62, 79, 82, 87, 110
Electron radius, classical, 93, 233
Electron temperature, catalog of measuring techniques for determining, 367
measurement by probes, 380, 385, 387
measurement by radiation, 243, 254, 255, 261, 265, 269, 287, 290, 294, 297, 302, 391
Elliptically polarized waves, 24, 29, 219, 227, 273; *see also* Circularly polarized waves
Emissivity, 264, 265, 267, 269, 270, 271, 284
effect of antenna gain on, 264, 265
effect of surface reflection on, 266, 269
relation to absorptivity, 270, 287, 289
see also Absorptivity
Energy, electron, 74
loss by bremsstrahlung, 256
loss by collision, 60
loss by cyclotron radiation, 272
spacecharge wave, 187, 234, 236
Ergiebigkeit, 259, 261
Euler's constant, 87
Evanescent wave, 8; *see also* Tunneling
Extinction coefficient, 398; *see also* Attenuation index
Extraordinary wave, 26, 34, 48, 53, 134, 161, 220
in warm plasma, 104, 111

Faraday rotation, 19, 223, 322, 373
Far field of antenna, 146, 341; *see also* Antennas
Field particle, 58
Field strength, measurement of, 367, 387, 388
Filters, band rejection, 237, 299, 319
frequency diplexer, 316, 318
mode, 177, 307, 310

Filters, resonant cavity, 299, 325
waveguide, 229, 319
Fine-scale mixing, 114
Fizeau effect, 228
f-Number of lens, 147
Fokker-Planck equation, 81, 186
Force laws, interparticle, 62, 63
Fourier analysis, 230, 246, 302
Fraunhofer diffraction, 146, 341; *see also* Antennas
Free-free transitions, 245; *see also* Bremsstrahlung
Free-space beams, 117, 141; *see also* Antennas
Frequencies, special, 34, 53
Frequency, collision, *see* Collision frequency
complex, 185, 188
control of, 351; *see also* Automatic frequency control
critical (for self-absorption), 266
cyclotron, harmonics of, 191, 276, 302, 304
cyclotron (or gyro), 15, 52, 272
hybrid, 35, 53, 181, 220
Larmor, 15
plasma, 3, 52
propagation as function of, 9, 10, 35, 36, 54, 56
resonant cavity, 157
Frequency bands, EIA, 306
Frequency diversity, 197, 199, 216
Frequency spectrum, due to fluctuating plasma, 229, 231
for cyclotron radiation, 191, 228, 304
for synchrotron radiation, 276, 278
of scattered wave, 93, 235
Fresnel zones, 142, 143
antenna using, 332
interferences of, 198

g and *h* Correction factors, 74, 75, 85, 274
Gain of antenna, 243
dependence of emissivity on, 264, 265
Gamma functions, 72
Gamma rays, *see* X-rays
γ_E Correction factor, 84
Gaunt factor, 86, 248
connection with ln Λ, 253, 262
high frequency, low temperature, 249
quantum mechanical form, 252
shielding correction, 252, 253
temperature correction, 249, 253
Gaussian shape factor, 274
Geometrical optics limit, 119, 146, 150
Geometrical optics of cylindrical plasma, 137
Gray body radiation, 244, 257, 261; *see also* Blackbody radiation
Group velocity, 5, 11, 46, 168, 178, 187, 398
Growth, wave amplitude, 185, 190, 236, 260, 286; *see also* Damping
Gyration, sense of, 15
Gyro frequency, *see* Cyclotron frequency
Gyroradius (Larmor radius), 88, 96, 97, 190

Hall current probes, 367, 387; *see also* Field strength; Magnetic probes
Handedness of circular polarization, 14, 15, 40
Hankel functions, 249
Hard sphere interaction, 61, 63
Harmonic generation, in plasma, 92, 93, 302, 345
with ferrites, 345, 352
with semiconductors, 345, 351
Heating, plasma, 91
"High" frequencies, 9, 72, 87
Horn antenna, 143, 197, 204, 215, 237, 292, 322, 329, 360
as feed to dielectric rod, 224, 309, 334, 340
as feed to lens, 218, 311, 333
as feed to reflector, 336, 337
circular waveguide, 322, 324, 328
Hot plasma, 95, 115
Huygens wavelet, 45, 281
Hybrid resonance frequency, lower, 53
upper, 35, 53, 181, 220, 298
Hydromagnetic theory, 66, 67, 98

Impact parameter, 58
classes in coulomb collisions, 81

Impact parameter, cutoffs, 85
for 90° collision, 80, 85
Incoherent radiation, 242; *see also* Radiation
Incoherent scattering, 93, 232, 366; *see also* Scattering
Index, attenuation, 7, 165, 398
Faraday rotation, 19, 224
growth, 186, 236
refractive, *see* Refractive index
Induced absorption and emission, 259
Inelastic collisions, 62; *see also* Collisions
Infrared probing, 368, 373; *see also* Optical probing; Radiometer
Inhomogeneity broadening, 275, 293, 299; *see also* Broadening
Inhomogeneous plasmas, cutoff regions in, 125, 191, 292, 304
nonlinearities in, 93
propagation in, 130, 135
see also Boundaries
Instability, driven by electron beam, 285, 300
electrostatic, 185, 188, 235, 286, 300
hydromagnetic, 226, 372, 387
two-stream, 189, 300
velocity-space, 190, 302
see also Turbulence; Spacecharge waves
Intensity, specific, 257, 270; *see also* Radiation
Interaction, electron beam–plasma wave, 185, 189, 190, 235, 300; *see also* Growth; Beam-plasma interaction; Instability
Interference, due to internal reflections, 129, 131, 240, 334, 342, 361
Fresnel, 145, 198, 332
fringes, 198, 202, 207, 216, 371, 373
stray, *see* Pickup
Interferometer, Fabry-Perot, 369, 389
fringe-shift, 206
Mach-Zehnder, 200, 367, 369, 371
microwave, 119, 200
polar-plot display, 210
streak, 370, 373
zebra stripe, 206
Intermediate frequencies, 8
Intermediate frequencies, of superhet receiver, 295, 299, 349, 353
Internal reflections, 126, 129, 131
attenuation by, 141
interferences from, 129, 131, 240, 334, 342, 361
Interparticle force laws, 62, 63
Ion density, measurement of, 367, 380, 386, 389; *see also* Electron density
Ion motions, conductivity with, 51, 380
dielectric constant with, 52
oblique propagation with, 56
principle waves with, 52
Ion temperature, measurement of, 367, 387, 389
Ion waves, *see* Spacecharge waves
Ionosphere, cross-modulation in, 92
propagation in, 225, 312
scattering from, 93, 232
Isotropic medium, propagation in, 133, 396

Johnson noise, 245, 346, 349
Junction, directional coupler, 193, 201, 315, 322
fin-line coupler, 200, 219, 223, 317, 322
hybrid, 315, 316
magic tee, 315
turnstile, 315, 323, 324

Kinetic (Vlasov) equation, 67, 184
Kinetic theory, 66, 104
Kirchhoff's law, 244, 270, 274, 277, 292
Klystron, 201, 206, 208, 218, 237, 295, 344; *see also* Transmitter
Kramers-Kronig dispersion relations, 115

Landau (collisionless) damping, in fluctuating plasma, 231
of electromagnetic waves, 96, 114, 226, 231, 275, 283, 293
of spacecharge waves, 185, 190, 232
Langevin equation, 12
Langmuir probe, 378
circuits for data reduction using, 379, 382

Langmuir probe, current-voltage curves of, 378, 383
double probe, 384
floating potential of, 380, 384
magnetic field effects on, 383, 385
saturation current of, 380, 382, 385
single probe, 301, 360, 378
typical configurations of, 215, 360, 379
Laplacian operator, 77, 188
Larmor frequency, 15; *see also* Cyclotron frequency
Larmor radius (gyroradius), 88, 96, 97, 190
Laser, 369
emission wavelengths, 370
interferometer using, 371
Legendre functions, 69
Lenses, microwave, 146, 150, 218, 311, 331, 333; *see also* Antennas
Linear electromagnetic medium, 393
Linearity, criterion for, 89
Linearly polarized wave, 26, 40
Lines, optical emission, 368, 388
resonance, *see* Resonance; Broadening
transmission, *see* Transmission lines; Waveguide
Liouville theorem, 67
ln Λ, 85, 87
connection with Gaunt factor, 253, 262
high frequency, low temperature, 87, 88
quantum correction, 86, 88, 89
shielding correction, 86, 88, 89
Spitzer's, 78, 80, 85, 86, 266
Lorentz conductivity, 6, 71
Lorentz dielectric constant, 6, 70, 179
Lorentz-Lorenz formula, 401
Lorentz plasma, 1, 6, 12, 85
Lorentz polarization correction, 24, 401
Lorentz shape factor, 274
Loschmidt's constant, 59
Loss factor, 394
Loss tangent, 394
"Low" frequencies, 8, 72, 87
Lower hybrid frequency, 53; *see also* Hybrid resonance frequency
Luxembourg effect (cross-modulation), 91, 229
collisionless, 231

Magnetic beach, 127, 293
Magnetic bremsstrahlung, 272; *see also* Cyclotron radiation
Magnetic field, measurement of, 367, 387, 388
propagation as function of, 16, 17, 27, 109
propagation in, 12, 18, 27, 40, 44, 55, 76, 88, 106, 219, 223, 226, 228, 293
Magnetic mirror, 97, 292
propagation through, 223, 228, 295
radiation from, 292, 295, 297, 302
Magnetic moment, 96
Magnetic probes, 367, 387
Hall current, 387
miniature coil, 387
Rogowsky loop, 387
three dimensional, 387
see also Field strength
Magnetrons, 345; *see also* Transmitters; Microwave sources
Magnetization vector, 97, 393
Matrix form of tensor, 22, 29, 31, 105, 407
Maxwell-Boltzmann population distribution, 259
Maxwell condition, 71
Maxwellian velocity distribution, 68, 71
Maxwell's equations, 392
Mean free path, 59; *see also* Collision frequency
Microscopic fields in a medium, 400
Microwave components (hardware), 201, 205, 207, 211, 215, 218, 237, 238, 288, 305–344
antennas and radiators, 196, 207, 218, 224, 226, 292, 301, 327
couplers, 193, 201, 207, 237, 300, 315, 317, 323
filters, 237, 318
frequency diplexer, 199, 316
hybrid junction, 218, 315, 323
mixer, 207, 237, 288, 289, 295, 299, 315, 351, 353

Microwave components (hardware), phase shifter, 201, 207, 212, 314
polarization diplexer, 200, 223, 300, 316, 322
polarizer, 319, 322, 324
resonant cavity, 155–163, 297, 324
waveguide, 204, 207, 305–312
Microwave sources, millimeter waves, 344, 345; *see also* Klystron; Magnetron; Transmitter; Backward-wave oscillator; Traveling-wave tubes
Mirror, magnetic, 97, 223, 228, 292, 297, 302
parabolic, 336, 337
Mixers (frequency converters), balanced, 237, 295, 299, 315, 349
for swept frequency receiver, 289, 299
harmonic, 349
parametric, 351
receivers using, 237, 288, 295, 299, 353
Mobility, 393
Mode cutoff, 165, 169, 179, 297, 310; *see also* Cutoff conditions
Modulation, collisionless Luxembourg, 231
cross, 91, 229
frequency spectrum due to, 229, 231
Luxembourg, 89, 91
of scattered waves, 235
phase, due to plasma fluctuations, 93, 229
Moments of velocity distribution function, 69, 98
Momentum lost in collision, 60
Momentum transfer, collision frequency for, 60, 64
cross section for, 60
Momentum transport, equation of, 99
Monochrometer, 369, 388, 390; *see also* Optical spectroscopy
Motion, equation of, 6, 12, 64, 99

Neutrality, departure of plasma from, 78
90° Deflection time, 81
Noise temperature, 290, 349, 355
of plasma radiation, 242, 290, 299, 353
of standard source, 244, 266, 355
Nonlinear effects, 89, 229, 234
Nonreciprocity, due to electron drift, 171, 182, 228
due to Faraday rotation, 20, 223
Normalization of velocity distribution function, 69

Oblique propagation to magnetic field, 38–41, 49, 50, 190, 227
with ion motions, 56
Ohm's law, 21, 51, 99, 393
Omega-beta diagram (Brillouin), 10, 11, 102, 167, 177, 187, 398, 399
Opacity, plasma, 197, 244, 258, 293, 298
Optical depth, 258, 265, 292, 298; *see also* Absorption length; Attenuation length
Optical (infrared) probing, 368
by Faraday rotation, 373
by scattering, 232, 367
interferometers for, 369, 374
light sources for, 370
measurement of refractive index by, 369
using lasers, 369
Optical spectroscopy, 388
atom identification by, 388
Balmer series of, 367, 391
continua in, 388, 391
doppler broadening in, 367, 389, 390
measurement of line shape in, 388
Stark broadening in, 367, 388
Zeeman line splitting in, 388
Optimization of antennas, 148; *see also* Antennas
Orbit theory, 66
Ordered component of velocity, 64
Ordinary wave, 11, 26, 34, 49, 53, 220
in warm plasma, 103, 111
Oscillator, backward-wave (BWO), 289, 299, 344
local, in superhet, 237, 295, 344, 351, 353
tunnel diode, 345, 352

Oscillator, voltage-tuned, 289, 299, 302, 344, 351
see also Microwave sources; Transmitters

Parseval's theorem, 246
Permeability, magnetic, 96, 393
Permittivity, 179, 393; *see also* Dielectric constant
Phase anomalies, at focus of antenna, 145, 150
due to multiple transmission paths, 132, 152, 204
in Faraday rotation measurement, 219
Phase coefficient, 397
of electromagnetic wave, 5, 165
of spacecharge wave, 173, 177, 181, 185, 190, 235
vector, 46, 188, 235
see also Propagation coefficient
Phase factor, for plane wave, 21, 397, 404
Phase mixing, 114, 232, 293; *see also* Landau damping
Phase scrambling, 232, 293
Phase shift, 118, 119, 121, 123, 126, 129
at optical frequencies, 369, 373
in moving medium, 174, 182, 229
in nonuniform medium, 214, 220
measurements of, 166, 200, 206, 210, 221, 229
Phase shifter, electronic, 168, 315
line stretcher, 315
waveguide, 314, 318
Phase space, 66
Phase velocity, 5, 11, 45, 397
calculated from ω-β diagram, 10, 174, 187
of spacecharge waves, 171, 177, 181, 185, 187, 235
relation to ray velocity, 46
Phase-velocity surface, 43–46, 55
Phasor, 13
Photon emission, 259
Pickup, stray, 205, 300, 348, 354, 364
Planck function, 243, 260, 261
Plasma, confinement of, 97, 210, 221, 226, 272, 292
Lorentz, 1, 6, 12, 85
production of, 194, 213, 221, 223, 226, 293, 301, 302, 360
Plasma analogs, 151
Plasma frequency, 3, 52, 178, 186
Plasma oscillations, 4, 86, 87, 92, 94, 95, 102, 103, 112, 170, 175, 185, 235, 285, 286, 300; *see also* Spacecharge waves
Poisson distribution, 65
Poisson's equation, 77
Polarizability, 401
Polarization coefficient, 24
Polarization correction, Lorentz, 24, 401
Polarization diplexer, 200, 223, 300, 316, 322
Polarization of waves, linear, 24, 40
circular, 12, 40, 108, 160, 223, 292
elliptical, 24, 29, 219, 227, 273
rotation of, 19, 224
Polarization vector, dipole, 393
Power factor, 394
Poynting vector, 45, 133, 230
Pressure tensor, 99
Principal waves, 34, 36, 37
including ion motions, 52, 54
see also Characteristic waves
Probability of collision, 59
Probes, ballistic, 387
conductivity, 374, 386
electromagnetic, 226, 234
Langmuir, 215, 301, 360, 378
magnetic, 367, 387
movable, 341, 360
optical beam, 368
resonant, 386
spacecharge wave, 182, 360, 379, 386
waveguide, 224, 334, 340
Profile, measurement of electron density, 123, 212, 219, 221, 224
Propagation, angle of, 21, 38, 49, 227
as function of electron density, 11, 28, 35, 37, 47–50, 56, 194, 214, 225

Propagation, as function of frequency, 9, 10, 35, 36, 54, 56
at angle to magnetic field, 38–41, 49, 50, 56, 190, 227
in drifting plasma, 228
in inhomogeneous plasma, 130, 212
in Lorentz plasma, 6
in magnetized plasma, 12, 18, 27, 40, 41, 44, 55, 76, 88, 106
in nonmagnetized plasma, 4, 87, 112
in waveguide, 155, 163, 297
through fluctuating plasma, 229
Propagation coefficient, 5, 397, 404
for spacecharge waves, 177, 185, 190
summary of computation for, 76, 87
vector, 21, 46, 188, 235, 404

QL and *QT* approximations, 38, 292

Radiance, 257
Radiation, at angle to magnetic field, 227, 298
blackbody, 242, 266, 269, 287, 297
bremsstrahlung, 245, 248, 254, 256, 263, 391
by electron-electron collisions, 256
Cerenkov, 96, 114, 280, 282
Cillie, 251, 263, 266, 269
coherent, 242, 285, 299
cyclotron, 272, 274, 278, 284, 292, 297, 302
cyclotron-frequency harmonic, 191, 275, 304
determination of T_e by, 293, 298
from finite plasma, 263, 264, 269, 278, 287, 298
impurity, 256, 388
grey body, 244, 257, 261
incoherent, 242
instability-generated, 286, 300
measurement of, 289, 292, 297, 353, 391
nonthermal, 242, 285, 299, 302
recombination, 388, 391
relation to absorption, 270, 287, 289
specific intensity of, 257
synchrotron, 272, 275, 276, 278, 292, 302
Radiation, thermal, 242
see also Bremsstrahlung; Cyclotron radiation; Emissivity
Radiation measurements, 287
from finite, free-space plasma, 263, 264, 269, 278, 287, 298
in resonant cavity, 297
in waveguide, 295, 297
see also Radiation; Radiometers
Radiation transport, 257
Radiators, *see* Antennas; Probes
Radiometer, calibration of, 290, 355
coherent detection, 298, 353
Dicke, 298, 353
direct detection, 288, 295, 300, 353
infrared, 373
swept frequency, 289, 295, 299, 302
Range of measurable electron densities, 121, 122, 366, 370
Ray surface, 45, 46
Ray velocity, 46
Rayleigh-Jeans approximation, 87, 243, 251, 254, 265
Receivers, crystal-video, 195, 200, 218, 346, 348
microwave, 289, 295, 346
noise in, 346, 355
performance measurements of, 355
radiometer, *see* Radiometer
superheterodyne, 204, 232, 288, 295, 349, 353
Reduced mass, 52
Reflection coefficient, cavity, 157, 162
plasma, 128–131, 194, 199, 267, 270, 287
Reflections, from small plasma column, 239, 240
internal, multiple, 126, 129, 131, 204, 240, 298, 342
measurement of, 193, 195, 289, 298, 361
see also Scattering
Refraction, attenuation by, 137, 140
Refractive index, 5, 7, 93, 398
as function of propagation angle, 23, 38, 42, 45, 49, 56
complex, 7, 398
contour maps of, 47–50
for characteristic waves, 23, 34, 52

Refractive index, for cyclotron wave, 15, 35, 47, 53, 108, 110
for extraordinary wave, 26, 35, 48, 53, 111, 220
for Faraday rotation, 19, 219, 224
for ordinary wave, 26, 35, 48, 53
in fluctuating medium, 230
in moving medium, 229
in warm plasma, 108, 109, 111, 116
Refractive-index surface, 42, 45
Relativistic effects, 115, 275, 284
Relaxation time constant, 68, 92
of tuned circuit, 156, 205, 364
relation to cross-modulation, 92, 230, 231
Resistivity, surface, 305, 361
tensor, 21, 29
waveguide, 305, 307
see also Conductivity
Resonance, cavity, 157
cyclotron, 18, 84, 91, 92, 110, 279
dipole (perpendicular), 178, 241
hybrid, 34, 53, 181, 220, 298
Resonance conditions, 18, 28, 34–39, 44, 53–56, 125, 279
Resonance frequency, shift of, as function of propagation angle, 38, 42, 49
Rogowsky loop, 368, 387; *see also* Field strength; Magnetic probes
Rotating coordinates, 31
Rotating unit vectors, 13, 31
Runaway electrons, 285, 300
Rutherford scattering formula, 62
Rydberg energy constant, 87, 252

Scattering, angle of, 58, 233, 235
Bragg, 235
cross section for, 93, 232, 233
enhanced, 94, 236
experiments on, 232, 237, 239, 241, 366
from plasma column, 235, 240, 241
from plasma fluctuations, 234, 236
incoherent, 93, 232
optical, 367
stray, 195, 204, 227, 232, 236, 361
Thomson, 93, 232
Schlieren photography, 372, 374
Sellmeier formula, 402
Sharp boundaries, cylindrical plasma with, 130, 137, 138, 175
slab plasma with, 127
Sheath, between plasma and conductor, 78, 386
effects on Langmuir probes, 380, 384, 386
effects on plasma radiation, 302
oscillations in, 300, 386
Shielding, correction to Gaunt factor, 252, 253
correction to ln Λ, 86, 89
debye, 76, 82, 256, 320
Shock waves, measurement of intensity of, 387
measurement of velocity of, 368, 373, 374
Skin depth, 400
in metals, 305, 307
in plasma, 8, 10
see also Attenuation length
Skin effect, 8, 306
Slab plasma, diffusely bounded, 120
propagation through, 120, 126, 127, 131, 212
radiation from, 263, 264, 269, 278, 298
sharply bounded, 127
transmission coefficient for, 129, 131, 298
validity of model for, 150, 151
Slowness surface, 42, 45
Snell's law, 257
Sources, plasma, 293, 301; *see also* Plasma, production of
Spacecharge, 2, 132, 172
Spacecharge waves, 170
body, 155, 181, 235
coupling to electromagnetic radiation, 182, 227, 286, 300, 302
dipole resonance frequency of, 179, 235, 241
dispersion equation for, 177, 184
fast and slow, 171
group velocity of, 174, 187
growth of, 185, 188, 236
in bounded plasma, 175

Spacecharge waves, in drifting plasma, 171, 182
in fluctuating plasma, 229, 232, 241
in plasma in magnetic field, 179, 188, 191
in warm plasma, 183, 189
Landau damping of, 185, 189, 232
ω-β diagram for, 174, 177, 181, 190
phase velocity of, 185, 236
probes for, 360, 379, 386
propagation coefficient for, 173, 177, 182, 185, 187, 190
related to electrostatic instabilities, 185, 189, 234
surface, 155, 176, 182
see also Plasma oscillations
Spatial dispersion, 100, 405
Spatial distribution, of electron density, 123, 161, 212, 214, 218, 222
measurement of, 123, 212, 219, 221, 224
Special electron densities, 35, 53
Special frequencies, 34, 53
Specific heats, ratio of, 99
Spectroscopic measurements, *see* Optical spectroscopy
Spectrum, frequency, *see* Frequency spectrum
Spherical harmonics, 68
Spitzer's ln Λ, 78, 80, 85, 86, 226
Spontaneous emission, 259
Standing wave, 129, 157, 162, 400
Standing-wave ratio, 128, 157
Stimulated absorption and emission, 259
Superthermal electrons, 285, 300, 302
Surface reflection, effect of gradient on, 195, 199
effect on emissivity, 197, 266, 269
Susceptibility, 393, 401
Synchrotron radiation, 272, 275, 292, 302
power radiated as, 275
spectrum of, 276, 278
see also Cyclotron radiation; Radiation

Temperature, blackbody, 243, 298
electron, *see* Electron energy; Electron temperature
noise, 290, 299, 349, 353, 355
radiation, 242
Tensor, hermitian, 407
inverse or reciprocal, 21, 29, 33, 408
symmetric, 407
unit, 23, 30, 408
Tensors, uses of, 22, 29, 31, 51, 105, 407
Test particle, 58
Thermal radiation, 242; *see also* Radiation
Thermal velocity, 74, 86; *see also* Electron energy; Velocity
Thomson scattering, 93, 232; *see also* Scattering
Three frequency regions, 7
Threshold signal sensitivity, 346, 347; *see also* Receivers
Time constant, relaxation, 68, 92, 230, 231
tuned circuit, 156, 205, 364
video, 346, 364
Total collision cross section, 59; *see also* Cross section
Total collision frequency, 59; *see also* Collision frequency
Transconductance, *see* Interaction; Modulation
Transit-time broadening, 274; *see also* Broadening
Transmission, ducted, 48, 182, 225, 297
free-space beam, 117, 141
see also Propagation
Transmission coefficient, 128–131, 267, 270
measurement of 192–212
of plasma in waveguide, 155, 163, 298
of plasma slab, 129, 131, 298
Transmission lines, 305
attenuation in, 166, 306, 308
free-space link, 311, 312
special waveguide, 307, 320
waveguide, 165, 305
see also Waveguides

Transmitter, microwave, 193, 212, 237, 295, 344
  frequency control of, 208, 237, 295, 351
  modulation of, 204, 206, 208, 295
  see also Microwave sources
Transparent medium, radiation from, 245, 254, 263; *see also* Bremsstrahlung; Radiation
Traveling-wave tubes, 344, 345, 348; *see also* Backward-wave oscillator; Microwave sources; Transmitter
Tunnel diodes, as amplifiers, 352
  as oscillators, 345
Tunneling, of radiation, 127, 292
  through cut-off regions, 127, 227, 228
Turbulence, instability-generated, 197, 234, 372
  measurement of, 227, 234, 366, 372, 387

Unit vectors, rotating, 13, 31
Unitary matrix transformation, 33, 106
Upper hybrid frequency, 35, 53, 181, 220, 298

Vacuum considerations, 356
  ultra-high, 357
Velocity, electron thermal, 74, 86
  group, 5, 11, 46, 168, 178, 187, 398
  ion, 51, 367
  ordered component of, 64
  phase, 5, 11, 45, 171, 187, 397
  see also Electron energy
Velocity dependence of collision frequency, 63, 72, 92
Velocity distribution function, 64, 66, 92, 104, 183
  double-humped, 185, 189, 234, 286
  Maxwellian, 68, 71, 186, 189
  measurement of, 297, 367
  moments of, 69
  normalization of, 69
Viscous damping, representation of collisions by, 6, 64; *see also* Collisional damping
Vlasov (kinetic) equation, 67, 184
Voight line shape, 275, 298; *see also* Broadening; Optical spectroscopy
Voltage standing-wave ratio (VSWR), 128, 157

Wanted wave, 91
Warm plasma, 95, 109
Wave, characteristic, 24, 38
  cyclotron, 15, 35, 114, 181, 224
  evanescent, 8
  extraordinary, 26, 34, 48, 53, 111, 134, 161, 220
  in warm plasma, 108, 111, 116
  ordinary, 11, 26, 34, 49, 53, 111, 220
  principal, 34, 52
  spacecharge, 170, 175, 181, 188, 191, 235
  surface, 155, 176, 182
  velocity of, 5, 11, 45, 168, 178, 187, 397
  whistler, 18, 48, 182, 225, 297
Wave equation, 396, 404
Wave impedance, 91, 127, 133, 400
Wave-normal surface, 42, 45, 55
Wave polarization coefficient, 24
Wave propagation, *see* Propagation
Waveguide, attenuation in, 165, 166, 306, 308
  beyond cutoff, 8
  dielectric, 224, 310, 311, 334
  elliptical, 320
  materials for, 306, 307
  modes of, 165, 307–310
  ω-β diagram for, 167, 170
  plasmas in, 163, 168, 297
  propagation coefficient of, 165, 298
  radiation measurements in, 297
  spacecharge wave, 155, 174, 178, 235
  special modes of, 309–312
  standard bands, 306
  see also Transmission lines
Wavelength, free-space, 397
  guide, 165–167
Wave number, 7, 397
Whistlers (whistler mode), 18, 48, 182, 225, 297
  damping of, 114, 185, 226
Windows, for atmospheric propagation, 312
  waveguide vacuum, 197, 333, 357
WKB approximation, 119, 125

X-rays, measurement of, 297, 367, 391